The Dissertation Committee for Aboulghasem Kazemi Nia Korrani Certifies that this is the approved version of the following dissertation:

Mechanistic Modeling of Low Salinity Water Injection

Committee:

Kamy Sepehrnoori, Supervisor

Mojdeh Delshad

Kishore K. Mohanty

David DiCarlo

Gary R. Jerauld

Mohammad H. Kalaei

Mechanistic Modeling of Low Salinity Water Injection

by

Aboulghasem Kazemi Nia Korrani, B.E.; M.S.

Dissertation

Presented to the Faculty of the Graduate School of

The University of Texas at Austin

in Partial Fulfillment

of the Requirements

for the Degree of

Doctor of Philosophy

The University of Texas at Austin

December 2014

Dedication

To my parents, brothers, and sisters

Acknowledgements

It is a great honor for me to express my sincere gratitude to my supervising professor, Dr. Kamy Sepehrnoori, for his excellent guidance, patience, support, and encouragement. I have learned a lot from his keen observations, scientific intuition, and vast knowledge. It was a privilege to have had an opportunity to work with him.

I greatly appreciate David L. Parkhurst of the United States Geological Survey for his four years of continuous advice, direction, and support in coupling IPhreeqc with both the UTCOMP and UTCHEM simulators. David responded to more than hundred emails of mine and I really acknowledge his patience with my basic questions. Without his help the coupling of IPhreeqc with the simulators, which is the main part of my dissertation, would not have been possible.

I appreciate the time, valuable comments, and feedback of my committee members Dr. Mojdeh Delshad, Dr. Gary Jerauld, Dr. Kishore Mohanty, Dr. David DiCarlo, and Dr. Mohammad H. Kalaei. Special thanks go to Dr. Chowdhury Mamun for his review and comments of my dissertation. I also enjoyed technical discussion with Dr. Abdoljalil Varavei.

I would like to acknowledge the staff of the Petroleum and Geosystems Engineering Department at The University of Texas at Austin, Dr. Roger Terzian, Tim Guinn, John Cassibry, Michelle Mason, Phyllis Harmon, Joanna Castillo, Frankie Hart, Mary Pettengill, and Glen Baum for their technical and administrative support.

I express my extreme appreciation to Raymond Choo, EOR Deployment Manager, and Dr. Gary R. Jerauld, Reservoir Engineering Advisor, for the opportunity to intern at BP America Inc. Inclusion of the hydrocarbon phase effect on the aqueous-rock geochemistry was implemented in UTCOMP-IPhreeqc during my internship with BP.

I appreciate my close friend Mojtaba Ghasemi Doroh for his help in parallelizing the geochemistry module of the UTCOMP-IPhreeqc and UTCHEM-IPhreeqc simulators. Also, I have enjoyed helpful technical discussions with my great friends Mohsen Rezaveisi, Hamidreza Lashgari, Saeedeh Mohebbinia, and Javad Behseresht. I acknowledge Wensi Fu in providing user's manual and technical guide for UTCOMP-IPhreeqc.

I will definitely miss my great officemates Wei Yu, Mahmoud Shakiba, Ali Abouie, Shayan Tavassoli, Jose Sergio, Hamidreza Lashgari, Emad Al-Shalabi, Reza Ganjdenesh, Walter Fair, Yifei Xu, and Wensi Fu.

I would like to thank my friends Mohsen Rezaveisi, Mojtaba Ghasemi Doroh, Javad Behseresht, Saeedeh Mohebbinia, Amir Frooqnia, Rohollah Abdollah-Pour, Amir Kianinejad, Behzad Eftekhari, Ali Goudarzi, Mahdy Shirdel, Hamed Darabi, Ali Moinfar, Mohsen Taghavifar, Mehdi Haghshenas, Soheil Ghanbarzadeh, Morteza Elahi Naraghi, Amirreza Rahmani, Ali Farhadinia, Mohammad Lotfollahi, Mohammadreza Beigi, Mahdi Haddad, Saeid Enayat-Pour, Ehsan Saadat-Pour, Rouzbeh Ghanbarnezhad, Amin Ettehadtavakkol, Ahmad Sakhaee-Pour, Abdolhamid Hadibeik, Zoya Heidari, Vahid Shabro, Ali Rasheed, Akand Islam, Ali Afshaar-Pour, Mehran Hosseini, Ayaz Mehmani, Yashar Mehmani, Maryam Mirabolghasemi, Alireza Sanaei, Mohammad Eshkalak, Masoud Behzadi, and Pooneh Hosseininoosheri as well as many other friends and classmates whom I did not name explicitly.

I express my gratitude to Abu Dhabi National oil Company (ADNOC) along with the member of companies of Reservoir Simulation Joint Industry Project (RSJIP) at The University of Texas at Austin for their financial support for this research.

Mechanistic Modeling of Low Salinity Water Injection

Aboulghasem Kazemi Nia Korrani, Ph.D.

The University of Texas at Austin, 2014

Supervisor: Kamy Sepehrnoori

Low salinity waterflooding is an emerging enhanced oil recovery (EOR) technique in which the salinity of the injected water is substantially reduced to improve oil recovery over conventional higher salinity waterflooding. Although there are many low salinity experimental results reported in the literature, publications on modeling this process are rare. While there remains some debate about the mechanisms of low salinity waterflooding, the geochemical reactions that control the wetting of crude oil on the rock are likely to be central to a detailed description of the process. Since no comprehensive geochemical-based modeling has been applied in this area, we decided to couple a state-of-the-art geochemical package, IPhreeqc, developed by the United States Geological Survey (USGS) with UTCOMP, the compositional reservoir simulator developed at the Center for Petroleum and Geosystems Engineering in The University of Texas at Austin.

A step-by-step algorithm is presented for integrating IPhreeqc with UTCOMP. Through this coupling, we are able to simulate homogeneous and heterogeneous (mineral dissolution/precipitation), irreversible, and ion-exchange reactions under non-isothermal, non-isobaric and both local-equilibrium and kinetic conditions. Consistent with the literature, there are significant effects of water-soluble hydrocarbon components (e.g.,

CO_2, CH_4, and acidic/basic components of the crude) on buffering the aqueous pH and more generally, on the crude oil, brine, and rock reactions. Thermodynamic constrains are used to explicitly include the effect of these water-soluble hydrocarbon components. Hence, this combines the geochemical power of IPhreeqc with the important aspects of hydrocarbon flow and compositional effects to produce a robust, flexible, and accurate integrated tool capable of including the reactions needed to mechanistically model low salinity waterflooding. The geochemical module of UTCOMP-IPhreeqc is further parallelized to enable large scale reservoir simulation applications.

We hypothesize that the total ionic strength of the solution is the controlling factor of the wettability alteration due to low salinity waterflooding in sandstone reservoirs. Hence, a model based on the interpolating relative permeability and capillary pressure as a function of total ionic strength is implemented in the UTCOMP-IPhreeqc simulator. We then use our integrated simulator to match and interpret a low salinity experiment published by Kozaki (2012) (conducted on the Berea sandstone core) and the field trial done by BP at the Endicott field (sandstone reservoir).

On the other hand, we believe that during the modified salinity waterflooding in carbonate reservoirs, calcite is dissolved and it liberates the adsorbed oil from the surface; hence, fresh surface with the wettability towards more water-wet is created. Therefore, we model wettability to be dynamically altered as a function of calcite dissolution in UTCOMP-IPhreeqc. We then apply our integrated simulator to model not only the oil recovery but also the entire produced ion histories of a recently published coreflood by Chandrasekhar and Mohanty (2013) on a carbonate core.

We also couple IPhreeqc with UTCHEM, an in-house research chemical flooding reservoir simulator developed at The University of Texas at Austin, for a mechanistic integrated simulator to model alkaline/surfactant/polymer (ASP) floods. UTCHEM has a

comprehensive three phase (water, oil, microemulsion) flash calculation package for the mixture of surfactant and soap as a function of salinity, temperature, and co-solvent concentration. Similar to UTCOMP-IPhreeqc, we parallelize the geochemical module of UTCHEM-IPhreeqc. Finally, we show how apply the integrated tool, UTCHEM-IPhreeqc, to match three different reaction-related chemical flooding processes: ASP flooding in an acidic active crude oil, ASP flooding in a non-acidic crude oil, and alkaline/co-solvent/polymer (ACP) flooding.

Table of Contents

List of Tables

List of Figures

Chapter 1: Introduction

This chapter discusses the main objectives and the overall scope of this dissertation. Moreover, we briefly describe the structure and different chapters of this dissertation.

1.1 DESCRIPTION OF THE PROBLEM

Waterflooding as a secondary oil recovery technique is still the most common and versatile method since 1865. This is on account of various reasons, ranging from high efficiency in displacing light to medium gravity crude oils, ease of injection into oil-bearing formations, availability and low cost water to lower the project capital and operating costs. This obviously leads to favorable economics compared to other improved oil recovery (IOR) methods. However, in recent years a tertiary effect of waterflooding has been observed, depending on the composition and the salinity of the injected water. Literature shows that the adjustment of injected brine composition of a mature waterflood can cause an increase in oil production. This means that the quality of injected water is as important as the quantity and the former should be monitored. If the salinity of the injected water is controlled the process is called low salinity waterflooding. This technique is known as LoSal®[1], SmartWater Flood[2], Smart Water[3], Advanced Ion

Note: Throughout this dissertation care was taken to cite the trademarks properly. However, the author disclaims responsibility for specifying which trademarks are owned by which companies.

[1] LoSal® is a trademark of BP p.l.c
[2] SmartWater Flood was proposed by Saudi Aramco people (Yousef *et al.*, 2010; 2012)
[3] Smart Water is frequently used by Austad and his co-researchers at the University of Stavanger (Austad *et al.*, 2010; 2011)

Management[SM1], Designer Waterflooding[TM2], and Modified Salinity Flooding[TM3] in the literature. We refer to this process as low salinity waterflooding (mainly for sandstones) or modified salinity waterflooding (mainly for carbonates) in this dissertation.

It is not until relatively recently that it has begun to be thought of waterflooding as a chemical as well as a physical process where the ionic composition of the brine can impact oil recovery by changing wettability (Yildiz and Morrow, 1996; Tang and Morrow 1996). Evidence from the laboratory and field studies have definitively shown that using low salinity can substantially increase oil recovery compared to conventional high salinity waterflooding, with incremental recovery in the range of 5% to 40% of the base waterflood (Tang and Morrow 1996; Webb *et al.*, 2004; McGuire *et al.*, 2005; Webb *et al.*, 2005; Robertson, 2007; Lager *et al.*, 2008a; Lager *et al.*, 2008b; Patil *et al.*, 2008; Seccombe *et al.*, 2008; Pu *et al.*, 2010; Seccombe *et al.*, 2010; Vledder *et al.*, 2010; Rivet *et al.*, 2010; Nasralla *et al.*, 2011a; 2011b; Mahani *et al.*, 2011; Hadia *et al.*, 2011; Lager *et al.*, 2011; Callegaro *et al.*, 2013 Austad *et al.*, 2008; Chandrasekhar and Mohanty, 2013; Chandrasekhar, 2013; Alotaibi *et al.*, 2010; Al-Attar *et al.*, 2013; Gupta *et al.*, 2011; Hognesen *et al.*, 2005; Fathi *et al.*, 2012; Romanuka *et al.*, 2012; Zhang *et al.*, 2007; Austad *et al.*, 2005; Austad *et al.*, 2011; Strand *et al.*, 2006; Tweheyo *et al.*, 2006; Shariatpanahi *et al.*, 2011; Fernø *et al.*, 2011; Sultani *et al.*, 2012; Rezaei Gomari and Hamouda, 2006; Hamouda *et al.*, 2008; Gupta and Mohanty; 2011; Chukwudeme and Hamouda, 2009). Some of these reports are discussed later.

Optimization of any EOR processes requires a predictive model. A predictive model is also needed to fully understand the underlying mechanisms driving the EOR

[1] Advanced Ion Management is the service mark of Exxon Mobil
[2] Designer Waterflooding is the trademark of Shell
[3] Modified salinity flooding[TM] is used in Zekri *et al.* (2011).

processes. Unfortunately, publications on modeling low salinity waterflooding are limited. It is widely believed that low salinity waterflooding changes wettability through geochemical reactions (Lager *et al.*, 2008a; Austad *et al.*, 2010; Pu *et al.*, 2010; Farooq *et al.*, 2011; Nasralla *et al.*, 2011a; 2011b; RezaeiDoust *et al.*, 2011; Fjelde *et al.*, 2012; Brady and Krumhansl, 2012; Dang *et al.*, 2013; Emadi and Sohrabi, 2013; Austad *et al.*, 2008; Fathi *et al.*, 2012; Strand *et al.*, 2006; Austad *et al.*, 2005). Hence, mechanistic modeling of this process is possible only by modeling geochemical reactions. To the best author's knowledge, there is no comprehensive geochemical-based reservoir simulation model in the industry for low salinity waterflooding. Models proposed for low salinity waterflooding are not mechanistic (i.e., no geochemistry modeling is included) (Jerauld *et al.*, 2008; Wu and Bai, 2009; Gupta *et al.*, 2011; Aladasani *et al.*, 2012; Al-Shalabi *et al.*, 2014a) or they are simple in the sense of geochemistry or reservoir simulation (Omekeh *et al.*, 2011; Dang *et al.*, 2013; Al-Shalabi *et al.*, 2014b).

1.2 RESEARCH OBJECTIVES

In this dissertation, we model low salinity waterflooding mechanistically and comprehensively based on the geochemical reactions. In line with several experimental observations published in the literature we hypothesize that wettability alteration is the underlying mechanism in low (or modified) salinity waterflooding. Hence, the key objective in our approach is to link the water-rock chemistry to changes in the state of a rock (e.g., wettability). Because geochemical reactions are the basis for this mechanistic modeling, we would need a geochemical engine to handle complicated geochemical reactions of the process. Toward this goal, we coupled IPhreeqc (Charlton and Parkhurst, 2011), developed by the United States Geological Survey (USGS), with UTCOMP, a compositional reservoir simulator, developed in The University of Texas at Austin, to

build a robust, accurate, and flexible integrated tool for modeling low salinity waterflooding. IPhreeqc is used in our modeling because we need a robust state-of-the-art geochemical package to handle complex geochemical reactions involved in this process. This geochemical package was coupled with a reservoir simulator to expand its capability from one-dimensional and single-phase to multi-dimensional and multi-phase oil field reactive-transport problems (IPhreeqc can model single-phase and one-dimensional reactive-transport problems). We intentionally used a compositional reservoir simulator for this purpose to include the buffering effect of commonly occurring hydrocarbon phase components (e.g., CO_2, CH_4, and acidic/basic) on the aqueous-rock geochemistry. In other words, we model reactive transport processes along with phase equilibrium calculation in an EOS compositional model. We then apply our integrated tool (i.e., UTCOMP-IPhreeqc) to model low salinity waterflooding in both sandstone and carbonate reservoirs.

1.3 BRIEF DESCRIPTION OF CHAPTERS

Chapter 2 discusses with details all implementations applied in UTCOMP towards building a comprehensive simulator for modeling low (or modified) salinity waterflooding. The chapter includes the formulation (i.e., the mass conservation equation) implemented in UTCOMP to transport the geochemical species. EQBATCH (Bhuyan, 1989) is then coupled with UTCOMP to handle geochemical reactions. However, the physics included in EQBATCH is limited and also EQBATCH is not robust due to numerical convergence problems. To tackle the issues involved in EQBATCH, IPhreeqc (Charlton and Parkhurst, 2011) is integrated with UTCOMP that provides a complete geochemical package to model geochemical reactions. On the other hand, compare with UTCOMP-EQBATCH, UTCOMP-IPhreeqc requires more

computational time and computer memory. Hence, we parallelize the geochemistry module of UTCOMP-IPhreeqc for large-scale reservoir simulation applications.

Chapter 3 presents the low salinity waterflooding in sandstone reservoirs. In this chapter we first review the literature on the laboratory works, field applications, and models proposed in sandstone formations. A mechanistic model, based on the total ionic strength of the solution, is then implemented in UTCOMP-IPhreeqc to relate the wettability alteration to geochemical reactions. Finally, we apply our integrated tool to match and interpret a low salinity coreflood published by Kozaki (2012) and the field trial at the Endicott field.

Chapter 4 discusses the modified salinity waterflooding in carbonate reservoirs. Similar to Chapter 3, we first review the literature and then implement a model, based on calcite dissolution, in UTCOMP-IPhreeqc for modified salinity waterflooding in carbonates. Finally we validate the model implemented in UTCOMP-IPhreeqc against a coreflood published by Chandrasekhar and Mohanty (2013).

Chapter 5 describes the procedure through which IPhreeqc is coupled with UTCHEM, an in-house research chemical flooding reservoir simulator developed in The University of Texas at Austin, towards a mechanistic simulator for modeling Alkaline/Surfactant/Polymer (ASP) floods. Similar to UTCOMP-IPhreeqc, we parallelize the geochemistry module of UTCHEM-IPhreeqc. UTCHEM-IPhreeqc is then applied to match three different reaction-related chemical flooding processes: ASP flooding in an acidic active crude oil, ASP flooding in a non-acidic crude oil, and alkaline/co-solvent/polymer (ACP) flooding.

Chapter 6 illustrates capability of the UTCHEM-IPhreeqc and UTCOMP-IPhreeqc integrated simulators to model variety of reactive-transport problems (other than

low salinity waterflooding and chemical floods) including scale depositions and groundwater modeling.

Chapter 7 presents the summary of the dissertation and the concluding remarks. We further propose some recommendations that can be accomplished for further enhancements in both UTCOMP-IPhreeqc and UTCHEM-IPhreeqc simulators.

Appendix A briefly explains geochemical concepts used throughout this dissertation. Appendix B provides sample input files for UTCOMP-EQBATCH and UTCHEM-EQBATCH simulators. Appendix C presents a simplified code along with a verification case showing how methods available in IPhreeqc are applied to communicate between this geochemical package and a client simulator (i.e., UTCOMP or UTCHEM). Appendix D illustrates the detailed computational flowchart applied in UTCOMP-IPhreeqc. Appendix E provides UTCOMP-IPhreeqc input files of a sample case. Moreover, Appendix E shows how gridblocks geochemistry data are stored in the computer memory; how geochemistry of gridblocks are modified in each simulation time step; how IPhreeqc outputs are organized in the computer memory to be transferred to UTCOMP. The parallel version of the simplified code, provided in Appendix C, is given in Appendix F. Included in Appendix F is also a case that verifies our parallelization procedure and shows the decrease in computational time due to the parallel processing. Appendix G provides command lines implemented in UTCOMP-IPhreeqc that store gridblocks geochemistry data from the computer memory into a file to resume the simulation (i.e., simulation restart files). Finally, Appendix H provides the UTCHEM-IPhreeqc input files applied to model the ACP coreflood presented in Chapter 5.

Chapter 2: Towards a Mechanistic Tool for Modeling Low Salinity Waterflooding[1]

As discussed in Chapter 1, we believe that mechanistic modeling of low (or modified) salinity waterflooding is possible only through consideration of geochemical reactions. Hence, to comprehensively model this process, we first implement the mass conservation equation in UTCOMP, The University of Texas at Austin in-house compositional reservoir simulator (Chang, 1990), in order to model the transport of geochemical elements (e.g., Na, Ca, Mg, S, C, etc.) in this simulator. Geochemical species are not like inactive tracers. Hence, a geochemical engine should also be included in the modeling simulator (i.e., UTCOMP) to determine the equilibrium state in terms of geochemistry in reservoir gridblocks at each time step. Towards this goal, we couple EQBATCH, a previously developed geochemical module by Bhuyan (1989) at The University of Texas at Austin, to UTCOMP. To make the simulator more flexible, robust, and accurate, we also integrate IPhreeqc (Charlton and Parkhurst, 2011), the modules-based version of PHREEQC, the USGS geochemical package (Parkhurst and Appelo,

[1] Some parts of Chapters 2 and 3 are published in the following citation:

Korrani, A. K. N., Jerauld, G. R., and Sepehrnoori, K. 2014. Coupled Geochemical-Based Modeling of Low Salinity Waterflooding. SPE Improved Oil Recovery Symposium, Tulsa, Oklahoma, USA, 12-16 April. http://dx.doi.org/10.2118/169115-MS.

Below briefly describes nature of coathors'contribution.

- Gray R. Jerauld: The idea of expanding UTCOMP-IPhreeqc from single-phase to multi-phase reactive-transport problems through considering the fugacity, including the acid/basic component using the pseudo-fugacity concept, set up the TDRM scripts and modified some parts of the TDRM code to do low salinity waterflooding, performing the original runs in the history matching of Endicott trial, and revising the manuscript.

- Kamy Sepehrnoori: The idea of coupling PHREEQC with UTCOMP for mechanistic modeling of low salinity water injection, technical support, and revising the manuscript.

1999; 2013), to UTCOMP. One of the hypotheses we make in this dissertation is that the wettability alteration is the underlying mechanism in low salinity waterflooding. Hence, to enable applying UTCOMP-IPhreeqc for mechanistic modeling of low salinity waterflooding, a wettability alteration model, based on the interpolating technique, is included in this integrated simulator.

Although IPhreeqc provides a complete geochemical package for geochemical modeling, UTCOMP-IPhreeqc requires more computer memory and computational time compared with UTCOMP-EQBATCH. To tackle this issue, we parallelize the geochemistry module of UTCOMP-IPhreeqc. There are other capabilities (e.g., restart option and expanding the UTCOMP-IPhreeqc simulator to be used along with Top-Down Reservoir Modeling, BP's history matching tool (Williams *et al.*, 2004; Jerauld *et al.*, 2010)) that we added to the UTCOMP-IPhreeqc simulator. What follows below presents the description of entire set of features included in UTCOMP towards a mechanistic simulator for low (or modified) salinity waterflooding.

2.1 UTCOMP DESCRIPTION

UTCOMP is a non-isothermal, three-dimensional, equation-of-state, implicit in pressure and explicit compositions (IMPEC), compositional reservoir simulator developed upon extensive research, at The University of Texas at Austin (Chang, 1990; Khan, 1992; Xiao, 1994; Cheng *et al.*, 2000; Vikas, 2002; Ghasemi Doroh, 2012; Li, 2012; Darabi, 2014; Korrani, 2014b; Mohebbinia *et al.*, 2013; Mohebbinia, 2013; Shirdel, 2013; Rezaveisi *et al.*, 2014a; 2014b; Shakiba, 2014; UTCOMP Technical Documentation, 2011). UTCOMP is capable of modeling up to four-phase (an aqueous, a gas, and two liquid hydrocarbon phases) flow behavior. This simulator has been

developed as general purpose code for miscible and immiscible gas injection EOR processes.

Figure 2-1 gives the simplified UTCOMP flowchart where we start the simulation at time t after the initialization step is completed. In the initialization step, gridblock pressures are corrected for gridblock depths; phase behavior calculation is performed using the overall hydrocarbon mole fractions provided by the user; constant terms of the transmissibilities are calculated.

After the initialization step, pressure equation is solved implicitly. The UTCOMP pressure equation is derived based on the fact that the pore volume should be filled completely by the total fluid volume (Chang, 1990):

$$V_t\left(P,\vec{N}\right)=V_P\left(P\right), \tag{2.1}$$

where

$V_t =$ total fluid volume (ft^3)

$V_p =$ pore volume (ft^3)

$P =$ pressure (psi)

$\vec{N} =$ component moles

In Eq. (2.1), the pore volume is only a function of pressure while the occupying fluids depend on both the pressure and total number of moles of each component. After the rigorous calculation, the final pressure equation, according to UTCOMP, is as follows (Chang, 1990):

$$\left(V_p^0 c_f - \frac{\partial V_t}{\partial P}\right)\left(\frac{\partial P}{\partial t}\right) - 0.006328 V_b \sum_{i=1}^{n_c+1} \bar{V}_{ti} \vec{\nabla} \bullet \sum_{j=1}^{n_p} \vec{\vec{k}} \lambda_{rj} \xi_j x_{ij} \nabla P$$
$$= 0.006328 V_b \sum_{i=1}^{n_c+1} \bar{V}_{ti} \vec{\nabla} \bullet \sum_{j=1}^{n_p} \vec{\vec{k}} \lambda_{rj} \xi_j x_{ij} \left(\nabla P_{c2j} - \gamma_j \nabla D\right) \qquad (2.2)$$
$$+ V_b \sum_{i=1}^{n_c+1} \bar{V}_{ti} \vec{\nabla} \bullet \sum_{j=1}^{n_p} \phi \xi_j S_j \vec{\vec{K}} \nabla x_{ij} + \sum_{i=1}^{n_c+1} \bar{V}_{ti} q_i,$$

where

$V_p^0 =$ pore volume at reference pressure (ft^3)

$c_f =$ formation compressibility (psi^{-1})

$V_t =$ total fluid volume (ft^3)

$P =$ pressure (psi)

$t =$ time (day)

$V_b =$ bulk volume (ft^3)

$n_c =$ number of components

$\bar{V}_{ti} =$ the partial derivative of total fluid volume with respect to component i (ft^3/lbmole)

$n_p =$ number of phases

$\vec{\vec{k}} =$ absolute permeability diagonal tensor (md)

$\lambda_{rj} =$ relative mobility of phase j (cp^{-1})

$\zeta_j =$ molar density of phase j (lbmoles/ft^3)

$x_{ij} =$ mole fraction of component i in phase j

$P_{c2j} =$ capillary pressure of phase 2 and phase j (psi)

$\gamma_j =$ specific weight of phase j (psi/ft)

$D =$ depth from the datum plane (ft)

$\phi =$ porosity (fraction)

$\vec{\vec{K}} =$ dispersion tensor (ft^2/day)

$S_j =$ saturation of phase j

$q_i =$ molar flowrate of component i (lbmoles/day)

The value of 0.006328 in Eq. (2.2) is the conversion factor from Darcy units to field units. All the terms in the right hand side of Eq. (2.2) are known from the previous time step and pressure is the only unknown in the left hand side (coefficients are calculated using the previous time step data). After discretization of the pressure equation, a linear system of NB (number of gridblocks) equations needs to be solved for the gridblock pressures. Discritization of the pressure equation is well documented in Chang (1990) and is not repeated here.

Once the gridblock pressures are updated, mass conservation equation is solved to explicitly calculate the total moles of hydrocarbon components. Mass conservation equation for each component in UTCOMP is as follows (Chang, 1990):

$$\frac{\partial N_i}{\partial t} - V_b \vec{\nabla} \bullet \left[\sum_{j=1}^{n_p} 0.006328 \zeta_j \vec{\vec{k}} \lambda_{rj} x_{ij} \left(\nabla P_j - \gamma_j \nabla D \right) + \phi \zeta_j S_j \vec{\vec{K}}_{ij} \nabla x_{ij} \right] - q_i = 0 \qquad (2.3)$$

$$for\ i = 1, 2, ..., n_c, \mathrm{n_{c+1}},$$

where

$N_i =$ number of moles of component i (lbmoles)

$t =$ time (day)

$V_b =$ bulk volume (ft^3)

$n_p =$ number of phases

ζ_j = molar density of phase *j* (lbmoles/ft^3)

$\vec{\vec{k}}$ = absolute permeability diagonal tensor (md)

λ_{rj} = relative mobility of phase *j* (cp^{-1})

x_{ij} = mole fraction of component *i* in phase *j* (lbmoles/lbmoles)

P = pressure (psi)

γ_j = specific weight of phase *j* (psi/ft)

D = depth from the datum plane (ft)

ϕ = porosity (fraction)

S_j = saturation of phase *j*

$\vec{\vec{K}}$ = dispersion tensor (ft^2/day)

q_i = molar flowrate of component *i* (lbmoles/day)

The equation above is written in terms of total moles (in lbmoles) per unit time (i.e., day); q_i is positive if the component *i* is injected and negative if the component is produced. Dispersion is described by the Fick's law and the full dispersion tensor is modeled for the physical dispersion.

$$\vec{\vec{K}} = \begin{bmatrix} K_{xx,ij} & K_{xy,ij} & K_{xz,ij} \\ K_{yx,ij} & K_{yy,ij} & K_{yz,ij} \\ K_{zx,ij} & K_{zy,ij} & K_{zz,ij} \end{bmatrix}, \tag{2.4}$$

where

$\vec{\vec{K}}$ = dispersion tensor (ft^2/day)

K_{xx}, K_{yy}, K_{zz} = diagonal elements of the dispersion tensor for component *i* in phase *j* (ft^2/day)

$K_{xy,ij}, K_{yx,ij},$
$K_{xz,ij}, K_{zx,ij}, =$
$K_{yz,ij}, K_{zy,ij}$ off-diagonal elements of the dispersion tensor for component *i* in phase *j* (ft^2/day)

Molecular diffusion and mechanical dispersion contribute to all the elements of the above tensor. The mass conservation equation is discretized and then solved explicitly in UTCOMP (see Chang (1990) for details of discritization).

Next step in the UTCOMP computational flowchart is to determine number of hydrocarbon phases and their amounts and phase compositions using the flash calculation. UTCOMP employs two widely used Peng-Robinson (Peng and Robinson, 1976) and Modified Redlich-Kwong (Turek *et al.*, 1984) cubic equation of states. Stability analysis is performed prior to flash calculation and the latter determines the number of equilibrium phases evolving from the mixture at given temperature, pressure, and overall fluid compositions. UTCOMP also has the capability of three-hydrocarbon phase equilibrium calculation to properly model the CO_2-EOR at temperatures below about 120 ^oF (UTCOMP Technical Documentation, 2011). Other than conventional phase equilibrium calculation methods, reduced phase equilibrium calculatutions are also implemented in UTCOMP (Okuno *et al.*, 2010). Furthermore, Rezaveisi *et al.* (2014a; 2014b) implemented several robust tie-line-based phase equilibrium calculation methods in UTCOMP. Noteworthy, Mohebbinia (2013) implemented four-phase flash calculation in UTCOMP by introducing the water component in the phase equilibrium calculation. Once UTCOMP finishes the flash calculation, phase properties (e.g., molar and mass densities) are evaluated and consequently phase saturations are calculated. The phase saturations are then used to calculate the relative permeability and capillary pressure. For non-isothermal cases, the energy balance equation is solved to compute gridblock

temperatures. The module for solving the energy balance equation was recently implemented in UTCOMP by Darabi (2014). It should be noted that the UTCOMP version used in this dissertation is isothermal. Finally, reservoir rock (e.g., porosity) and fluid properties (e.g., viscosity) are updated for the new component compositions, pressure, and temperature. The same algorithm will be followed for the next time-step until the end of the simulation. A detailed description of UTCOMP can be found in Chang (1990) and the UTCOMP Technical Documentation (2011). It is worth noting that UTCOMP has been recently enhanced with Embedded Discrete Fracture Model (EDFM) to handle complex fracture geometries (Shakiba, 2014).

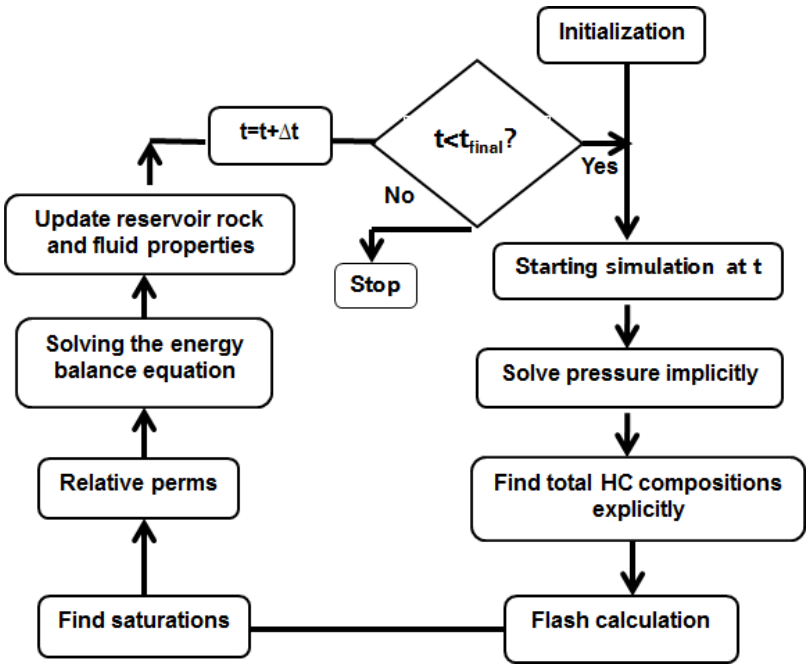

Figure 2-1: Simplified UTCOMP calculation flowchart.

2.2 IMPLEMENTATION OF THE TRANSPORT OF GEOCHEMICAL SPECIES IN UTCOMP

The main goal in this dissertation is to model the low (or modified) salinity waterflooding mechanistically based on the geochemical reactions. Towards this goal, a geochemical module should be augmented in the UTCOMP computational algorithm to solve the mass conservation equation and handle the geochemical reactions involved in the process. Hence, in the first step, the transport of geochemical elements needs to be transcribed into the UTCOMP simulator. In other words, besides the hydrocarbon components, the mass conservation equation should be solved for the geochemical species at each time step. Once at each time step the element concentrations are known for gridblocks, a geochemical package is required to find the equilibrium state at each gridblock.

Although the conservation equation should be solved for any component present in the system, rather than solving the mass conservation equation for the entire fluid species, it is common that the mass conservation equation be solved for the master elements. In other words, if for example, an aqueous phase contains Na^+, $NaHSO_4$, NaCl, Na_2CO_3, Na_2SO_4, $NaHCO_3$, CO_3^{-2}, HCO_3^-, HSO_4^-, SO_4^{-2}, HCl, H^+, and OH^- fluid species, rather than solving the mass conservation equation for all the fluid species, the mass conservation equation is solved only for the constituting elements of the fluid species (i.e., Na, S, Cl, C, H, and O). This approach is applied in the works of Bhuyan (1989), Parkhurst *et al.* (2010), and Wei (2011; 2012). In this approach the lumped element concentration is evaluated from the fluid species using the stoichiometric coefficient multiplies by the fluid species concentration. For example, the lumped concentration of the sodium element for the above mentioned aqueous species is calculated as follows:

$$C_{Na} = C_{Na^+} + C_{NaCl} + 2C_{Na_2CO_3} + 2C_{Na_2SO_4} + C_{NaHSO_4} + C_{NaHCO_3}. \quad (2.5)$$

Using the same concept, the concentrations of the other geochemical elements constituting the fluid species (i.e., S, Cl, C, H, and O) are evaluated. The mass conservation equation is solved for the lumped element concentrations and the newly calculated concentrations are fed to a geochemical engine to find the new equilibrium state. This assumption is valid if the molecular diffusion of the entire set of fluid species is the same. It should be also noted that using this approach accelerates the computational time because the mass conservation equation is solved for less number of components.

Considering the assumption addressed above, a new module is implemented in UTCOMP to solve the mass conservation equation for geochemical elements. We further assume that the geochemical elements are transported only through the aqueous phase. However, as we discuss later (cf. Section 2.7.1) aqueous species can interact with hydrocarbon components (such as CO_2, CH_4, H_2S and acidic/basic components) during the batch reaction calculation. Shown in Figure 2-2 is the UTCOMP algorithm after the implementation of the mass conservation equation for the geochemical elements.

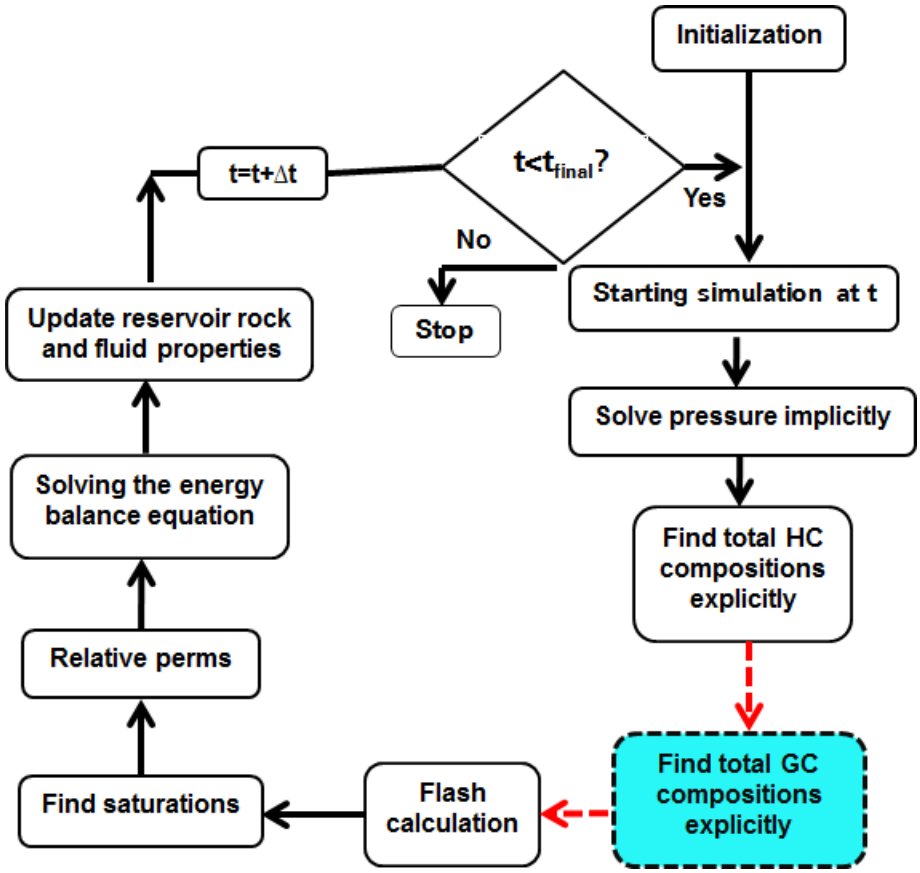

Figure 2-2: Simplified UTCOMP calculation flowchart after implementation of the transport of geochemical species.

Eq. (2.6) presents the mass conservation equation to be solved for the geochemical species:

$$\frac{\partial N_i}{\partial t} + V_b \sum_{j=1}^{n_p} \vec{\nabla} \bullet \left(\rho_j x_{ij} \vec{u}_j - \phi \rho_j S_j \vec{\vec{K}}_{ij} \nabla x_{ij} \right) - q_i = 0 \quad for\, i = 1, 2, ..., n_{gc}, \tag{2.6}$$

where

$N_i =$ moles of geochemical species i (lbmoles)

$t =$ time (day)

V_b = bulk volume (ft^3)

ρ_j = mass density of phase *j* (lb/ft^3)

x_{ij} = geochemical species concentration (lbmoles/lb)

$\vec{u}_j$ = total flux of phase *j* (ft/day)

ϕ = porosity (fraction)

S_j = saturation of phase *j* (fraction)

$\vec{\vec{K}}_{ij}$ = dispersion tensor (ft^2/day)

q_i = molar flowrate of geochemical species *i* (lbmoles/day)

n_{gc} = number of geochemical species

The mass conservation equation solved for the geochemical species is very similar to the one solved for the hydrocarbon components (i.e., Eq. (2.3)). However, Eq. (2.6) is written based on phase mass densities rather than phase molar densities used in Eq. (2.3). It is worth mentioning that although we assume geochemical species remain with the aqueous phase, Eq. (2.6) is still written in the full form that includes all the phases.

Although in reality transport and chemical reactions occur simultaneously, similar to PHAST, we separate the transport and the geochemistry and solve the coupled system through a sequential non-iterative approach (SNIA). PHAST is the USGS groundwater simulator (Parkhurst *et al.*, 2010). In this approach, no chemical reactions are included when solving the mass conservation equation. In other words, geochemical species are treated as inactive tracers when solving the mass conservation equation. This approach is non-iterative because no iteration is performed between the transport and geochemical reactions.

Total flux of phase *j* is defined as Eq. (2.7):

$$\vec{u}_j = -0.006328\vec{\vec{k}}\lambda_{rj}\left(\nabla P_j - \gamma_j \nabla D\right), \tag{2.7}$$

where

$\vec{u}_j =$ total flux of phase *j* (ft/day)

$\vec{\vec{k}} =$ absolute permeability diagonal tensor (md)

$\lambda_{rj} =$ relative mobility of phase *j* (cp^{-1})

$P_j =$ pressure of phase *j* (psi)

$\gamma_j =$ specific weight of phase *j* (psi/ft)

$D =$ depth from the datum plane (ft)

Substituting the total flux of phase *j* (i.e., Eq. (2.7)) in the mass conservation equation (i.e., Eq. (2.6)) results in

$$\frac{\partial N_i}{\partial t} - V_b \sum_{j=1}^{n_p} \vec{\nabla} \bullet \left[0.006328 \rho_j x_{ij} \vec{\vec{k}} \lambda_{rj} \left(\nabla P_j - \gamma_j \nabla D \right) \right] - V_b \sum_{j=1}^{n_p} \vec{\nabla} \bullet \left[\phi \rho_j S_j \vec{\vec{K}}_{ij} \nabla x_{ij} \right] - q_i = 0 \quad for\, i = 1, 2, ..., n_{gc}. \tag{2.8}$$

All the terms are defined in Eqs. (2.6) and (2.7). Transmissibilities in different directions are defined as follows (equations are taken from Chang (1990) and modified for the phase mass densities):

$$\left(T_j\right)^n_{x\pm 1/2} = \left(\lambda_{rj}\rho_j\right)^n_{x\pm 1/2} \frac{2\Delta y \Delta z}{\left(\frac{\Delta x}{k_x}\right)_x + \left(\frac{\Delta x}{k_x}\right)_{x\pm 1}}, \tag{2.9}$$

$$\left(T_j\right)^n_{y\pm1/2} = \left(\lambda_{rj}\rho_j\right)^n_{y\pm1/2} \frac{2\Delta x\Delta z}{\left(\frac{\Delta y}{k_y}\right)_y + \left(\frac{\Delta y}{k_y}\right)_{y\pm1}}, \tag{2.10}$$

$$\left(T_j\right)^n_{z\pm1/2} = \left(\lambda_{rj}\rho_j\right)^n_{z\pm1/2} \frac{2\Delta x\Delta y}{\left(\frac{\Delta z}{k_z}\right)_z + \left(\frac{\Delta z}{k_z}\right)_{z\pm1}}, \tag{2.11}$$

where

$\left(T_j\right)_{m\pm1/2}$ = transmissibility of phase *j* in m direction (lb/day/psi)

k_x, k_y, k_z = absolute permeability in the *x*-, *y*-, and *z*-directions (md)

$\Delta x, \Delta y, \Delta z$ = grid size in the *x*-, *y*-, and *z*-directions (ft)

The physical dispersion term containing a full tensor can be expanded as follows (the equation is taken from Chang (1990) and modified for the phase mass densities):

$$\begin{aligned}
&\vec{\nabla}\bullet\left[\phi\rho_j S_j \vec{\vec{K}}_{ij} \nabla x_{ij}\right] = \\
&\frac{\partial}{\partial x}\left[\phi\rho_j S_j\left(K_{xx,ij}\frac{\partial x_{ij}}{\partial x} + K_{xy,ij}\frac{\partial x_{ij}}{\partial y} + K_{xz,ij}\frac{\partial x_{ij}}{\partial z}\right)\right] \\
&+\frac{\partial}{\partial y}\left[\phi\rho_j S_j\left(K_{yx,ij}\frac{\partial x_{ij}}{\partial x} + K_{yy,ij}\frac{\partial x_{ij}}{\partial y} + K_{yz,ij}\frac{\partial x_{ij}}{\partial z}\right)\right] \\
&+\frac{\partial}{\partial z}\left[\phi\rho_j S_j\left(K_{zx,ij}\frac{\partial x_{ij}}{\partial x} + K_{zy,ij}\frac{\partial x_{ij}}{\partial y} + K_{zz,ij}\frac{\partial x_{ij}}{\partial z}\right)\right].
\end{aligned} \tag{2.12}$$

Using the central difference scheme of discritization, the physical dispersion term is approximated as shown below (the equations below are taken from Chang (1990) and modified for the phase mass densities):

$$\vec{\nabla}\bullet\left[\phi\rho_j S_j \vec{\vec{K}}_{ij}\vec{\nabla}x_{ij}\right] \approx \Delta J^n_{xij} + \Delta J^n_{yij} + \Delta J^n_{zij}, \tag{2.13}$$

where

$$\begin{aligned}
\Delta J^n_{xij} &= J^n_{(x+1/2)ij} - J^n_{(x-1/2)ij} \\
&= \frac{1}{\Delta x_x}\left[2\left(\rho_j\phi S_j K_{xx,ij}\right)^n_{x+1/2}\frac{\left(x_{ij}\right)^n_{x+1} - \left(x_{ij}\right)^n_x}{\Delta x_x + \Delta x_{x+1}}\right. \\
&\quad + \left(\rho_j\phi S_j K_{xy,ij}\right)^n_{x+1/2}\frac{\left(x_{ij}\right)^n_{(x+1/2)(y+1)} - \left(x_{ij}\right)^n_{(x+1/2)(y-1)}}{\Delta y_y + 0.5\left(\Delta y_{y+1} + \Delta y_{y-1}\right)} \\
&\quad \left. + \left(\rho_j\phi S_j K_{xz,ij}\right)^n_{x+1/2}\frac{\left(x_{ij}\right)^n_{(x+1/2)(z+1)} - \left(x_{ij}\right)^n_{(x+1/2)(z-1)}}{\Delta z_z + 0.5\left(\Delta z_{z+1} + \Delta z_{z-1}\right)}\right] \\
&\quad - \frac{1}{\Delta x_x}\left[2\left(\rho_j\phi S_j K_{xx,ij}\right)^n_{x-1/2}\frac{\left(x_{ij}\right)^n_x - \left(x_{ij}\right)^n_{x-1}}{\Delta x_x + \Delta x_{x-1}}\right. \\
&\quad + \left(\rho_j\phi S_j K_{xy,ij}\right)^n_{x-1/2}\frac{\left(x_{ij}\right)^n_{(x-1/2)(y+1)} - \left(x_{ij}\right)^n_{(x-1/2)(y-1)}}{\Delta y_y + 0.5\left(\Delta y_{y+1} + \Delta y_{y-1}\right)} \\
&\quad \left. + \left(\rho_j\phi S_j K_{xz,ij}\right)^n_{x-1/2}\frac{\left(x_{ij}\right)^n_{(x-1/2)(z+1)} - \left(x_{ij}\right)^n_{(x-1/2)(z-1)}}{\Delta z_z + 0.5\left(\Delta z_{z+1} + \Delta z_{z-1}\right)}\right],
\end{aligned} \tag{2.14}$$

$$
\begin{aligned}
\Delta J^{n}_{yij} &= J^{n}_{(y+1/2)ij} - J^{n}_{(y-1/2)ij} \\
&= \frac{1}{\Delta y_y}\Bigg[\left(\rho_j \phi S_j K_{yx,ij}\right)^{n}_{y+1/2} \frac{\left(x_{ij}\right)^{n}_{(y+1/2)(x+1)} - \left(x_{ij}\right)^{n}_{(y+1/2)(x-1)}}{\Delta x_x + 0.5\left(\Delta x_{x+1} + \Delta x_{x-1}\right)} \\
&\quad + 2\left(\rho_j \phi S_j K_{yy,ij}\right)^{n}_{y+1/2} \frac{\left(x_{ij}\right)^{n}_{y+1} - \left(x_{ij}\right)^{n}_{y}}{\Delta y_y + \Delta y_{y+1}} \\
&\quad + \left(\rho_j \phi S_j K_{yz,ij}\right)^{n}_{y+1/2} \frac{\left(x_{ij}\right)^{n}_{(y+1/2)(z+1)} - \left(x_{ij}\right)^{n}_{(y+1/2)(z-1)}}{\Delta z_z + 0.5\left(\Delta z_{z+1} + \Delta z_{z-1}\right)} \Bigg] \\
&\quad - \frac{1}{\Delta y_y}\Bigg[\left(\rho_j \phi S_j K_{yx,ij}\right)^{n}_{y-1/2} \frac{\left(x_{ij}\right)^{n}_{(y-1/2)(x+1)} - \left(x_{ij}\right)^{n}_{(y-1/2)(x-1)}}{\Delta x_x + 0.5\left(\Delta x_{x+1} + \Delta x_{x-1}\right)} \\
&\quad + 2\left(\rho_j \phi S_j K_{yy,ij}\right)^{n}_{y-1/2} \frac{\left(x_{ij}\right)^{n}_{y} - \left(x_{ij}\right)^{n}_{y-1}}{\Delta y_y + \Delta y_{y-1}} \\
&\quad + \left(\rho_j \phi S_j K_{yz,ij}\right)^{n}_{y-1/2} \frac{\left(x_{ij}\right)^{n}_{(y-1/2)(z+1)} - \left(x_{ij}\right)^{n}_{(y-1/2)(z-1)}}{\Delta z_z + 0.5\left(\Delta z_{z+1} + \Delta z_{z-1}\right)} \Bigg],
\end{aligned}
\tag{2.15}
$$

$$
\begin{aligned}
\Delta J^{n}_{zij} &= J^{n}_{(z+1/2)ij} - J^{n}_{(z-1/2)ij} \\
&= \frac{1}{\Delta z_z}\left[\left(\rho_j \phi S_j K_{zx,ij}\right)^{n}_{z+1/2} \frac{\left(x_{ij}\right)^{n}_{(z+1/2)(x+1)} - \left(x_{ij}\right)^{n}_{(z+1/2)(x-1)}}{\Delta x_x + 0.5\left(\Delta x_{x+1} + \Delta x_{x-1}\right)} \right. \\
&+ \left(\rho_j \phi S_j K_{zy,ij}\right)^{n}_{z+1/2} \frac{\left(x_{ij}\right)^{n}_{(z+1/2)(y+1)} - \left(x_{ij}\right)^{n}_{(z+1/2)(y-1)}}{\Delta y_y + 0.5\left(\Delta y_{y+1} + \Delta y_{y-1}\right)} \\
&+ \left. 2\left(\rho_j \phi S_j K_{zz,ij}\right)^{n}_{z+1/2} \frac{\left(x_{ij}\right)^{n}_{z+1} - \left(x_{ij}\right)^{n}_{z}}{\Delta z_z + \Delta z_{z+1}} \right] \\
&- \frac{1}{\Delta z_z}\left[\left(\rho_j \phi S_j K_{zx,ij}\right)^{n}_{z-1/2} \frac{\left(x_{ij}\right)^{n}_{(z-1/2)(x+1)} - \left(x_{ij}\right)^{n}_{(z-1/2)(x-1)}}{\Delta x_x + 0.5\left(\Delta x_{x+1} + \Delta x_{x-1}\right)} \right. \\
&+ \left(\rho_j \phi S_j K_{zy,ij}\right)^{n}_{z-1/2} \frac{\left(x_{ij}\right)^{n}_{(z-1/2)(y+1)} - \left(x_{ij}\right)^{n}_{(z-1/2)(y-1)}}{\Delta y_y + 0.5\left(\Delta y_{y+1} + \Delta y_{y-1}\right)} \\
&+ \left. 2\left(\rho_j \phi S_j K_{zz,ij}\right)^{n}_{z-1/2} \frac{\left(x_{ij}\right)^{n}_{z} - \left(x_{ij}\right)^{n}_{z-1}}{\Delta z_z + \Delta z_{z-1}} \right].
\end{aligned}
\tag{2.16}
$$

Considering the transmissibility equations (Eqs. (2.9) through (2.11)) and the approximations for the physical dispersion term (Eqs. (2.14) through (2.16)) one can rewrite the mass conservation equation as

$$
\begin{aligned}
N^{n+1}_i = N^{n}_i + \Delta t \left\{ \sum_{j=1}^{n_p} \left[\Delta\left(x_{ij} T_j\right)^{n} \Delta\left(P^{n+1} + P^{n}_{c2\,j}\right) - \Delta\left(x_{ij} T_j \gamma_j\right)^{n} \Delta D \right]_i \right. \\
\left. + V_b \sum_{j=1}^{n_p} \left(\Delta J^{n}_{xij} + \Delta J^{n}_{yij} + \Delta J^{n}_{zij}\right) + q \right\} \qquad for\, i = 1, \ldots, n_{gc},
\end{aligned}
\tag{2.17}
$$

where the pressure and gravity terms are discretized as follows:

$$
\begin{aligned}
&\Delta\left(x_{ij}T_j\right)^n \Delta\left(P^{n+1}+P^n_{c2\,j}\right)= \\
&\quad \left(x_{ij}T_j\right)^n_{x+1/2}\left[\left(P^{n+1}+P^n_{c2\,j}\right)_{x+1}-\left(P^{n+1}+P^n_{c2\,j}\right)_{x}\right] \\
&\quad -\left(x_{ij}T_j\right)^n_{x-1/2}\left[\left(P^{n+1}+P^n_{c2\,j}\right)_{x}-\left(P^{n+1}+P^n_{c2\,j}\right)_{x-1}\right] \\
&\quad +\left(x_{ij}T_j\right)^n_{y+1/2}\left[\left(P^{n+1}+P^n_{c2\,j}\right)_{y+1}-\left(P^{n+1}+P^n_{c2\,j}\right)_{y}\right] \\
&\quad -\left(x_{ij}T_j\right)^n_{y-1/2}\left[\left(P^{n+1}+P^n_{c2\,j}\right)_{y}-\left(P^{n+1}+P^n_{c2\,j}\right)_{y-1}\right] \\
&\quad +\left(x_{ij}T_j\right)^n_{z+1/2}\left[\left(P^{n+1}+P^n_{c2\,j}\right)_{z+1}-\left(P^{n+1}+P^n_{c2\,j}\right)_{z}\right] \\
&\quad +\left(x_{ij}T_j\right)^n_{z-1/2}\left[\left(P^{n+1}+P^n_{c2\,j}\right)_{z}-\left(P^{n+1}+P^n_{c2\,j}\right)_{z-1}\right],
\end{aligned}
\tag{2.18}
$$

$$
\begin{aligned}
&\Delta\left(x_{ij}T_j\gamma_j\right)^n \Delta D= \\
&\quad \left(x_{ij}T_j\gamma_j\right)^n_{x+1/2}\left[D_{x+1}-D_x\right]-\left(x_{ij}T_j\gamma_j\right)^n_{x-1/2}\left[D_x-D_{x-1}\right] \\
&\quad +\left(x_{ij}T_j\gamma_j\right)^n_{y+1/2}\left[D_{y+1}-D_y\right]-\left(x_{ij}T_j\gamma_j\right)^n_{y-1/2}\left[D_y-D_{y-1}\right] \\
&\quad +\left(x_{ij}T_j\gamma_j\right)^n_{z+1/2}\left[D_{z+1}-D_z\right]-\left(x_{ij}T_j\gamma_j\right)^n_{z-1/2}\left[D_z-D_{z-1}\right],
\end{aligned}
\tag{2.19}
$$

Notations used in this dissertation are consistent with those applied in Chang (1990). Both higher- and lower-order schemes of discretization are considered for the geochemical species. More details on discretizing different terms in the mass conservation equation are provided in Chang (1990). Moreover, the tracer module implemented in UTCOMP by Maroongroge (1994) was very helpful to develop a stand-alone module for solving the mass conservation equation of the geochemical species.

The new implementation in UTCOMP is verified against the analytical solution of the convective-diffusion (CD) (for 1D and single-phase case) and also against UTCHEM, an in-house research chemical flooding reservoir simulator developed at The University

of Texas at Austin (Delshad *et al.*, 1996), for a complicated multi-dimensional and multi-phase case.

The CD equation describes conservation of the displacing component with mass concentration of C (Lake 1989) as

$$\phi \frac{\partial C}{\partial t} + u \frac{\partial C}{\partial x} - \phi K_L \frac{\partial^2 C}{\partial x^2} = 0, \tag{2.20}$$

where

$\phi =$ porosity (fraction)

$t =$ time (day)

$C =$ mass concentration (lb/lb or lbmoles/lb)

$u =$ bulk fluid velocity (ft/day)

$x =$ distance (ft)

$K_L =$ longitudinal dispersion coefficient (ft^2/day)

To derive Eq. (2.20), it is assumed that fluid and rock are incompressible; mixing is ideal; and a single phase flows.

Eq. (2.21) gives the dimensionless form of CD equation (Lake, 1989).

$$\frac{\partial C_D}{\partial t_D} + \frac{\partial C_D}{\partial x_D} - \frac{1}{N_{Pe}} \frac{\partial^2 C_D}{\partial x_D^2} = 0, \tag{2.21}$$

where

$C_D = \frac{C - C_o}{C_J - C_o} =$ dimensionless concentration

$t_D = \frac{ut}{\phi L} =$ dimensionless time

$x_D = \frac{x}{L} =$ dimensionless distance

$N_{Pe} = \frac{uL}{\phi K_L} =$ dimensionless Peclet number

$C_0 =$ initial tracer concentration (lb/lb or lbmoles/lb)

$C_J =$ injected tracer concentration (lb/lb or lbmoles/lb)

$u =$ Darcy velocity (ft/day)

$L =$ reservoir length (ft)

$K_L =$ longitudinal dispersion coefficient (ft^2/day)

Because the above partial differential equation (PDE) is second order in space and first order in time, obviously one initial and two boundary conditions are required to solve the equation. The CD equation can be solved analytically for the following initial and boundary conditions (Eq. (2.22)):

$$\begin{cases} C_D(x_D, 0) = 0, & x_D \geq 0 \\ C_D(x_D \to \infty, t_D) = 0, & t_D \geq 0 \\ C_D(0, t_D) = 1, & t_D \geq 0 \end{cases}, \tag{2.22}$$

and the analytical solution is (Lake, 1989):

$$C_D = \frac{1}{2} erfc\left(\sqrt{\frac{N_{Pe}}{t_D}} \times \frac{x_D - t_D}{2}\right) + \frac{e^{x_D N_{Pe}}}{2} erfc\left(\sqrt{\frac{N_{Pe}}{t_D}} \times \frac{x_D + t_D}{2}\right). \tag{2.23}$$

Second term in Eq. (2.23) is neglected and this makes the concentration profile symmetric. In fact, the second term in Eq. (2.23) exponentially approaches zero at large x_D and N_{Pe} values no matter what (Lake, 1989). For 1D flow, the longitudinal dispersion coefficient K_L is given by

$$\frac{K_L}{D_o} = C_1 + C_2 \left(\frac{|v| D_p}{D_o} \right)^{\beta}, \tag{2.24}$$

where

$K_L =$ longitudinal dispersion coefficient (ft^2/day)

$D_o =$ effective binary molecular diffusion coefficient between the miscible and displacing and displaced fluids (ft^2/day)

$C_1, C_2, \beta =$ properties of the permeable medium and the flow regime

$D_p =$ average particle diameter (ft)

If the interstitial velocity is greater than about 3 cm/day, the local mixing term in the equation dominates the first term (Lake, 1989); hence,

$$K_L = \frac{D_o}{\phi F} + C_2 \left(\frac{|v| D_p}{D_o} \right)^{\beta} D_o \cong \alpha_l |v|, \tag{2.25}$$

where

$K_L =$ longitudinal dispersion coefficient (ft^2/day)

$\alpha_L =$ the longitudinal dispersivity (ft)

$v =$ interstitial velocity (ft/day)

Thus the dimensionless Peclet number now becomes independent of the velocity as

$$N_{Pe} = \frac{L}{\alpha_L}. \tag{2.26}$$

A 1D case study (shown in Figure 2-3) is designed using UTCOMP and the analytical solution. Ba is the only tracer element considered with initial and injected concentrations of 0 and 1, respectively.

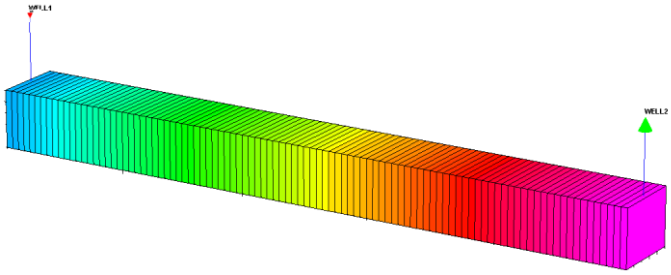

Figure 2-3: 1D model to verify the transport of geochemical species in UTCOMP against the analytical solution.

Figures 2-4 and 2-5 verify UTCOMP normalized concentration profiles against the analytical solution at different injected pore volumes of 0.2, 0.5, and 0.8 (N_{Pe}=100) and different Peclet numbers of 10, 100, and 1000 (t_D=0.5).

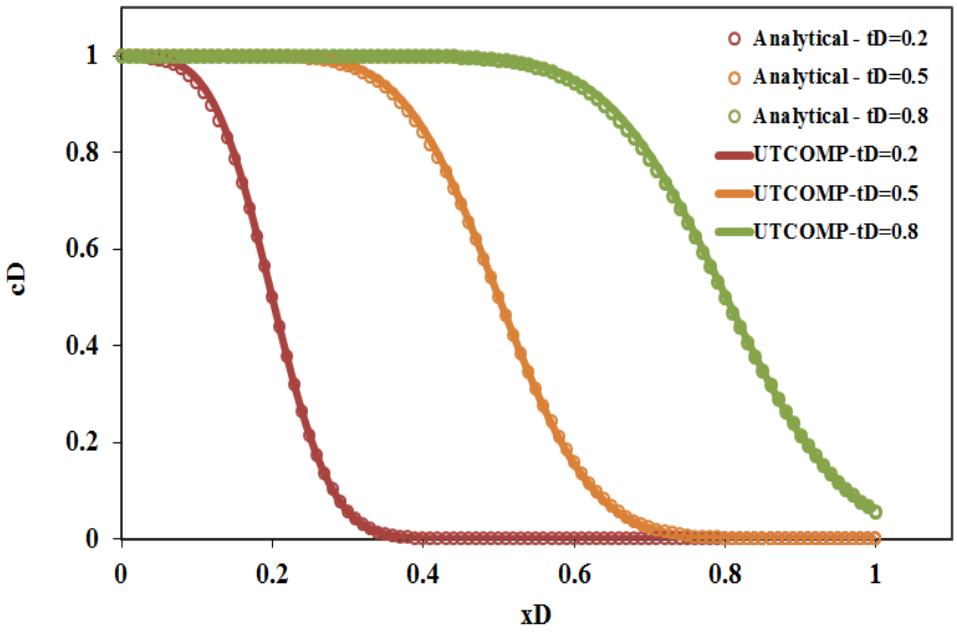

Figure 2-4: Verification of the UTCOMP normalized concentration profiles against the analytical solution at N_{Pe}=100 but different injected pore volumes.

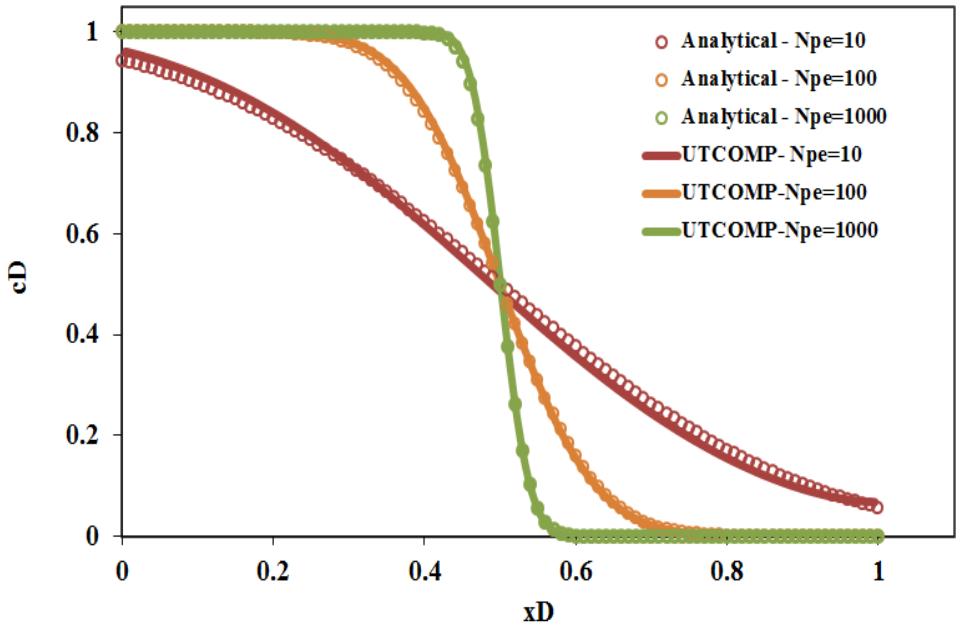

Figure 2-5: Verification of the UTCOMP normalized concentration profiles against the analytical solution at t_D=0.5 but different dimensionless Peclet numbers.

The implementation in UTCOMP was also verified against the UTCHEM tracer module for a complicated case.

Some points should be considered when verifying UTCOMP against UTCHEM. UTCHEM (version 2011) is a chemical flooding simulator with no gas phase flow (the gas phase flow module was recently implemented in UTCHEM by Lashgari, 2014). Hence, initial pressure and the producing bottomhole pressures are considered above the bubble point pressure and no gas is evolved from the crude oil. Therefore, only two phases (i.e., water and oil) flow in UTCOMP and UTCHEM.

For heterogeneous cases, care must be taken to assign the same properties (e.g., porosity, absolute permeabilities, initial water saturation, etc.) to reservoir gridblocks in UTCOMP and UTCHEM. Both UTCOMP and UTCHEM read the gridblock properties through a linear vector from the input file. Properties are then assigned to the gridblocks with the order defined in these simulators. The fastest direction in UTCHEM is the *x*-direction, the *y*-direction varies next fastest, and the *z*-direction varies the slowest (UTCHEM User's Guide, 2011). However, in UTCOMP, the *y*-direction is the fastest moving grid, then *z*-direction, and *x*-direction is the slowest (UTCOMP User's Guide, 2012). For example, for *xy*-2D cases, porosity and absolute permeability matrices in the UTCHEM input file are the transpose of those placed in the UTCOMP input file.

In the UTCHEM simulator, gridblocks with porosity less than 0.01 or absolute permeability in the *x*-direction less than 1×10^{-5} md are considered as inactive cells. If either of the conditions holds (i.e., porosity less than 0.01 or absolute permeability less than 1×10^{-5} md) then water saturation, porosity, and absolute permeability in both *x* and *y* directions are internally modified to 1.0, 0.01, and 1×10^{-5} md, respectively (UTCHEM User's Guide (2000), see also the resread.f routine in the UTCHEM source code). This

assumption has not been included in the UTCOMP reservoir simulator. Hence, to make UTCOMP and UTCHEM consistent in this regards, we need to make sure that the porosities and the absolute permeabilities of the entire gridblocks are above 0.01 and 1×10^{-5} md, respectively.

Oil viscosity is another point that should be emphasized in this validation. In UTCHEM, oil and water viscosities are constant and are input parameters (of course, they are functions of the gridblock temperature), whereas in UTCOMP, water viscosity is the only phase viscosity that is constant. Hydrocarbon phase viscosities are functions of phase compositions and are calculated using compositional correlations, such as Lohrenz *et al.* (1964) (UTCOMP Technical Documentation, 2011). To make the oil viscosity consistent in UTCHEM and UTCOMP simulators, we temporarily skip the compositional viscosity calculation in the UTCOMP code and assign constant oil viscosity, identical to the input in the UTCHEM input file. We could also handle the discrepancy between UTCOMP and UTCHEM oil viscosity as follows: by considering a synthetic oil in UTCOMP and then through tuning the critical volume (V_C) of hydrocarbon components, we can achieve the same oil viscosity used in UTCHEM[1].

UTCOMP always corrects gridblock pressures for gridblock depths (i.e., potential rather than pressure is applied for the calculation). To be consistent with UTCOMP, the "IDEN" flag in the UTCHEM input file is also considered to be 2. Through this we make UTCHEM use potential rather than pressure in its calculation. However, this introduces another inconsistency between UTCHEM and UTCOMP. In UTCHEM oil density is constant and its dependency to the pressure is defined through the oil compressibility

[1] Personal communication with G. R. Jerauld. 2013. Houston: BP America Inc.

factor, whereas in UTCOMP, oil density at each gridblock is evaluated using oil composition obtained from the flash calculation (see dens.f routine of UTCOMP). Because we consider reservoir pressure to be always above the saturation (or bubble point) pressure, during the entire simulation, oil composition hence remains unchanged and is identical to the initial oil composition. However, oil density in UTCOMP still changes as a function of gridblock pressure (oil compressibility is zero in the UTCHEM input file). Hence, some discrepancies are expected between UTCOMP and UTCHEM results for 3D cases.

Automatic time stepping can be applied in both the UTCHEM and UTCOMP simulators. Because reservoir pressure is above the bubble point pressure the ISINGLE keyword in the UTCOMP input file is equal to 1 to skip the phase equilibrium calculation and accelerate the simulation. Peaceman wellbore model (Peaceman, 1978) is used in both UTCHEM and UTCOMP.

Considering all the remarks discussed above, a 3D very heterogeneous and non-isotropic case is modeled using UTCOMP and UTCHEM (see Figure 2-6 for the reservoir geometry and wells pattern). Tables 2-1 and 2-2 present detailed reservoir characteristics and recurrent data for the case considered, respectively. Oil and water relative permeability data are provided in Table 2-3. Figures 2-7 through 2-10 illustrate the porosity and the absolute permeability maps (in *x*- and *y*-direction). Six injection wells, injecting Na, Ca, and Ba at different concentrations into the reservoir, and four production wells are operating with constant bottomhole pressure of 3000 psi (see Table 2-2). Wells are perforated in all layers. It is worth mentioning that although Ba, Na, and Ca are geochemical species, no geochemical calculations are performed in UTCOMP and

UTCHEM and these species are treated as inactive tracers. Initial concentrations of the geochemical species are reported in Table 2-4.

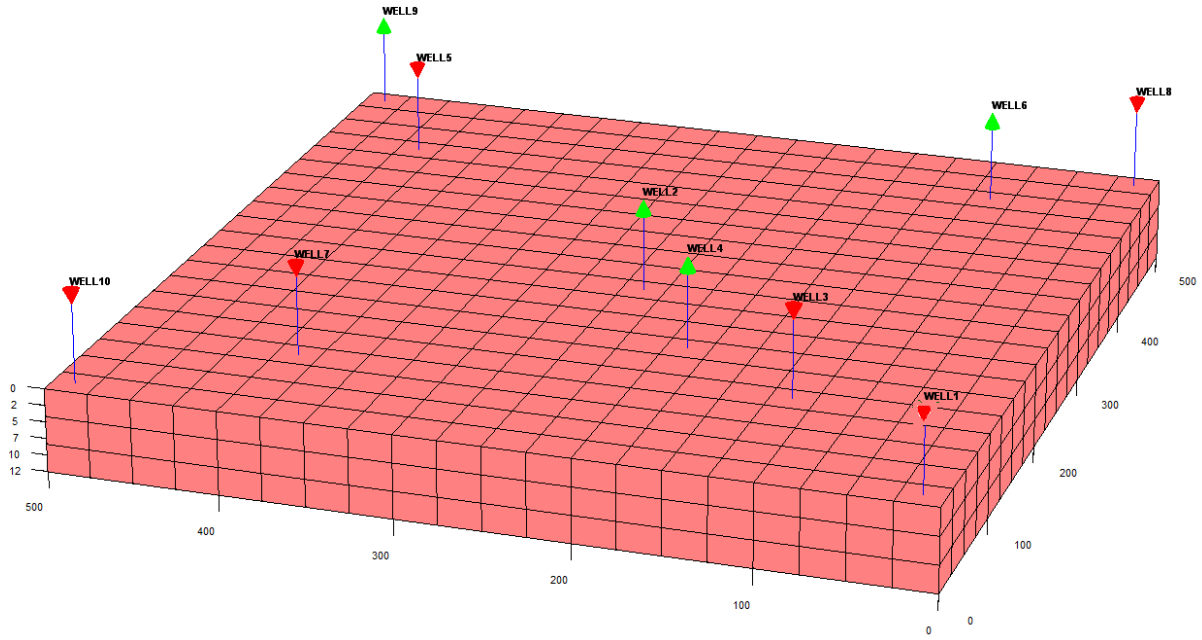

Figure 2-6: Well locations in the 3D case considered to verify the implementation of the transport of geochemical species in UTCOMP against UTCHEM.

Table 2-1: Reservoir characteristics for 3D considered to verify the implementation of the transport of geochemical species in UTCOMP against UTCHEM

No. of gridblocks		1200 (20×20×3)	
Δx(ft)		25.0	
Δy(ft)		25.0	
Δz(ft)		4.0	
Permeability (md)	*x*-direction	Heterogeneous	
	y-direction	Heterogeneous	
	z-direction	Heterogeneous	
Porosity		Heterogeneous	
Rock compressibility (psi^{-1})		0.	
Water compressibility (psi^{-1})		0.	
Initial water saturation		0.45	
Irreducible water saturation		0.2	
Reservoir temperature (^oF)		105	
Initial pressure (psi)		4000.0	
Reservoir depth (ft)		0.	
Water viscosity (cp)		0.79	
Oil viscosity (cp)		6.3	
Number of wells		10	6 injectors
			4 producers
Simulation time(days)		1000.0	

Table 2-2: Wells condition and injecting element concentrations for the 3D case

Well No.	I	J	Perforated Layer	r_w (ft)	Type	Operating Condition	Concentration (meq/ml)		
							Ba	Na	Ca
1	1	1	1-3	0.33	Inj.	Q_w=300 bbl/Day	0.02	0.	0.05
2	10	10	1-3	0.33	Prod.	BHP=3000 psia	-	-	-
3	5	5	1-3	0.33	Inj.	Q_w=300 bbl/Day	0.2	0.3	0.75
4	8	7	1-3	0.33	Prod.	BHP=3000 psia	-	-	-
5	18	17	1-3	0.33	Inj.	Q_w=300 bbl/Day	1.0	0.78	0.4
6	4	18	1-3	0.33	Prod.	BHP=3000 psia	-	-	-
7	16	4	1-3	0.33	Inj.	Q_w=300 bbl/Day	0.02	0.	0.05
8	1	20	1-3	0.33	Inj.	Q_w=300 bbl/Day	0.02	0.	0.05
9	20	20	1-3	0.33	Prod.	BHP=3000 psia	-	-	-
10	20	1	1-3	0.33	Inj.	Q_w=300 bbl/Day	0.2	0.	0.5

Table 2-3: Corey's parameters for oil and water relative permeabilities

Residual saturation	Water	0.2
	Oil	0.2
Exponent	Water	1.5
	Oil	2.5
Endpoint	Water	0.21
	Oil	0.7

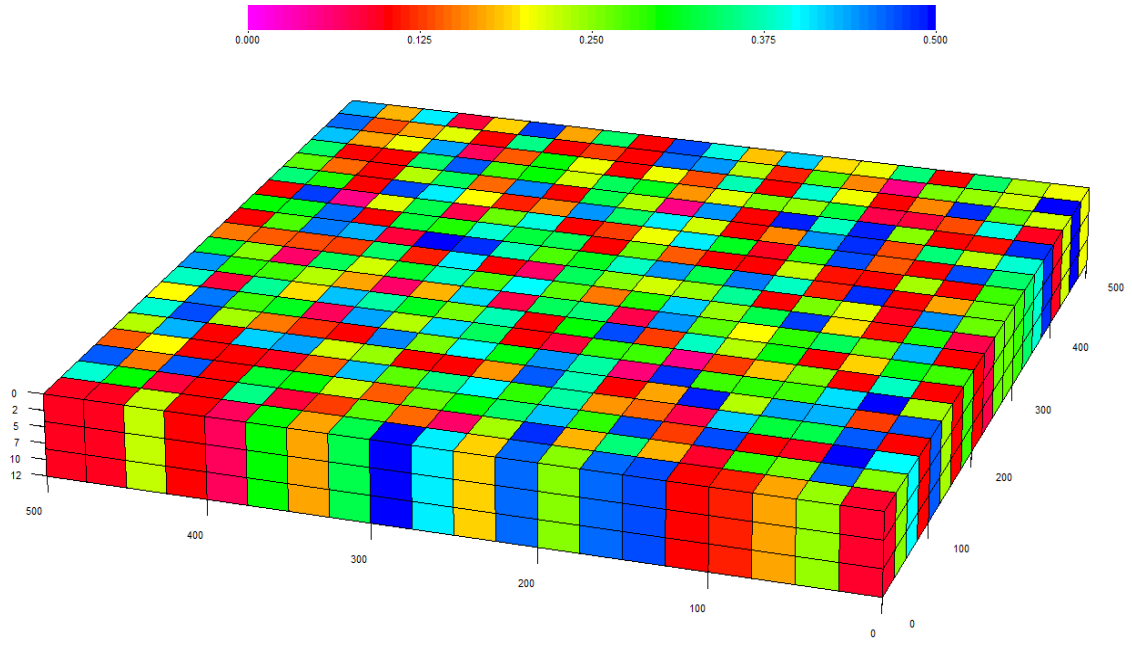

Figure 2-7: Distribution of porosity for the 3D case.

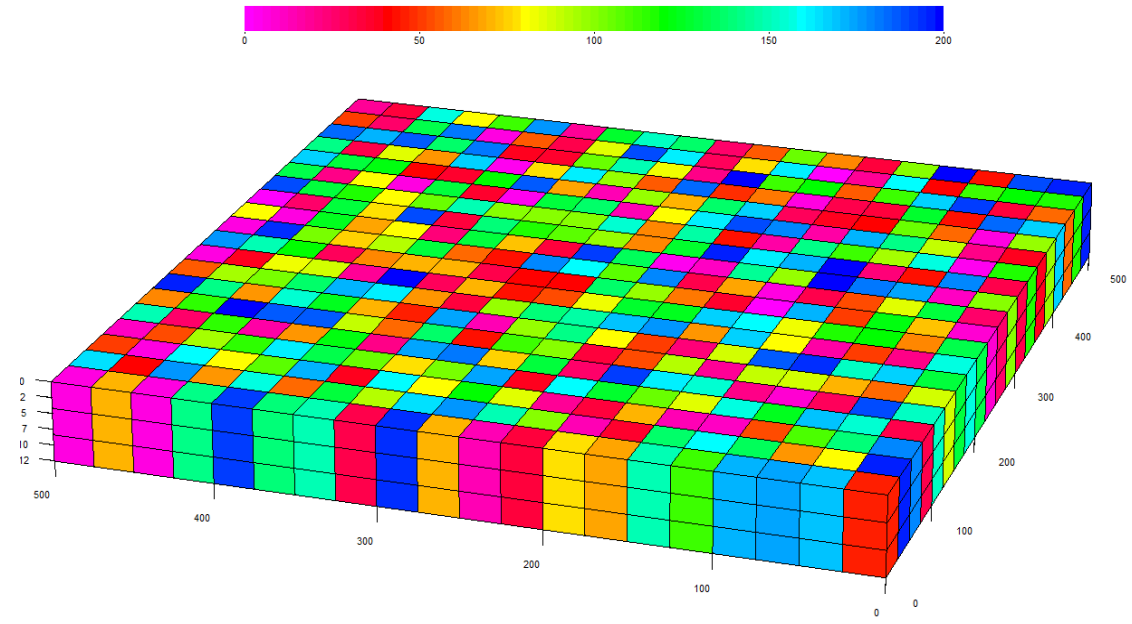

Figure 2-8: Distribution of the absolute permeability (in md) in the *x*-direction for the 3D case.

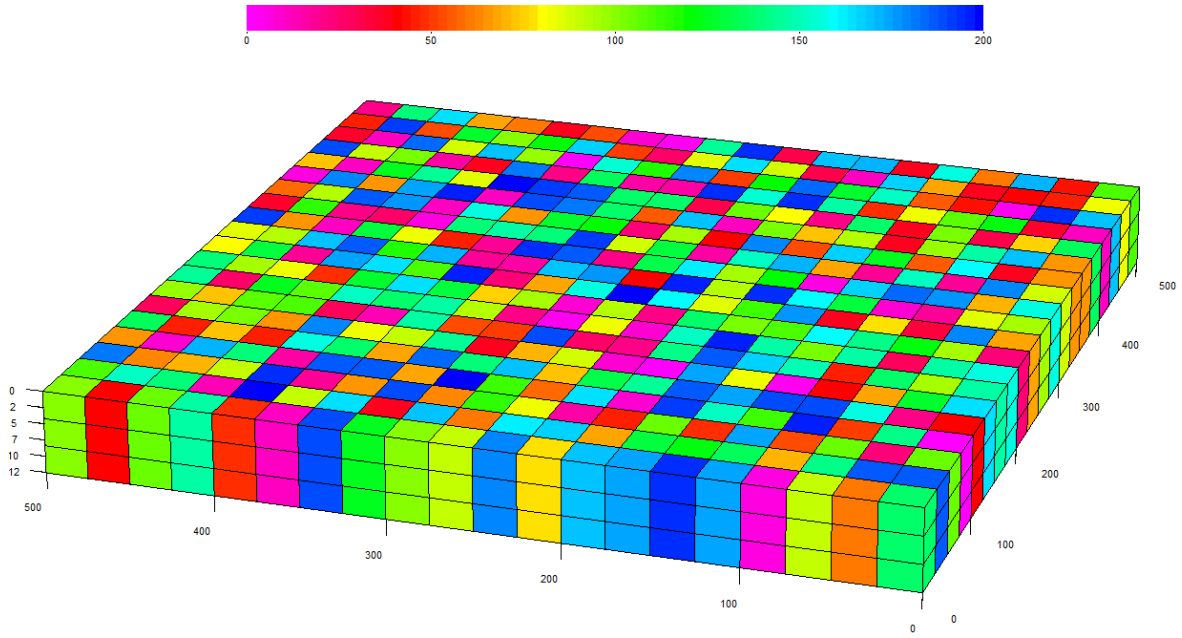

Figure 2-9: Distribution of the absolute permeability (in md) in the *y*-direction for the 3D case.

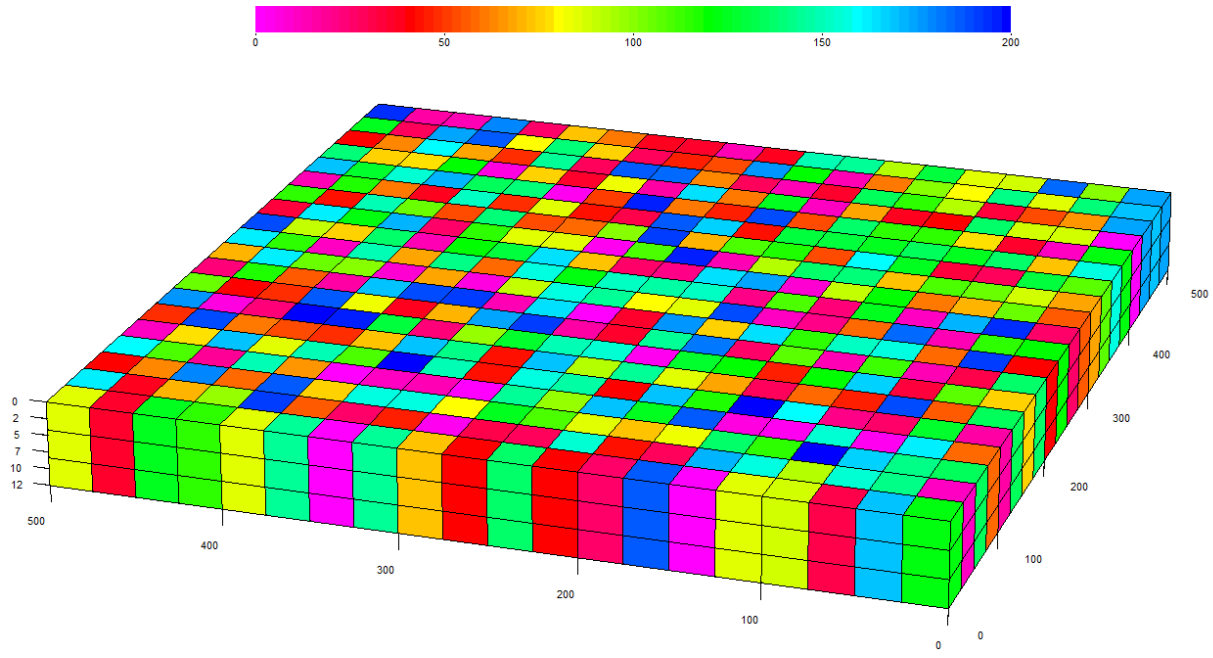

Figure 2-10: Distribution of the absolute permeability (in md) in the *z*-direction for the 3D case.

Table 2-4: Initial concentrations of geochemical elements

	Ba	Na	Ca
Initial concentration (meq/ml)	0.	0.1	0.

Figures 2-11 and 2-12 compare UTCOMP results for cumulative oil recovery and average reservoir pressure against those of the UTCHEM simulator, respectively. Also, Figures 2-13 through 2-17 present UTCOMP and UTCHEM simulation results for concentration histories of Ba, Na, and Ca as well as pressure and water saturation at two different gridblocks of (4,9,2) and (3,7,2).

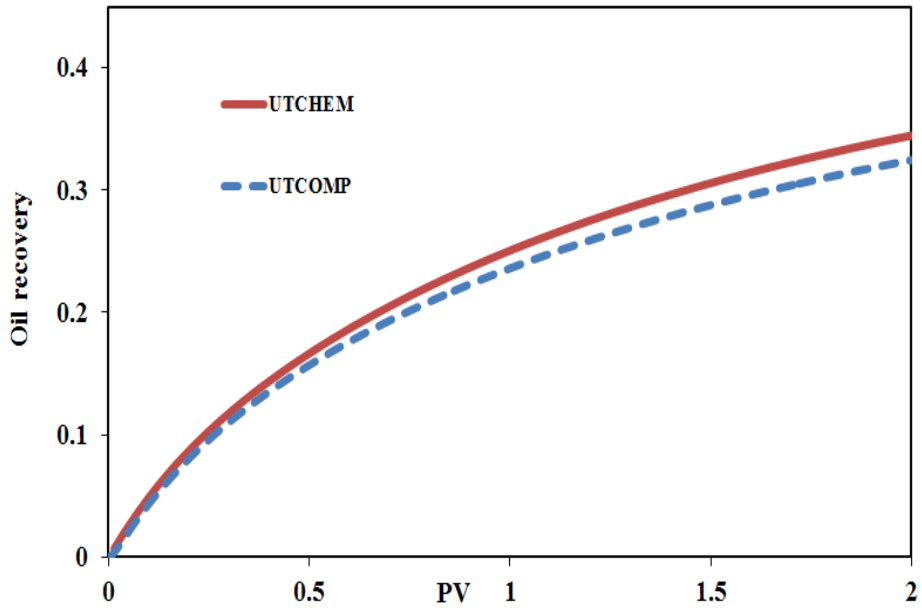

Figure 2-11: Oil recovery of the 3D case (verification of the mass conservation equation implemented in UTCOMP for the geochemical elements against UTCHEM).

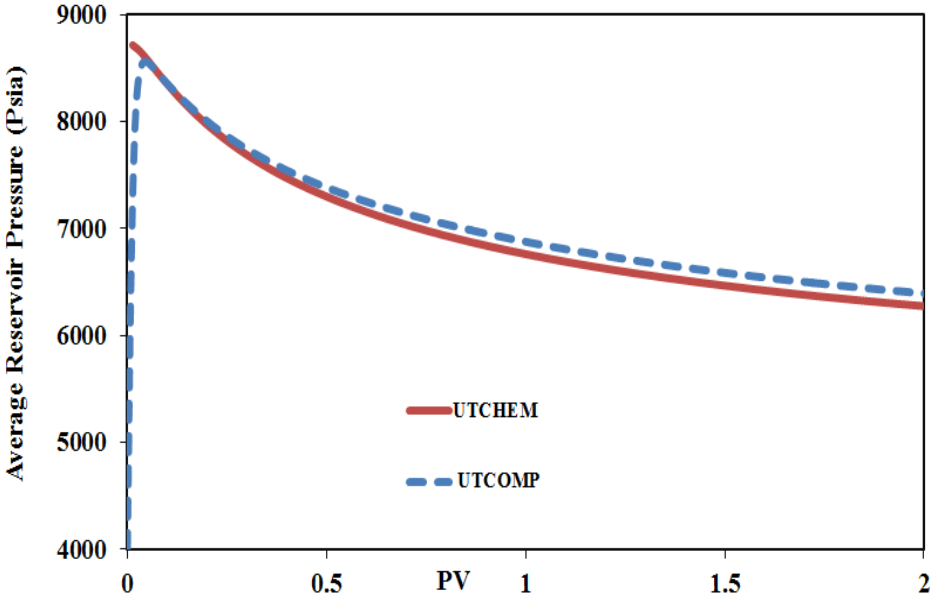

Figure 2-12: Average reservoir pressure of the 3D case (verification of the mass conservation equation implemented in UTCOMP for the geochemical elements against UTCHEM).

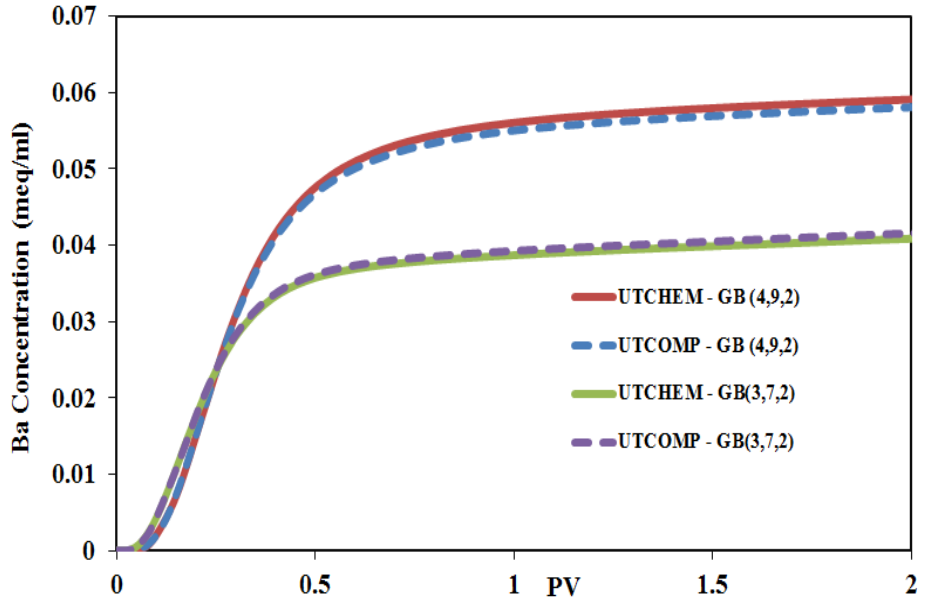

Figure 2-13: Ba concentration histories at two gridblocks of the 3D case (verification of the mass conservation equation implemented in UTCOMP for the geochemical elements against UTCHEM).

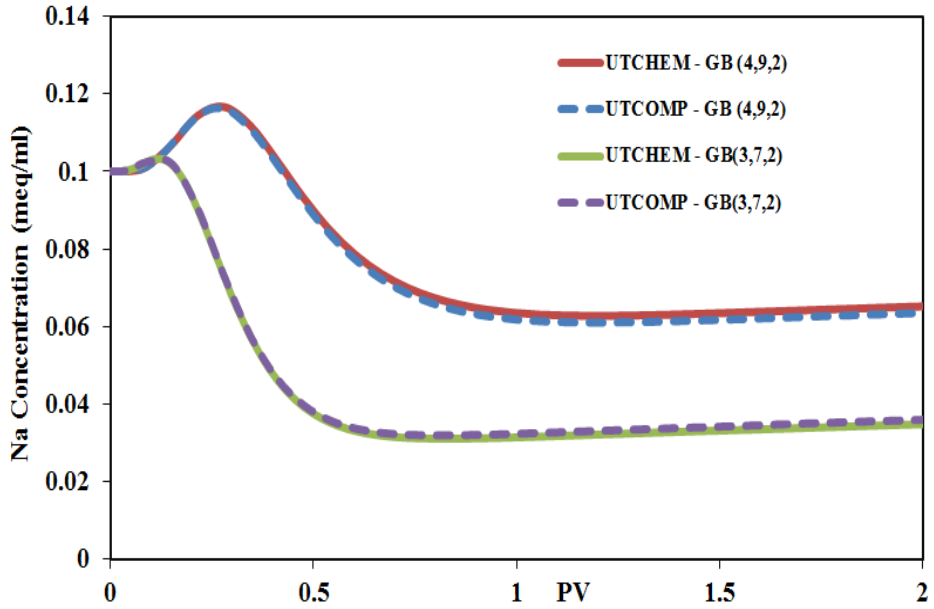

Figure 2-14: Na concentration histories at two gridblocks of the 3D case (verification of the mass conservation equation implemented in UTCOMP for the geochemical elements against UTCHEM).

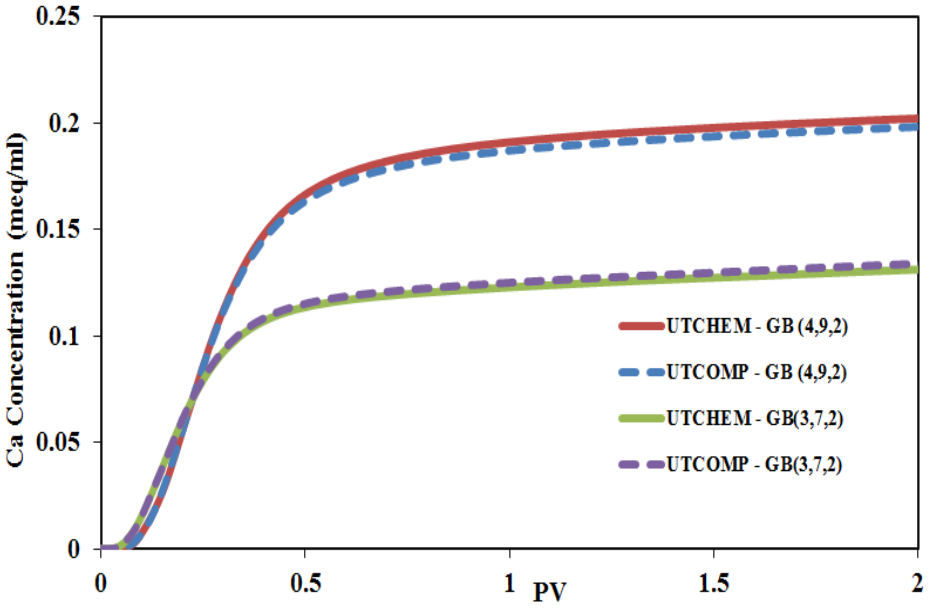

Figure 2-15: Ca concentration histories at two gridblocks of the 3D case (verification of the mass conservation equation implemented in UTCOMP for the geochemical elements against UTCHEM).

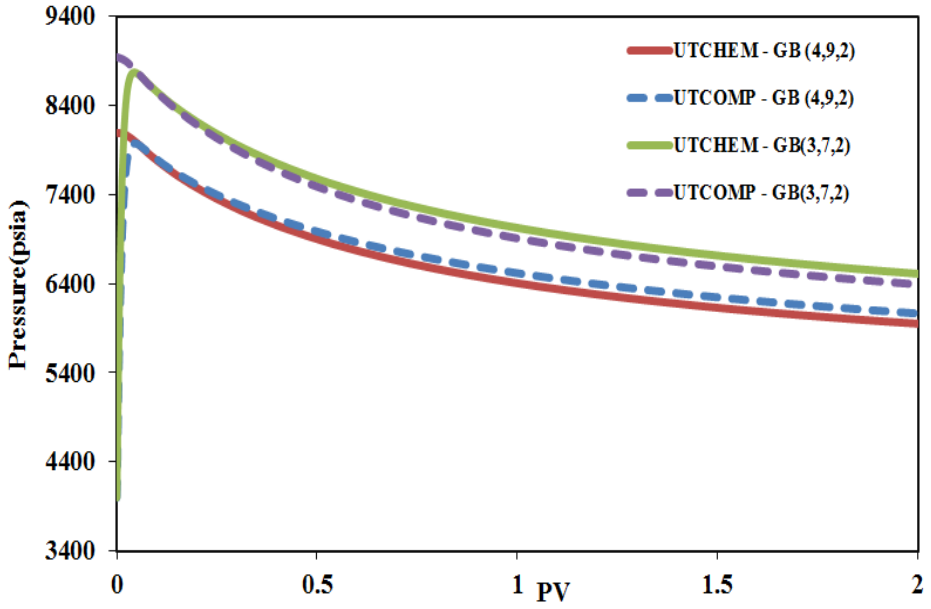

Figure 2-16: Pressure histories at two gridblocks of the 3D case (verification of the mass conservation equation implemented in UTCOMP for the geochemical elements against UTCHEM).

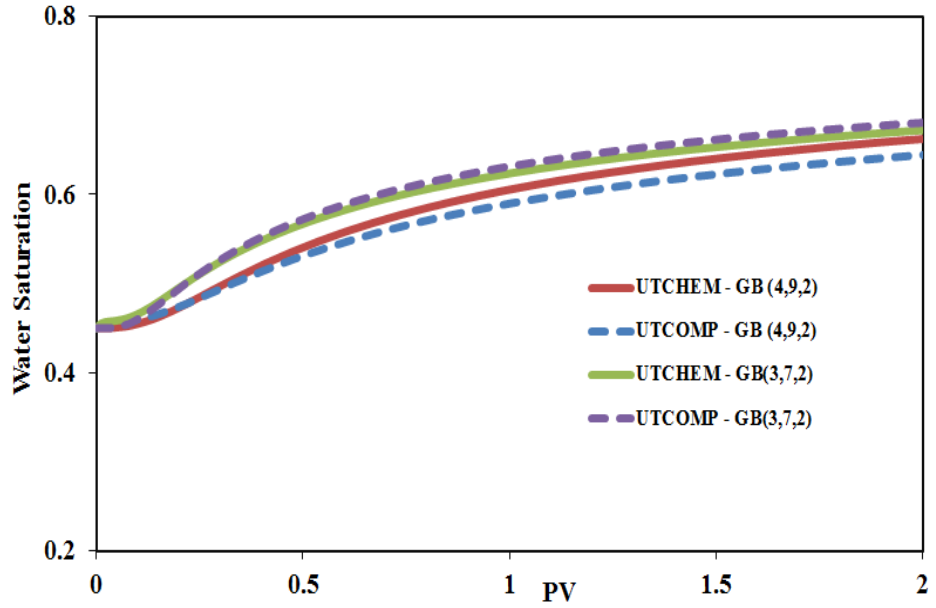

Figure 2-17: Water saturation histories at two gridblocks of the 3D case (verification of the mass conservation equation implemented in UTCOMP for the geochemical elements against UTCHEM).

As discussed above, discrepancies between UTCOMP and UTCHEM results in 3D cases are because of the fact that the oil density is treated differently in UTCOMP and UTCHEM simulators. To confirm this, rather than considering three layers, only the first layer (i.e., a 2D case) is considered in the simulation. Also, we modify the injection rates from 300 bbl/day per injection well to 100 bbl/day per injection well.

Figures 2-18 and 2-19 present cumulative oil recovery and average pressure of the 2D case and Figures 2-20 through 2-24 illustrate concentration histories of Ba, Na, and Ca along with pressure and water saturation at gridblocks (4,9,1) and (3,7,1). As the figures show, results are in very good agreement between the UTCOMP and UTCHEM simulators for the 2D case.

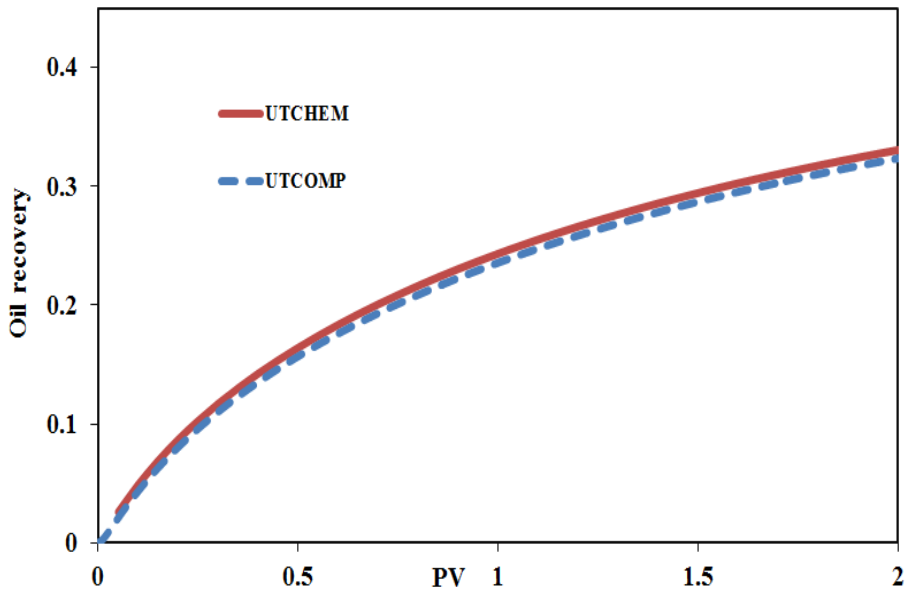

Figure 2-18: Oil recovery of the 2D case (verification of the mass conservation equation implemented in UTCOMP for the geochemical elements against UTCHEM).

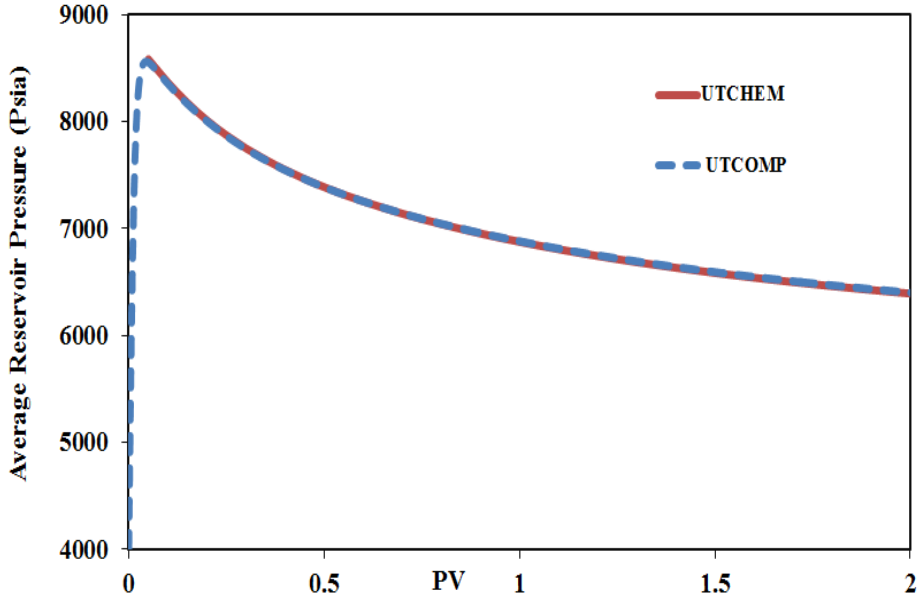

Figure 2-19: Average reservoir pressure of the 2D case (verification of the mass conservation equation implemented in UTCOMP for the geochemical elements against UTCHEM).

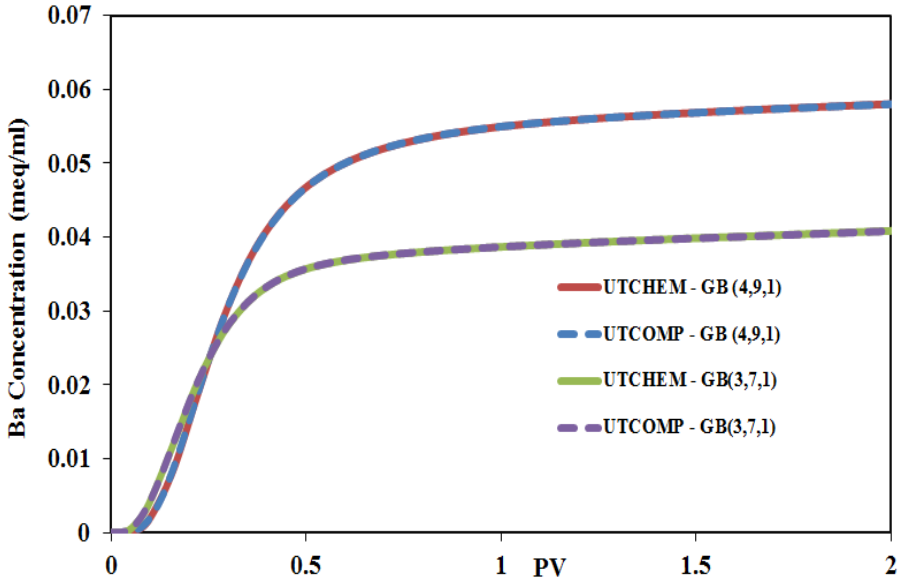

Figure 2-20: Ba concentration histories at two gridblocks of the 2D case (verification of the mass conservation equation implemented in UTCOMP for the geochemical elements against UTCHEM).

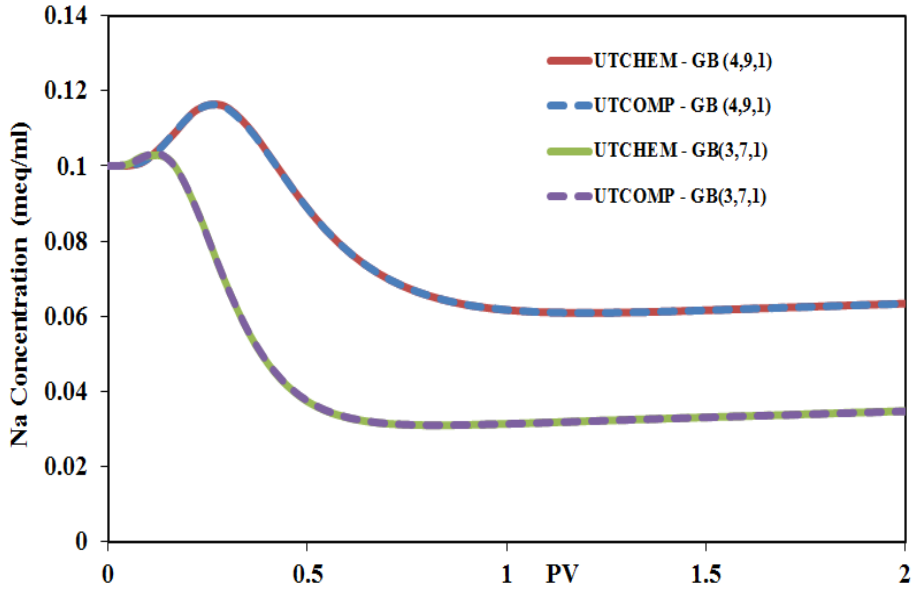

Figure 2-21 Na concentration histories at two gridblocks of the 2D case (verification of the mass conservation equation implemented in UTCOMP for the geochemical elements against UTCHEM).

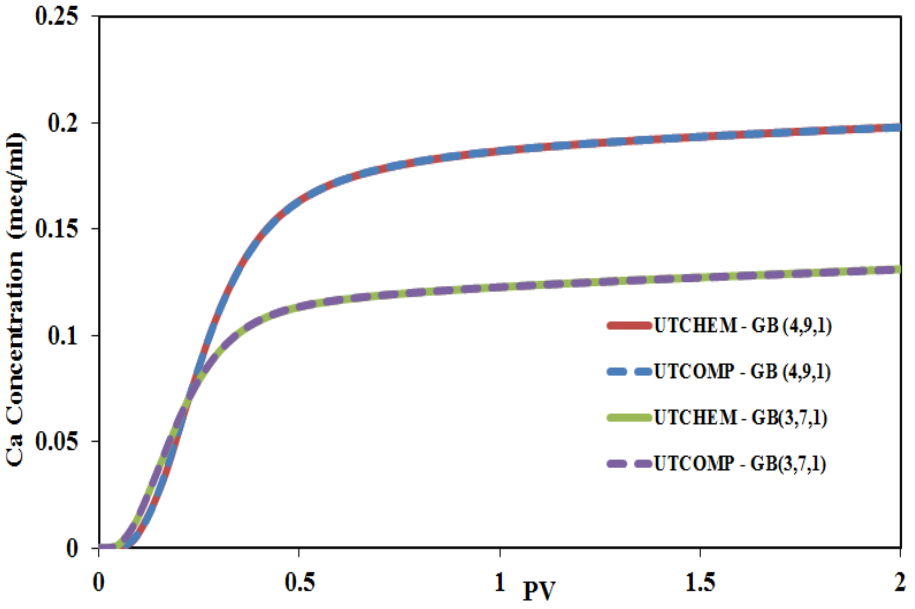

Figure 2-22: Ca concentration histories at two gridblocks of the 2D case (verification of the mass conservation equation implemented in UTCOMP for the geochemical elements against UTCHEM).

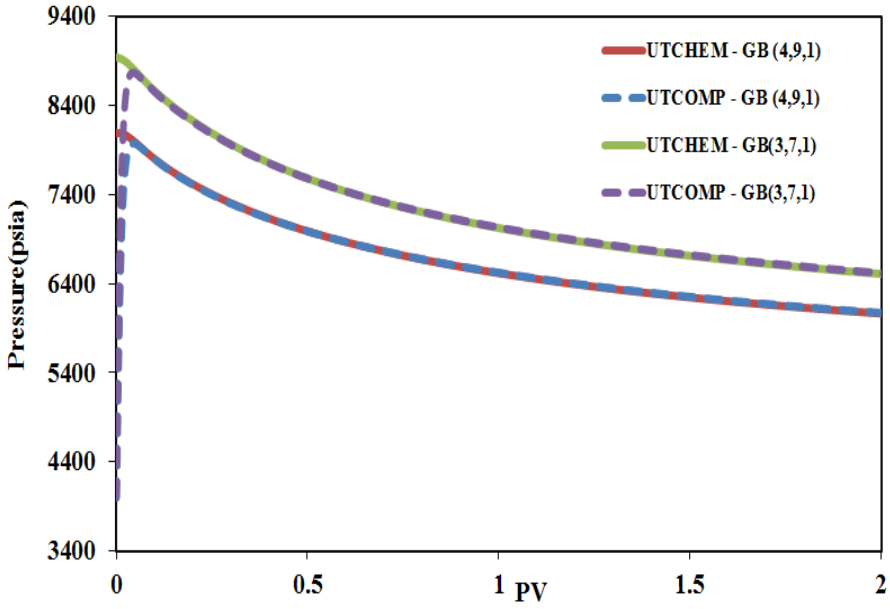

Figure 2-23: Pressure histories at two gridblocks of the 2D case (verification of the mass conservation equation implemented in UTCOMP for the geochemical elements against UTCHEM).

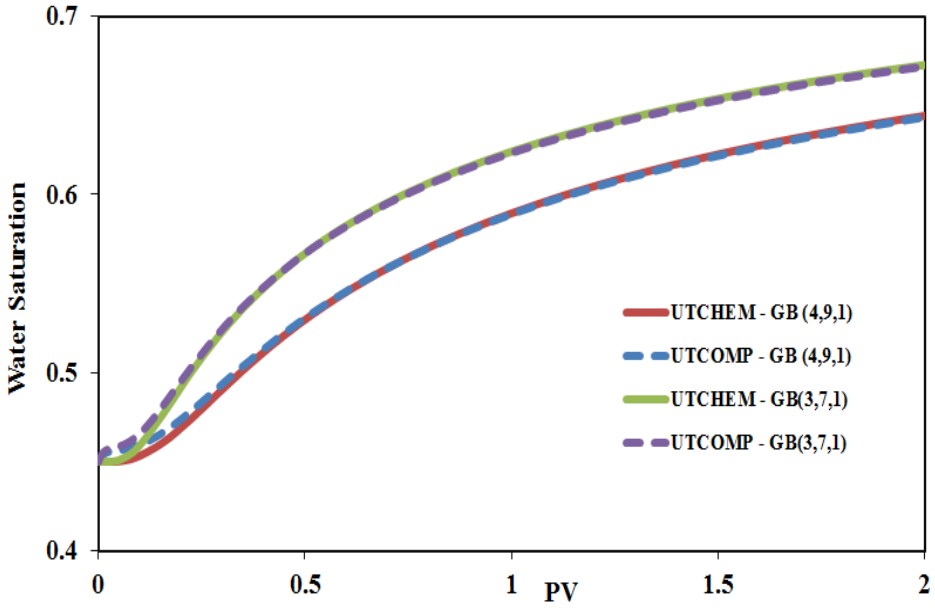

Figure 2-24: Water saturation histories at two gridblocks of the 2D case (verification of the mass conservation equation implemented in UTCOMP for the geochemical elements against UTCHEM).

The same 2D case described above is also used to verify the total variation diminishing (TVD) higher-order scheme of discretization implemented in UTCOMP for the geochemical species against the UTCHEM simulator (see Liu *et al.* (1994) for the TVD higher-order discretization scheme). Figures 2-25 through 2-31 compare the UTCOMP and UTCHEM results (the "TVD higher-order" and "lower-order" methods are simply labeled as "higher-order" and "lower-order" in the figures, respectively). Figures 2-27 through 2-31 are plotted for gridblock (4,9,1). Obviously, the discrepancy between the higher-order and the lower-order methods is because of numerical dispersion. It is assumed that the TVD higher-order method is numerical dispersion-free, whereas, the dispersivity coefficient introduced to the problem by applying the lower-order method is approximately $\Delta x/2$ (Δx is the gridblock length in each direction).

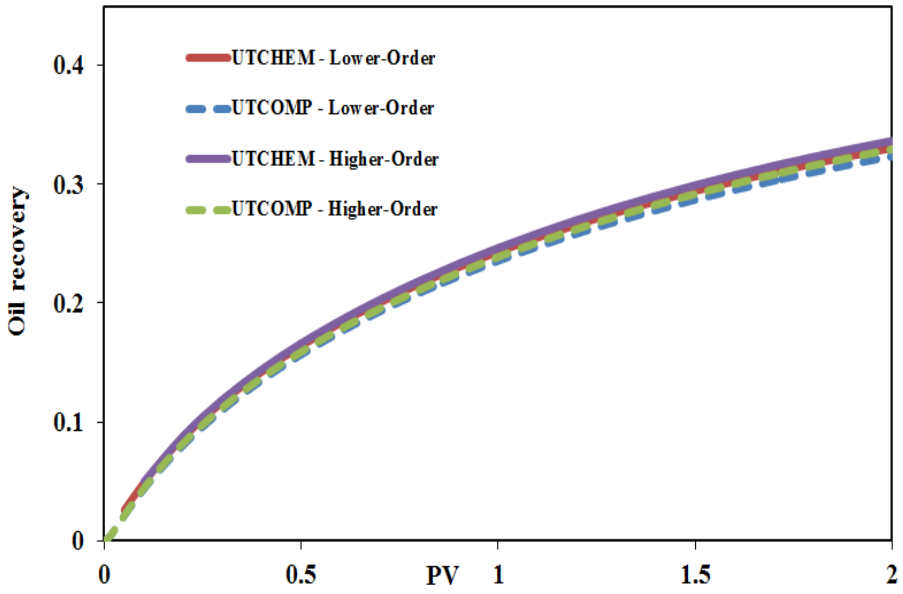

Figure 2-25: Oil recovery of the 2D case using higher- and lower-order methods (verification of the mass conservation equation implemented in UTCOMP for the geochemical elements against UTCHEM).

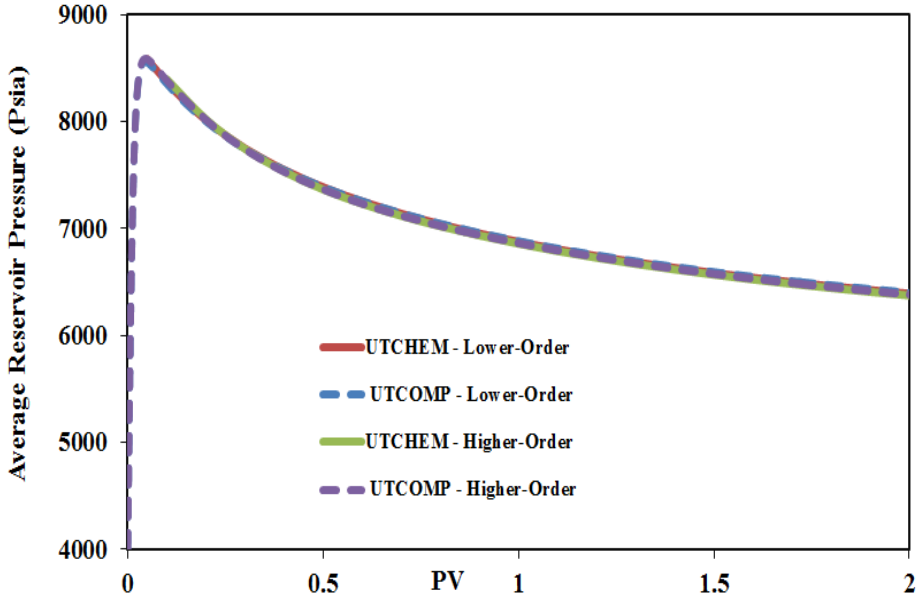

Figure 2-26: Average reservoir pressure of the 2D case using higher- and lower-order methods (verification of the mass conservation equation implemented in UTCOMP for the geochemical elements against UTCHEM).

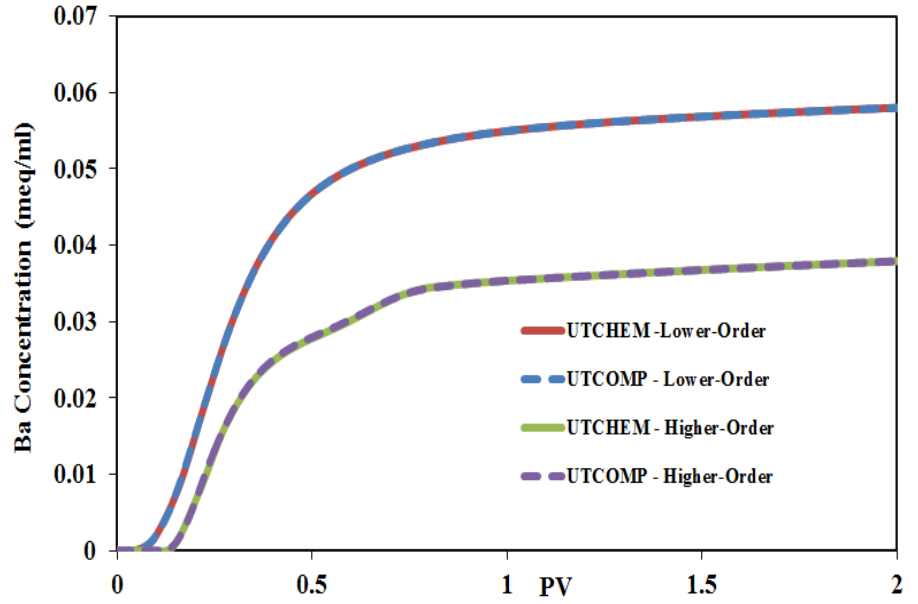

Figure 2-27: Ba concentration history at gridblock (4,9,1) of 2D case using higher- and lower-order methods (verification of the mass conservation equation implemented in UTCOMP for the geochemical elements against UTCHEM).

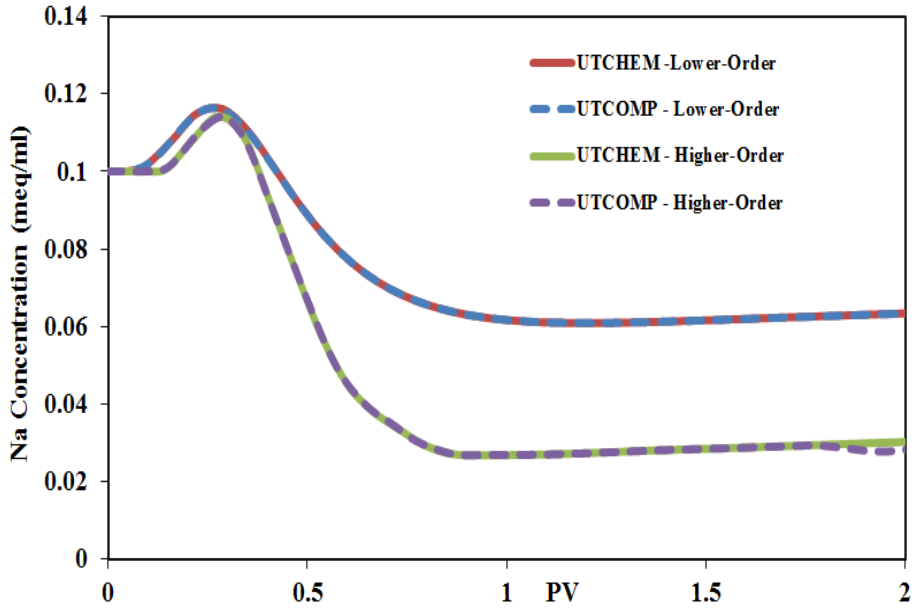

Figure 2-28: Na concentration history at gridblock (4,9,1) of 2D case using higher- and lower-order methods (verification of the mass conservation equation implemented in UTCOMP for the geochemical elements against UTCHEM).

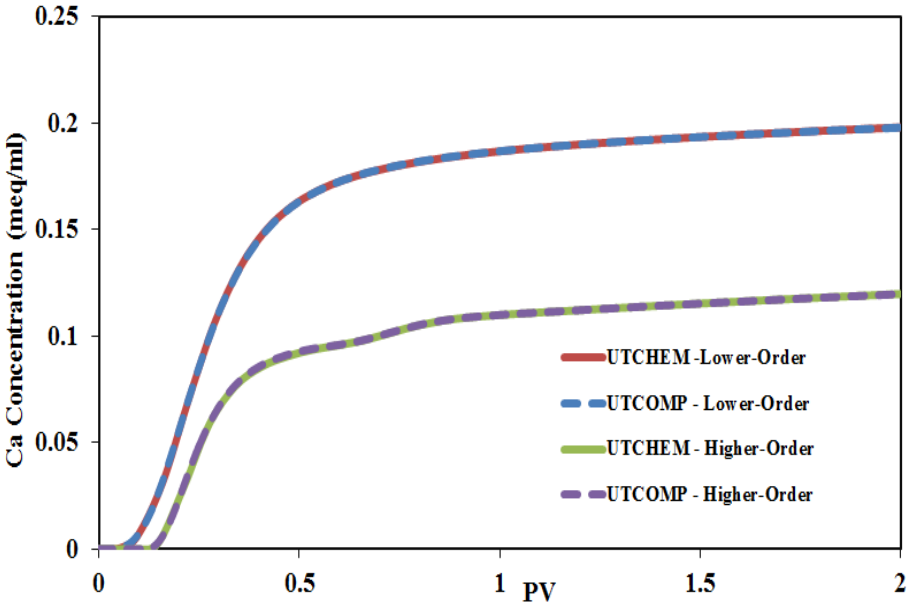

Figure 2-29: Ca concentration history at gridblock (4,9,1) of 2D case using higher- and lower-order methods (verification of the mass conservation equation implemented in UTCOMP for the geochemical elements against UTCHEM).

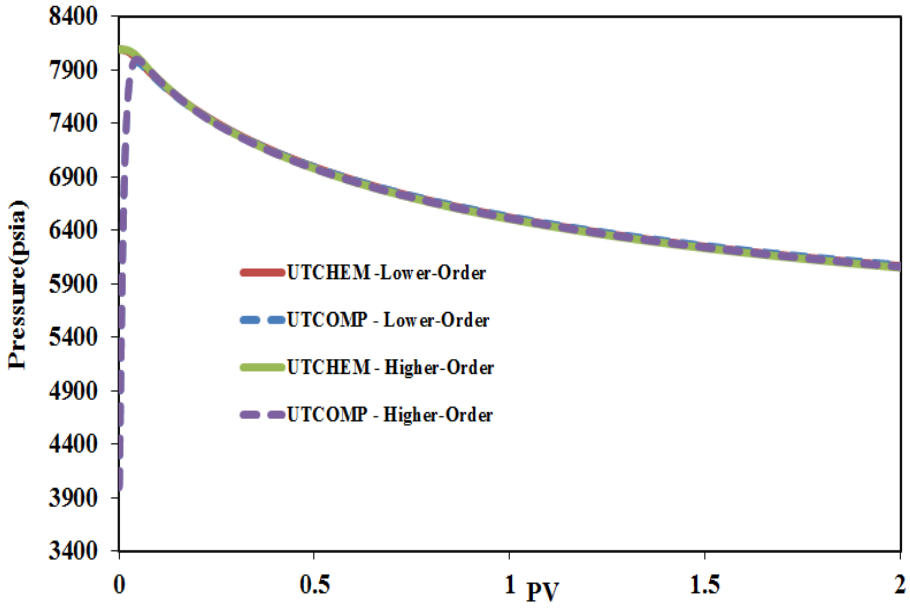

Figure 2-30: Pressure history at gridblock (4,9,1) of 2D case using higher- and lower-order methods (verification of the mass conservation equation implemented in UTCOMP for the geochemical elements against UTCHEM).

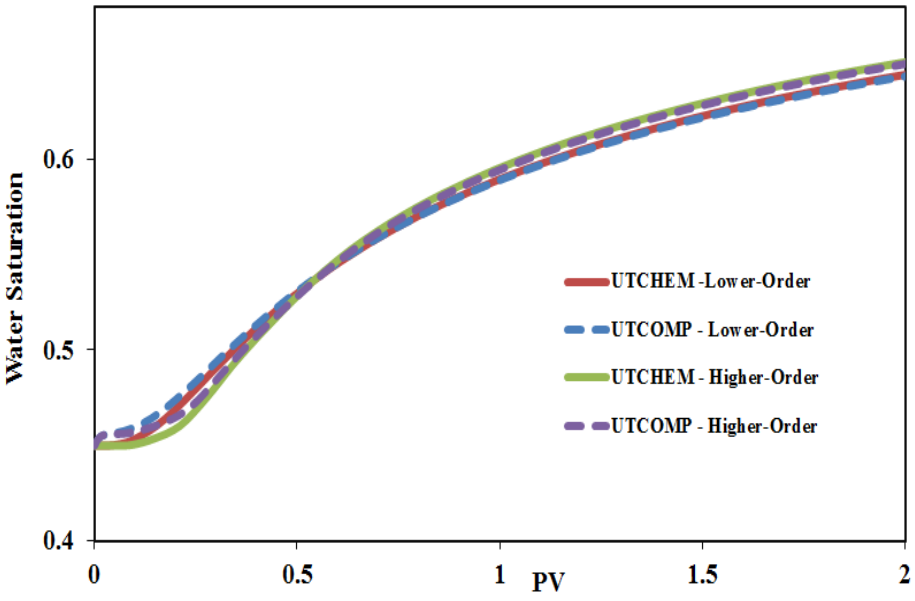

Figure 2-31: Water saturation history at gridblock (4,9,1) of 2D case using higher- and lower-order methods (verification of the mass conservation equation implemented in UTCOMP for the geochemical elements against UTCHEM).

2.3 BATCH REACTION CALCULATION

Geochemical species are not like inactive tracers; they in fact interact with other geochemical species present in the system through geochemical reactions. Hence, after solving the mass balance equation for the geochemical species and evaluating the new geochemical element concentrations in each gridblcok, geochemical reactions between the elements must be taken into account. We treat each gridblock as a batch cell. Batch reaction can simply be conceptualized as a solution plus a set of reactants put into a beaker and allowed to react (Zhu and Anderson, 2002). All of the moles of elements in the solution and in the reactants are combined in the beaker and a new system is calculated.

We explain the batch reaction calculation through a simple example. Let us assume that an aqueous solution containing Ba, S(6), Na, and Cl with certain concentrations is poured into a beaker. We further assume that followings are the only geochemical reactions occurring in the aqueous phase:

$$Na^{+} + Cl^{-} \rightleftharpoons NaCl, \tag{2.27}$$

$$Na^{+} + SO_4^{-2} \rightleftharpoons Na_2SO_4, \tag{2.28}$$

$$Na^{+} + SO_4^{-2} \rightleftharpoons NaSO_4^{-}, \tag{2.29}$$

$$Ba^{+2} + 2Cl^{-} \rightleftharpoons BaCl_2, \tag{2.30}$$

$$Ba^{+2} + SO_4^{-2} \rightleftharpoons BaSO_4(aq). \tag{2.31}$$

We also add some $BaSO_4$(s) solid to the beaker. The $BaSO_4$(s) reaction is shown in Eq. (2.32).

$$Ba^{+2} + SO_4^{-2} \rightleftharpoons BaSO_4(s)\downarrow. \quad (2.32)$$

The equilibrium state of the system is determined if concentrations of Na^+, Cl^-, NaCl, SO_4^{-2}, Na_2SO_4, $NaSO_4^{-1}$, Ba^{+2}, $BaCl_2$, and $BaSO_4$(aq), existing in the aqueous phase, and the new concentration of $BaSO_4$(s) (some of the barium sulfate may be precipitated or dissolved) are known. In other words, 10 equations are required to define a unique solution for the equilibrium state of the batch cell.

Four equations can be set up using the material balance for each element, which simply suggests that the initial mole for each element should be conserved during the geochemical calculations. Material balance equations for this simple case can be written as follows:

$$n_{Na_{initial}} = n_{Na^+} + n_{NaCl} + 2n_{Na_2SO_4} + n_{NaSO_4^{-1}}, \quad (2.33)$$

$$n_{Cl_{initial}} = n_{Cl^-} + n_{NaCl} + 2n_{BaCl_2}, \quad (2.34)$$

$$n_{S(6)_{initial}} = n_{SO4^{-2}} + n_{Na_2SO_4} + n_{NaSO_4^{-1}} + n_{BaSO_4}, \quad (2.35)$$

$$n_{Ba_{initial}} = n_{Ba^{+2}} + n_{BaSO_4} + n_{BaCl_2}. \quad (2.36)$$

Another five equations are defined through mass-action reactions occurring in the aqueous phase.

$$K_1 = \frac{\left[NaCl\right]}{\left[Na^{+}\right]\left[Cl^{-}\right]}, \tag{2.37}$$

$$K_2 = \frac{\left[Na_2SO_4\right]}{\left[Na^{+}\right]^2\left[SO_4^{-2}\right]}, \tag{2.38}$$

$$K_3 = \frac{\left[NaSO_4^{-}\right]}{\left[Na^{+}\right]\left[SO_4^{-2}\right]}, \tag{2.39}$$

$$K_4 = \frac{\left[BaCl_2\right]}{\left[Ba^{+2}\right]\left[Cl^{-}\right]^2}, \tag{2.40}$$

$$K_5 = \frac{\left[BaSO_4(aq)\right]}{\left[Ba^{+2}\right]\left[SO_4^{-2}\right]}. \tag{2.41}$$

In the equations above brackets represent the molality concentrations of the species. The last required equation is obtained using the solubility product of the solid phase present in the system (see Eq. (2.42)).

$$\left[Ba^{+2}\right]\left[SO_4^{-2}\right] \le K_{sp}. \tag{2.42}$$

If the solid is not present, the corresponding solubility product constraint is inequality; if the solid is present, the constraint is equality (Bhuyan, 1989).

Eqs. (2.33) through (2.42) can be rearranged as follows:

$$n_{Na_{initial}} - \left(n_{Na^{+}} + n_{NaCl} + 2n_{Na_2SO_4} + n_{NaSO_4^{-1}}\right) = 0, \tag{2.43}$$

$$n_{Cl_{initial}} - \left(n_{Cl^-} + n_{NaCl} + 2n_{BaCl_2} \right) = 0, \tag{2.44}$$

$$n_{S(6)_{initial}} - \left(n_{SO4^{-2}} + n_{Na_2SO_4} + n_{NaSO_4^{-1}} + n_{BaSO_4} \right) = 0, \tag{2.45}$$

$$n_{Ba_{initial}} - \left(n_{Ba^{+2}} + n_{BaSO_4} + n_{BaCl_2} \right) = 0, \tag{2.46}$$

$$K_1 \left[Na^+ \right] \left[Cl^- \right] - \left[NaCl \right] = 0, \tag{2.47}$$

$$K_2 \left[Na^+ \right]^2 \left[SO_4^{-2} \right] - \left[Na_2 SO_4 \right] = 0, \tag{2.48}$$

$$K_3 \left[Na^+ \right] \left[SO_4^{-2} \right] - \left[NaSO_4^- \right] = 0, \tag{2.49}$$

$$K_4 \left[Ba^{+2} \right] \left[Cl^- \right]^2 - \left[BaCl_2 \right] = 0, \tag{2.50}$$

$$K_5 \left[Ba^{+2} \right] \left[SO_4^{-2} \right] - \left[BaSO_4(aq) \right] = 0, \tag{2.51}$$

$$\left[Ba^{+2} \right] \left[SO_4^{-2} \right] \leq K_{sp}, \tag{2.52}$$

where K_i's and K_{SP} are pressure- and temperature-dependent and can be found in the literature for each reaction.

The above ten equations (i.e., Eqs. (2.43) through (2.52)) should be solved for ten unknowns. These equations are highly coupled and nonlinear. Iterative methods like the Newton-Raphson method can be used to find the solution to this highly nonlinear set of equations.

In Eqs. (2.43) through (2.52), molalities are considered in the mass-action equations; however, molalities can be applied in ideal cases where the salinity of solution is very low. The deviation from the ideal case is taken into account through the ion

activity coefficient. Hence, ion activity coefficient multiplied by the molality is applied for the mass-action reactions. The ion activity coefficient of a species multiplied by its molality is called ion activity of that species (see Appendix A for basic geochemical concepts). The concept of ion activity coefficient for the geochemical species in the aqueous phase is equivalent to the fugacity coefficient for the hydrocarbon components (Zhu and Anderson, 2002). What follows below presents Eqs. (2.47) through (2.52) with the ion activity coefficient included:

$$K_1\left\{\gamma_{Na^+}\left[Na^+\right]\right\}\left\{\gamma_{Cl^-}\left[Cl^-\right]\right\}-\left\{\gamma_{NaCl}\left[NaCl\right]\right\}=0, \tag{2.53}$$

$$K_2\left\{\gamma_{Na^+}\left[Na^+\right]\right\}^2\left\{\gamma_{SO_4^{-2}}\left[SO_4^{-2}\right]\right\}-\left\{\gamma_{Na_2SO_4}\left[Na_2SO_4\right]\right\}=0, \tag{2.54}$$

$$K_3\left\{\gamma_{Na^+}\left[Na^+\right]\right\}\left\{\gamma_{SO_4^{-2}}\left[SO_4^{-2}\right]\right\}-\left\{\gamma_{NaSO_4^-}\left[NaSO_4^-\right]\right\}=0, \tag{2.55}$$

$$K_4\left\{\gamma_{Ba^{+2}}\left[Ba^{+2}\right]\right\}\left\{\gamma_{Cl^-}\left[Cl^-\right]\right\}^2-\left\{\gamma_{BaCl_2}\left[BaCl_2\right]\right\}=0, \tag{2.56}$$

$$K_5\left\{\gamma_{Ba^{+2}}\left[Ba^{+2}\right]\right\}\left\{\gamma_{SO_4^{-2}}\left[SO_4^{-2}\right]\right\}-\left\{\gamma_{BaSO_4(aq)}\left[BaSO_4(aq)\right]\right\}=0, \tag{2.57}$$

$$\left[\gamma_{Ba^{+2}}Ba^{+2}\right]\left[\gamma_{SO_4^{-2}}SO_4^{-2}\right]\le K_{sp}, \tag{2.58}$$

where γ_i's are the activity coefficients of the aqueous species *i*. Davies (Davies, 1962; Parkhurst and Appelo, 1999; 2013) or the extended or WATEQ Debye-Huckel equation (extended form of Debye-Huckel model (Debye and Huckel, 1954)) are the models through which the activity coefficients can be evaluated. These models are presented below.

Davies equation (Davies, 1962; Parkhurst and Appelo, 1999; 2013):

$$\log \gamma_i = -Az_i^2 \left(\frac{\sqrt{I}}{1+\sqrt{I}} - 0.3I \right). \quad (2.59)$$

Extended or WATEQ Debye-Huckel equation (Truesdell and Jones, 1974; Parkhurst and Appelo, 1999; 2013):

$$\log \gamma_i = -\frac{Az_i^2 \sqrt{I}}{1+Ba_i^o \sqrt{I}} + b_i I, \quad (2.60)$$

where

$\gamma_i =$ activity coefficient of the aqueous or exchange species *i*

$z_i =$ ionic charge of aqueous phase species *i*

$A, B =$ constants dependent only on temperature (see Appendix A for the temperature dependency)

$a_i^o, b_i =$ ion-specific parameters

$I =$ total ionic strength of the solution (mol/kgw)

The total ionic strength of the solution is function of the entire aqueous species concentrations and defined as Eq. (2.61):

$$I = \frac{1}{2} \sum_i C_i z_i^2, \quad (2.61)$$

where

$C_i =$ molality of species *i* (moles/kgw)

Davies (Davies, 1962; Parkhurst and Appelo, 1999; 2013) and Extended or WATEQ Debye-Huckel models (Truesdell and Jones, 1974; Parkhurst and Appelo, 1999; 2013) are discussed with more details later (cf. Section 2.8 and Chapter 5).

Including ion activity coefficients in mass-action equations introduces more non-linearity to the set of equations. The reason is each species appears in the equations encompasses a coefficient, which is a function of entire existing species present in the aqueous solution. To this end, in situations the salinity is not low enough to apply molalities, Eqs. (2.43) through (2.46), along with Eqs. (2.53) through (2.58), are solved to find the equilibrium state of the batch cell.

The batch calculation discussed above can be expanded to include other geochemical features, such as surfactant cation associated, surface complexation, kinetic, and exchange reactions. Further details of the batch reaction can be found in Parkhurst and Appelo (1999; 2013) and Bhuyan (1989).

EQBATCH (Bhuyan, 1989) is a geochemical module that performs batch reaction calculation. We integrate EQBATCH to UTCOMP to apply the batch reaction calculation for each reservoir gridblock at each time step. What follows below describes this geochemical module and the procedure through which we couple EQBATCH to UTCOMP.

2.4 COUPLING EQBATCH WITH UTCOMP

EQBATCH is a geochemical package developed in The University of Texas at Austin by Bhuyan (1989) and later generalized (UTCHEM Technical Documentation, 2000). The original intention for developing EQBATCH was modeling ASP floods with some limited reactions that may have significant impact on the process. EQBATCH takes into the account not all but essential geochemical reactions involved in the ASP flooding

such as soap generation, alkali precipitation with aqueous divalents, and alkaline consumption in ion exchange reactions. The EQBATCH formulations are well documented in Bhuyan (1989). The EQBTACH related routines (i.e., georead.f, gauss.f, solve.f, jacup.f, manipl.f, reactr.f, renam1.f, renam2.f, totals.f, and alloc3.f) are publicly available through the free version of UTCHEM (visit Center for Petroleum and Geosystems Engineering website[1] to download the UTCHEM free version). More details on EQBATCH will be presented in Chapter 5. We couple EQBATCH with UTCOMP to calculate the equilibrium state in terms of geochemistry for gridblocks at each time step.

The structure of geochemistry section in the UTCOMP-EQBATCH input file is very close to that of UTCHEM-EQBATCH (a sample input file will be provided later). In this dissertation, both "UTCHEM" and "UTCHEM-EQBATCH" refer to the same version of UTCHEM. In fact, UTCHEM-EQBATCH is used to emphasize on the geochemical engine (i.e., EQBATCH) applied in the UTCHEM simulator. We applied some modifications to make the input file consistent with the other sections in the UTCOMP input file. Furthermore, since no surfactant phase behavior calculation is performed in UTCOMP, when integrating EQBATCH to UTCOMP, oil acidic/aqueous reaction (partitioning and dissociation reaction of the oil acidic component) and surfactant cation associated reactions are excluded from this geochemical module (i.e., EQBATCH). It should be noted that in UTCHEM-EQBATCH, the entire set of non-reacting ions is lumped and transported through the component number 5. The concentration for the lumped species is required for the batch reaction calculation if the charge balance or oxygen balance is desired. The initial and injecting concentrations of the non-reacting element in UTCOMP-EQBATCH are the last value entered at the

[1] http://www.cpge.utexas.edu/

corresponding places where other element concentrations are entered in the input file. In UTCOMP-EQBATCH, ion compositions of the injected water are entered right after the injection flowrates.

We verify UTCOMP-EQBATCH against UTCHEM-EQBATCH for two different case studies.

Case 1

Case 1 is aqueous single-phase with 100 gridblocks in *x*-direction. Table 2-5 presents the case descriptions. This case is based on the example 45 of the UTCHEM simulator (released along with the free version of UTCHEM). The dimensionless Peclet number is 40 which includes the physical dispersion coefficient of 0.08 ft and the numerical dispersion of 0.02 ft (based on the gridblock length in the flow direction which is 0.04 ft). Injection rate is 4×10^{-5} bbl/day and the production well is operating at constant bottomhole pressure of 4890 psi. No exchange reaction is included in the model. Because UTCOMP always performs the phase equilibrium calculation for the hydrocarbon phase, initial concentration for the entire hydrocarbon components cannot be zero. In other words, the initial water saturation cannot be exactly 1.0 in UTCOMP. To tackle this issue, 0.999 is used for the initial water saturation. Tables 2-6 and 2-7 present aqueous and solid reactions along with the equilibrium constants, respectively. Because gridblock pore volumes are fully saturated with the aqueous phase, units of moles/pore volume and meq/pore volume for the solids and exchange species, respectively, are equal to moles/kgw and meq/kgw ("kgw" is kilogram of water). Initial element concentrations in the aqueous phase and solid concentrations are reported in Tables 2-8 and 2-9, respectively. Input files for both UTCHEM-EQBATCH and UTCOMP-EQBATCH are provided in Appendix B.

Figures 2-32 through 2-43 compare UTCOMP-EQBATCH histories of produced ions from the 100th gridblock against those of the UTCHEM-EQBATCH simulator. As the figures illustrate, UTCOMP-EQBTACH matches the UTCHEM-EQBATCH simulation results very well.

Table 2-5: Reservoir characteristics for 1D case

No. of gridblocks		100 (100×1×1)
Δx(ft)		0.04
Δy(ft)		0.15
Δz(ft)		0.15
Permeability (md)	*x*-direction	100
Porosity		0.25
Rock compressibility (psi^{-1})		0.
Water compressibility (psi^{-1})		0.
Initial water saturation		1.0 (0.999 in UTCOMP)
Irreducible water saturation		0.05
Reservoir temperature (^oF)		212.0
Initial pressure (psi)		4890.0
Reservoir depth (ft)		0.
Water viscosity (cp)		0.79
Number of wells	2	1 injector
		1 producer
Simulation time(PV)		1.5

Table 2-6: Aqueous reactions

Reaction	K_{eq}	Reaction	K_{eq}
$H_2O \rightleftharpoons H^+ + OH^-$	$10^{-14.0}$	$Pb^{+2} + 4Cl^- \rightleftharpoons PbCl_4^{-2}$	$10^{1.38}$
$H_4SiO_4 \rightleftharpoons H^+ + H_3SiO_4^-$	$10^{-9.93}$	$Pb^{+2} + 2CO_3^{-2} \rightleftharpoons Pb(CO_3)_2^{-2}$	$10^{10.64}$
$Mg^{+2} + H_2O \rightleftharpoons Mg(OH)^+ + H^+$	$10^{-11.79}$	$Pb^{+2} + H_2O \rightleftharpoons Pb(OH)^+ + H^+$	$10^{-7.71}$
$Mg^{+2} + CO_3^{-2} \rightleftharpoons MgCO_3$	$10^{2.98}$	$2Pb^{+2} + H_2O \rightleftharpoons Pb_2OH^{+3} + H^+$	$10^{-6.36}$
$Mg^{+2} + H^+ + CO_3^{-2} \rightleftharpoons MgHCO_3^+$	$10^{11.40}$	$Pb^{+2} + SO_4^{-2} \rightleftharpoons PbSO_4$	$10^{2.75}$
$Mg^{+2} + SO_4^{-2} \rightleftharpoons MgSO_4$	$10^{2.25}$	$Pb^{+2} + CO_3^{-2} \rightleftharpoons PbCO_3$	$10^{7.24}$
$Ca^{+2} + H_2O \rightleftharpoons Ca(OH)^+ + H^+$	$10^{-12.60}$	$Pb^{+2} + 2SO_4^{-2} \rightleftharpoons Pb(SO_4)_2^{-2}$	$10^{3.47}$
$Ca^{+2} + H^+ + CO_3^{-2} \rightleftharpoons CaHCO_3^+$	$10^{11.33}$	$Pb^{+2} + H^+ + CO_3^{-2} \rightleftharpoons PbHCO_3^+$	$10^{13.20}$
$Ca^{+2} + CO_3^{-2} \rightleftharpoons CaCO_3$	$10^{3.15}$	$H^+ + CO_3^{-2} \rightleftharpoons HCO_3^-$	$10^{10.33}$
$Ca^{+2} + SO_4^{-2} \rightleftharpoons CaSO_4$	$10^{2.31}$	$2H^+ + CO_3^{-2} \rightleftharpoons H_2CO_3$	$10^{16.68}$
$Na^+ + CO_3^{-2} \rightleftharpoons NaCO_3^-$	$10^{1.27}$	$H^+ + SO_4^{-2} \rightleftharpoons HSO_4^-$	$10^{1.99}$
$Na^+ + H^+ + CO_3^{-2} \rightleftharpoons NaHCO_3$	$10^{10.28}$	$Cr(OH)_2^+ + 2H^+ \rightleftharpoons 2H_2O + Cr^{+3}$	$10^{9.62}$
$Na^+ + SO_4^{-2} \rightleftharpoons NaSO_4^-$	$10^{0.7}$	$Cr(OH)_2^+ + H^+ \rightleftharpoons H_2O + Cr(OH)^{+2}$	$10^{5.62}$
$Al^{+3} + H_2O \rightleftharpoons Al(OH)^{+2} + H^+$	$10^{-4.99}$	$Cr(OH)_2^+ + 2H^+ + Cl^- \rightleftharpoons H_2O + CrCl^{+2}$	$10^{9.37}$
$Al^{+3} + 2H_2O \rightleftharpoons Al(OH)_2^+ + 2H^+$	$10^{-10.10}$	$Cr(OH)_2^+ + 2H^+ + 2Cl^- \rightleftharpoons 2H_2O + CrCl_2^+$	$10^{8.66}$
$Al^{+3} + SO_4^{-2} \rightleftharpoons AlSO_4^+$	$10^{3.02}$	$Cr(OH)_2^+ + 2H^+ + SO_4^{-2} \rightleftharpoons CrSO_4^+ + 2H_2O$	$10^{10.97}$
$Al^{+3} + 2SO_4^{-2} \rightleftharpoons Al(SO_4)_2^-$	$10^{4.92}$	$Cr(OH)_2^+ + H^+ + SO_4^{-2} \rightleftharpoons CrOHSO_4 + H_2O$	$10^{8.28}$
$Pb^{+2} + Cl^- \rightleftharpoons PbCl^-$	$10^{1.60}$	$2Cr(OH)_2^+ + 2H^+ + SO_4^{-2} \rightleftharpoons Cr_2(OH)_2SO_4^{+2} + 2H_2O$	$10^{16.16}$
$Pb^{+2} + 2Cl^- \rightleftharpoons PbCl_2$	$10^{1.8}$	$2Cr(OH)_2^+ + 2H^+ + 2SO_4^{-2} \rightleftharpoons Cr_2(OH)_2(SO_4)_2 + 2H_2O$	$10^{17.93}$
$Pb^{+2} + 3Cl^- \rightleftharpoons PbCl_3^-$	$10^{1.70}$		

Table 2-7: Solid reactions

Solid Name	Reaction	K_{SP}
Calcite	$CaCO_3 \rightleftharpoons Ca^{+2} + CO_3^{-2}$	$10^{-8.47}$
Gibbsite	$Al(OH)_3 + 3H^+ \rightleftharpoons Al^{+3} + 3H_2O$	$10^{8.77}$
Gypsum	$CaSO_4.2H_2O \rightleftharpoons Ca^{+2} + SO_4^{-2} + 2H_2O$	$10^{-4.85}$
SiO_2(a)	$SiO_2 + 2H_2O \rightleftharpoons H_4SiO_4$	$10^{-2.71}$
Cerrusite	$PbCO_3 \rightleftharpoons Pb^{+2} + CO_3^{-2}$	$10^{-13.13}$
Anglesite	$PbSO_4 \rightleftharpoons Pb^{+2} + SO_4^{-2}$	$10^{-7.79}$
$Cr(OH)_3$	$Cr(OH)_3 + H^+ \rightleftharpoons Cr(OH)_2^+ + H_2O$	$10^{-0.75}$

Table 2-8: Ion compositions for the initial and injected waters

	$C_{initial}$ (meq/ml)	$C_{injection}$ (meq/ml)
Cr^{+3}	3.00×10^{-08}	3.00×10^{-04}
H^+	1.53×10^{-02}	$1.66\times10^{+00}$
Pb^{+2}	2.00×10^{-08}	2.00×10^{-05}
Mg^{+2}	4.00×10^{-03}	4.00×10^{-03}
Ca^{+2}	1.55×10^{-02}	4.80×10^{-02}
Na^+	1.30×10^{-03}	1.30×10^{-03}
Al^{+3}	3.36×10^{-08}	5.04×10^{-03}
Si^{+4}	7.80×10^{-03}	7.80×10^{-03}
Cl^-	1.30×10^{-03}	1.30×10^{-03}
CO_3^{-2}	1.13×10^{-02}	4.80×10^{-02}
SO_4^{-2}	1.32×10^{-02}	9.01×10^{-03}
O^{-2}	Oxygen balance is applied	
Non-reacting ion	2.54×10^{-03}	4.83×10^{-02}

Table 2-9: Initial concentration of solids

	$C_{initial}$ (mole/kgw)
Calcite	1.83×10^{-02}
Gibbsite	2.50×10^{-03}
Gypsum	8.99×10^{-04}
SiO_2(a)	3.98×10^{-01}
Cerrusite	$0.00\times10^{+00}$
Anglesite	$0.00\times10^{+00}$
$Cr(OH)_3$	$0.00\times10^{+00}$

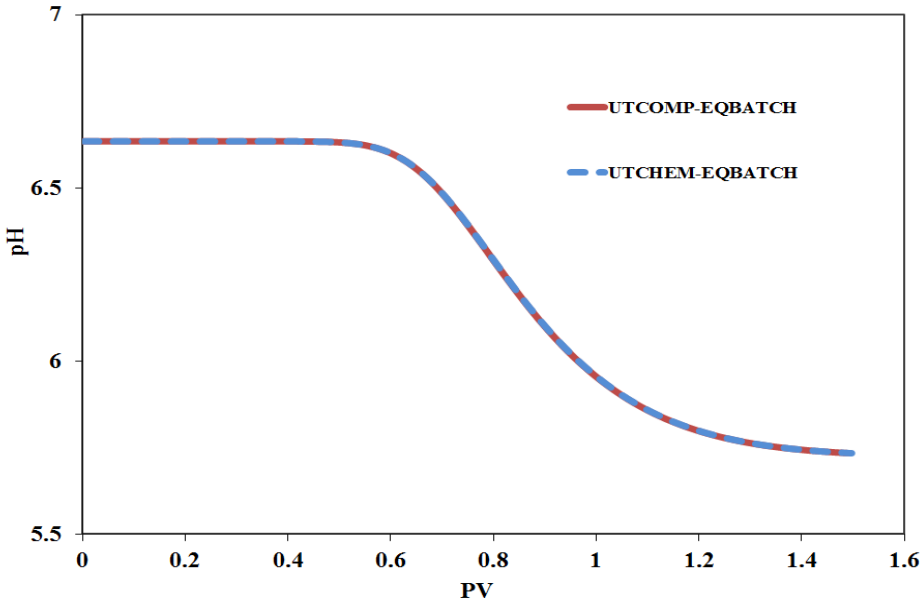

Figure 2-32: History of effluent pH (UTCOMP-EQBATCH verification against UTCHEM-EQBATCH).

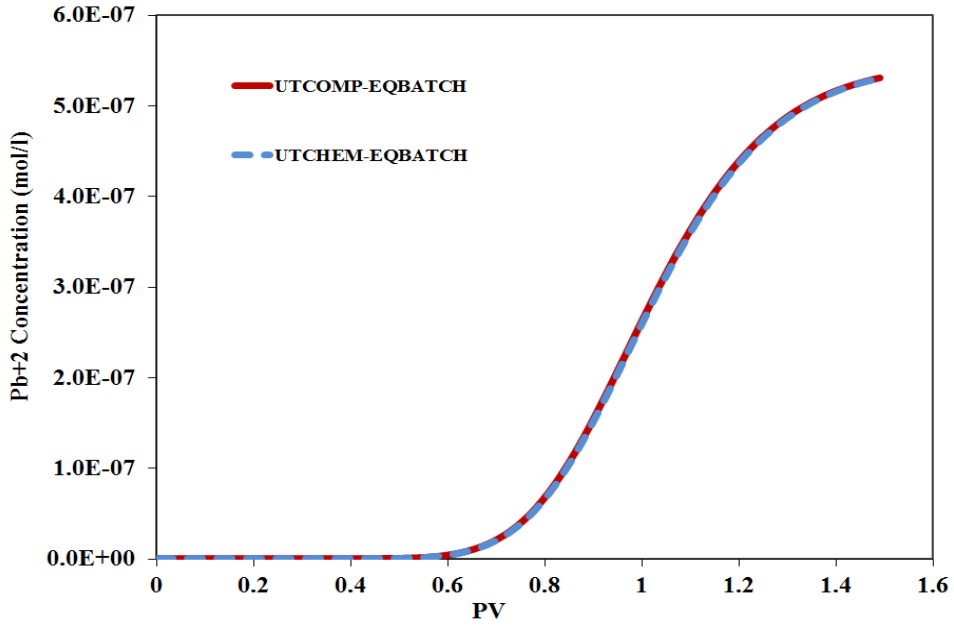

Figure 2-33: History of effluent Pb^{+2} concentration (UTCOMP-EQBATCH verification against UTCHEM-EQBATCH).

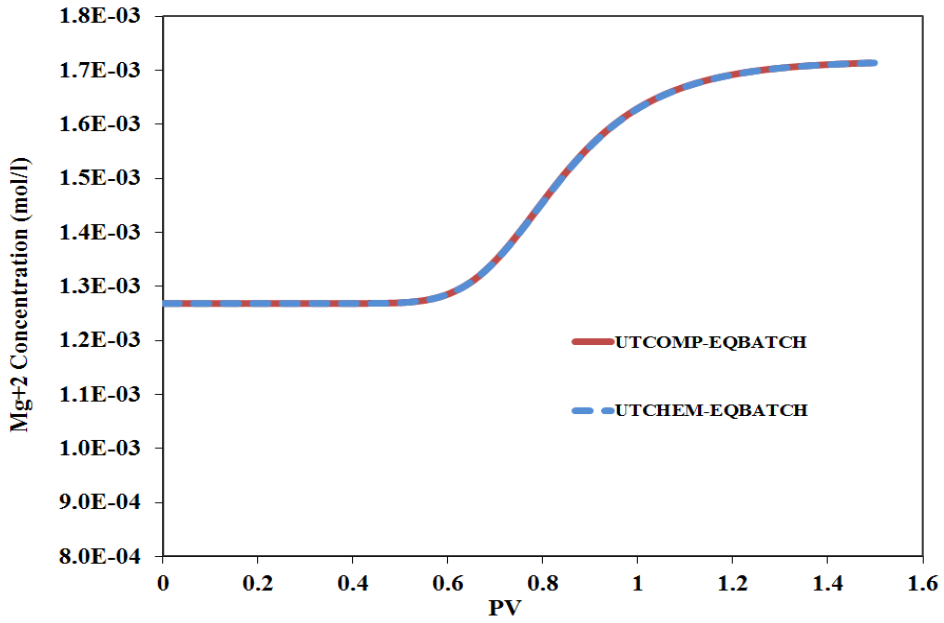

Figure 2-34: History of effluent Mg^{+2} concentration (UTCOMP-EQBATCH verification against UTCHEM-EQBATCH).

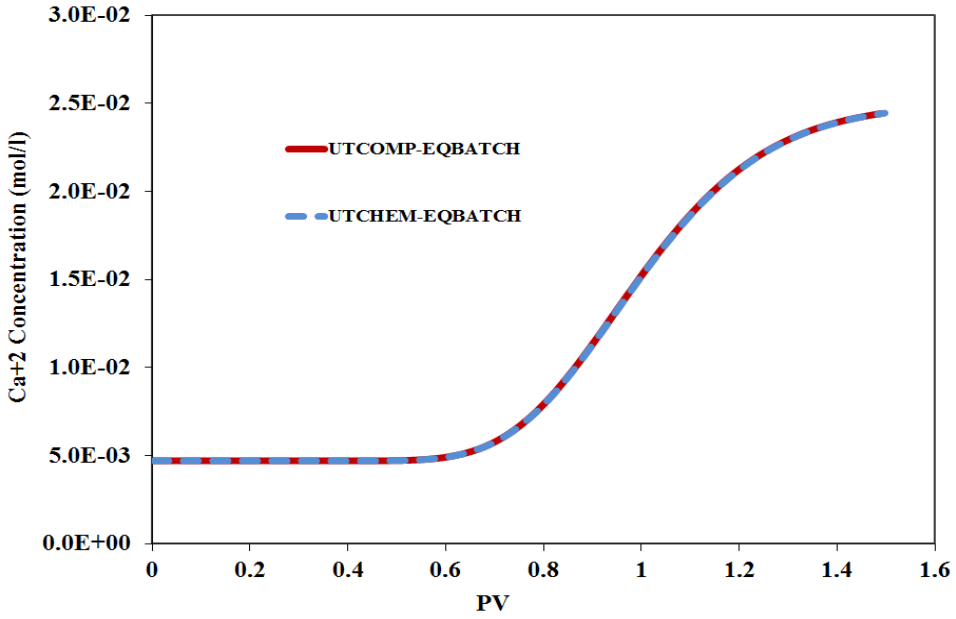

Figure 2-35: History of effluent Ca^{+2} concentration (UTCOMP-EQBATCH verification against UTCHEM-EQBATCH).

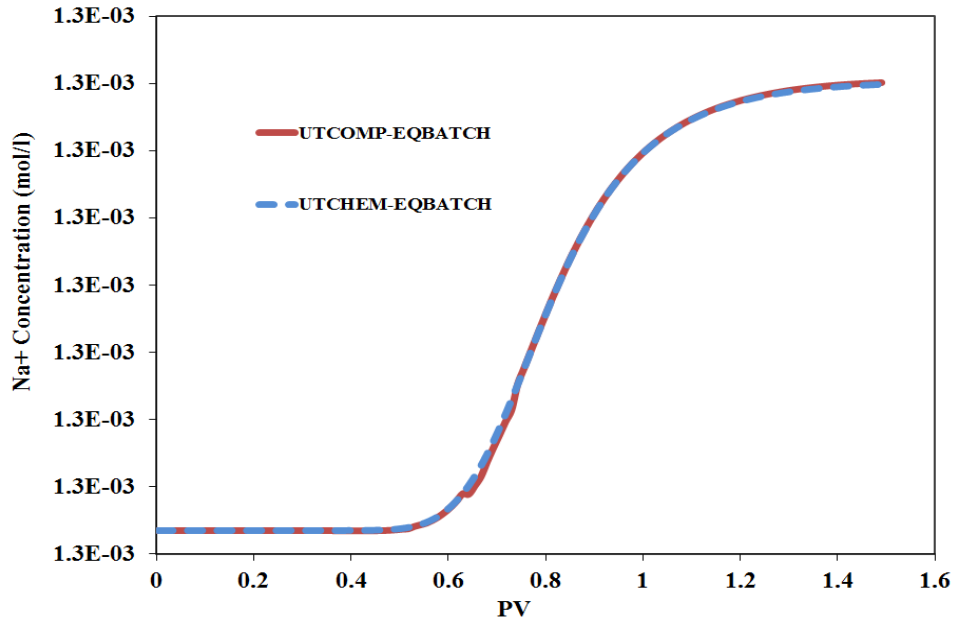

Figure 2-36: History of effluent Na^{+} concentration (UTCOMP-EQBATCH verification against UTCHEM-EQBATCH).

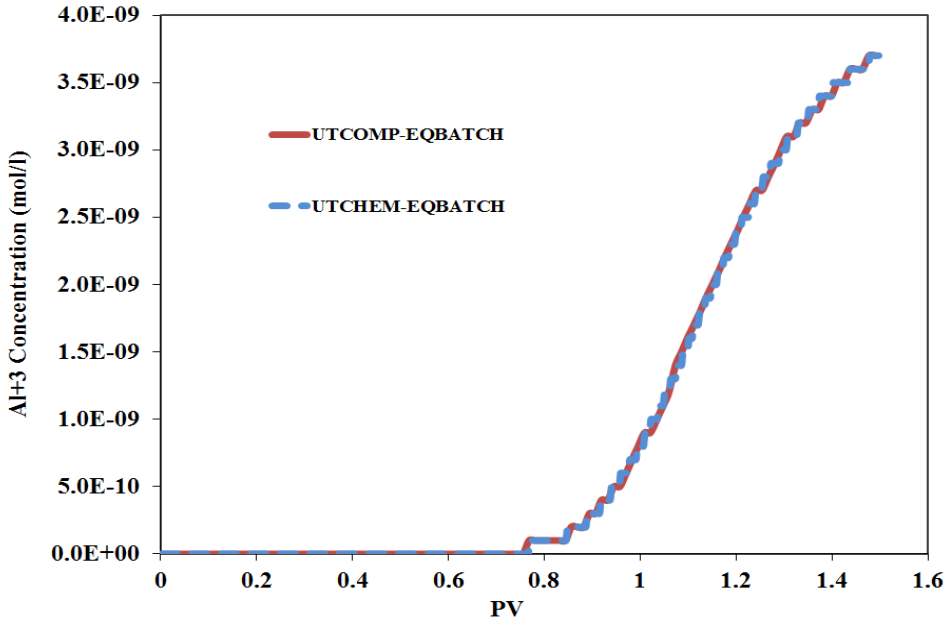

Figure 2-37: History of effluent Al^{+3} concentration (UTCOMP-EQBATCH verification against UTCHEM-EQBATCH).

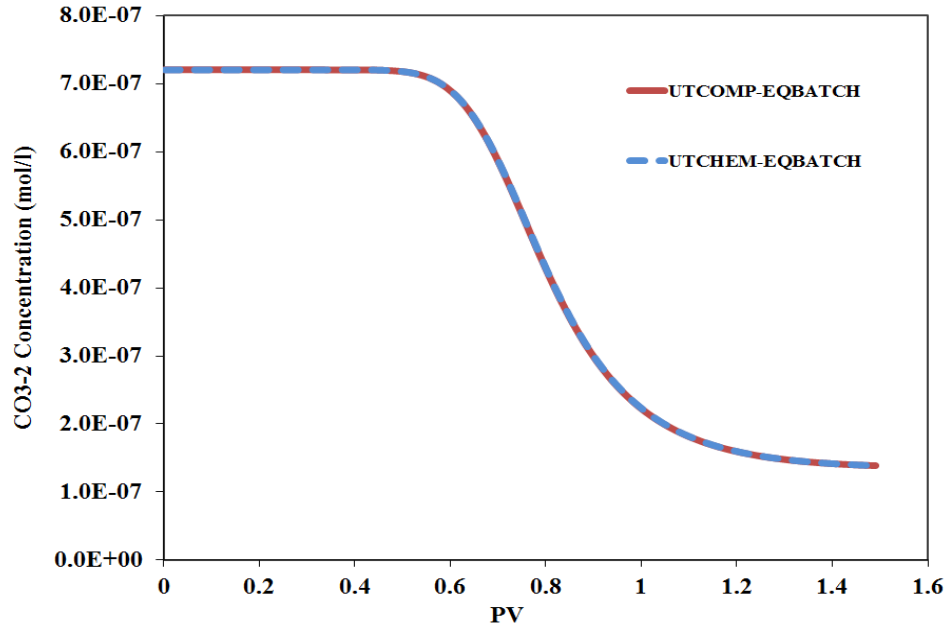

Figure 2-38: History of effluent CO_3^{-2} concentration (UTCOMP-EQBATCH verification against UTCHEM-EQBATCH).

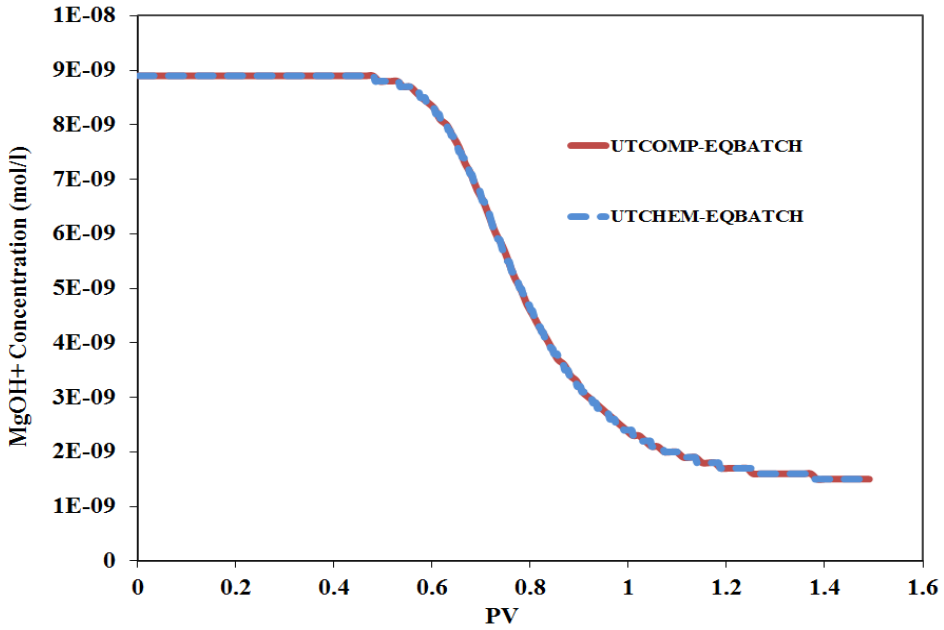

Figure 2-39: History of effluent $MgOH^+$ concentration (UTCOMP-EQBATCH verification against UTCHEM-EQBATCH).

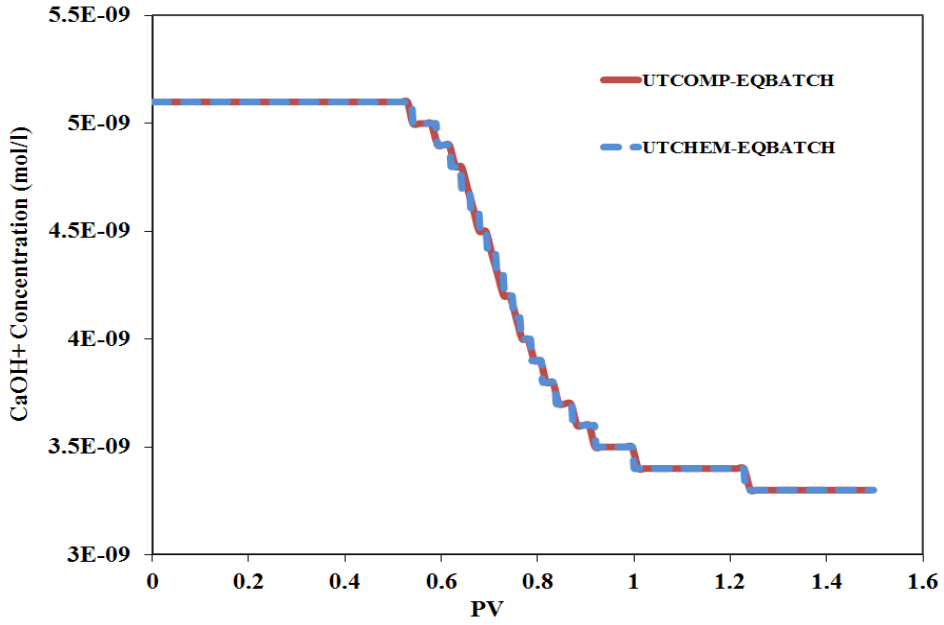

Figure 2-40: History of effluent $CaOH^+$ concentration (UTCOMP-EQBATCH verification against UTCHEM-EQBATCH).

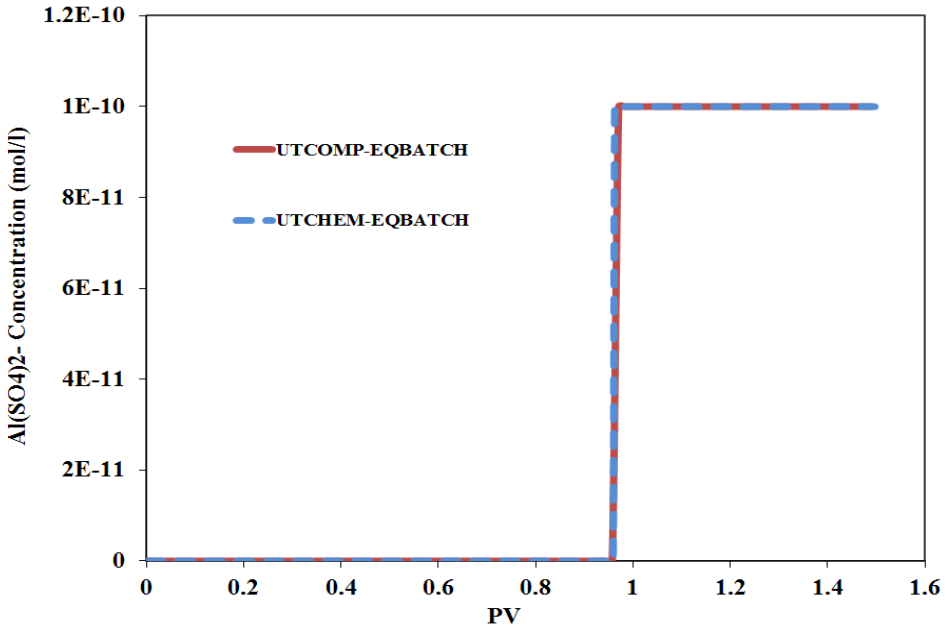

Figure 2-41: History of effluent $Al(SO_4)_2^-$ concentration (UTCOMP-EQBATCH verification against UTCHEM-EQBATCH).

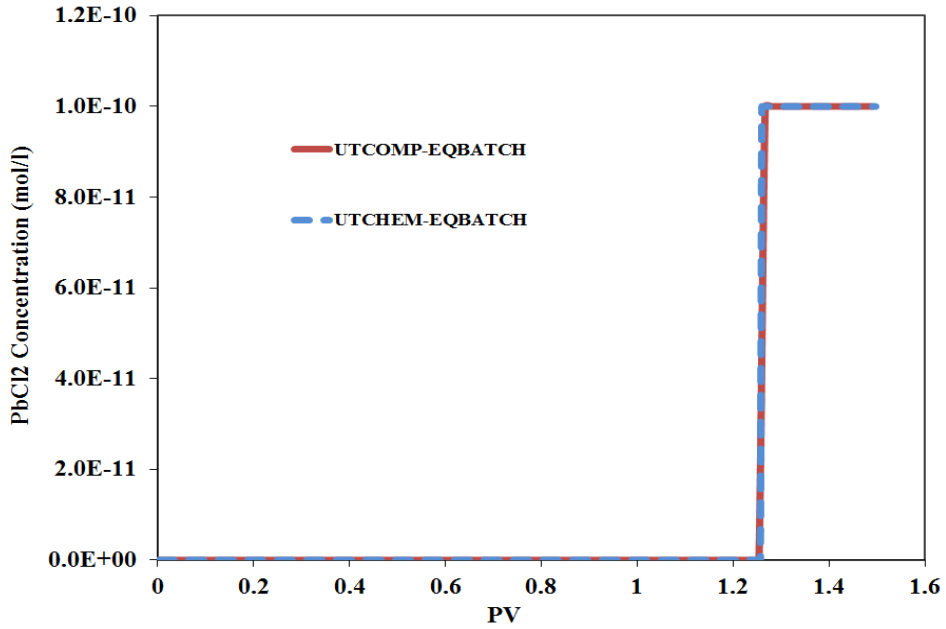

Figure 2-42: History of effluent $PbCl_2$ concentration (UTCOMP-EQBATCH verification against UTCHEM-EQBATCH).

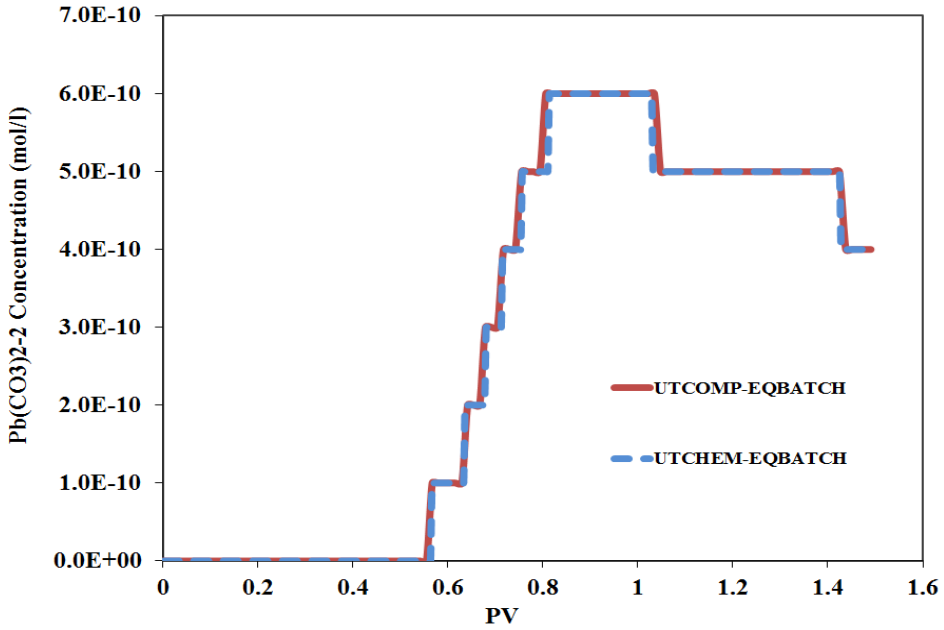

Figure 2-43: History of effluent $Pb(CO_3)_2^{-2}$ concentration (UTCOMP-EQBATCH verification against UTCHEM-EQBATCH).

Case 2

We also verify UTCOMP-EQBATCH against the UTCHEM-EQBATCH simulator for a case with exchange reactions and the charge balance option included. This case includes two exchange reactions and concentration for the chloride is adjusted to make the solution balanced in charge. Table 2-10shows the case description. Aqueous, solid, and exchange reactions considered in this case are illustrated in Table 2-11, Table 2-12, and Table 2-13, respectively. Initial and injecting ion compositions are reported in Table 2-14. In fact, the case is flushed with the pure water. Tables 2-15 and 2-16 present the initial solid and exchange species concentrations, respectively. Cation exchange capacity (CEC) of the exchanger site is 0.1 moles/kgw (see Table 2-17). Injection rate is 4×10^{-5} bbl/day and the production well is operating with the constant bottomhole pressure of 4890.0 psi. The dimensionless Peclet number is 111.1 (the physical

dispersivity coefficient is 0.016 ft and the approximated numerical dispersion coefficient is 0.02 ft). Figures 2-44 through 2-51 compare UTCOMP-EQBATCH produced ion histories for some aqueous species against the UTCHEM-EQBATCH outputs.

Included in Figures 2-44 through 2-51 are results for the case in which two-phase flow is applied in both UTCHEM-EQBATCH and UTCOMP-EQBATCH. The initial water saturation is 0.6 (everything else is identical to that described for Case 2) and there is no interaction between the oleic and aqueous phases. In other words, oleic and aqueous phases are two separate phases being transported in UTCOMP or UTCHEM. As shown in the figures, UTCOMP-EQBATCH matches the UTCHEM-EQBATCH results very well for both single-phase and two-phase flow cases.

Comparison of the ion histories of the two-phase flow with those of the single-phase flow reveals the fact that even when no interaction is assumed between the aqueous and oleic phases (e.g., dead oil), modeling ion histories of a two-phase flow case using a single-phase geochemical package (e.g., PHREEQC, Parkhurst and Appelo, 2013) might introduce significant errors in interpreting the results. The difference between ion histories of multi-phase with those of single-phase reactive-transport problems is more pronounced if the oleic phase (i.e., live oil containing soluble hydrocarbon components) interacts with the aqueous phase (discussed in Chapter 3).

Table 2-10: Reservoir characteristics for 1D verification case

No. of gridblocks		100 (100×1×1)	
Δx(ft)		0.04	
Δy(ft)		0.15	
Δz(ft)		0.15	
Permeability (md)	*x*-direction	100	
Porosity		0.25	
Rock compressibility (psi^{-1})		0.	
Water compressibility (psi^{-1})		0.	
Initial water saturation		1.0 (0.999 in UTCOMP)	
Irreducible water saturation		0.05	
Reservoir temperature (^{o}F)		212.0	
Initial pressure (psi)		4890.0	
Reservoir depth (ft)		0.	
Water viscosity (cp)		0.79	
Number of wells		2	1 injector
			1 producer
Simulation time(PV)		0.5	

Table 2-11: Aqueous reactions

Reaction	K_{eq}
$H_2O \rightleftharpoons H^+ + OH^-$	$10^{-14.0}$
$SO_4^{-2} + H^+ \rightleftharpoons HSO_4^-$	$10^{1.988}$
$Ca^{+2} + SO_4^{-2} \rightleftharpoons CaSO_4$	$10^{2.30}$
$Na^+ + SO_4^{-2} \rightleftharpoons NaSO_4^-$	$10^{0.7}$
$Na^+ + CO_3^{-2} \rightleftharpoons NaCO_3^-$	$10^{1.27}$
$Na^+ + H^+ + CO_3^{-2} \rightleftharpoons NaHCO_3$	$10^{10.079}$
$H^+ + CO_3^{-2} \rightleftharpoons HCO_3^-$	$10^{10.329}$
$Ca^{+2} + CO_3^{-2} \rightleftharpoons CaCO_3$	$10^{3.224}$
$Ca^{+2} + H_2O \rightleftharpoons CaOH^+ + H^+$	$10^{-12.78}$
$Ca^{+2} + CO_3^{-2} + H^+ \rightleftharpoons CaHCO_3^+$	$10^{11.435}$
$Ca^{+2} + SO_4^{-2} + H^+ \rightleftharpoons CaHSO_4^+$	$10^{3.068}$
$Na^+ + H_2O \rightleftharpoons NaOH + H^+$	$10^{-24.0}$

Table 2-12: Solid reactions

Solid reaction	K_{SP}
$CaSO_4(S) \rightleftharpoons Ca^{+2} + SO_4^{-2}$	$10^{-4.36}$
$CaCO_3(S) \rightleftharpoons Ca^{+2} + CO_3^{-2}$	$10^{-8.48}$

Table 2-13: Exchange reactions

Exchange Reaction	K_{ex}
$Na^+X^- + H^+ \rightleftharpoons H^+X^- + Na^+$	$10^{1.0}$
$2Na^+X^- + Ca^{+2} \rightleftharpoons Ca^+X_2^- + Na^+$	$10^{0.8}$

Table 2-14: Ion compositions of initial and injected waters

	$C_{initial}$ (meq/ml)	$C_{injection}$ (meq/ml)
H	$1.11\times10^{+02}$	$1.11\times10^{+02}$
Ca	2.18×10^{-01}	0.
S	1.83×10^{-02}	0.
Na	1.00×10^{-01}	0.
CO_3^{-2}	2.00×10^{-02}	0.
Cl	Charge balance element	
Non-reacting ion	2.00×10^{-01}	0.

Table 2-15: Initial solid concentrations

	$C_{initial}$ (mole/kgw)
Anhydrite	9.09×10^{-02}
Calcite	1.00×10^{-01}

Table 2-16: Initial concentration of the exchange species

	$C_{initial}$ (mole/kgw)
HX	0.
CaX_2	0.
NaX	0.

Table 2-17: Cation exchange capacity of the exchanger site

	Cation Exchange capacity (mole/kgw)
Exchanger	0.1

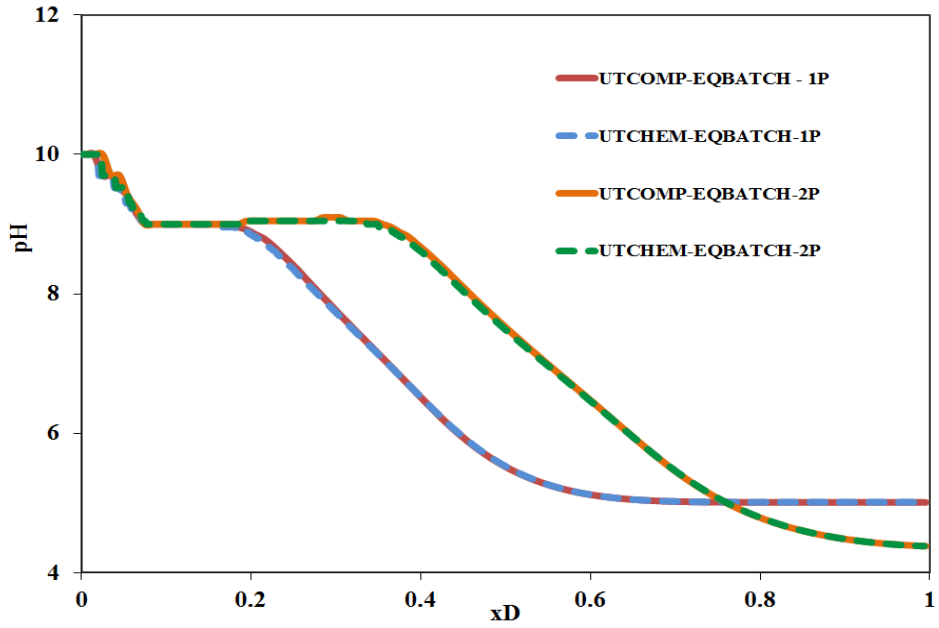

Figure 2-44: History of effluent pH (UTCOMP-EQBATCH verification against UTCHEM-EQBATCH for two-phase and single-phase cases).

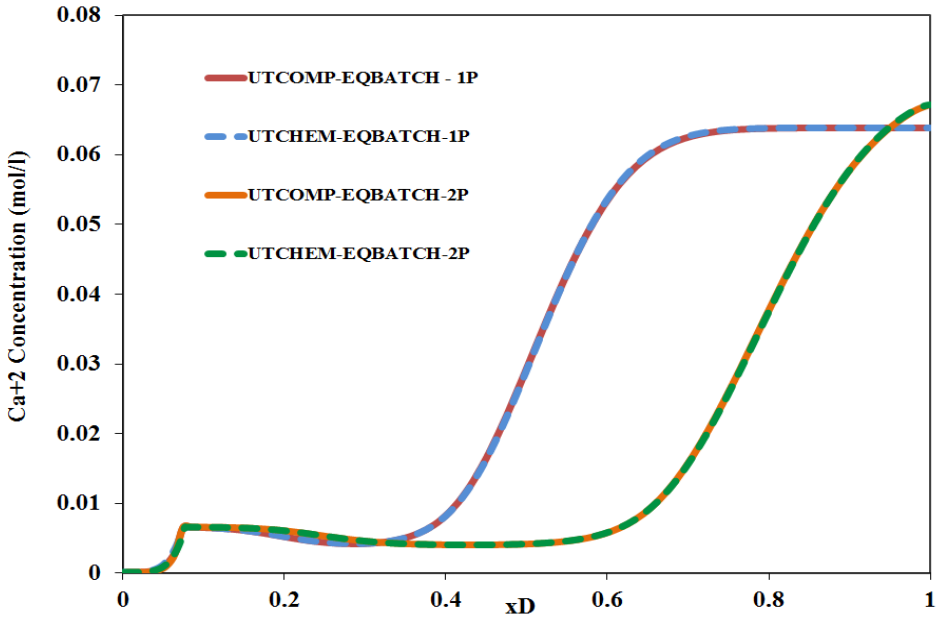

Figure 2-45: History of effluent Ca^{+2} concentration (UTCOMP-EQBATCH verification against UTCHEM-EQBATCH for two-phase and single-phase cases).

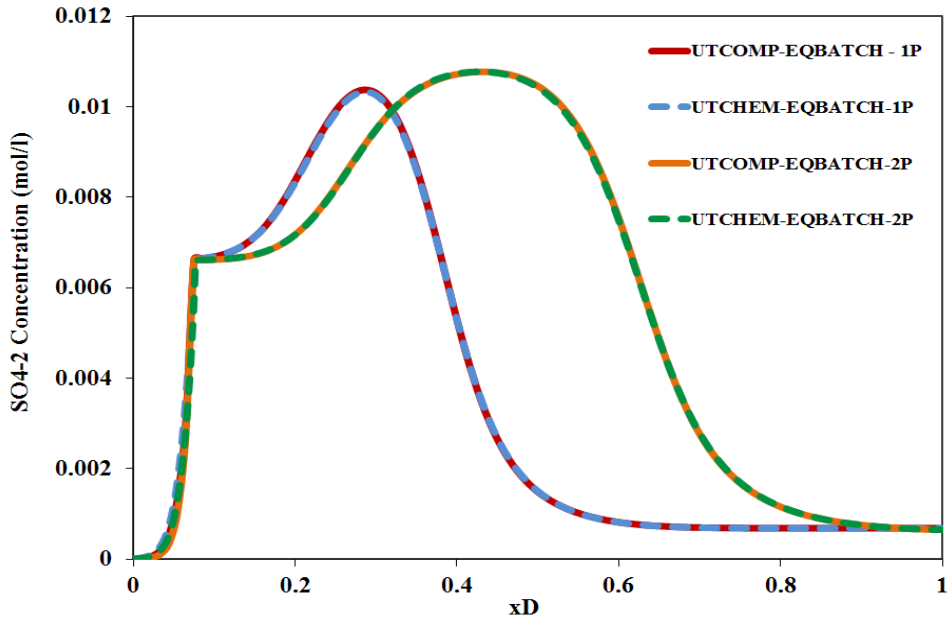

Figure 2-46: History of effluent SO_4^{-2} concentration (UTCOMP-EQBATCH verification against UTCHEM-EQBATCH for two-phase and single-phase cases).

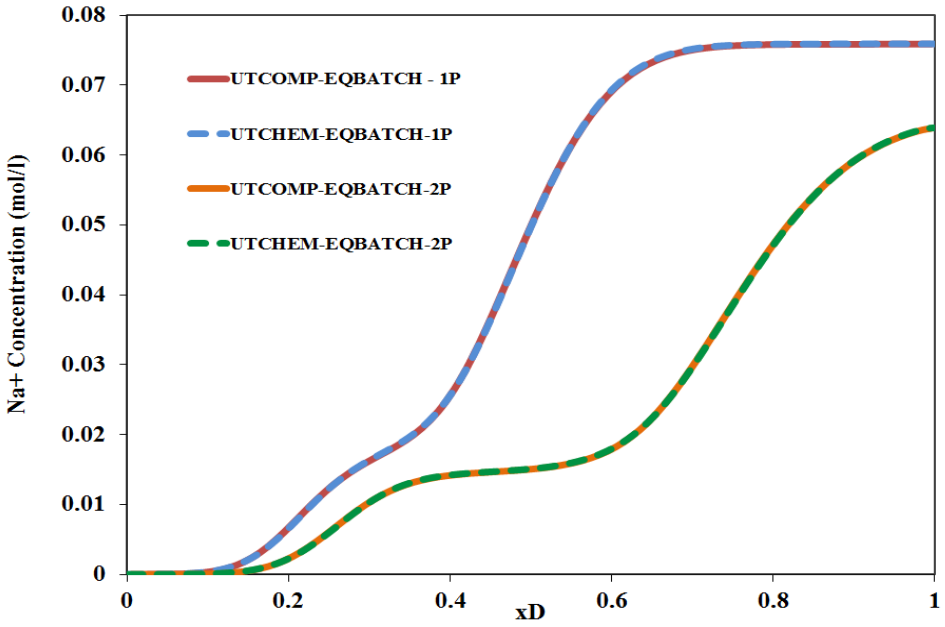

Figure 2-47: History of effluent Na^+ concentration (UTCOMP-EQBATCH verification against UTCHEM-EQBATCH for two-phase and single-phase cases).

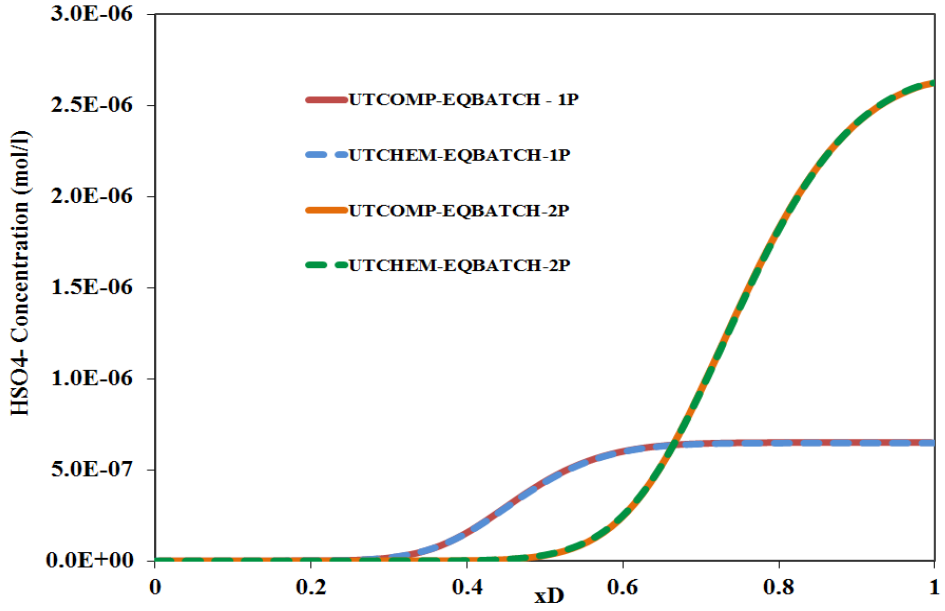

Figure 2-48: History of effluent HSO_4^- concentration (UTCOMP-EQBATCH verification against UTCHEM-EQBATCH for two-phase and single-phase cases).

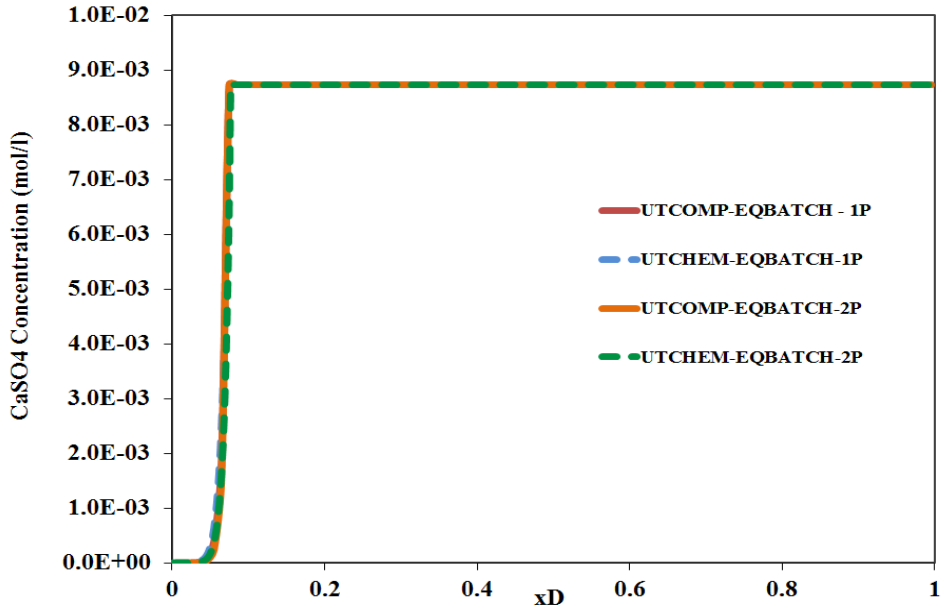

Figure 2-49: History of effluent $CaSO_4$ concentration (UTCOMP-EQBATCH verification against UTCHEM-EQBATCH for two-phase and single-phase cases).

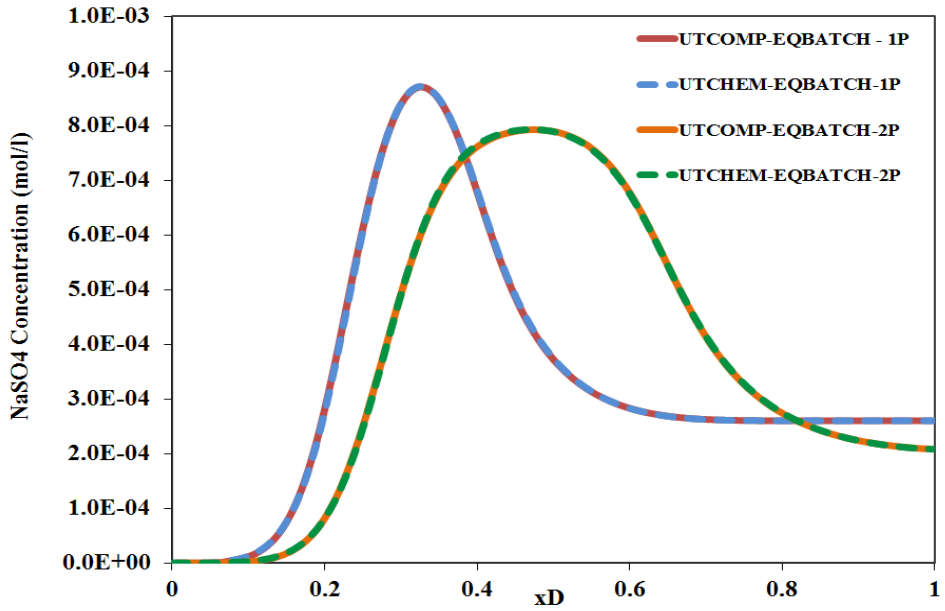

Figure 2-50: History of effluent $NaSO_4$ concentration (UTCOMP-EQBATCH verification against UTCHEM-EQBATCH for two-phase and single-phase cases).

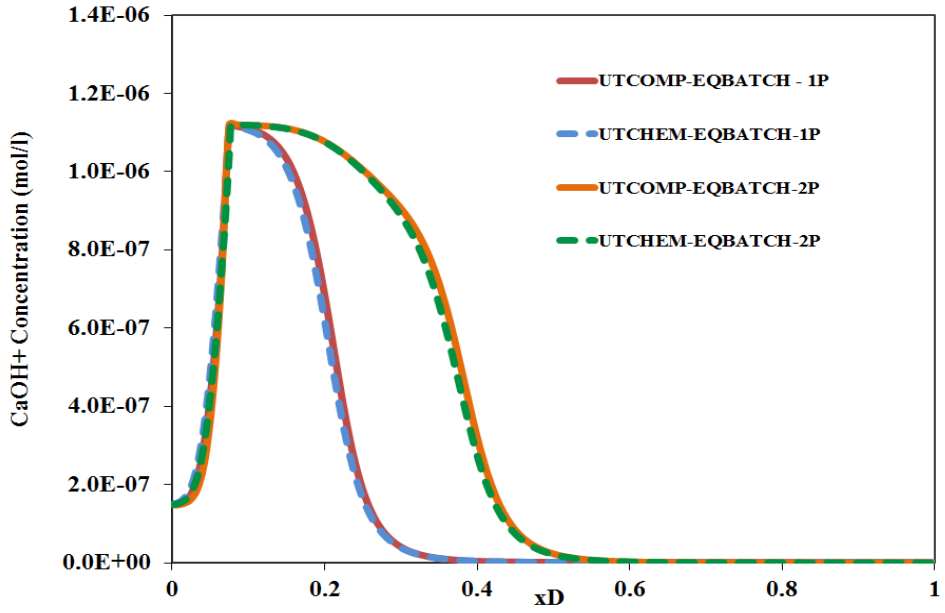

Figure 2-51: History of effluent $CaOH^+$ concentration (UTCOMP-EQBATCH verification against UTCHEM-EQBATCH for two-phase and single-phase cases).

Assumptions that have been made in developing EQBATCH, as well as limitations involved in this geochemical module, are listed below:

- Activity coefficients of all reactive species are unity so that molar concentrations replace activities in reaction equilibria calculations (ideal solution).
- The activity of water is equal to unity (ideal solution).
- Activity of the exchange species is equal to its molality.
- No redox reactions are present.
- All reactions are reversible.
- No surface complexation is allowed.
- All reactions attain thermodynamic equilibrium (no kinetics is allowed).

- Supersaturation and undersaturation of minerals are not included and saturation index of minerals is always zero.
- Equilibrium constants of geochemical reactions are independent of pressure and temperature.
- This geochemical module is not connected to a thermodynamic database and the users need to set up the input which can be tedious.
- No gas phase is allowed. Hence, the effect of soluble hydrocarbon components (e.g., CO_2, CH_4, and H_2S) cannot be included in geochemical calculations. The significant effect of the hydrocarbon phase on the aqueous-rock geochemistry is discussed in Chapter 3.
- No Hetrogeneity in the mineralogy can be applied. In other words, gridblocks are initially identical in EQBATCH.
- EQBATCH is not robust due to numerical convergence problems.

Rather than enhancing EQBATCH to take into account some of the crucial geochemical aspects required for the reactive-transport modeling (such as ion activity coefficients, surface complexation, kinetics, inclusion of the hydrocarbon phase effect in geochemical calculations, etc.), we decided to couple a more comprehensive geochemical package to UTCOMP. It is worth noting that Luo *et al.* (2015) included the ion activity coefficients in the EQBATCH geochemical module.

Table 2-18 is taken from Zhu and Anderson (2002) where they compare capabilities of several geochemical packages available (i.e., MINTEQA2, PHREEQC, EQ3/6, and GWB, Geochemist's WorkBench®[1]). Among these geochemical packages, PHREEQC has more capabilities. In fact, modeling the surface complexation (triple-

[1] Geochemist's WorkBench® is a registered trademark of Aqueous Solutions LLC

layer) and pitzer activity coefficient models are now available in PHREEQC version 3.1.1.8288 (July, 2014). However, this does not mean that no more features have been added to the other geochemical packages presented in the table (as the reference where the table is taken from is fairly old).

Table 2-18: Capabilities in different geochemical packages (Zhu and Anderson, 2002)

Functions		MINTEQA2	PHREEQC	EQ3/6	GWB
Types of rxn	aqueous speciation	√	√	√	√
	pptn/dissolution	√	√	√	√
	solid solutions		√	√	
	ion-exchange	√	√		
	surface complexation				
	constant capacitance	√			
	double layer	√	√		√
	triple layer	√			
Act. coefficient	Davis	√	√	√	√
Models	B-dot		√	√	√
	Pitzer			√	√
Redox	disequilibrium		√		√
Gas phase		√	√	√	√
Reaction path	mixing/titration		√	√	√
models	flow through		√	√	√
	flush		√		√
	dump option		√		√
	fixed activity/fugacity		√	√	√
	slide activity/fugacity		√		√
	change of temperature		√	√	√

Based on the discussion above, PHREEQC is now a complete geochemical package that provides all the essential capabilities required for comprehensive reactive-transport modeling. What follows below presents more details on PHREEQC.

2.5 PHREEQC DESCRIPTION

PHREEQC (**pH**-**RE**dox-**EQ**uilibrium in **C** programing language) is a free, open-source state-of-the-art geochemical package of the USGS (Parkhurst and Appelo, 1999; 2013). It is based on the Fortran®[1] program PHREEQE (Parkhurst *et al.*, 1980) and supported by the USGS since 1980. PHREEQC is a very general and flexible tool for modeling reactive-transport studies with rich databases (Parkhurst and Appelo, 1999; 2013). Lawrence Livermore National Laboratory model and WATEQ4F models based on ion-association aqueous as well as the Pitzer specific-ion-interaction aqueous model and the SIT (Specific ion Interaction Theory) are the models through which ion-association aqueous can be modeled in PHREEQC. This geochemical package has the capability of equilibria calculation that includes aqueous, mineral, gas, solid-solution, surface-complexation, and ion-exchange equilibria; capabilities of speciation and saturation index calculation; batch-reaction and one-dimensional transport; reversible and irreversible reactions; kinetic reaction; mixing solutions; inverse modeling in which the temperature (van't Hoff expression or an analytical expression is used) and pressure effects are included (Parkhurst and Appelo, 1999; 2013). The importance of ion activities, temperature, and pressure in the reactive-transport modeling is investigated later.

If PHREEQC is coupled with a petroleum reservoir simulator, the entire geochemical capabilities of this geochemical simulator can be applied in a multi-dimensional and multi-phase reservoir simulator to comprehensively model reactive-related problems in the oil industry. We decided to couple PHREEQC with UTCOMP to combine the geochemical power of a state-of-the-art geochemical package with the

[1] Fortran® is a registered trademark of Intel Corporation

important aspects of hydrocarbon flow and compositional effects to mechanistically model low salinity waterflooding.

Soft coupling and hard coupling are two coupling approaches that can be applied to couple PHREEQC with UTCOMP. Compared to the hard coupling, soft coupling is easy to implement. In the soft coupling, reservoir simulator (i.e., UTCOMP) first writes the PHREEQC input file and then PHREEQC is run externally using the created input file to find the equilibrium state of all gridblocks. When PHREEQC is done with the calculation, the reservoir simulator reads the output of PHREEQC. Because of the writing and reading of the input and output files, soft coupling is computationally slow. On the other hand, in the hard coupling, the PHREEQC source code is modified to transfer data between the reservoir simulator and PHREEQC through the computer memory. Although the hard coupling is preferred for the sake of computational speed, due to the complicated data structures in PHREEQC and data dependencies between these structures, hard coupling is difficult to program (Charlton and Parkhurst, 2011). Figure 2-52 summarizes the soft and hard coupling approaches of PHREEQC to client software (Muller *et al*., 2011).

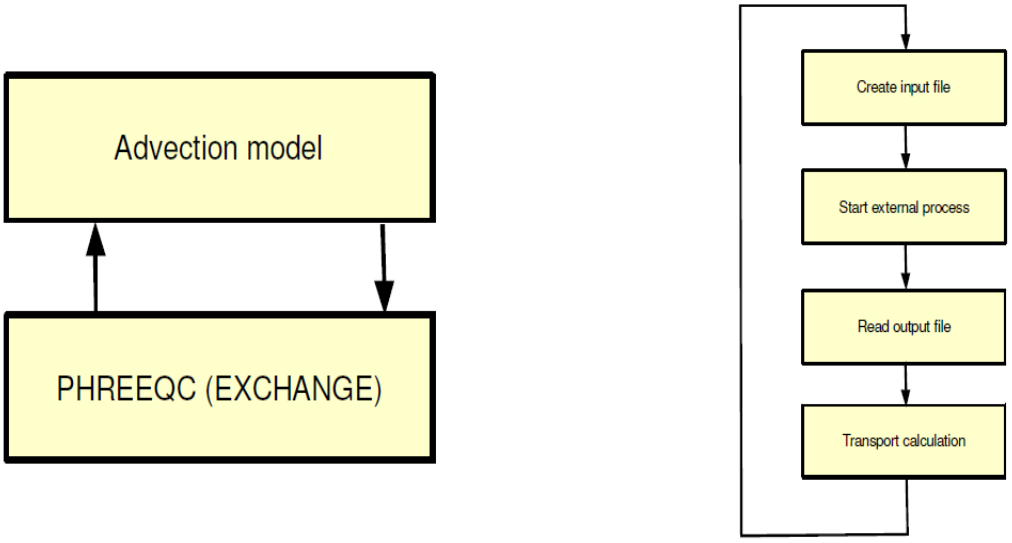

Figure 2-52: Conceptual hard coupling (left panel) (e.g., IPhreeqc coupling, discussed in Section 2.6) and soft coupling with PHREEQC (right panel) (Muller *et al.*, 2011).

PHREEQC has been previously coupled with MPRS, Shell's in-house reservoir simulator (Wei, 2011; 2012). Later Farajzadeh *et al.* (2012) expanded MPRS-PHREEQC for mechanistic modeling of ASP processes. However, from the papers published on MPRS-PHREEQC it is not clear how the coupling is applied in their integrated simulator.

To address the difficulties discussed above concerning coupling method, the USGS released IPhreeqc, with all the PHREEQC capabilities, designed to be integrated with any transport simulator (Charlton and Parkhurst, 2011).

2.6 IPHREEQC DESCRIPTION

IPhreeqc is free and open-source modules of the PHREEQC geochemical package (Parkhurst and Appelo, 1999; 2013) designed to be used in scripting languages and integrated into C++, C, and Fortran® programs (Charlton and Parkhurst, 2011). IPhreeqc is identical to PHREEQC in modeling capability. In fact, the "I" in IPhreeqc stands for

"Interface[1]". Hence, IPhreeqc provides an interface through which a client simulator can easily and efficiently communicate with the PHREEQC geochemical package.

In using IPhreeqc, all data transfer between reservoir simulator and PHREEQC is achieved through a well-defined set of methods without writing and reading files (similar to the hard coupling approach) (Charlton and Parkhurst, 2011). Coupling with IPhreeqc makes the simulation runs roughly an order of magnitude faster compared to soft coupling with PHREEQC (Muller *et al.*, 2011). It should be noted that the gained speedup for IPhreeqc over PHREEQC is not only because of skipping writing and reading of files but also because of the followings: 1) IPhreeqc loads the database once throughout the entire simulation (compare with soft coupling with PHREEQC in which database is loaded at each time step) and 2) compared with PHREEQC which evaluates the solution speciation at each time step, IPhreeqc performs the solution speciation once and only at the first time step. For the rest of simulations, IPhreeqc modifies the solution speciation rather than recalculating it. The latter is the most important aspect through which IPhreeqc accelerates the simulation. For IPhreeqc to skip the solution speciation calculations at each time step, it is necessary to transport H, O, and charge imbalance, in addition to any other elements in the system to maintain complete solution composition and correct charge imbalances. This will be discussed with more details later (cf. Section 2.7).

Muller *et al.* (2011) compared the computational times for the direct use of PHREEQC and the different coupling methods. In their study, direct use of PHREEQC was considered as the base case for the comparison. The bar plot labeled "CPP" in Figure

[1] Personal communication with D. L. Parkhurst of the USGS. 2014 (through email).

2-53 stands for the case where IPhreeqc is coupled with the client software written in the C++ programming language. “COM” (Component Object Model) is for the case in which IPhreeqc COM interfaces with Python. “DLL” (Dynamically Linked Library) is for the case where IPhreeqc is coupled with client software written in Python and the last, the soft coupling is labeled as “external” in this figure.

As we can see from Figure 2-53 the CPU time decreases about 8 times for the case where IPhreeqc is used as a dynamically linked library (DLL) to client software compared to the case where PHREEQC is soft coupled.

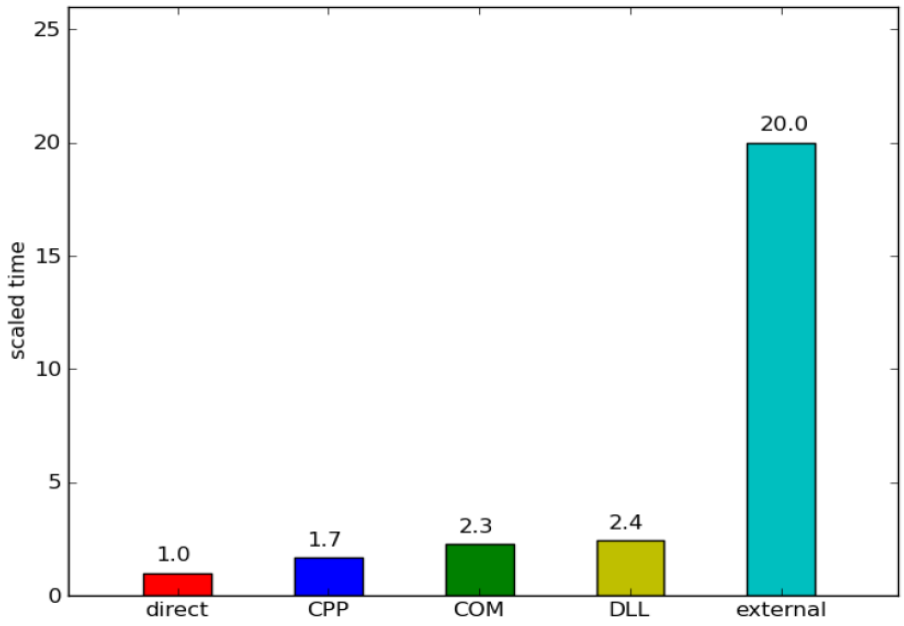

Figure 2-53: Comparing computational times for different coupling approaches (normalized with the direct use of PHREEQC) (Muller *et al.* (2011)).

IPhreeqc is being widely integrated with several transport simulators to embed an exhaustive geochemistry in different research areas (Wissmeier and Barry, 2011; Nardi *et*

al., 2012; Huber *et al.*, 2012; Elakneswaran and Ishida, 2014; Nardi *et al.*, 2014). To this end, due to the advantages of IPhreeqc over PHREEQC in terms of the coupling, we follow a step-by-step approach to couple IPhreeqc with UTCOMP. The coupling approach will be presented in sections below.

2.7 COUPLING IPHREEQC WITH UTCOMP

The way by which a reactive-transport problem is designed in UTCOMP-IPhreeqc has been tried to be very close to PHAST (Parkhurst *et al.*, 2010). In UTCOMP-IPhreeqc, transport-related parameters are defined in "INPUT.DAT" which is the main UTCOMP input file (equivalent to *prefix*.trans.dat in PHAST). In modeling reactive-transport problems, IGEOCHEM flag is "true" in this input file. Through using another flag (i.e., IPhreeqc_FLAG) the users can define if EQBATCH (coupled with UTCOMP in Section 2.4) or IPhreeqc is applied to the simulation.

Complete geochemistry information is provided through four input files in the UTCOMP-IPhreeqc simulator. What follows below is a brief description of the UTCOMP-IPhreeqc geochemistry input files:

- GCINPUT.DAT: through this input file the users can control UTCOMP-IPhreeqc output files (ion histories and maps; aqueous histories and maps; solid histories and maps; surface histories and maps; exchange histories and maps). Moreover, number of hydrocarbon components to be included in geochemical calculations (cf. Section 2.7.1) is defined in this file.
- IPhreeqc_Database.DAT (equivalent to phast.dat in PHAST): is the main geochemistry database required by IPhreeqc. Usually one of the geochemistry databases released along with PHREEQC is used (e.g., phreeqc.dat, pitzer.dat, etc.).

- IPhreeqc_Database.inc: additional geochemical reactions can be defined in this input file. Obviously, the same reactions can be also added in the "IPhreeqc_Database.DAT file".
- IPhreeqc_INPUT.DAT (equivalent to *prefix*.chem.dat in PHAST): is the input file through which the users define initial cells conditions and injected solutions. The format of this input file is identical to the PHREEQC input file. Hence, all the PHREEQC capabilities are functional in this input file to define the initial and injection solutions. Aqueous solutions (using **SOLUTION**) for cells 1 through NB (NB is number of gridblocks) must be defined in this input file. In other words, initial aqueous solutions of all the gridblocks must be initially defined. Cells may be heterogeneous in terms of geochemistry. For clarity, IPhreeqc/PHREEQC keywords are all capital letters and in bold font in this dissertation (e.g., **SOLUTION**, **EQUILIBRIUM_PHASES**). Injection solutions are also defined in the IPhreeqc_INPUT.DAT file and the solution numbers are given in the INPUT.DAT file where the injection flowrates is provided (similar to PHAST).

In using IPhreeqc, batch cells (i.e., each reservoir gridblock is treated as a batch cell) are completely defined in the IPhreeqc_INPUT.DAT input file using **SOLUTION** (to define aqueous ion compositions, temperature, and pressure, etc.), **EQUILIBRIUM_PHASES** (to define the solid phases initially present or later appear), **EXCHANGE** (to define ion-exchange sites), **KINETICS** (to define kinetic reaction), and **SURFACE** (to define the surface complex) keywords.

In the initialization step, *CreateIPhreeqc* (italic expressions containing several words capitalized in the first letter are IPhreeqc methods) of IPhreeqc is first used to

define an IPhreeqc module in the computer memory (see Table A.1 provided in Charlton and Parkhurst (2011) for complete list of methods available for a Fortran® IPhreeqc module). *LoadDatabase* is then applied to load the thermodynamic database (i.e., IPhreeqc_Database.DAT file) in the just created IPhreeqc module.

We always store the following dummy reaction along with the database to better numerical convergence:

```
SOLUTION_SPECIES; H2O + 0.01e- = H2O-0.01; log_k -9
```

The dummy reaction above is suggested in the PHREEQC user manual (Parkhurst and Appelo, 2013). To store any data in the IPhreeqc module, *AccumulateLine* is used. For example, what follows below shows the process of accumulating in the computer memory the dummy reaction given above.

```
Ierr=AccumulateLine(Id_phreeqc_initialization,'SOLUTION_SPE
CIES;H2O + 0.01e- = H2O-0.01; log_k -9')
```

If the IPhreeqc_Database.inc file exists in the run directory, it will be also stored in the memory. After accumulating all the geochemical reaction required, we load IPhreeqc_INPUT.DAT input file in the IPhreeqc module through using *AccumulateLine* and **INCLUDE$** keywords available in IPhreeqc. *RunAccumulated*, *GetComponentCount*, and *GetComponent* are applied to obtain the number and name of geochemical species, respectively. Using the number of geochemical species, we allocate the entire variables involved in geochemical calculations.

At later time steps, we just modify the previously defined batch cells for any changes occurring in solution, solid phase, exchange site, kinetic reaction, or surface complex using **SOLUTION_MODIFY**, **EQUILIBRIUM_PHASES_MODIFY**,

EXCHANGE_MODIFY, **KINETICS_MODIFY**, and **SURFACE_MODIFY**, respectively. In this coupling approach, once the concentrations of aqueous geochemical species are calculated, the IPhreeqc input is stored in the computer memory using *AccumulateLine* method available in IPhreeqc. IPhreeqc module is then run using *RunAccumulated* method to calculate the new equilibrium state for all batch cells. Finally, *GetSelectedOutputColumnCount*, *GetSelectedOutputRowCount*, and *GetSelectedOutputValue* methods are used to transfer the IPhreeqc's outputs to UTCOMP.

As mentioned earlier, besides the total moles of geochemical elements existing in the aqueous phase, total moles of hydrogen and oxygen and charge balance must be transported in order to maintain complete solution composition and correct charge imbalances in IPhreeqc. **TOTMOLE("H")**, **TOTMOLE("O")**, and **CHARGE_BALANCE** available in IPhreeqc returns total moles of hydrogen and oxygen along with the charge balance of each batch cell, respectively.

Charge balance is treated similar to other geochemical elements (e.g., Ca, Na, H, etc.) present in the system. The same as other geochemical elements, mass balance equation is solved for the charge balance. However, care must be taken to the fact that contrary to the geochemical element concentrations that must be always positive, charge balance can have negative values (if the sum equivalent of anions present in the gridblock is greater than that for cations). Hence, mass balance equation for the charge balance is solved regardless if it is negative or positive[1]. A simplified code is provided in Appendix C that shows how we use the methods available in IPhreeqc to communicate between this

[1] Personal communication with D. L. Parkhurst of the USGS. 2014 (through email).

geochemical package and a client simulator (i.e., UTCOMP) through the computer memory. This simplified code is the expanded version of advect.f90 example file released with IPhreeqc (Charlton and Parkhurst, 2011). Basically, we apply the same approach in the UTCOMP-IPhreeqc (and later in Chapter 5 for UTCHEM-IPhreeqc) simulator. However, compared with the simplified code that simple cell shifting is applied to introduce the transport into the problem, in the UTCOMP-IPhreeqc simulator, the mass conservation equation (i.e., Eq. (2.17)) is solved to transport geochemical species. No physical dispersion has been included in the simplified code provided in Appendix C.

Because IPhreeqc automatically saves moles of the solid phases; moles of ions on exchange sites; and moles of surface complexes after each batch cell calculation, hence, it is often the case that only aqueous phase is modified at each time step using the **SOLUTION_MODIFY** keyword (Charlton and Parkhurst, 2011; Korrani *et al.*, 2013). Later we also use **EQUILIBRIUM_PHASES_MODIFY** to include the hydrocarbon phase effect on the aqueous-rock geochemistry.

2.7.1 Including the Hydrocarbon Phase Effect on the Aqueous-Rock Geochemistry

Several researchers have investigated the impact of water-soluble hydrocarbon phase components on multi-phase reactive-transport. In particular, the significant effect of CO_2 on the reactive-transport modeling has been extensively studied in the research area of the CO_2 storage and sequestration (Nghiem *et al.*, 2004; Cantucci *et al.*, 2009; Xiao *et al.*, 2009; Xu *et al.*, 2010; Liu *et al.*, 2010; Zhang *et al.*, 2011; Xu *et al.*, 2011). CO_2 dissolves in the aqueous phase, particularly at high reservoir pressure, and carbonic acid is formed. As a result, not only the pH of the system will be affected but also carbonate anion in the system can interact with the cations present in the water to form insoluble carbonates. Zhang *et al.* (2012) discussed the importance of the hydrocarbon

phase effect on the aqueous-rock geochemistry. They believe in the multi-phase reactive-transport modeling, hydrocarbon does not have to come into the sight through an additional phase but, as a geochemical entity. Hydrocarbon components can coat mineral surfaces and reduce the effective surface area of the mineral for precipitation and dissolution (Zhang *et al.*, 2012). Also, hydrocarbon components can directly affect the mineral dissolution/precipitation (as discussed above for CO_2).

Acidic/basic components of the crude oil can also exchange between the hydrocarbon and aqueous phases (Havre *et al.*, 2003; Austad *et al.*, 2010; RezaeiDoust *et al.*, 2011). Broadly speaking, acidic components refer to all carboxylic acids with the general formula of RCOOH existing in the crude oil. These components can be found in the resin and asphaltene fractions (Farooq *et al.*, 2011). The importance of these components has been highly emphasized for years for processes such as alkaline and alkaline/surfactant/polymer floodings (deZabala *et al.*, 1982; Bhuyan, 1989; Mohammadi *et al.*, 2009). The significant role of acidic components during ASP floods is discussed with more details in Chapter 5. On the other hand, hetrocylic aromatic compounds with one nitrogen atom and one or more aromatic rings are referred to as basic components (Farooq *et al.*, 2011). Acidic/basic components have been recently studied to interpret the underlying mechanisms behind the low salinity water injection (Austad *et al.*, 2010; RezaeiDoust *et al.*, 2011; Farooq *et al.*, 2011). For these reasons, it is clear that water soluble hydrocarbon components are an integral part of multi-phase reactive-transport.

UTCOMP is a compositional reservoir simulator capable of modeling the effects of soluble hydrocarbon gas components (e.g., CH_4 and CO_2) and acidic/basic components of the hydrocarbon phase. Based on the discussion above, there are two types of hydrocarbon components that should be taken into considerations for proper multi-phase

oil-field reactive-transport modeling: 1) Soluble hydrocarbon components (e.g., CH_4 and CO_2) 2) Acidic/basic components.

IPhreeqc/PHREEQC can be used to properly take into account the effect of the hydrocarbon phase on the aqueous-rock geochemistry. Figure 2-54 compares the IPhreeqc/PHREEQC simulated results for the CO_2 solubility in the aqueous phase against the measured values at different temperatures and high range of pressure values. As the figure presents, IPhreeqc/PHREEQC predicts the solubility of CO_2 in the aqueous phase fairly well. Moreover, IPhreeqc/PHREEQC considers the hydrocarbon solubility reactions along with other reaction occurring in the aqueous phase. Hence, the calculated CO_2 solubility in the aqueous phase is somehow salinity dependent.

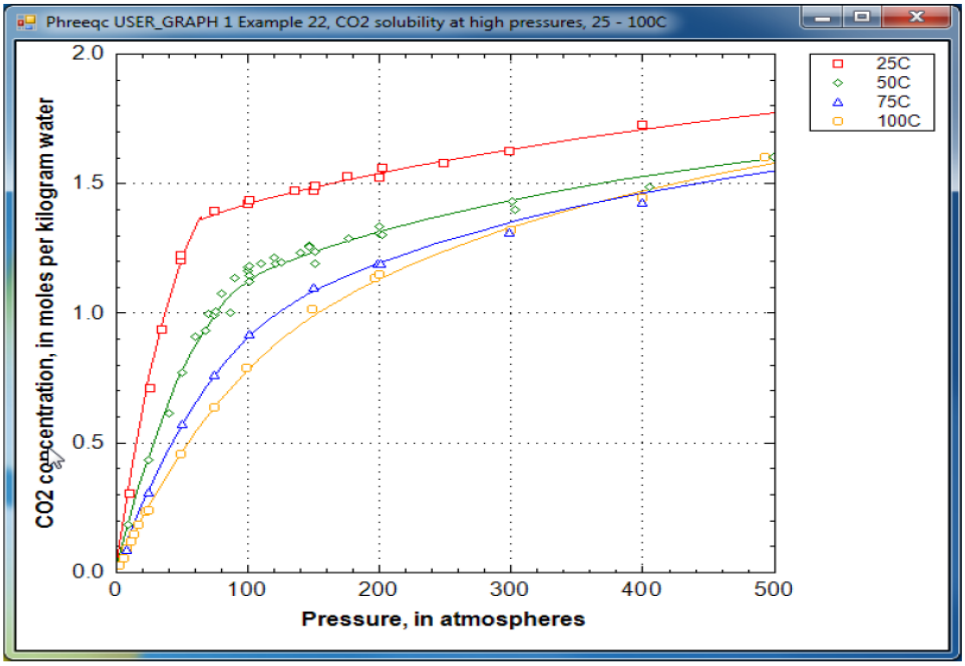

Figure 2-54: PHREEQC simulated results against the measured values for the CO_2 solubility in the aqueous phase (Parkhurst and Appelo, 2013).

Different approaches can be followed to take the effect of the soluble hydrocarbon components into account: the sequential iterative approach (Mangold *et al.*, 1991; Yeh *et al.*, 1991) and the simultaneous solution method (also referred as fully-coupled approach) (Steefel *et al.*, 1992; Nghiem *et al.*, 2004). In the sequential iterative approach, flow equation and geochemistry equations are in an iteration loop and solved separately and sequentially until the convergence achieved. On the other hand, in the fully-coupled approach, Newton's method is applied to solve system of equations (flow and geochemistry reactions) simultaneously (Nghiem *et al.*, 2004). It appears the sequential iterative approach uses much less computer memory than a fully-coupled approach. The sequential iterative approach is followed in this work. Below presents how UTCOMP-IPhreeqc was developed to take into account the effect of the hydrocarbon phase in geochemical calculations.

Soluble hydrocarbon components (CH_4 and CO_2)

Basic thermodynamic concept that a soluble hydrocarbon component will have identical fugacities in oil, gas, and water phases is used to model the solubility of gases. For example, at the equilibrium, the fugacity of the CO_2 and CH_4 components should be the same in all three phases of gas, oil, and water phase.

$$\begin{aligned} f^{o}_{CO2} &= f^{g}_{CO2} = f^{w}_{CO2}, \\ f^{o}_{CH4} &= f^{g}_{CH4} = f^{w}_{CH4}. \end{aligned} \tag{2.62}$$

Acidic/ Basic Components

Figure 2-55 presents how acidic/basic components partition between the aqueous and oleic phases and consequently affect the aqueous-rock geochemistry state.

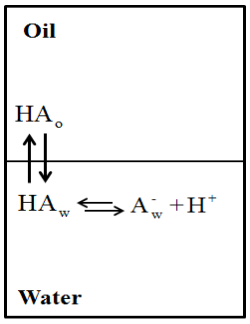

Figure 2-55: Equilibrium in water/oil/naphthenic acid systems at low pH (Havre *et al.*, 2003).

Acidic and basic components are partitioned between the aqueous and hydrocarbon phases as given in the following equation (Bhuyan 1989; Havre *et al.*, 2003):

$$HA_w = HA_o. \tag{2.63}$$

This geochemical reaction is known as partitioning reaction with the equilibrium constant shown below:

$$K_{wo} = \frac{[HA_w]}{[HA_o]}, \tag{2.64}$$

where

$[HA_w]$ = concentration of the acidic component in the aqueous phase (mole/l)

$[HA_o]$ = concentration of the acidic component in the oleic phase (mole/l)

K_{wo} = partition coefficient

The partitioned acid in the aqueous phase will dissociate in the aqueous phase according to Eq. (2.65):

$$HA_w = A_w^- + H^+. \tag{2.65}$$

With the reaction constant following the equilibrium relationship (Bhuyan 1989; Havre *et al.*, 2003):

$$K_a = \frac{[H^+][A_w^-]}{[HA_w]}. \tag{2.66}$$

The IPhreeqc database is modified to include the acidic/basic geochemical reactions along with the other reactions in UTCOMP-IPhreeqc. A new component, A_w, is defined using **SOLUTION_MASTER_SPECIES** to be representative of the acidic/basic component. Moreover, **SOLUTION_SPECIES** is used to include the association reaction of the acidic/basic component. Oil-aqueous partitioning reaction of the acidic/basic component is rearranged as follows before implementation in the IPhreeqc database:

$$\mathrm{K_{wo}} = \frac{[\mathrm{HA_w}]}{[\mathrm{HA_o}]}, \tag{2.67}$$

$$[\mathrm{HA_w}] = \mathrm{K_{wo}}[\mathrm{HA_o}], \tag{2.68}$$

$$\frac{\mathrm{grmole\,HA_w}}{\mathrm{Lit\,of\,water}} = \mathrm{K_{wo}}\frac{\mathrm{grmole\,HA_o}}{\mathrm{Lit\,of\,oil}}, \tag{2.69}$$

$$\frac{\mathrm{lbmole\,HA_w}}{\mathrm{ft^3\,of\,water}} = \mathrm{K_{wo}}\frac{\mathrm{lbmole\,HA_o}}{\mathrm{ft^3\,of\,oil}}, \tag{2.70}$$

$$\frac{1}{\rho_w\left(\frac{\mathrm{lb\,of\,water}}{\mathrm{ft^3\,of\,water}}\right)}\frac{\mathrm{lbmole\,HA_w}}{\mathrm{ft^3\,of\,water}} = \mathrm{K_{wo}}\frac{\mathrm{lbmole\,HA_o}}{\mathrm{ft^3\,of\,oil}}\frac{1}{\rho_w\left(\frac{\mathrm{lb\,of\,water}}{\mathrm{ft^3\,of\,water}}\right)}, \tag{2.71}$$

$$\frac{\text{gr of HA}_w}{\text{gr of water}} = K_{wo} \frac{x_{Aw}\left(\text{lbmole of oil-phase}\right)}{\text{ft}^3 \text{ of oil}} \frac{1}{\rho_w}, \tag{2.72}$$

$$\frac{\text{gr of HA}_w}{\text{Kg of water}} = 1000 K_{wo} \frac{x_{Aw}\bar{\rho}_o}{\rho_w}, \tag{2.73}$$

$$\text{molality of HA}_w = 1000 K_{wo} \frac{x_{Aw}\bar{\rho}_o}{\rho_w}, \tag{2.74}$$

where

x_{Aw} = mole fraction of the acidic/basic component in the oil phase (acidic/basic component is defined as a hydrocarbon component in the UTCOMP input file)

$\bar{\rho}_o$ = molar density of the oil phase (lbmole/ft^3)

ρ_w = mass density of the water phase (lb/ft^3)

Eq. (2.74) is now consistent with the solubility reaction of IPhreeqc shown in Eq. (2.75).

$$m_i \gamma_i = K_H \varphi_i P, \tag{2.75}$$

where

m_i = molality of species *i* (mol/kgw)

γ_i = activity coefficient of species *i* in water

K_H = equilibrium constant

P = partial pressure (atm)

φ_i = fugacity coefficient (which is 1.0 if the ideal gas law is applied) (Parkhurst and Appelo, 2013)

Comparing Eq. (2.75) with Eq. (2.74) leads us to this conclusion where, if a new phase (HA_w) with the equilibrium constant of $1000K_{wo}$ is defined in IPhreeqc then, $\frac{x_{Aw}\overline{\rho}_o}{\rho_w}$ of the acidic/basic component can be treated similar to the partial pressure (or fugacity) of the soluble hydrocarbon components. Eq. (2.75) is also generalized with the water activity coefficient (γ_i) included. Hence, the solubility reaction of IPhreeqc can be applied for both soluble hydrocarbon components as well as the acidic/basic components. Therefore, **PHASES** of IPhreeqc is used to define a new phase, HA_w, with equilibrium constant of $1000K_{wo}$ and during the simulation we treat $\frac{x_{Aw}\overline{\rho}_o}{\rho_w}$ of the acidic/basic components the same as hydrocarbon component fugacities. Hereafter, we refer to the term $\frac{x_{Aw}\overline{\rho}_o}{\rho_w}$ as pseudo-fugacity. Because the formulation in the UTCHEM and UTCOMP simulators are different, the acidic component is treated differently in UTCHEM-IPhreeqc for mechanistic modeling of ASP floods. This is discussed with details in Chapter 5.

GAS_PHASE (at constant pressure), **GAS_PHASE** (at constant volume), and **EQUILIBRIUM_PHASES** are the three options by which a gas phase can be defined in IPhreeqc (Parkhurst and Appelo, 2013). Shown in below is how a gas phase in contact with an aqueous phase is defined using these options.

```
GAS_PHASE
     -fixed_volume
     -volume
     -temperature
     CO2(g)       -moles
     H2S(g)         -moles
     CH4(g)       -moles
```

```
END

GAS_PHASE
     -fixed_pressure
    -pressure
    -temperature
    CO2(g)       -moles
    H2S(g)         -moles
    CH4(g)       -moles
END

EQUILIBRIUM_PHASES
    CO2(g)  Log(PCO2)    -moles
END
```

To be consistent with the fugacity calculation in UTCOMP, complete composition of the gas phase must be defined if **GAS_PHASE** keyword (either at constant pressure or constant volume) is used in IPhreeqc, whereas the **EQUILIBRIUM_PHASES** keyword provides the opportunity to define individual gas components at desired partial pressures. Because limited number of hydrocarbon phase components (and not the entire components) with certain fugacities are interested in terms of multi-phase reactive-transport modeling hence, **EQUILIBRIUM_PHASES** keyword is the only suitable option for our purpose. Moreover, ideal gas law (Henry's law) is applied in IPhreeqc and component fugacities (rather than partial pressures) are considered in **EQUILIBRIUM_PHASES**. IPhreeqc applies ideal gas law, rather than the Peng-Robinson equation-of-state (Peng and Robinson, 1976), if critical temperatures and pressures of the hydrocarbon phase components are not defined in the database (Parkhurst and Appelo, 2013). The same rigorous approach is used for the components in the oil phase if the hydrocarbon phase is oil single-phase.

Figure 2-56 gives a simplified UTCOMP flowchart after coupling with IPhreeqc and including the hydrocarbon phase effect on the aqueous-rock geochemistry (a more

detailed algorithm is provided in Appendix D). In this computational algorithm, after solving the mass conservation equation for hydrocarbon components and geochemical elements, **SOLUTION_MODIFY** is used to modify the aqueous phase for the updated total moles of the geochemical elements. **EQUILIBRIUM_PHASES_MODIFY** is then applied to update fugacities, pseudo-fugacities, and total moles of the hydrocarbon phase components in contact with the aqueous phase. While the updated total moles are used, fugacities and pseudo-fugacities have not been updated yet. Once all the required information is stored in the computer memory, IPhreeqc is run to find the new equilibrium state of the system. According to applied assigned fugacities, hydrocarbon phase components dissolve into the aqueous phase or evolve from the aqueous phase into the hydrocarbon phase. Total moles of the hydrocarbon phase components are then updated in UTCOMP for any changes occurred (**EQUI_DELTA** of IPhreeqc returns this for each component) and consequently flash calculations for the hydrocarbon phase are performed. New calculated fugacities (and pseudo-fugacities) of the hydrocarbon phase components are compared with the previous fugacities (and pseudo-fugacities) used in the geochemical calculations. If the difference is greater than a desired tolerance, fugacities, pseudo-fugacities, and total moles of the hydrocarbon phase components are restored in the computer memory for the IPhreeqc calculation and the iteration loop is followed until convergence is achieved. For the cases studied, bisection method turns out to be more efficient than successive substitution for updating the fugacities of the next iteration. Broadly speaking, to account for the solubility of hydrocarbon phase components, the flash calculation module in UTCOMP was modified to two sequential flash calculations (hydrocarbon-aqueous phase and oil-gas flash calculations). The developed modules in UTCOMP were written in a general way to account for the effects

of arbitrary number of hydrocarbon phase components (for example, H_2S along with CO_2 and CH_4) on the multi-phase reactive-transport modeling. After convergence is achieved in the flash module, hydrocarbon phase properties (e.g., molar and mass densities) are evaluated and subsequently phase saturations are calculated. Rest of the computational algorithm was previously discussed.

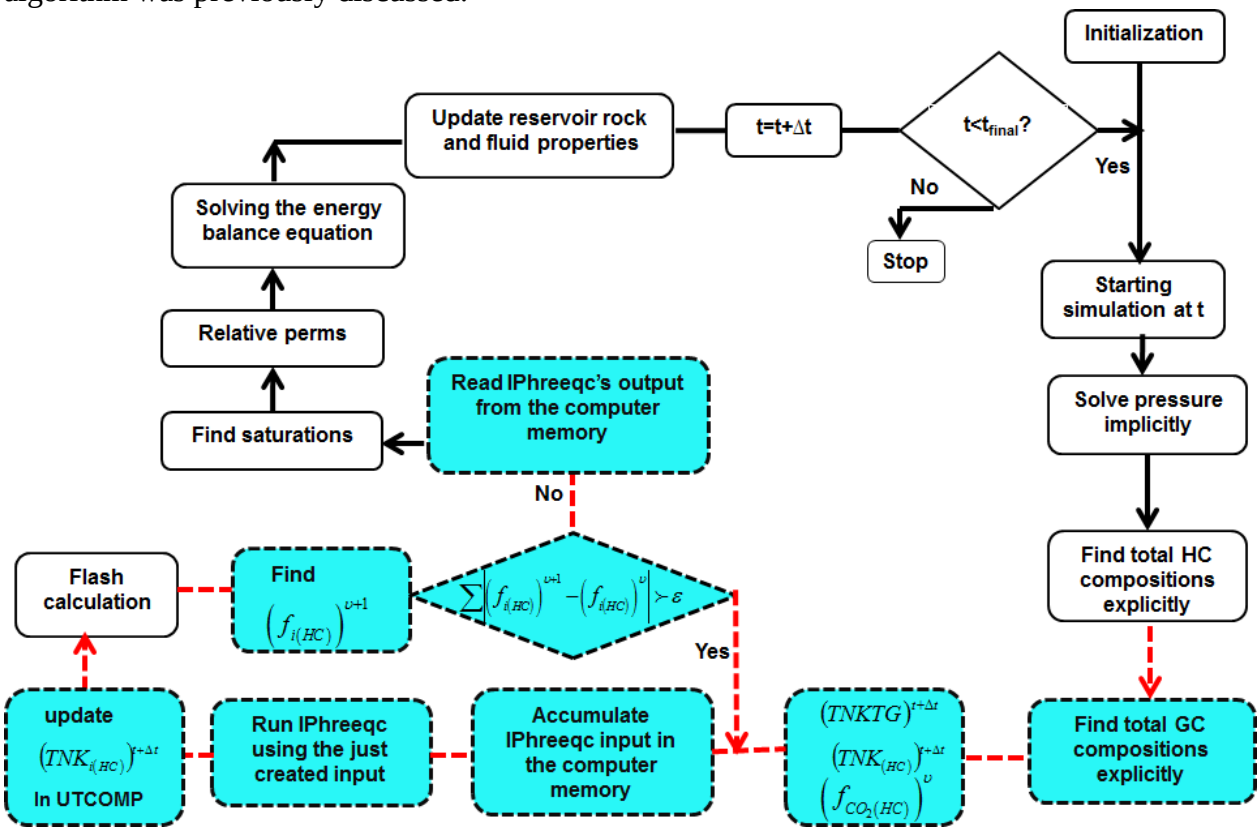

Figure 2-56: Simplified UTCOMP-IPhreeqc calculation flowchart with the hydrocarbon phase effect on the aqueous-rock geochemistry included.

It should be noted that very similar to PHAST (Parkhurst *et al.*, 2010), batch cell calculations in UTCOMP-IPhreeqc are based on 1 Kg of water. Hence, before going to the geochemistry module, total moles of the entire geochemical species and total moles of

all the hydrocarbon components (if the hydrocarbon phase effect is included in the geochemical calculations) of gridblocks are divided by water mass existing in each gridblock. When UTCOMP-IPhreeqc is done with the geochemical calculation, total moles of geochemical species and hydrocarbon components (if the effect is included on the aqueous-rock geochemistry) are multiplied by water mass of gridblocks. The reason for this is the fact that IPhreeqc/PHREEQC works the best if water mass is within a couple of orders of magnitude of 1 Kg[1]. Contrary to PHAST (Parkhurst *et al.*, 2010) where concentrations of geochemical species are used for the transport, the UTCOMP mass conservation equations (for hydrocarbon; tracers; geochemical components) are solved based on the total moles. Noteworthy, in UTCOMP-IPhreeqc, except where the iteration is followed to make identical component fugacities among the phases, finding new equilibrium states of gridblocks is not performed one by one. At each time step, we modify all the gridblocks in the memory (using *AccumulateLine*) and then run IPhreeqc (using *RunAccumulated*) to find new equilibrium states of the entire gridblocks. This accelerates the simulation to some extent.

For single-phase cases (only aqueous phase) or two-phase cases with dead oil (with insignificant amount of soluble hydrocarbon components), the effect of the hydrocarbon phase on the aqueous-rock geochemistry is negligible. If this is the case, the phase composition calculation of the hydrocarbon and the aqueous phases are independent; hence, the computational algorithm shown in Figure 2-57 (rather than the one presented in Figure 2-56) is followed in UTCOMP-IPhreeqc. This computational algorithm is very close to that of UTCHEM-IPhreeqc described in Chapter 5.

[1] Personal communication with D. L. Parkhurst of the USGS. 2014 (through email).

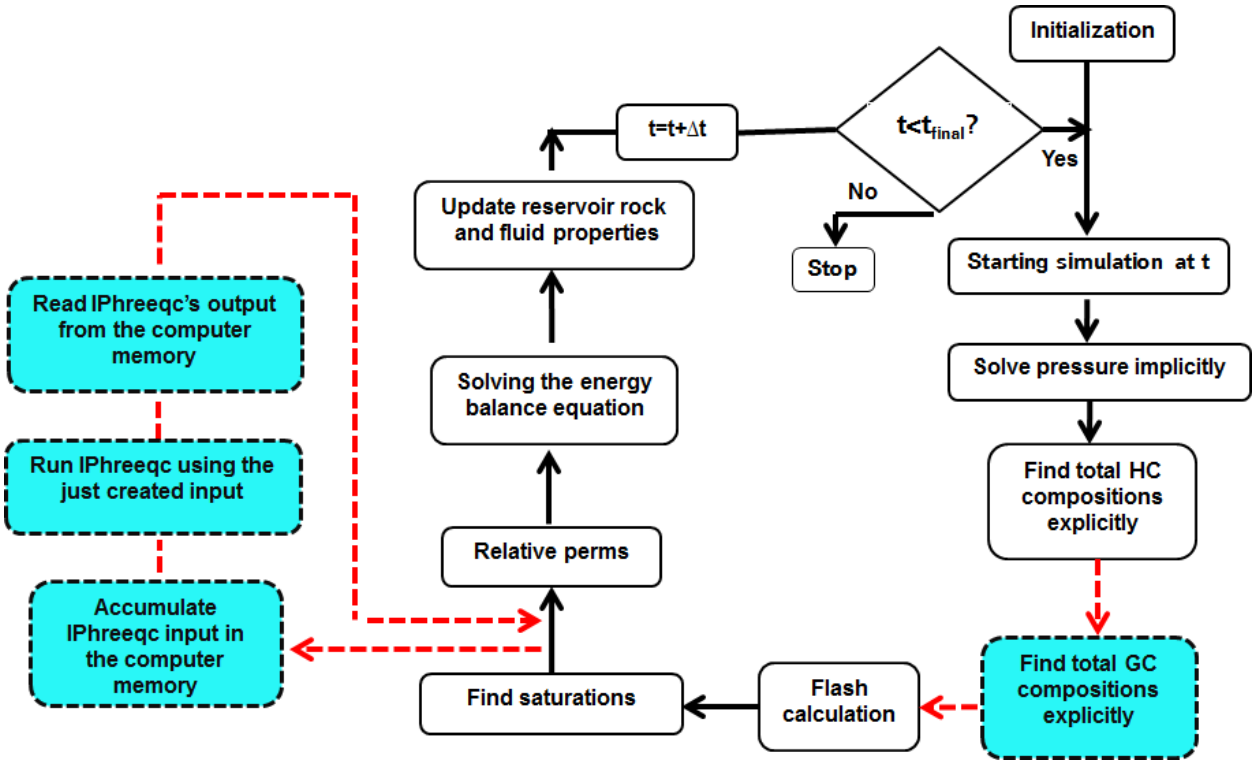

Figure 2-57: Simplified UTCOMP-IPhreeqc calculation flowchart when the effect of the hydrocarbon phase on the aqueous-rock geochemistry is neglected.

2.7.2 UTCOMP-IPhreeqc Verifications

We verify our integrated simulator, UTCOMP-IPhreeqc, against PHREEQC's single-phase and one-dimensional reactive-transport case studies. First, we make sure that the transports are identical in both UTCOMP-IPhreeqc and PHREEQC; second, we introduce geochemical reactions to verify the reactive-transport.

Verification of UTCOMP-IPhreeqc against PHREEQC - Transport

A 1D test case with 100 gridblocks was set up with injecting in the 1st gridblock and producing from the 100th gridblock. As mentioned previously, in order to model a single-phase flow in UTCOMP, initial water saturation is considered 0.999 in all

gridblocks. Barium is the only element considered in this case and the IPhreeqc and PHREEQC geochemical database was modified to make sure that no reaction occurs. Since there is no reaction, barium is like a conservative tracer where it can also be verified against the analytical solution (previously discussed in Section 2.2). The dispersion coefficient, injection rate, gridblock size in the direction of flow, gridblock cross-sectional area perpendicular to the flow, and porosity are considered in the way that dispersivity is independent of the fluid velocity (discussed in Section 2.2). It should be noted that the lower-order method (i.e., one-point upstream weighted method) of discretization is applied in UTCOMP-IPhreeqc. The numerical dispersion for the lower-order method is approximated as $\Delta x/2$ (Δx is the gridblock size in the flow direction). We assume PHREEQC is numerical dispersion free. Below shows how we assign identical dimensionless Peclet numbers between UTCOMP-IPhreeqc and PHREEQC.

$$\left(\frac{N\Delta x}{\alpha_{physical} + \frac{\Delta x}{2}} \right)_{\text{UTCOMP-IPhreeqc}} = \left(\frac{N\Delta x}{\alpha_{physical}} \right)_{\text{PHREEQC}} . \qquad (2.76)$$

In Eq. (2.76), "N" is the number of gridblocks in UTCOMP-IPhreeqc and PHREEQC (for the case studied, N = 100 in both UTCOMP-IPhreeqc and PHREEQC). Figure 2-58 compares the barium concentration history at the last gridblock (i.e., 100^{th}) of UTCOMP-IPhreeqc, PHREEQC, and the analytical solution at two different Peclet numbers of 125 and 500.

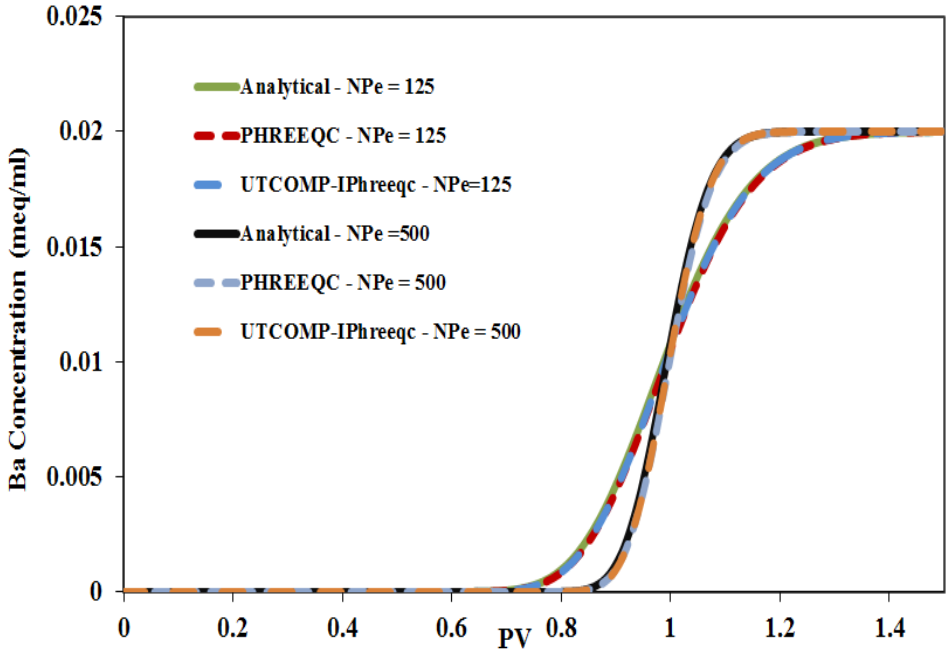

Figure 2-58: Ba elemental concentration at 100th gridblock in UTCOMP-IPhreeqc, PHREEQC, and the analytical solution for two Peclet numbers of 125 and 500.

Verification of UTCOMP-IPhreeqc against PHREEQC - Reactive-Transport

UTCOMP-IPhreeqc has been verified against PHREEQC for several reactive-transport cases; two realistic cases are presented in this dissertation. In the first case, UTCOMP-IPhreeqc is verified for the example problem 11 from Parkhurst and Appelo (2013). A 1D case with 40 cells is designed. Cells are initially saturated with a solution of sodium-potassium-nitrate (see Table 2-19 for ion compositions of the initial water) and they are in equilibrium with a cation-exchanger (with the cation exchange capacity of 0.0011 moles/kgw). Three pore volumes of calcium chloride ($CaCl_2$) solution is then injected into the column (see Table 2-19 for the ion compositions of the water injected). Appendix E provides UTCOMP-IPhreeqc input files for this case; how cells data are

stored in the computer memory (presented only for one cell); how UTCOMP-IPhreeqc modifies the cell data at each time step; how the IPhreeqc's output file is organized in the computer memory to be read by UTCOMP, respectively. Included in this Appendix is also the PHREEQC input file. Figures 2-59 and 2-60 verify the UTCOMP-IPhreeqc results against PHREEQC for two different Peclet numbers of infinity (or dispersion free case) and 40, respectively.

Table 2-19: Ion compositions for initial and injected waters

Ion	Initial	Injected
pH	adjusted for charge balance	
pe	12.5 $O_2(g)$ -0.68	
Na (mmol/kgw)	1.0	0.
K(mmol/kgw)	0.2	0.
N(5) (mmol/kgw)	1.2	0.
Ca(mmol/kgw)	-	0.6
Cl (mmol/kgw)	-	1.2

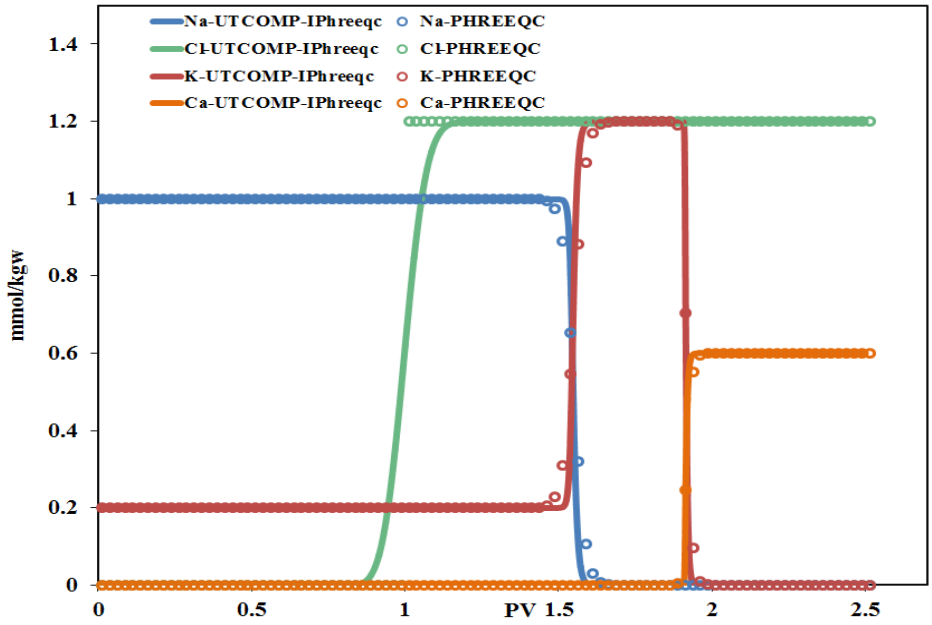

Figure 2-59: UTCOMP-IPhreeqc verification for example problem 11 of PHREEQC (Parkhurst and Appelo, 2013) at $N_{Pe}=\infty$.

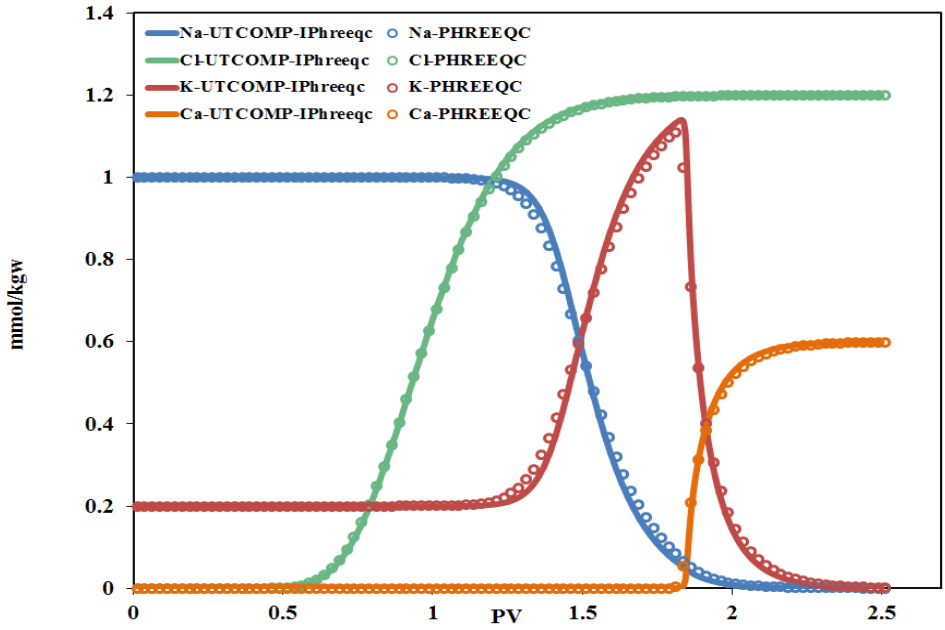

Figure 2-60: UTCOMP-IPhreeqc verification for example problem 11 of PHREEQC (Parkhurst and Appelo, 2013) at $N_{Pe}=40$.

To obtain very good agreements between the integrated simulator (i.e., UTCOMP-IPhreeqc) and PHREEQC (particularly pH and redox potential, pe), the geochemical elements, including the total H and O as well as the charge imbalance, must be transported with very high precision, at least by 13 digits (Wissmeier and Barry, 2010; Appelo and Rolle, 2010; Korrani *et al*., 2013; Korrani *et al.*, 2014c). If the transport simulator is in Fortran® programming language (i.e. in UTCOMP or UTCHEM discussed in Chapter 5), DOUBLE PRECISION (or REAL*8) is used.

In the second case, we verify UTCOMP-IPhreeqc against PHREEQC for a more realistic case with more complexity in reactive-system. 1D single-phase with 100 gridblocks is set up in both UTCOMP-IPhreeqc and PHREEQC. Endicott connate water (see Table 2-20 for the ion compositions) is assumed to be initially present (chloride concentration is adjusted to make the solutions charge-balanced). More description of Endicott is provided in Chapter 3. Table 2-21 shows the list of possible solid phases modeled in this verification case (considering connate water, seawater, produced and low salinity water compositions for Endicott). Initial mole and saturation index (SI) of solid phases are assumed to be zero. Saturation index of a solid phase is the logarithm of ratio of ionic products over the solid solubility product (see Appendix A for basic geochemical concepts). The dimensionless Peclet number is 125 in this case.

Table 2-20: Endicott water compositions (McGuire *et al.*, 2005; Korrani *et al.*, 2014a)

Elements	Ion compositions (mg/l)			
	Connate water	Sea water	Produced water (High salinity)	Low salinity
Al	0.0	0.5	0.0	0.0
Ba	7.0	0.02	0.55	0.048
B	0.	0.0	57.0	0.22
Ca	320.0	401.67	158.0	28.8
Fe^{+2}	10.0	0.3	0.0	0.0
Li	0.0	0.0	2.09	0.0
Mg	48.0	1265	386.0	4.4
Mn^{+2}	0.0	0.05	0.184	0.0
P	0.0	0.0	0.0	1.2
K	110.0	386.33	174.0	3.3
Si	0.0	2.0	0.0	0.0
Na	11850.0	10812.0	9796.0	56.1
Sr	24.0	7.38	6.9	0.1
Zn	0.0	0.5	0.0	0.0
HCO_3^-	2000.0	147.02	1920	146
Br	0.0	67.63	0.0	0.0
Cl	17275.0	18963.83	15262.0	49.0
F	0.0	0.81	0.0	0.0
S(6)	63.0	2645.83	510.0	27.0
TDS	31707.0	34700.87	28272.724	316.168

Table 2-21: All potential solids considering Endicott water compositions

No.	Solid Name	No.	Solid Name	No.	Solid Name
1	Anhydrite	18	Melanterite	35	Chrysotile
2	Aragonite	19	Pyrite	36	Fluorite
3	Barite	20	Siderite	37	Gibbsite
4	Calcite	21	Strontianite	38	Hausmannite
5	Celestite	22	Sulfur	39	Illite
6	Dolomite	23	Sylvite	40	K-feldspar
7	Fe(OH)3(a)	24	Witherite	41	K-mica
8	FeS(ppt)	25	Al(OH)3(a)	42	Kaolinite
9	Goethite	26	Albite	43	Manganite
10	Gypsum	27	Alunite	44	Pyrochroite
11	Halite	28	Anorthite	45	Pyrolusite
12	Hematite	29	Ca-Montmorillonite	46	Quartz
13	Jarosite-K	30	Chalcedony	47	Rhodochrosite
14	Mackinawite	31	Chlorite(14A)	48	Sepiolite
15	Smithsonite	32	SiO2(a)	49	Sepiolite(d)
16	Sphalerite	33	Talc	50	Willemite
17	Zn(OH)2(e)	34	Hydroxyapatite		

This case is flooded for 3.0 PV of waters with different compositions (first, 0.5 PV seawater, then 0.5 PV produced water (or high salinity water), 0.5 PV low salinity water, and finally with 1.5 PV produced water). Figure 2-61 shows the sequence of injections.

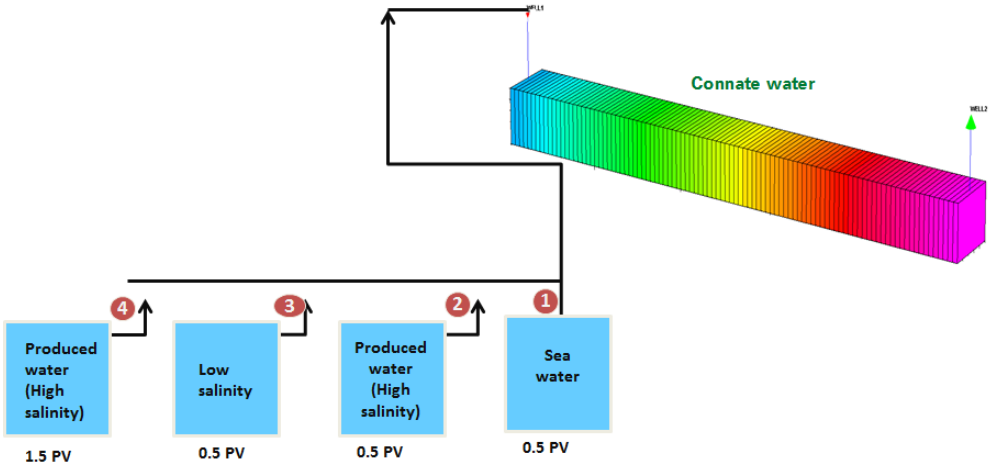

Figure 2-61: Sequence of injecting different Endicott water compositions in a 1D case to verify UTCOMP-IPhreeqc against PHREEQC.

The default PHREEQC database, phreeqc.dat, (provided in Appendix E) is used in this modeling and around 200 geochemical reactions are activated during this process. Figures 2-62 through 2-73 present the verification results between UTCOMP-IPhreeqc and PHREEQC for effluent Na^{+}, Ca^{+2}, Cl^{-}, SO_4^{-2}, HSO_4, $CaSO_4$, Ba^{+2}, HCO_3^{-}, Fe^{+2}, Mg^{+2}, and Sr^{+2} as well as the pH histories of the aqueous solution. As these figures demonstrate, very good agreement between results of UTCOMP-IPhreeqc and PHREEQC results were achieved.

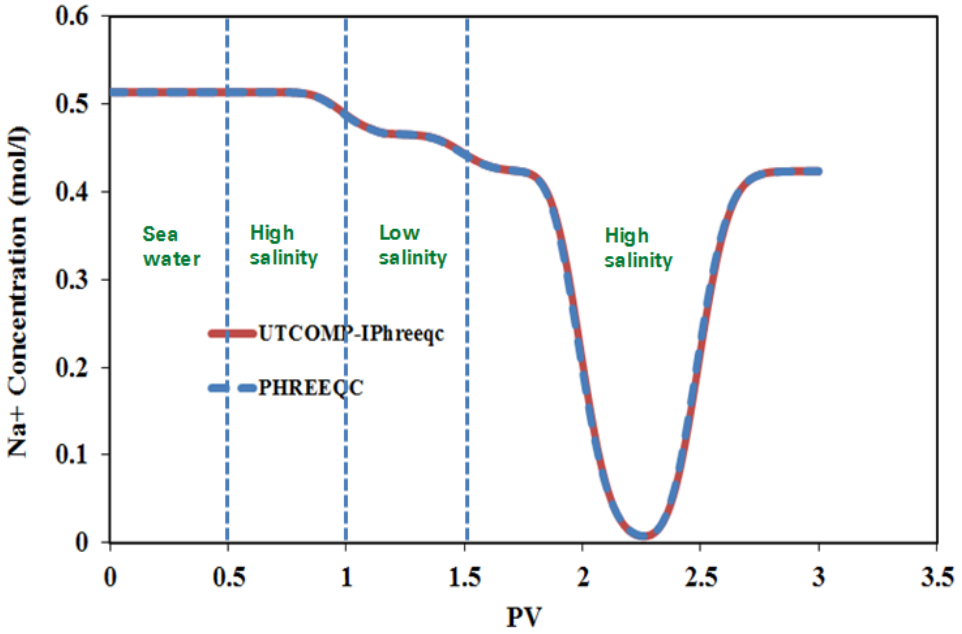

Figure 2-62: History of effluent Na^{+} concentration (UTCOMP-IPhreeqc verification against PHREEQC).

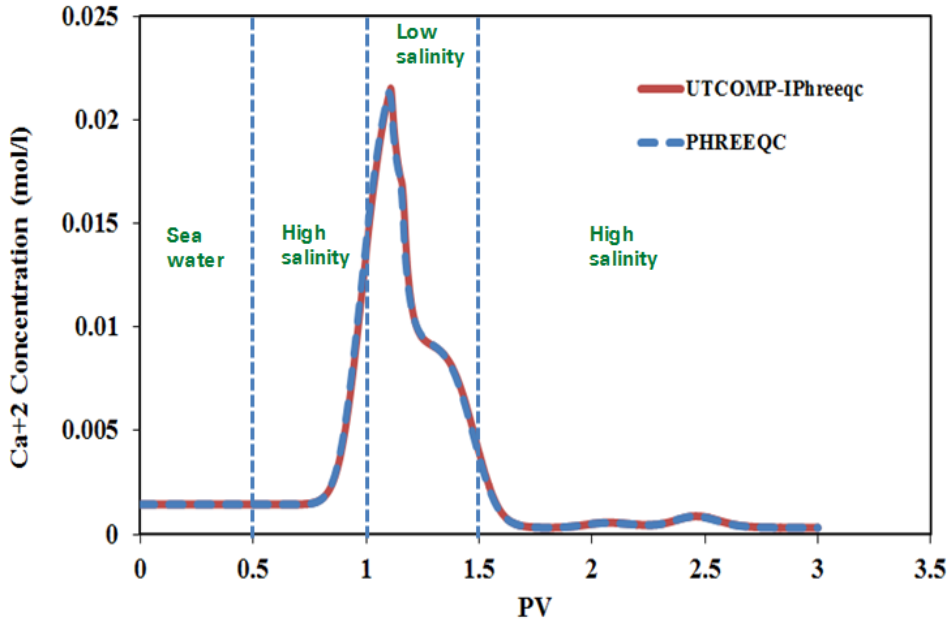

Figure 2-63: History of effluent Ca^{+2} concentration (UTCOMP-IPhreeqc verification against PHREEQC).

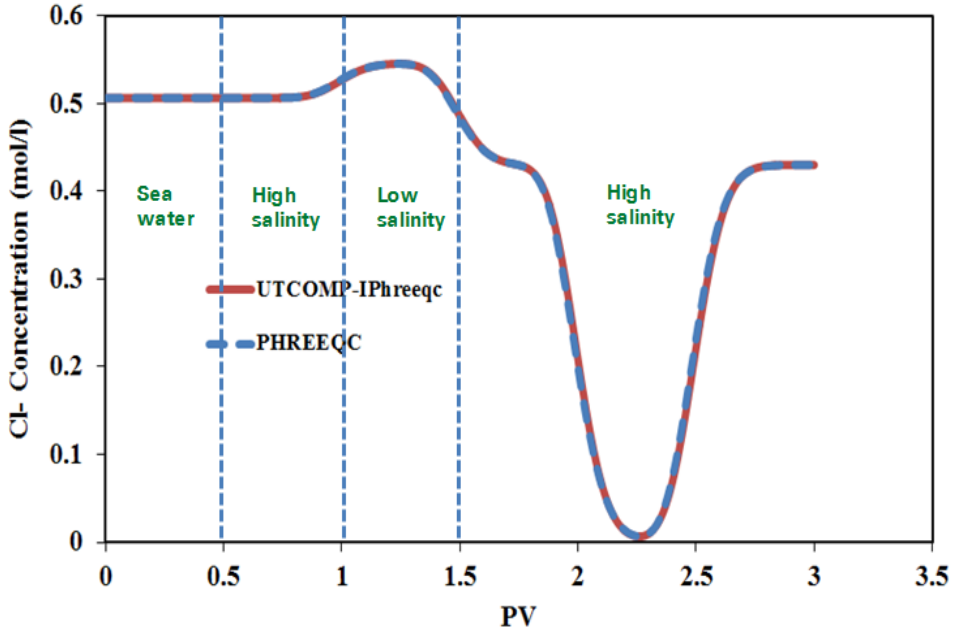

Figure 2-64: History of effluent Cl^- concentration (UTCOMP-IPhreeqc verification against PHREEQC).

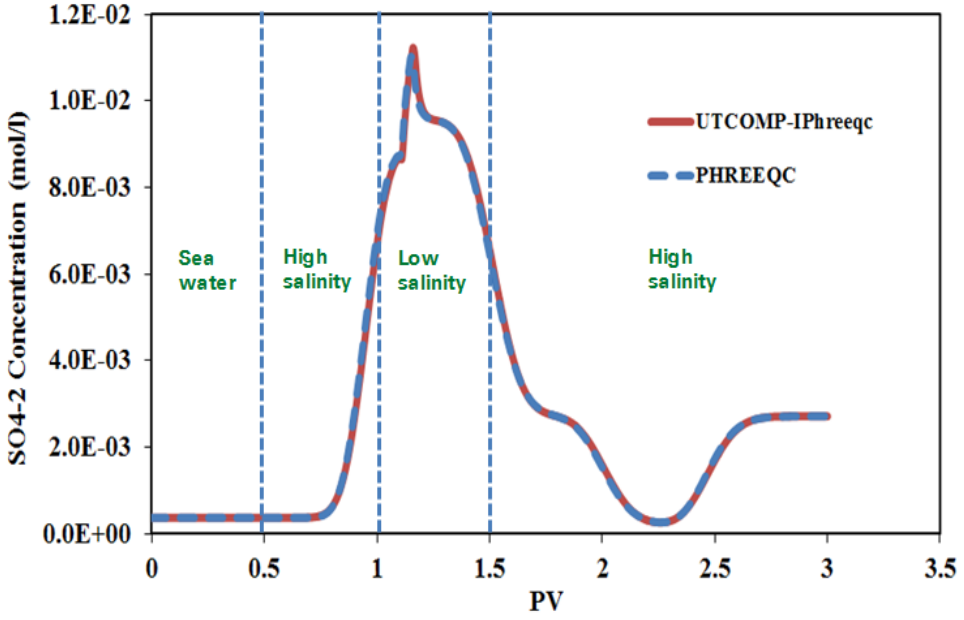

Figure 2-65: History of effluent SO_4^{-2} concentration (UTCOMP-IPhreeqc verification against PHREEQC).

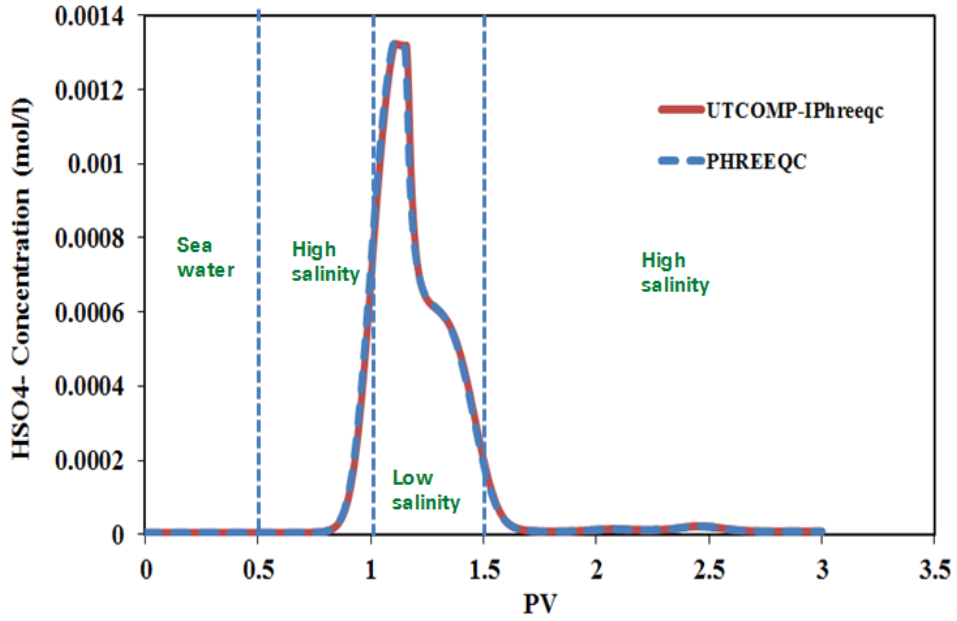

Figure 2-66: History of effluent HSO_4^- concentration (UTCOMP-IPhreeqc verification against PHREEQC).

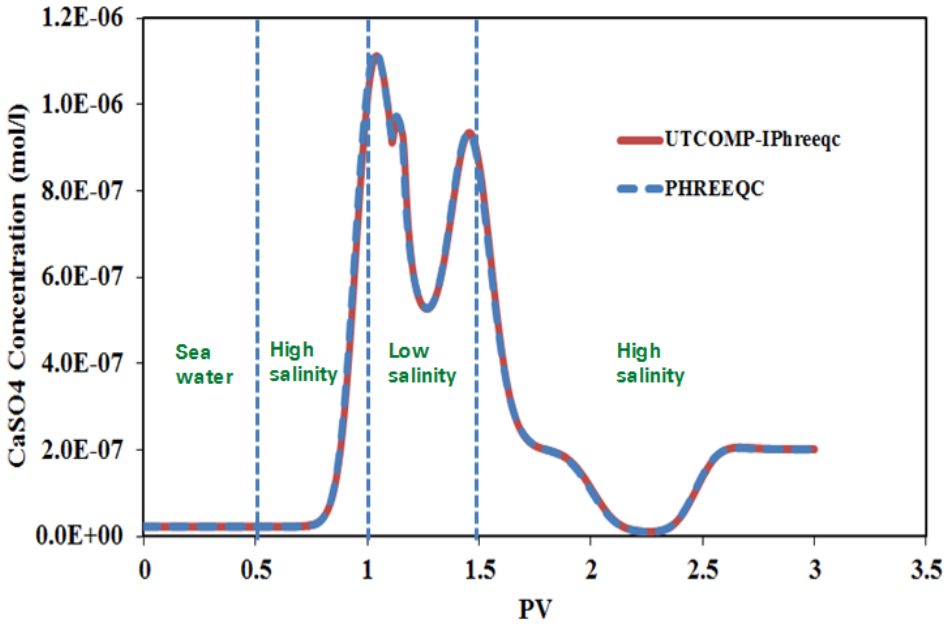

Figure 2-67: History of effluent $CaSO_4$ concentration (UTCOMP-IPhreeqc verification against PHREEQC).

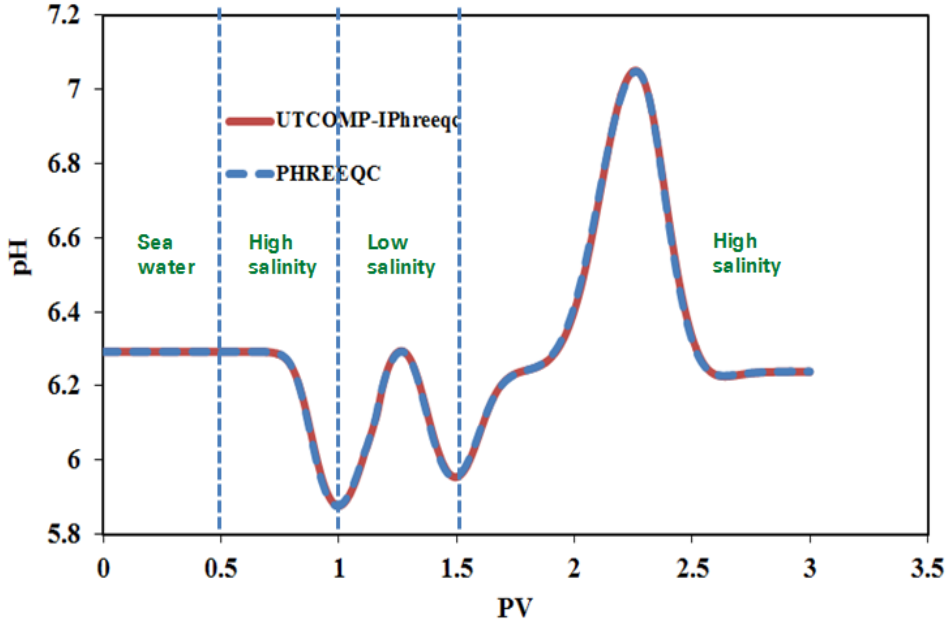

Figure 2-68: History of effluent pH (UTCOMP-IPhreeqc verification against PHREEQC).

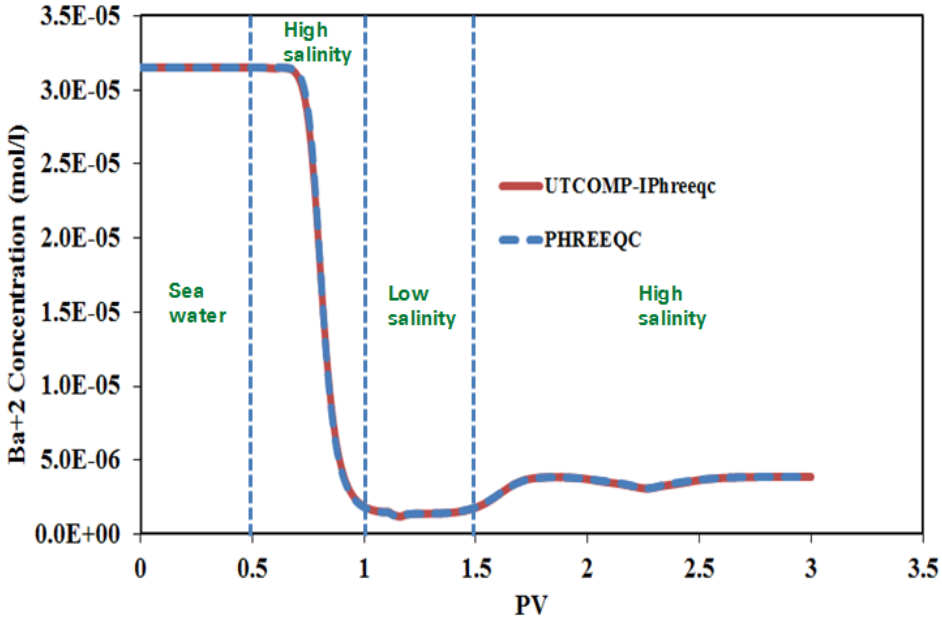

Figure 2-69: History of effluent Ba^{+2} concentration (UTCOMP-IPhreeqc verification against PHREEQC).

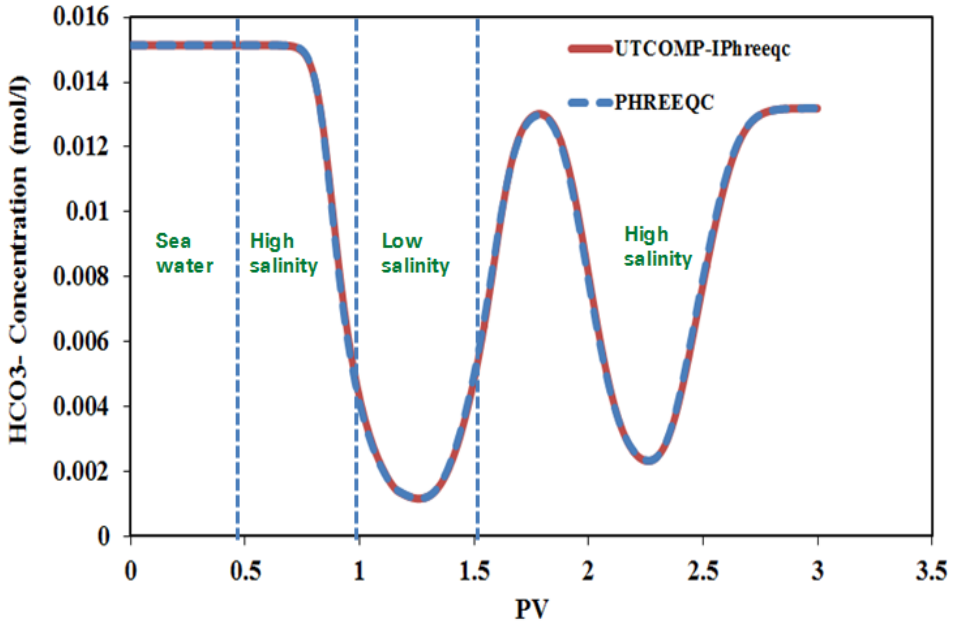

Figure 2-70: History of effluent HCO_3^- concentration (UTCOMP-IPhreeqc verification against PHREEQC).

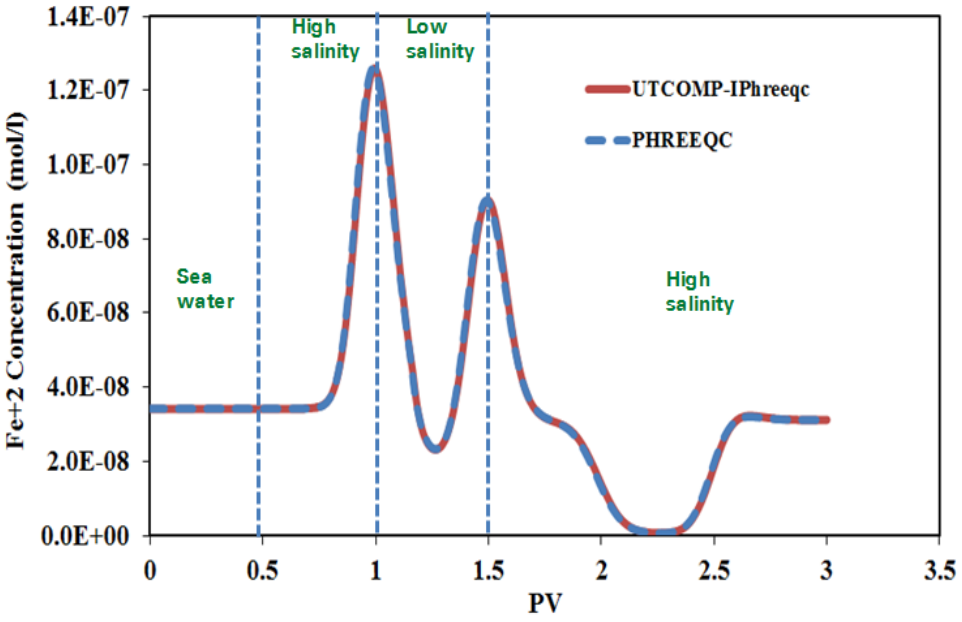

Figure 2-71: History of effluent Fe^{+2} concentration (UTCOMP-IPhreeqc verification against PHREEQC).

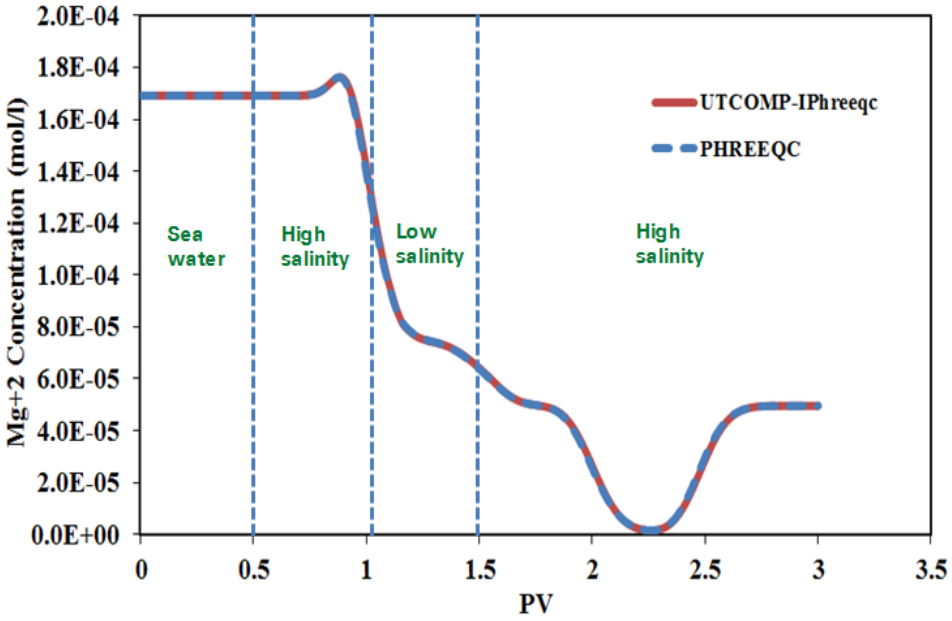

Figure 2-72: History of effluent Mg^{+2} concentration (UTCOMP-IPhreeqc verification against PHREEQC).

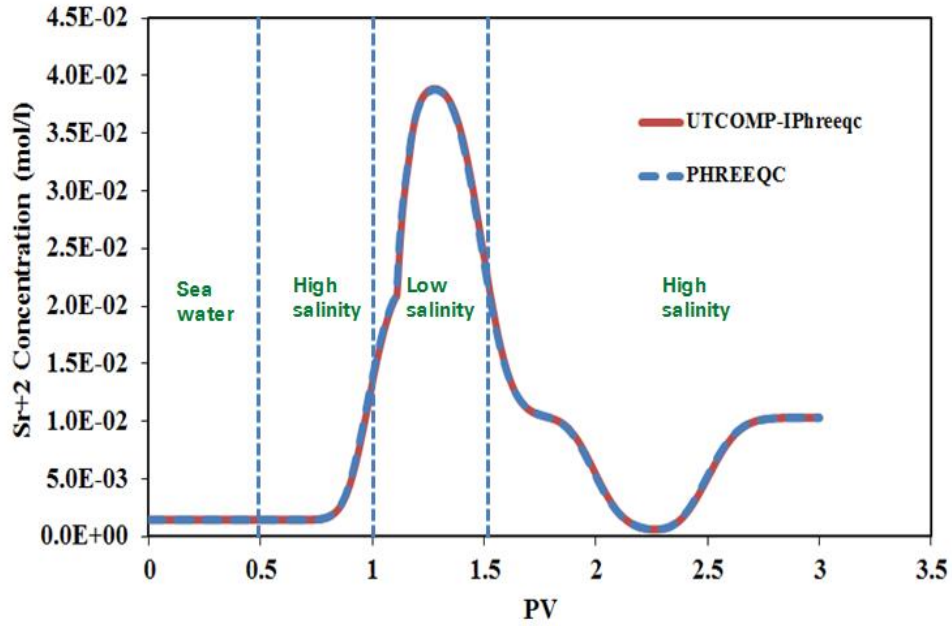

Figure 2-73: History of effluent Sr^{+2} concentration (UTCOMP-IPhreeqc verification against PHREEQC).

It should be noted that de Bruin (2012) coupled IPhreeqc with his simplified transport code based on Buckley-Leverett equation (Buckley and Leverett, 1941) to expand the IPhreeqc capability from single-phase to multi-phase flow (still limited to one-dimensional cases) and model low salinity waterflooding. However, based on the description documented, it appears that IPhreeqc was applied improperly in de Bruin (2012)'s work. Although charge balance, total hydrogen, and total oxygen must be transported when using IPhreeqc (as discussed in our coupling approach), it seems that de Bruin (2012) ignored this important fact and instead, they used water mass (or water saturation) for IPhreeqc batch reactions. That is why his coupled simplified transport code with IPhreeqc does not match the PHREEQC results appropriately for single-phase and one-dimensional cases (see de Bruin, 2012).

By coupling IPhreeqc with UTCOMP, the entire geochemical capabilities of IPhreeqc/PHREEQC can be used in a multi-dimensional and multi-phase reservoir simulator for a comprehensive simulation of reactive-transport flow. Next section gives the results of sensitivity analyses to investigate the importance of including ion activities rather than molalities, and temperature and pressure effects on the reactive-transport modeling.

2.8 SIGNIFICANCE OF ION ACTIVITY IN GEOCHEMICAL MODELING

The ion activity measures the deviation from the ideal behavior of a component in an aqueous solution (Zhu and Anderson, 2002). IPhreeqc uses the ion activities (real solution) rather than ion concentrations (ideal solution) in finding the equilibrium state of a system. IPhreeqc has the options of using Davies (Davies, 1962; Parkhurst and Appelo, 1999; 2013) or the extended or WATEQ Debye-Huckel (Truesdell and Jones, 1974; Parkhurst and Appelo, 1999; 2013) equation to calculate the activity coefficients. Pitzer

and SIT aqueous-association models can be also used through two separate databases released with IPhreeqc. The Davies and WATEQ Debye-Huckel models are presented below:

Davies equation (Davies, 1962; Parkhurst and Appelo, 1999; 2013):

$$\log \gamma_i = -Az_i^2 \left(\frac{\sqrt{I}}{1+\sqrt{I}} - 0.3I \right). \tag{2.77}$$

Extended or WATEQ Debye-Huckel equation (Truesdell and Jones, 1974; Parkhurst and Appelo, 1999; 2013):

$$\log \gamma_i = -\frac{Az_i^2 \sqrt{I}}{1+Ba_i^o \sqrt{I}} + b_i I, \tag{2.78}$$

where

γ_i = activity coefficient of the aqueous or exchange species *i*

z_i = ionic charge of aqueous phase species *i*

I = ionic strength of solution (mol/kgw)

A, B = constants dependent only on temperature (see Appendix A for the temperature dependency)

a_i^o, b_i = ion-specific parameters

Unless otherwise specified in the IPhreeqc database file or the input data set, Davies equation is used for the calculation of ion activity coefficients. For uncharged species, the first term of the activity coefficient in the WATEQ Debye-Huckel equation is zero. Unless defined in the input file or database file, b_i is assumed to be 0.1 for all the uncharged species (Parkhurst and Appelo, 1999; 2013).

To show the importance of ion activity on geochemistry state of a system, a two-phase 1D coreflood is designed using UTCOMP-IPhreeqc. Initial oil saturation in the core is 0.7 (dead-oil with no hydrocarbon-aqueous interaction) (see Table 2-22 for the case descriptions) and is initially saturated with the produced water of the South American reservoir (see Table 2-23, Kazempour *et al.*, 2013). Aragonite, calcite, celestite, dolomite, halite, strontianite, sylvite, and witherite are the minerals considered. Except calcite and dolomite with initial concentration of 0.1 moles/kg of water, initial concentrations for other minerals are zero. It is also assumed that a cation-exchanger with cation exchange capacity (CEC) of 0.01 moles/kgw is at equilibrium with the initial solution. Injection rate is 0.0023 ft^3/day and the producing well is operating with the constant bottomhole pressure of 4000.0 psi. The core is then flooded with the following sequence of waters 0.7 PV IW1 followed by 0.7 PV PW1 and 0.7 SW1. Water ion compositions are shown in Table 2-23. Two cases are compared. In one case, the IPhreeqc database ("phreeqc.dat" is used in this simulation) is modified to make the ion activity coefficients very close to one (ideal solution) for all the components in the aqueous solution (by considering 1×10^9 for a_i and zero for b_i in the WATEQ Debye-Huckel activity coefficient model[1]; this trick is discussed in Chapter 5 where we verify UTCHEM-IPhreeqc against UTCHEM-EQBATCH). However, in the second case, the "phreeqc.dat" database with no modification is used in the simulation.

[1] Personal communication with D. L. Parkhurst of the USGS. 2014 (through email).

Table 2-22: Reservoir characteristics for 1D verification case

No. of gridblocks		100 (100×1×1)
Δx(ft)		0.04
Δy(ft)		0.15
Δz(ft)		0.15
Permeability (md)	*x*-direction	100.0
Porosity		0.25
Rock compressibility (psi^{-1})		0.
Water compressibility (psi^{-1})		0.
Initial water saturation		0.3
Irreducible water saturation		0.2
Initial pressure (psi)		4000.0
Reservoir depth (ft)		0.
Water viscosity (cp)		0.79
Oil viscosity (cp)		6.3
Number of wells	2	1 injector
		1 producer
Simulation time(PV)		2.1

Table 2-23: Water analysis for South American formation (in ppm) (Kazempour *et al.*, 2013)

Ions	Produced water (PW1)	Injection water (IW1)	Fresh water (SW1)
Na^{+}	2430	2083	40
K^{+}	66	75	< 5
Ca^{+2}	300	310	12
Mg^{+2}	47	50	3
Ba^{+2}	20	70	-
Sr^{+2}	26	28	1
Cl^{-}	4343	3926	18
SO_4^{-2}	-	-	7
HCO_3^{-}	512	928	110
TDS	8410	7680	215

Figures 2-74 through 2-81 compare the ion histories of some aqueous species along with the pH of the produced aqueous solution. Figures 2-82 and 2-83 also present solid concentrations (in moles/kgw) of calcite and dolomite in the 1st gridblock, which is the injection gridblock. These figures clearly emphasize the importance of inclusion of the ion activity coefficients in the reactive-transport modeling.

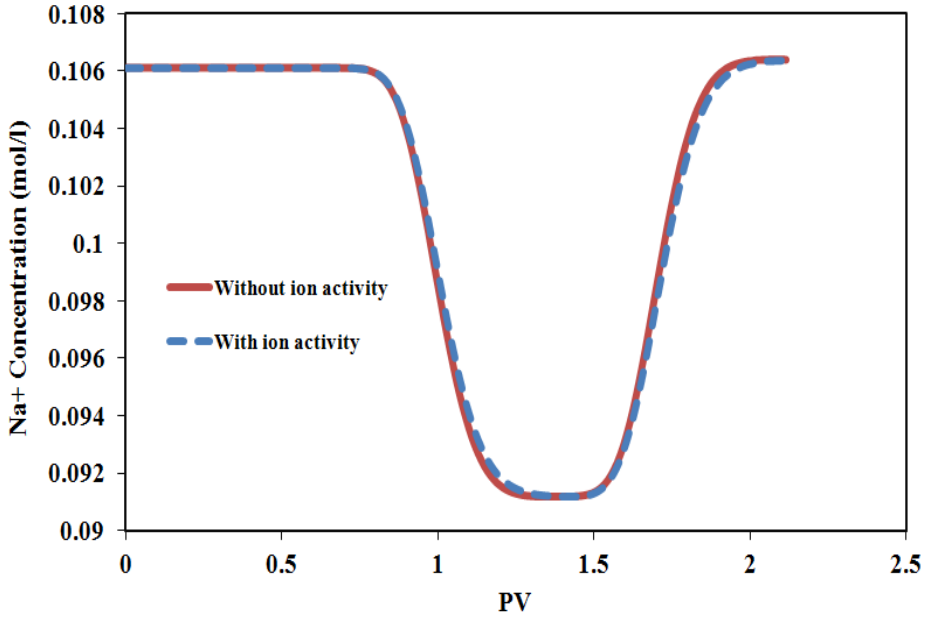

Figure 2-74: History of effluent Na^{+} concentration (significance of the ion activity coefficients in the reactive-transport modeling).

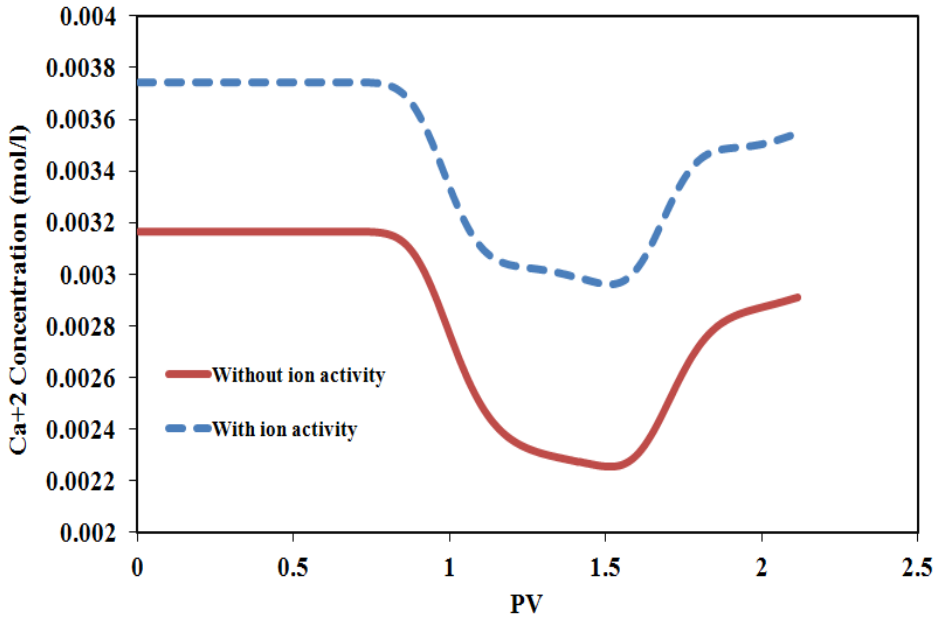

Figure 2-75: History of effluent Ca^{+2} concentration (significance of the ion activity coefficients in the reactive-transport modeling).

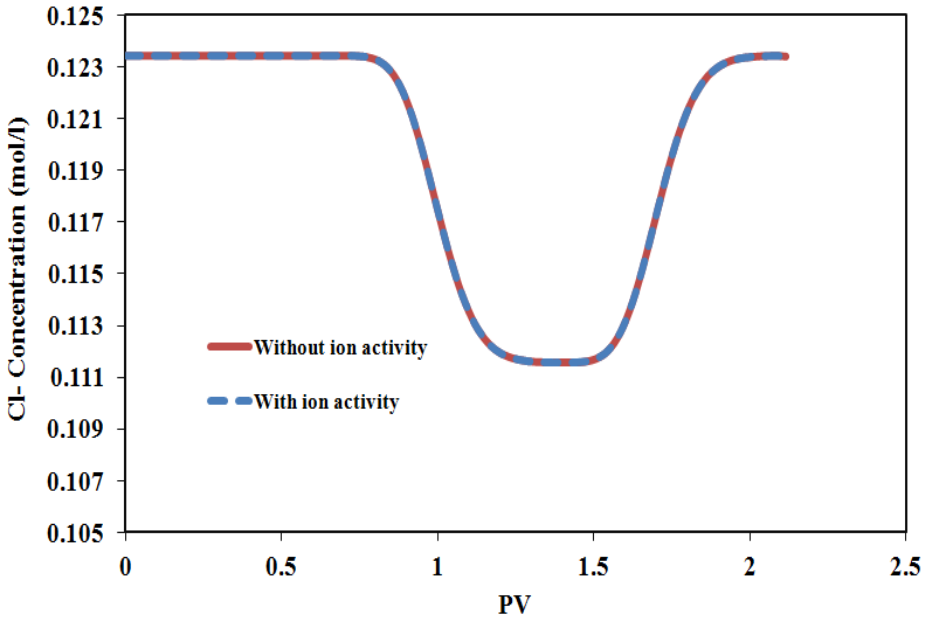

Figure 2-76: History of effluent Cl^- concentration (significance of the ion activity coefficients in the reactive-transport modeling).

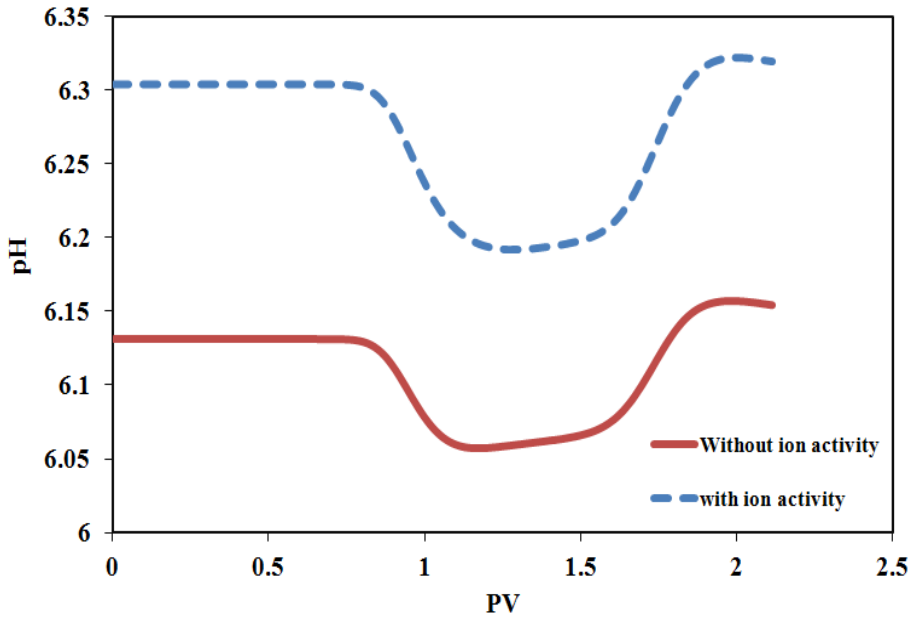

Figure 2-77: History of effluent pH (significance of the ion activity coefficients in the reactive-transport modeling).

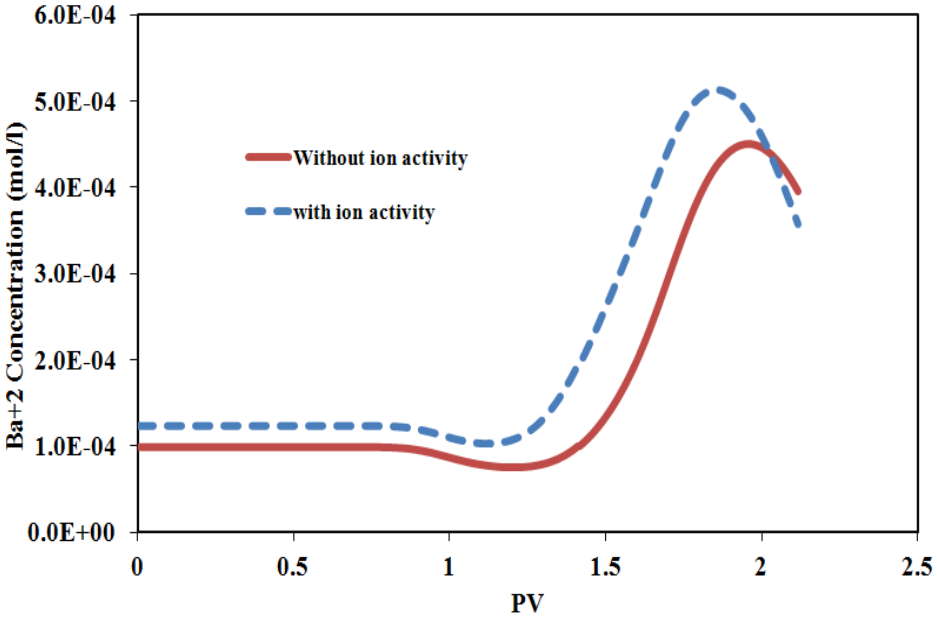

Figure 2-78: History of effluent Ba^{+2} concentration (significance of the ion activity coefficients in the reactive-transport modeling).

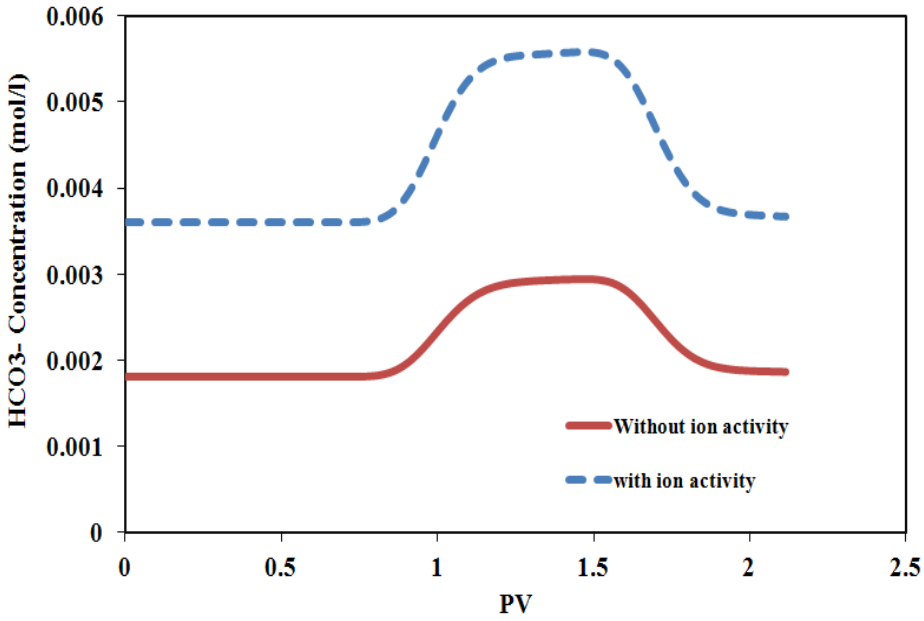

Figure 2-79: History of effluent $HCO3^{-}$ concentration (significance of the ion activity coefficients in the reactive-transport modeling).

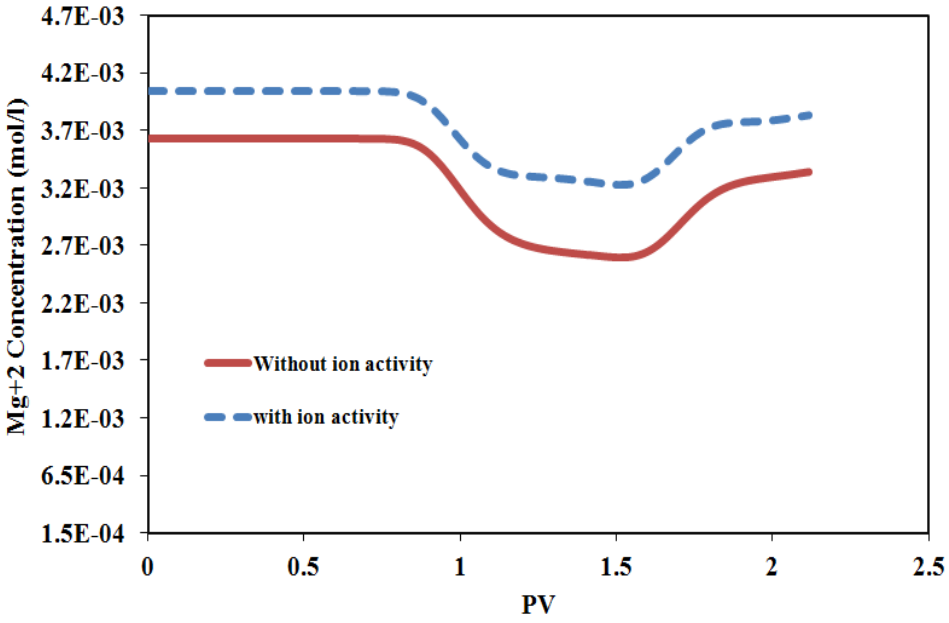

Figure 2-80: History of effluent Mg^{+2} concentration (significance of the ion activity coefficients in the reactive-transport modeling).

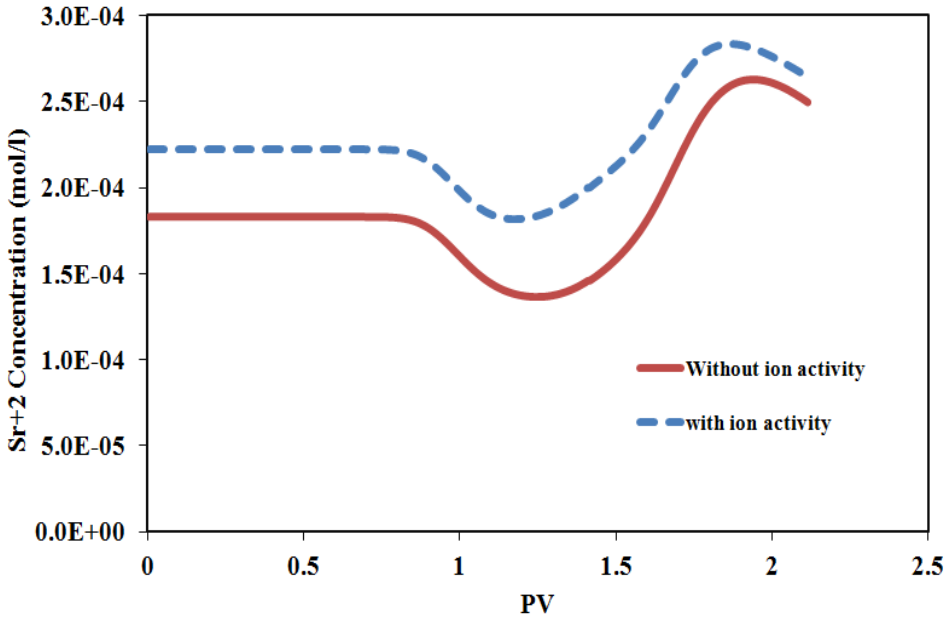

Figure 2-81: History of effluent Sr^{+2} concentration (significance of the ion activity coefficients in the reactive-transport modeling).

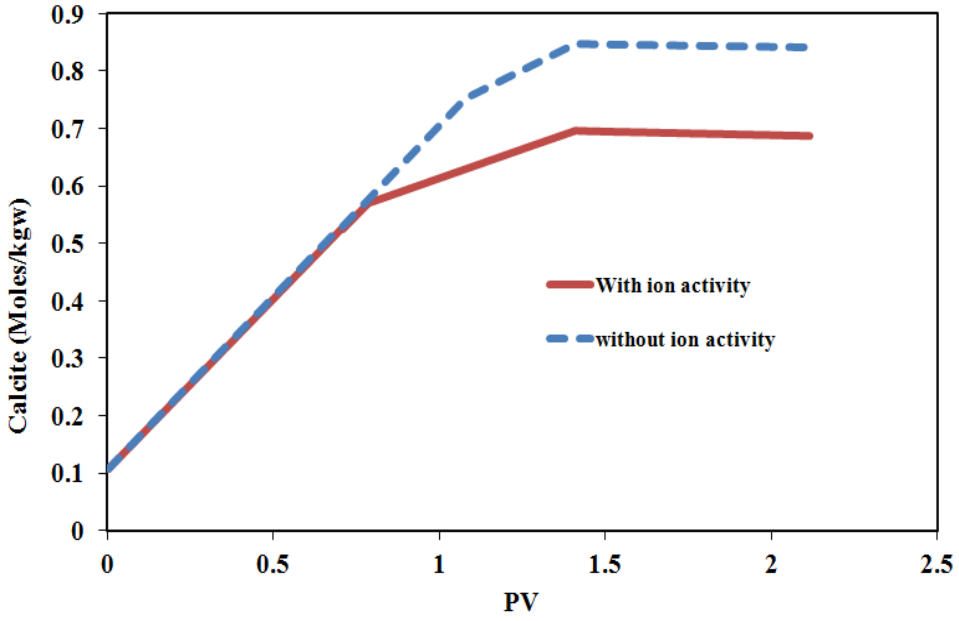

Figure 2-82: History of calcite concentration in the first gridblock (significance of the ion activity coefficients in the reactive-transport modeling).

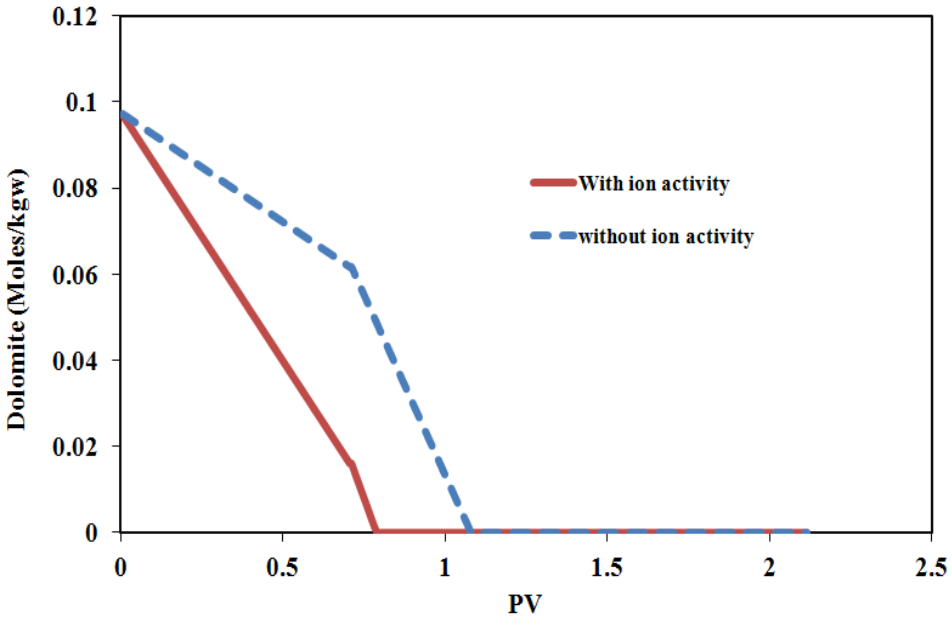

Figure 2-83: History of dolomite concentration in the first gridblock (significance of the ion activity coefficients in the reactive-transport modeling).

2.9 SIGNIFICANCE OF TEMPERATURE AND PRESSURE IN GEOCHEMICAL MODELING

IPhreeqc/PHREEQC uses the van't Hoff expression or an analytical expression to define the temperature dependency of the equilibrium constants. The van't Hoff equation is presented in Eq. (2.79).

$$Log\, K_T = Log\, K_{298} - \frac{\Delta_r H^0_{298}}{2.3025R}\left(\frac{1}{T} - \frac{1}{298.15}\right), \tag{2.79}$$

where

K_T = equilibrium constant at temperature T

K_{298} = equilibrium constant at 298 K

$\Delta H_r{}^o{}_{298}$ = the standard enthalpy change of the process (j/mole)

R = gas constant (8.314 j/mol/K)

T = temperature (K)

The van't Hoff model is often a useful approximation over small temperature intervals (Zhu and Anderson, 2002; Parkhurst and Appelo, 1999; 2013).

An analytical expression, shown in Eq. (2.80), for the temperature dependence of logarithm of the equilibrium constant for a reaction may also be defined in IPhreeqc through the "**-ANALYTICAL_EXPRESSION**" keyword (Parkhurst and Appelo, 1999; 2013). In this model, at each temperature, log K is directly calculated using Eq. (2.80).

$$Log_{10}\, K = A_1 + A_2 T + \frac{A_3}{T} + A_4 Log_{10} T + \frac{A_5}{T^2}, \tag{2.80}$$

where

A_1 through A_5 = constants

T = temperature (K)

Reaction constants for species and solubilities of minerals can also be defined as functions of pressure in IPhreeqc. This dependency is defined using molar volume of the solids together with the volumes of the solute species as in Eq. (2.81) (Parkhurst and Appelo, 2013):

$$Log\, K_P = Log\, K_{P=1} - \frac{\Delta V_r}{2.303RT}(P-1), \tag{2.81}$$

where

P = pressure (atm)

T = temperature (K)

ΔV_r = volume change of the reaction (cm^3/mol)

R = gas constant (82.06 atm cm^3 mol^{-1} K^{-1})

A sensitivity study is conducted to investigate the importance of temperature and pressure on the aqueous-rock geochemistry. The two-phase 1D coreflood with the descriptions mentioned above is again considered in UTCOMP-IPhreeqc. In one stage of this sensitivity analysis, keeping the average pressure of the system constant (very close to 1 atm), coreflooding is done at three different temperatures of 50, 100, and 150^{o}C (the initial and injection water temperatures are the same). In the second step of this sensitivity analysis, temperature of the initial (connate) water and all the injection waters are constant and equal to 25^{o}C, while we compare three different average pressures of 14.7, 3000, and 6000 psi. Figures 2-84 through 2-91 demonstrate ion histories of aqueous

species as well as the pH of the produced solution with different temperatures. Figures 2-92 and 2-93 present calcite and dolomite mineral concentrations (mol/kgw) at the injection gridblock. Except the Na and Cl elements which are not reactive (particularly Cl), the effect of the temperature on the aqueous-rock geochemistry is significant in ion histories of the other aqueous species including the pH, and solids concentrations (i.e., calcite and dolomite solids). As expected, the temperature does not show the same effect on the aqueous ion histories, pH and the mineral concentrations. For example, by increasing the temperature, ion concentrations for Ca^{+2}, Ba^{+2}, and Sr^{+2} decrease while the Mg^{+2} concentration increases or, although by increasing the temperature the calcite solubility decreases, the dolomite solubility increases.

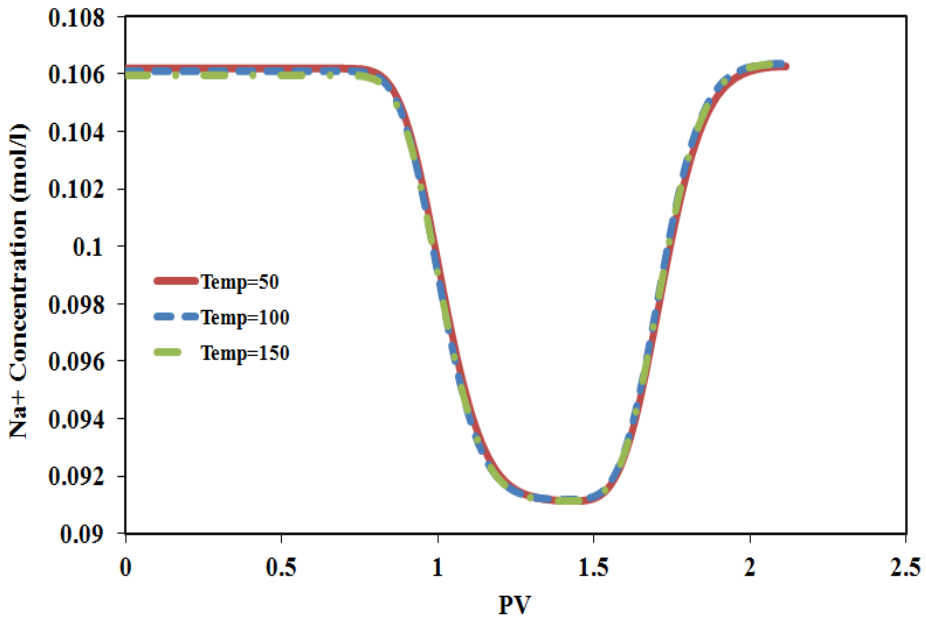

Figure 2-84: History of effluent Na^{+} concentration (significance of the temperature in the reactive-transport modeling).

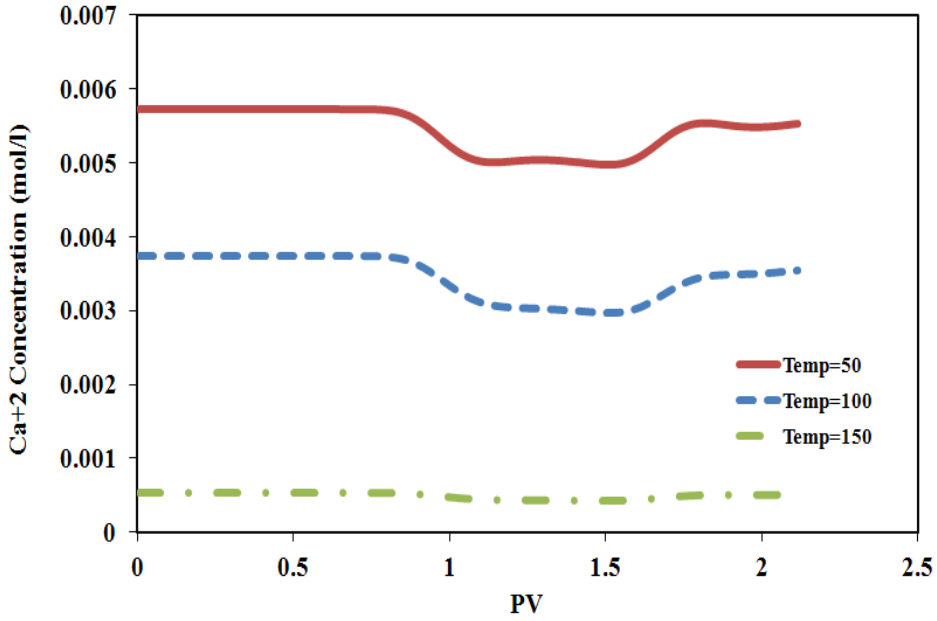

Figure 2-85: History of effluent Ca^{+2} concentration (significance of the temperature in the reactive-transport modeling).

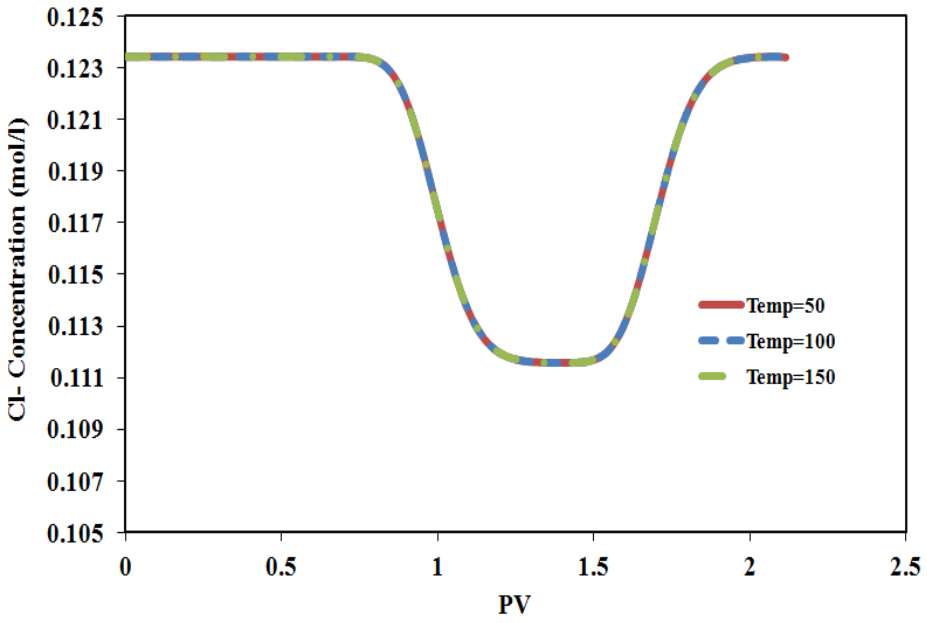

Figure 2-86: History of effluent Cl^{-} concentration (significance of the temperature in the reactive-transport modeling).

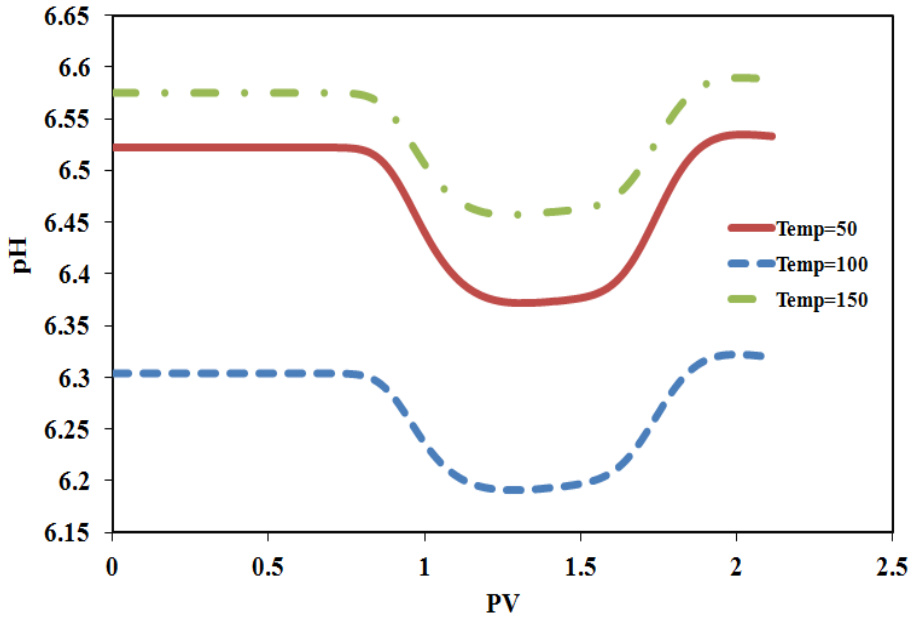

Figure 2-87: History of effluent pH (significance of the temperature in the reactive-transport modeling).

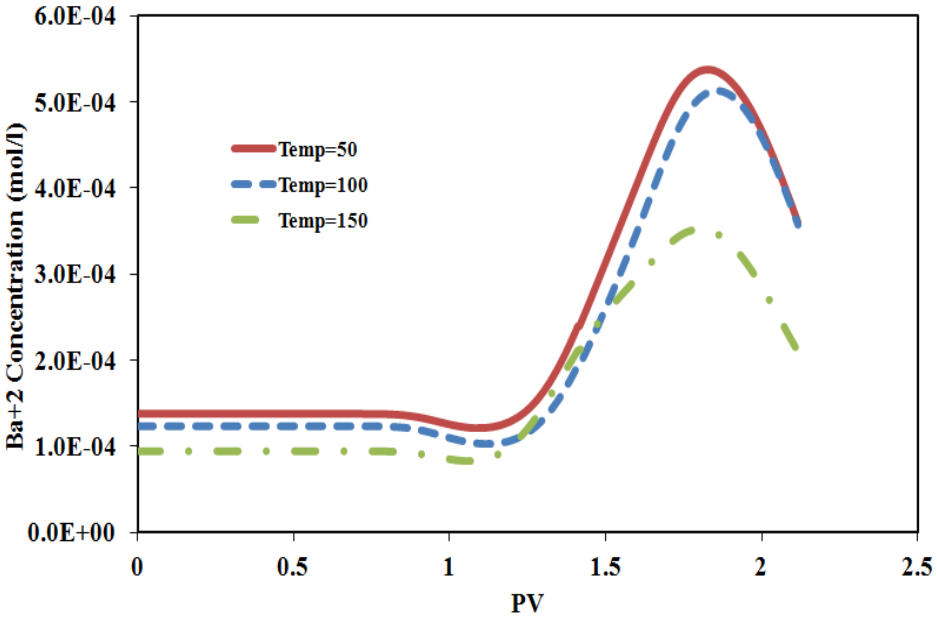

Figure 2-88: History of effluent Ba^{+2} concentration (significance of the temperature in the reactive-transport modeling).

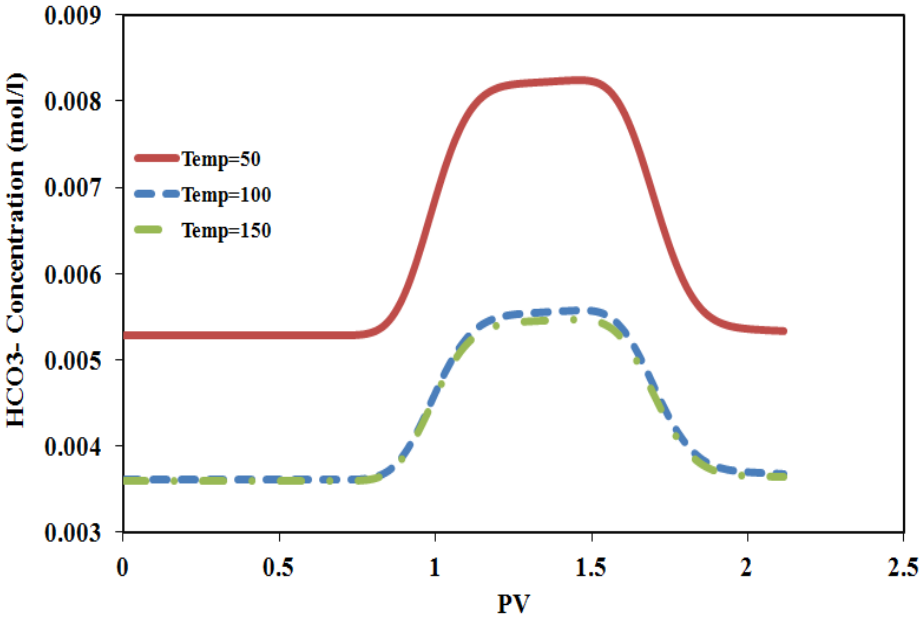

Figure 2-89: History of effluent HCO_3^- concentration (significance of the temperature in the reactive-transport modeling).

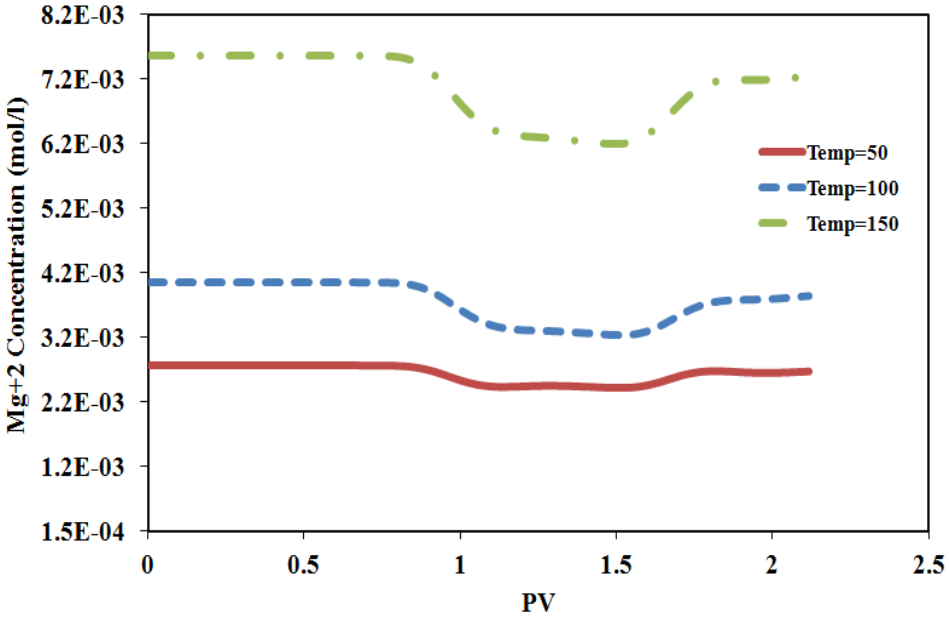

Figure 2-90: History of effluent Mg^{+2} concentration (significance of the temperature in the reactive-transport modeling).

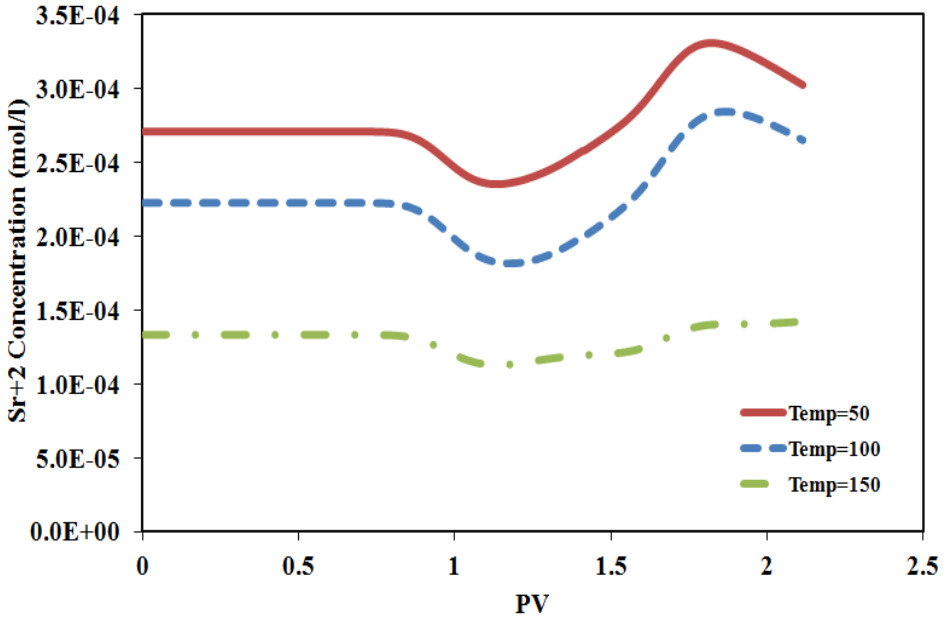

Figure 2-91: History of effluent Sr^{+2} concentration (significance of the temperature in the reactive-transport modeling).

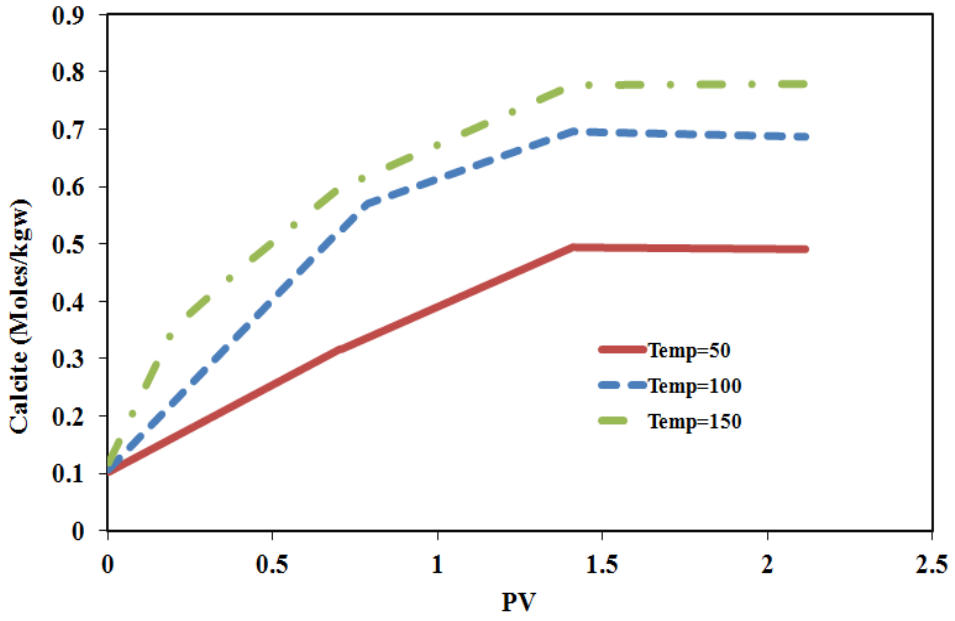

Figure 2-92: History of calcite concentration in the first gridblock (significance of the temperature in the reactive-transport modeling).

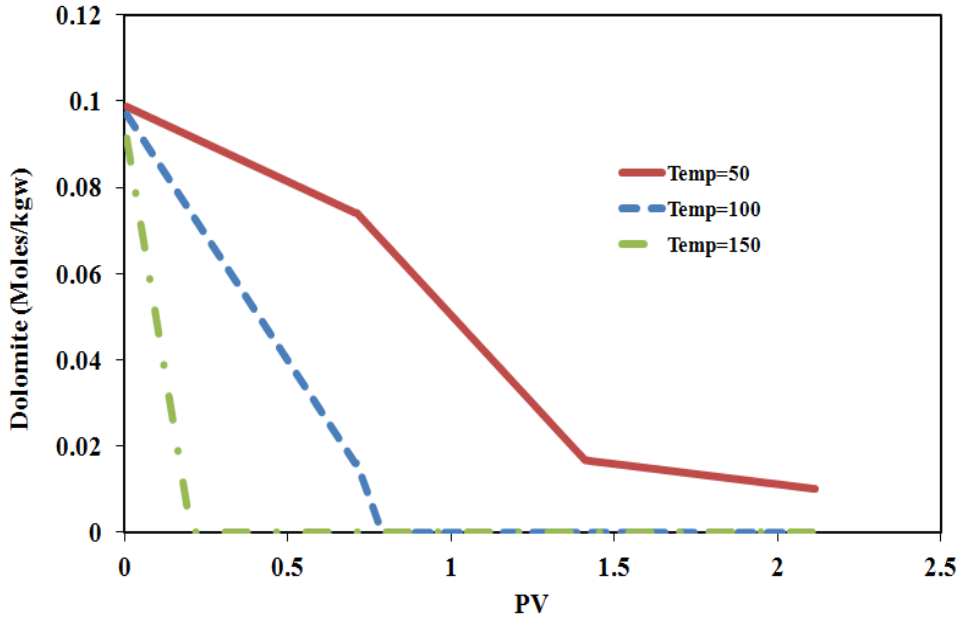

Figure 2-93: History of dolomite concentration in the first gridblock (significance of the temperature in the reactive-transport modeling).

For the case studied, the effect of pressure on the aqueous-rock geochemistry is not as pronounced as the temperature effect (see Figures 2-94 through 2-101 for the ion histories and pH of the aqueous solution produced from the 100th gridblock). Calcite and dolomite concentrations in the 1st gridblock are also presented in Figures 2-102 and 2-103. Although by increasing the average pressure, concentrations of Ca^{+2}, pH, HCO_3^-, Sr^{+2}, Ba^{+2} are affected to some extent, the change in the calcite and dolomite solubilities can be ignored.

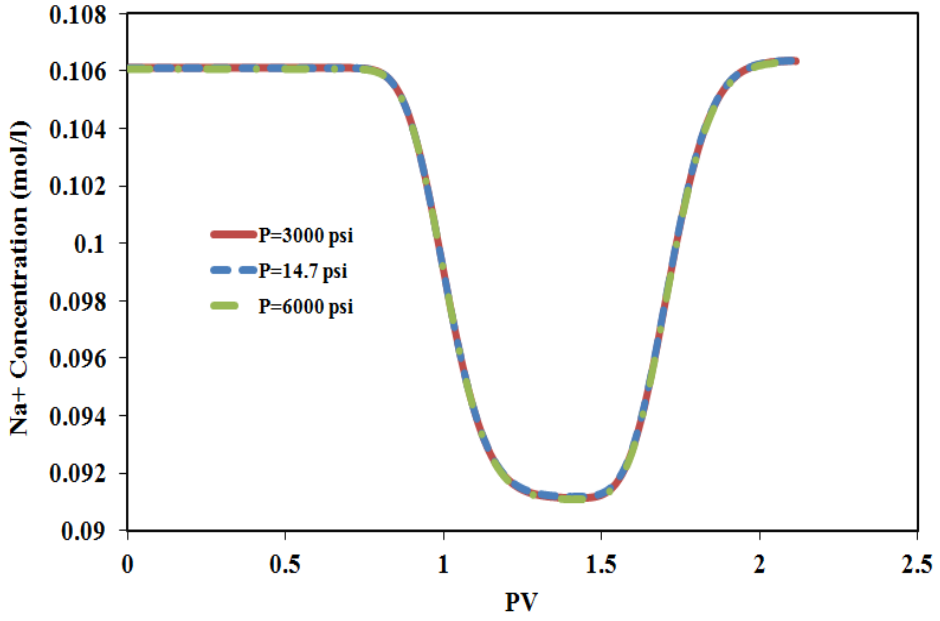

Figure 2-94: History of effluent Na^{+} concentration (significance of the pressure in the reactive-transport modeling).

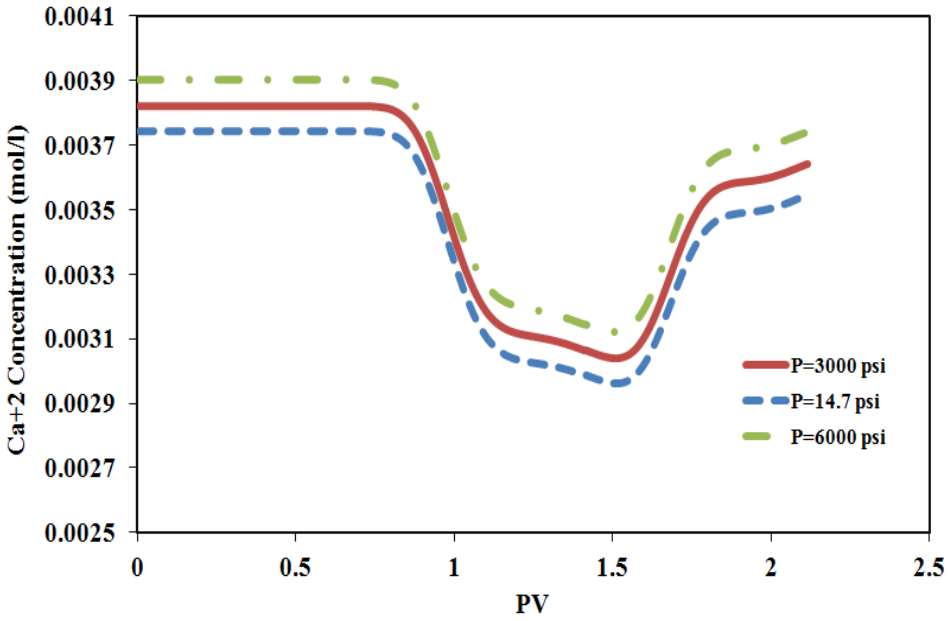

Figure 2-95: History of effluent Ca^{+2} concentration (significance of the pressure in the reactive-transport modeling).

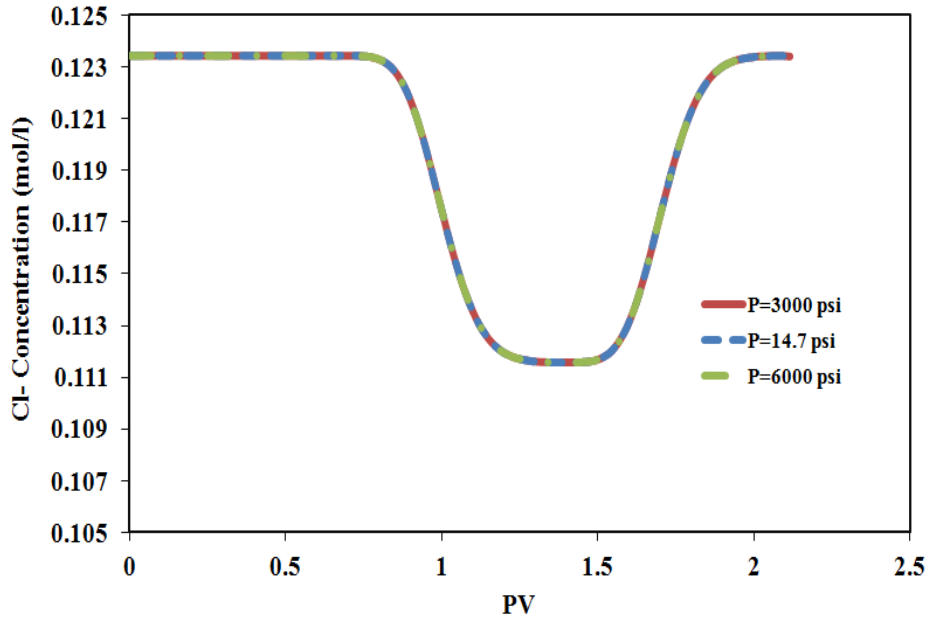

Figure 2-96: History of effluent Cl^- concentration (significance of the pressure in the reactive-transport modeling).

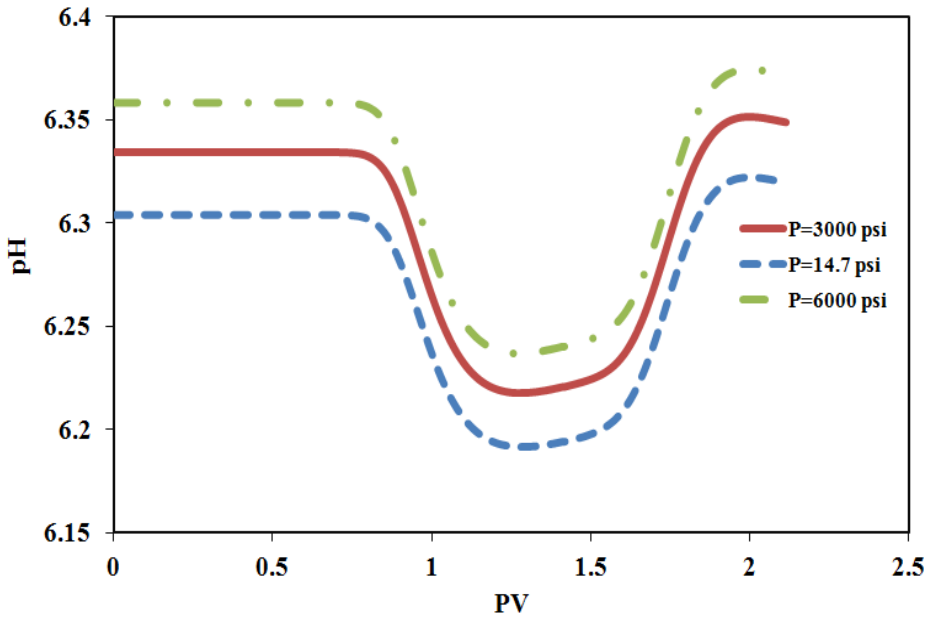

Figure 2-97: History of effluent pH (significance of the pressure in the reactive-transport modeling).

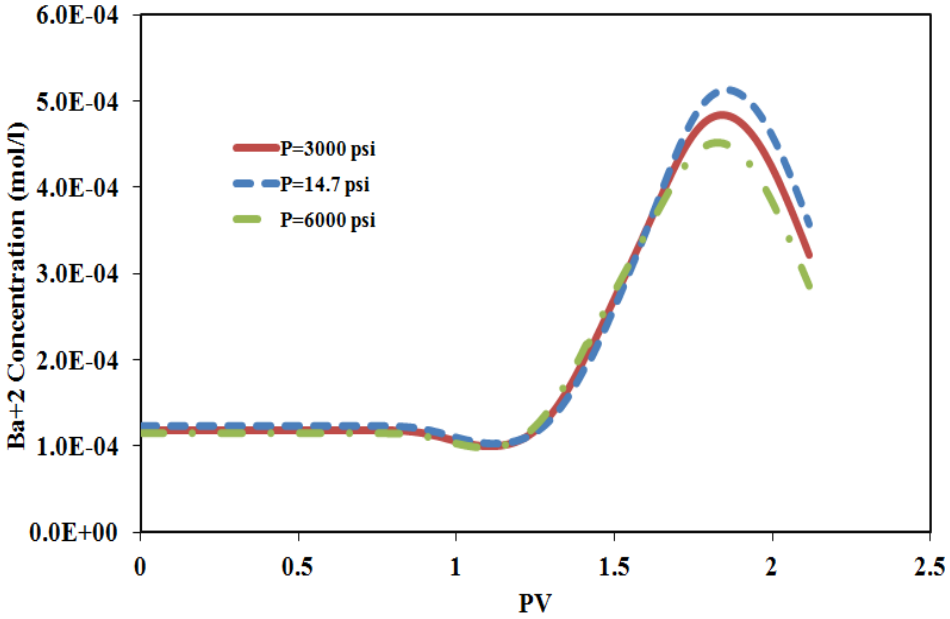

Figure 2-98: History of effluent Ba^{+2} concentration (significance of the pressure in the reactive-transport modeling).

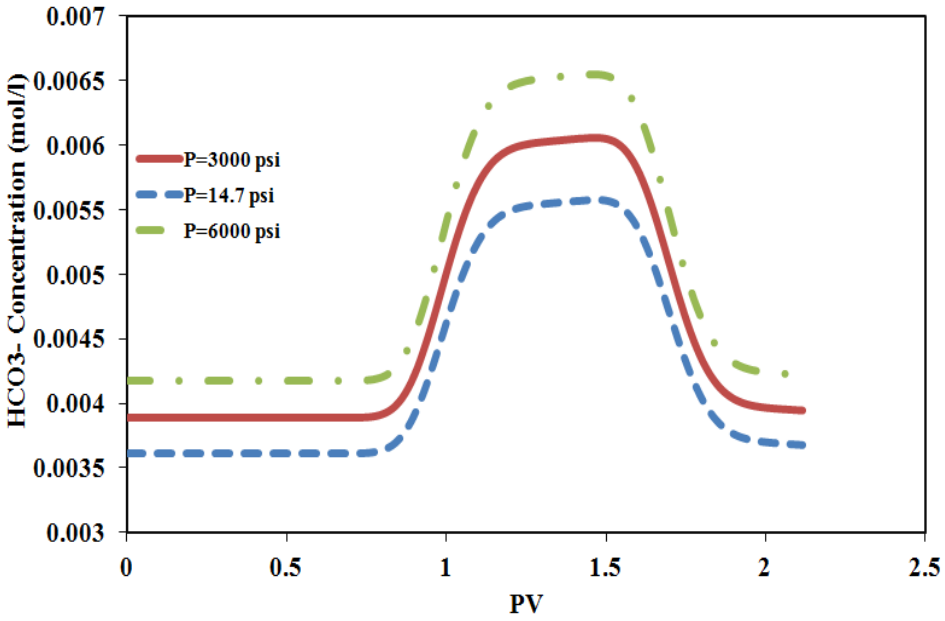

Figure 2-99: History of effluent HCO_3^- concentration (significance of the pressure in the reactive-transport modeling).

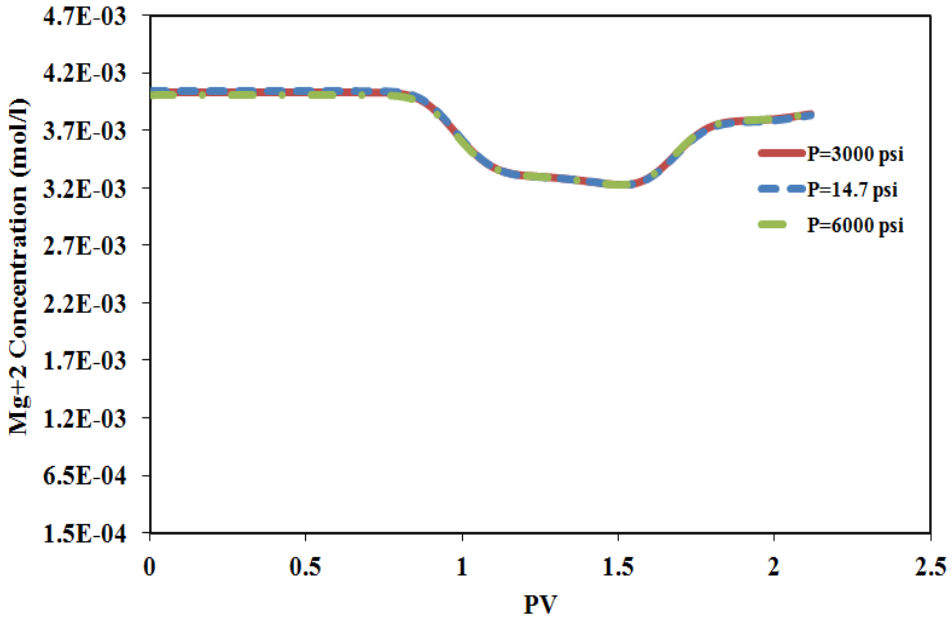

Figure 2-100: History of effluent Mg^{+2} concentration (significance of the pressure in the reactive-transport modeling).

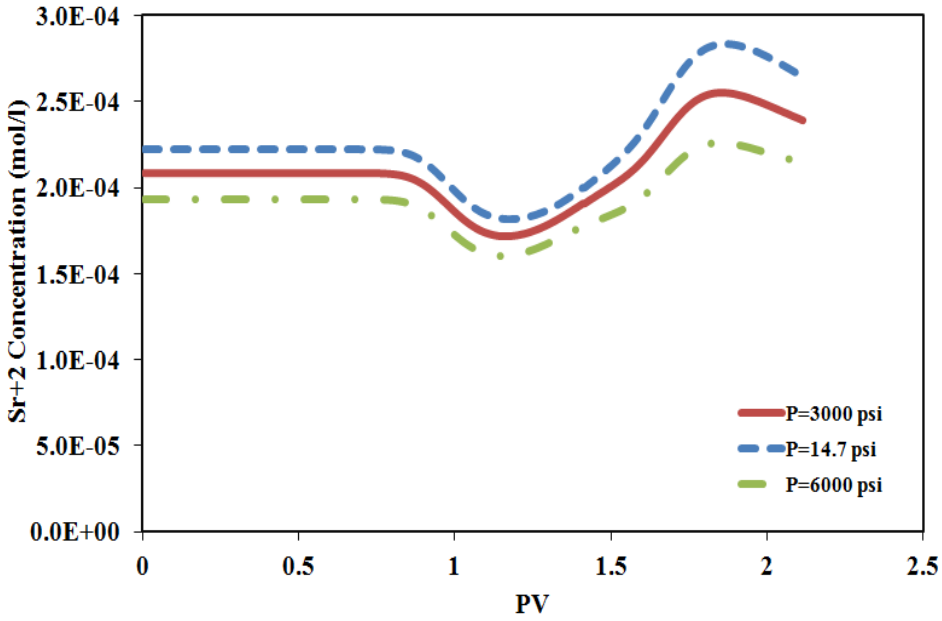

Figure 2-101: History of effluent Sr^{+2} concentration (significance of the pressure in the reactive-transport modeling).

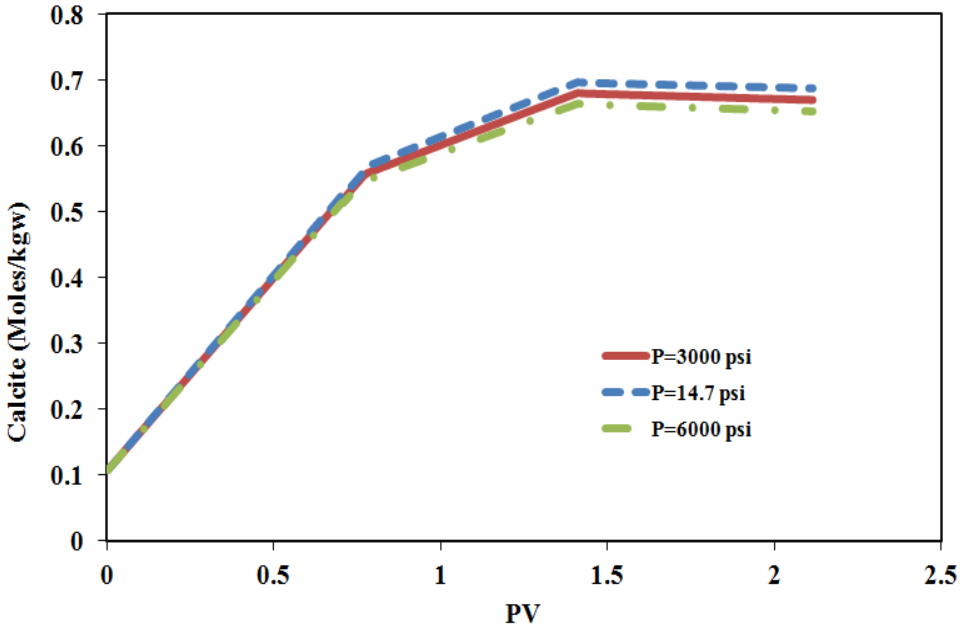

Figure 2-102: History of calcite concentration in the first gridblock (significance of the pressure in the reactive-transport modeling).

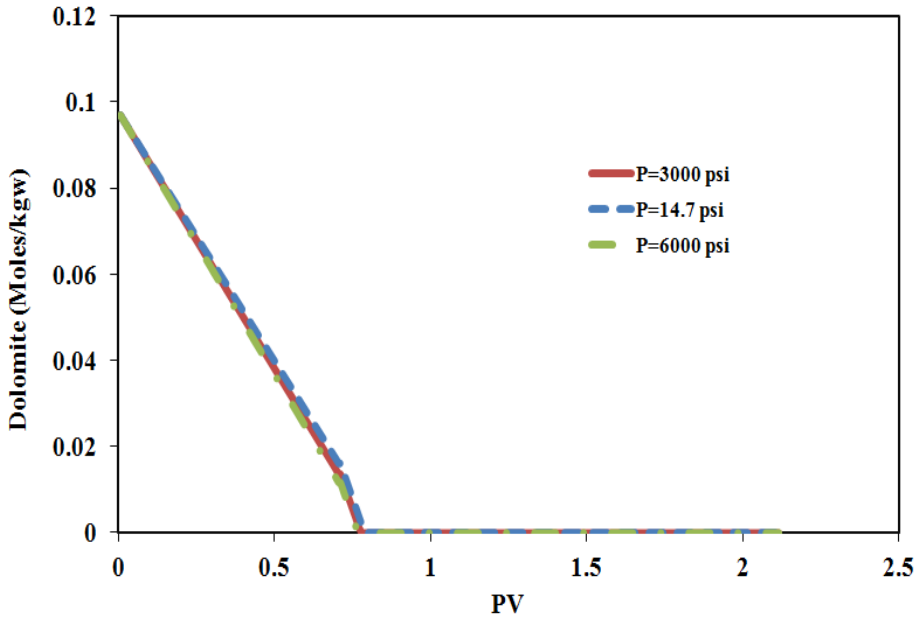

Figure 2-103: History of effluent dolomite concentration in the first gridblock (significance of the pressure in the reactive-transport modeling).

It should be emphasized that the conclusions drawn from the sensitivity studies regarding the change in ion histories and solids precipitation as a function pressure and temperature should not be generalized. The purpose of these sensitivity studies is to show the importance of the inclusion of ion activity coefficients and the temperature and the pressure effects on the aqueous-rock geochemistry. It should be noted that similar results can be reproduced using UTCHEM-IPhreeqc (Korrani *et al.*, 2014c).

2.10 UTCOMP-IPHREEQC USING HIGHER-ORDER METHOD

For a reason unclear to the author, some oscillations appeared in histories of ions with low concentrations (less than 10^{-6}) when the higher-order discretization method (hereafter, simply called higher-order method) is applied in UTCOMP-IPhreeqc. The higher-order method is applied in the UTCOMP input file through the IUPSTW flag. UTCOMP has four different schemes of discretization (IUPSTW = 1 through 4) (see Chang (1990) and UTCOMP Technical Documentation (2011) for the discretization details). Later we show that this issue is not limited to the UTCOMP-IPhreeqc simulator and that perhaps it is a general issue for reactive-transport modeling.

We apply the higher-order method in UTCOMP-IPhreeqc and rerun Case 2 (with the Endicott water compositions) modeled in Section 2.7.2. We believe that the total variation diminishing (TVD) higher-order method (i.e., IUPSTW = 4 in UTCOMP) avoids all the dispersion due to numerical discretization. Hence, Eq. (2.82) (rather than Eq. (2.76)) is applied to consider identical Peclet numbers in UTCOMP-IPhreeqc and PHREEQC. No physical dispersion is included in the model. Hence, the dimensionless Peclet number is infinite. Here we refer to third-order TVD method simply as the higher-order method.

$$\left(\frac{N\Delta x}{\alpha_{physical}}\right)_{\text{UTCOMP-IPhreeqc}} = \left(\frac{N\Delta x}{\alpha_{physical}}\right)_{\text{PHREEQC}} . \qquad (2.82)$$

Figures 2-104 through 2-115 show histories of some fluid species and pH of the solution produced from the case. As the figures illustrate, when the higher-order method is applied in UTCOMP-IPhreeqc, this integrated simulator does not match the PHREEQC's results very well for low concentration ions (including the solution pH which is in fact the decimal logarithm of reciprocal of the hydrogen ion activity, Zhu and Anderson, 2002). Noteworthy, the fact that UTCOMP-IPhreeqc fairly well matches the PHREEQC's output for the chloride ion (as an inactive geochemical species) reveals that, Peclet numbers are almost identical in UTCOMP-IPhreeqc and PHREEQC. Hence, the discrepancies observed are not due to different Peclet numbers in UTCOMP-IPhreeqc and PHREEQC simulators.

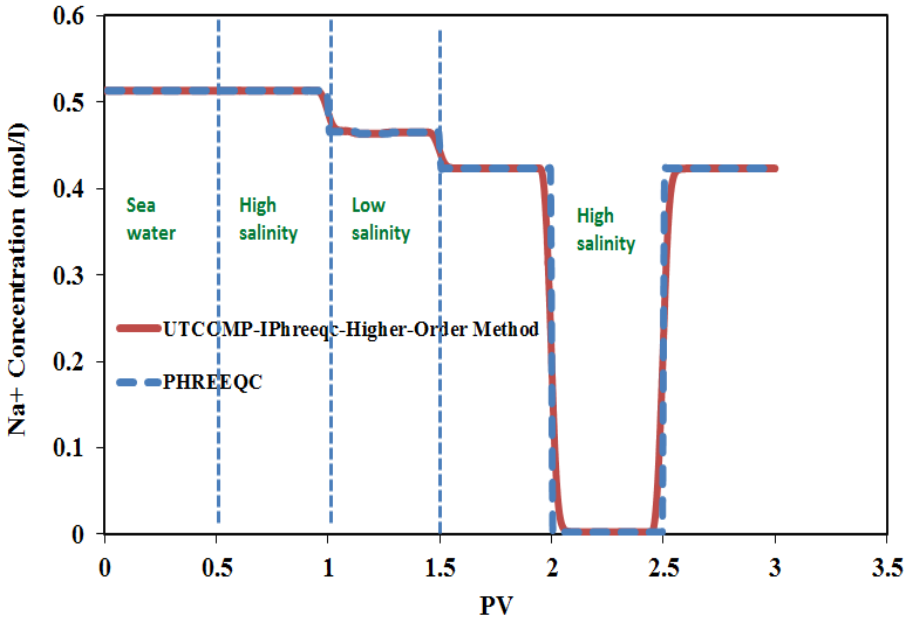

Figure 2-104: Simulation results for the Na^+ concentration history of the effluent solution using UTCOMP-IPhreeqc with the higher-order method and PHREEQC.

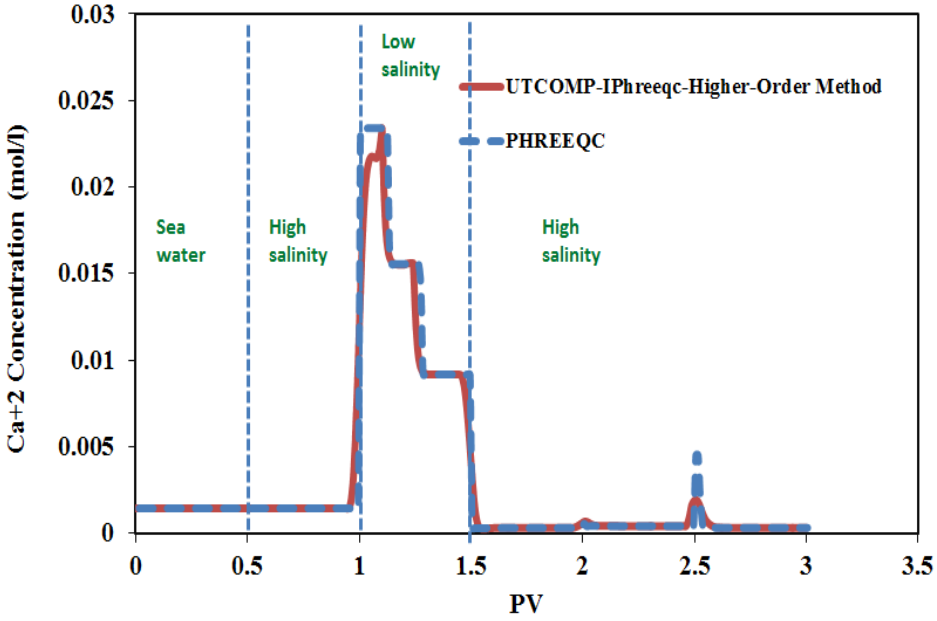

Figure 2-105: Simulation results for the Ca^{+2} concentration history of the effluent solution using UTCOMP-IPhreeqc with the higher-order method and PHREEQC.

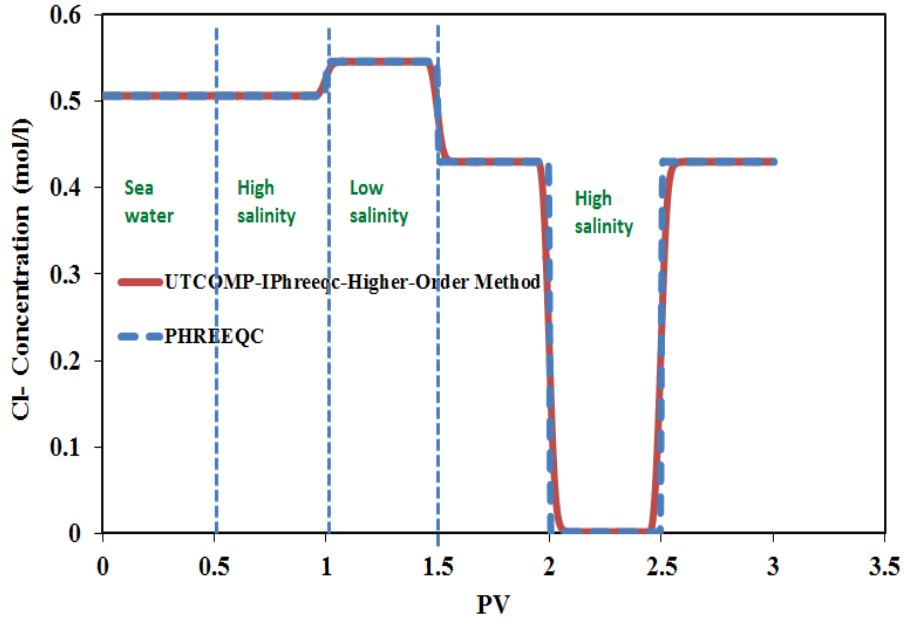

Figure 2-106: Simulation results for the Cl^{-} concentration history of the effluent solution using UTCOMP-IPhreeqc with the higher-order method and PHREEQC.

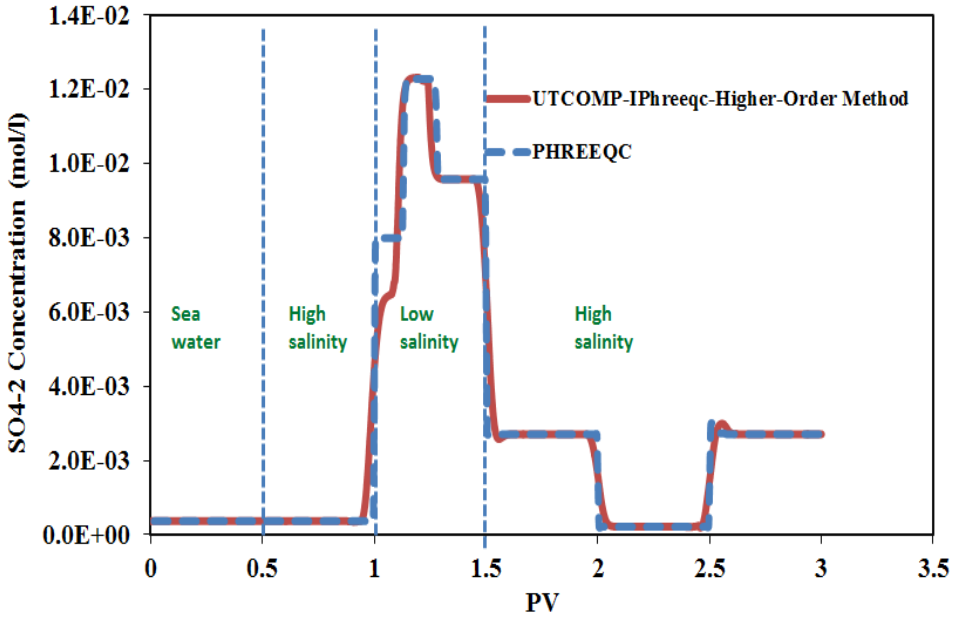

Figure 2-107: Simulation results for the SO_4^{-2} concentration history of the effluent solution using UTCOMP-IPhreeqc with the higher-order method and PHREEQC.

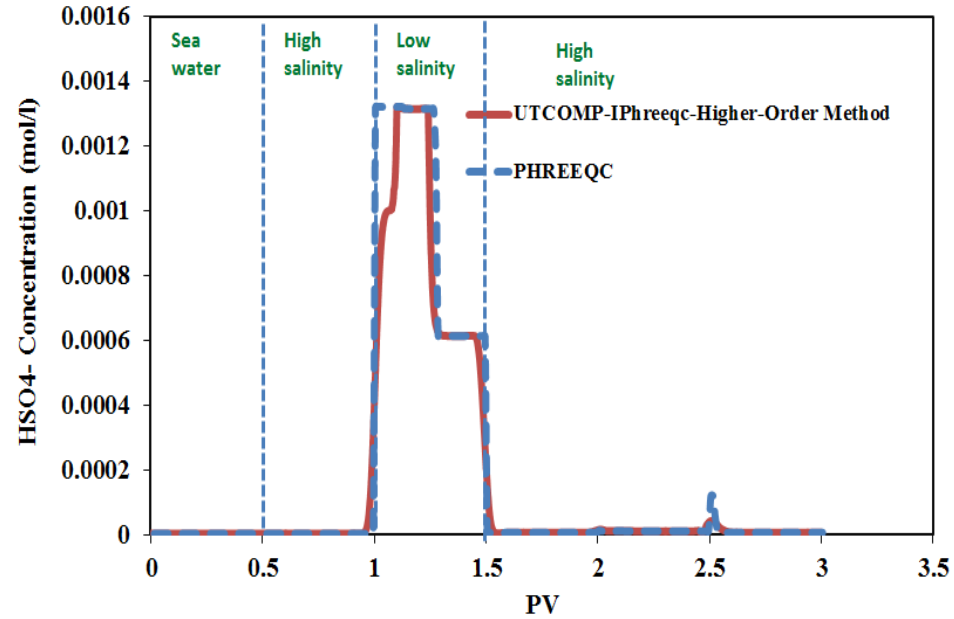

Figure 2-108: Simulation results for the HSO_4^{-1} concentration history of the effluent solution using UTCOMP-IPhreeqc with the higher-order method and PHREEQC.

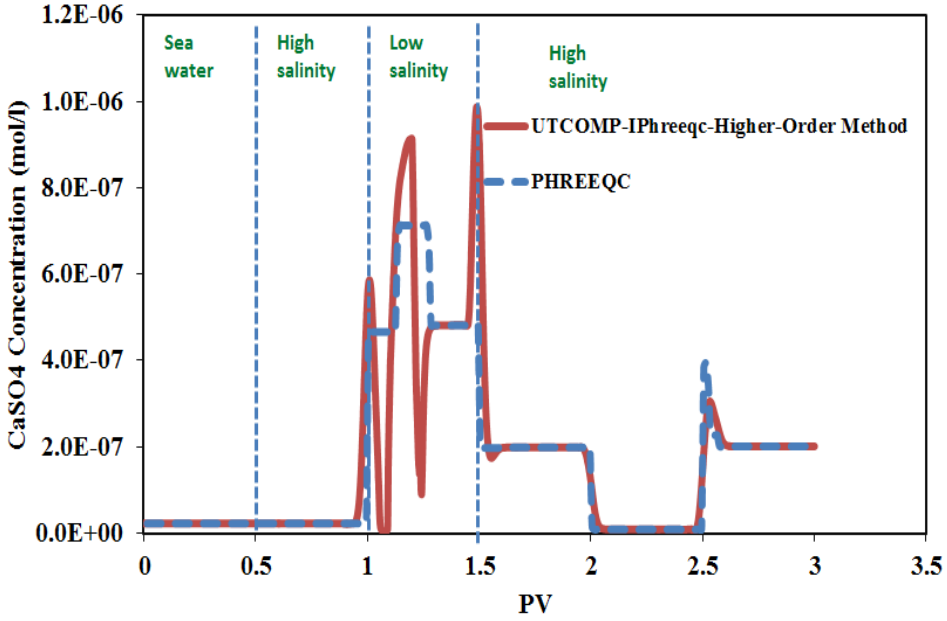

Figure 2-109: Simulation results for the $CaSO_4$ concentration history of the effluent solution using UTCOMP-IPhreeqc with the higher-order method and PHREEQC.

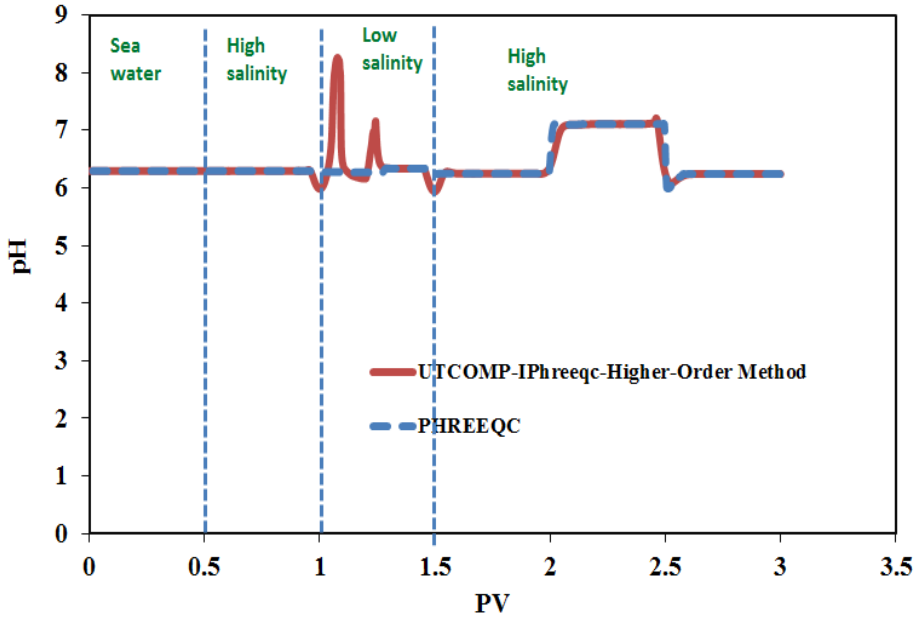

Figure 2-110: Simulation results for the pH history of the effluent solution using UTCOMP-IPhreeqc with the higher-order method and PHREEQC.

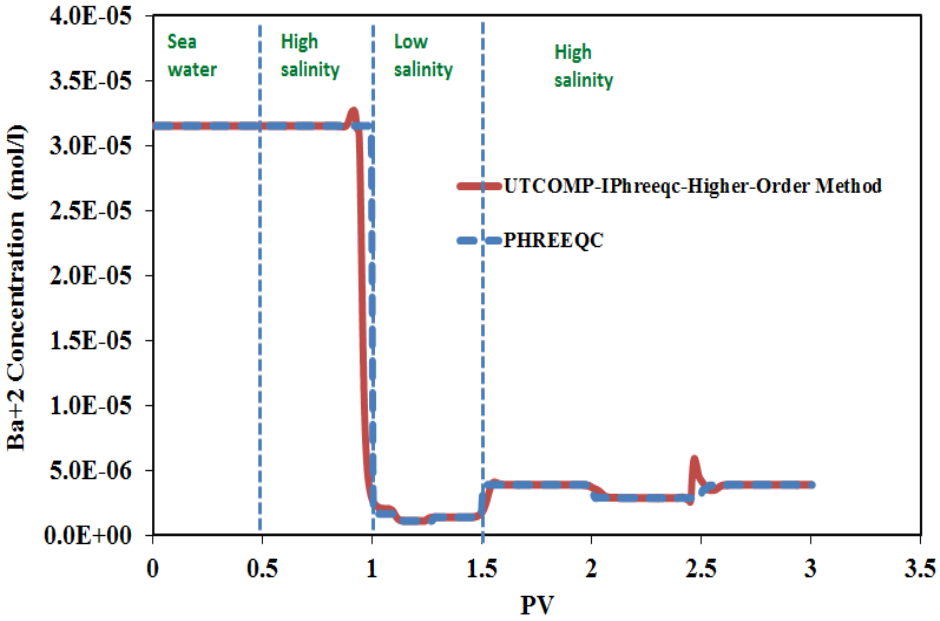

Figure 2-111: Simulation results for the Ba^{+2} concentration history of the effluent solution using UTCOMP-IPhreeqc with the higher-order method and PHREEQC.

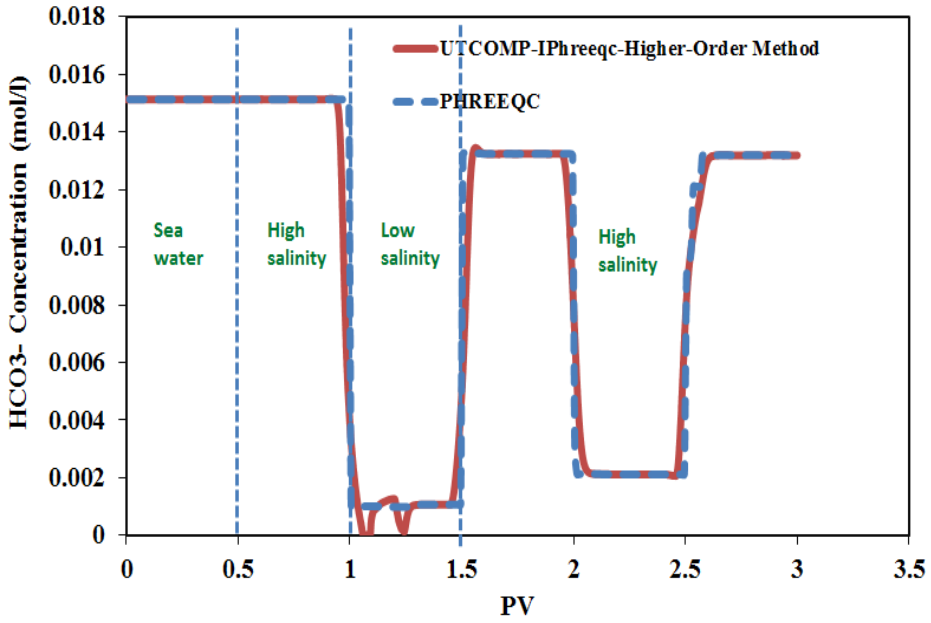

Figure 2-112: Simulation results for the HCO_3^- concentration history of the effluent solution using UTCOMP-IPhreeqc with the higher-order method and PHREEQC.

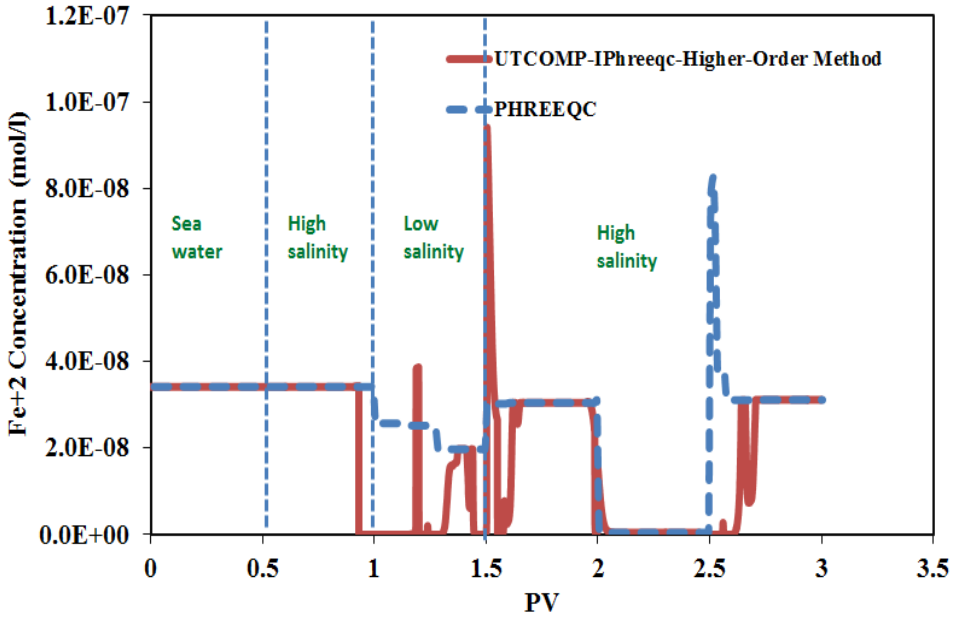

Figure 2-113: Simulation results for the Fe^{+2} concentration history of the effluent solution using UTCOMP-IPhreeqc with the higher-order method and PHREEQC.

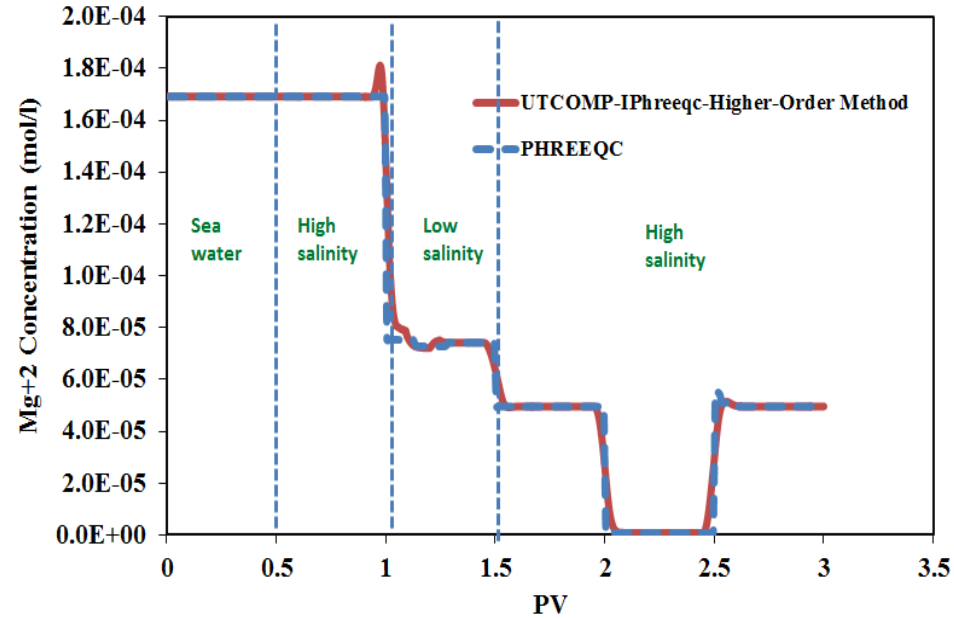

Figure 2-114: Simulation results for the Mg^{+2} concentration history of the effluent solution using UTCOMP-IPhreeqc with the higher-order method and PHREEQC.

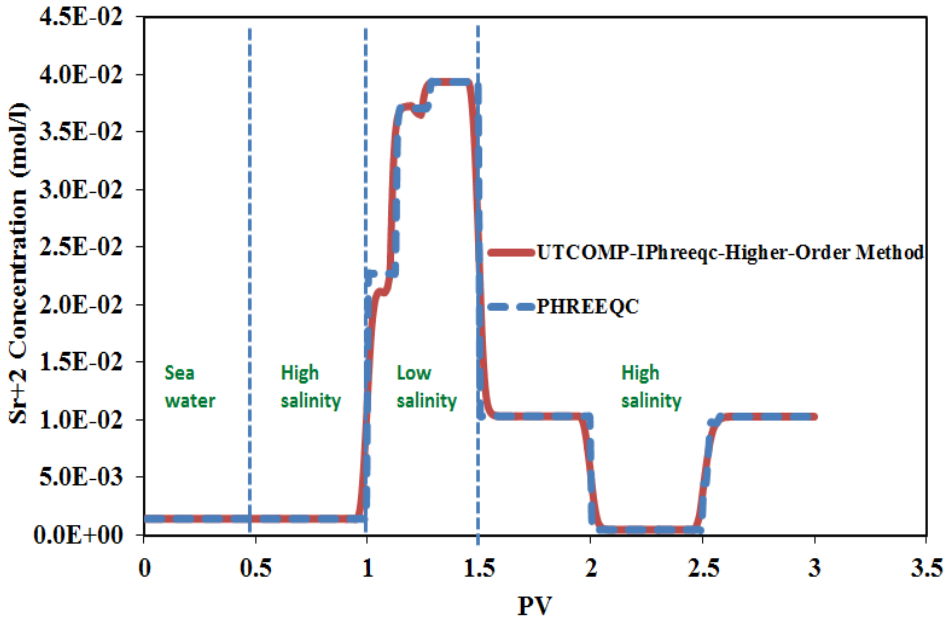

Figure 2-115: Simulation results for the Sr^{+2} concentration history of the effluent solution using UTCOMP-IPhreeqc with the higher-order method and PHREEQC.

A simple case is designed in UTCOMP-/UTCHEM-IPhreeqc, UTCOMP-/UTCHEM-EQBATCH, and PHREEQC to investigate if the problem is because of inherent nature of the higher-order method or the procedure applied to integrate IPhreeqc with UTCOMP. IPhreeqc was integrated with UTCHEM to comprehensively model ASP floods. Details on UTCHEM-IPhreeqc are well documented in Chapter 5. Two aqueous reactions (shown in Table 2-24) and the anhydrite reaction (shown in Table 2-25) are included in the model. Table 2-26 presents ion compositions of initial and injecting waters. Initial anhydrite concentration is 0.091 moles/kgw. For the sake of comparison with EQBATCH, IPhreeqc and PHREEQC are forced to apply molalities rather than ion activities in geochemical calculations. As discussed in Section 2.4, EQBATCH (version 2011) considers molalities rather than ion activities for geochemical calculations.

IPhreeqc/PHREEQC multiplies molality times the ion activity coefficient to find the ion activity (see Appendix A). Hence, to make ion activity coefficients equal to one, the WATEQ Debye-Huckel's model is applied in IPhreeqc/PHREEQC with high value for a_i^0 and zero for b_i (also pointed out in Section 2.8). No Exchange reaction is included in the model because to the best of author's knowledge there is no way through that activity coefficient calculation of IPhreeqc/PHREEQC can be completely ignored for the exchange species. In fact, even if the WATEQ Debye-Huckel activity coefficients are forced to be one for the exchange species, IPhreeqc/PHREEQC still uses the equivalent fractions for the exchange species while EQBATCH applies the molalities in the geochemical calculations. Furthermore, the IPhreeqc/PHREEQC database is modified to consider only the geochemical reactions shown in Tables 2-24 and 2-25. We comprehensively discuss the difference between EQBATCH and IPhreeqc/PHREEQC in Chapter 5.

Table 2-24: Aqueous reaction

Reaction	K_{SP}
$SO_4^{-2} + H^+ \rightleftharpoons HSO_4^-$	$10^{1.988}$
$Ca^{+2} + SO_4^{-2} \rightleftharpoons CaSO_4$	$10^{2.3}$

Table 2-25: Solid reaction

Solid Name	**Reaction**	K_{SP}
Anhydrite	$CaSO_4 \rightleftharpoons Ca^{+2} + SO_4^{-2}$	$10^{-4.360}$

Table 2-26: Ion compositions of initial and injected waters

Ion	$C_{Initial}$ (mol/kgw)	$C_{Injected}$ (mol/kgw)
Ca	0.11	0.
S	0.0092	0.
Cl	charge balance element	

Figures 2-116 through 2-120 compare simulation results of produced Ca^{+2}, SO_4^{-2}, HSO_4^{-1}, $CaSO_4$, and pH using the UTCOMP-/UTCHEM-IPhreeqc, UTCOMP-/UTCHEM-EQBATCH simulators with the higher-order method against PHREEQC outputs.

Although the results of the simulators are in agreement for Ca^{+2}, SO_4^{-2}, $CaSO_4$ fluid species, the discrepancies among these tools are highly pronounced for HSO_4^{-1} and pH. However, UTCOMP-EQBATCH matches UTCOMP-IPhreeqc outputs and also we obtain identical results using UTCHEM-EQBATCH and UTCHEM-IPhreeqc. Hence, even if the oscillation observed in UTCOMP-IPhreeqc or UTCHEM-IPhreeqc is due to a potential programming bug, the programming bug should be in the module where the higher-order method is applied, not the IPhreeqc coupling related routines. The difference between the higher-order method implemented in UTCOMP and the previously developed module in UTCHEM is in order of 10^{-6}. That is why UTCOMP-IPhreeqc/-EQBATCH does not reproduce the UTCHEM-IPhreeqc/-EQBATCH results. It is worth mentioning that if the lower-order method (i.e., one-point upstream weighted method) is applied instead, the results for all the five simulators (i.e., UTCOMP-/UTCHEM-IPhreeqc, UTCOMP-/UTCHEM-EQBATCH, and PHREEQC) match fairly well (see Figures 2-121 through 2-125).

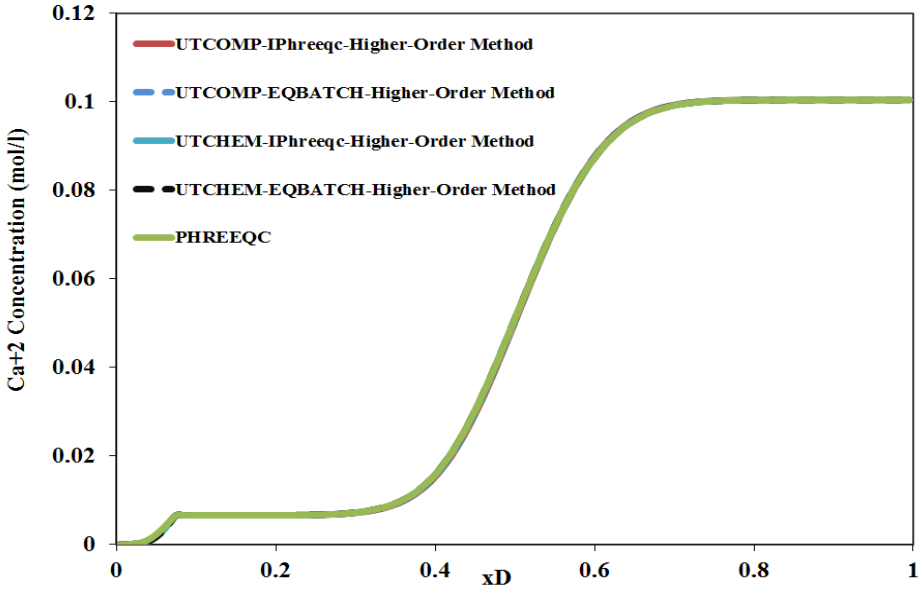

Figure 2-116: Simulation results for the Ca^{+2} concentration profile at 0.5 PV using UTCOMP-/UTCHEM-IPhreeqc and UTCOMP-/UTCHEM-EQBATCH with the higher-order method and PHREEQC.

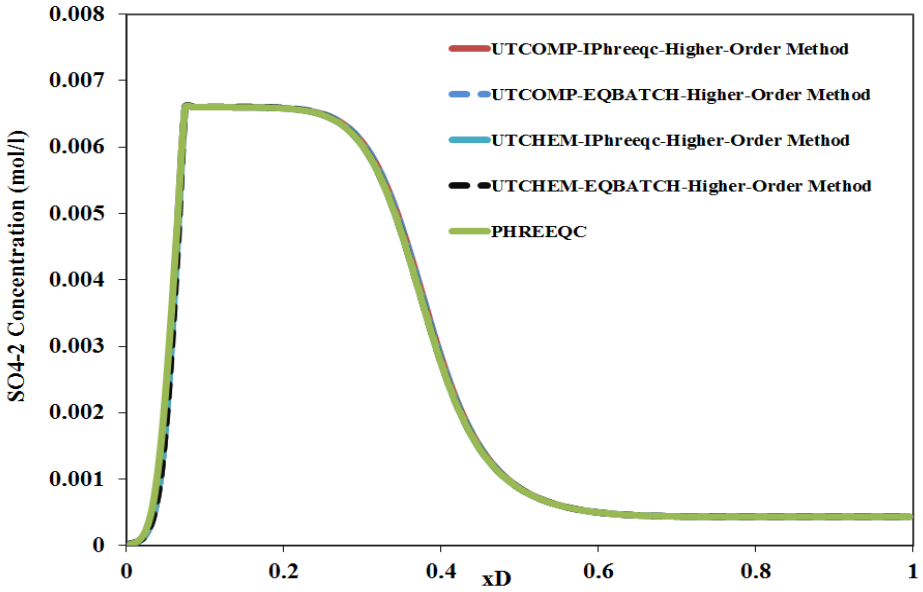

Figure 2-117: Simulation results for the SO_4^{-2} concentration profile at 0.5 PV using UTCOMP-/UTCHEM-IPhreeqc and UTCOMP-/UTCHEM-EQBATCH with the higher-order method and PHREEQC.

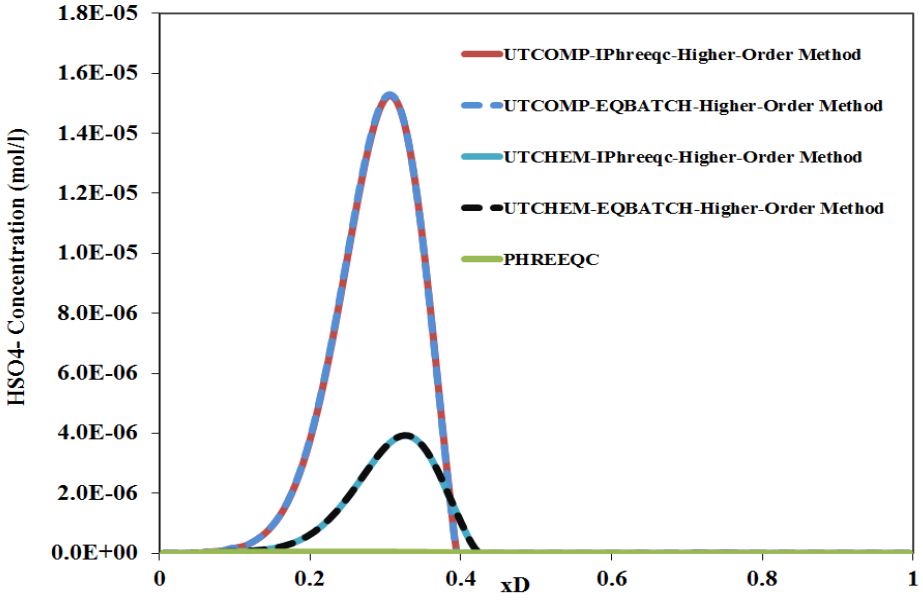

Figure 2-118: Simulation results for the HSO_4^{-1} concentration profile at 0.5 PV using UTCOMP-/UTCHEM-IPhreeqc and UTCOMP-/UTCHEM-EQBATCH with the higher-order method and PHREEQC.

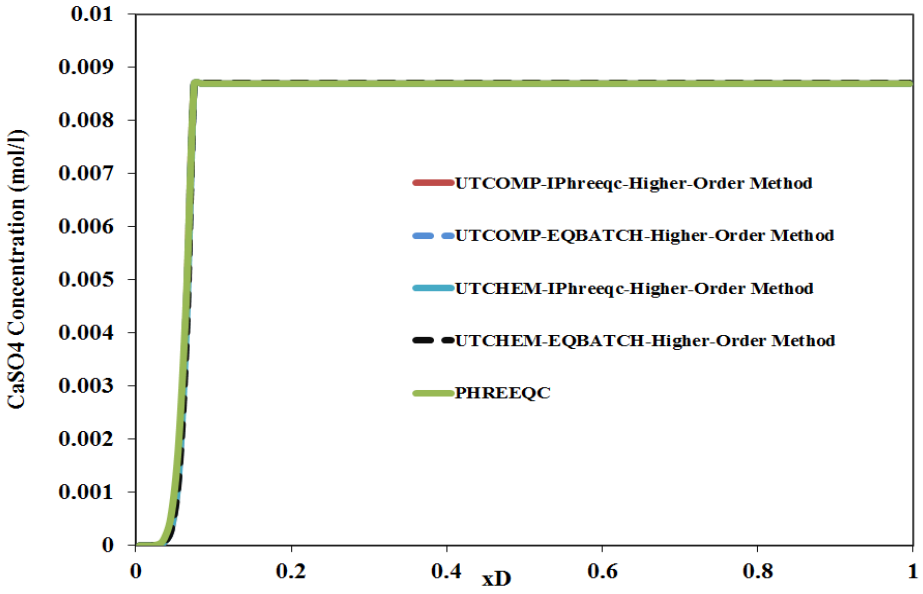

Figure 2-119: Simulation results for the $CaSO_4$ concentration profile at 0.5 PV using UTCOMP-/UTCHEM-IPhreeqc and UTCOMP-/UTCHEM-EQBATCH with the higher-order method and PHREEQC.

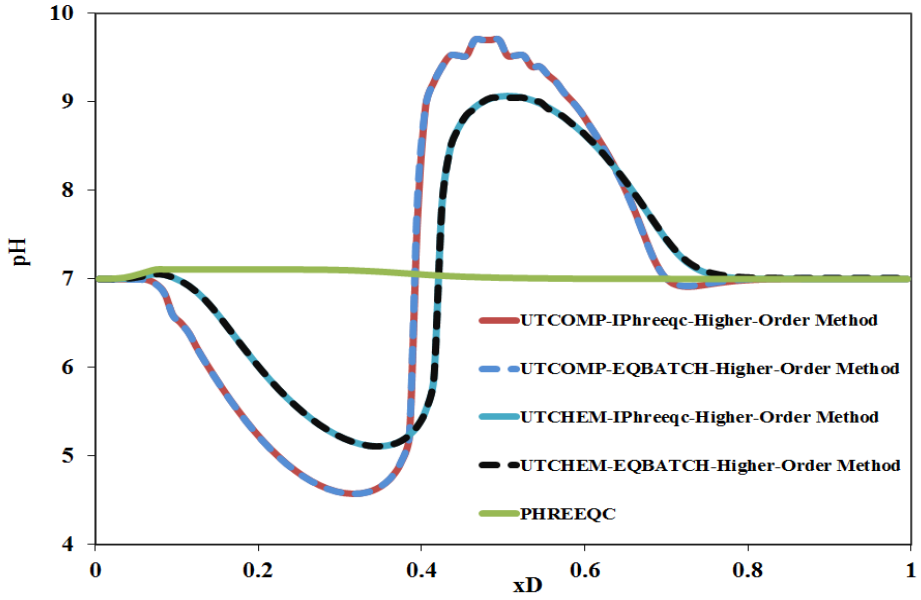

Figure 2-120: Simulation results for the pH profile at 0.5 PV using UTCOMP-/UTCHEM-IPhreeqc and UTCOMP-/UTCHEM-EQBATCH with the higher-order method and PHREEQC.

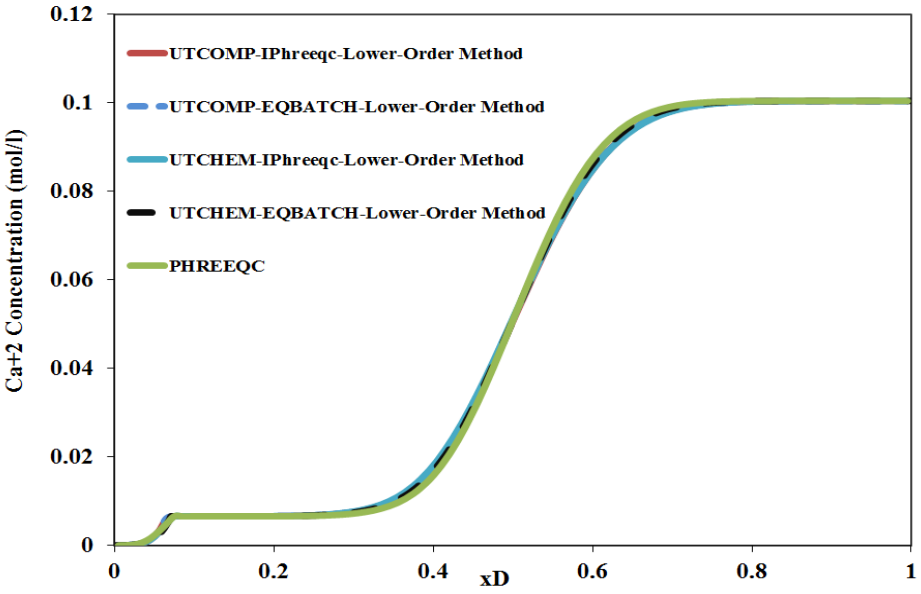

Figure 2-121: Simulation results for the Ca^{+2} concentration profile at 0.5 PV using UTCOMP-/UTCHEM-IPhreeqc and UTCOMP-/UTCHEM-EQBATCH with the lower-order method and PHREEQC.

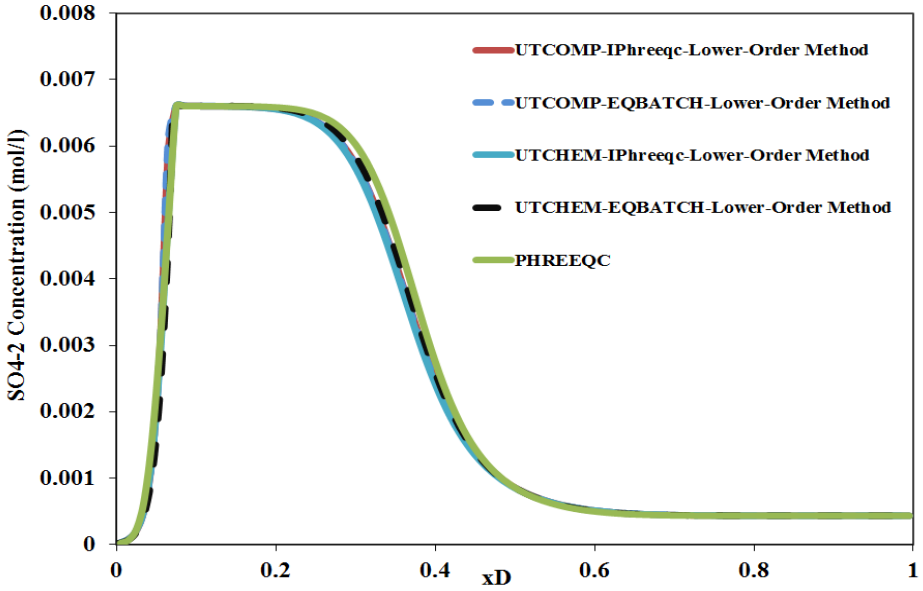

Figure 2-122: Simulation results for the SO_4^{-2} concentration profile at 0.5 PV using UTCOMP-/UTCHEM-IPhreeqc and UTCOMP-/UTCHEM-EQBATCH with the lower-order method and PHREEQC.

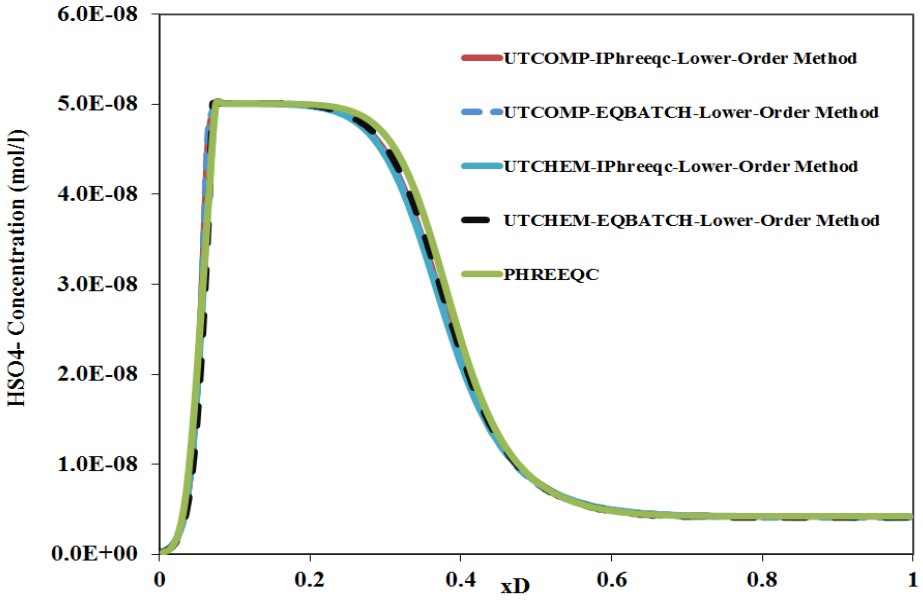

Figure 2-123: Simulation results for the HSO_4^{-1} concentration profile at 0.5 PV using UTCOMP-/UTCHEM-IPhreeqc and UTCOMP-/UTCHEM-EQBATCH with the lower-order method and PHREEQC.

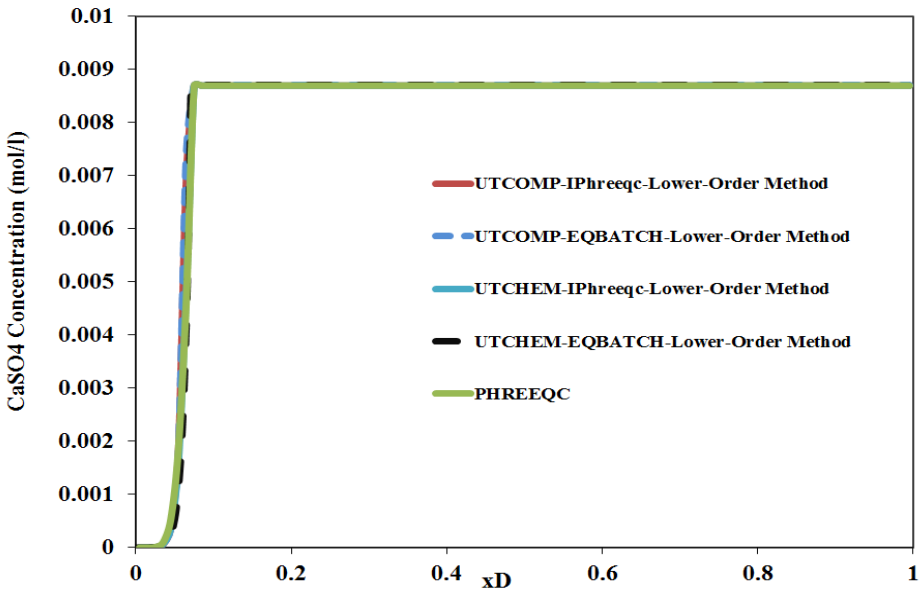

Figure 2-124: Simulation results for the $CaSO_4$ concentration profile at 0.5 PV using UTCOMP-/UTCHEM-IPhreeqc and UTCOMP-/UTCHEM-EQBATCH with the lower-order method and PHREEQC.

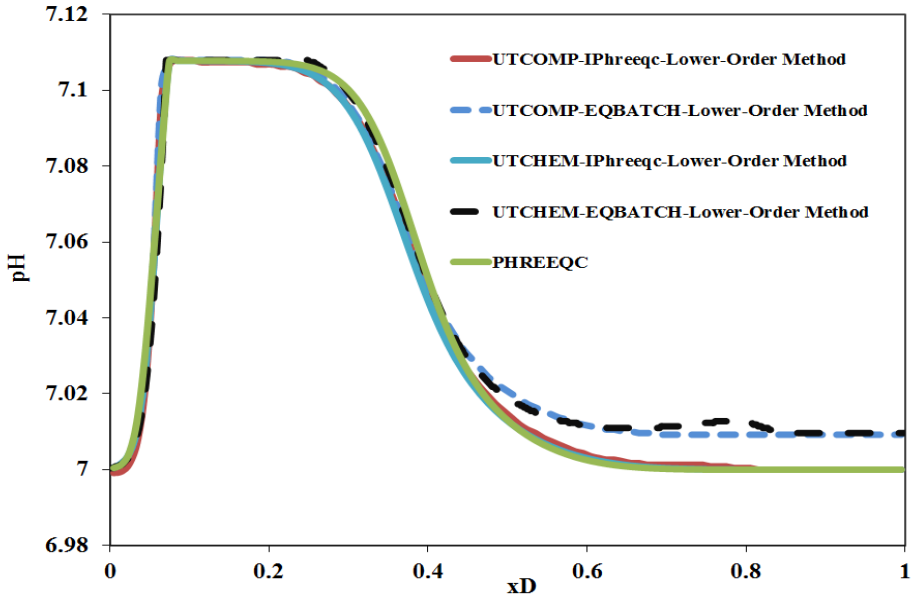

Figure 2-125: Simulation results for the pH profile at 0.5 PV using UTCOMP-/UTCHEM-IPhreeqc and UTCOMP-/UTCHEM-EQBATCH with the lower-order method and PHREEQC.

The oscillation in pH or ions with small concentration is not always observed. To confirm this, Case 2 presented in Section 2.4 is used in UTCOMP-/UTCHEM-EQBATCH, UTCOMP-/UTCHEM-IPhreeqc, and PHREEQC. As previously discussed, if an exchange site is included into a model, there is no way through which we can obtain the same results using EQBATCH (coupled with UTCHEM or UTCOMP) and IPhreeqc (coupled with UTCHEM and UTCOMP). Hence, here we exclude the exchange reactions from Case 2.

Figures 2-126 through 2-138 present histories of pH and some of the fluid species produced from the case. As the figures illustrate, although the higher-order method is applied in UTCOMP-/UTCHEM-IPhreeqc, UTCOMP-/UTCHEM-EQBATCH, these simulators match the PHREEQC's results fairly well for a complicated case. Once again, we emphasize on the fact that ion activity coefficients of aqueous species are forced to be one in the IPhreeqc/PHREEQC thermodynamic database in order to apply molalities rather than ion activities for geochemical calculations (similar to EQBATCH).

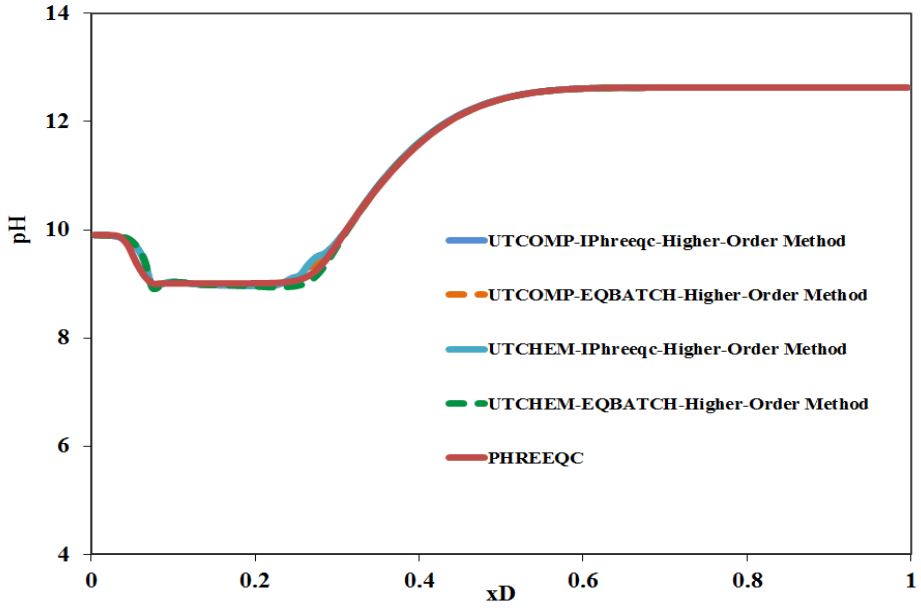

Figure 2-126: Simulation results for pH profile at 0.5 PV using UTCOMP-/UTCHEM-IPhreeqc and UTCOMP-/UTCHEM-EQBATCH with the higher-order method and PHREEQC.

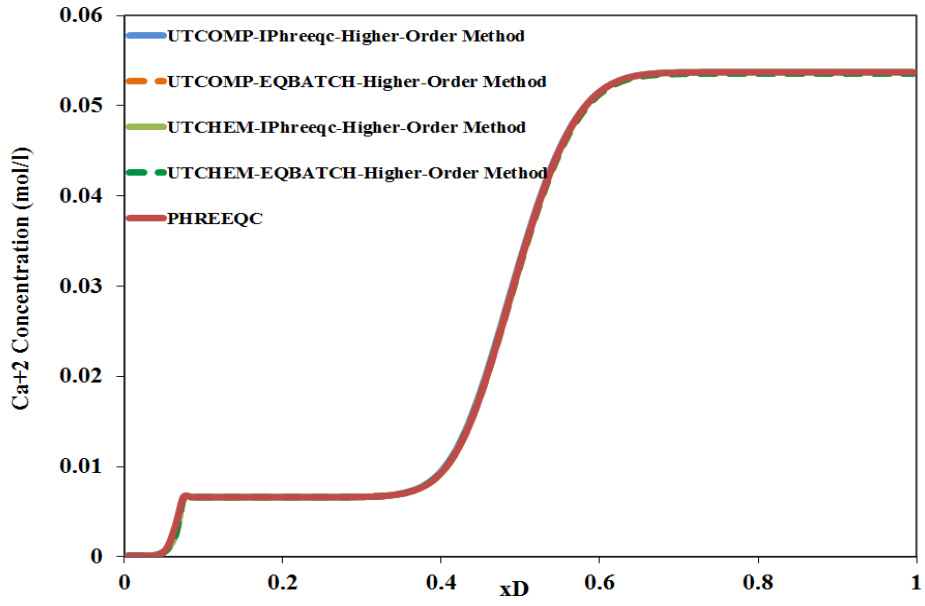

Figure 2-127: Simulation results for the Ca^{+2} concentration profile at 0.5 PV using UTCOMP-/UTCHEM-IPhreeqc and UTCOMP-/UTCHEM-EQBATCH with the higher-order method and PHREEQC.

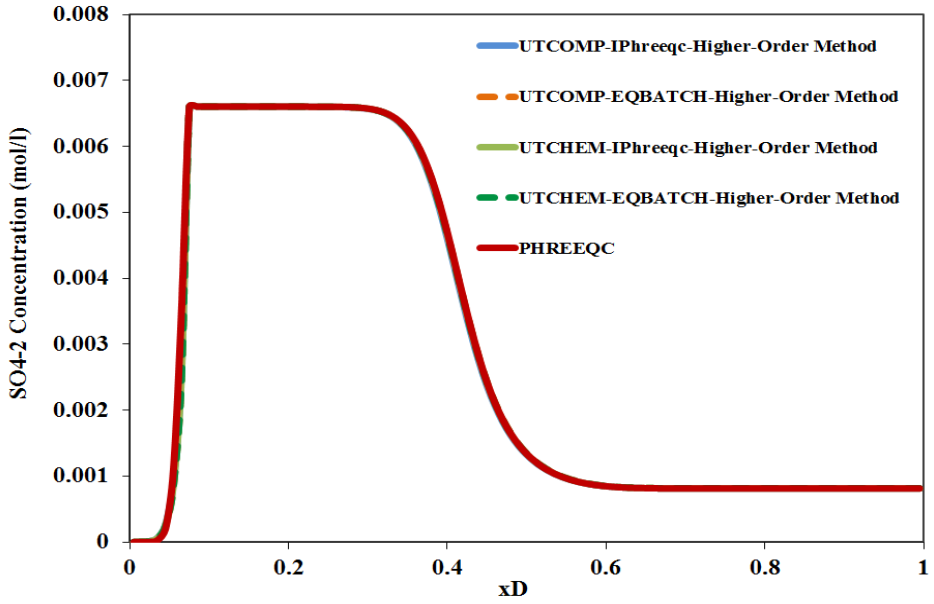

Figure 2-128: Simulation results for the SO_4^{-2} concentration profile at 0.5 PV using UTCOMP-/UTCHEM-IPhreeqc and UTCOMP-/UTCHEM-EQBATCH with the higher-order method and PHREEQC.

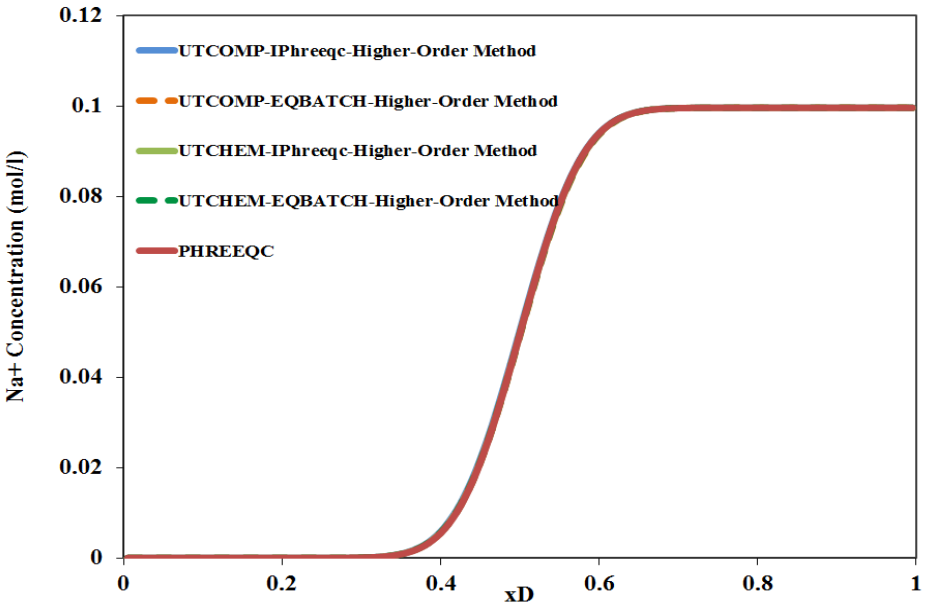

Figure 2-129: Simulation results for the Na^+ concentration profile at 0.5 PV using UTCOMP-/UTCHEM-IPhreeqc and UTCOMP-/UTCHEM-EQBATCH with the higher-order method and PHREEQC.

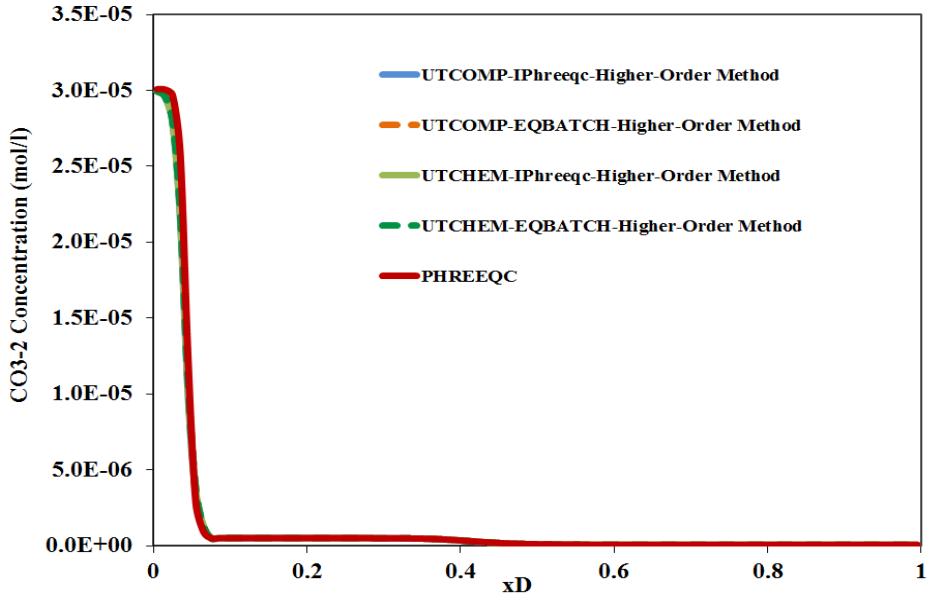

Figure 2-130: Simulation results for the CO_3^{-2} concentration profile at 0.5 PV using UTCOMP-/UTCHEM-IPhreeqc and UTCOMP-/UTCHEM-EQBATCH with the higher-order method and PHREEQC.

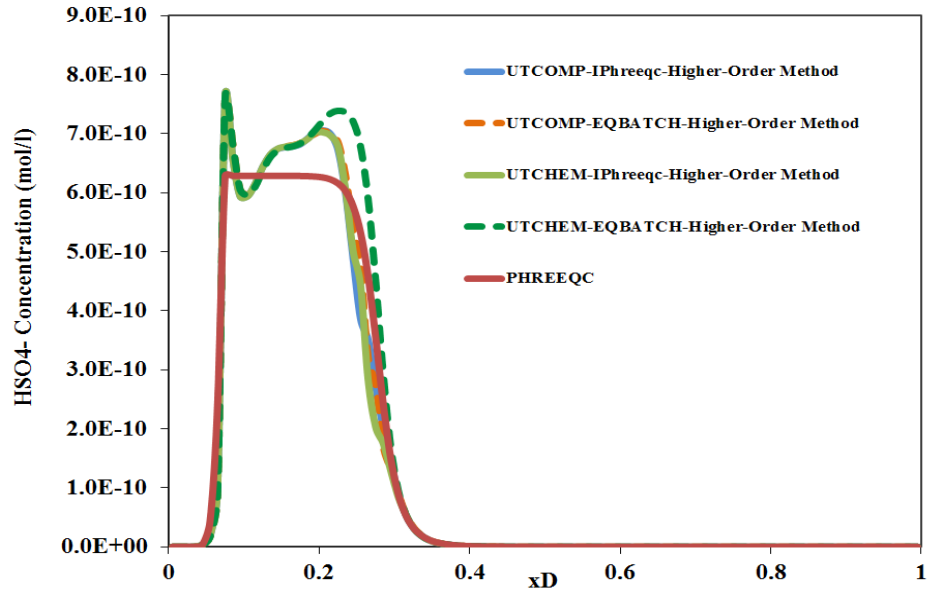

Figure 2-131: Simulation results for the HSO_4^{-1} concentration profile at 0.5 PV using UTCOMP-/UTCHEM-IPhreeqc and UTCOMP-/UTCHEM-EQBATCH with the higher-order method and PHREEQC.

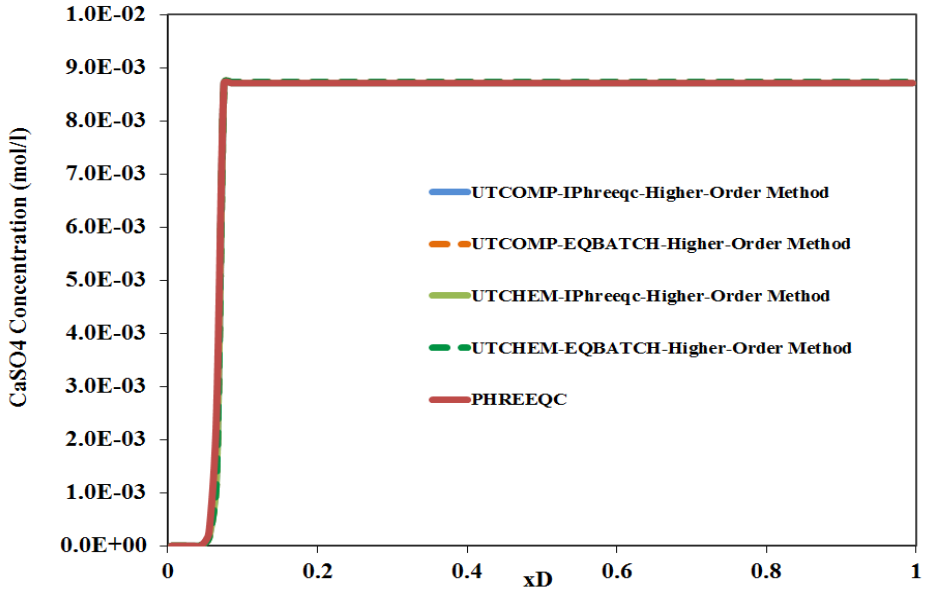

Figure 2-132: Simulation results for the $CaSO_4$ concentration profile at 0.5 PV using UTCOMP-/UTCHEM-IPhreeqc and UTCOMP-/UTCHEM-EQBATCH with the higher-order method and PHREEQC.

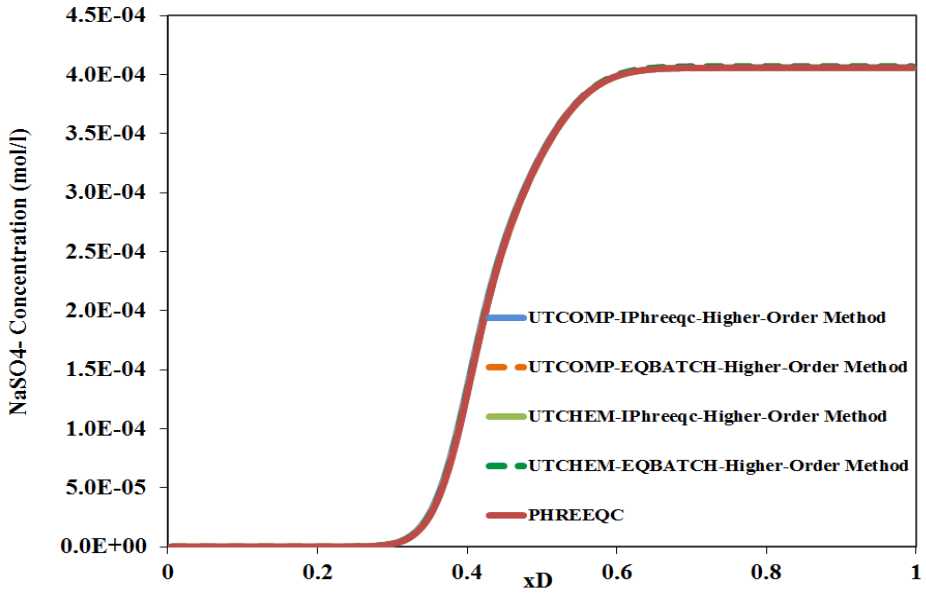

Figure 2-133: Simulation results for the $NaSO_4^-$ concentration profile at 0.5 PV using UTCOMP-/UTCHEM-IPhreeqc and UTCOMP-/UTCHEM-EQBATCH with the higher-order method and PHREEQC.

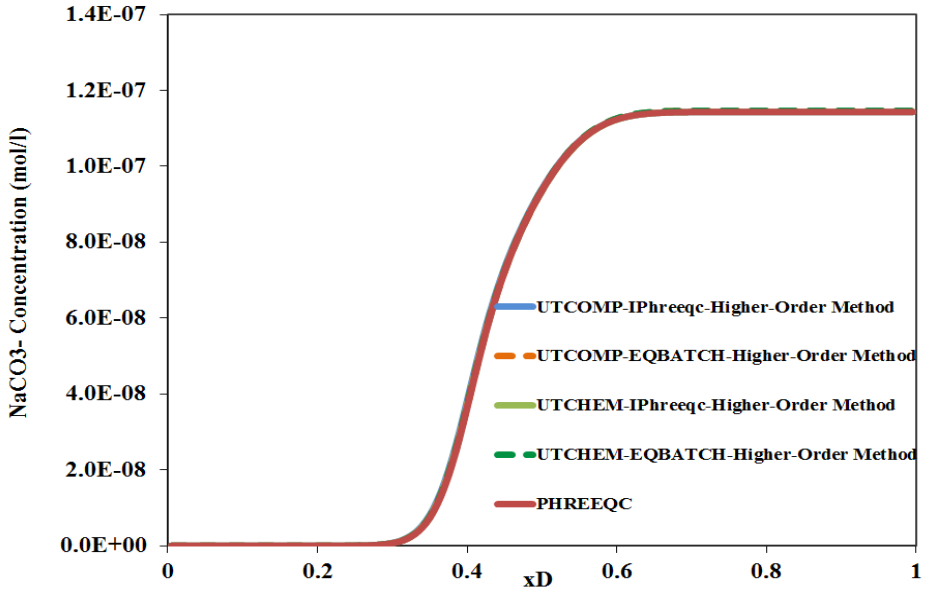

Figure 2-134: Simulation results for the $NaCO_3^-$ concentration profile at 0.5 PV using UTCOMP-/UTCHEM-IPhreeqc and UTCOMP-/UTCHEM-EQBATCH with the higher-order method and PHREEQC.

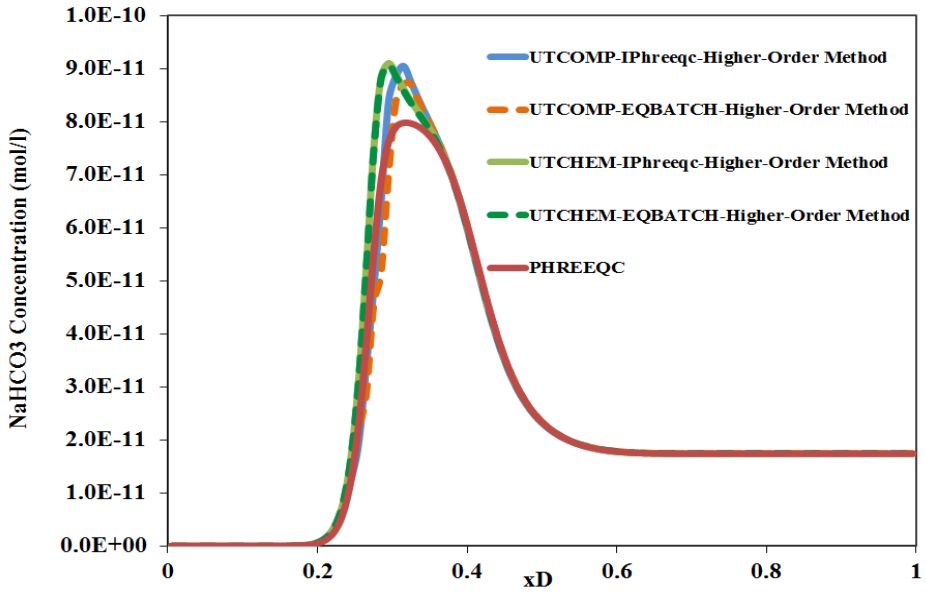

Figure 2-135: Simulation results for the $NaHCO_3$ concentration profile at 0.5 PV using UTCOMP-/UTCHEM-IPhreeqc and UTCOMP-/UTCHEM-EQBATCH with the higher-order method and PHREEQC.

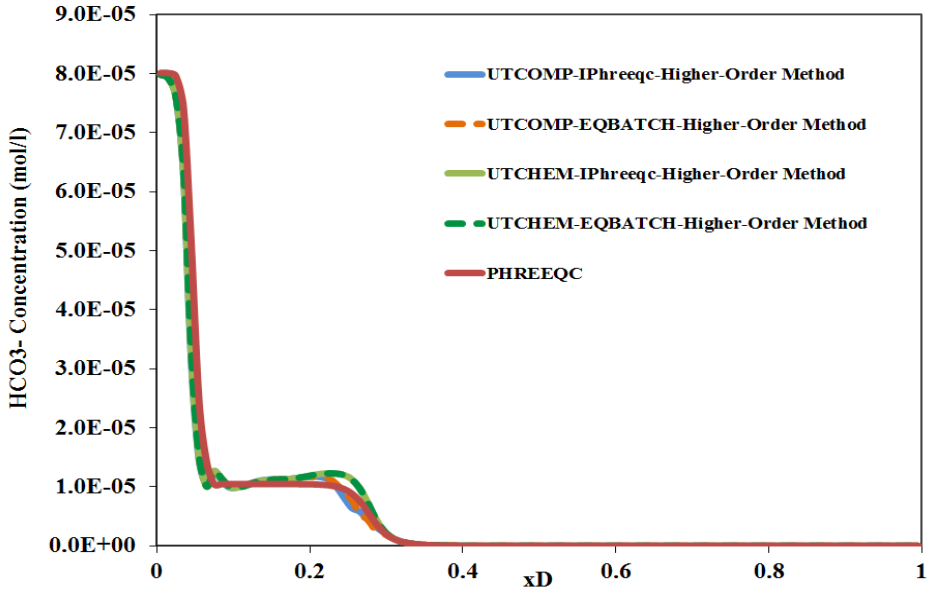

Figure 2-136: Simulation results for the HCO_3^{-1} concentration profile at 0.5 PV using UTCOMP-/UTCHEM-IPhreeqc and UTCOMP-/UTCHEM-EQBATCH with the higher-order method and PHREEQC.

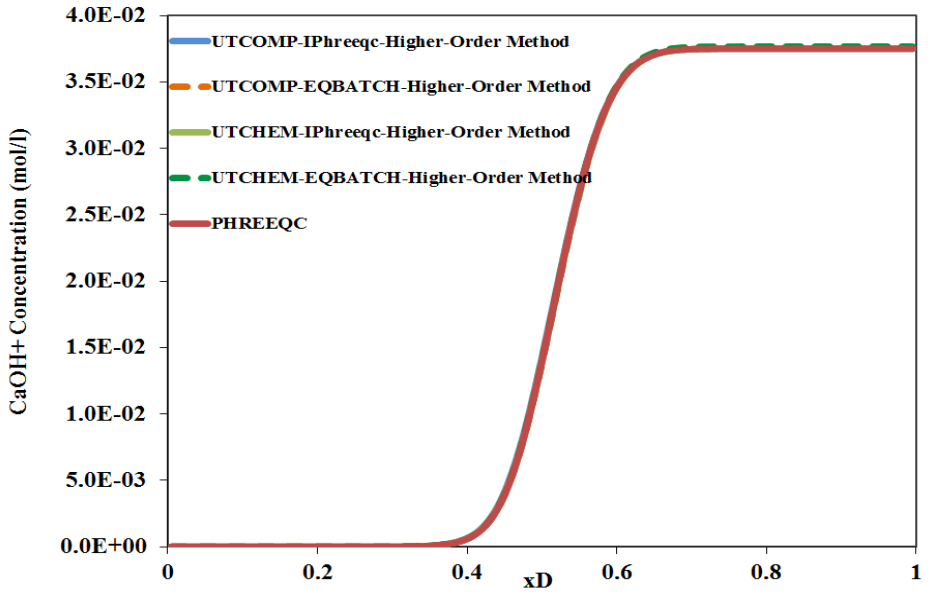

Figure 2-137: Simulation results for the $CaOH^+$ concentration profile at 0.5 PV using UTCOMP-/UTCHEM-IPhreeqc and UTCOMP-/UTCHEM-EQBATCH with the higher-order method and PHREEQC.

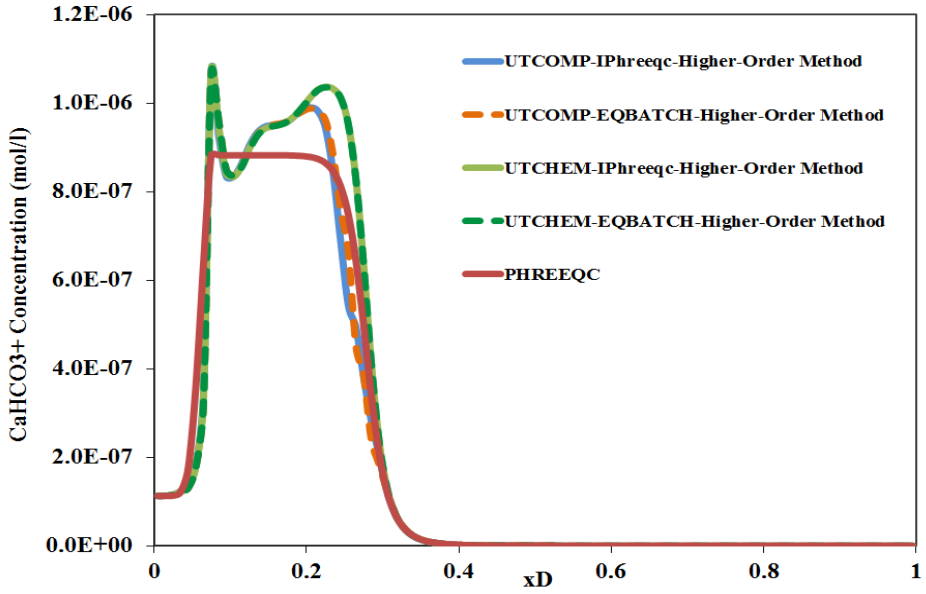

Figure 2-138: Simulation results for the $CaHCO_3^+$ concentration profile at 0.5 PV using UTCOMP-/UTCHEM-IPhreeqc and UTCOMP-/UTCHEM-EQBATCH with the higher-order method and PHREEQC.

Out of the four schemes of discretization available in UTCOMP (IUPSTW = 1 through 4) and UTCHEM (IDISP = 0 through 3), UTCOMP-IPhreeqc with IUPSTW = 1 and UTCHEM-IPhreeqc with IDISP = 0 are the only options that always match PHREEQC results. Oscillations in low concentration ions are worse when IUPSTW = 3 is applied compared with IUPSTW = 2. IUPSTW = 4 shows the worst oscillations.

Broadly speaking, schemes of discretization other than the lower-order method (i.e., one-point upstream weighted method) are not recommended to model processes in which fluid species with low concentrations play a significant role in the physics of the process. For example, geochemistry, particularly pH of the aqueous solution, is the fundamental basis for high-pH flooding or ASP processes. Hence, using the higher-order scheme of discretization to model these processes might lead to misleading results. High pH values (usually above 11) are considered in high-pH flooding or ASP processes. The

pH value, say 11, by definition means the hydrogen ion activity of 10^{-11}. For the time being, UTCOMP-/UTCHEM-IPhreeqc stops if methods other than the lower-order method are considered for the simulation. Hereafter in this dissertation the lower-order scheme is applied in all the simulation runs.

2.11 IMPLEMENTATION OF WETTABILITY ALTERATION MODULE IN UTCOMP-IPHREEQC

One of the hypotheses made in this dissertation is that the wettability alteration is the underlying mechanism behind low (or modified) salinity waterflooding. This hypothesis is based on several experimental observations published in the literature (more details are provided in Chapters 3 and 4). Hence, to be able to apply UTCOMP-IPhreeqc for mechanistic modeling of low salinity waterflooding, a wettability alteration model should be included in this integrated simulator.

The wettability alteration model based on the interpolating technique is implemented in the UTCOMP-IPhreeqc simulator. In this modeling approach, a single set of oil-wet curves corresponding to the oil-wet condition and another set corresponding to the water-wet condition are considered and then during the simulation, the altered relative permeabilities or capillary pressure are computed as weighted averages between two previously defined oil-wet and water-wet curves (see Eqs. (2.83) and (2.84)).

$$k_{rl}^{altered} = \left(1-\theta_1\right)k_{rl}^{initial} + \theta_1 k_{rl}^{final}, \tag{2.83}$$

$$P_c^{altered} = \left(1-\theta_2\right)P_c^{initial} + \theta_2 P_c^{final}, \tag{2.84}$$

where

$\theta_1, \theta_2 =$ process dependent interpolation factors

k_{rl} = relative permeability of the phase l

P_c = capillary pressure (psi)

The interpolating technique was implemented in UTCHEM to model the wettability alteration due to chemical floods such as surfactant and alkaline flooding (Najafabadi, 2009; Anderson, 2006; Goudarzi *et al.*, 2012; 2013). For example, in one of the mechanistic model implemented in UTCHEM, the interpolating parameter is defined as a function of adsorbed surfactant on the rock surface. Through this model, wettability alteration due to the surfactant flooding is introduced. In other words, the more surfactant adsorbed on the grain, the more chance there is to change the wettability of the rock from mixed-wet toward water-wet (Najafabadi, 2009; Anderson, 2006; Goudarzi *et al.*, 2012; 2013).

In UTCOMP-IPhreeqc when phase saturations are known for reservoir gridblocks, they are used to separately calculate "initial" and "final" relative permeabilities and capillary pressure. Routines to evaluate the "initial" and "final" relative permeabilities and capillary pressure are basically the same except different relative permeability parameters are applied. For example, residual saturations, endpoints, and exponents if the Corey's model is considered. These parameters are defined by the users in the UTCOMP input file. The calculated "initial" and "final" relative permeabilities and capillary pressure are used along with the interpolating parameter in a separate routine (i.e., wetmodel.f in UTCOMP-IPhreeqc) to evaluate the "altered" relative permeabilities and capillary pressure using Eqs. (2.83) and (2.84). In fact, the "altered" relative permeabilities are applied for the transmissibility and subsequently the gridblocks pressure calculations.

In this work we assume the same interpolating parameter for the relative permeability and the capillary pressure (i.e., $\theta_1 = \theta_2$). Based on the literature (discussed in Chapters 3 and 4), the underlying mechanisms for low salinity water injection in sandstone and carbonate reservoirs are different. Hence, to introduce this discrepancy in the model, we define different interpolating parameters for sandstone (see Chapter 3) and carbonate (see Chapter 4) reservoirs.

The wettability alteration module implemented in UTCOMP is not limited to modeling the low salinity waterflooding, but can be also applied to model the wettability alteration due to other processes. For example, Mohebbinia (2013) and Mohebbinia *et al.* (2014) applied the UTCOMP wettability alteration module to model wettability alteration due to the asphaltene deposition on the rock surface. It is widely accepted that when asphaltene is deposited on the rock surface, it changes the rock wettability from the water-wet condition towards the oil-wet condition. Noteworthy, to model wettability alteration due to asphaltene deposition, the initial set of relative permeabilities is water-wet and the final set is oil-wet (just the opposite of low salinity waterflooding).

Two different scenarios are applied to verify the wettability alteration model implemented in the UTCOMP-IPhreeqc simulator.

Case 1

In the first scenario; a heterogeneous 2D case is designed in UTCOMP-IPhreeqc. Table 2-27 presents the case descriptions. Barium (Ba), sodium (Na), and calcium (Ca) are the geochemical species present in the connate water and also injected with different concentrations into the reservoir (through the 6 injection wells included in the case). Tables 2-28 and 2-29 illustrate ion compositions of geochemical species for initial and injecting waters, respectively. This case is heterogeneous in porosity and absolute

permeability (in both *x* and *y* directions). Isotropic permeability is assumed. Figure 2-139 shows the map for the *x*- and *y*-direction permeabilities and Figure 2-140 presents the porosity distribution map. The injection pattern is line drive with 6 injection and 3 production wells (see Figure 2-141). The capillary pressure is assumed to be zero. Initial and final sets of relative permeability curves are identical (Corey's relative permeability model is applied with the parameters shown in Table 2-30) and the interpolating parameter for the relative permeability is constant and equal to 0.3. This case is verified against an identical case but without wettability alteration and only with one set of relative permeability curves. In fact, because the initial and final sets of relative permeability curves are identical for the case with the wettability alteration, results for this case should match those of the case with one set of relative permeability (i.e., no wettability alteration is applied).

Figures 2-142 through 2-148 demonstrate results of the case with the wettability alteration included (shown with IWALT=1 in the figures) with those from the case without wettability alteration (shown with IWALT =0 in the figures). Figures 2-142 and 2-143 show oil recovery and average reservoir pressure and Figures 2-144 through 2-148 present the ion histories of Ba, Na, and Ca; pressure; water saturation at two gridblocks of (50,30,1) and (30,50,1). As the figures show, results are identical for the cases compared.

Table 2-27: Reservoir characteristics for 3D verification case

No. of gridblocks		10000 (100×100×1)	
Δx(ft)		25.0	
Δy(ft)		25.0	
Δz(ft)		20.0	
Permeability (md)	*x*-direction	Heterogeneous	
	y-direction	Heterogeneous	
Porosity		Heterogeneous	
Rock compressibility (psi^{-1})		0.	
Water compressibility (psi^{-1})		0.	
Initial water saturation		0.25	
Irreducible water saturation		0.25	
Reservoir temperature (^oF)		105.0	
Initial pressure (psi)		1100.0	
Reservoir depth (ft)		0.	
Water viscosity (cp)		0.79	
Oil viscosity (cp)		6.3	
Number of wells		9	6 injectors
			3 producers
Simulation time(PV)		2.0	

Table 2-28: Initial concentration for the geochemical elements

	Ba	Na	Ca
Initial concentration (meq/ml)	0.	0.1	0.1

Table 2-29: Wells condition and injecting element concentrations for 3D case

Well No.	I	J	Perforated layer	r_w (ft)	Type	Operating Condition	Concentration (meq/ml)		
							Ba	Na	Ca
1	10	10	1-1	0.33	Inj.	Q_w=200 bbl/Day	0.02	0.	0.05
2	10	90	1-1	0.33	Inj.	Q_w=200 bbl/Day	0.2	0.3	0.75
3	90	10	1-1	0.33	Inj.	Q_w=200 bbl/Day	1.1	0.48	0.2
4	90	90	1-1	0.33	Inj.	Q_w=200 bbl/Day	0.2	0.	0.5
5	50	50	1-1	0.33	Prod.	BHP=1000 psia	-	-	-
6	90	50	1-1	0.33	Inj.	Q_w=200 bbl/Day	0.2	0.	0.5
7	10	50	1-1	0.33	Inj.	Q_w=200 bbl/Day	0.02	0.	0.05
8	50	90	1-1	0.33	Prod.	BHP=1000 psia	-	-	-
9	50	10	1-1	0.33	Prod.	BHP=1000 psia	-	-	-

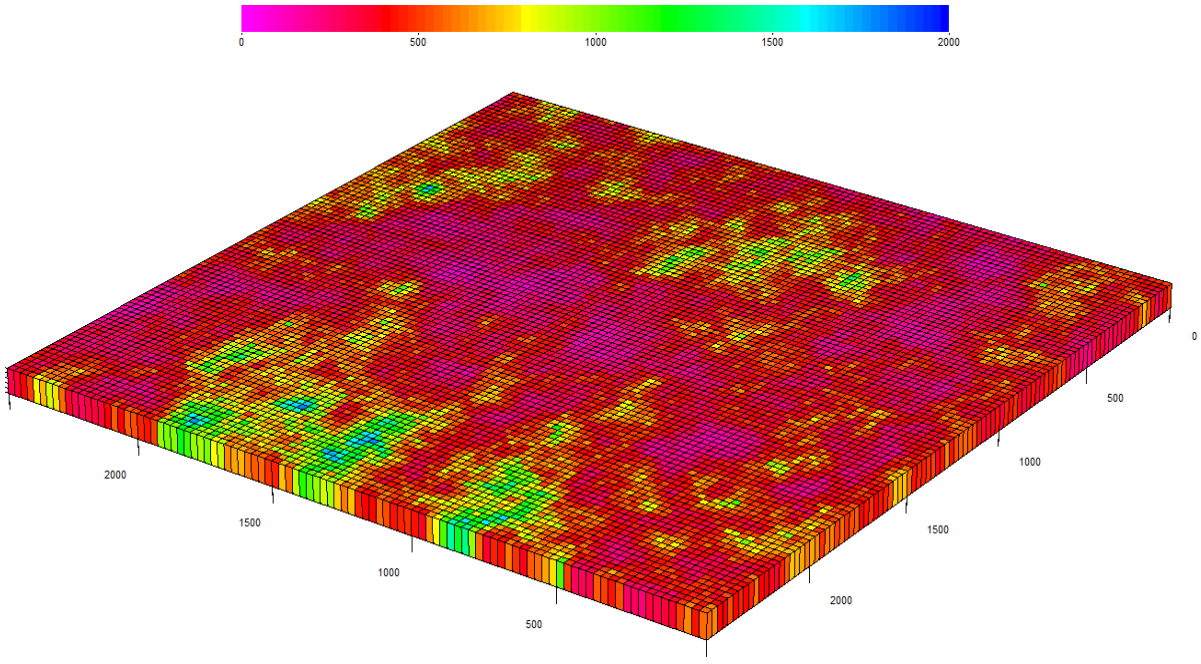

Figure 2-139: Distribution of permeabilities (in md) in *x* and *y* directions for the 2D case.

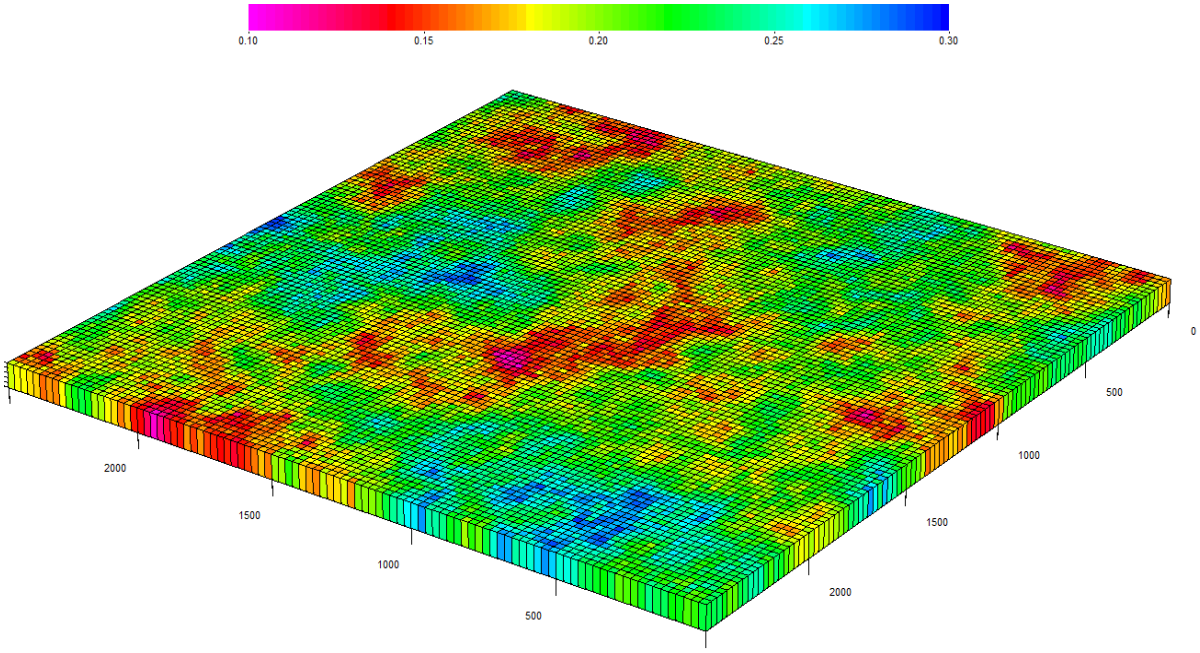

Figure 2-140: Distribution of porosity for the 2D case.

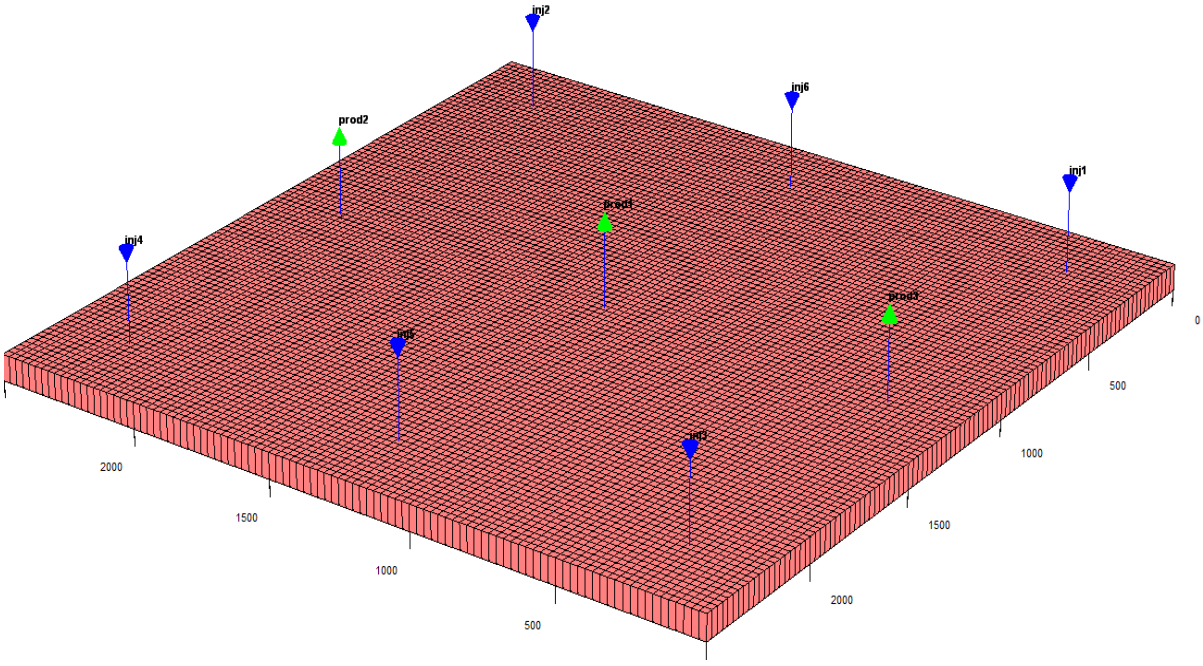

Figure 2-141: Well locations in the 2D case considered to verify the implementation of the wettability alteration module in UTCOMP.

Table 2-30: Corey's parameters of the initial set of relative permeability

Residual saturation	Water	0.25
	Oil	0.2
Exponent	Water	1.5
	Oil	2.5
Endpoint	Water	0.21
	Oil	0.7

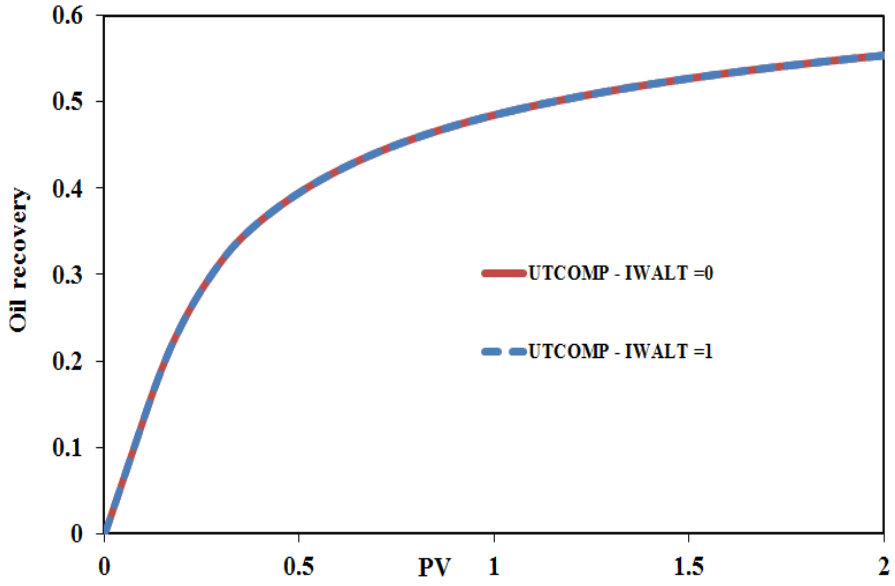

Figure 2-142: Oil recovery (verification of the wettability alteration module implemented in UTCOMP). IWALT=0: no wettability alteration is modeled; IWALT=1: wettability alteration is applied with identical initial and altered sets of relative permeabilities.

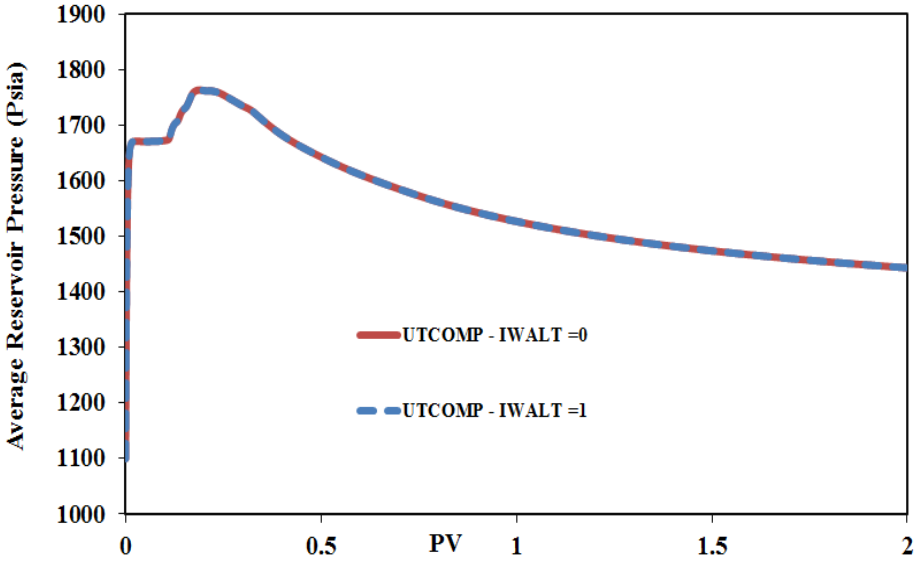

Figure 2-143: Average reservoir pressure (verification of the wettability alteration module implemented in UTCOMP). IWALT=0: no wettability alteration is modeled; IWALT=1: wettability alteration is applied with identical initial and altered sets of relative permeabilities.

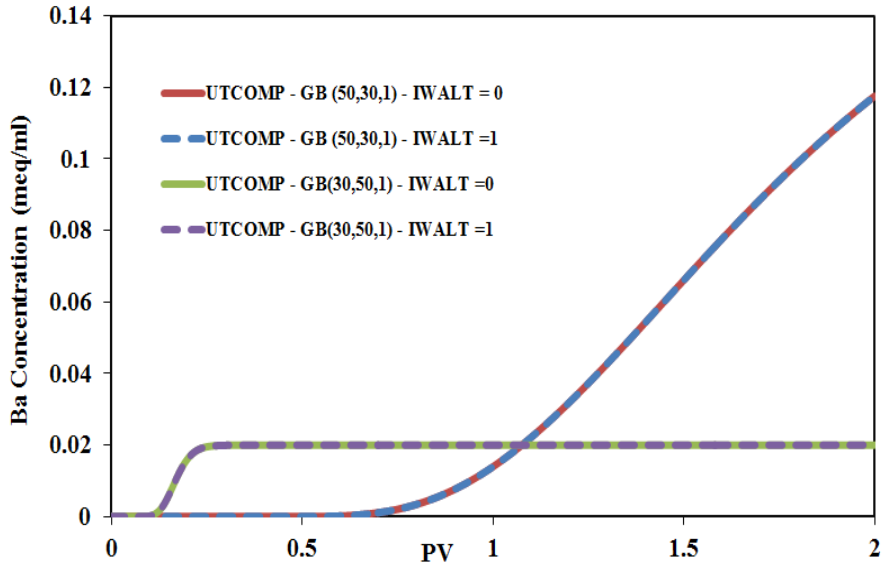

Figure 2-144: Ba concentration histories of two gridblocks (verification of the wettability alteration module implemented in UTCOMP). IWALT=0: no wettability alteration is modeled; IWALT=1: wettability alteration is applied with identical initial and altered sets of relative permeabilities.

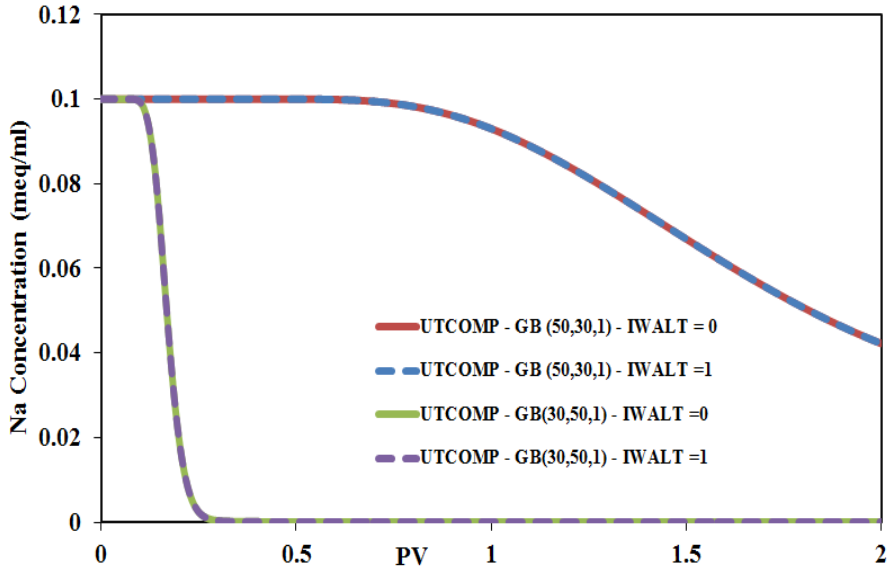

Figure 2-145: Na concentration histories of two gridblocks (verification of the wettability alteration module implemented in UTCOMP). IWALT=0: no wettability alteration is modeled; IWALT=1: wettability alteration is applied with identical initial and altered sets of relative permeabilities.

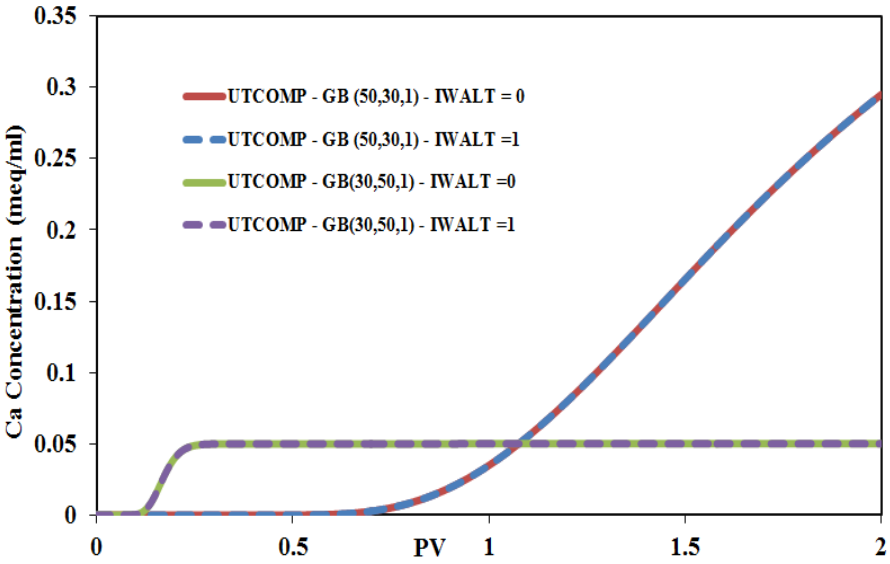

Figure 2-146: Ca concentration histories of two gridblocks (verification of the wettability alteration module implemented in UTCOMP). IWALT=0: no wettability alteration is modeled; IWALT=1: wettability alteration is applied with identical initial and altered sets of relative permeabilities.

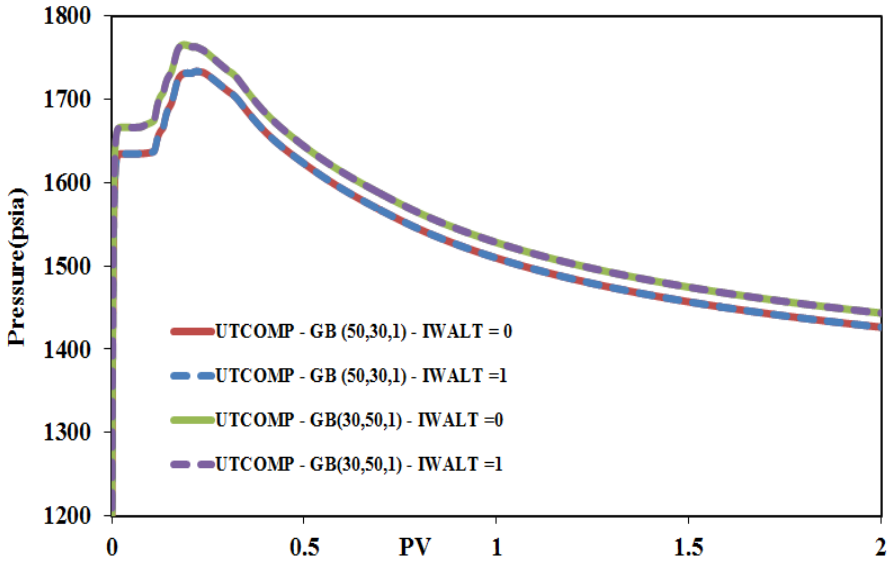

Figure 2-147: Pressure histories of two gridblocks (verification of the wettability alteration module implemented in UTCOMP). IWALT=0: no wettability alteration is modeled; IWALT=1: wettability alteration is applied with identical initial and altered sets of relative permeabilities.

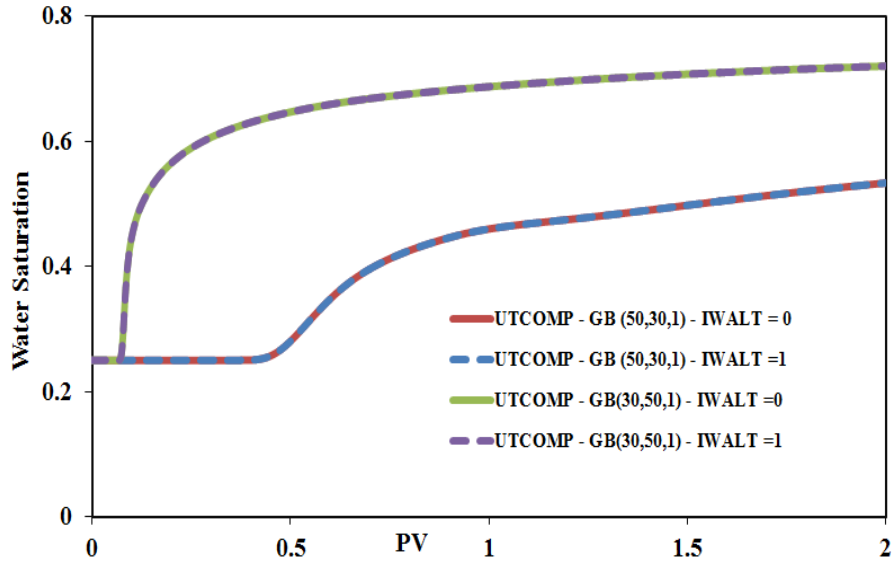

Figure 2-148: Water saturation histories of two gridblocks (verification of the wettability alteration module implemented in UTCOMP). IWALT=0: no wettability alteration is modeled; IWALT=1: wettability alteration is applied with identical initial and altered sets of relative permeabilities.

Case 2

In the second scenario; the implemented wettability alteration module in the UTCOMP-IPhreeqc integrated simulator is verified against the UTCHEM simulator. Towards this goal, the case described above (i.e., Case 1) is also designed using UTCHEM. Initial and final sets of relative permeability curves are now different. Table 2-30 and Table 2-31present the Corey's parameters for the initial and final sets of relative permeability curves, respectively (Figure 2-149 provides the plot). All the notes discussed in Section 2.2 are taken into consideration when comparing UTCHEM to UTCOMP-IPhreeqc. Moreover, because the case considered is a 2D case, the small discrepancy in terms of the oil gravity between UTCHEM and UTCOMP-IPhreeqc is eliminated (discussed in Section 2.2). The interpolating parameter is 0.5 in both UTCHEM and UTCOMP-IPhreeqc simulators. It is worth noting that in UTCHEM by default the wettability alteration with constant interpolating parameter is applied only for the surfactant flooding. Hence, we temporarily change the "wetmodel.f" routine of UTCHEM to consider the constant interpolating parameter even in the absence of the surfactant. The following presents the temporary changes applied in the UTCHEM source code:

Originally in the "wetmodel.f" routine:

```
      IF (IWALF.EQ.0) THEN
         DO 20 I = 1,NBL
            IF (CTOT(I,3).GT.EPSME) IWTHIS(I) = 1
            IF (IWTHIS(I).EQ.1) THEN
            DO 25 L = 1,NPHAS
               RPERM(I,L) = FW1*RPERMW(I,L)+(1-
FW1)*RPERM(I,L)
               PRC(I,L) = PCW1*PRCW(I,L)+(1-PCW1)*PRC(I,L)
 25          CONTINUE
            ENDIF
```

```
 20       CONTINUE
       ENDIF
```

is temporarily changed to:

```
       IF (IWALF.EQ.0) THEN
          DO 20 I = 1,NBL
CC              IF (CTOT(I,3).GT.EPSME) IWTHIS(I) = 1
CC              IF (IWTHIS(I).EQ.1) THEN
              DO 25 L = 1,NPHAS
                 RPERM(I,L) = FW1*RPERMW(I,L)+(1-
FW1)*RPERM(I,L)
                 PRC(I,L) = PCW1*PRCW(I,L)+(1-PCW1)*PRC(I,L)
 25           CONTINUE
CC             ENDIF
 20       CONTINUE
       ENDIF
```

Figures 2-150 through 2-156 verify UTCOMP-IPhreeqc results (i.e., dashed lines) against UTCHEM (i.e., solid lines) outputs. Included in these figures are also results for the case in which no wettability alteration ($\theta_1 = \theta_2 = 0$) is considered in the UTCHEM and UTCOMP-IPhreeqc simulators.

Because only three geochemical elements (i.e., Ba, Na, and Ca) are included in the two cases considered for the verification, the IPhreeqc database is modified in the way that no extra geochemical calculations are performed. This speeds up the simulation in UTCOMP-IPhreeqc to some extent.

Table 2-31: Final set of relative permeability

Residual saturation	Water	0.2
	Oil	0.1
Exponent	Water	2.5
	Oil	1.5
Endpoint	Water	0.1
	Oil	0.85

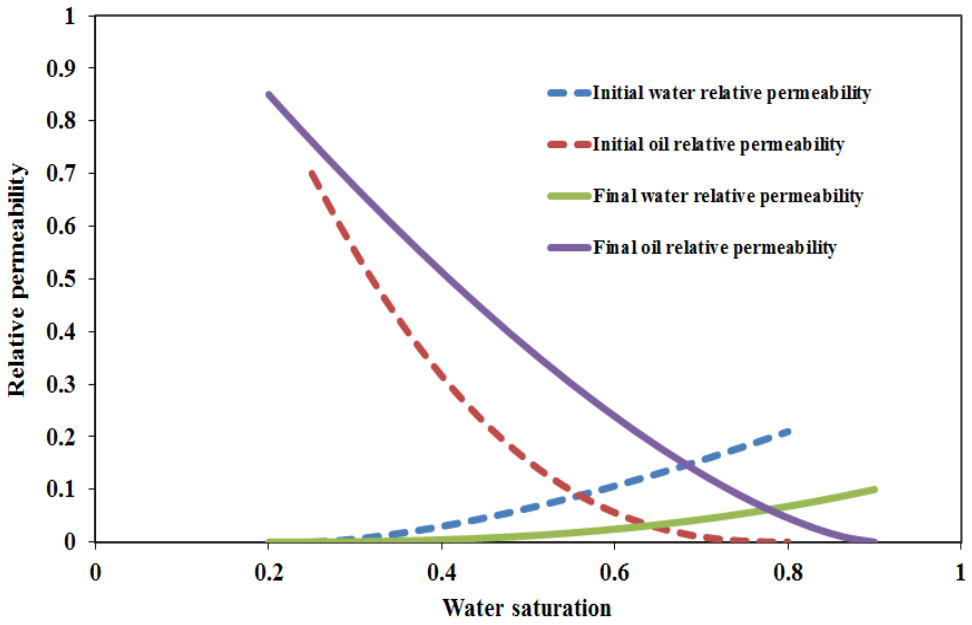

Figure 2-149: Initial (dashed lines) and final (solid lines) relative permeabilities.

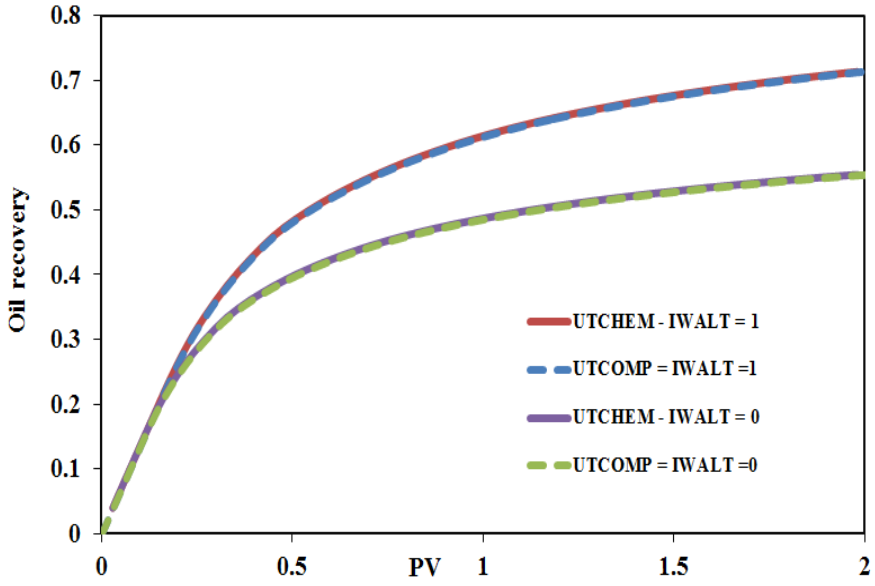

Figure 2-150: Oil recovery (verification of the wettability alteration module implemented in UTCOMP against UTCHEM). IWALT=0: no wettability alteration is modeled; IWALT=1: wettability alteration is included in the model.

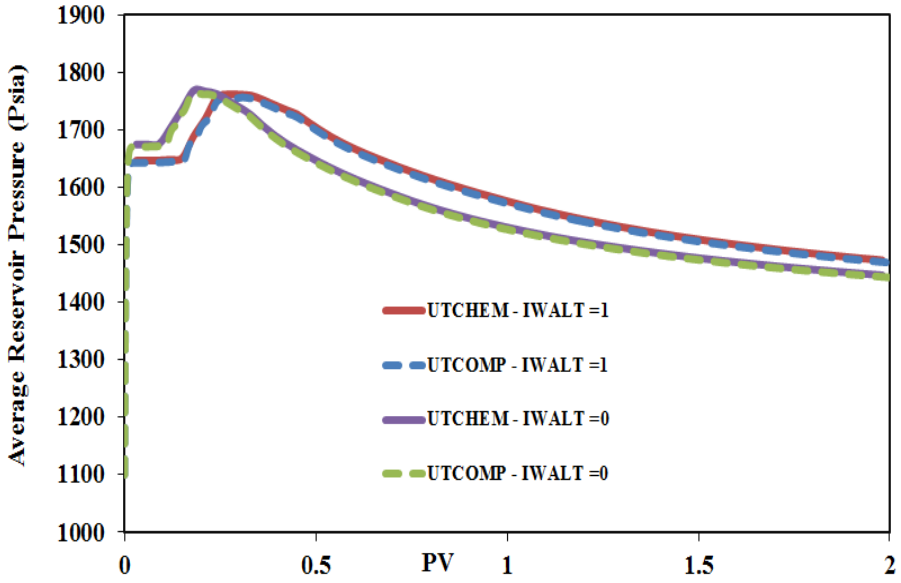

Figure 2-151: Average reservoir pressure (verification of the wettability alteration module implemented in UTCOMP against UTCHEM). IWALT=0: no wettability alteration is modeled; IWALT=1: wettability alteration is included in the model.

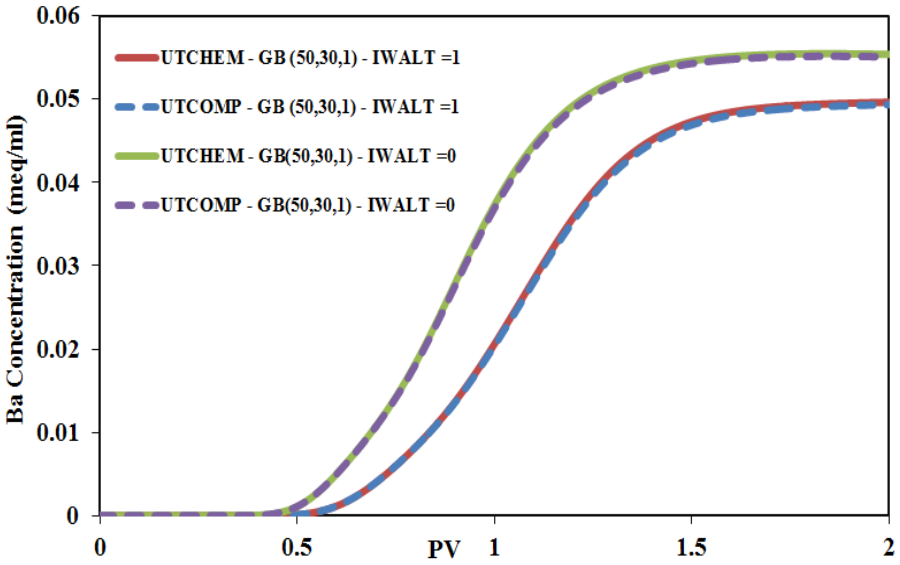

Figure 2-152: Ba concentration histories at two gridblocks (verification of the wettability alteration module implemented in UTCOMP against UTCHEM). IWALT=0: no wettability alteration is modeled; IWALT=1: wettability alteration is included in the model.

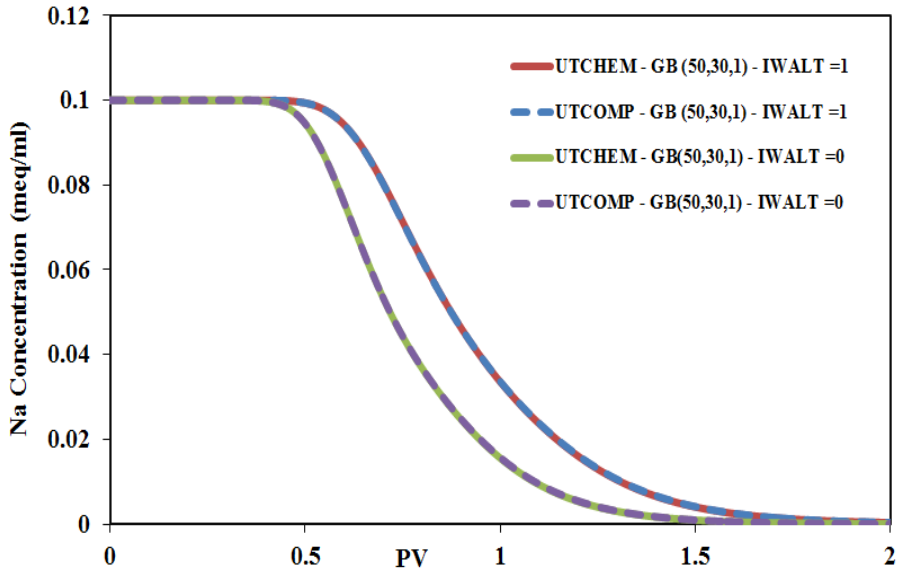

Figure 2-153: Na concentration histories at two gridblocks (verification of the wettability alteration module implemented in UTCOMP against UTCHEM). IWALT=0: no wettability alteration is modeled; IWALT=1: wettability alteration is included in the model.

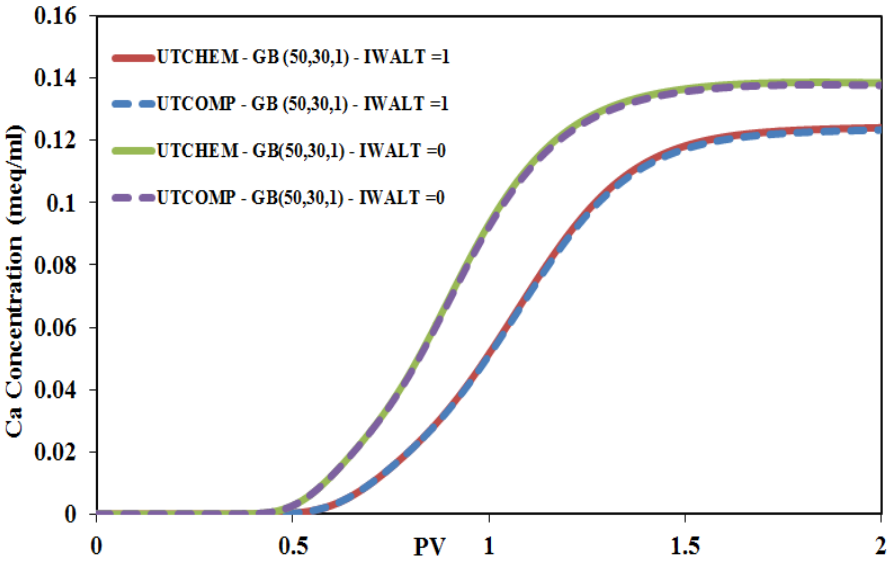

Figure 2-154: Ca concentration histories at two gridblocks (verification of the wettability alteration module implemented in UTCOMP against UTCHEM). IWALT=0: no wettability alteration is modeled; IWALT=1: wettability alteration is included in the model.

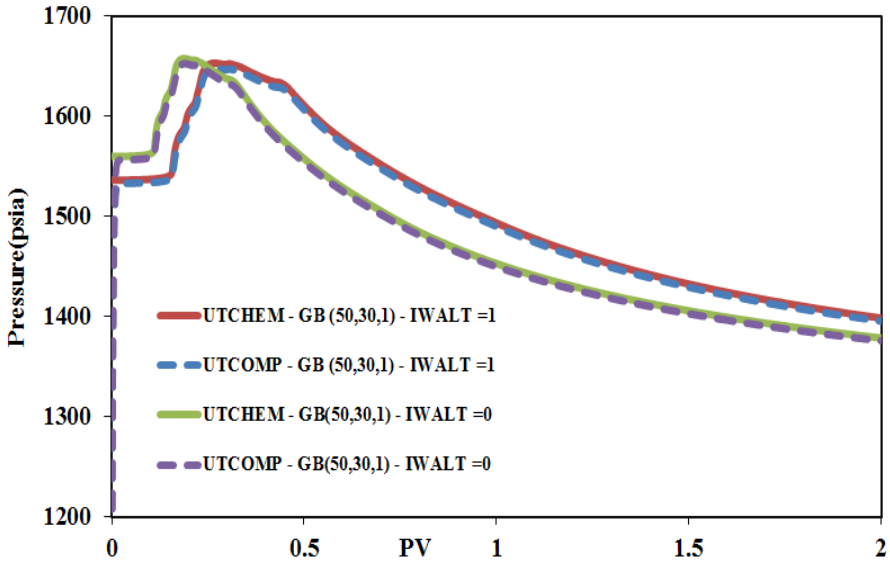

Figure 2-155: Pressure histories at two gridblocks (verification of the wettability alteration module implemented in UTCOMP against UTCHEM). IWALT=0: no wettability alteration is modeled; IWALT=1: wettability alteration is included in the model.

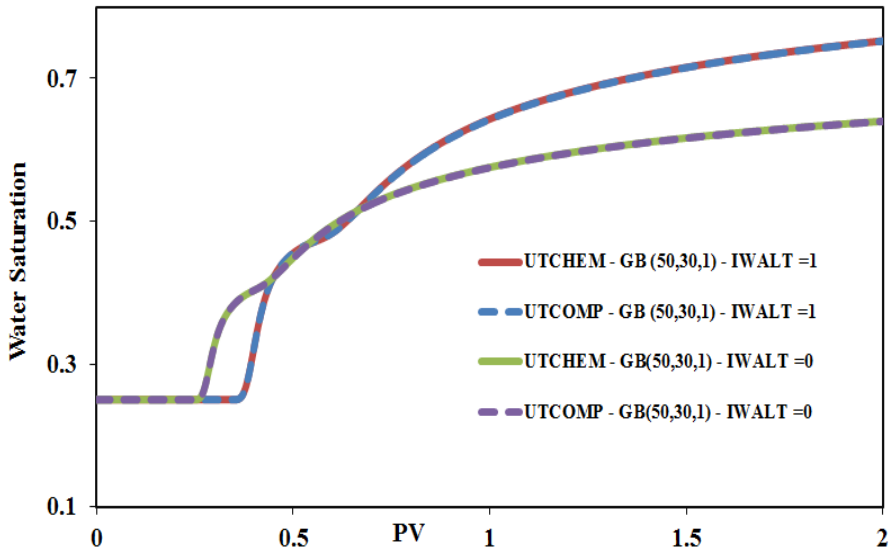

Figure 2-156: Water saturation histories at two gridblocks (verification of the wettability alteration module implemented in UTCOMP against UTCHEM). IWALT=0: no wettability alteration is modeled; IWALT=1: wettability alteration is included in the model.

2.12 PARALLELIZATION OF THE UTCOMP-IPHREEQC HYDROCARBON-AQUEOUS PHASE COMPOSITION CALCULATION MODULE

IPhreeqc is a complete geochemical package that overcomes all the EQBATCH limitations for comprehensive reactive-transport modeling. However, although an efficient algorithm was followed to couple IPhreeqc with UTCOMP, using IPhreeqc for geochemical calculations requires more computational time for the simulation. The increase in CPU time in UTCOMP-IPhreeqc is consistent with that of PHAST where the required computational time for the geochemistry calculation is at least twice of the total time spent on other calculations (i.e., flow and transport) (Parkhurst *et al.*, 2010). To tackle this issue and enhance UTCOMP-IPhreeqc to large-scale reservoir simulation, we parallelize the geochemistry module of this integrated simulator.

Figure 2-157 illustrates the computational algorithm applied in PHAST (Parkhurst *et al.*, 2010). In this computational algorithm, multiple computing processors (or simply "processors") are initialized at the beginning of the simulation. However, except the geochemistry section in which the task is distributed among the processors (master and slave processors), master processor performs all the other calculations including solving the pressure matrix, mass conservation equation, and reporting the output results.

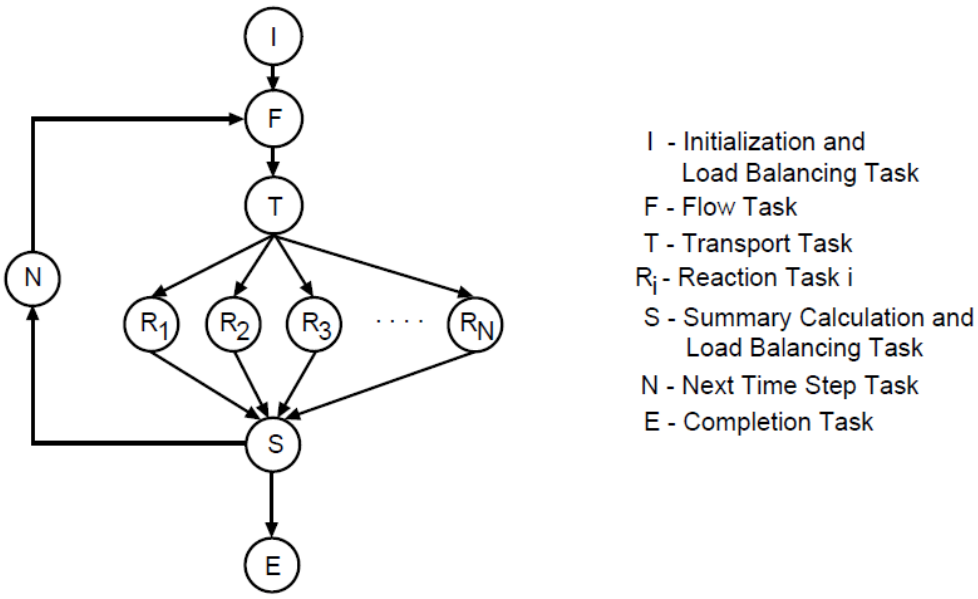

Figure 2-157: Computational algorithm of parallel-processing version of PHAST (Parkhurst *et al.*, 2010)

We apply the similar approach to parallelize the phase composition calculation (aqueous and hydrocarbon) module in UTCOMP-IPhreeqc. Massage Passing Interface (MPI) (Barney, 2009) is used as the parallel processing interface. MPI_INIT, MPI_COMM_RANK, and MPI_COMM_SIZE available in MPI are applied to initialize and assigning the ranks to the processors. Master processor (processor with the rank 0 is

considered as the master processor) performs the entire calculations such as reading the input files, allocating the variables, setting up the pressure matrix, solving the pressure matrix, and calculating the total moles of the hydrocarbon and geochemical species (i.e., solving the mass conservation equation) till it reaches the phase composition calculation module. Within the time period that the master processor performs the calculations, all the other processors (i.e., slave processors) have skipped the calculations and are waiting for the master processor before getting into the geochemistry module. MPI_BARRIER of MPI is used to block the slave processors until the master processor reaches the routine. Once the master processor joins the slave processors, it shares the updated geochemistry data (MPI_SEND and MPI_RECV of MPI are used for sharing the data among the processors) and then all the processors (including the master processor) perform the thermodynamic calculation of the phases for certain number of gridblocks. It should be noted that some of the data is transferred from the master processor to the slave ones once and only in the first time step; however, there are some data that needs to be updated in the slave processors at each time step. For example, number of geochemical elements involved in the simulation is constant during the simulation. Hence, the master processor sends the number of geochemical species to the slave processors in the first time step. On the other hand, total moles of the geochemical species in each gridblock are updated at each time step by solving the mass conservation equation. Hence, we need to update the total moles of the geochemical elements in the slave processors at each time step. This will be discussed with more details later.

Another point is the number gridblocks assigned to each computing processor. If the number of gridblocks is divisible by the number of processors, then equal number of gridblocks is assigned for each processor. Otherwise, some processors have an extra

gridblock for thermodynamic calculations. For example, if the number of gridblocks and the number of processors (including the master processor) are 100 and 7, respectively; in the geochemistry module, two processors perform the calculations for 15 gridblocks and the other 5 processors have 14 gridblocks for the calculation. The reason for having this flexibility is the fact that when evaluating the thermodynamic equilibrium of either aqueous or hydrocarbon phase, reservoir gridblocks are independent and treated as batch cells.

All the computing processors call the same routines for phase composition calculations (either hydrocarbon or the aqueous phase). "Do loops" in these routines are all from 1 to NB where NB is the local number of gridblocks in each processor. We change the number of gridblocks in the master processor to the local value before it starts the phase composition calculation. Number of gridblocks in the master processor is returned back to the main number of gridblocks when it finishes with the phase composition calculations.

Computational times required for the thermodynamic calculations of gridblocks are not identical. Some gridblocks require more iterations in IPhreeqc or between UTCOMP and IPhreeqc (based on the algorithm shown in Figure 2-56) to converge to the solution. Hence, the total computational time that takes for each processor to finish the phase composition calculations of its entire assigned gridblocks might not be the same for all the processors. However, if a processor finishes the calculations sooner compared with other processors, it should wait for other processors to finish their tasks as well. When all the processors are done with their calculations, the equilibrium data of the gridblocks assigned to the slave processors are transferred to the master processor. Slave processors

are now free and will be waiting for the master processor to perform the rest of calculations and reach the phase composition calculation module again.

2.12.1 Parallelization of the UTCOMP-IPhreeqc Hydrocarbon Phase Composition Calculation Module

As shown in Figure 2-56, if the effect of the hydrocarbon phase on the aqueous-rock geochemistry is included in the model, UTCOMP-IPhreeqc follows a sequential iterative scheme between the hydrocarbon flash calculation of UTCOMP and the aqueous phase flash calculation of IPhreeqc (finding the equilibrium state of the aqueous is a kind of flash calculation in the aqueous phase). The sequential iterative algorithm is followed to make fugacities identical (within a desired tolerance) among the phases. If multiple processors are applied, the same solution scheme should be applied in each processor. Hence, the hydrocarbon flash calculation module of UTCOMP should be also parallelized along with the IPhreeqc coupling related routines. If the effect of the hydrocarbon phase on the aqueous-rock geochemistry is not included in the model, parallelization is applied only for the phase composition calculation of the aqueous phase and no longer for the hydrocarbon phase. Hence, in this case the entire hydrocarbon flash calculations are performed by the master processor.

To parallelize the hydrocarbon flash calculation module of UTCOMP-IPhreeqc, the thermodynamic properties of hydrocarbon components that remain unchanged during the simulation, such as T_c (critical temperature), P_c (critical pressure), V_c (critical volume), and ω (acentric factor), are shared with the slave processors by the master processor only at the first time step. On the other hand, total moles of the hydrocarbon components are transferred from the master processor to the slave processor in each time step. When all the processors finish the hydrocarbon phase behavior calculation, the slave

processors send the equilibrium data of their local gridblocks to the master processor. These data are: number of phases in each gridblock, component compositions of the phases, phase compressibility factors, and phase mole ratios.

A synthetic case is designed to verify the procedure through which we parallelized the hydrocarbon phase behavior module of UTCOMP-IPhreeqc. The geochemistry option is set zero (IGEOCHEM = 0 in the UTCOMP input file) in this case. Tables 2-32 and 2-33 show case descriptions and the initial overall mole fraction of the hydrocarbon components, respectively. This case is a homogeneous quarter five-spot pattern (see Figure 2-158) with one well at a corner injecting 5 MMScf/day mixture of C_1-C_3 (0.8-0.2 overall mole fraction) and the other well at the opposite corner producing from the reservoir at the constant bottomhole pressure of 3100.0 psi. Figures 2-159 through 2-162 show oil recovery, average reservoir pressure, and gas and oil surface production rates when different number of computing processors is used. Figures 2-163 and 2-164 show oil and gas saturation maps of the first layer at 0.1 PV using 1, 6, and 10 processors. As Figures 2-159 through 2-164 demonstrate, results are in very good agreements when different number processors are applied for the hydrocarbon phase behavior calculation. Table 2-34 presents the computational time spent in the hydrocarbon flash calculation module and also the total computational time using different number of processors. Simulations are run on two different clusters of processors (i.e., TACC-Lonestar cluster and PETROS). TACC (Texas Advanced Computing Center) is a high performance computing center owned by The University of Texas at Austin. Lonestar has 1888 compute nodes with two 6-cores per node (22656 CPU cores in total). Each node in the Lonestar 64-bit has 24 gigabytes memory with the frequency of the cores (clock-speed) of 3.33 GHz (TACC, 2014). PETROS is the Unix-

based in-house cluster of processors in the Petroleum and Geosystems Engineering (PGE) department of The University of Texas at Austin. PETROS has 32 compute nodes with 4 processors (128 CPU cores in total) with the frequency of 2.73 GHz in each node. Each computing nodes in PETROS has 16 gigabytes of memory.

Figure 2-165 presents the total computational time and the time spent in the phase behavior calculation module (CPU times obtained from TACC are used). Speedup plot is provided in Figure 2-166. Speedup is computational time using one processor over the computational time for the parallel run (using multiple processors).

Table 2-32: Reservoir characteristics for the 3D case

No. of gridblocks		9600 (40×40×6)	
Δx(ft)		75.0	
Δy(ft)		75.0	
Δz(ft)		50.0	
Permeability (md)	*x*-direction	100.0	
	y-direction	100.0	
	z-direction	100.0	
Porosity		0.3	
Rock compressibility (psi^{-1})		50.0×10^{-6}	
Water compressibility (psi^{-1})		3.0×10^{-6}	
Initial water saturation		0.25	
Irreducible water saturation		0.25	
Reservoir temperature (^{o}F)		150.0	
Initial pressure (psi)		3100.0	
Reservoir depth (ft)		0.	
Water viscosity (cp)		1.0	
Number of wells		2	1 injector
			1producer
Simulation time(PV)		1.0	

Table 2-33: Overall mole fraction of initial and injected hydrocarbon components

Component	$Z_{initial}$	$Z_{injected}$
C_1	0.5	0.8
C_3	0.03	0.2
C_6	0.07	-
C_{10}	0.2	-
C_{15}	0.15	-
C_{20}	0.05	-

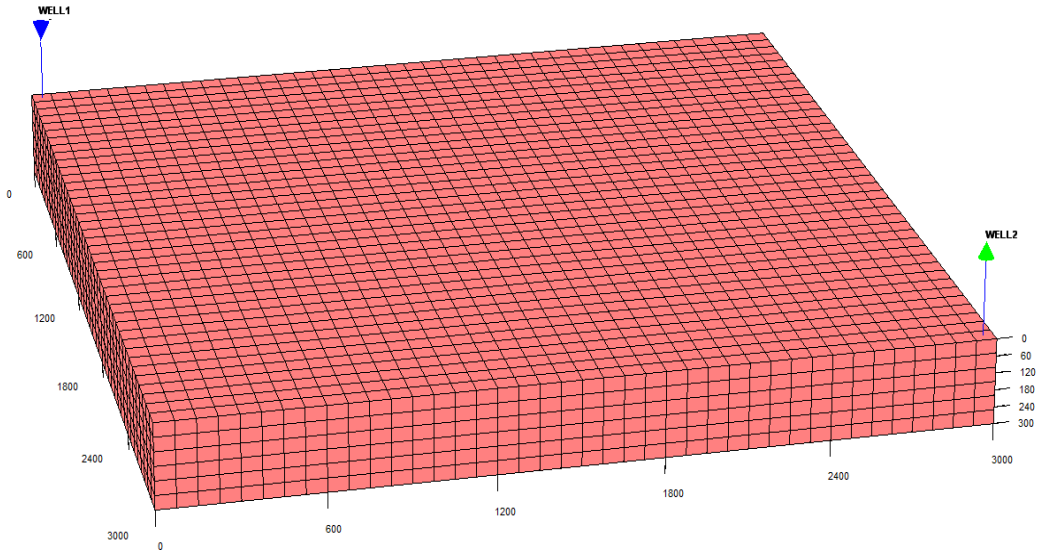

Figure 2-158: Well locations in the 3D case considered to verify the parallelization of the hydrocarbon phase behavior calculation in UTCOMP.

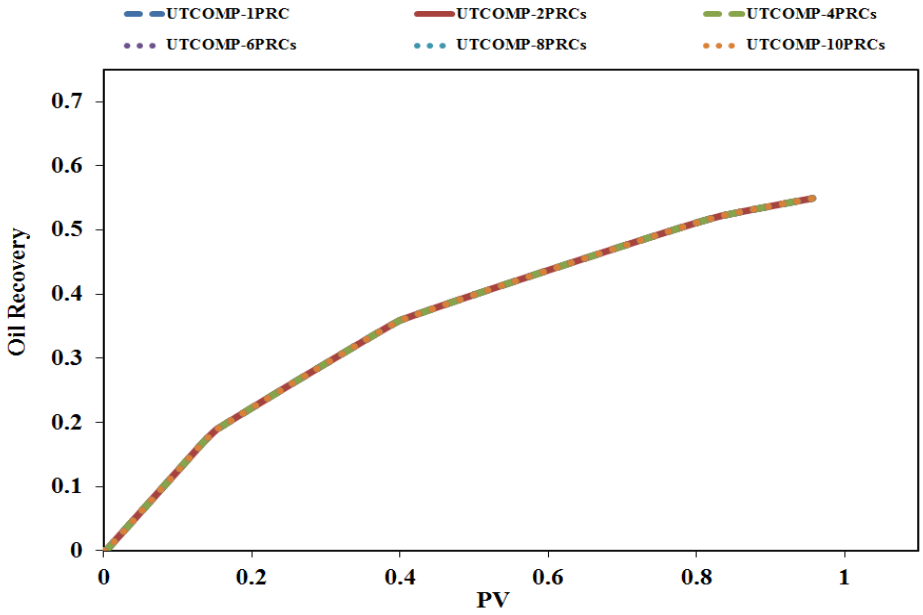

Figure 2-159: Oil recovery (using UTCOMP-IPhreeqc with multiple processors for the hydrocarbon phase composition calculations).

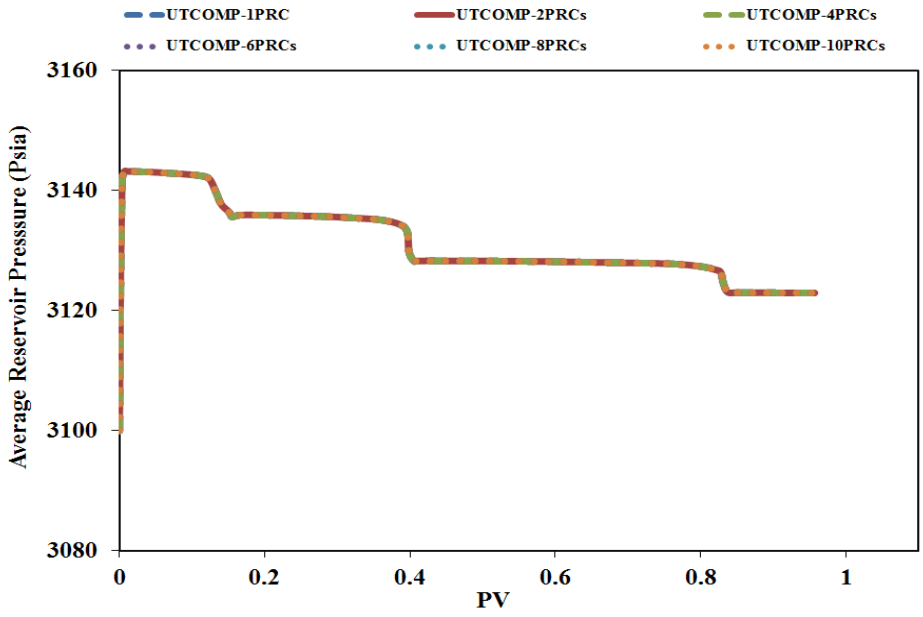

Figure 2-160: Average reservoir pressure (using UTCOMP-IPhreeqc with multiple processors for the hydrocarbon phase composition calculations).

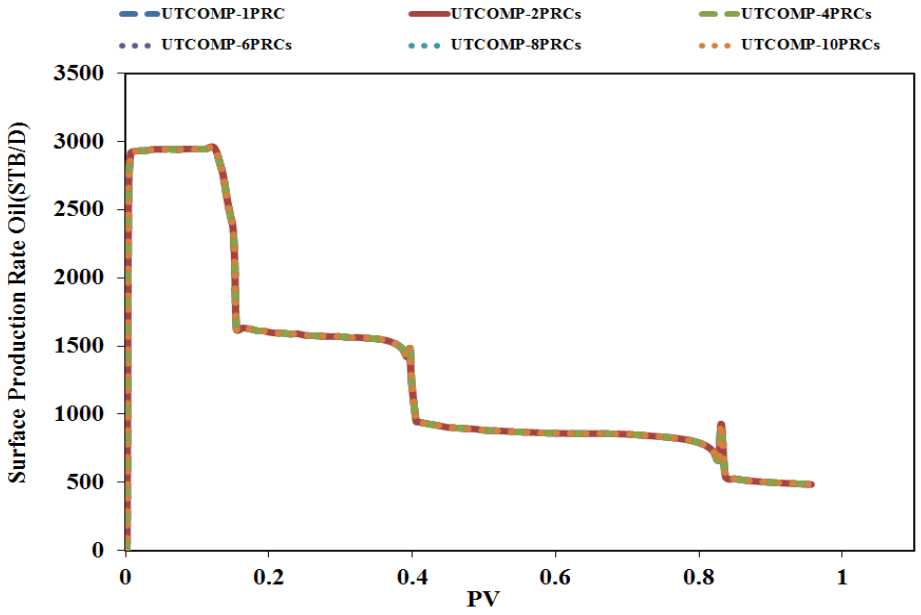

Figure 2-161: Oil surface production rate (using UTCOMP-IPhreeqc with multiple processors for the hydrocarbon phase composition calculations).

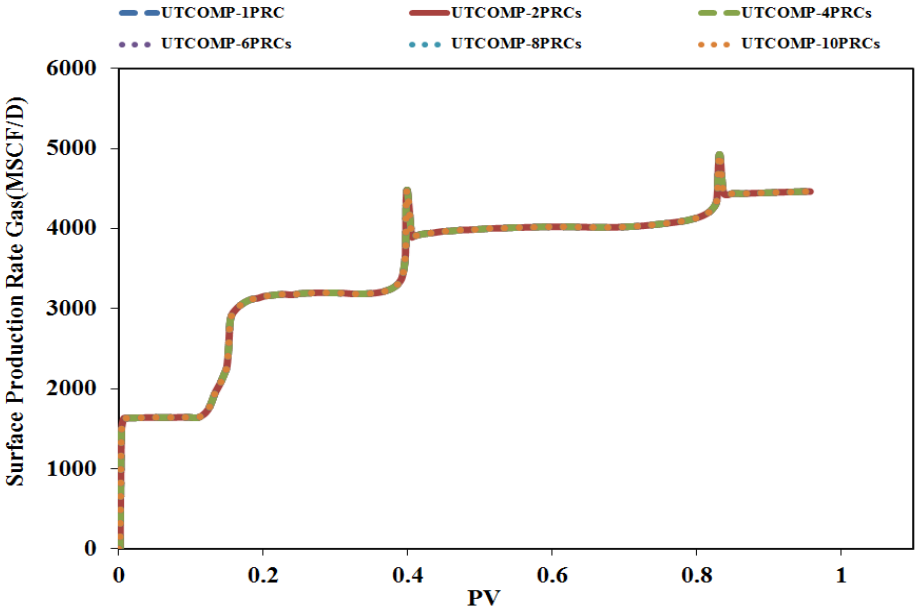

Figure 2-162: Gas surface production rate (using UTCOMP-IPhreeqc with multiple processors for the hydrocarbon phase composition calculations).

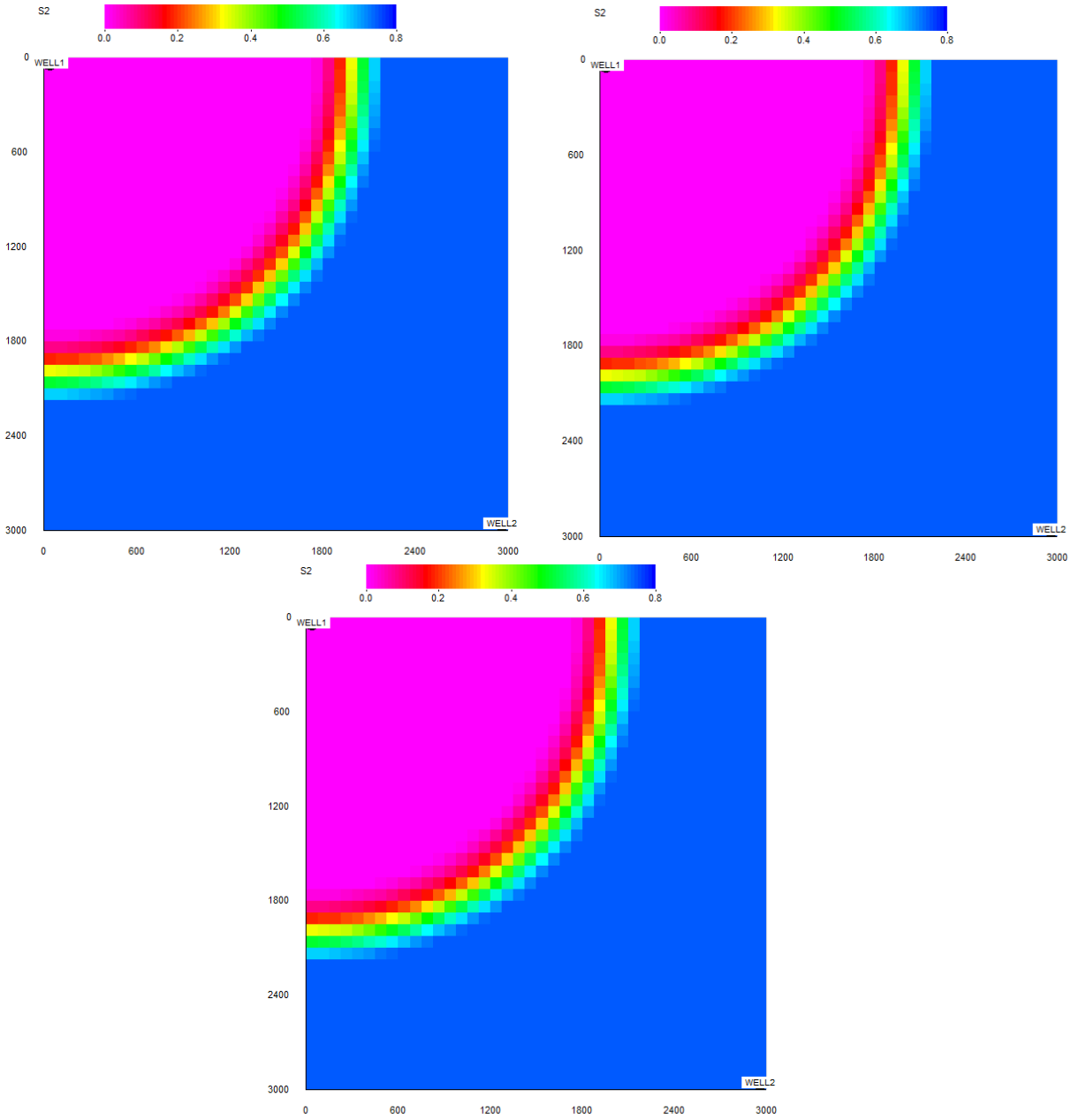

Figure 2-163: Oil saturation map of the first layer at 0.1 PV (using UTCOMP-IPhreeqc with 1 processor (top-left panel), 6 processors (top-right panel), and 10 processors (bottom panel) for the hydrocarbon phase composition calculations).

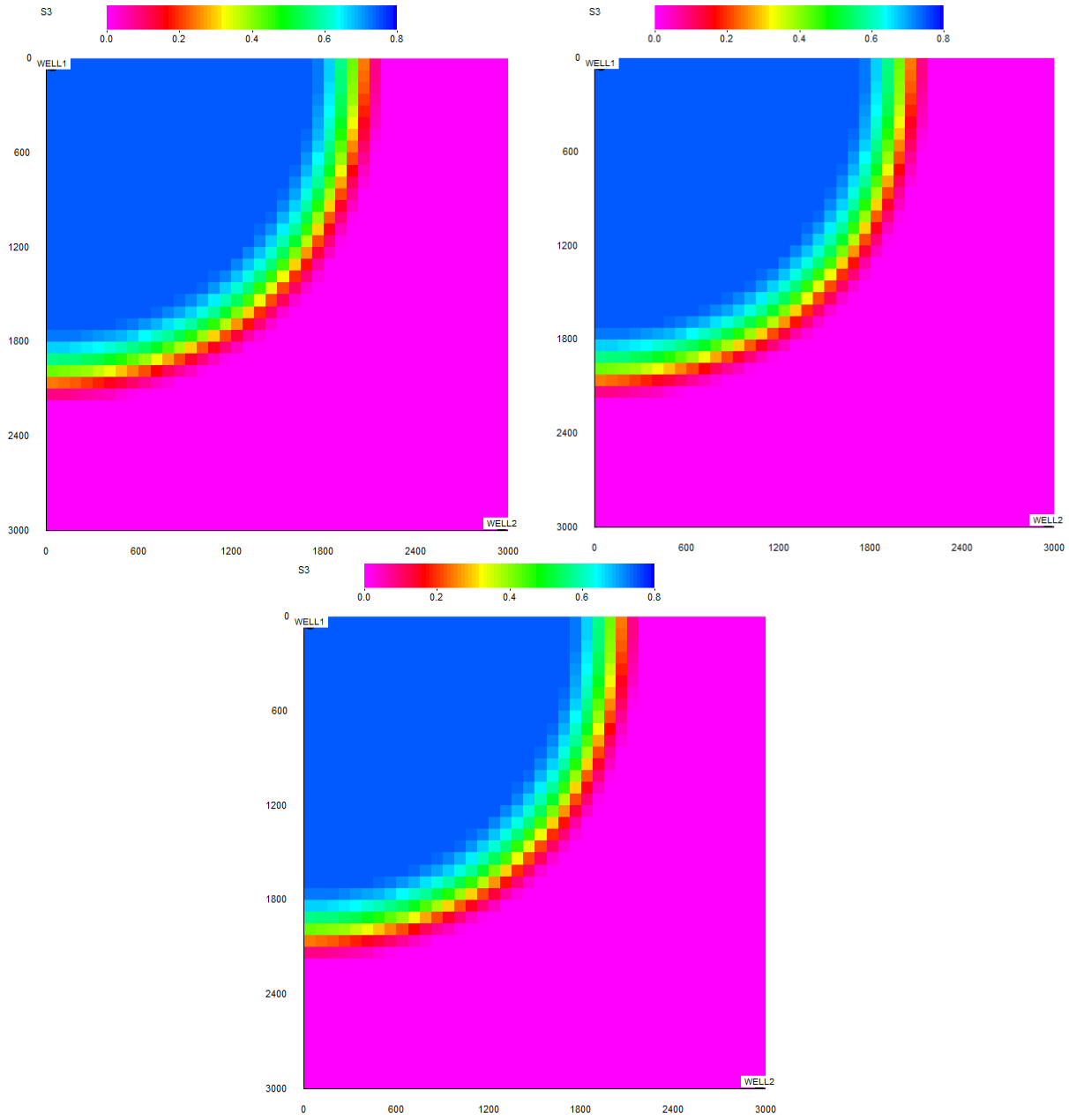

Figure 2-164: Gas saturation map of the first layer at 0.1 PV (using UTCOMP-IPhreeqc with 1 processor (top-left panel), 6 processors (top-right panel), and 10 processors (bottom panel) for the hydrocarbon phase composition calculations).

Table 2-34: Total computational time and the time spent for the hydrocarbon phase composition calculations

	PETROS		TACC-Lonestar	
No. of Processor(s) in UTCOMP	Phase behavior computational time (seconds)	Total computational time (seconds)	Phase behavior computational time (seconds)	Total computational time (seconds)
1PRC	2450.04	4730.21	1512.07	2233.0
2PRCs	1352.1	3625.82	792.27	1514.0
4PRCs	756.5	3000.37	433.69	1155.0
6PRCs	700.28	2817.06	311.80	1034.0
8PRCs	660.13	2888.86	249.93	971.0
10PRCs	756.05	3031.51	227.34	972.0

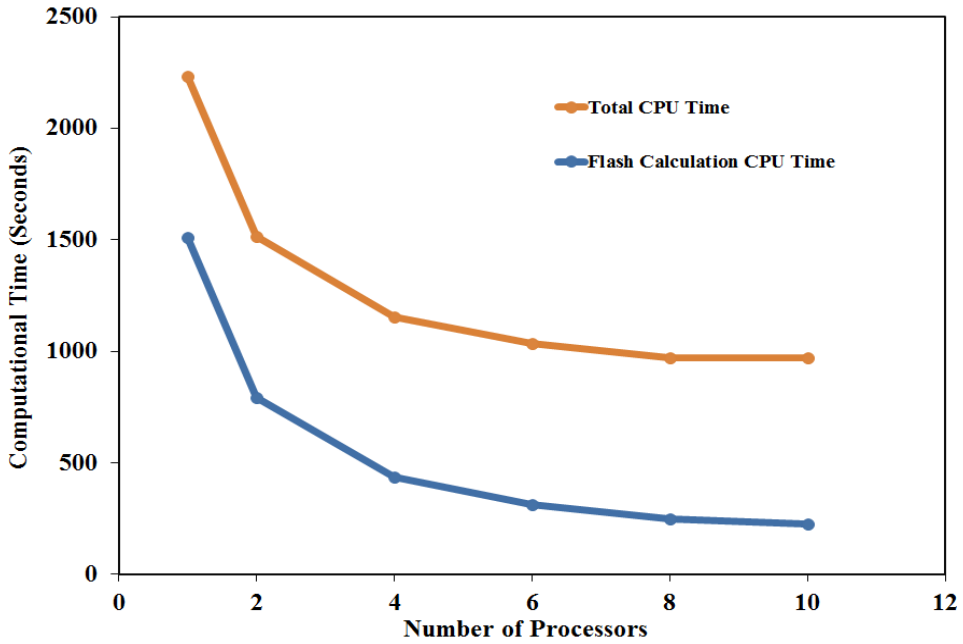

Figure 2-165: Total computational time and the time spent for the hydrocarbon phase composition calculations versus number of processors.

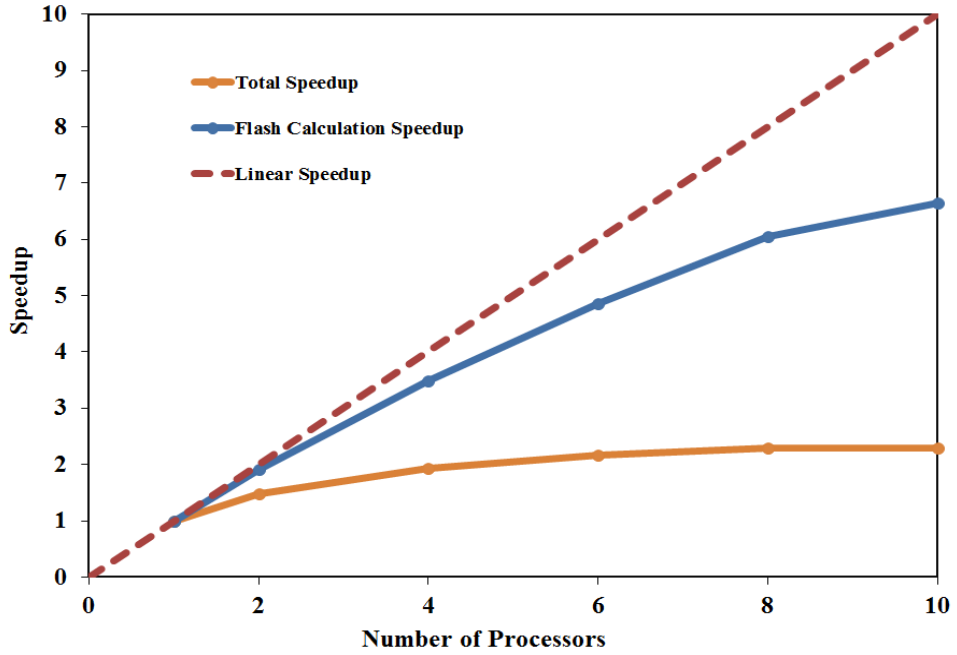

Figure 2-166: Speedup curve for the total simulation and hydrocarbon phase composition calculations versus number of processors.

Using robust solvers for parallel processing is highly recommended. PETSc (Portable Extensible Toolkit for Scientific computation) (Brown, 2010) is applied over the two UTCOMP solvers based on biconjucate gradient algorithm (i.e., IPRESS=3 in the UTCOMP input file) and biconjucate gradient squared algorithm (i.e., IPRESS=4 in the UTCOMP input file). PETSc is a comprehensive package for solving the linear and non-linear system of equations and has been developed in the Argonne National Laboratory (Brown, 2010).

2.12.2 Parallelization of the UTCOMP-IPhreeqc Aqueous Phase Composition Calculation Module

IPhreeqc (Charlton and Parkhurst, 2011) has been designed very intelligently making the parallelization straightforward. IPhreeqc modules are independent; hence,

each processor has its own IPhreeqc module and performs part of geochemical calculation tasks of the aqueous phase (Parkhurst and Appelo, 2011). What follows below presents the procedure through which we parallelized the aqueous phase composition calculation module in UTCOMP-IPhreeqc.

At the first time step all the slave processors create their own IPhreeqc modules using *CreateIPhreeqc* method of IPhreeqc. Subsequently slave processors load the IPhreeqc thermodynamic database using *LoadDatabase*. The geochemistry information of the entire gridblocks is then accumulated in the slave processors (i.e., IPhreeqc_INPUT.DAT is stored in the memory of processors using *AccumulateLine* and **INCLUDE$**). Each processor keeps the information of its assigned gridblocks; information of the extra gridblocks is deleted from the processors (using **DELETE** available in IPhreeqc). The master processor distributes the total moles of geochemical elements (to be used along with **SOLUTION_MODIFY** for each gridblock), mole fraction of the geochemical species in the aqueous phase, water saturations, and pressures among the slave processors at each time step. Appendix F provides the parallel version of the simplified code previously presented in Appendix C. Included in Appendix F is also a sample case study that verifies the parallel version of the simplified code using different number of processors.

Hereafter in this dissertation "the parallel version of UTCOMP-IPhreeqc" and, later in Chapter 5, "the parallel version of UTCHEM-IPhreeqc" mean the UTCOMP-IPhreeqc and UTCHEM-IPhreeqc simulators which are parallel in only the phase composition calculations (hydrocarbon and aqueous phases).

Verification of the Parallel version of UTCOMP-IPhreeqc

Several case studies (1D, 2D, and 3D) are presented below that show the benefits in terms of the computational time due to the parallelization of the phase composition calculation in the UTCOMP-IPhreeqc simulator. For all the cases presented below Na^{+}, Ca^{+2}, Cl^{-}, SO_4^{-2}, HSO_4^{-1}, $CaSO_4$, Ba^{+2}, HCO_3^{-1}, Fe^{+2}, Mg^{+2}, Sr^{+2}, and pH histories were verified when different number of processors is applied. However, only pH value (representative of an ion (i.e., H^{+}) with small concentration) and chloride concentrations (representative of a non-reacting ion or a tracer-like geochemical species) are presented.

All simulations presented below were run on Lonestar cluster of TACC (see Section 2.12.1 for TACC characteristics). The upper limit for the jobs submitted to TACC is 24 hours. Hence, for simulation runs that take more than 24 hours, the UTCOMP-IPhreeqc restart option (cf. Section 2.13) is used to resume the simulation. The restart files are stored each 500 time steps. We believe that using the restart option should not introduce more than 5% error in the computational times.

1D Case Studies

Case 1

A 1D case with 100 gridblocks (see Figure 2-167) is designed using the parallel version of the UTCOMP-IPhreeqc simulator. The case descriptions are shown in Table 2-35. Calcite and dolomite are the solids present in the system. Saturation indices for these solids are -0.4 and 0.4, respectively. The pitzer.dat database of IPhreeqc is used in this simulation. About 0.5 of the "SW/50" is injected first and then chased with 0.6 PV of the "FB" (formation water). Table 2-36 presents ion compositions for the "SW/50" and "FB" waters. Injection flowrate is constant and equal to 4×10^{-5} bbl/day and the production well is operating with the constant bottomhole pressure of 4890 psi.

This simulation is performed using UTCOMP-IPhreeqc with 1, 2, 4, 6, 8, and 10 processors. Histories of the chloride ion and pH produced from the core are shown in Figures 2-168 and 2-169, respectively. We obtain identical results for arbitrary number of processors. Table 2-37 shows the total computational time and time spent solely in the geochemistry module versus the number of processors and Figure 2-170 gives the plot. Figure 2-171 illustrates the speedup plot.

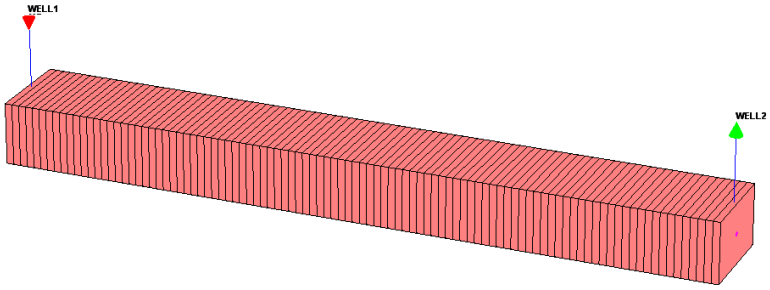

Figure 2-167: 1D case with 100 gridblocks (1 injector and 1 producer).

Table 2-35: Case descriptions for the 1D Case

No. of gridblocks		100 (100×1×1)
Δx(ft)		0.04
Δy(ft)		0.15
Δz(ft)		0.15
Permeability (md)	*x*-direction	100
Porosity		0.25
Rock compressibility (psi^{-1})		0.
Water compressibility (psi^{-1})		0.
Initial water saturation		0.999
Irreducible water saturation		0.05
Reservoir temperature (^oF)		212.0
Initial pressure (psi)		4890.0
Reservoir depth (ft)		0.
Water viscosity (cp)		0.79
Number of wells	2	1 injector
		1 producer
Simulation time(PV)		1.1

Table 2-36: Formation brine (FB) and SW/50 ion concentrations (from Chandrasekhar, 2013)

Ion	Formation brine (FB) (ppm)	SW/50 (ppm)
Na^{+}	49933	274
Mg^{+2}	3248	32.4
Ca^{+2}	14501	10.42
Cl^{-}	111810	489.36
SO_4^{-2}	234	66.2
HCO_3^{-}	-	-
Ionic strength (mol/kgw)	3.658	0.017
TDS (mg/L)	179730	872

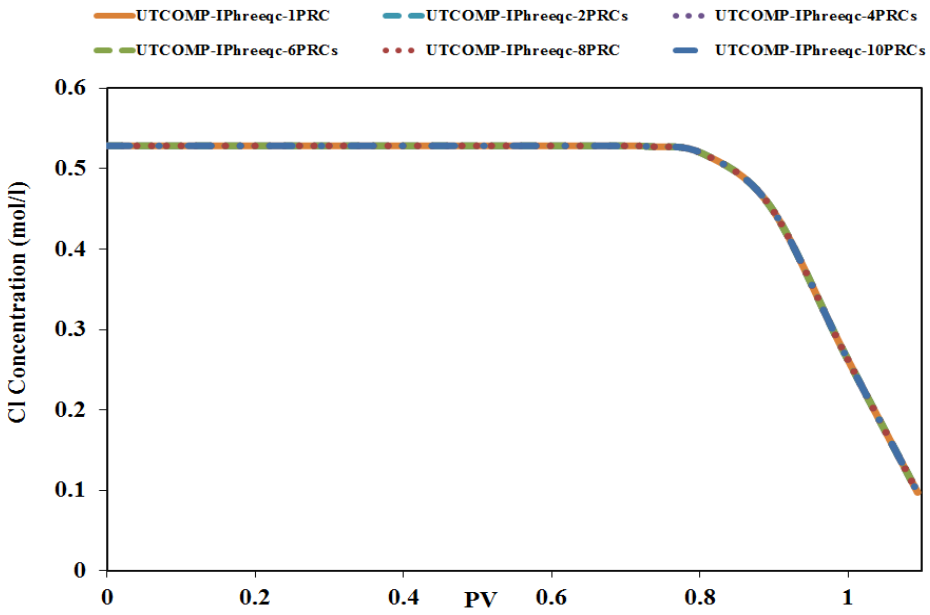

Figure 2-168: Case 1- produced chloride concentration history (using UTCOMP-IPhreeqc with multiple processors for geochemical calculations).

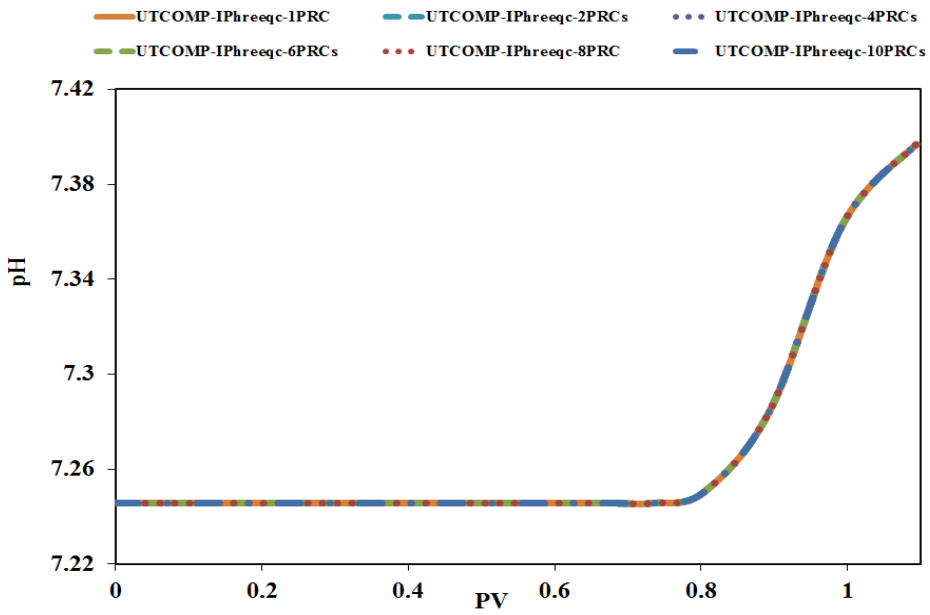

Figure 2-169: Case 1- produced pH history (using UTCOMP-IPhreeqc with multiple processors for geochemical calculations).

Table 2-37: Case 1- total computational time and the time spent for the aqueous composition calculations

No. of processor(s) in UTCOMP-IPhreeqc	CPU time spent in geochemistry (seconds)	Total computational time (seconds)
1PRC	194.8279	199
2PRCs	109.3308	112
4PRCs	64.33192	68
6PRCs	51.05515	54
8PRCs	44.24679	48
10PRCs	41.31858	44

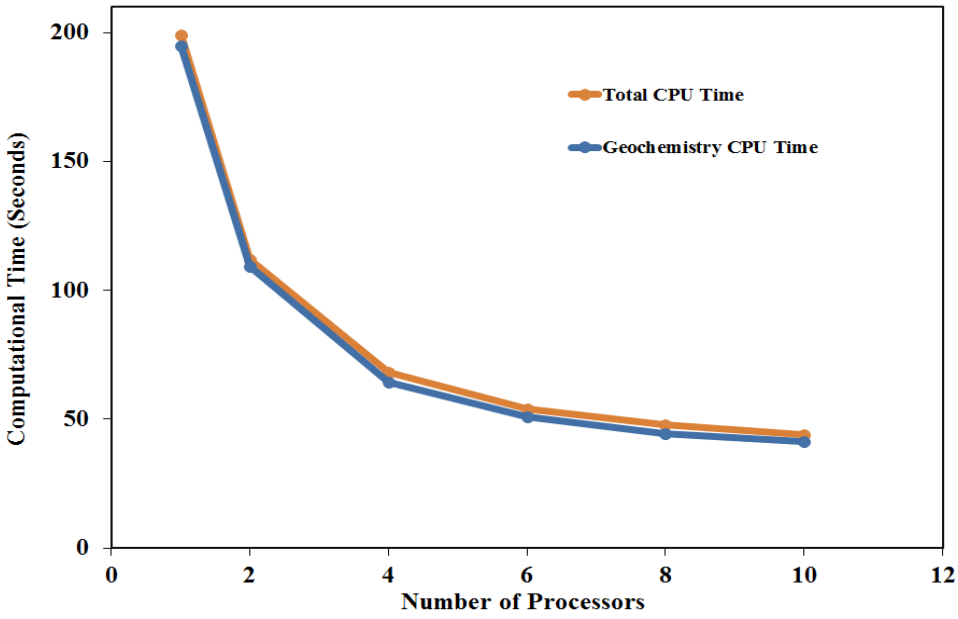

Figure 2-170: Case 1- total computational time and the time spent for the aqueous composition calculations versus number of processors.

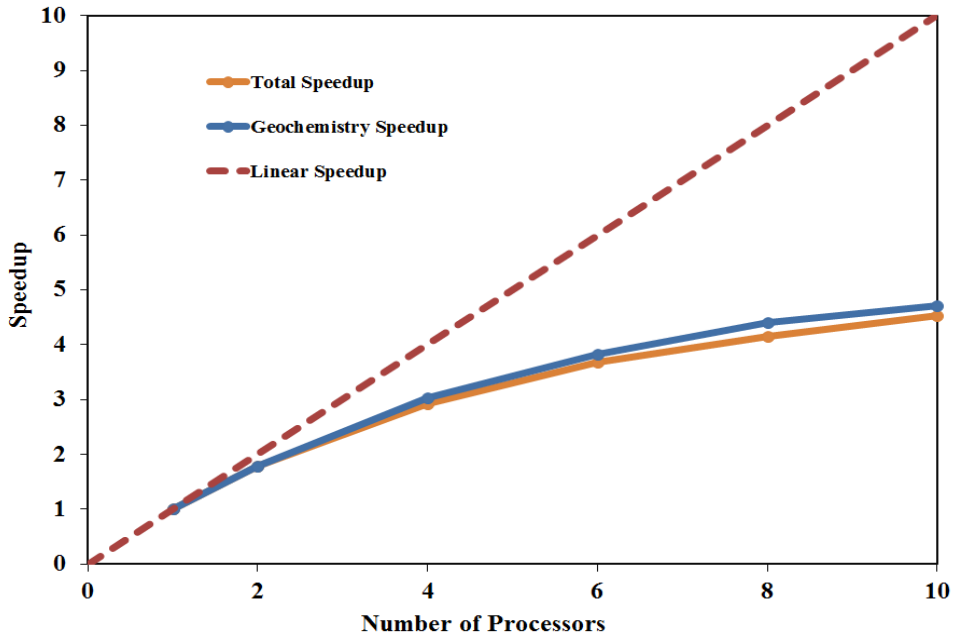

Figure 2-171: Case 1- speedup curve for the total simulation and aqueous phase composition calculations versus number of processors.

Computational time for modeling a reactive-transport problem using UTCOMP-IPhreeqc highly depends on the initial and injecting aqueous ion compositions and number of gridblocks. To confirm this, two different scenarios are modeled. In the first scenario, Case 1 is considered and number of gridblocks is increased to 1000 (i.e., Case 2). In the second scenario, both 100 and 1000 gridblocks are run using the Endicott water ion compositions (i.e., Cases 3 and 4).

Case 2

Case 2 is identical to the Case 1 except the number of gridblocks in this case is 1000 (we enlarge Case 1 rather than refining it). Table 2-38 shows the total computational time and the time spent for geochemical calculations. Figure 2-172 presents the plot of computational times versus the number of processors. Speedup is shown in Figure 2-173. The computational times reported in Table 2-37 should not be directly compared with those of Table 2-38. Because, although the injection rate in Case 1 and Case 2 is identical, total pore volume of Case 2 is 10 times of that in Case 1 (i.e., 1000 gridblocks in Case 2 versus 100 gridblocks in Case 1). Hence, it takes about 10 times to inject 1.1 PV in Case 2 compared with Case 1. Therefore, the CPU times presented in Table 2-38 should be divided by 10 before comparing the values reported in Table 2-37. For the case studied, the dependency of computational time is almost a linear function of the number of gridblocks.

Table 2-38: Case 2- total computational time and the time spent for the aqueous composition calculations

No. of processor in UTCOMP-IPhreeqc	CPU time spent in geochemistry (seconds)	Total computational time (seconds)
1PRC	18359.04	18695
2PRCs	9588.363	9925
4PRCs	5422.25	5758
6PRCs	4110.603	4448
8PRCs	3490.897	3826
10PRCs	3142.104	3545

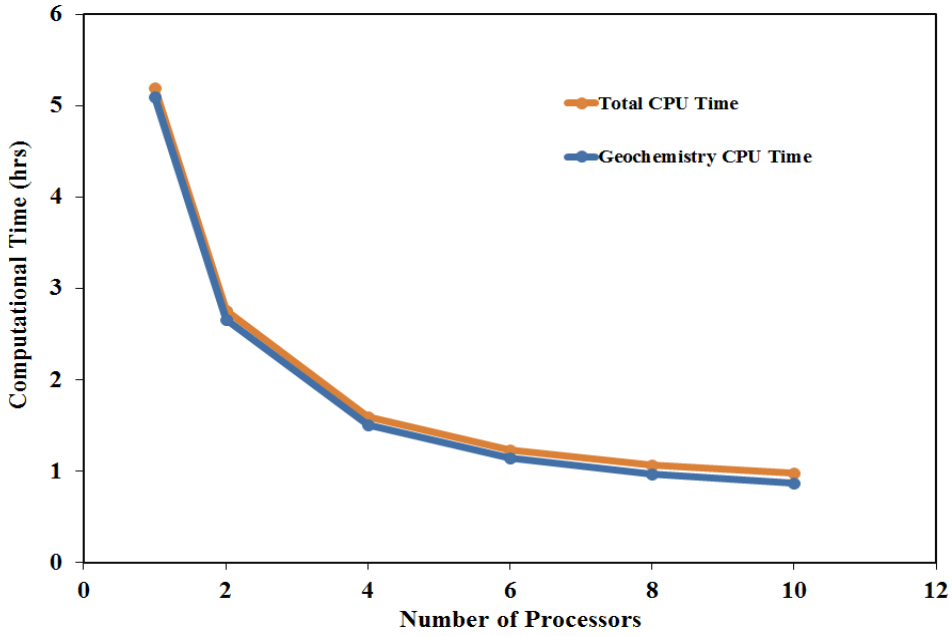

Figure 2-172: Case 2- Total computational time and the time spent for the aqueous composition calculations versus number of processors.

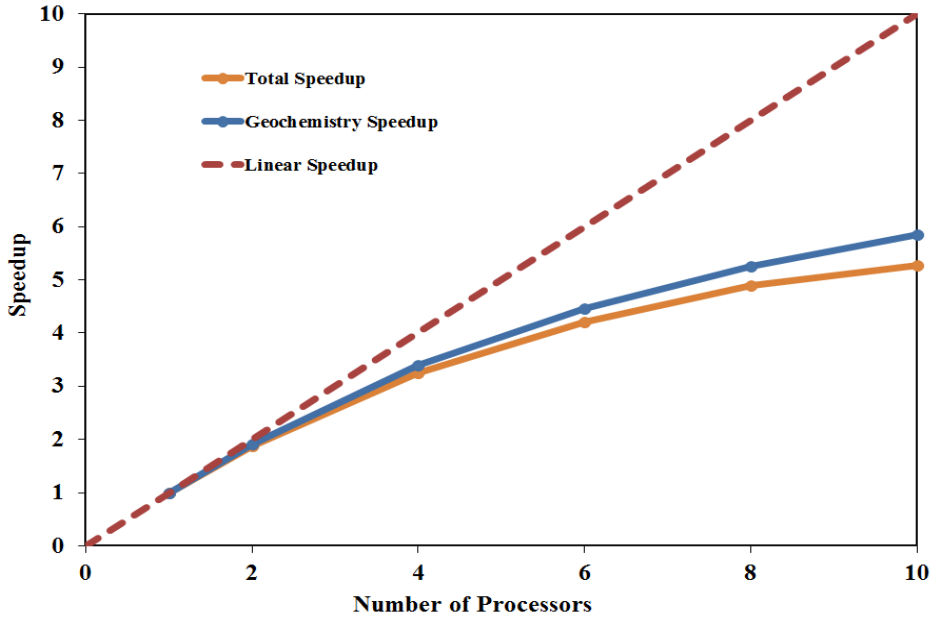

Figure 2-173: Case 2- speedup curve for the total simulation and aqueous phase composition calculations versus number of processors.

Case 3

Descriptions for this case are identical to those of Case 1 (see Table 2-35). However, the geochemistry of the problem is different. This case is initially filled with the Endicott connate water (Endicott water compositions were shown in Table 2-20). All the potential minerals considering Endicott waters compositions (see Table 2-21) are included in the model. This case is flooded with 0.5 PV, 0.5 PV, 0.5 PV, and 1.5 PV of Endicott seawater, Endicott produced water (or high salinity water), Endicott low salinity water, and Endicott high salinity water, respectively. The phreeqc.dat database of IPhreeqc is used in the simulation. Figures 2-174 and 2-175 compare histories of pH and the chloride ion produced from this case using different number of processors. Results are in very good agreements using UTCOMP-IPhreeqc with different number of processors. Computational time of the entire simulation and also the time spent in the geochemistry

module are reported in Table 2-39 (Figure 2-176 shows the plot). Figure 2-177 illustrates the speedup of the total simulation and the geochemistry module. As Figure 2-177 shows, speedup for the entire simulation is very close to that of the geochemistry module. This clearly reveals the fact that most of the computational time is spent for geochemical calculations. Comparison of the computational times reported in Table 2-39 with those of Table 2-37 clearly reveals the high dependency of the CPU time, required to model a reactive-transport problem, to the geochemistry of the problem. It is worth mentioning that as we applied the automatic time stepping option of UTCOMP-IPhreeqc to model both Case 1 and Case 3, some portion of the difference in the CPU times may be due to different time steps in the two cases.

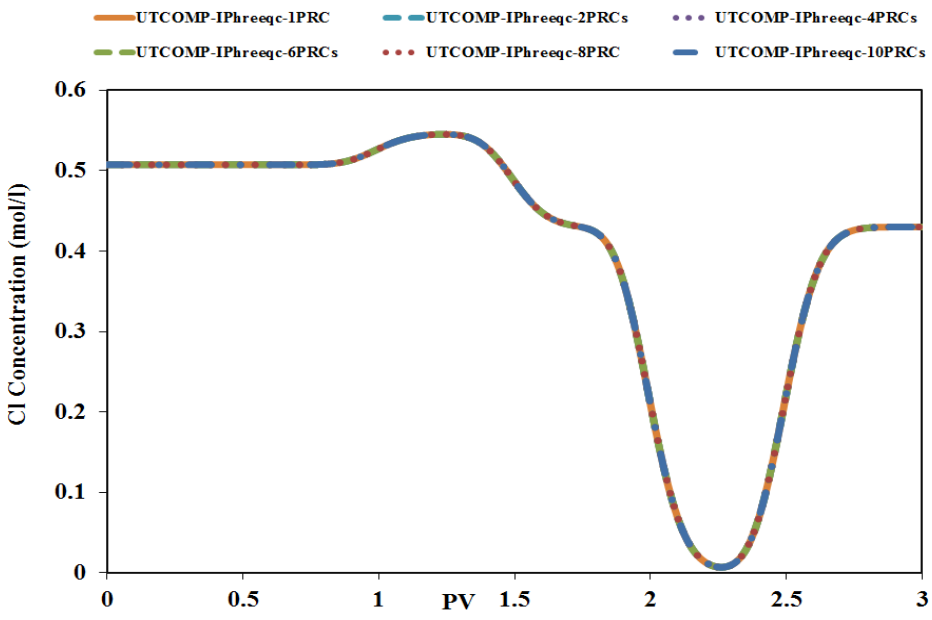

Figure 2-174: Case 3- produced chloride concentration history (using UTCOMP-IPhreeqc with multiple processors for geochemical calculations).

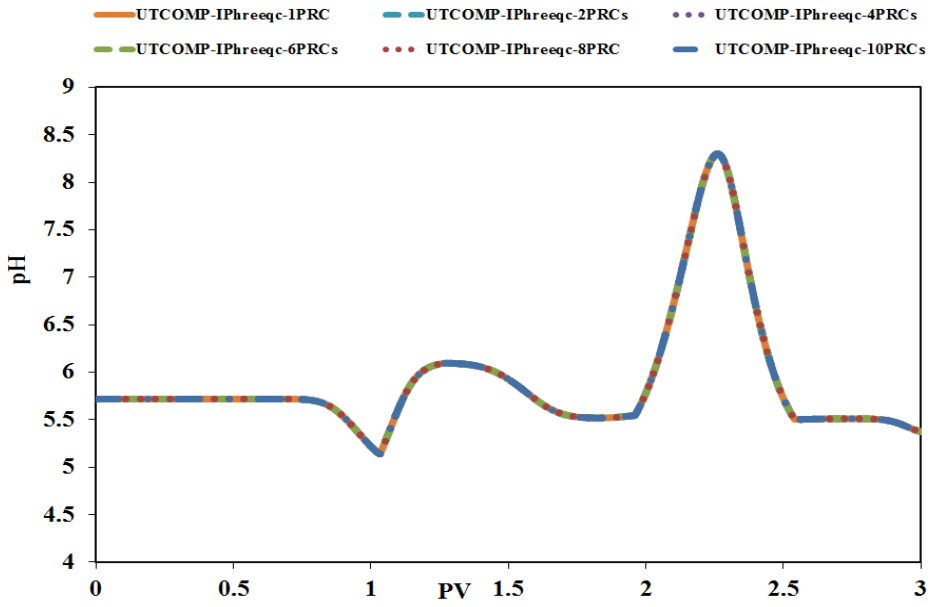

Figure 2-175: Case 3- produced pH history (using UTCOMP-IPhreeqc with multiple processors for geochemical calculations).

Table 2-39: Case 3- total computational time and the time spent for the aqueous composition calculations

No. of processor(s) in UTCOMP-IPhreeqc	CPU time spent in geochemistry (seconds)	Total computational time (seconds)
1PRC	7457.906	7503
2PRCs	4000.51	4046
4PRCs	2265.906	2313
6PRCs	1691.573	1744
8PRCs	1375.574	1426
10PRCs	1190.969	1244

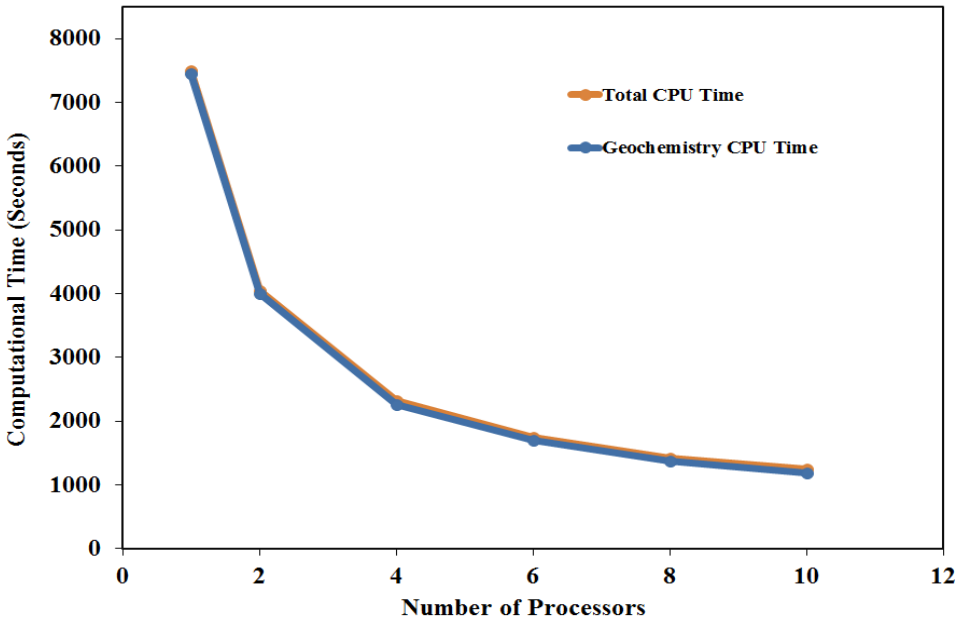

Figure 2-176: Case 3- total computational time and the time spent for the aqueous composition calculations versus number of processors.

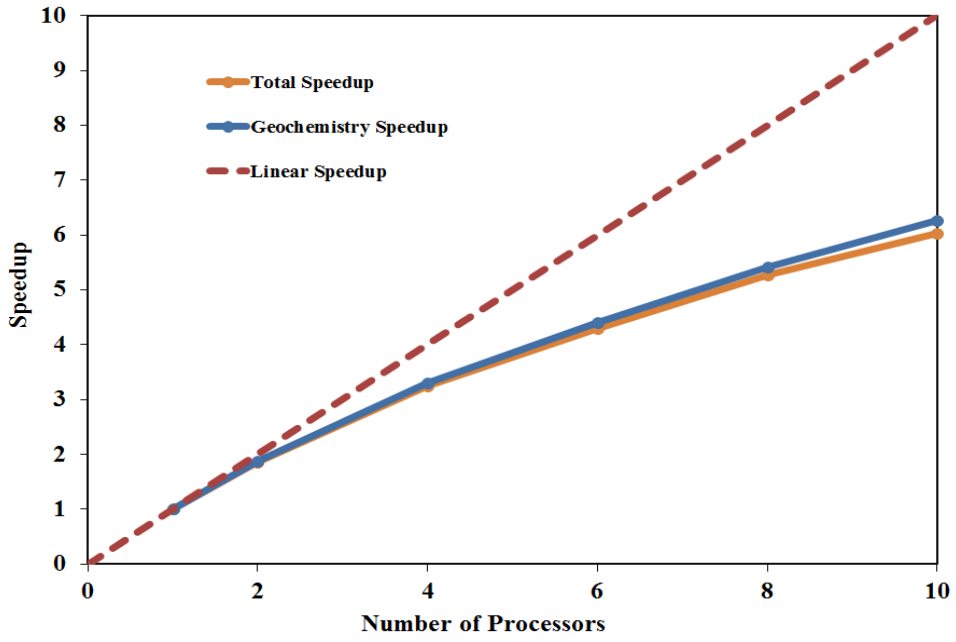

Figure 2-177: Case 3- speedup curve for the total simulation and aqueous phase composition calculations versus number of processors.

Case 4

Case 3 is modified for the number of gridblocks and the injected pore volumes. Number of gridblocks in Case 4 is 1000 and all the waters are injected for 0.1 PV with the sequence as applied in Case 3. Table 2-40 shows the total computational time and the time spent in the geochemistry module versus the number of processors used (see Figure 2-178 for the plot). Figure 2-179 gives the speedup plot.

Table 2-40: Case 4- total computational time and the time spent for the aqueous composition calculations

No. of processor(s) in UTCOMP-IPhreeqc	CPU time spent in geochemistry (seconds)	Total computational time (seconds)
1PRC	66461.63	66931
2PRCs	36814.33	37226
4PRCs	21775.61	22185
6PRCs	15746.58	16156
8PRCs	12688.96	13099
10PRCs	10602.76	11060
20PRCs	6712.145	7133
30PRCs	5572.182	5997
40PRCs	4947.919	5446
50PRCs	4467.391	4975

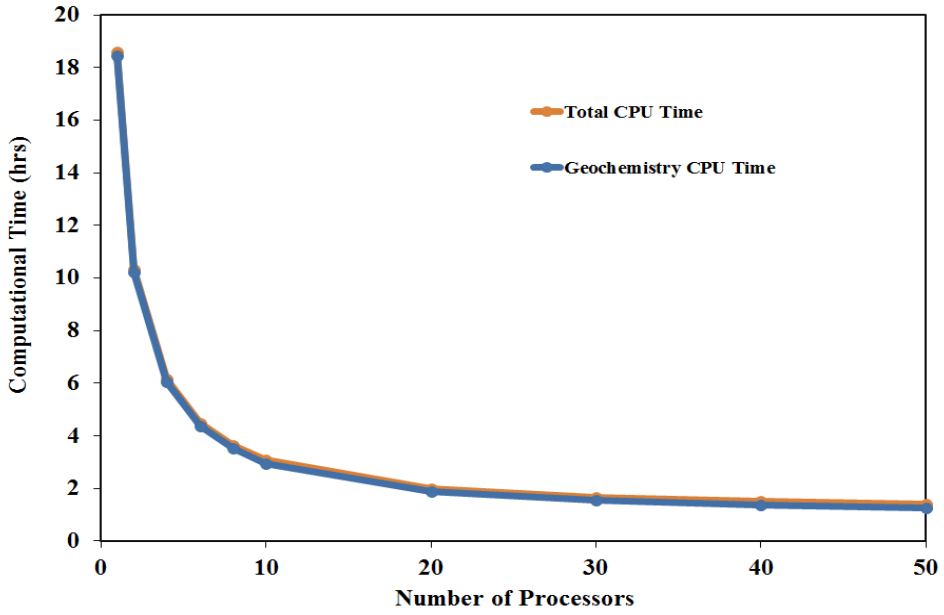

Figure 2-178: Case 4- total computational time and the time spent for the aqueous composition calculations versus number of processors.

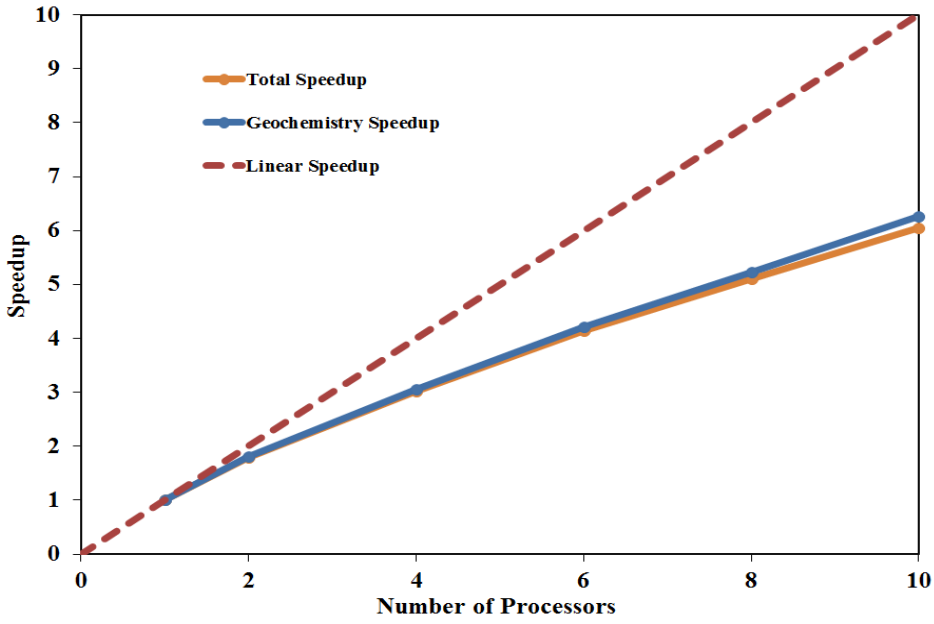

Figure 2-179: Case 4- speedup curve for the total simulation and aqueous phase composition calculations versus number of processors.

2D Case Studies

Case 5

A 2D case is designed using UTCOMP-IPhreeqc. Table 2-41 shows the reservoir descriptions and Figure 2-180 presents the well pattern. A large number of injection wells is included in the model to disturb the geochemistry equilibrium state of more gridblocks at each time step. Obviously, as the number of injection wells increases, the wall-clock time required to simulate the case also decreases. In fact, because higher amount of water is injected into the reservoir per time step, simulation time required to inject certain amount (say 1 PV) of water into the reservoir becomes less. It should be noted that rather than using several vertical wells in a line drive pattern, a horizontal well could be also applied.

"FB" with the ion compositions shown in Table 2-36 is the connate water. Calcite and dolomite are the solids present in the system. Saturation indices for these solids are -0.4 and 0.4, respectively. The phreeqc.dat database of IPhreeqc is applied for the simulation. Although this case is a two-phase case with live-oil, the hydrocarbon effect on the aqueous-rock geochemistry is neglected. All the injection wells are injecting "SW/50" at constant flowrate of 200 bbl/day and production wells are operating at the constant bottomhole pressure of 1000.0 psi. The sequence of water flooding is as follows: 0.5 PV of "SW/50" is injected first and then followed by 0.5 PV of the "FB" water.

Figures 2-181 and 2-182 show the histories of the chloride ion and pH of the aqueous solution for the gridblock (12,12,1). These figures verify the parallel version of UTCOMP-IPhreeqc when different number of processors is applied. Table 2-42 and Figure 2-183 show the computational time of the total simulation and the phase

composition calculation module when different number of computing processors is applied. Figure 2-184 presents the plot of speedup.

Table 2-41: Case descriptions for the 2D Case

No. of gridblocks		900 (30×30×1)	
Δx(ft)		25.0	
Δy(ft)		25.0	
Δz(ft)		20.0	
Permeability (md)	*x*-direction	300.0	
	y-direction	300.0	
Porosity		0.25	
Rock compressibility (psi^{-1})		0.	
Water compressibility (psi^{-1})		0.	
Initial water saturation		0.25	
Irreducible water saturation		0.25	
Reservoir temperature (^oF)		105.0	
Initial pressure (psi)		1100.0	
Reservoir depth (ft)		0.	
Water viscosity (cp)		0.79	
Number of wells		25	15 injectors
			10 producers
Simulation time(PV)		1.0	

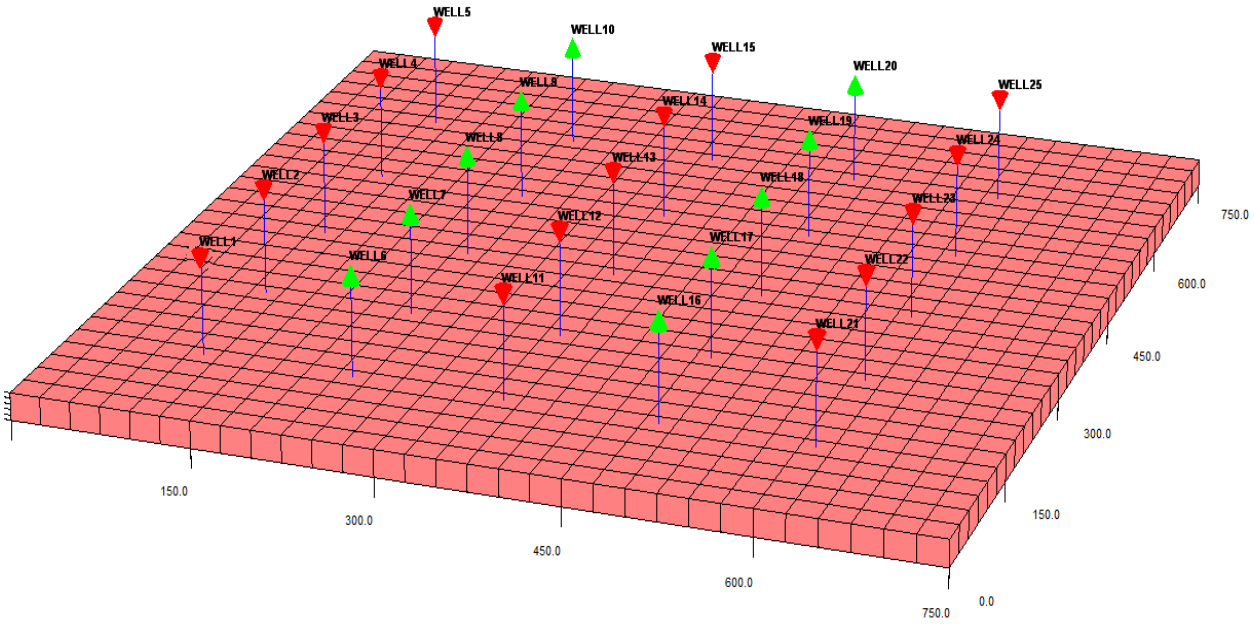

Figure 2-180: 2D case with 900 gridblocks (15 injectors and 10 producers).

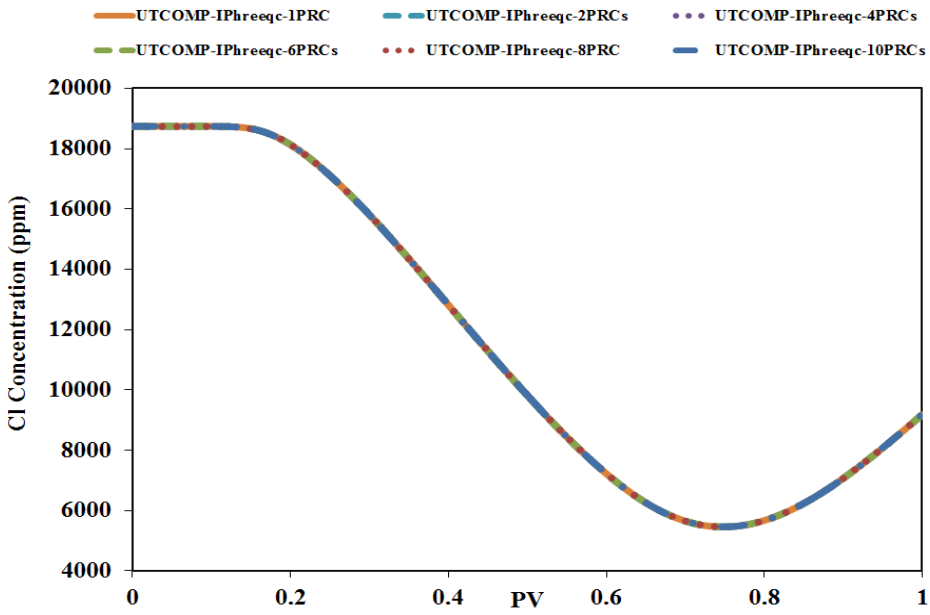

Figure 2-181: Case 5- chloride concentration history at gridblock (12,12,1) (using UTCOMP-IPhreeqc with multiple processors for geochemical calculations).

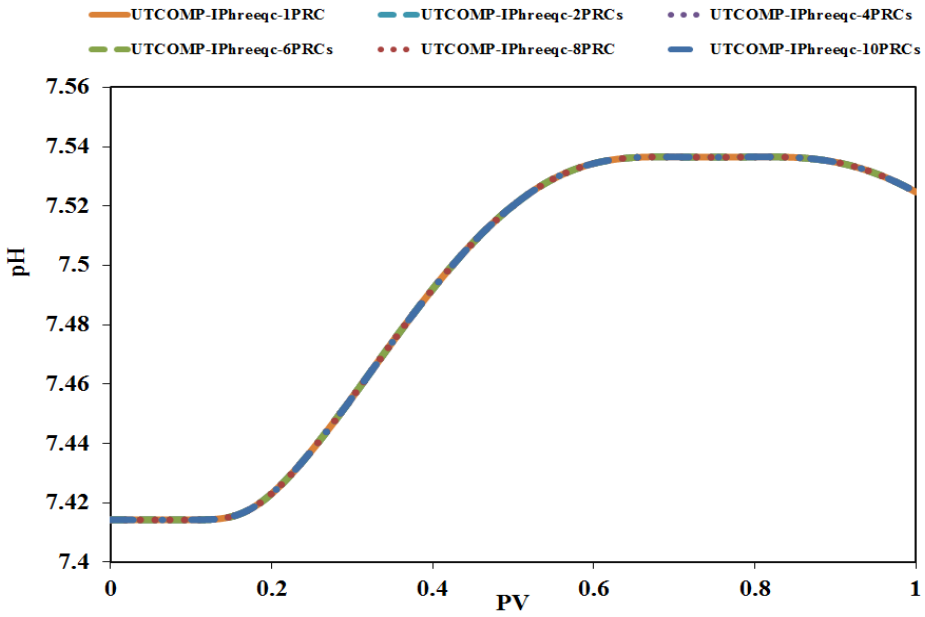

Figure 2-182: Case 5- pH history at gridblock (12,12,1) (using UTCOMP-IPhreeqc with multiple processors for geochemical calculations).

Table 2-42: Case 5- total computational time and the time spent for the aqueous composition calculations

No. of processor(s) in UTCOMP-IPhreeqc	CPU time spent in geochemistry (seconds)	Total computational time (seconds)
1PRC	1697.47	1724
2PRCs	872.46	899
4PRCs	470.03	497
6PRCs	347.26	375
8PRCs	280.04	308
10PRCs	242.78	274
12PRCs	223.33	256

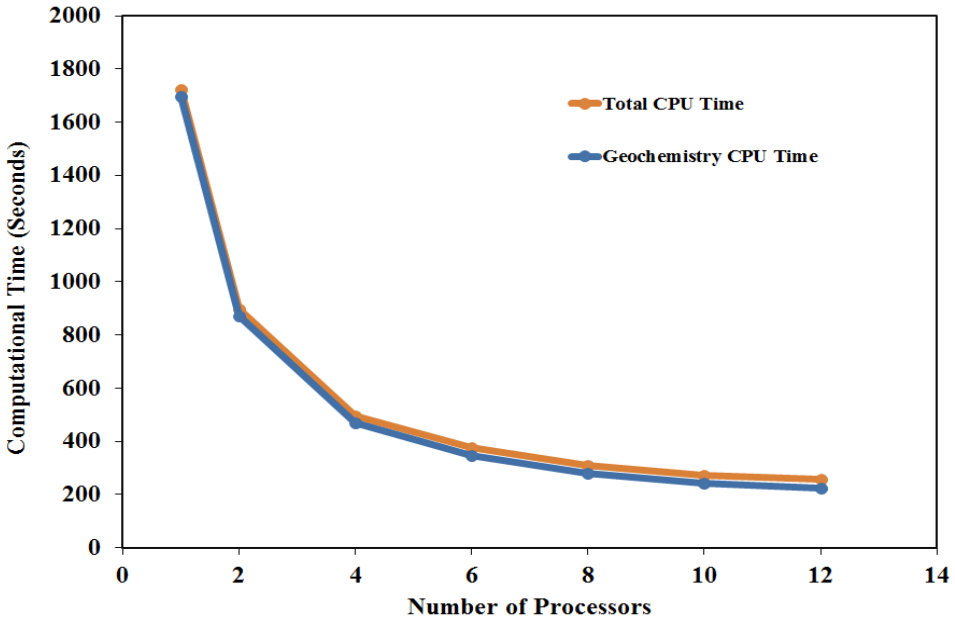

Figure 2-183: Case 5- total computational time and the time spent for the aqueous composition calculations versus number of processors.

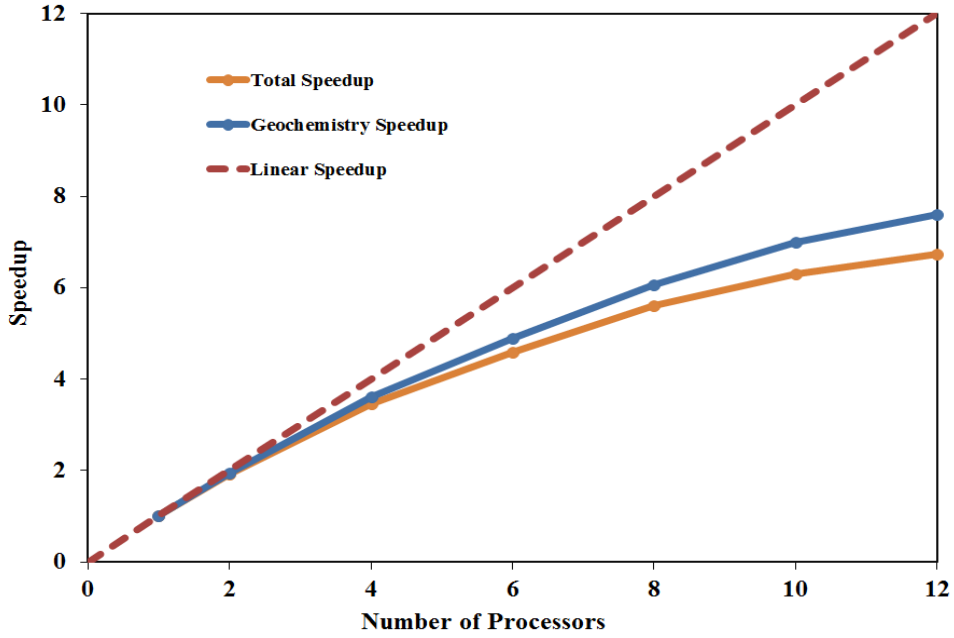

Figure 2-184: Case 5- speedup curve for the total simulation and aqueous phase composition calculations versus number of processors.

Case 6

Case 6 is identical to Case 5 except in number of gridblocks and number of wells. The number of gridblocks and number of wells in Case 6 are 10000 (100×100×1) and 81 wells (45 injectors and 36 producers), respectively (see Figure 2-185). Figures 2-186 and 2-187 verify the parallel version of UTCOMP-IPhreeqc for histories of the chloride ion and pH at the gridblock (30,20,1). The total simulation time using different number of processors is shown in Table 2-43 (see Figure 2-188 for the plot). Figure 2-189 shows the speedup of the total simulation time. As this figure shows, up to 12 processors, we observe super-linear speedup. The reason for the super-linear speedup lies in efficiencies related to usage of cache memory. This occurs when the size of the problem is greater than the CPU cache memory. Hence, by using larger number of processors, we in fact break down the size of problem per processor (Ghasemi Doroh, 2012). The super-linear speedup in parallelization is discussed with details in the works of Abate *et al.* (2001) and Ghasemi Doroh (2012).

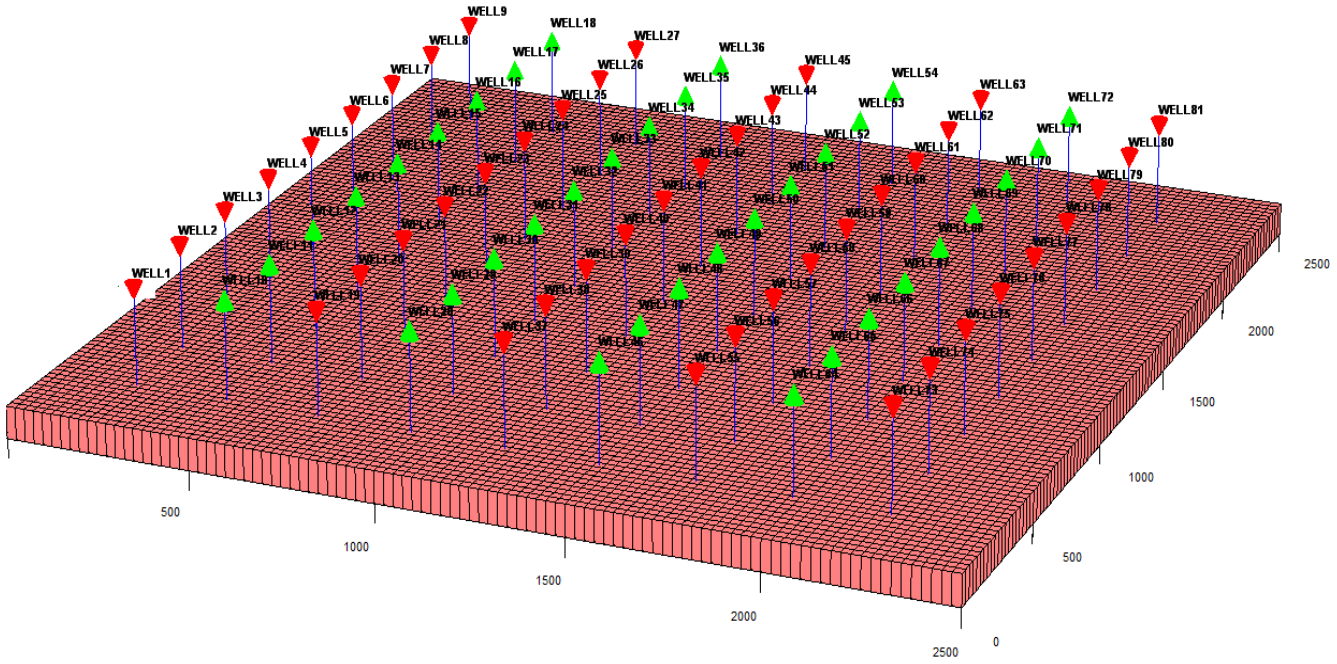

Figure 2-185: 2D case with 10000 gridblocks (45 injectors and 36 producers).

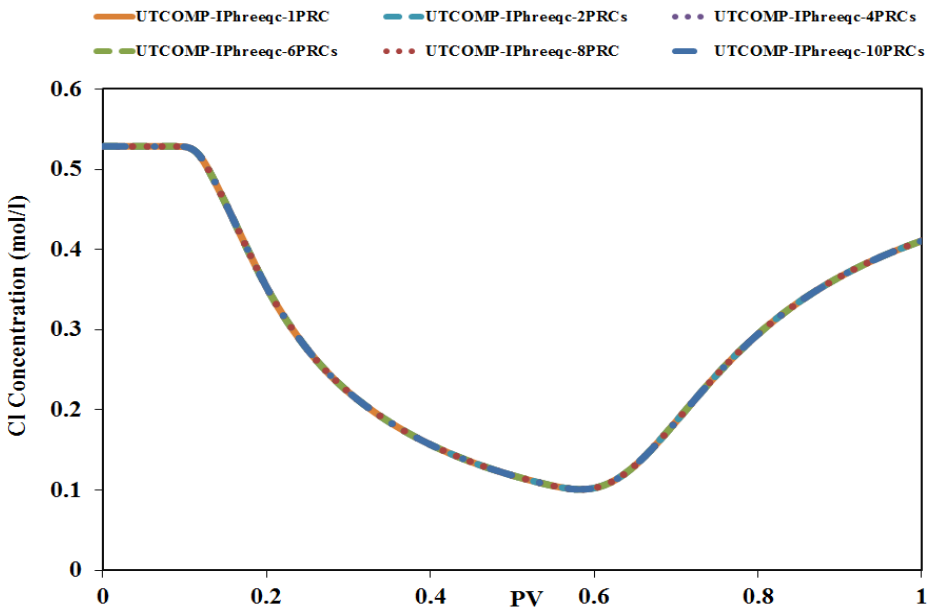

Figure 2-186: Case 6- chloride concentration history at gridblcok (30,20,1) (using UTCOMP-IPhreeqc with multiple processors for geochemical calculations).

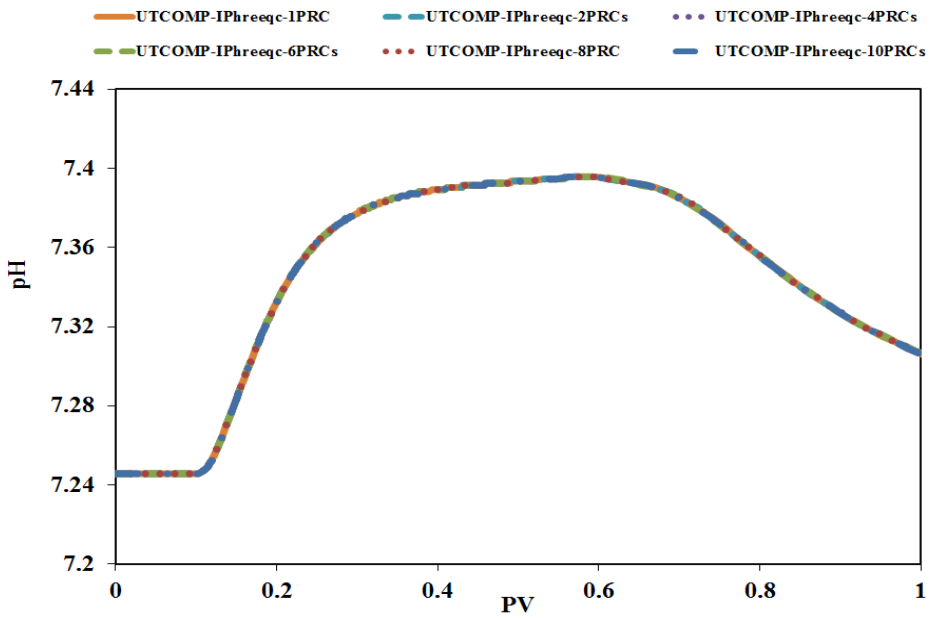

Figure 2-187: Case 6- pH history at gridblcok (30,20,1) (using UTCOMP-IPhreeqc with multiple processors for geochemical calculations).

Table 2-43: Case 6- total computational time

No. of Processor(s) in UTCOMP-IPhreeqc	Total computational time (hrs)
1PRC	99.30
2PRCs	40.85
4PRCs	18.85
6PRCs	13.11
8PRCs	10.37
10PRCs	8.98
12PRCs	7.95
16PRCs	6.86
20PRCs	6.11
24PRCs	5.70
30PRCS	5.25
40PRCs	4.82
50PRCs	4.56
60PRCs	4.45
100PRCs	4.36

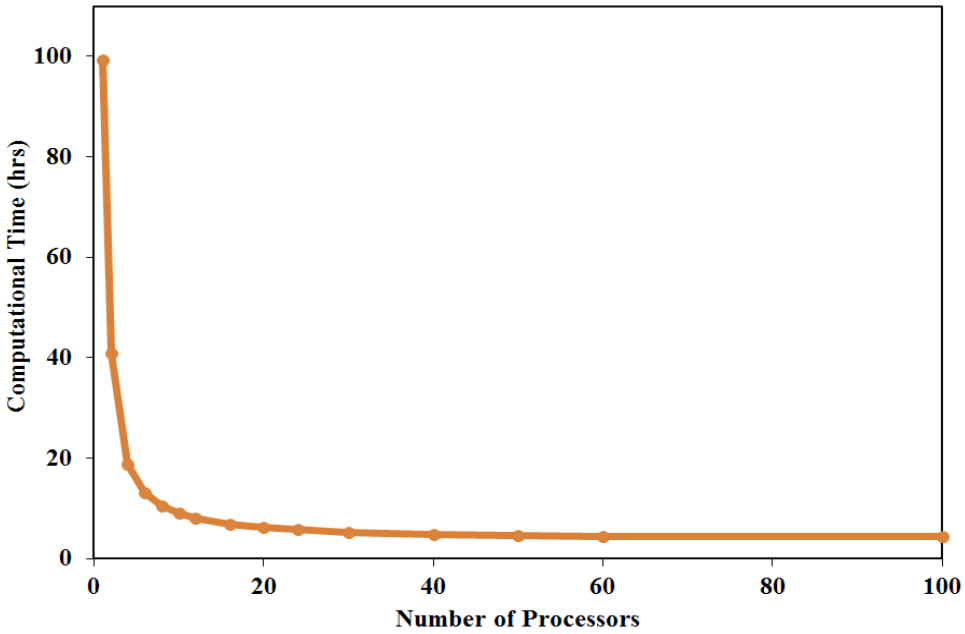

Figure 2-188: Case 6- total computational time versus number of processors.

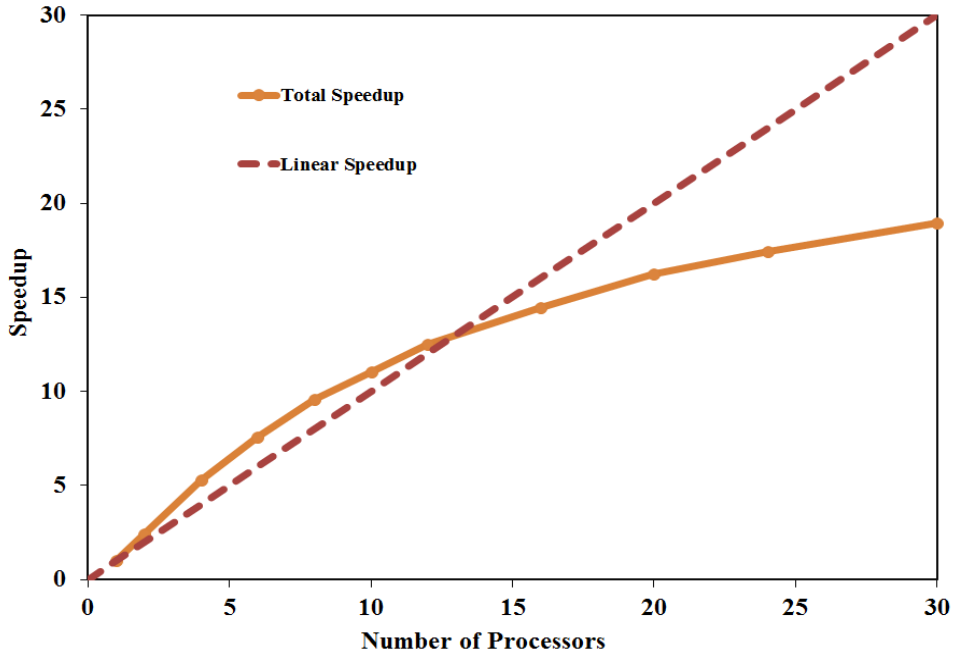

Figure 2-189: Case 6- speedup curve for the total simulation versus number of processors.

Case 7

Case 7 is designed to investigate the effect of the hydrocarbon phase on the computational time, when included in geochemical calculations. Everything in Case 7 is identical to that of Case 6 except that in Case 7, the effect of CO_2 of the hydrocarbon phase on the aqueous-rock geochemistry is included in the model. Table 2-44 shows the overall mole fraction and some important thermodynamic properties of the hydrocarbon components used in the case. Histories of the chloride ion and pH at the gridblock (30,20,1), the same gridblcok used for the verification in Case 6, are shown in Figures 2-190 and 2-191, respectively. Comparing Figure 2-191 with Figure 2-187 clearly shows the buffering effect of CO_2 on the pH of the aqueous solution.

Table 2-44: Overall mole fraction and thermodynamic properties of hydrocarbon components

Component	Overall Mole Fraction	Pc (psi)	Tc(^{o}R)
CO_2	0.0337	1069.87	547.56
C_1	0.0861	667.20	343.08
C_2-C_3	0.1503	652.56	619.57
C_4-C_6	0.1671	493.07	833.80
C_7-C_{15}	0.3304	315.44	1090.35
C_{16}-C_{27}	0.1611	239.90	1351.83
C_{28}	0.0713	238.12	1696.46

Table 2-45 reports the computational time for Case 7 using UTCOMP-IPhreeqc with different number of processors. As the table shows, through parallelization we can significantly decrease the computational time to model reactive-transport problems. Figures 2-192 and 2-193 present the plots of the total computational time and the speedup versus the number of processors, respectively. Included in these figures is the computational times for the case in which the effect of the hydrocarbon phase on the

aqueous-rock geochemistry is ignored (i.e., the Case 6 results). Based on the results presented in Figures 2-192 and 2-193, we can conclude that benefits due to parallelizing the phase composition calculation module of UTCOMP-IPhreeqc are significantly pronounced when the hydrocarbon phase effect is included in geochemical calculations. When the hydrocarbon phase effect is included in the case, we obtain super-linear speedup up to 50 computing processors. However, we believe that as the case becomes larger, using the restart option introduces more errors in the computed CPU times (say less than 6 processors).

It should be noted that the speedup curve of Case 7 is evaluated by considering the CPU time of UTCOMP-IPhreeqc-2PRCs as the base case. Hence, rather than the actual computational time of 242.71 hours for UTCOMP-IPhreeqc-1PRC, 155.92 hours ($2\times CPU_{UTCOMP\text{-}IPhreeqc\text{-}2PRCs}=2\times 77.96$ hours) is used in the calculation. By comparing the computational times reported in Table 2-43 (without the hydrocarbon phase effect included) with those documented in Table 2-45 (with the hydrocarbon phase effect included) one can conclude that inclusion of the hydrocarbon phase effect in geochemical calculations slows down the simulation by a factor of about 2-2.5. However, we need to note that the automatic time stepping option is applied in these simulations (MDT=1 in the UTCOMP input file). Hence, the time step might not increase in one case (say the case with the hydrocarbon phase effect included) as it builds up in another case (without the hydrocarbon phase effect included). Two more cases (i.e., Cases 11 and 12) are presented later to discuss the hydrocarbon phase effect on the computational time and time stepping.

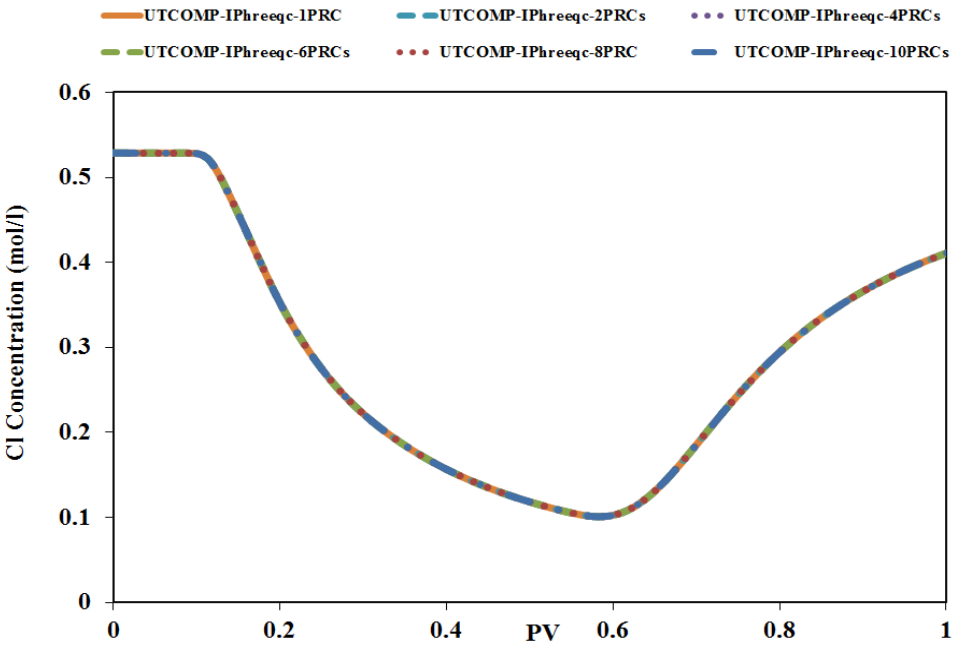

Figure 2-190: Case 7- chloride concentration history at gridblcok (30,20,1) (using UTCOMP-IPhreeqc with multiple processors for geochemical calculations).

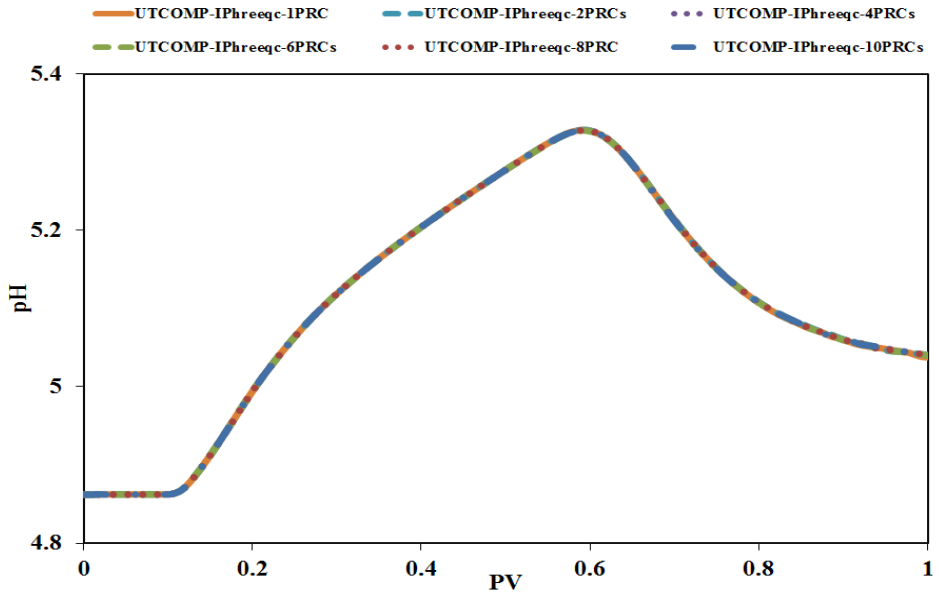

Figure 2-191: Case 7- pH history at gridblcok (30,20,1) (using UTCOMP-IPhreeqc with multiple processors for geochemical calculations).

Table 2-45: Case 7- total computational time

No. of processor(s) in UTCOMP-IPhreeqc	Total computational time (hrs)	Total computational time (days)
1PRC	242.71	10.11
2PRCs	77.96	3.25
4PRCs	27.71	1.15
6PRCs	16.45	0.69
8PRCs	11.92	0.50
10PRCs	9.76	0.41
12PRCs	7.90	0.33
16PRCs	5.99	0.25
20PRCs	5.13	0.21
24PRCs	4.46	0.19
30PRCS	4.11	0.17
40PRCs	3.26	0.14
50PRCs	3.01	0.13
60PRCs	2.84	0.12
100PRCs	2.39	0.10

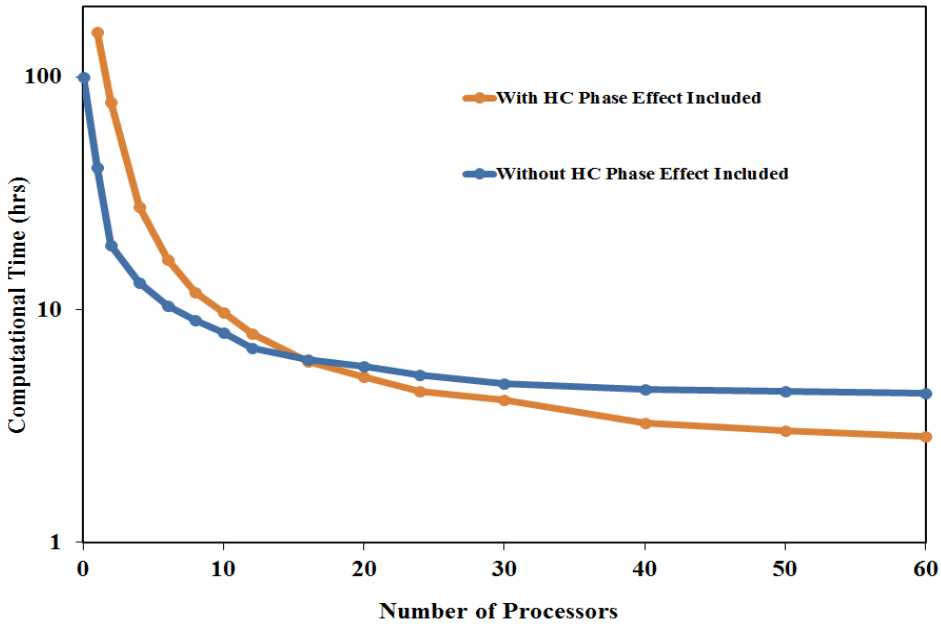

Figure 2-192: Case 7- total computational time versus number of processors for cases with and without the hydrocarbon phase effect included in the geochemical calculations.

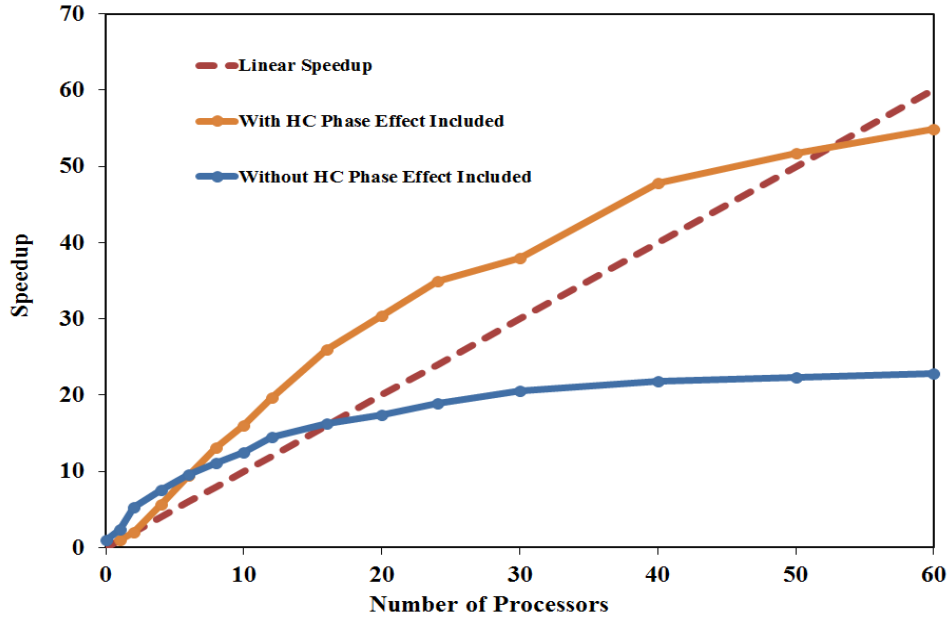

Figure 2-193: Case 7- speedup curves versus number of processors for cases with and without the hydrocarbon phase effect included in the geochemical calculations.

3D Case Studies

Case 8

Case 8 is identical to Case 5 except in this case four numerical layers are considered in *z*-direction. The reservoir geometry and the well pattern are provided in Figure 2-194 (number of gridblocks are 3600 (30×30×4) in Case 8). The histories of the chlorine ion and pH of the aqueous solution at gridblock (14,14,2) are shown in Figures 2-195 and 2-196, respectively. Total simulation time and the time spent in the geochemistry module are reported in Table 2-46 (Figure 2-197 provides the plot) and Figure 2-198 illustrates the speedup curve. Comparison of Figure 2-198 with Figure 2-184 reveals the fact that as the number of gridblocks increases, the speedup achieved through the parallelization approaches to the linear speedup.

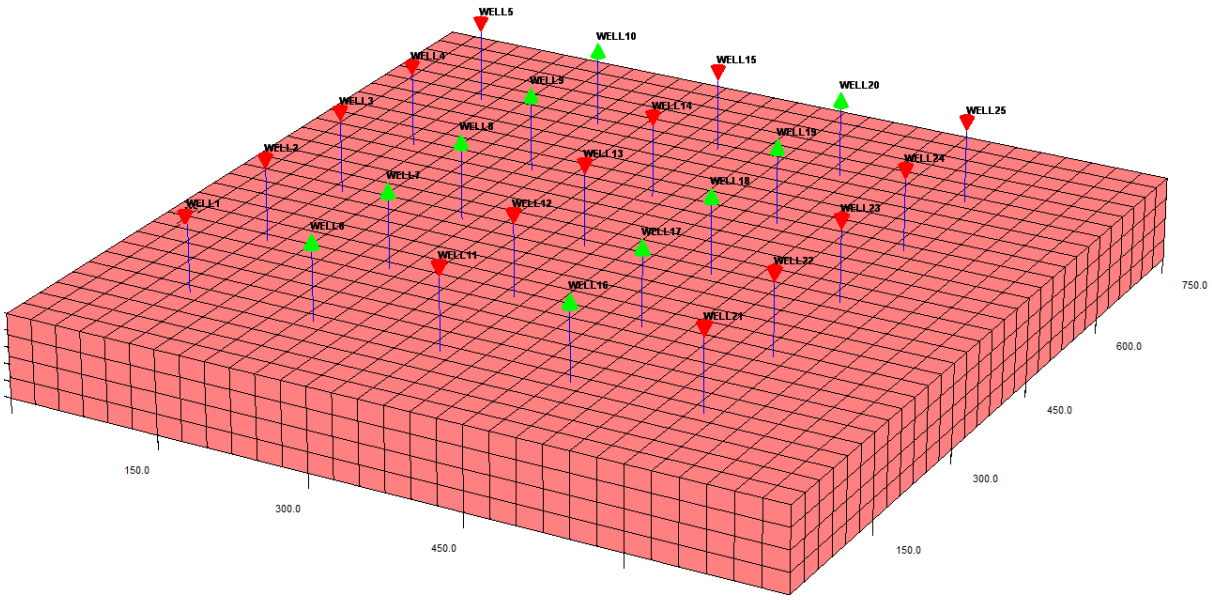

Figure 2-194: 3D case with 3600 gridblocks (15 injectors and 10 producers).

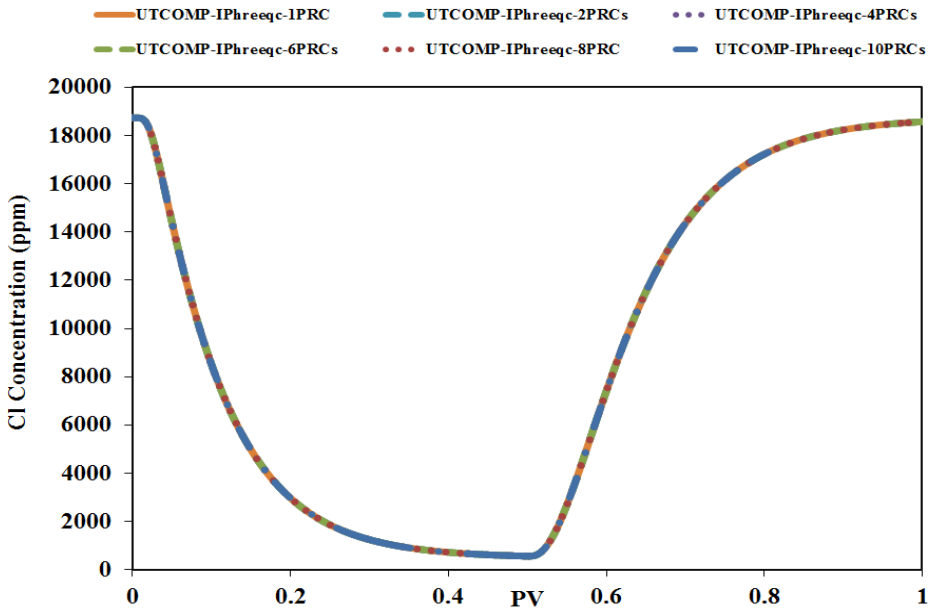

Figure 2-195: Case 8- chloride concentration history at gridblock (14,14,2) (using UTCOMP-IPhreeqc with multiple processors for geochemical calculations).

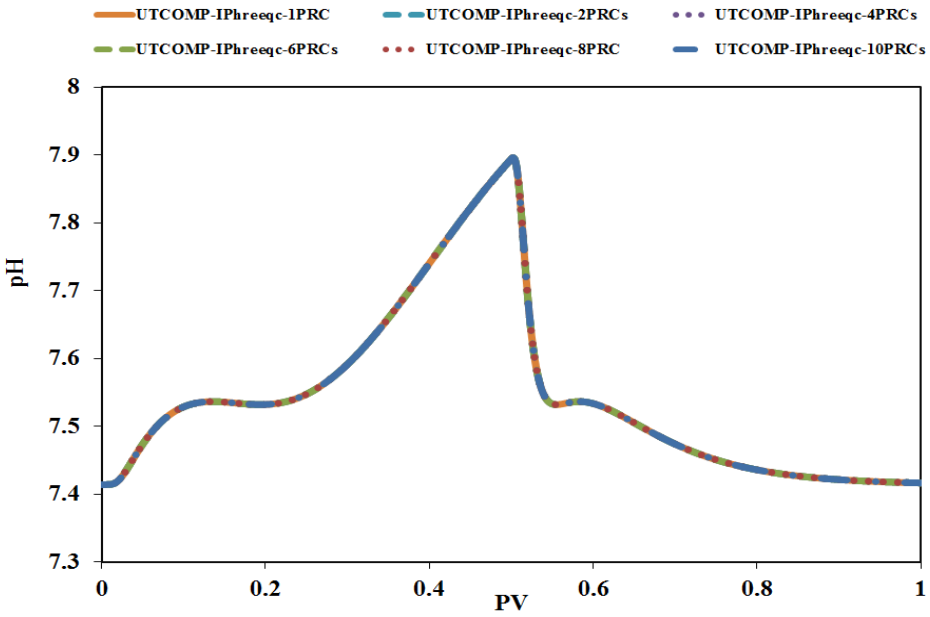

Figure 2-196: Case 8- pH history at gridblock (14,14,2) (using UTCOMP-IPhreeqc with multiple processors for geochemical calculations).

Table 2-46: Case 8- total computational time and the time spent for the aqueous composition calculations

No. of processor(s) in UTCOMP-IPhreeqc	CPU time spent in geochemistry (seconds)	Total computational time (seconds)
1PRC	23692	23307.61
2PRCs	11528	11142.99
4PRCs	6293	5863.49
6PRCs	4534	4149.849
8PRCs	3732	3348.51
10PRCs	3318	2932.35
12PRCs	3070	2676.69
16PRCs	2661	2277.73
20PRCs	2487	2100.39

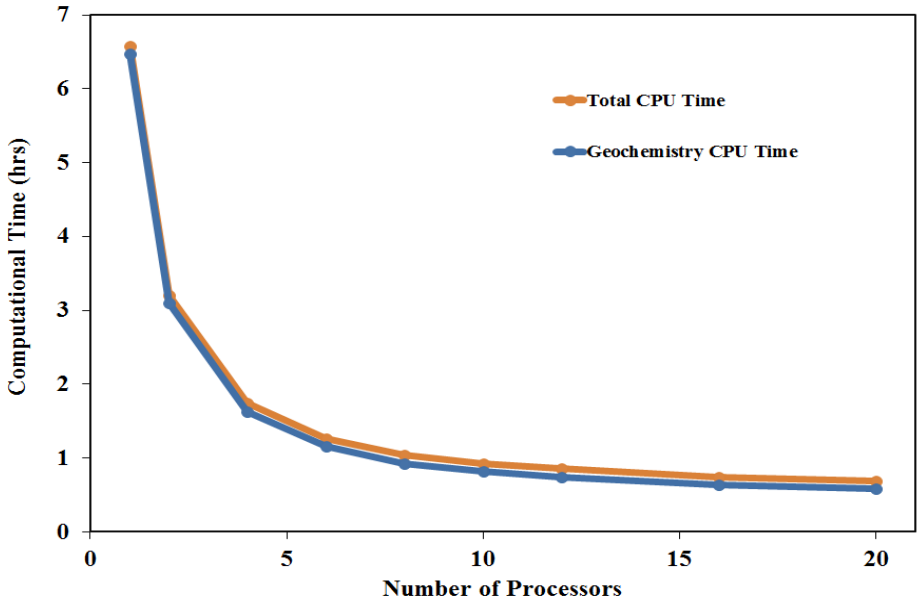

Figure 2-197: Case 8- total computational time and the time spent for the aqueous phase composition calculations versus number of processors.

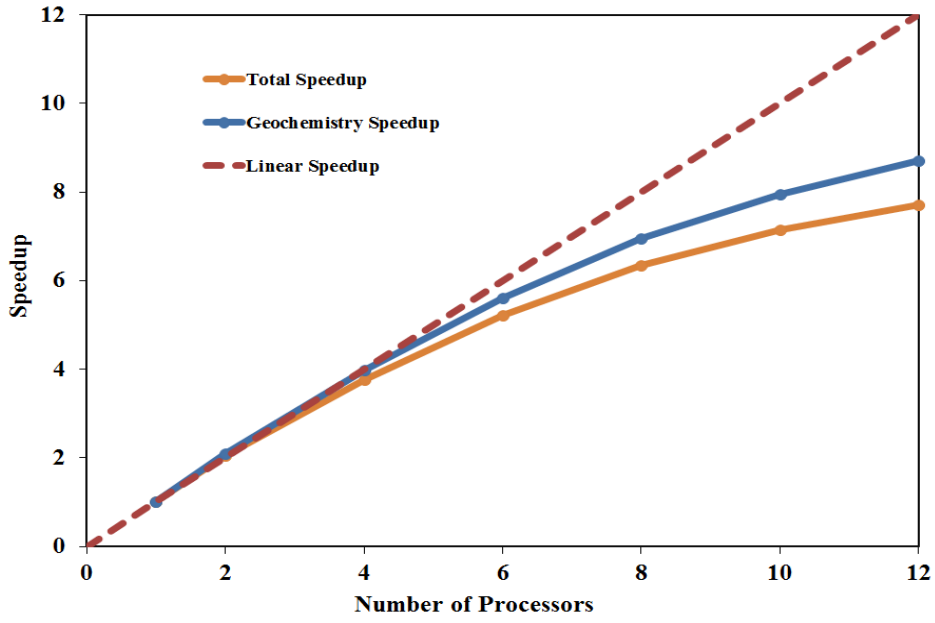

Figure 2-198: Case 8- speedup curve for the total simulation and aqueous phase composition calculations versus number of processors.

Case 9

Case 9 is similar to Case 6 except 2 numerical layers are considered in the model (see Figure 2-199 for the reservoir geometry and well pattern). Number of gridblocks in Case 9 is 20000 (100×100×2).

Figures 2-200 and 2-201 verify the parallel version of UTCOMP-IPhreeqc for the chloride concentration and pH at gridblock (10,10,1). Table 2-47 provides the total computational time using different number of processors (see Figure 2-202 for the plot). The speedup curve is also presented in Figure 2-203.

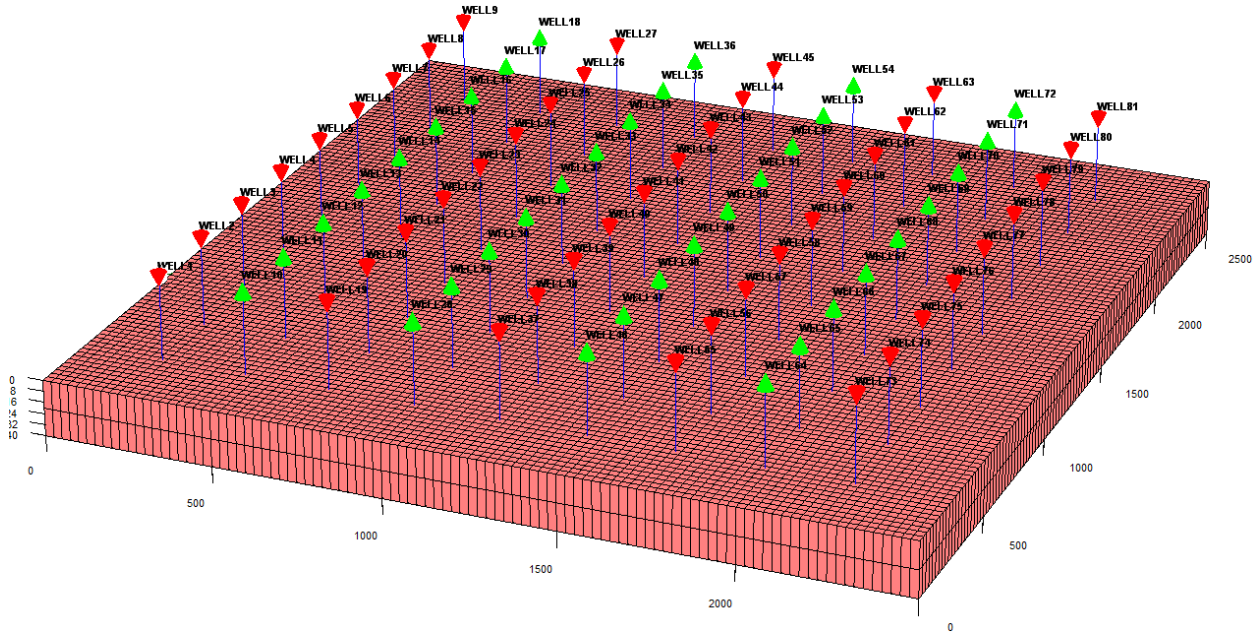

Figure 2-199: 3D case with 20000 gridblocks (45 injectors and 36 producers).

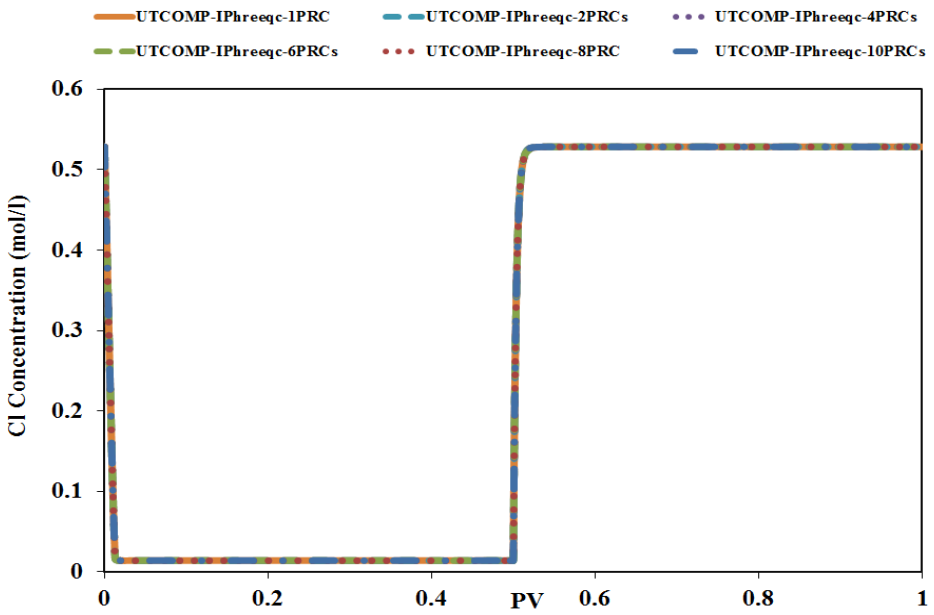

Figure 2-200: Case 9- chloride concentration history at gridblock (10,10,1) (using UTCOMP-IPhreeqc with multiple processors for geochemical calculations).

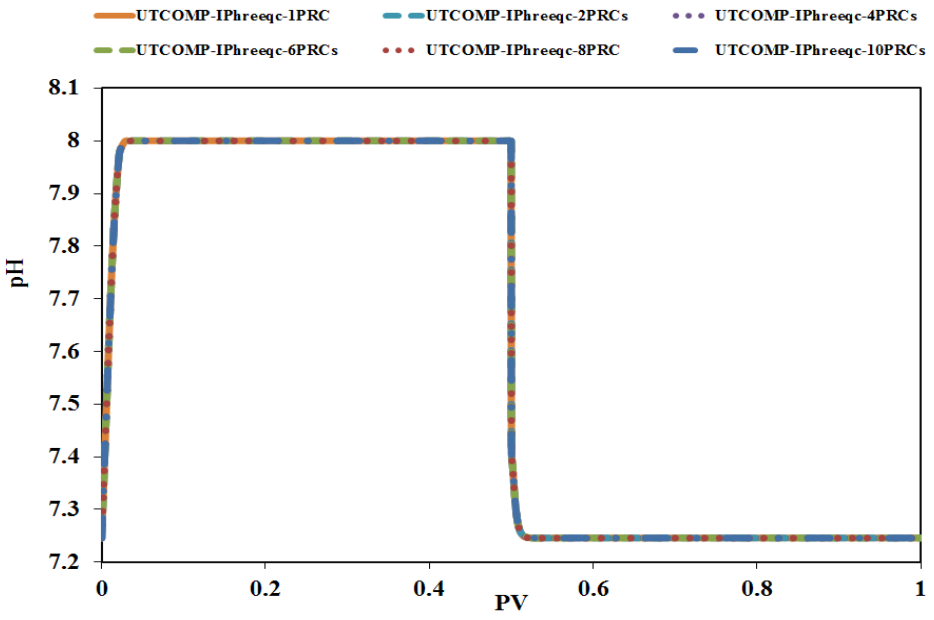

Figure 2-201: Case 9- pH history at gridblock (10,10,1) (using UTCOMP-IPhreeqc with multiple processors for geochemical calculations).

Table 2-47: Case 9- total computational time

No. of processor(s) in UTCOMP-IPhreeqc	Total computational time (hrs)	Total computational time (days)
1PRC	412.71	17.20
2PRCs	155.43	6.48
4PRCs	63.30	2.64
6PRCs	40.82	1.70
8PRCs	31.99	1.33
10PRCs	26.57	1.11
12PRCs	23.44	0.98
16PRCs	19.43	0.81
20PRCs	17.31	0.72
30PRCs	14.70	0.61
40PRCs	13.59	0.57
60PRCs	12.28	0.51
80PRCs	11.72	0.49
100PRCs	11.47	0.48

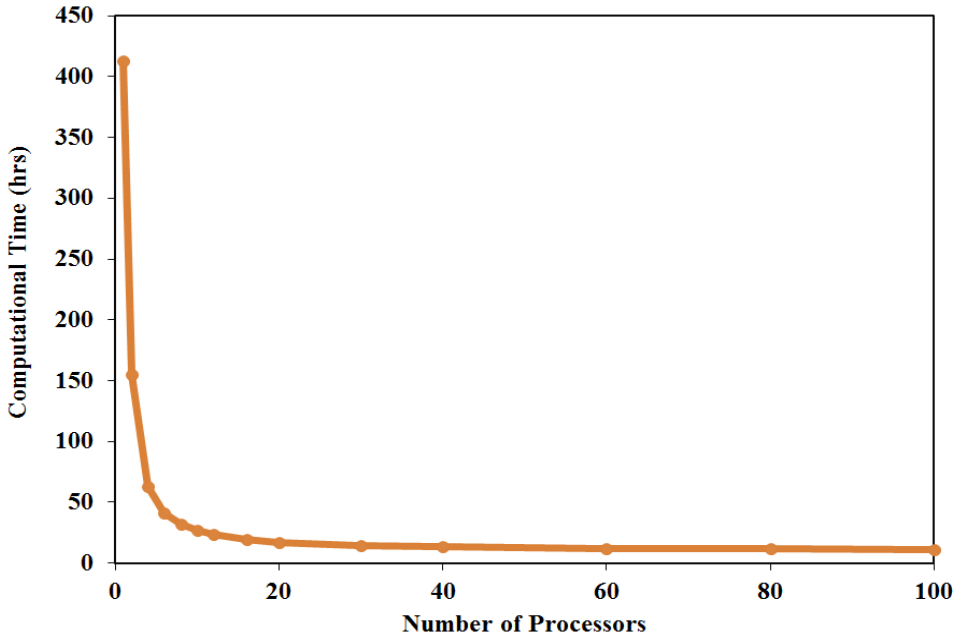

Figure 2-202: Case 9- total computational time versus number of processors.

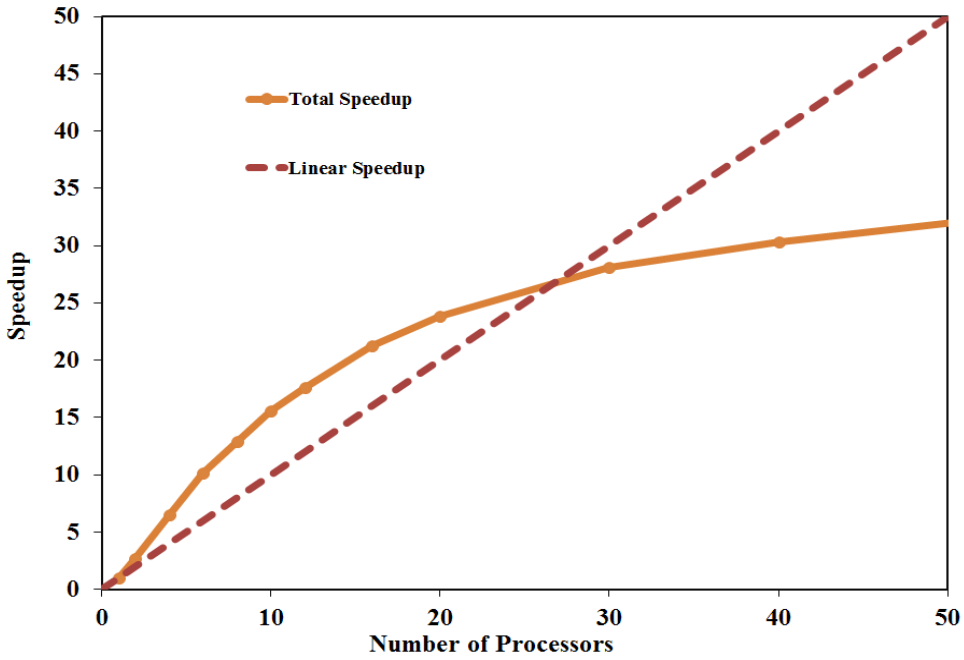

Figure 2-203: Case 9- speedup curve for the total simulation versus number of processors.

Case 10

Case 9 is repeated when 3 numerical layers are included in the model (number of gridblocks = 30000, 100×100×3). Histories for the chloride ion and pH of the aqueous solution at gridblock (30,20,2) are shown in Figures 2-204 and 2-205, respectively (using 2, 10, 20, 30, 50, and 100 processors). Table 2-48 and Figure 2-206 present the total computational time and Figure 2-207 provides the speedup curve. As Table 2-48 shows, by applying 20 processors the simulation time decreases from 45.5 days to about 1.3 days. To plot the speedup curve, the total simulation time of UTCOMP-IPhreeqc-2PRCs is considered as the base case.

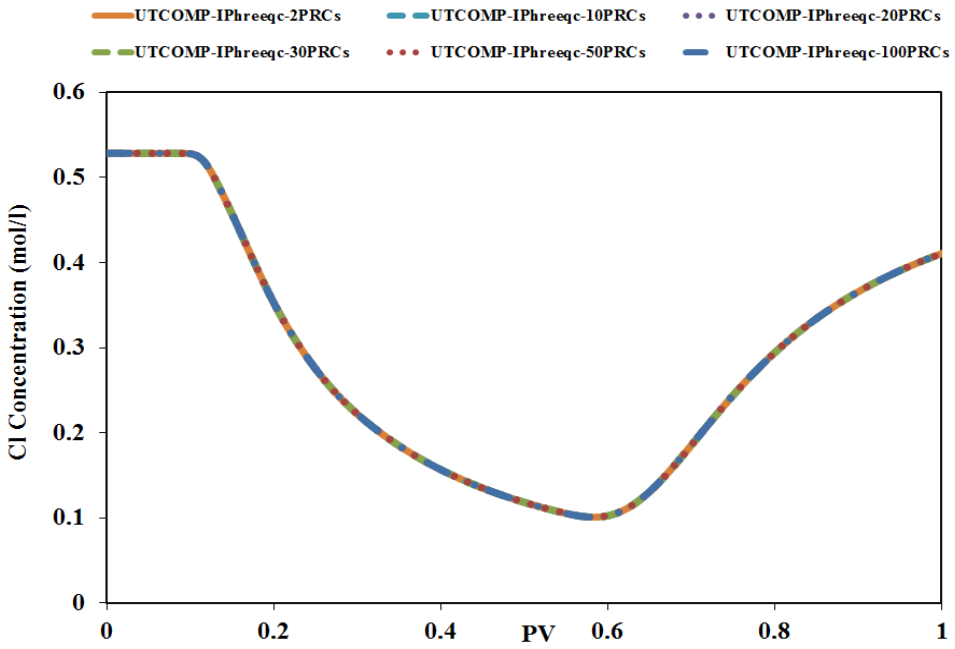

Figure 2-204: Case 10- chloride concentration history at gridblock (30,20,2) (using UTCOMP-IPhreeqc with multiple processors for geochemical calculations).

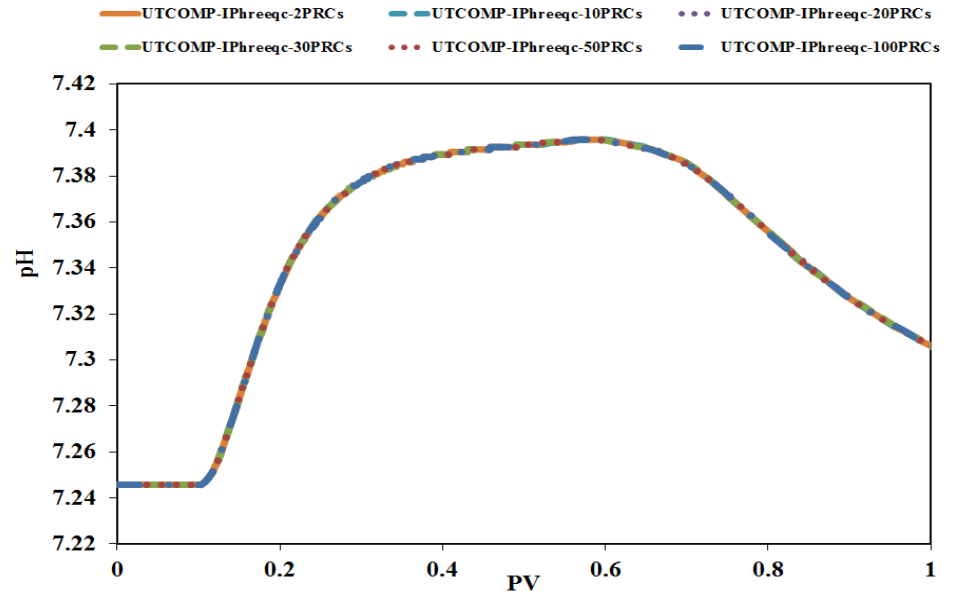

Figure 2-205: Case 10- pH history at gridblock (30,20,2) (using UTCOMP-IPhreeqc with multiple processors for geochemical calculations).

Table 2-48: Case 10- total computational time

No. of processor(s) in UTCOMP-IPhreeqc	Total computational time (hrs)	Total computational time (days)
1PRC	1090.58	45.44
2PRCs	356.25	14.84
4PRCs	129.11	5.38
6PRCs	82.47	3.44
8PRCs	61.30	2.55
10PRCs	50.18	2.09
12PRCs	44.48	1.85
16PRCs	36.10	1.50
20PRCs	31.71	1.32
30PRCs	24.30	1.01
40PRCs	24.30	1.01
50PRCs	22.78	0.95
60PRCs	22.29	0.93
80PRCs	21.18	0.88
100PRCs	20.26	0.84
252PRCs	19.75	0.82

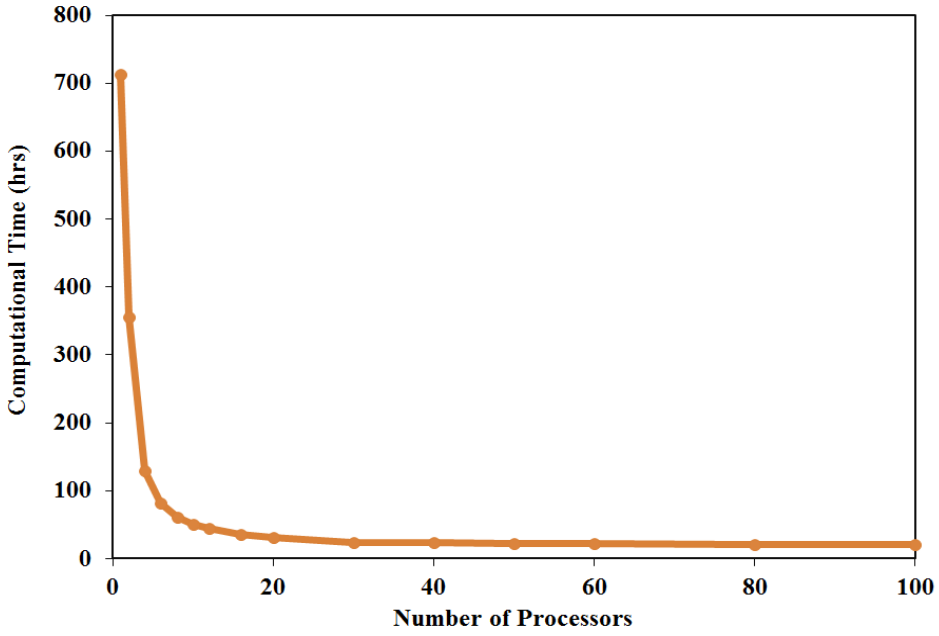

Figure 2-206: Case 10- total computational time versus number of processors.

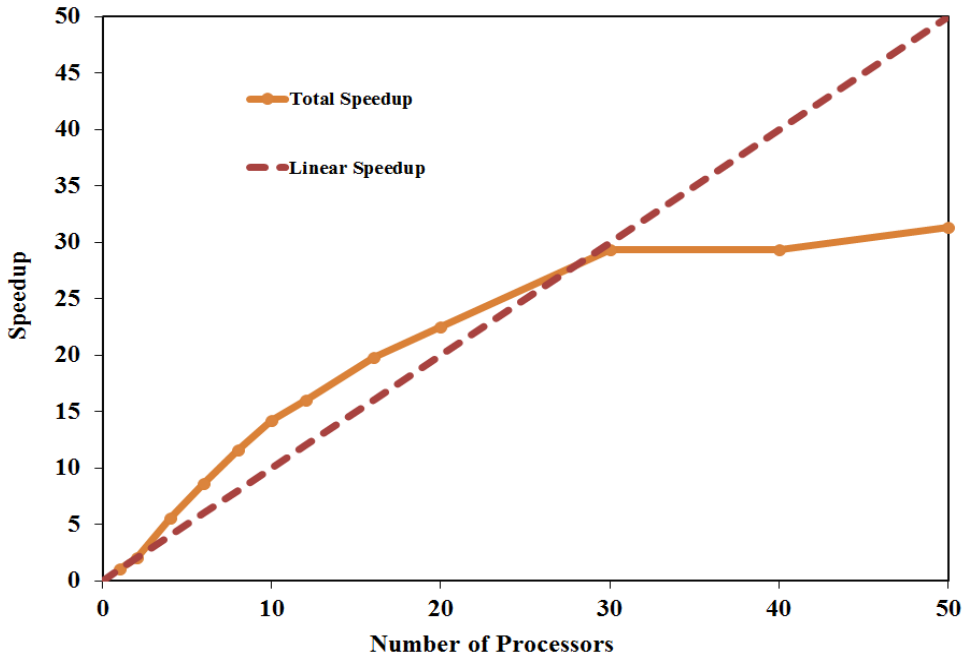

Figure 2-207: Case 10- speedup curve for the total simulation versus number of processors.

Based on the results presented for Cases 6, 7, 9, and 10, we observe super-linear speedup when the number of gridblocks is greater than 10000. Moreover, the speedup due to parallelization is more pronounced for cases with the hydrocarbon phase effect included in geochemical calculations.

Two more cases are designed to investigate the effect of the hydrocarbon phase on the computational time and time stepping, when included in geochemical calculations.

Case 11

Case 1 is modified to include the effect of the soluble hydrocarbon components on the aqueous-rock geochemistry. Hence, initial water saturation is modified to 0.2 in Case 11 (S_{wi} = 0.999 in Case 1). Only the effect of the CO_2 component of the hydrocarbon phase is included in geochemical calculations. Table 2-49 compares the total

computational time for the case with the hydrocarbon-CO_2 effect on the aqueous-rock geochemistry included against the case in which the hydrocarbon-CO_2 effect is ignored. Results for both automatic and constant time stepping criteria are included in the table. For the automatic time stepping, maximum and minimum time steps are 0.1 and 0.0001 days, respectively, whereas, the time step is 0.01 days when constant time stepping criterion is applied. Figure 2-208 provides the plot of the total simulation time versus the number of processors. MDT in this figure refers to the flag in the UTCOMP input file through which the users assign automatic or constant time stepping criterion for the simulation (MDT =0 and 1 refer to constant time stepping and automatic time stepping, respectively). Figure 2-209 illustrates the speedup plot.

Based on the results presented for Case 11, three conclusions are drawn: 1) inclusion of the hydrocarbon phase on the aqueous-rock geochemistry slows down the simulation maximum by a factor of 1.3; 2) inclusion of the hydrocarbon phase appears not to change time step selection in UTCOMP; 3) we achieve more beneficial out of parallelizing the UTCOMP-IPhreeqc simulator for cases where the hydrocarbon-CO_2 effect is included (see Figure 2-209). The last point confirms our previous conclusion in Case 7.

We need to emphasize on the fact that these conclusions are solely for Case 11 and they may not be generalized to other cases.

Table 2-49: Case 11- total computational time using constant or automatic time stepping approaches for cases with and without the hydrocarbon phase effect included in aqueous-rock geochemistry

No. of processor(s) in UTCOMP-IPhreeqc	CPU time (seconds)			
	Automatic Time Stepping		Constant Time Step	
	With HC phase effect included	Without HC phase effect included	With HC phase effect included	Without HC phase effect included
1PRC	378	287	509	402
2PRCs	190	168	266	221
4PRCs	117	98	149	137
6PRCs	89	79	114	108
8PRCs	77	70	95	95
10PRCs	68	64	83	88

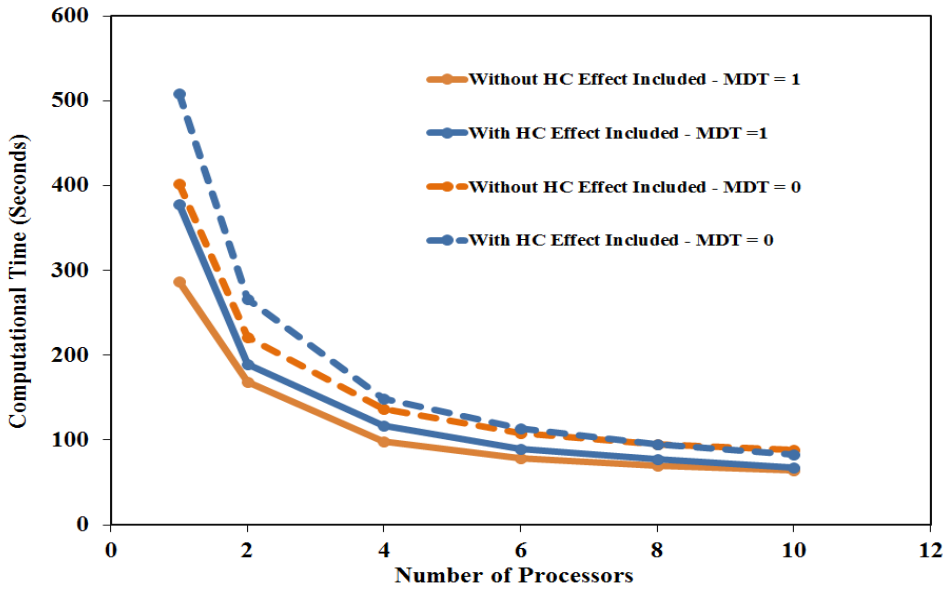

Figure 2-208: Case 11- total computational time using constant (MDT=0) or automatic time stepping (MDT=1) approaches for cases with and without the hydrocarbon phase effect included in aqueous-rock geochemistry.

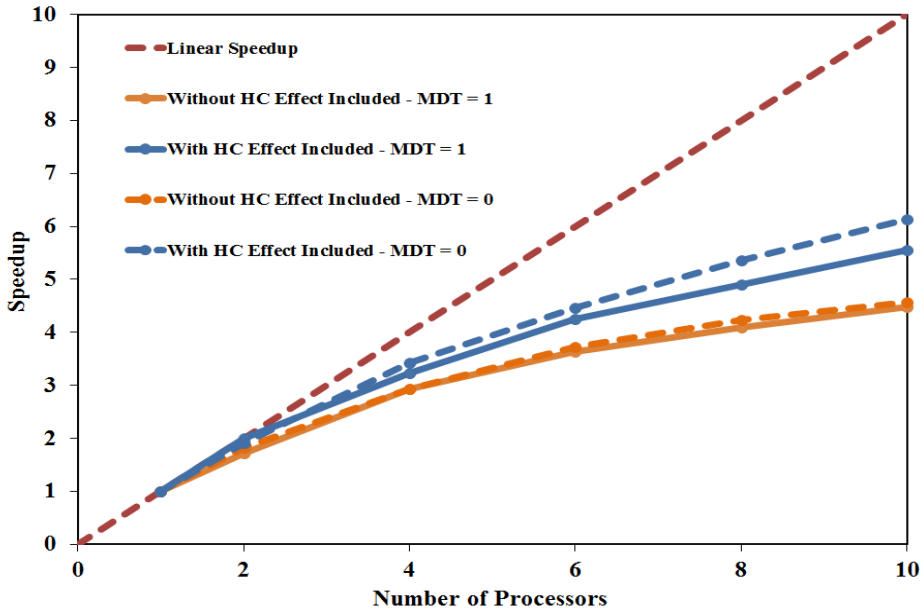

Figure 2-209: Case 11- speedup curves using constant (MDT=0) or automatic time stepping (MDT=1) approaches for cases with and without the hydrocarbon phase effect included in aqueous-rock geochemistry.

Case 12

Case 12 is modified from Case 3. Initial water saturation in Case 3 is changed to 0.5 and the hydrocarbon-CO_2 is included in phase composition calculation. Table 2-50 presents the total computational time when automatic or the constant time stepping criterion is applied in UTCOMP-IPhreeqc (plot is provided in Figure 2-210). It appears from the table that we did not choose appropriate time stepping criteria; hence, the total simulation time is higher when automatic time stepping is applied (although the opposite is expected). For the automatic time stepping, maximum and minimum time steps are 0.25 and 0.001 days, respectively. Whereas, when constant time stepping is applied, time step for the 1^{st} slug is 0.005 days and for the 2^{nd}, 3^{rd}, and 4^{th} slugs, 0.01 days is considered for the time step.

In this case, inclusion of the hydrocarbon phase effect in geochemical calculations slows down the simulation by a factor of 1.2. This factor is almost the same no matter if the automatic time or constant time stepping criterion is applied in UTCOMP-IPhreeqc.

Table 2-50: Case 12- total computational time using constant or automatic time stepping approaches for cases with and without the hydrocarbon phase effect included in aqueous-rock geochemistry

No. of processor(s) in UTCOMP-IPhreeqc	**CPU time (seconds)**			
	Automatic Time Stepping		Constant Time Step	
	With HC phase effect included	Without HC phase effect included	With HC phase effect included	Without HC phase effect included
1PRC	10206	8417	5658.0	4583.0
2PRCs	5519	4476	2997.0	2483.0
4PRCs	3105	2534	1662.0	1392.0
6PRCs	2288	1884	1215.0	1034.0
8PRCs	1877	1550	974.0	843.0
10PRCs	1587	1357	830.0	740.0

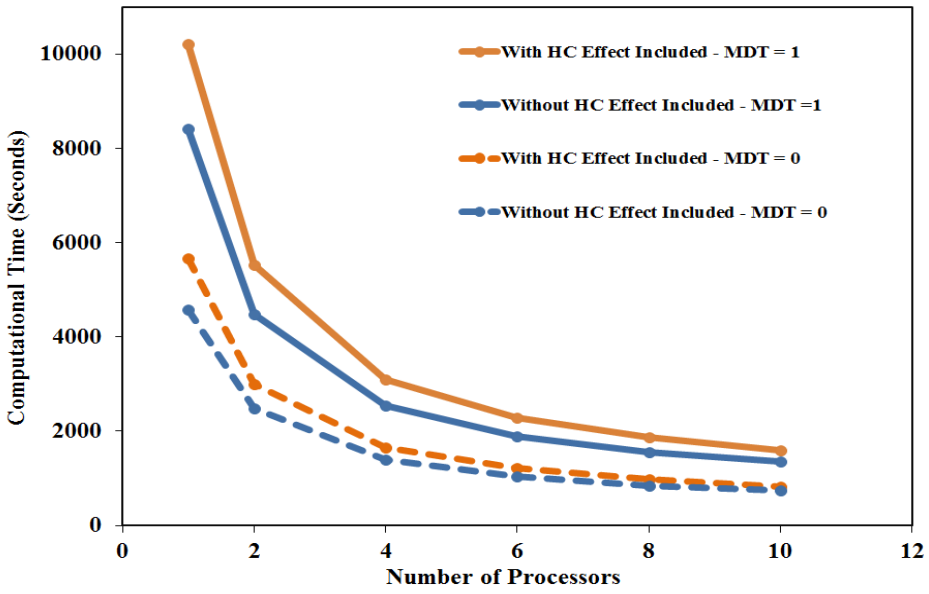

Figure 2-210: Case 12- total computational time using constant (MDT=0) or automatic time stepping (MDT=1) approaches for cases with and without the hydrocarbon phase effect included in aqueous-rock geochemistry.

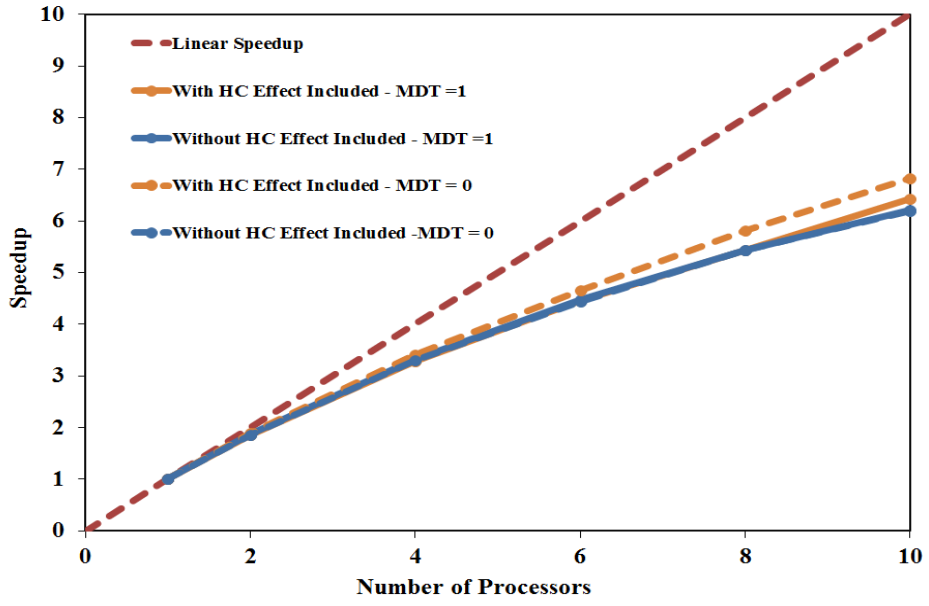

Figure 2-211: Case 12- speedup curves using constant (MDT=0) or automatic time stepping (MDT=1) approaches for cases with and without the hydrocarbon phase effect included in aqueous-rock geochemistry.

2.13 RESTART OPTION IN UTCOMP-IPHREEQC

Restart option is needed in a reservoir simulator, particularly if long simulation runs are desired. By using the restart option in the simulator, one can resume the simulation without the need to restart from the beginning. Moreover, the restart option can be also useful if, for any reason, simulation crashes before it finishes successfully. If this is the case, simulation can be resumed after some manipulation for example in the time stepping criteria. For a reservoir simulator to have the restart option, data required to run the simulator for a time step are stored in a file (usually a binary file) at certain frequencies. If a simulation run is to be resumed, the restart files (rather than the main input files) are used to initialize the reservoir parameters.

The UTCOMP simulator already has the restart option (implemented in UTCOMP by Chang, 1990). If ISTORE=1 in the UTCOMP input file, then during simulation runs, UTCOMP stores porosity, permeabilities, molar and mass densities, total moles of the hydrocarbon components, overall mole fractions, and total moles of the tracer components (if included in the model) at certain frequencies (defined through the NSTSKIP keyword in the input file by the user) in the restart file (i.e., TEST.STO). If restart option is applied in UTCOMP (i.e., ISTART=2), rather than INPUT.DAT (i.e., the main UTCOMP input file), the TEST.STO file is used for the initialization.

The main goal in this section is to include the restart option in the UTCOMP-IPhreeqc integrated simulator. To make the restart option available in UTCOMP-IPhreeqc, along with the other data stored in the TEST.STO file, total moles of geochemical species transported in UTCOMP as well as concentrations of the geochemical species in the aqueous phase should be stored in this file. Moreover, exactly at the same time at which UTCOMP writes the TEST.STO file, the geochemistry data

accumulated in the computer memory, used for the IPhreeqc calculations, should be dumped into a file (labeled as TESTGC.STO). Hence, if the restart option is applied in UTCOMP-IPhreeqc, TEST.STO (rather than INPUT.DAT) is used to initialize the transport related parameters and TESTGC.STO (rather than IPhreeqc_INPUT.DAT) is accumulated in the computer memory for the IPhreeqc to initialize the geochemistry of the gridblocks. We use **DUMP** along with *SetDumpFileOn*(ID_PHREEQC, .TRUE.) and *RunAccumulated* methods (ID_PHREEQC is the main IPhreeqc module ID in the UTCOMP-IPhreeqc simulator) available in IPhreeqc to get the geochemistry data of the gridblocks from the computer memory and store them in the TESTGC.STO file. Right after dumping the TESTGC.STO file, *SetDumpFileOn*(ID_PHREEQC, .FALSE.) should be used to disable continuous dumping of the geochemistry data from the computer memory for the later unnecessary time steps. In other words, we dump the geochemistry data with the same frequency by which the restart files are stored. Dumping the geochemistry data at each time step drastically slows down simulation runs.

Storing the TESTGC.STO file (i.e., the geochemistry restart file) becomes more complicated when multiple processors are used in the simulation. In this case, the master processor does not have the geochemistry information of the entire gridblocks but only of some of the gridblocks that it performs geochemical calculations for them (the same for slave processors). Hence, before the master processor writes the restart file (in general, in the parallel processing writing the output files should be done only through the master processor), it should first collect the geochemistry data accumulated in slave processors' memories.

We use *SetDumpStringOn*, *AccumulateLine*, *RunAccumulated*, *GetDumpStringLineCount*, *GetDumpStringLine* methods of IPhreeqc to get the

geochemistry data accumulated in each of the slave processor memories and save them in a temporary string variable. We then use MPI_SEND of MPI to send the string from the slave processors to the master processor. The master processor receives the massages from the slave processors using the MPI_RECV of MPI. **COPY** and **DELETE** methods available in IPhreeqc are applied in the master processor to put the geochemistry data in the actual order that they should be. For example, if 3 processors (ranked from 0 through 2) are considered to model a reactive-transport case with 75 gridblocks, each processor has the geochemistry data of 25 gridblocks. The processor with rank 0 (i.e., master processor) has the geochemistry data for the gridblocks 1 through 25 and gridblocks 26 through 50 and 51 through 75 are stored in the processors with rank 1 and 2, respectively. As mentioned previously, all the processors call the same routines with "do loops" starting from 1 through NB. Hence, the geochemistry data in all the processors (either slave or master) is from cell 1 through 25. Therefore, with massage received from a slave processor to the master, data should be sorted to the actual order. With this, geochemistry data of gridblocks 1 through 25 received from the processor with rank 1 and 2 are reordered to 26 through 50 and 51 through 75 gridblocks in the master processor, respectively. It is worth mentioning that in the master processor, ID_PHREEQC is the IPhreeqc module ID used for geochemical calculations, whereas ID_PHREEQC_STORE is the IPhreeqc module ID applied for storing the TESTGC.STO file (multiple independent IPhreeqc modules can be created in each processor using the *CreateIPhreeqc* method). In fact, data received from slave processors (for gridblocks 26 through 75) are directly accumulated in the ID_PHREEQC_STORE module. On the other hand, because the master processor already has geochemistry data of gridblocks 1 through 25, they are just transferred from the ID_PHREEQC module to the

ID_PHREEQC_STORE module. Once the master processor has all the data collected and reordered in the ID_PHREEQC_STORE module ID, **DUMP** is applied in the master processor that stores the geochemistry data in the TESTGC.STO file. Appendix G presents the command lines followed in UTCOMP-IPhreeqc to write the restart file when using the single- or multiple-processor code. Obviously, because the geochemistry data of the entire gridblocks are stored in a single file (rather than a strange approach in which each processor writes its own TESTGC.STO file), not necessarily the same number of processors should be considered if the restart files (i.e., TEST.STO and TESTGC.STO) are to be used later to resume the simulation.

If the restart option is applied in the parallel version of UTCOMP-IPhreeqc, only the master processor reads the TEST.STO file; however, all the processors (slaves and the master) read the TESTGC.STO file (rather than IPhreeqc_INPUT.DAT). The geochemistry data for extra gridblocks are then deleted from the processors. The reason that the slave processors do not read the TEST.STO file is that the slave processors are not involved in any calculations other than the phase composition calculations.

The implementation of the restart option in UTCOMP-IPhreeqc can be verified against the continuous simulation. Hence, we design a case using UTCOMP-IPhreeqc and run it for about 1.1 PV. The same case is then simulated for 0.1 PV and the UTCOMP-IPhreeqc restart files are used to resume the simulation to 0.2 PV. The same sequence is followed till 1.1 PV is injected into the reservoir. Table 2-51presents the case descriptions and well pattern is shown in Figure 2-212. Absolute permeability (in all directions) and porosity are heterogeneous and absolute permeabilities in the *x* and *y* directions are identical (see Figures 2-213 through 2-215 for porosity and permeability maps). The parallel version of UTCOMP-IPhreeqc is applied for the simulation and

different number of processors is considered to run each 0.1-PV subinterval. Wettability alteration (described in Section 2.11) is included in the model with the interpolating parameter as a function of the total ionic strength of the solution (the wettability alteration model is described in Chapter 3). “FB” is the connate water (see Table 2-52) and dolomite and calcite with the saturation index of -0.4 and 0.4, respectively, are the reservoir minerals. Rate for the injection wells is 200 bbl/day (“SW/50” shown in Table 2-52 is the injecting water) and the bottomhole pressure of the production wells is 1100.0 psi.

Figures 2-216 through 2-226 verify the average reservoir pressure, cumulative oil recovery, and some ion histories of two different gridblocks (i.e., (10,10,1) and (9,15,3)) of the continuous simulation with those of using the restart option.

Table 2-51: Reservoir characteristics for the 3D case

No. of gridblocks		7452 (46×54×3)	
Δx(ft)		25.0	
Δy(ft)		25.0	
Δz(ft)		4.0	
Permeability (md)	*x*-direction	Heterogeneous	
	y-direction	Heterogeneous	
	z-direction	Heterogeneous	
Porosity		Heterogeneous	
Rock compressibility (psi^{-1})		50.0×10^{-6}	
Water compressibility (psi^{-1})		0.0	
Initial water saturation		0.3	
Irreducible water saturation		0.2	
Reservoir temperature (^{o}F)		248.0	
Initial pressure (psi)		1100.0	
Reservoir depth (ft)		2500.0	
Water viscosity (cp)		0.79	
Number of wells		5	3 injectors
			2 producers
Simulation time(PV)		1.1	

Table 2-52: Formation brine (FB) and SW/50 ion concentrations (from Chandrasekhar, 2013). Ion concentrations are in ppm and the total ionic strength is in mol/kgw

Ion	FB	SW/50
Na^{+}	49933	274
Mg^{+2}	3248	32.4
Ca^{+2}	14501	10.42
Cl^{-}	111810	489.36
SO_4^{-2}	234	66.2
HCO_3^{-}	-	-
Total ionic strength	3.658	0.017
TDS (mg/L)	179730	872

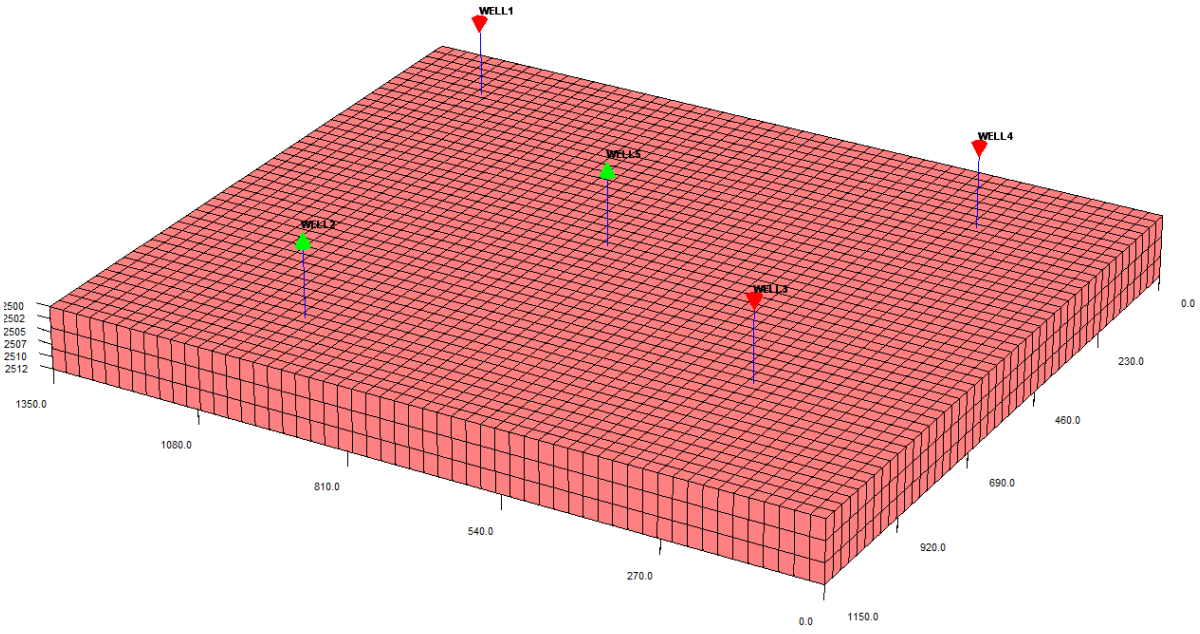

Figure 2-212: Well locations in the 3D case considered to verify the restart option implemented in UTCOMP-IPhreeqc.

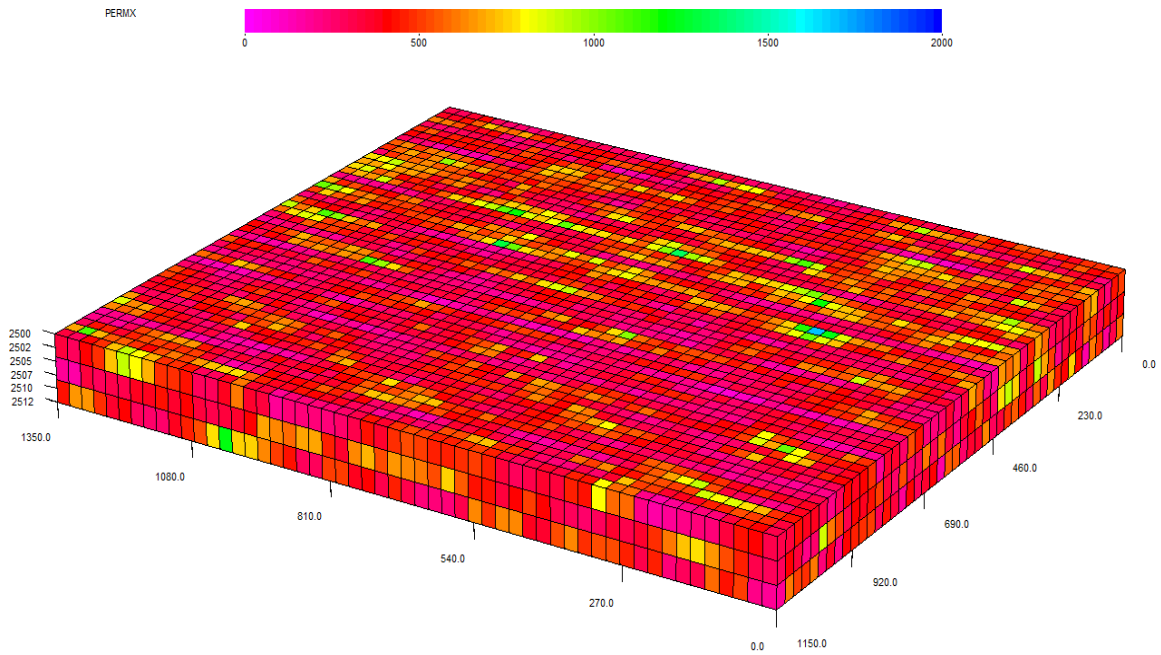

Figure 2-213: Absolute permeability (in md) distribution in *x* and *y* directions.

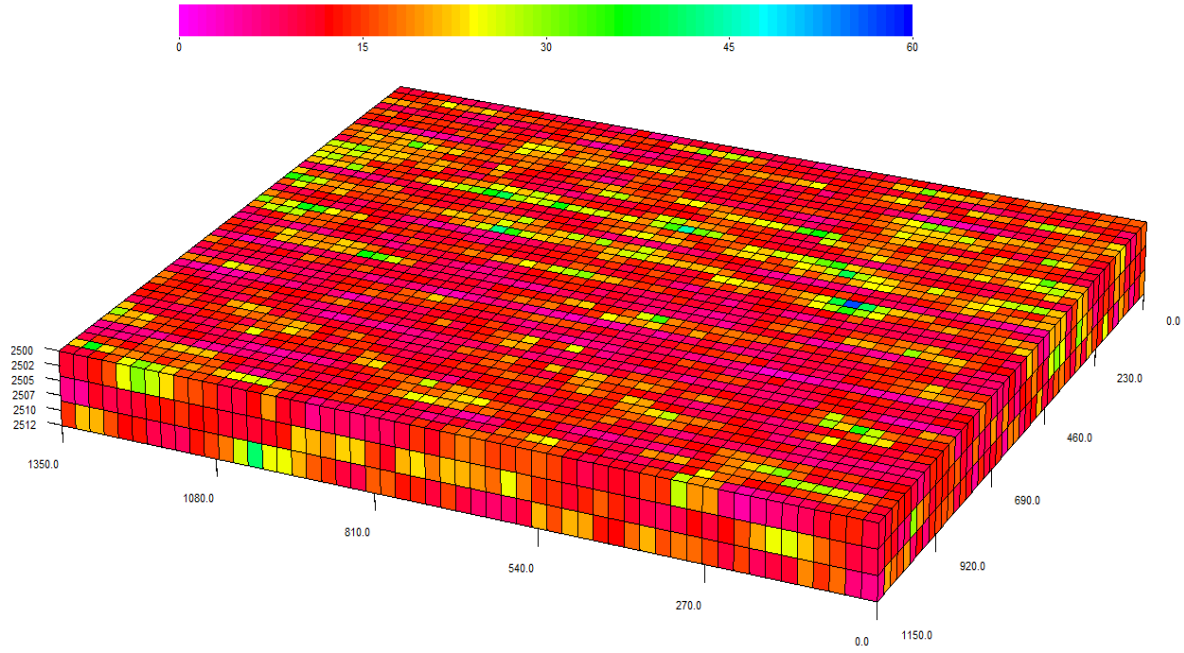

Figure 2-214: Absolute permeability (in md) distribution in *z*-direction.

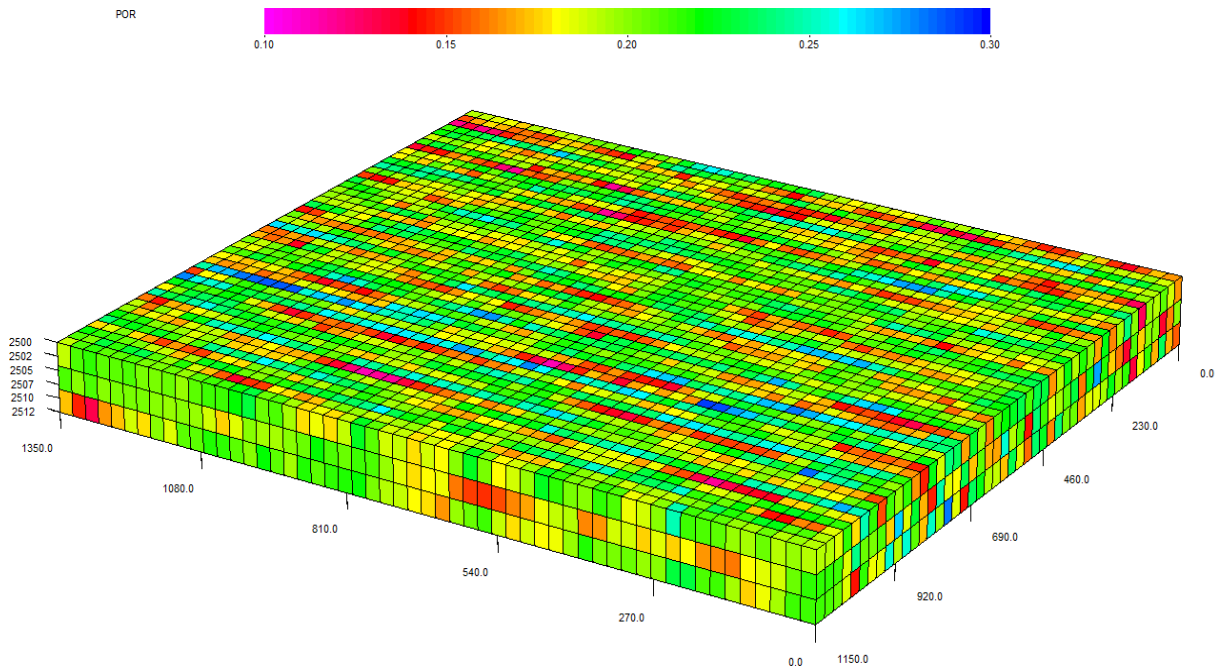

Figure 2-215: Porosity distribution.

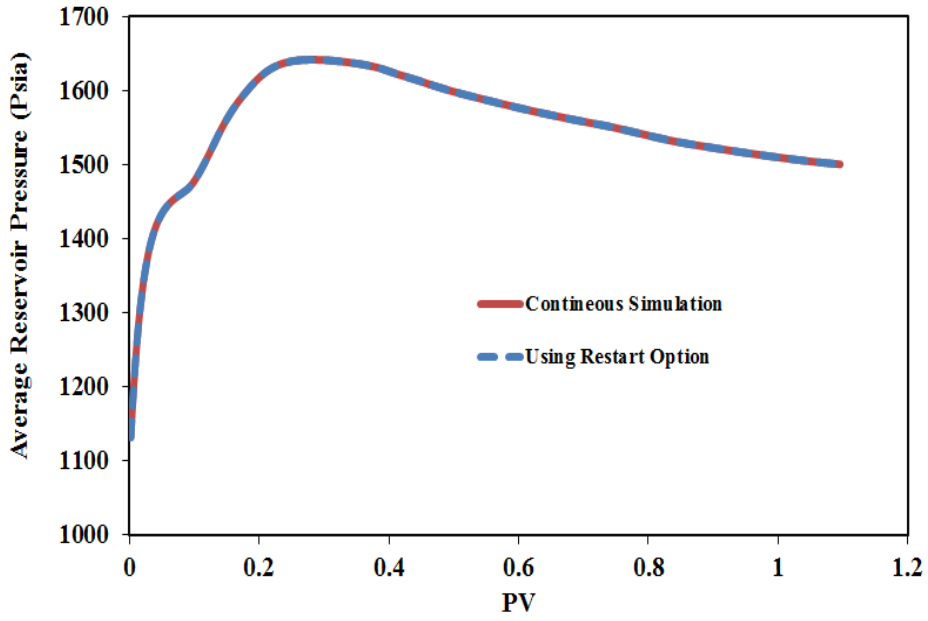

Figure 2-216: Average reservoir pressure (verification of the restart option implemented in UTCOMP-IPhreeqc).

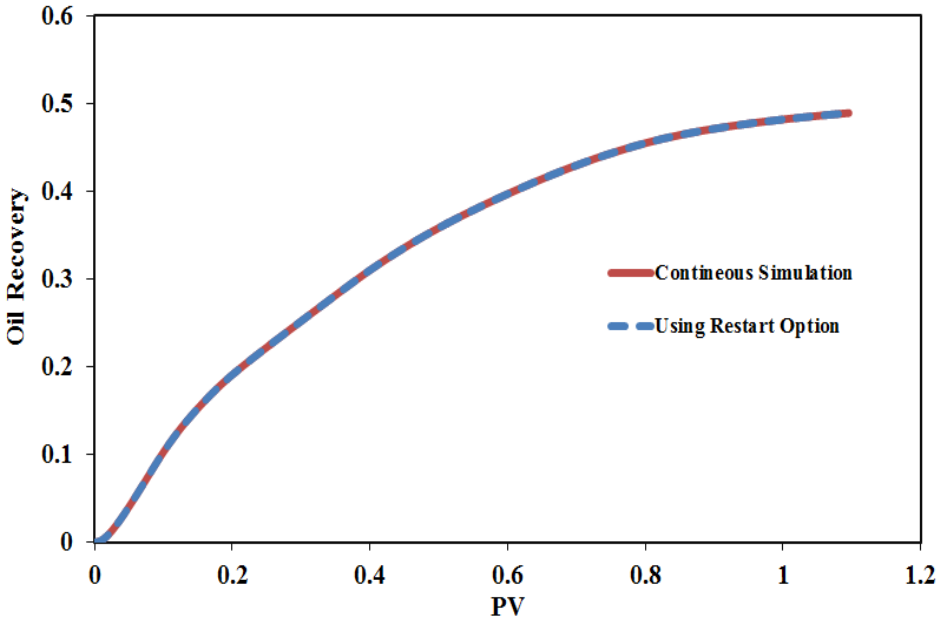

Figure 2-217: Oil recovery (verification of the restart option implemented in UTCOMP-IPhreeqc).

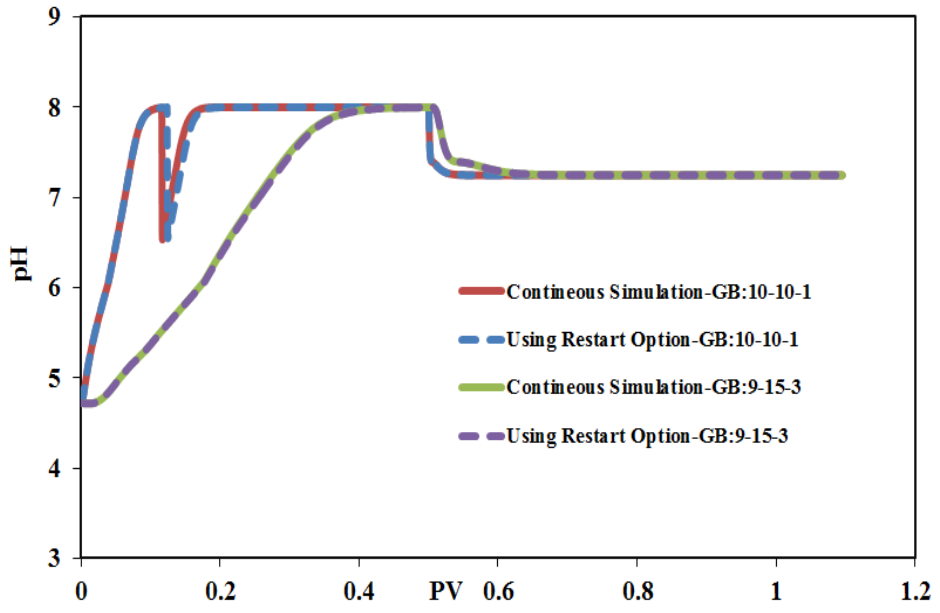

Figure 2-218: pH histories at two gridblocks (verification of the restart option implemented in UTCOMP-IPhreeqc).

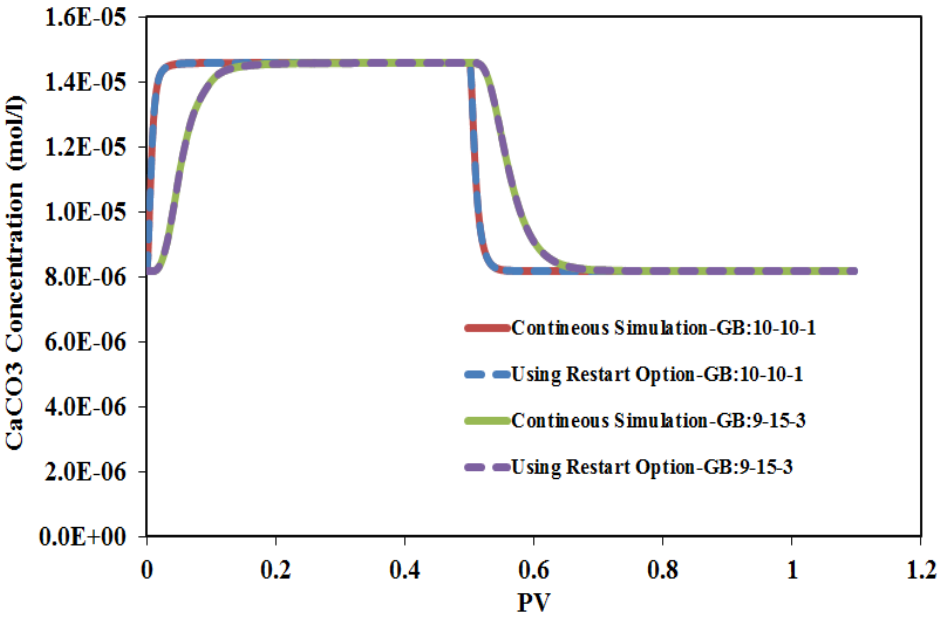

Figure 2-219: $CaCO_3$ concentration histories at two gridblocks (verification of the restart option implemented in UTCOMP-IPhreeqc).

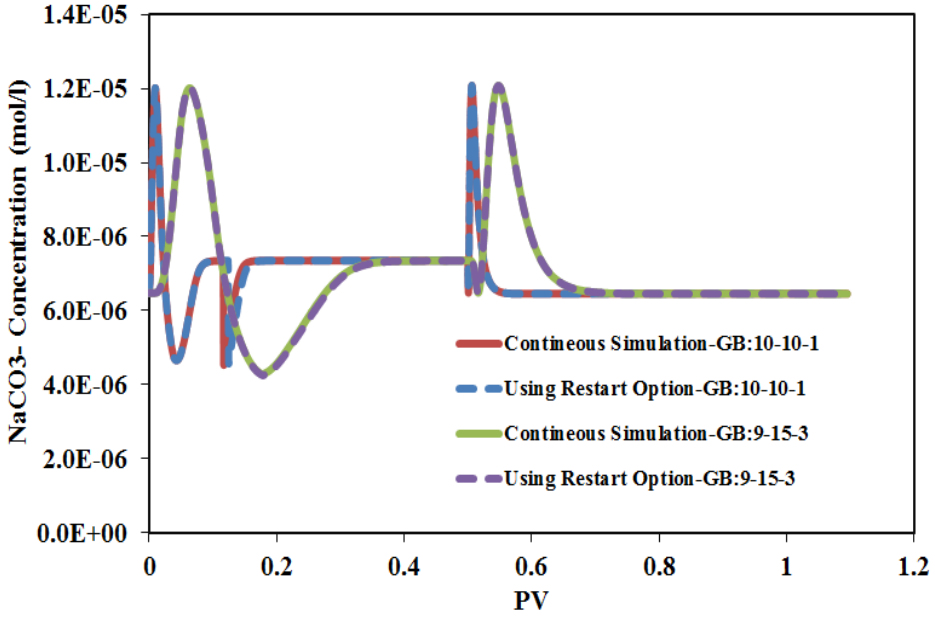

Figure 2-220: $NaCO_3^-$ concentration histories at two gridblocks (verification of the restart option implemented in UTCOMP-IPhreeqc).

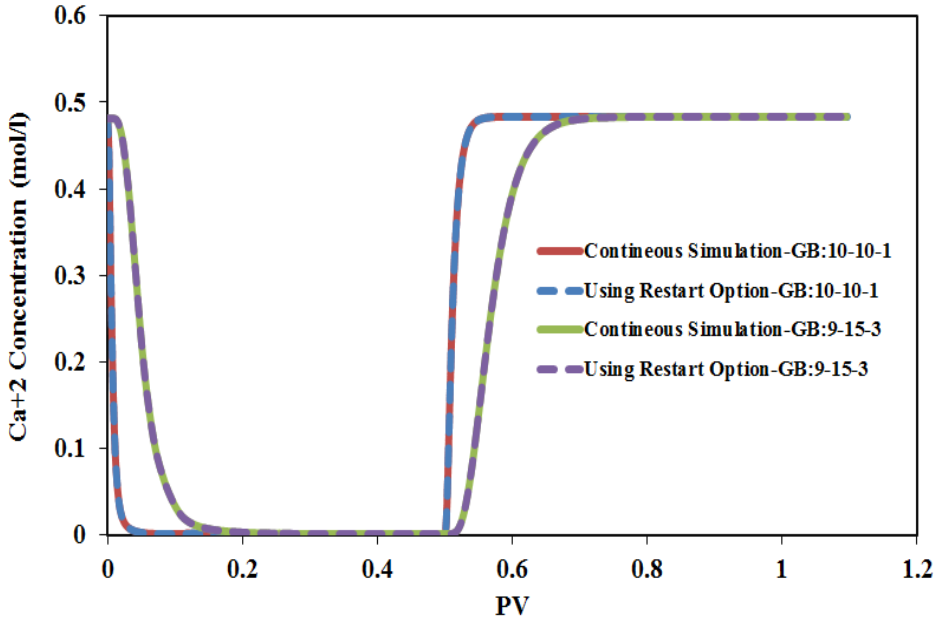

Figure 2-221: Ca^{+2} concentration histories at two gridblocks (verification of the restart option implemented in UTCOMP-IPhreeqc).

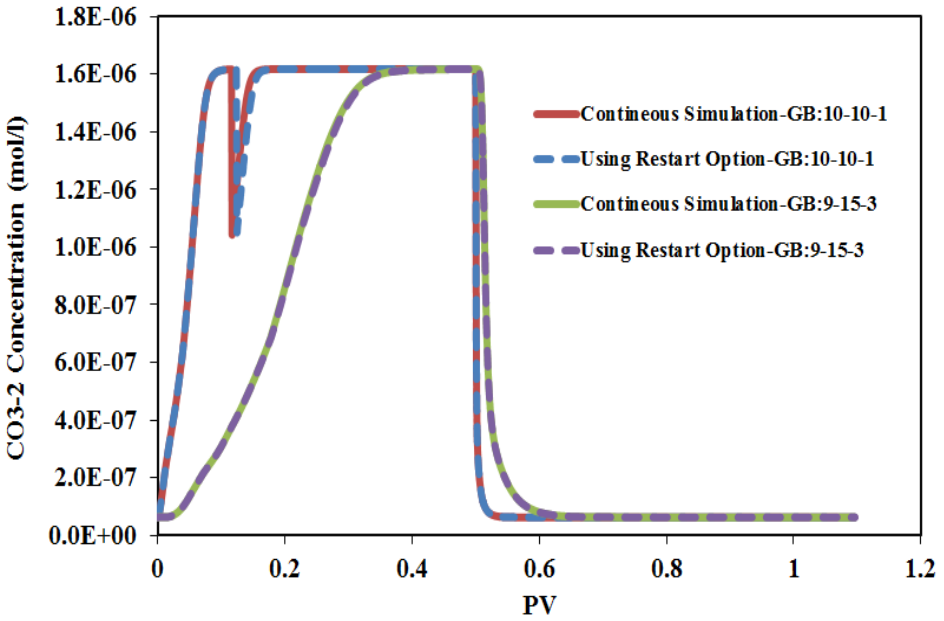

Figure 2-222: CO_3^{-2} concentration histories at two gridblocks (verification of the restart option implemented in UTCOMP-IPhreeqc).

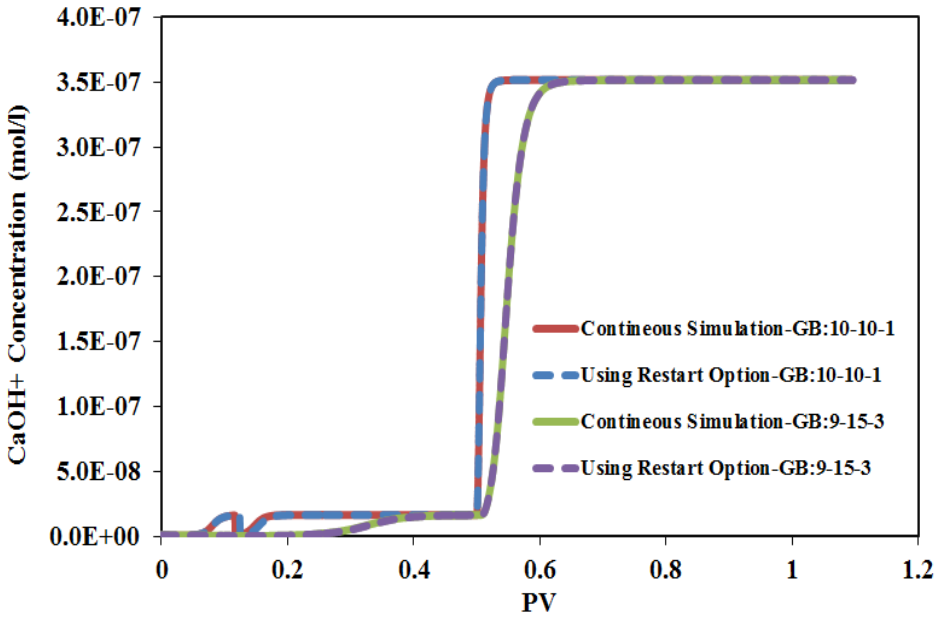

Figure 2-223: $CaOH^{+}$ concentration histories at two gridblocks (verification of the restart option implemented in UTCOMP-IPhreeqc).

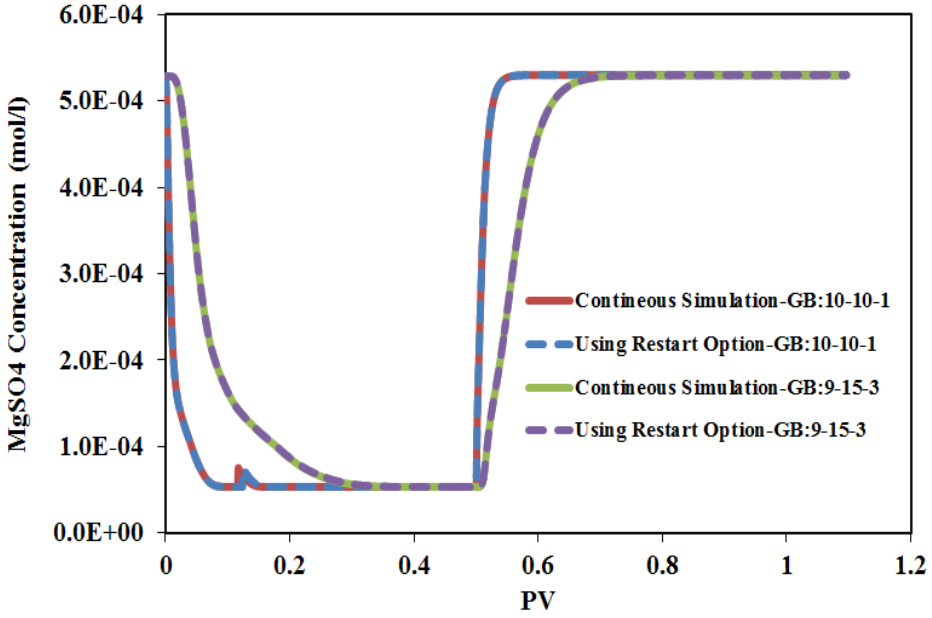

Figure 2-224: $MgSO_4$ concentration histories at two gridblocks (verification of the restart option implemented in UTCOMP-IPhreeqc).

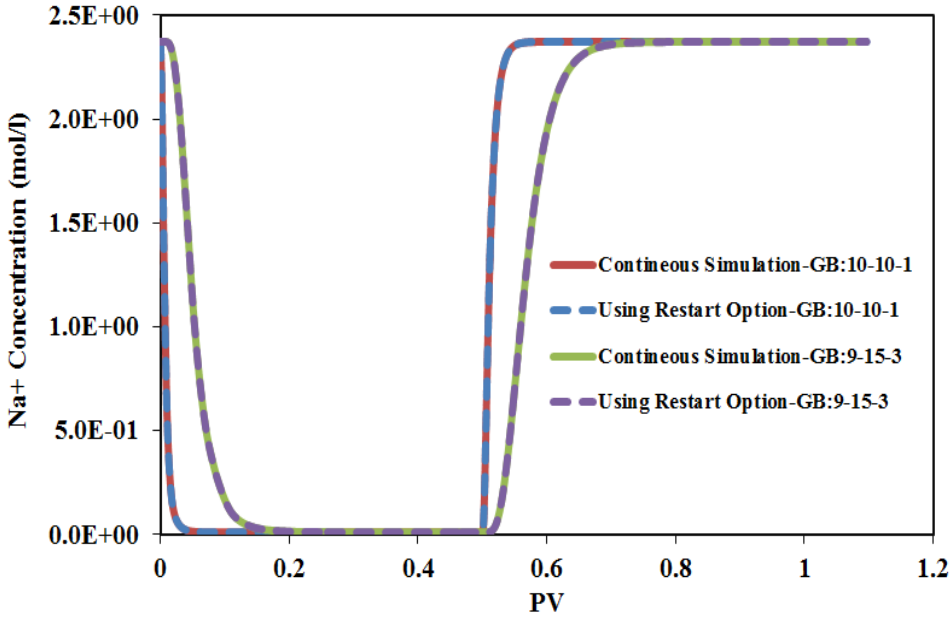

Figure 2-225: Na^{+} concentration histories at two gridblocks (verification of the restart option implemented in UTCOMP-IPhreeqc).

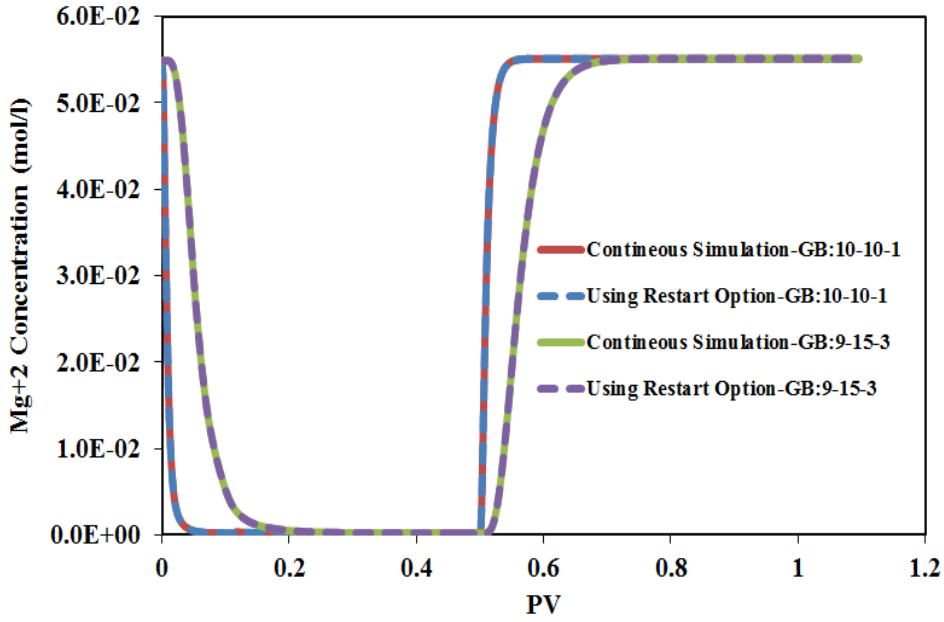

Figure 2-226: Mg^{+2} concentration histories at two gridblocks (verification of the restart option implemented in UTCOMP-IPhreeqc).

2.14 DEVELOPMENT OF UTCOMP-IPHREEQC TO BE USED ALONG WITH TDRM

UTCOMP-IPhreeqc is flexible enough that can be enhanced to be used along with any post-processing or history matching tool. For example, we added several routines to generate the appropriate output file read by a history matching tool called TDRM. TDRM (Top-Down Reservoir Modeling), developed by BP, for automatic history-matching. This history matching tool uses Genetic algorithm and the Nelder-Mead simplex to perform the automatic history matching (Williams *et al.*, 2004; Jerauld *et al.*, 2010). We take advantage of TDRM in modeling low salinity waterflooding of sandstone reservoirs (cf. Chapter 3).

Chapter 3: Mechanistic Modeling of Low Salinity Waterflooding in Sandstone Reservoirs

The goal of this chapter is to review the important findings published in the literature on low salinity waterflooding in sandstone formations. We then implement a mechanistic model proposed by Ligthelm *et al.* (2009) in UTCOMP-IPhreeqc (the integrated simulator developed in Chapter 2) to mechanistically model low salinity waterflooding in sandstone reservoirs. UTCOMP-IPhreeqc with the model implemented is then applied to model a coreflood published by Kozaki (2012) and the Endicott field trial.

3.1 Low Salinity Waterflooding in Sandstone Reservoirs

Increase in recovery of crude oil with decrease in salinity has been observed for numerous laboratory and field application waterfloods in sandstone formations. Some of these reports are discussed in the following sections.

3.1.1 Laboratory Works on Low Salinity Waterflooding in Sandstones

Tang and Morrow (1996) conducted coreflooding experiments in a sandstone core. They injected water with different salinities into the core consecutively. For the first cycle, water with salinity identical to the reservoir brine is injected into the core and then in the second cycle, water salinity was decreased to 0.1 of the initial formation salinity. In the last cycle, total salinity was kept the same as that in the second cycle but concentration ratio for the Ca/Na ions was increased to 10. Additional oil recovery after the injection of second cycle was 5.8% of the OOIP. However, no additional oil was recovered in the third cycle of injection.

Zhang *et al.* (2007)'s experimental results conducted on sandstone reservoir cores demonstrate that low salinity waterflooding can show promising results in both secondary and tertiary modes. Low salinity water (with the salinity of 1,479 ppm) when injected in tertiary mode, improves oil recovery by about 7-14% OOIP compare with the high salinity water (with salinity of 29,690 ppm). Moreover, the secondary oil recovery to low salinity water is significantly higher than that of high saline water. Change in pH of the effluent solution during the low saline waterflooding is negligible. On the other hand, pressure drop across the core increases during the process. Their experimental results also show no tertiary oil recovery when the low salinity water is switched with 8000 ppm sodium chloride. However, tertiary oil recovery substantially increases if the salinity of the sodium chloride solution is decreased to 1500 ppm.

Patil *et al.* (2008) presented coreflood results for low salinity water injection. This experiment was done in a secondary recovery mode using the core from in Alaska North Slope (ANS) formation. Brine salinity for the injected water ranged from 5,500 to 22,000 mg/l. All of their coreflood results confirm up to 20% reduction in oil saturation. They proposed wettability alteration as the main mechanism for low salinity water injection.

Cissokho *et al.* (2010) ran an experiment on an outcrop sandstone containing 9.2% total clay content (with no kaolinite). Their experimental results show that decreasing the salinity of the water, when injected in the tertiary mode, from 50 g/l to 1 g/l improves oil recovery by about 10% OOIP. Cissokho *et al.* (2010) observed increase in pH and pressure drop during low salinity waterflooding does not correlate with incremental oil recovery. Their experimental results also show that oil recovery due to low salinity waterflooding is a temperature-dependent process. While oil recovery in the

secondary mode is higher at elevated temperatures, moderate temperatures are more favorable in tertiary mode.

Rivet *et al.* (2010) conducted several corefloods to study the effect of low salinity waterflooding on oil recovery, residual oil saturation, and relative permeability curves. They observed a decrease in end-point water relative permeability and an increase in end-point oil relative permeability. The authors claimed that injecting low salinity brine produced a persistent wettability alteration that eliminates the dependency of the oil recovery to salinity in subsequent floods. No additional oil was recovered in cases where water is injected in the tertiary mode or when cores are strongly water-wet. They proposed wettability alteration as the main mechanism for low salinity water injection.

Experimental results documented by Gamage *et al.* (2011), conducted on Berea outcrop, show that low salinity waterflooding improves oil recovery in both secondary and tertiary modes (2-8% OOIP). However, incremental oil recovery is higher when low salinity water is injected in secondary mode. On the other hand, low salinity waterflooding improves oil recovery from the Minnelusa reservoir cores only when injected in secondary mode (10-22% OOIP). Gamage *et al.* (2011) also observed increase in pH of solution during low salinity water injection in both Berea outcrop and Minnelusa reservoir cores.

Hadia *et al.* (2011) conducted several corefloods on the Frøy reservoir cores. Their results show that injecting low salinity water decreases the residual oil saturation by 4-9% which leads in 6-14% OOIP incremental oil recovery. However, the incremental oil recovery in corefloods is along with substantial decrease in core permeabilities.

Nasralla *et al.* (2011c)'s experimental results conducted on eight Berea sandstone outcrop cores demonstrate that low salinity water, when injected in secondary mode,

significantly improves oil recovery (up to 22%) compare with seawater (with the salinity of 54,680). Deionized and aquifer (with the salinity of 5,436 mg/l) waters are used as the low salinity waters and salinity of formation water is 174,156ppm in this work. Interestingly enough, no additional oil recovery is produced when low saline water is injected in the tertiary mode. These results are confirmed using two different crude oils. Nasralla *et al.* (2011c) proposed cation exchange as the underlying mechanism behind low salinity waterflooding in sandstones.

3.1.2 Field Applications on Low Salinity Waterflooding in Sandstones

To confirm the lab results obtained for low salinity water injection, for the first time, Webb *et al.* (2004) conducted a log-inject-log through a clastic reservoir to see how low salinity water injection changes the remaining oil saturation near the wellbore. They observed a 25-50% reduction in residual oil saturation when low salinity water is injected into the reservoir. Waters with salinities of 220,000, 170,000, and 3,000 mg/l were injected in sequence into the reservoir. After stabilization of each test, the log-inject-log was run in the wellbore. Results show that the remaining oil saturation is not changed when waters with salinities of 220,000 and 170,000 mg/l are injected into the reservoir, while the remaining oil saturation significantly decreases, between 25-50%, for water with the salinity of 3,000 mg/l.

McGuire *et al.* (2005) ran single-well chemical tracer tests (SWCTT) in sandstone reservoirs in Alaska and showed that the lab results can be replicated in the field. This field test was run in the tertiary mode. Residual oil saturation was drastically reduced with an increase in oil recovery of 6 to 12 % of the original oil in place (OOIP).

Lager *et al.* (2008b) have reported another successful experience for low salinity water injection into an Alaskan reservoir. Low salinity water injection caused a

significant drop in the water oil ratio and the oil production rate was doubled during nearly 12 months of production. Although in some of the previous corefloodings, clay swelling or pore plugging was observed during low salinity water injection, Lager *et al.* (2008b) did not see any evidences of these issues during their field study.

Vledder *et al.* (2010) presented results for a full field-scale flood in Omar field in Syria. They described a field-scale proof of wettability alteration using low salinity water injection in mixed to oil-wet Omar sandstone formation. The reservoir has light oil with viscosity of 0.3 cp, formation water salinity of 90,000 mg/l, and bivalent cations of 5000 mg/l. Low salinity water was injected in the secondary mode using river water with salinity of 500 mg/l and less than 100 mg/l bivalent cations. Their results showed that an additional 10-15% of OOIP was recovered using low salinity water injection into mixed to oil-wet sandstone reservoirs

3.1.3 Modeling Low Salinity Waterflooding in Sandstone Reservoirs

The first model for low salinity waterflooding was proposed by Jerauld *et al.* (2008). This model applies the interpolating technique and makes oil and water relative permeabilities salinity-dependent between salinity thresholds. In fact, in this model, residual oil saturation is salinity dependent and interpolating parameter is defined as a function of residual oil saturation. Eqs. (3.1) through (3.5) present the Jerauld *et al.* (2008)'s model formulation:

$$k_{rw} = \theta k_{rw}^{HS}\left(S^*\right) + \left(1-\theta\right)k_{rw}^{LS}\left(S^*\right), \tag{3.1}$$

$$k_{row} = \theta k_{row}^{HS}\left(S^*\right) + \left(1-\theta\right)k_{row}^{LS}\left(S^*\right), \tag{3.2}$$

$$P_{cow} = \theta \times P_{cow}^{HS}(S^*) + (1-\theta) \times P_{cow}^{LS}(S^*), \tag{3.3}$$

$$\theta = (S_{orw} - S_{orw}^{LS}) / (S_{orw}^{HS} - S_{orw}^{LS}), \tag{3.4}$$

$$S^* = (S_o - S_{orw}) / (1 - S_{wr} - S_{orw}), \tag{3.5}$$

where

k_{rw} = relative permeability to water phase

k_{rw}^{HS} = relative permeability to water phase of high salinity set

k_{rw}^{LS} = relative permeability to water phase of low salinity set

θ = interpolation parameter ($\theta = 1$ for high salinity water and $\theta = 0$ for low salinity water)

k_{row} = relative permeability to oil phase

k_{row}^{HS} = relative permeability to oil phase of high salinity set

k_{row}^{LS} = relative permeability to oil phase of low salinity set

P_{cow} = oil/water capillary pressure (psi)

P_{cow}^{HS} = oil/water capillary pressure of high salinity set (psi)

P_{cow}^{LS} = oil/water capillary pressure of low salinity set (psi)

S_{orw} = residual oil saturation

S_{orw}^{LS} residual oil saturation to low salinity waterflood

S_{orw}^{HS} residual oil saturation to high salinity waterflood

S_{wr} = irreducible water saturation

Wu and Bai (2009) formulated a model that does not interpolate between two sets of relative permeabilities through an interpolating parameter. Similar to Jerauld *et al.* (2008)'s model, in this model, using the total salinity, residual oil saturation is interpolated between low salinity and high salinity residual oil saturations. However, the calculated residual oil saturation is then directly used to evaluate the relative permeabilities. Wu and Bai (2009)'s formulations are presented below:

$$k_{rw} = \left(\bar{S}_w\right)^{2+\varphi}\left[\bar{S}_w\left(X_c\right)\right], \tag{3.6}$$

$$k_{ro} = \left(\bar{S}_o\right)^{2}\left[1-\left(\bar{S}_w\right)^{\varphi}\right], \tag{3.7}$$

$$\bar{S}_w = \frac{S_w - S_{wr}}{1-S_{wr}}, \tag{3.8}$$

$$\bar{S}_o = \frac{S_o - S_{or}\left(X_c\right)}{1-S_{wr}}, \tag{3.9}$$

where

k_{rw} = relative permeability to water phase

φ = the Brooks-Corey exponential index

X_c = salt mass fraction in the aqueous phase

k_{ro} = relative permeability to oil phase

S_w = water saturation

S_{wr} = irreducible water saturation

S_{or} = residual oil saturation

Wu and Bai (2009) proposed the following correlation that makes the residual oil saturation salinity-dependent:

$$S_{or}\left(X_c\right) = S_{or1} + \frac{\left(-0.1083\right)\left(X_c\right)^2 + \left(1.244\right)\left(X_c\right) + \left(-4.694\times10^{-8}\right)}{X_c + 0.1353}\left(S_{or1} - S_{or2}\right), \qquad (3.10)$$

where

S_{or} = residual oil saturation

S_{or1} = residual oil saturation to high salinity waterflood (at high salt mass fraction X_{c1})

S_{or2} = residual oil saturation to low salinity waterflood (at high salt mass fraction X_{c2})

φ = the Brooks-Corey exponential index

X_c = salt concentration in the aqueous phase

k_{ro} = relative permeability to oil phase

S_w = water saturation

S_{wr} = irreducible water saturation

Omekeh *et al.* (2011) conducted a single-phase experiment in Berea sandstone cores using several brines with different ion compositions. Consistent with their experimental observations, they proposed a model for low salinity waterflooding. Their proposed model interpolates between two extreme sets of relative permeability and

capillary pressure with the interpolating parameter as a function of divalent cation desorption from the ion-exchanger.

Dang *et al.* (2013) modeled wettability alteration due to low salinity water waterflooding as a function of Ca^{2+} equivalent fraction on the ion exchanger. In this model as more Ca^{2+} ion adsorbs on the rock, wettability changes from oil-wet towards water-wet. Dang *et al.* (2013)'s model is also based on the interpolating technique between two extreme sets of relative permeability and capillary pressure.

3.2 MECHANISTIC MODELING USING UTCOMP-IPHREEQC

Sandstone reservoirs contain clays and clays are negatively charged. This provides an opportunity for positive ions (i.e., cations) to get close to the clay surface and adsorb on the surface. This is well illustrated in the work of Lee *et al.* (2010) (i.e., Figure 3-1a). It is believed that there are two layers of ions surrounding the clay surface. The first layer is "stern layer" and the second layer is called "diffuse layer." The stern layer contains only cations (i.e., Na^{+}, Ca^{+2}, Mg^{+2}, etc.) however, the diffuse layer is sufficiently far from the rock surface that even negative oil components might have the chance to enter. Negative oil components can attach to the divalents (i.e., Ca^{+2}, Mg^{+2}, etc.), present in the stern layer, and that makes the clay surface oil-wet. Figures 3-1b and 3-1c compare the thickness of double-layer (i.e., combination of stern and diffuse layers) when high and low salinity waters are in contact with the rock surface. As these figures demonstrate, during the low salinity waterflooding double-layer expands and that decreases the chance of oil components to get close to the stern layer and attach to the divalents. That is how low salinity waterflooding changes the wettability of the rock from oil-wet towards the water-wet condition.

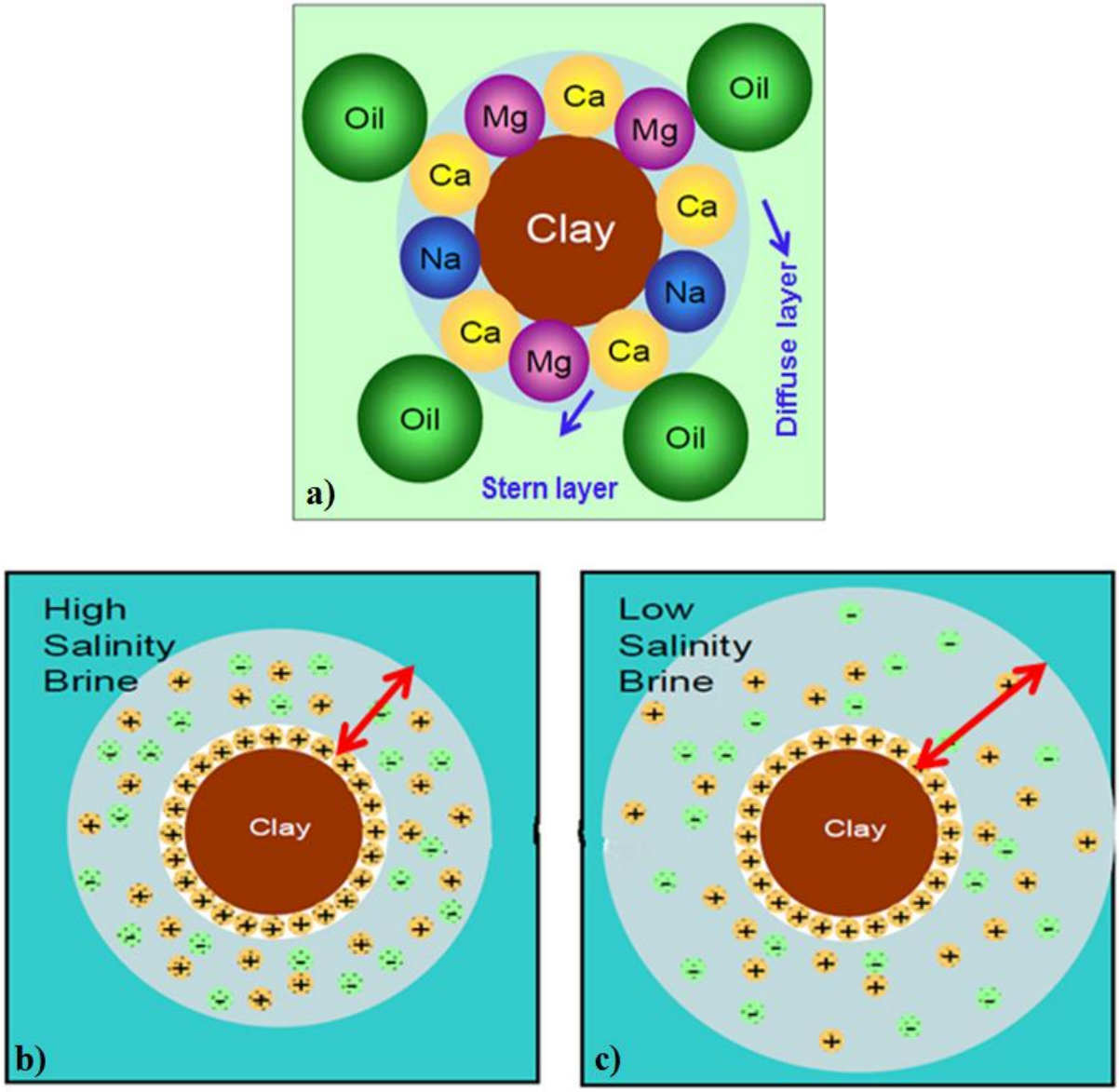

Figure 3-1: a) schematic of electric double-layer and oil components adsorbed to the divalents through the double-layer; b) the thickness of double-layer when high salinity water is in contact with the clay surface; c) the thickness of double-layer when low salinity water is in contact with the clay surface (figures are taken from Lee *et al.* (2010) with minor modifications).

A low salinity model is implemented in UTCOMP-IPhreeqc that relates rock wettability to geochemical calculations. This model is based on the interpolating technique with the interpolating parameter as a function of the total ionic strength (shown in Eq. (3.11)). Total ionic strength is believed to be the controlling parameter if the double-layer expansion is the dominant mechanism for low salinity waterflooding in sandstones. This philosophy is first proposed by Ligthelm *et al.* (2009) and later supported by Nasralla *et al.* (2011a; 2011b; 2011c)'s and Xie *et al*. (2014)'s experimental observations.

$$\theta = \frac{TIS_{\max} - TIS(x,t)}{TIS_{\max} - TIS_{\min}}, \tag{3.11}$$

where

$\theta =$ interpolating parameter

$TIS_{max} =$ total ionic strength value above which no wettability alteration is occurred

$TIS(x,t) =$ total ionic strength of each gridblock at certain simulation time

$TIS_{min} =$ total ionic strength value at which maximum wettability alteration is occurred

3.3 MULTI-PHASE REACTIVE-TRANSPORT MODELING IN UTCOMP-IPHREEQC

Before applying UTCOMP-IPhreeqc to model low salinity waterflooding in sandstone reservoirs, we demonstrate the significant effect of soluble hydrocarbon components on the aqueous-rock geochemistry. To study this, a 1D case is designed and three following cases are compared:

- The core is saturated with the Endicott live oil composition and the effect of the soluble hydrocarbon components (both CO_2 and CH_4) is included in multi-phase reactive-transport modeling.
- The core is saturated with the Endicott live oil composition and the aqueous and hydrocarbon phases are two separate phases with no interaction.
- The core is saturated with the Endicott dead oil composition (at 212ºF and 14.7 psi) and the effect of the soluble hydrocarbon components (both CO_2 and CH_4) is included on multi-phase reactive-transport modeling.

For all the three cases, initial oil saturation is 0.7 and the same injection sequence presented in Figure 2-61 is applied. We assumed the maximum and minimum thresholds as the corresponding total ionic strengths of Endicott diluted seawaters with total dissolved salts of 8000 and 2000 ppm, respectively. Table 3-1 presents the detailed ion compositions as well as the total ionic strengths for the seawater and diluted seawaters with the TDS of 8000 and 2000 ppm's. Maximum and minimum thresholds corresponding to these TDS values are 0.1478 and 0.03759 mol/kgw, respectively. In other words, Eq. (3.12) is the interpolating parameter considered in the simulation. Figure 3-2 shows the initial and altered oil and water relative permeability curves to be used along with the interpolating parameter to model the wettability alteration.

$$\theta = \frac{0.1478 - TIS(x,t)}{0.1478 - 0.03759}. \tag{3.12}$$

Figures 3-3 through 3-14 compare the predicted ion production of some aqueous ions for the cases considered. As expected, dead oil carries little soluble hydrocarbon

components hence, the effect of the hydrocarbon phase on the ion production is insignificant. This can be clearly seen in Figures 3-3 through 3-14 where the ion histories for the core “saturated with the live oil and no hydrocarbon interaction” are very close to the case “saturated with the dead oil and with hydrocarbon interaction”. However, except Na^+, which is essentially a tracer, the ion production of the core “saturated with the live oil and with hydrocarbon interaction” are significantly different than the other two cases. The initially produced ion concentrations are also different because the simulation starts at the equilibrium (aqueous phase is saturated with the fugacities of the soluble hydrocarbon components).

Figure 3-15 compares the oil recoveries of the three cases considered. Because the dead oil is more viscous than the live oil, the core saturated with the dead oil shows lower oil recovery compared to the other two cases with the live oil. The interesting point is the difference between the “live oil with HC interaction” and “live oil without HC interaction” cases. The CO_2 that dissolves into the aqueous phase from the hydrocarbon phase changes the total ionic strength of the aqueous phase which results in different breakthrough times and final oil recoveries between the two cases.

Table 3-1: Endicott seawater and diluted (2000 and 8000 ppm) waters composition

Elements	Ion compositions (mg/l)		
	Sea water	Diluted sea water (2000 ppm)	Diluted sea water (8000 ppm)
Al	0.5	0.028818	0.115271
Ba	0.02	0.001153	0.004611
B	0.0	0.0	0.0
Ca	401.67	23.15043	92.60171
Fe^{+2}	0.3	0.017291	0.069163
Li	0.0	0.0	0.0
Mg	1265	72.90883	291.6353
Mn^{+2}	0.05	0.002882	0.011527
P	0.0	0.0	0.0
K	386.33	22.2663	89.0652
Si	2.0	0.115271	0.461084
Na	10812.0	623.1544	2492.618
Sr	7.38	0.42535	1.701398
Zn	0.5	0.028818	0.115271
HCO_3^-	147.02	8.473563	33.89425
Br	67.63	3.897885	15.59154
Cl	18963.83	1092.989	4371.955
F	0.81	0.046685	0.186739
S(6)	2645.83	152.4936	609.9743
TDS	34700.87	2000	8000
Total ionic strength (mol/kgw)	0.6313	0.03759	0.1478

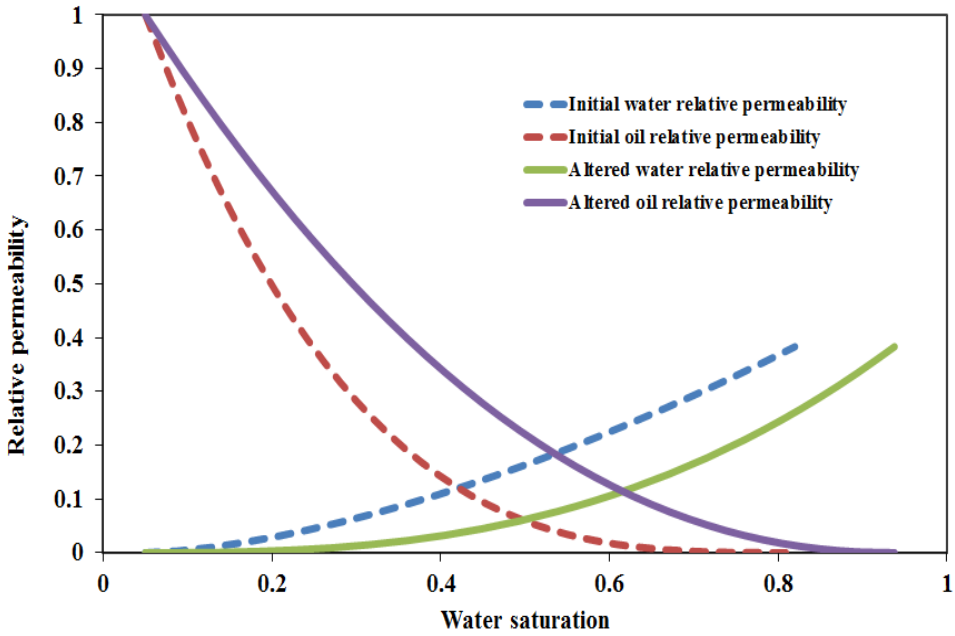

Figure 3-2: Initial and altered relative permeability curves.

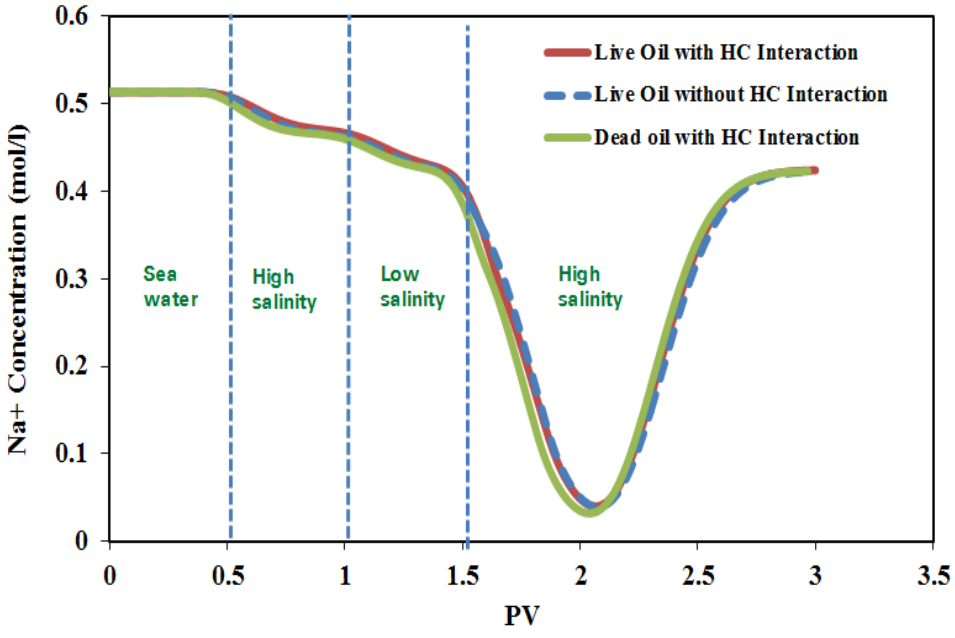

Figure 3-3: Na^{+} concentration history of the effluent solution (effect of the hydrocarbon phase on the aqueous-rock geochemistry).

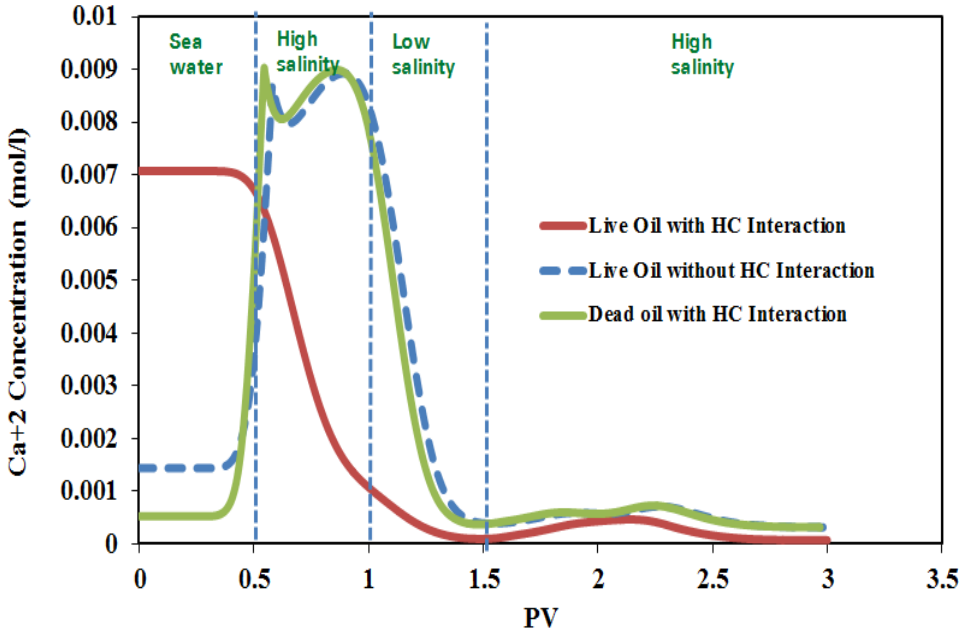

Figure 3-4: History of effluent Ca^{+2} concentration (effect of the hydrocarbon phase on the aqueous-rock geochemistry).

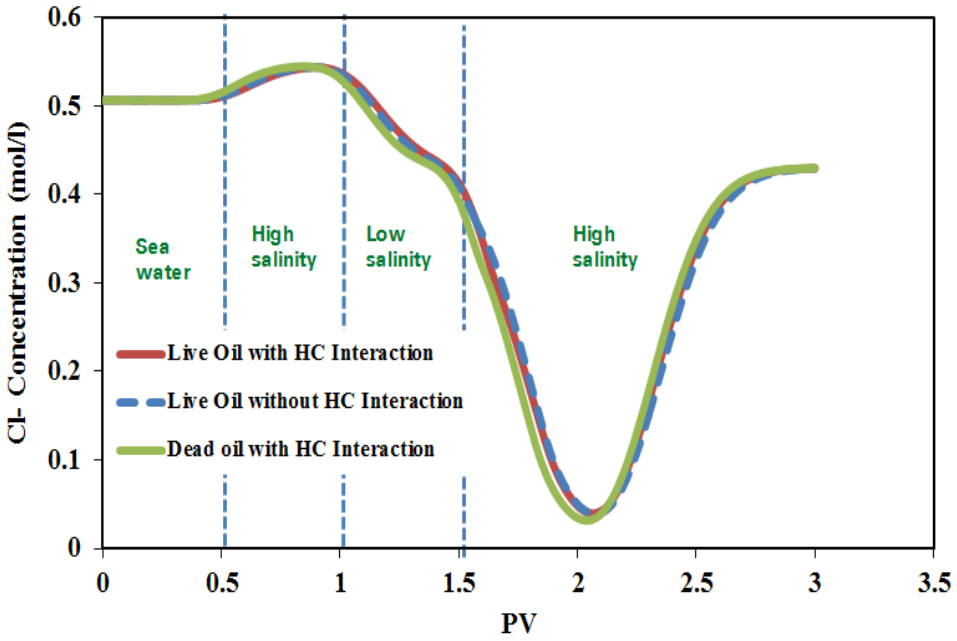

Figure 3-5: History of effluent Cl^{-} concentration (effect of the hydrocarbon phase on the aqueous-rock geochemistry).

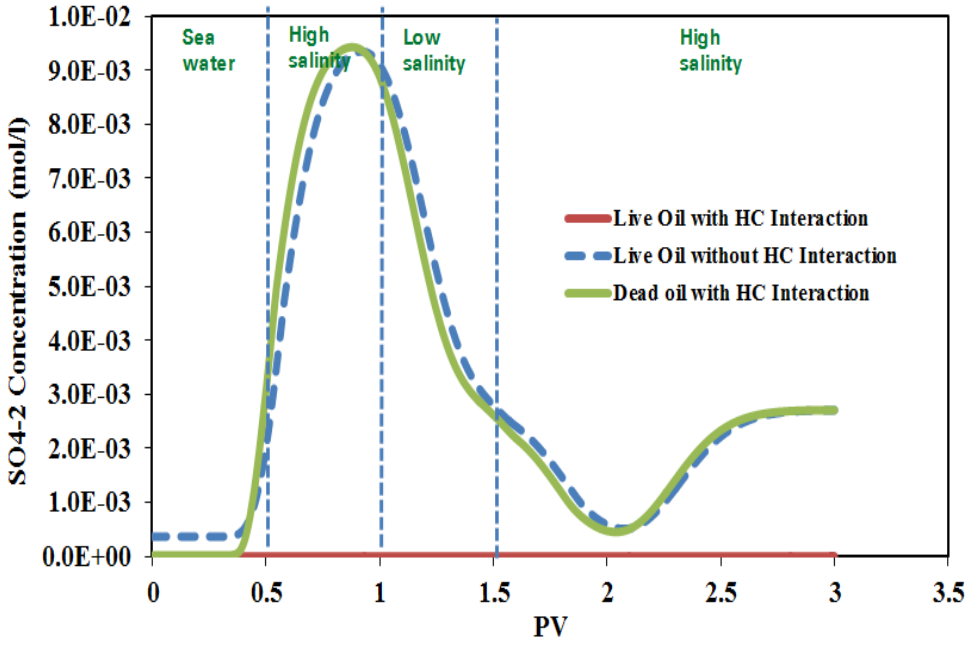

Figure 3-6: History of effluent SO_4^{-2} concentration (effect of the hydrocarbon phase on the aqueous-rock geochemistry).

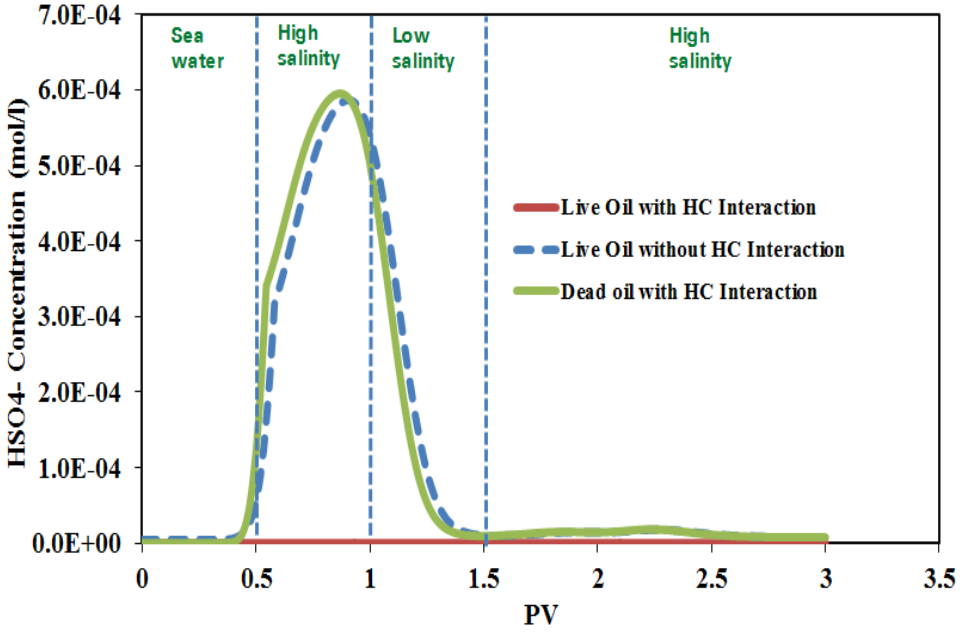

Figure 3-7: History of effluent HSO_4^- concentration (effect of the hydrocarbon phase on the aqueous-rock geochemistry).

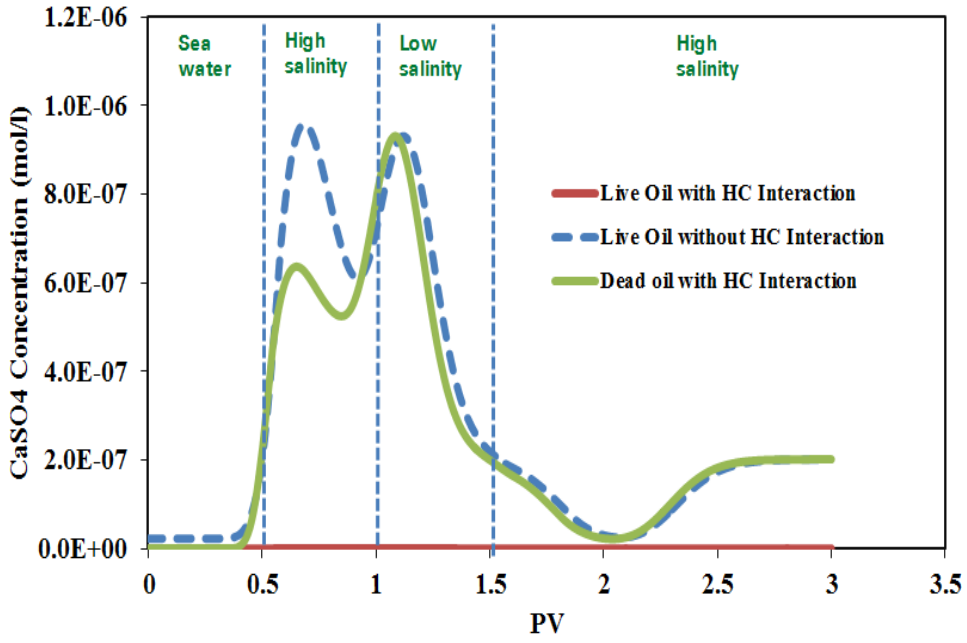

Figure 3-8: History of effluent $CaSO_4$ concentration (effect of the hydrocarbon phase on the aqueous-rock geochemistry).

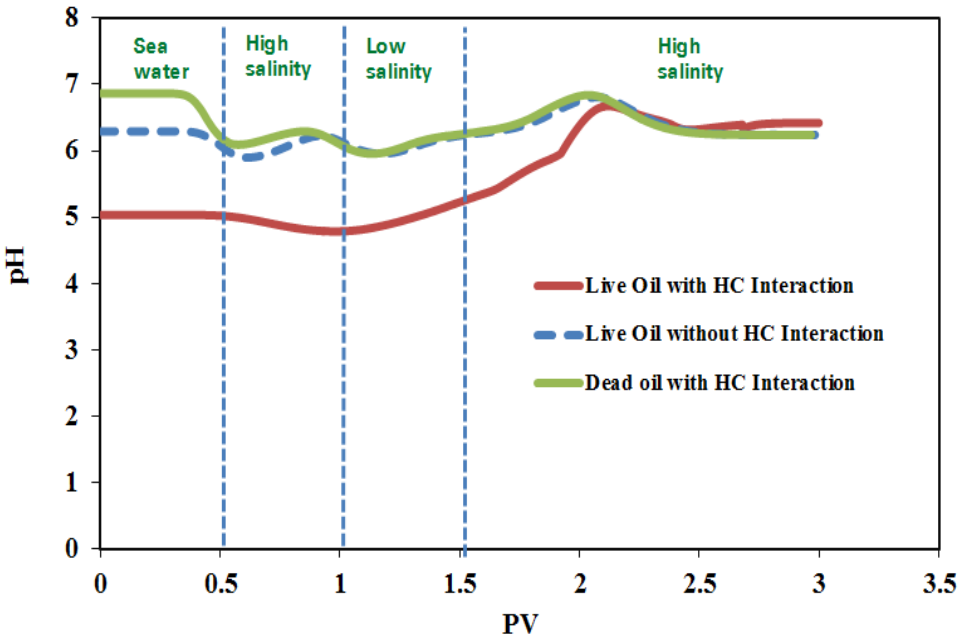

Figure 3-9: History of effluent pH (effect of the hydrocarbon phase on the aqueous-rock geochemistry).

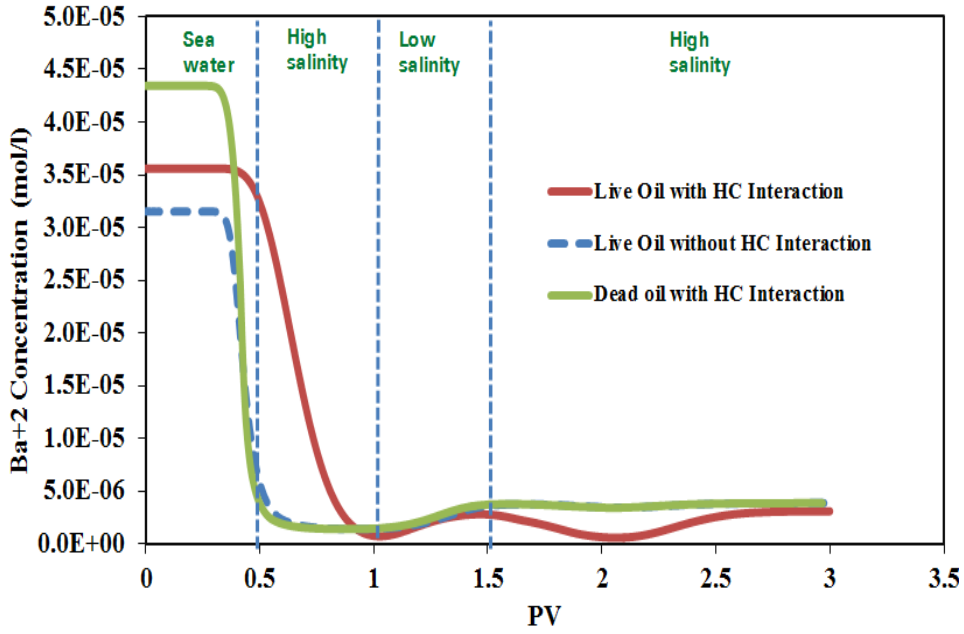

Figure 3-10: History of effluent $CaSO_4$ concentration (effect of the hydrocarbon phase on the aqueous-rock geochemistry).

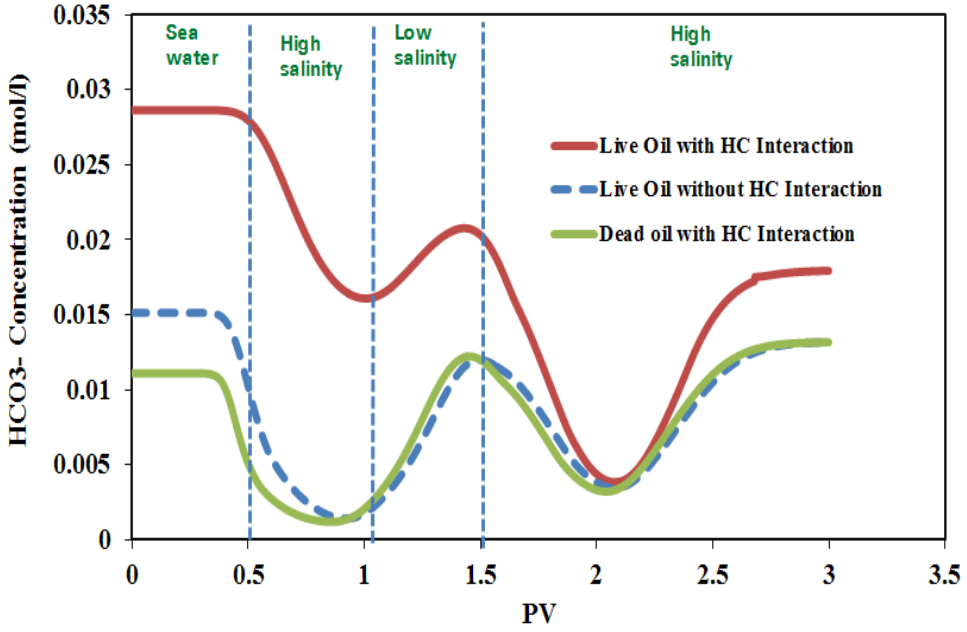

Figure 3-11: History of effluent HCO_3^- concentration (effect of the hydrocarbon phase on the aqueous-rock geochemistry).

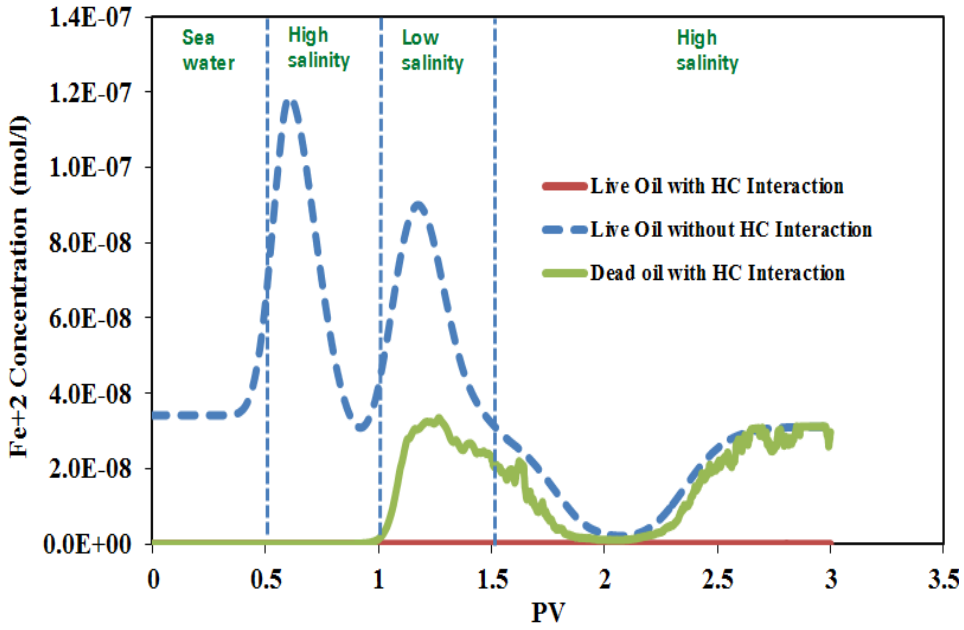

Figure 3-12: History of effluent Fe^{+2} concentration (effect of the hydrocarbon phase on the aqueous-rock geochemistry).

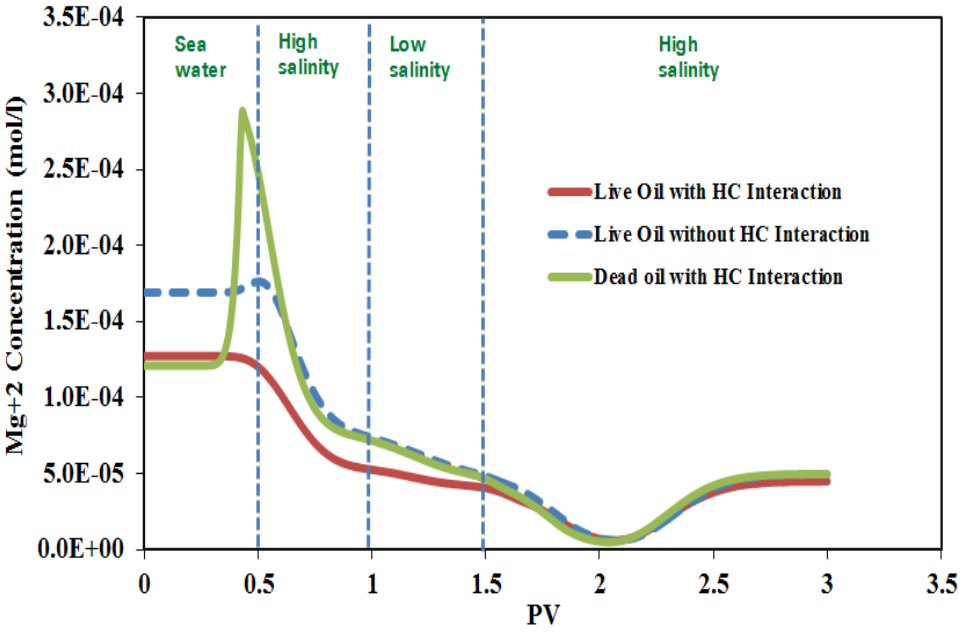

Figure 3-13: History of effluent Mg^{+2} concentration (effect of the hydrocarbon phase on the aqueous-rock geochemistry).

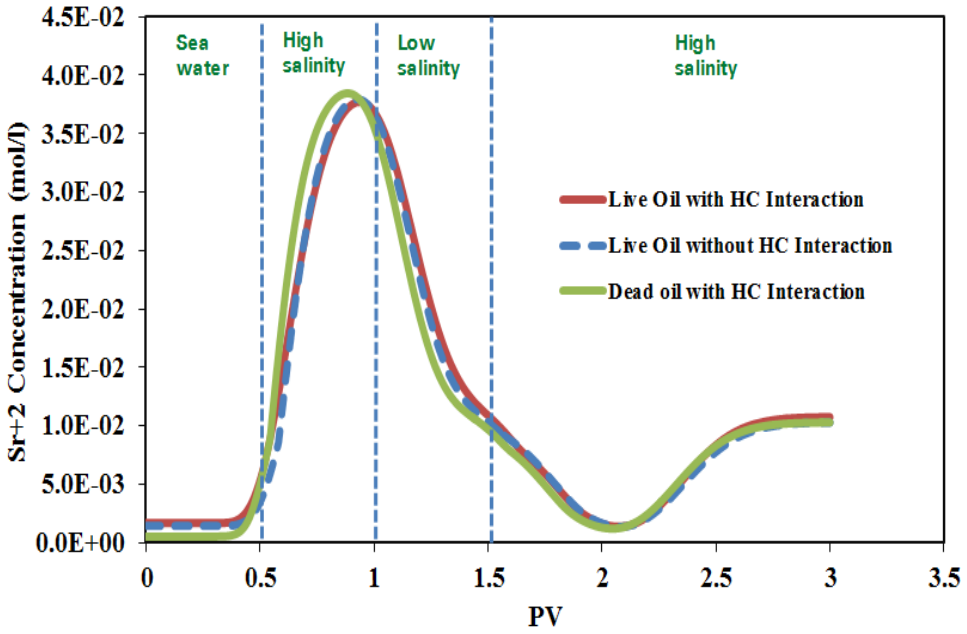

Figure 3-14: History of effluent Sr^{+2} concentration (effect of the hydrocarbon phase on the aqueous-rock geochemistry).

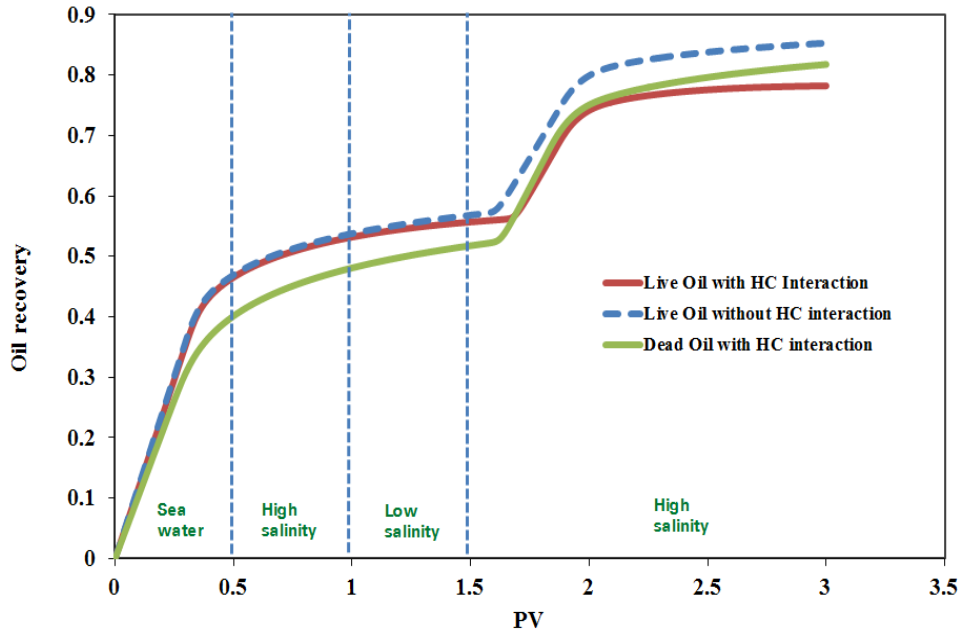

Figure 3-15: Effect of including the hydrocarbon phase in geochemistry calculation on oil recovery.

3.4 MODELING LOW SALINITY IN A SANDSTONE COREFLOOD

Kozaki (2012) reported two corefloods investigating low salinity water injection (labeled "Waterflood 1" and "Waterflood 2" in her thesis). In this work, two secondary high salinity waterfloods are compared against two secondary low salinity waterfloods. Figure 3-16 presents the experimental procedure.

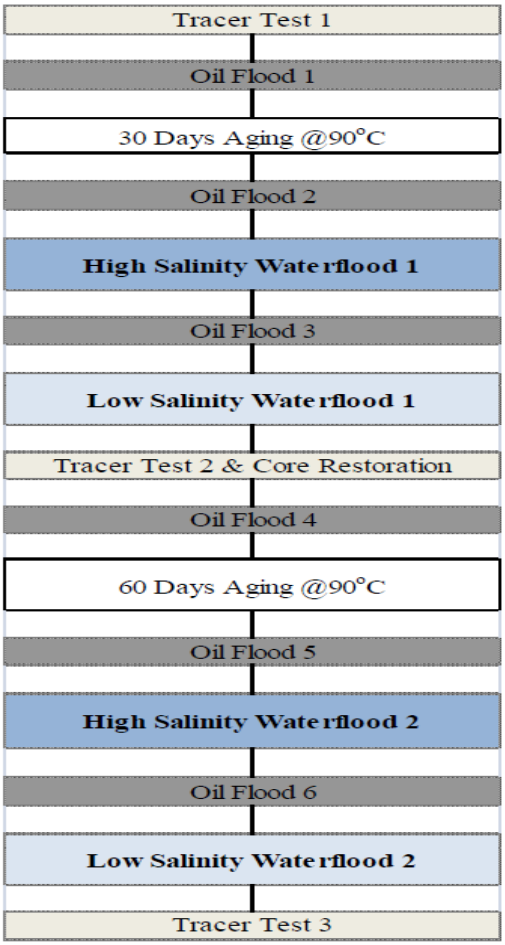

Figure 3-16: Experimental procedure followed in the work of Kozaki (2012).

Corefloods are all conducted on Berea sandstone core. High salinity and low salinity waters have the total dissolved salts of 33,793 ppm and 1,000 ppm, respectively. Table 3-2 presents the detailed fluid properties used in this experimental study. Further details about the corefloods are given in Kozaki (2012).

Table 3-2: Fluid properties for the experiment at 85 ^{o}C and 10 S^{-1} (Kozaki, 2012)

Synthetic Formation Brine (SFB)	Concentration	(ppm)	28620 650 2710 3890 33793	NaCl KCl CaCl2 MgCl2-6H2O TDS
	Viscosity	(cp)	0.47	
Low Salinity Brine (LSB)	Concentration	(ppm)	1000 1000	NaCl TDS
	Viscosity	(cP)	0.47	
Crude oil (Crude A)	Viscosity	(cp)	12	

We followed Kozaki (2011)'s experimental procedure to model the first set ("Waterflood 1") of this work. In the first step, tracer test was conducted to determine the pore volume of the core. Figure 3-17 shows measured values of normalized produced tracer concentration along with UTCOMP-IPhreeqc match and the analytical solution. It is worth mentioning that we believe the reported pore volume is overstated by 5% (we used 58.72 mL rather than reported value of 61.81 mL).

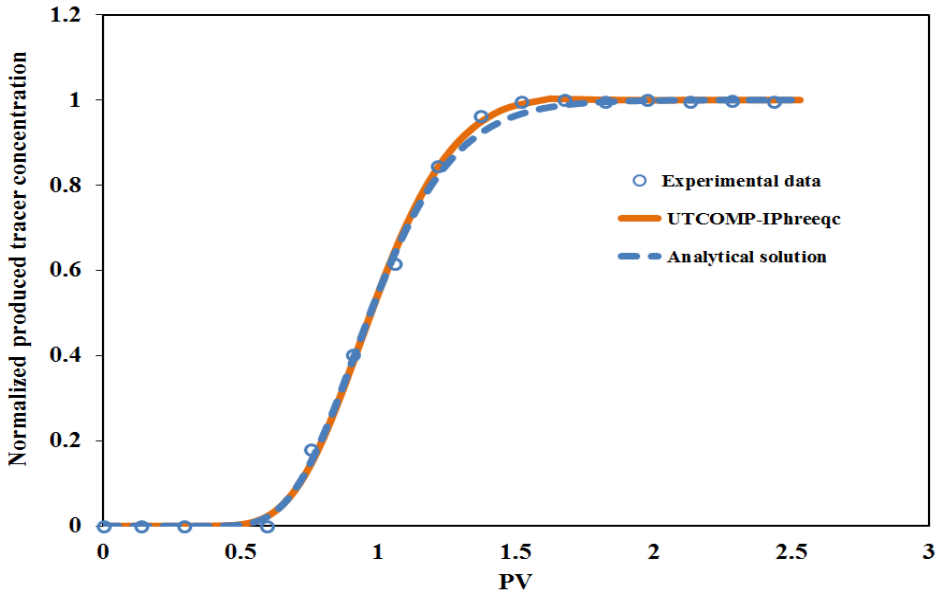

Figure 3-17: UTCOMP-IPhreeqc simulated result against the experimental normalized produced tracer concentration (Kozaki, 2012).

High Salinity Water Injection

UTCOMP-IPhreeqc is used to model the secondary high salinity waterflooding. A synthetic oil composition is used which reproduces the reported oil viscosity of 12 cp at 85 ^{o}C (oil viscosity is the only reported property of the oil used in the experiment). Initial oil saturation and oil end-point relative permeability are 0.78 and 0.45, respectively. The reported parameters (initial oil saturation and oil end-point relative permeability) are set and the other parameters, residual oil saturation, water end-point relative permeability, and exponents for oil and water relative permeabilities, are adjusted to get the best fit. Figures 3-18 and 3-19 show the match to oil recovery and produced ion histories, respectively. It should be noted that TDRM, BP's history matching tool, (Williams *et al.*, 2004; Jerauld *et al.*, 2010) is applied for assisted history matching (discussed in Chapter 2).

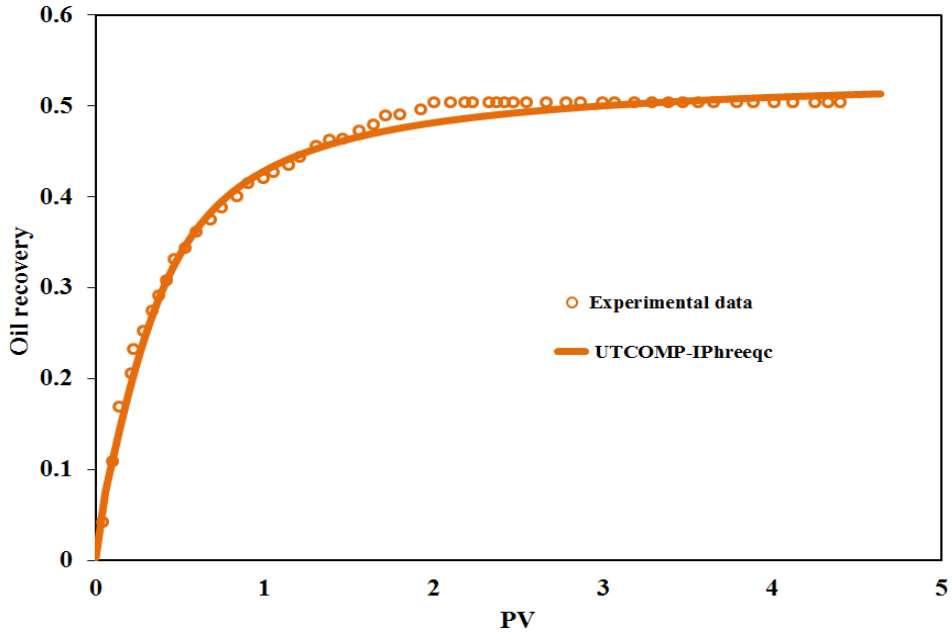

Figure 3-18: UTCOMP-IPhreeqc simulated result against the experimental oil recovery (Kozaki, 2012).

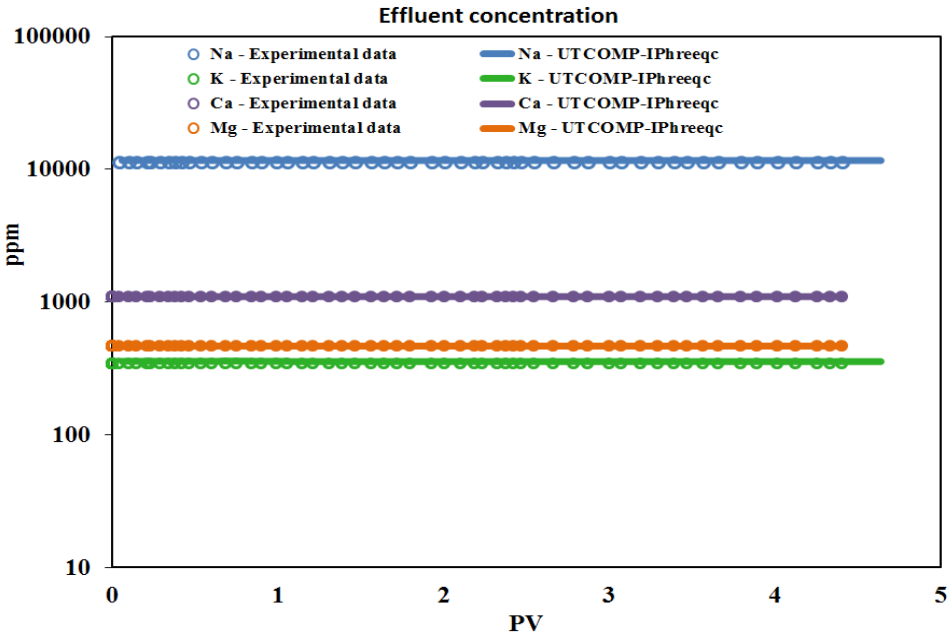

Figure 3-19: UTCOMP-IPhreeqc simulated result against the experimental ion histories (Kozaki, 2012).

Low Salinity Water Injection

After the high salinity waterflood, crude oil is injected into the core to establish the oil saturation (see Figure 3-16). Reported initial oil saturation and the oil end-point relative permeability are 0.74 and 0.48, respectively. Pure sodium chloride low salinity water, with the ion composition shown in Table 3-2, is then injected into the core for 9 PV. Different categories of parameters adjusted to get the best fit are

- **Initial set of relative permeability curves**: residual oil saturation, water end-point relative permeability, and oil and water relative permeability exponents (determined by matching the high salinity flood).
- **Interpolating parameter**: interpolating parameter is function of the total ionic strength (see Eq. (3.11)). Maximum and minimum thresholds are tuning parameters.
- **Altered set of relative permeability curves**: residual oil, oil and water exponents of the relative permeability, and water endpoints of the relative permeability.
- **Geochemistry of the rock**: kaolinite, illite, calcite, dolomite, and chlorite are only minerals that are affecting ion histories. The saturation indices of the minerals were used as matching parameters. An exchanger (initially at equilibrium with the solution) is also included. Cation exchange capacitance (CEC) of the exchanger is an adjusted parameter.

Figures 3-20 and 3-21 present UTCOMP-IPhreeqc simulated results for the oil recovery and produced ions, respectively. No history was reported for the pH of the effluent solution. However, Figure 3-22 illustrates the simulated pH of the effluent

solution. The increasing trend of pH during the low salinity flood is consistent with many in the literature (e.g., Cissokho *et al.*, 2010; Gamage *et al.*, 2011; Hamouda and Valderhaug, 2014; RezaeiDoust *et al.*, 2011; Aksulu *et al.*, 2012; Xie *et al.*, 2014). Including the exchanger and minerals are crucial to model the ion histories. Because the low salinity water contains only sodium and chloride, if no exchanger and soluble minerals were included, the effluent ion concentrations for calcium, magnesium, and potassium would approach zero after pushing out the connate water from the core. The dip in the ion concentrations of calcium and magnesium below the final value is due to ion exchange. Dissolution accounts for the continued production of ions not injected.

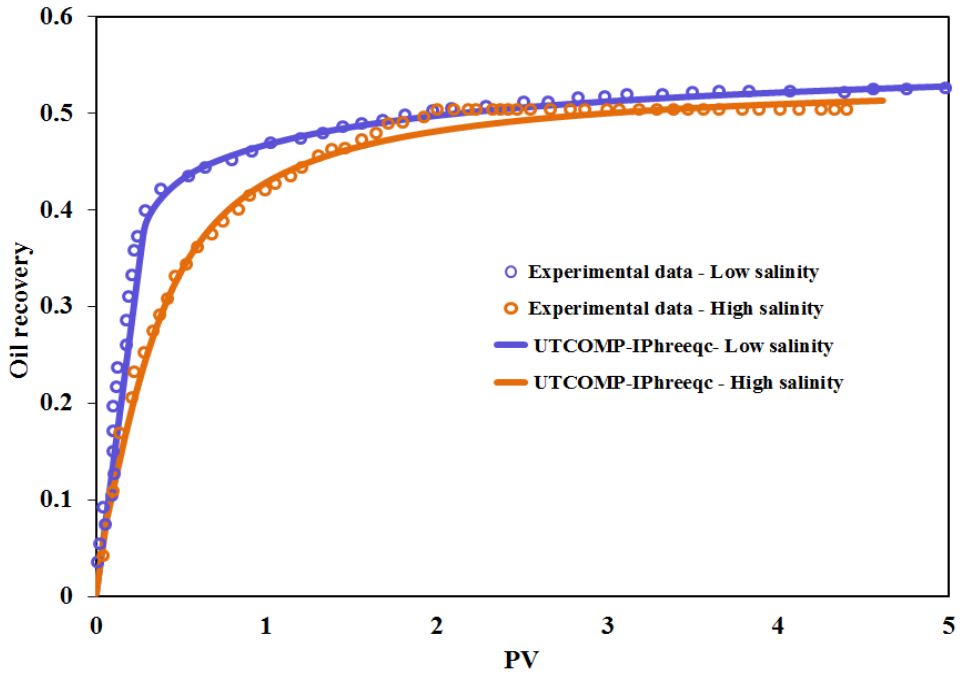

Figure 3-20: UTCOMP-IPhreeqc simulated results against the experimental high salinity and low salinity oil recoveries (Kozaki, 2012).

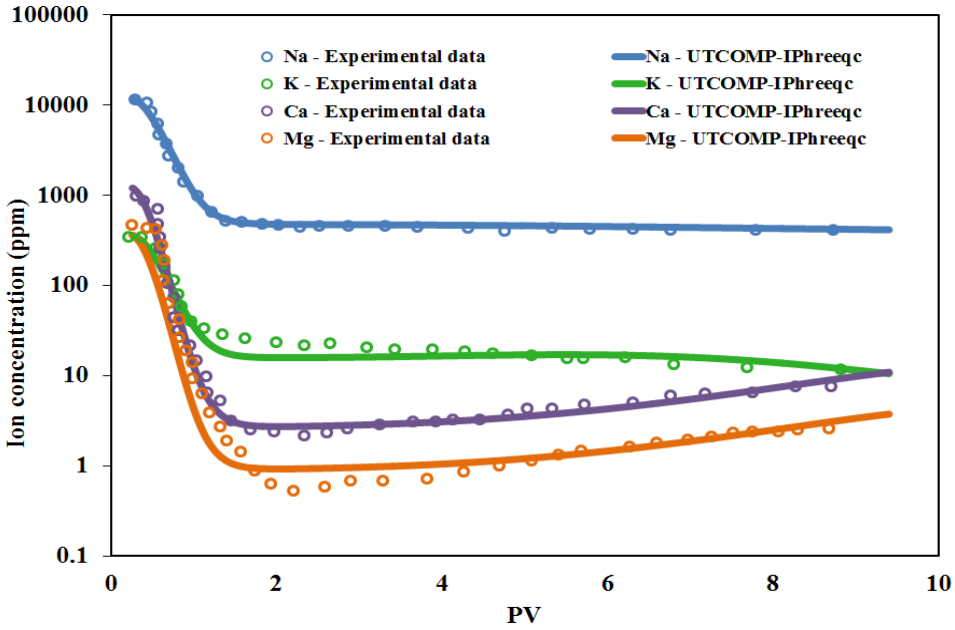

Figure 3-21: UTCOMP-IPhreeqc simulated result against the experimental ion concentrations during low salinity injection (Kozaki, 2012).

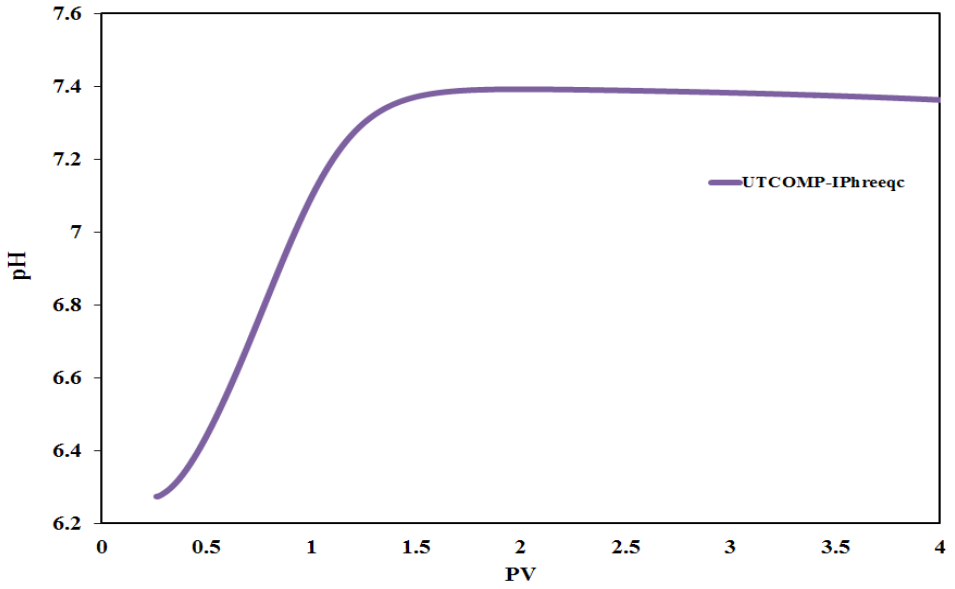

Figure 3-22: UTCOMP-IPhreeqc simulated result for the pH of the effluent solution during the low salinity injection.

To emphasize on the importance of geochemistry during the low salinity waterflood, the same case is simulated with no exchanger and minerals included (i.e., freshening case). Figures 3-23 through 3-27 show simulated ion histories of the freshening case against the measured data. Because the low salinity water contains only sodium and chloride (see Table 3-2) hence, as it is expected, the effluent ion histories for the calcium, magnesium, and potassium should approach to zero after pushing out the connate water from the core. This fact is consistent with the simulated results shown in Figures 3-24 through 3-26.

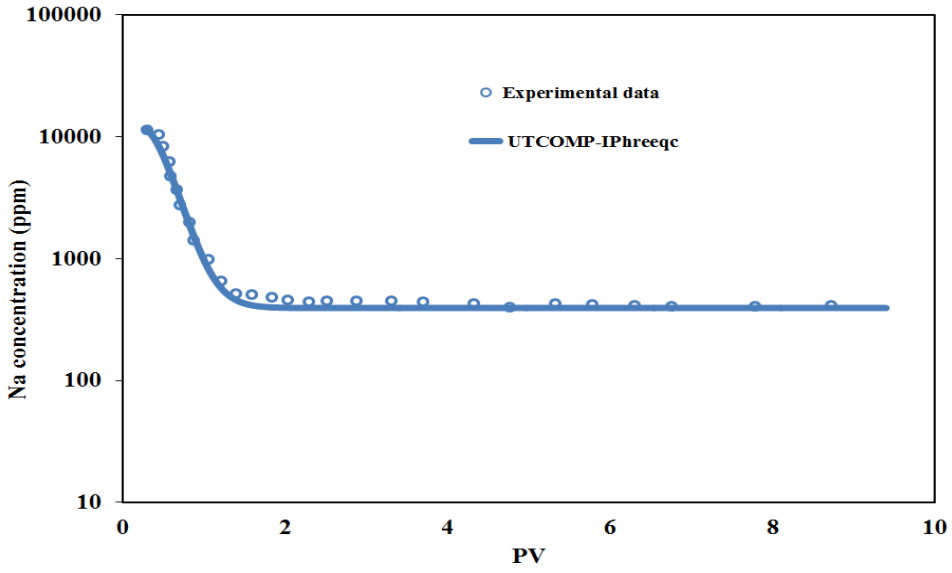

Figure 3-23: UTCOMP-IPhreeqc simulated result with no cation exchanger and minerals included against the experimental sodium concentration during the low salinity injection (Kozaki, 2012).

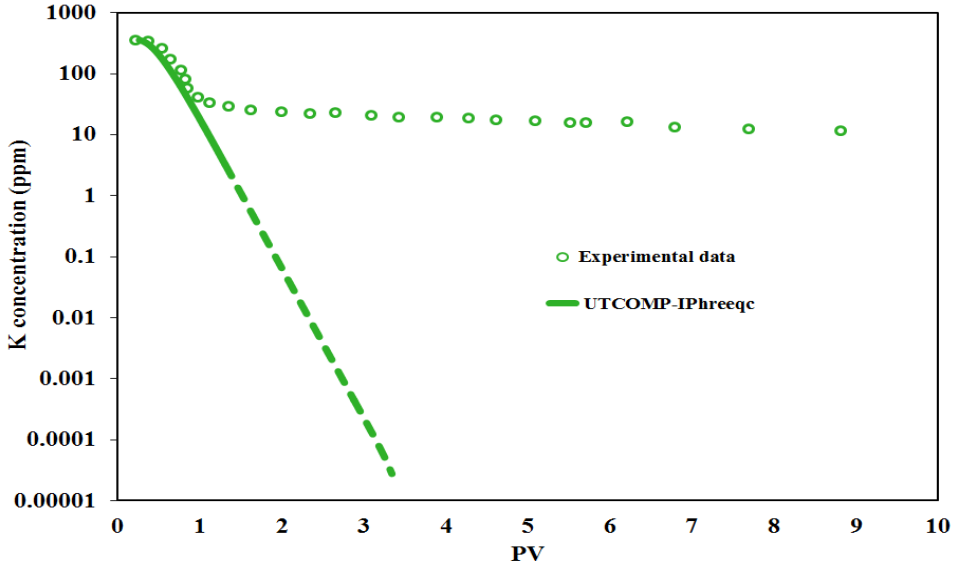

Figure 3-24: UTCOMP-IPhreeqc simulated result with no cation exchanger and minerals included against the experimental potassium concentration during the low salinity injection (Kozaki, 2012).

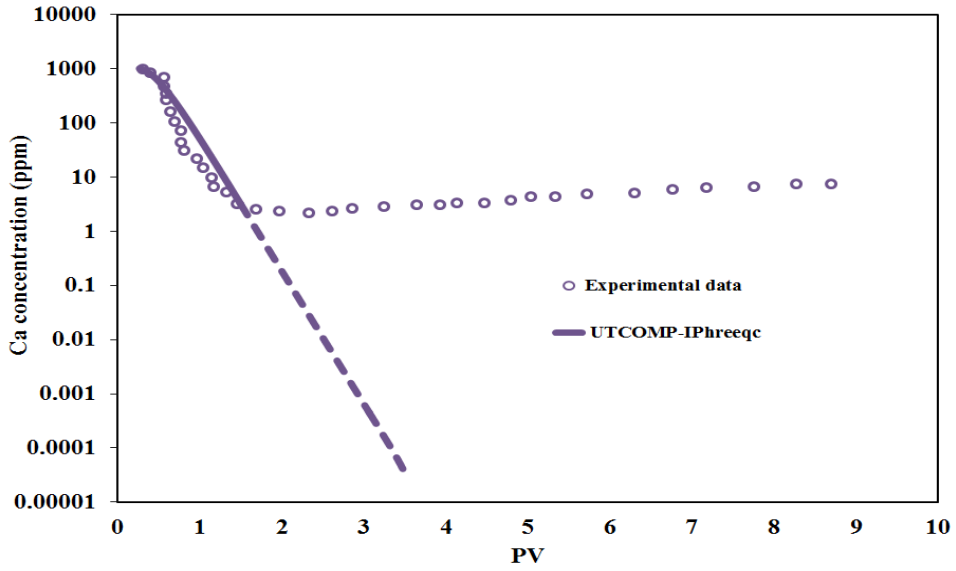

Figure 3-25: UTCOMP-IPhreeqc simulated result with no cation exchanger and minerals included against the experimental calcium concentration during the low salinity injection (Kozaki, 2012).

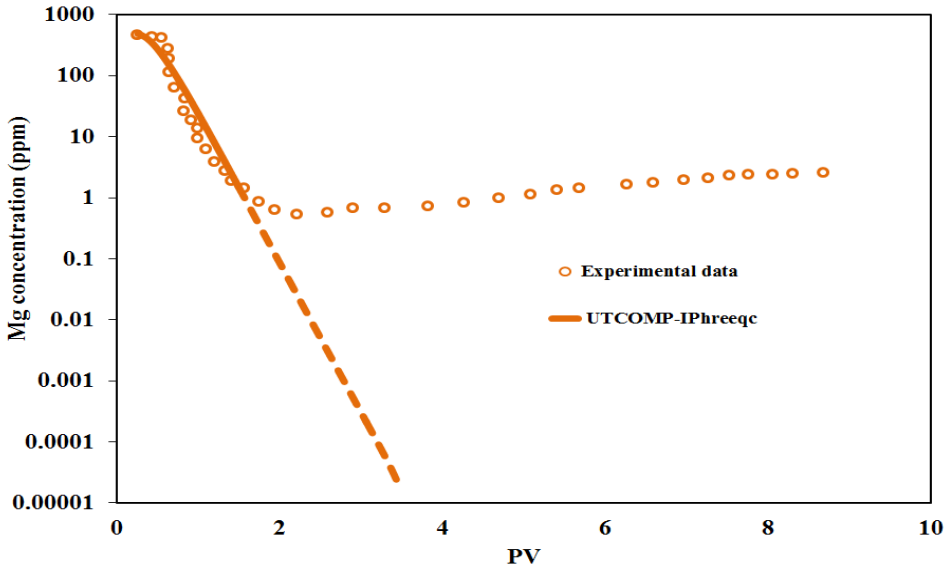

Figure 3-26: UTCOMP-IPhreeqc simulated result with no cation exchanger and minerals included against the experimental magnesium concentration during the low salinity injection (Kozaki, 2012).

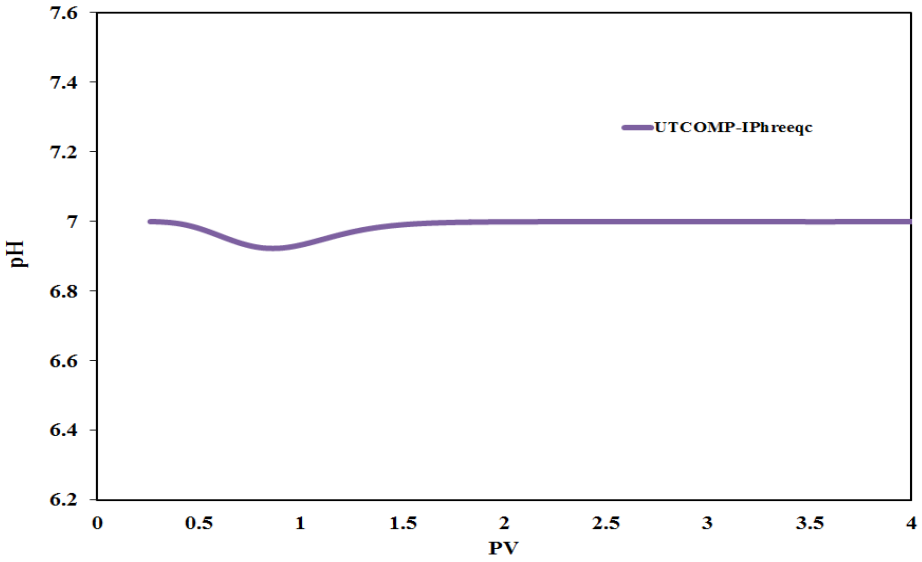

Figure 3-27: UTCOMP-IPhreeqc simulated result with no cation exchanger and minerals included for the pH of the effluent solution during the low salinity injection.

3.5 MODELING THE ENDICOTT FIELD TRIAL

Endicott, located on the North Slope of Alaska, is where the BP's first comprehensive inter-well field trial for low salinity EOR was implemented. After several studies including core measurements, single well chemical tracer tests (SWCTT), and simulations; reduced-salinity water injection in the Endicott pilot was put on the operation in June 2008 and continued for one year. In this pilot test, reduced-salinity water is injected through well "3-35" (see Figure 3-28) and production well is "3-37" which is 1040 ft far away (Seccombe *et al.*, 2010). Detailed ion compositions of the Endicott waters (connate, seawater, produced water, and low salinity) were previously presented in Table 2-20. Injecting the reduced-salinity water in this pilot test successfully decreased the residual oil saturation from 0.41 (before the low salinity injection) down to 0.27 (after the low salinity injection) (Seccombe *et al.*, 2010). More details about the field and the pilot can be found in the work of Seccombe *et al.* (2010) and lager *et al.* (2011).

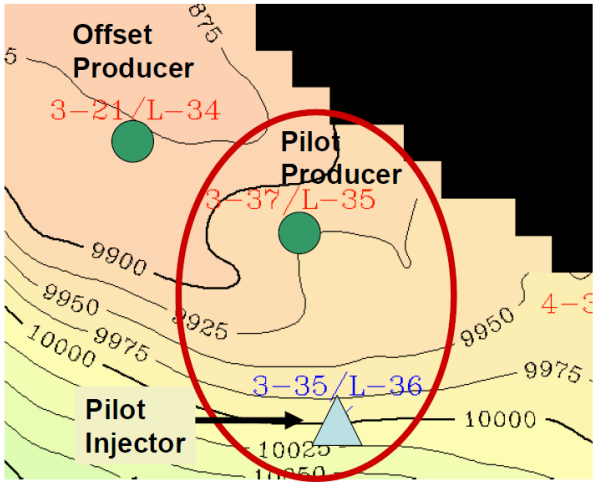

Figure 3-28: Endicott field trial map (Seccombe *et al.*, 2010).

Lager *et al.* (2011) applied the single-phase and one-dimensional reactive-transport capability of PHREEQC (Parkhurst and Appelo, 2013) and history matched the ion histories of the Endicott pilot. In this model, complex interaction between certain brine cations, the polar components in the oil, and the mineral surfaces is included by using a surface complexation model. Taking advantage of UTCOMP-IPhreeqc for modeling multi-phase and multi-dimensional oil-field problems with hydrocarbon buffering, we modeled both oil recovery and ion histories of the Endicott trial. We used the same form of surface complexation model proposed by Lager *et al.* (2011) and a 12-component Peng-Robinson equation of state (Peng and Robinson, 1976) characterization calibrated to Endicott oil in our work.

By accounting for effect of the region outside the pilot with a non-communicating layer, the Endicott pilot can be modeled with a cross-sectional model. Seccombe *et al.* (2010)'s compositional interpretation of the produced water reveals: the water production split is 55% from the pilot injector and 45% from outside the pilot region. Hence, injection rate and the thickness of the non-communicating layer are adjusted to satisfy the Seccombe *et al.* (2010)'s interpretation. A multilayer model was used because some degree of layering is apparent in the ion histories. Figure 3-29 shows the cross-sectional model used. TDRM (Williams *et al.*, 2004; Jerauld *et al.*, 2010) is applied for assisted history matching.

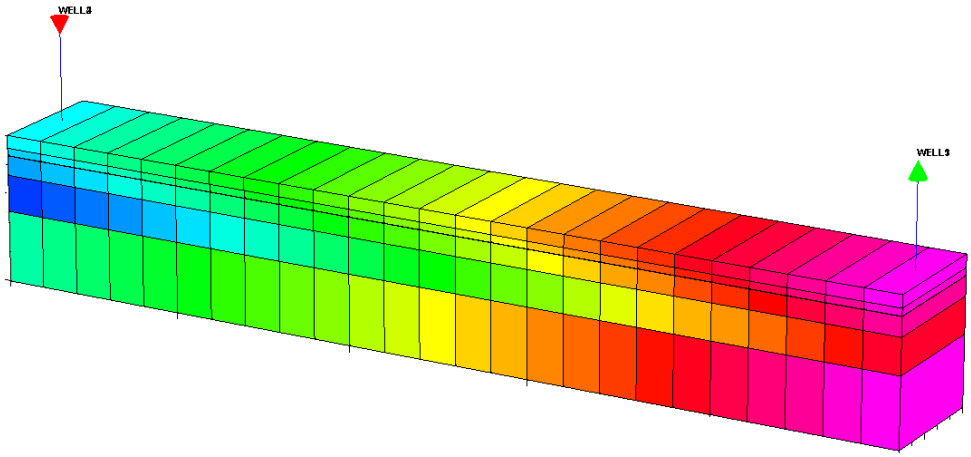

Figure 3-29: A cross-sectional case to model the Endicott inter-well field trial.

Figures 3-30 through 3-40 show the Endicott measured data as well as UTCOMP-IPhreeqc match for the watercut and produced ion histories for both cases of low salinity and a hypothetical high salinity waterflooding. The match to the ions is equivalent or better than obtained by Lager *et al.* (2011). The fact that the effects are seen in a 4 layer model demonstrates that the geochemical effects seen are robust – the details of the match are different from Lager *et al.* (2011)'s but the overall character is the same. An interesting improvement is that including the effect of the soluble hydrocarbon components on the aqueous-rock geochemistry leads to the correct trend for pH of the produced water (see Figure 3-40). Also included in the ion histories figures are ion histories of freshening model in which the surface complexation model and the exchanger are excluded from the model. As pointed out by Lager *et al.* (2011), alkalinity and iron match very poorly in the freshening model. Stabilized alkalinity during the low salinity flood is about 995 ppm in the freshening model while the measured value is around 1230 ppm. Furthermore, no peak is seen in the iron concentration history. The discrepancies

between the freshening and low salinity results demonstrate the importance of the geochemical reactions to low salinity waterflooding. Lager *et al.* (2011) studied four possibilities to interpret the increase in the alkalinity:

- Calcite and dolomite dissolution
- More CO_2 dissolution in the produced water due to the decrease in salinity of the water
- A possible mechanism linked to sulfate concentration
- Dissolution of the organic oils in the produced water due to the release of the polar components from the kaolinite

They concluded that the last possibility was the only feasible reason for the increase in the alkalinity. RezaeiDoust *et al.* (2011) on the other hand, believed the increase in alkalinity of the Endicott pilot during the low salinity water flooding is due to the presence of CO_2 in the reservoir. Our studies indicate RezaeiDoust *et al.* (2011) interpretations are not valid. For Endicott oil composition, temperature, and pressure; CO_2 fugacity can be estimated as 32.58 atm at the reservoir condition. The estimated solubility of CO_2 in the aqueous phase at the given fugacity and the Endicott reservoir temperature (with no salinity effect included) is roughly 0.36 mol/kgw (Duan and Sun, 2003; Parkhurst and Appelo, 2013). Including the impact of the CO_2 solubility on the geochemistry calculations, alkalinity increases by 63 ppm. For two reasons this is the maximum increase that can occur in the aqueous alkalinity due to the presence of CO_2. First, we estimated the solubility of CO_2 with no salinity effect included and, as the literature shows, CO_2 solubility in the aqueous phase decreases as the aqueous salinity increases (Duan and Sun, 2003). Second, the estimated value is at the reservoir condition while the alkalinity was measured at the separator condition with much lower CO_2

fugacity. Hence, we conclude that the 235 ppm increase (1230 ppm measured value versus 995 for the freshening case) in the alkalinity is too high to be interpreted due to the CO_2 solubility in the aqueous phase. Therefore, RezaeiDoust *et al.* (2011)'s interpretation is not valid.

RezaeiDoust *et al.* (2011)'s interpretation for the iron is not valid because a wrong reaction was addressed in their paper. The relevant reactions from the "phreeqc.dat" database of PHREEQC geochemical package (Parkhurst and Appelo, 2013) are

$$FeS + H^+ \rightleftharpoons Fe^{+2} + HS^- \qquad pK_a = 3.915, \tag{3.13}$$

$$Fe^{+2} + H_2O \rightleftharpoons FeOH^+ + H^+ \qquad pK_a = 9.5, \tag{3.14}$$

$$HS^- \rightleftharpoons S^{-2} + H^+ \qquad pK_a = 12.918, \tag{3.15}$$

$$H^+ + OH^- \rightleftharpoons H_2O \qquad pK_a = -14.0. \tag{3.16}$$

Summing all the reactions above will result in the following reaction:

$$FeS + OH^- \rightleftharpoons FeOH^+ + S^{-2} \qquad K_a = 10^{-12.333}. \tag{3.17}$$

The equilibrium constant of the reaction given in Eq. (3.17) shows, the solubility of the iron sulfide, FeS, does not increase by more than 5 orders of magnitude in the alkaline water. This observation is not consistent with the interpretation claimed in the work of RezaeiDoust *et al.* (2011).

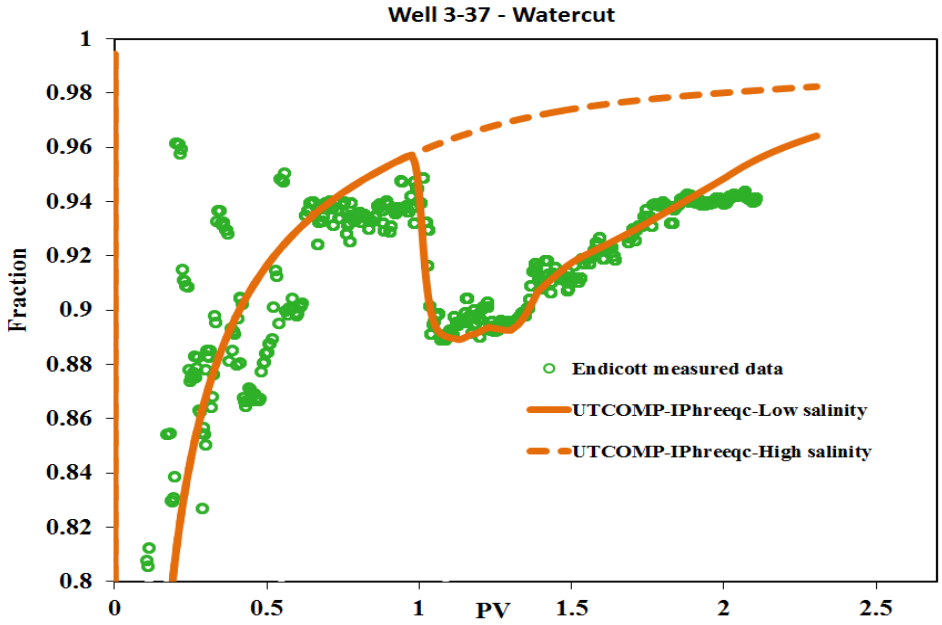

Figure 3-30: UTCOMP-IPhreeqc simulated results (high salinity and low salinity) against the measured water cut of the Endicott field trial.

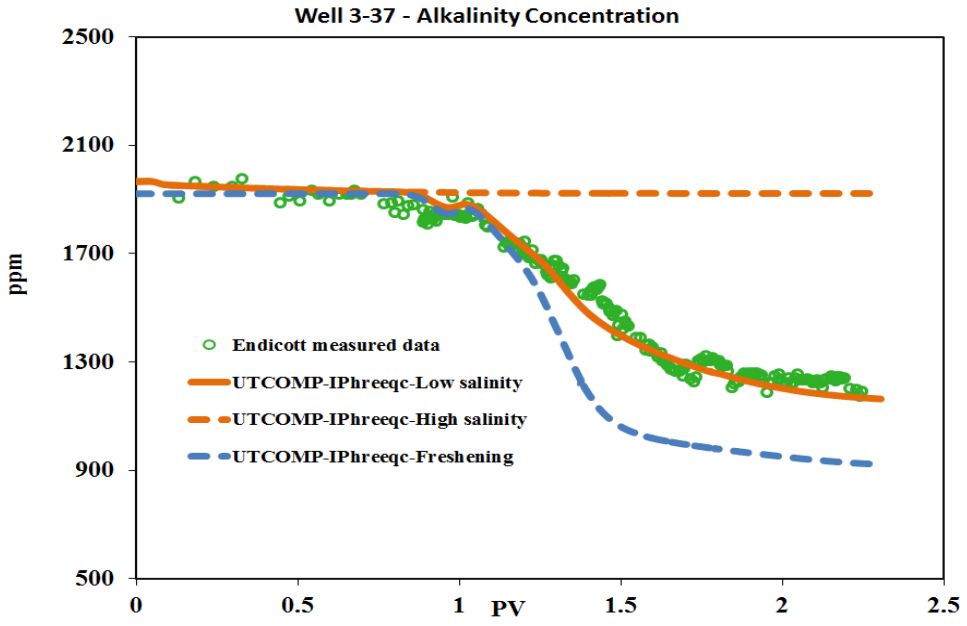

Figure 3-31: UTCOMP-IPhreeqc simulated results (high salinity, low salinity, and freshening) against the measured alkalinity concentration of the Endicott field trial.

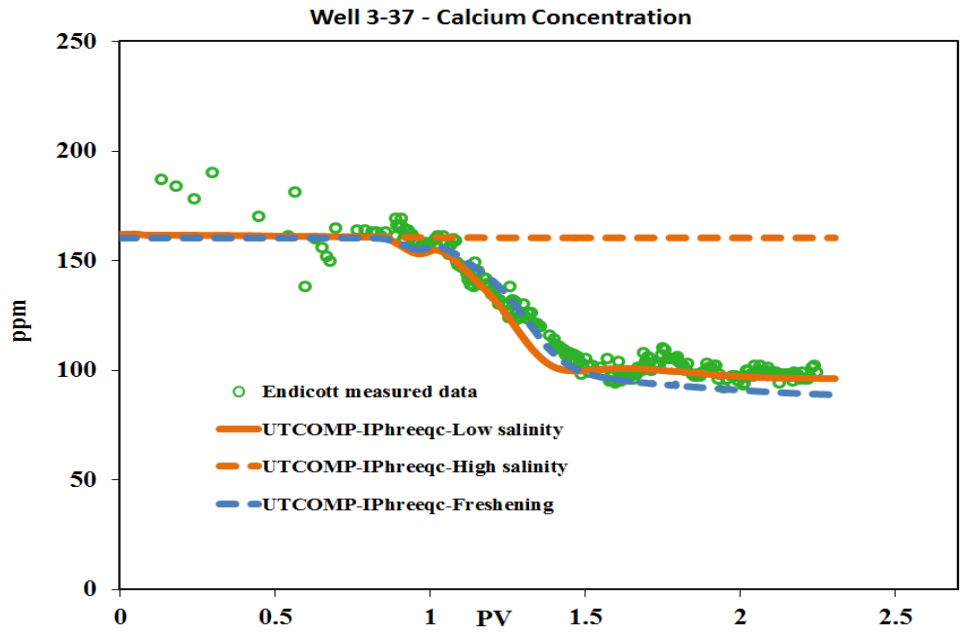

Figure 3-32: UTCOMP-IPhreeqc simulated results (high salinity, low salinity, and freshening) against the measured calcium concentration of the Endicott field trial.

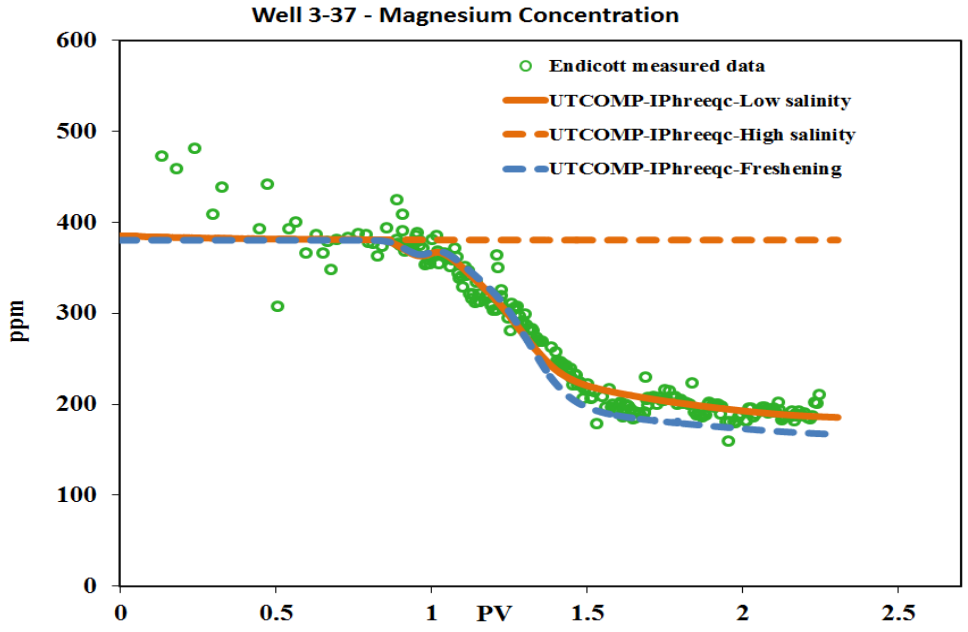

Figure 3-33: UTCOMP-IPhreeqc simulated results (high salinity, low salinity, and freshening) against the measured magnesium concentration of the Endicott field trial.

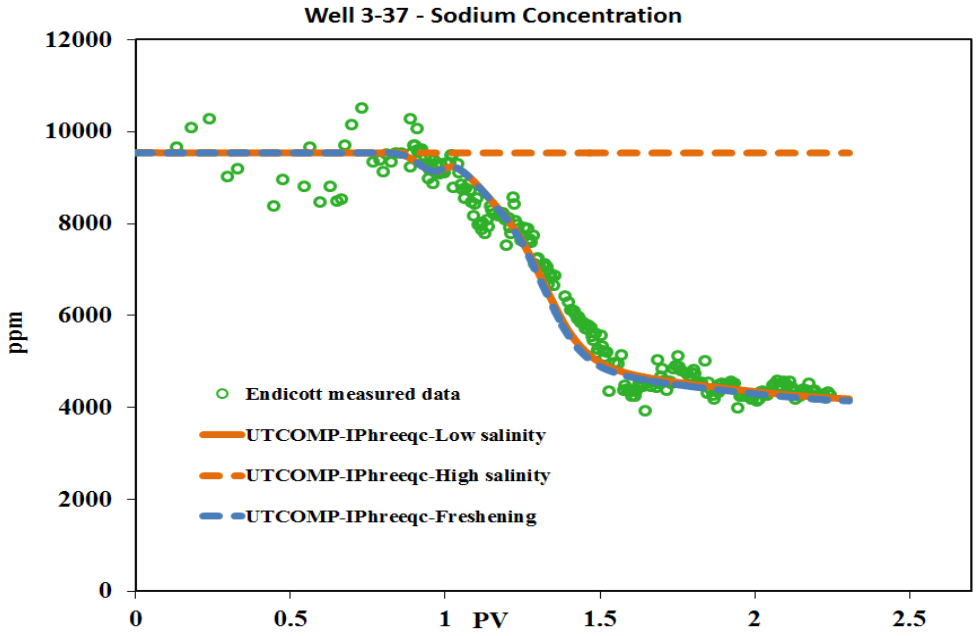

Figure 3-34: UTCOMP-IPhreeqc simulated results (high salinity, low salinity, and freshening) against the measured sodium concentration of the Endicott field trial.

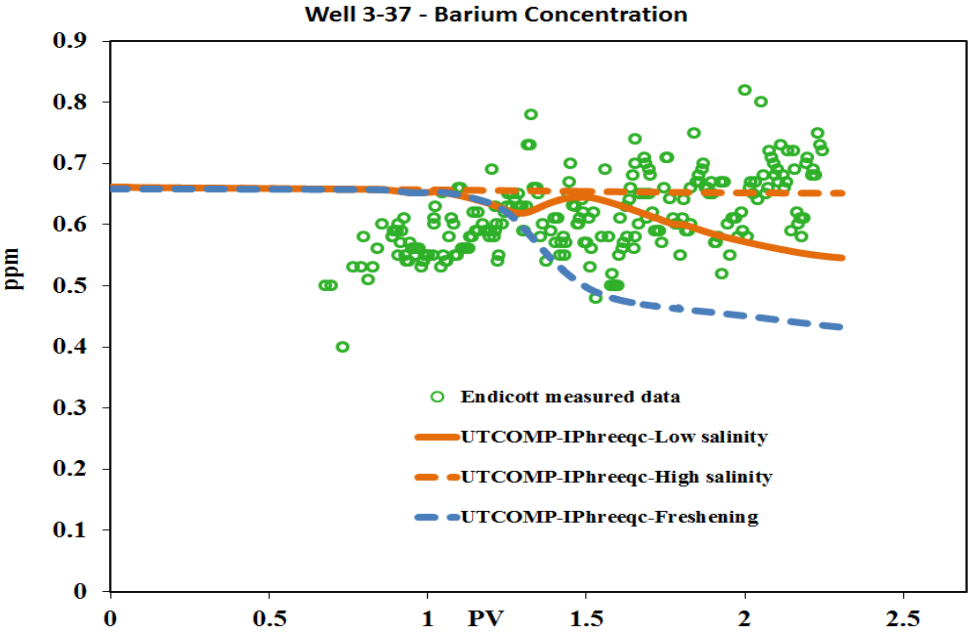

Figure 3-35: UTCOMP-IPhreeqc simulated results (high salinity, low salinity, and freshening) against the measured barium concentration of the Endicott field trial.

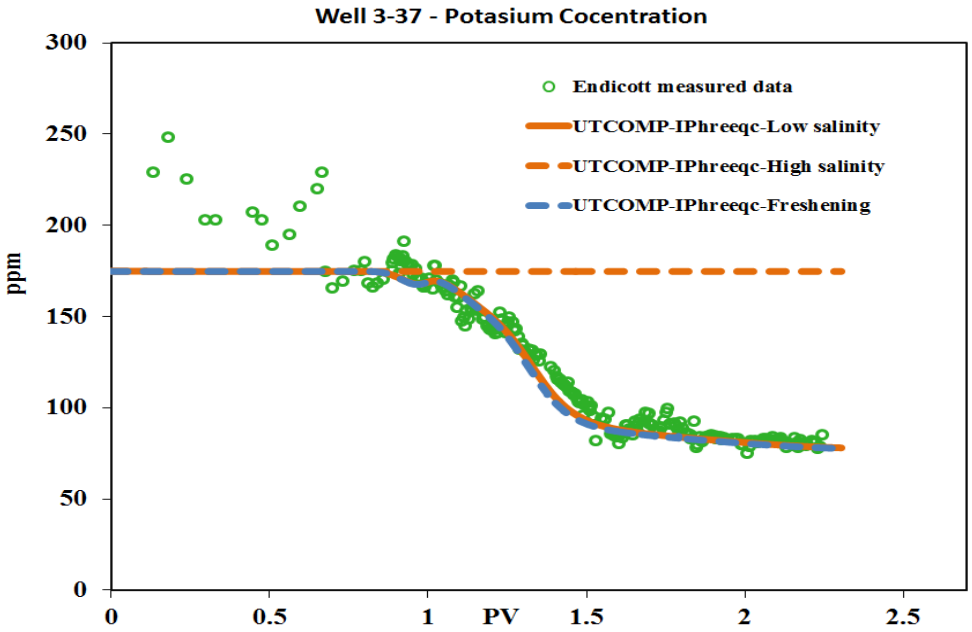

Figure 3-36: UTCOMP-IPhreeqc simulated results (high salinity, low salinity, and freshening) against the measured calcium concentration of the Endicott field trial.

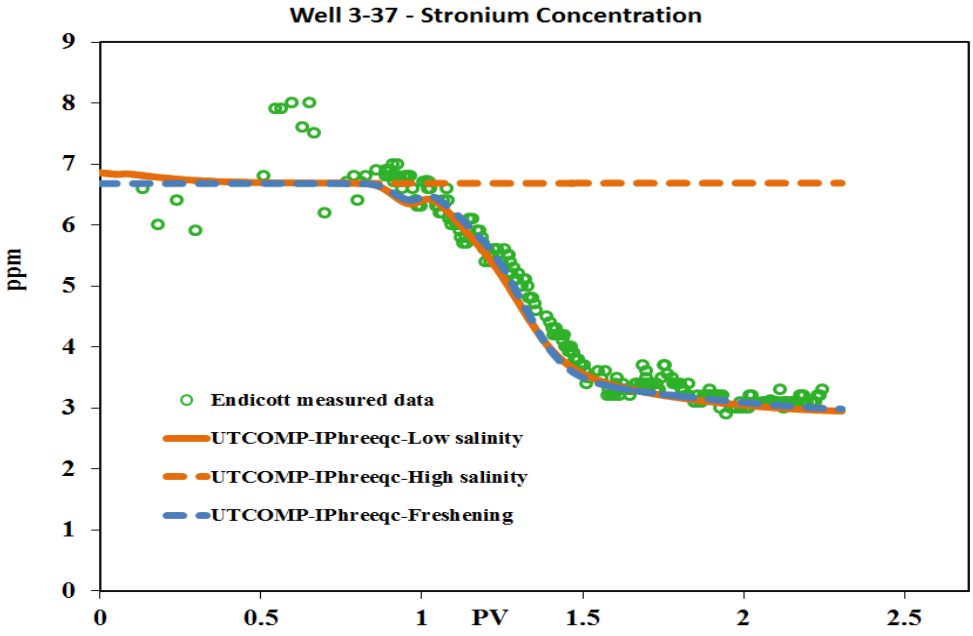

Figure 3-37: UTCOMP-IPhreeqc simulated results (high salinity, low salinity, and freshening) against the measured strontium concentration of the Endicott field trial.

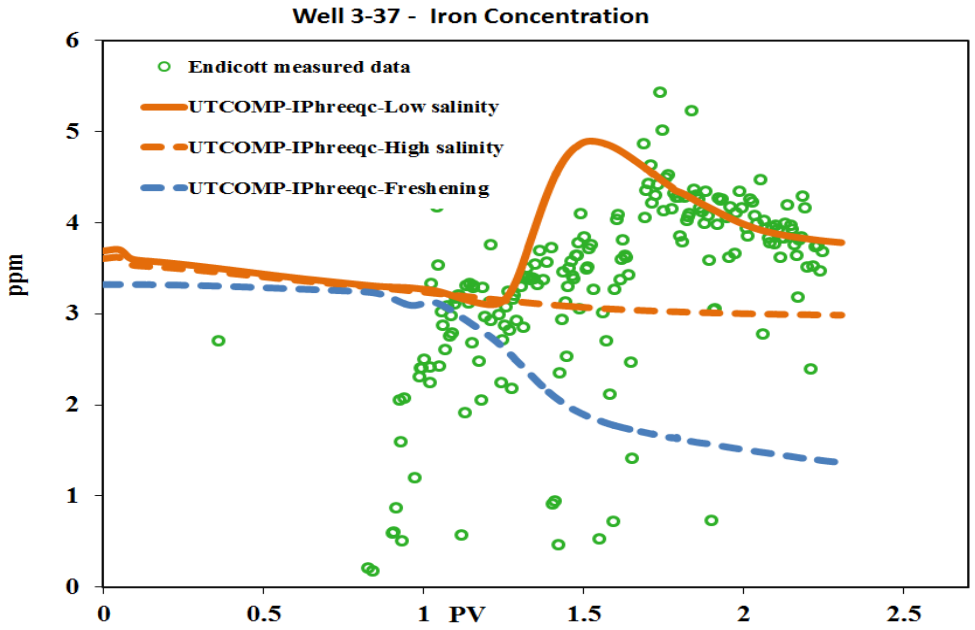

Figure 3-38: UTCOMP-IPhreeqc simulated results (high salinity, low salinity, and freshening) against the measured iron concentration of the Endicott field trial.

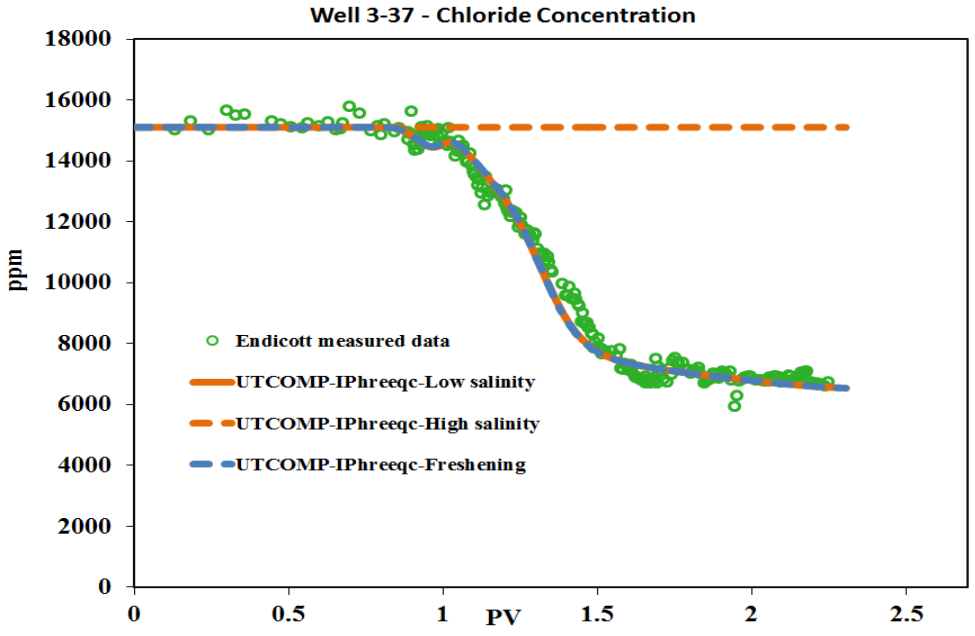

Figure 3-39: UTCOMP-IPhreeqc simulated results (high salinity, low salinity, and freshening) against the measured chloride concentration of the Endicott field trial.

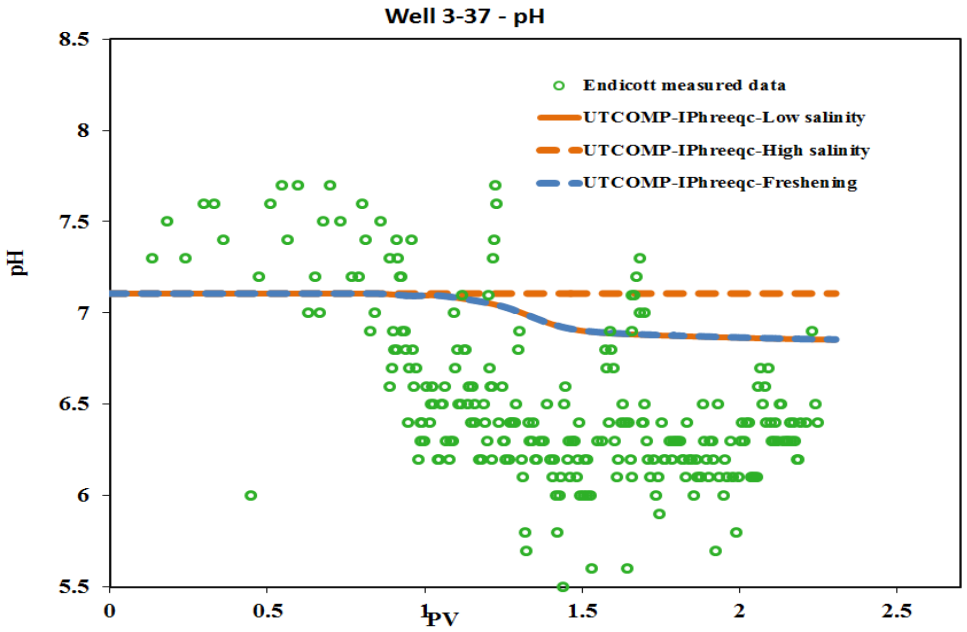

Figure 3-40: UTCOMP-IPhreeqc simulated results (high salinity, low salinity, and freshening) against the measured pH of the Endicott field trial.

3.6 IMPLEMENTATION OF OTHER MECHANISTIC MODELS IN UTCOMP-IPHREEQC

There are a number of more detailed approaches to modeling low salinity waterflooding that UTCOMP-IPhreeqc enables which have the potential to be more direct and mechanistic. We believe what makes a sandstone rock oil-wet is the attaching of the carboxylic branches through divalent cations on the rock surface (particularly the clay surface). When water with modified ion composition is injected into the reservoir, it disturbs the initial equilibrium established between crude oil, rock, and brine. Under favorable conditions, carboxylic-divalent (organometallic) complexes on the rock surface are exchanged with divalents with no attached carboxylic branch and/or monovalent ions. Hence, depending on how many of these organometallic complexes detached from the rock surface, the wettability of the rock is changed from oil-wet towards water-wet (see Figure 3-41).

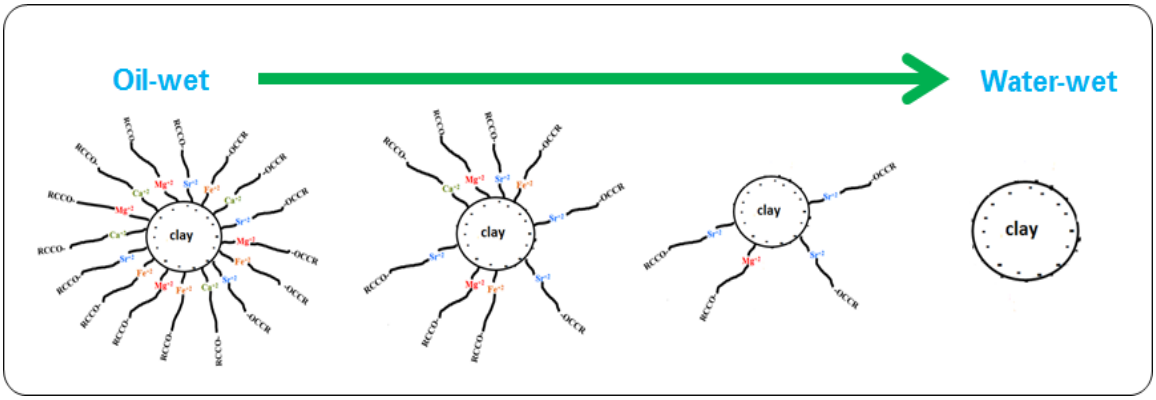

Figure 3-41: Schematic which qualitatively relates the wettability of a sandstone rock to number of organometallic complexes on the rock surface.

Clearly, there are a number of ways of modeling this process, depending on the details of the chemical mechanisms envisioned and the way this is translated into a change in wettability and ultimately changes in relative permeability and capillary pressure. UTCOMP-IPhreeqc provides a realistic tool to test ideas and ultimately choose the most effective approach. We explore a couple of approaches in this section.

Keeping the same concept, the interpolating parameter is defined as follows:

$$\theta = \frac{\zeta_{\max} - \zeta(x,t)}{\zeta_{\max} - \zeta_{\min}}, \tag{3.18}$$

where

$\zeta_{\max}$ = fraction of organometallic complexes on the exchanger above which no wettability alteration would occur

$\zeta(x,t)$ = fraction of organometallic complexes on the exchanger in each gridblock at

certain simulation time

ζ_{min} = fraction of organometallic complexes on the exchanger at which maximum wettability alteration would occur

ζ is given in Eq. (3.19).

$$\zeta = \frac{\left(FeA_wX + MgA_wX + CaA_wX + \cdots\right)}{CEC} = \frac{\sum_i I_i A_w X}{CEC}, \tag{3.19}$$

where

A_w = the carboxylic branch

X = exchanger site

I_i = divalent cations

CEC= the cation exchange capacity of the exchanger

The same philosophy is applied if the attachment of the oil component on the rock surface occurs through surface complexes, as proposed by Lager *et al.* (2011), rather than simple carboxylic-divalent complex. ζ for this case is the mole fraction of the oil component on the surface complex sites.

To test the model, a sensitivity analysis is performed to investigate how oil recovery behaves by changing different parameters in this mechanistic modeling approach. A coreflood is modeled using UTCOMP-IPhreeqc. Initial and altered oil and water relative permeability curves presented in Figure 3-2 are used. Sensitivity analysis is studied at both secondary and tertiary injection of low salinity water. Water initially present (S_{wi}=0.3) in the core is Endicott high salinity water (composition given in Table

2-20) and sequence of injected waters at secondary and tertiary injection modes are as follows (water compositions were given in Table 2-20):

- **Secondary mode**: 1) 3.5 PV of low salinity water
- **Tertiary mode**: 1) 1 PV of high salinity water 2) 1.7 PV of low salinity water 3) 0.8 PV of high salinity water

Sensitivity analysis is performed on the equilibrium constant of the organometallic complexes on the exchanger and ζ_{min} (minimum threshold) of Eq. (3.18). Affinities of the organometallic complexes towards the clay surface are expected to be related to the tendency of the constituting divalent cations of the organometallic complex. For example, CaA_w^+ has more tendency towards the clay surface than MgA_w^+ just because Ca^{+2} has more affinity towards the clay surface than Mg^{+2} (Austad *et al.*, 2010). However, in our sensitivity analysis we assume that all the organometallic complexes have the same affinity toward the rock surface (i.e., equilibrium constant of all the organometallic complexes on the exchanger is the same).

Table 3-3 shows different log(K) values of the organometallic complexes on the exchanger chosen for the sensitivity analysis purpose. Figures 3-42 and 3-43 demonstrate how differently oil recovery (at both secondary and tertiary injection modes) behaves by changing the log(K) of the organometallic complexes on the clay surface.

Table 3-3: Log(K) values of the organometallic complexes on the exchanger for chosen the sensitivity analysis purpose

	Case 1	Case 2	Base case	Case 3	Case 4	Case 5
Log(K)	0.5	0.7	0.9	1.0	1.2	1.3

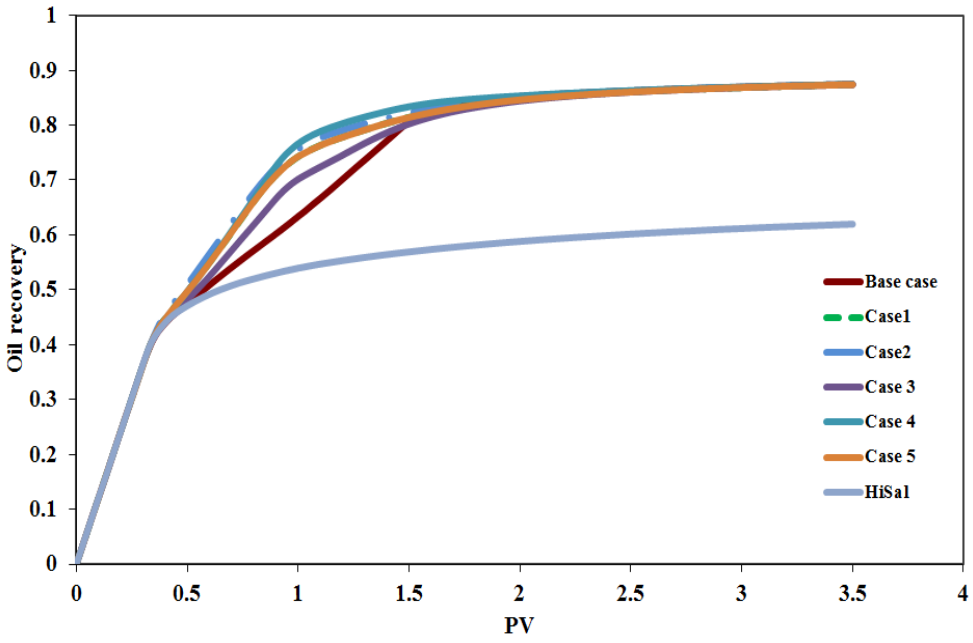

Figure 3-42: Oil recovery at the secondary injection mode (sensitivity analysis on log(K) of the organometallic complexes on the clay surface).

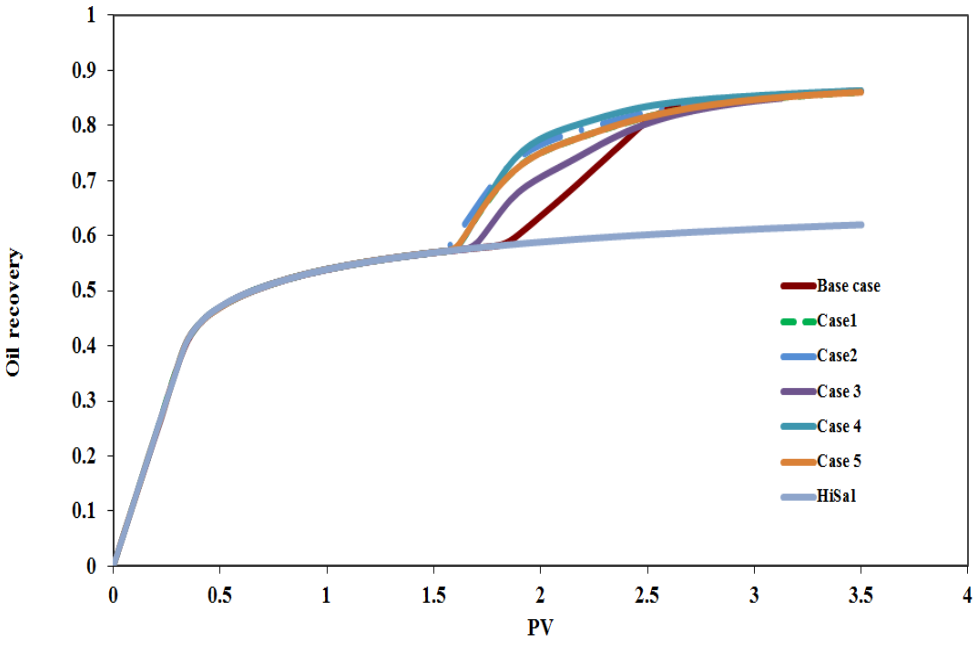

Figure 3-43: Oil recovery at the tertiary injection mode (sensitivity analysis on log(K) of the organometallic complexes on the clay surface).

Shown in Table 3-4 are different minimum threshold values chosen for the sensitivity analysis purpose. Oil recoveries at secondary and tertiary mode of injection are presented in Figures 3-44 and 3-45, respectively. It is difficult to differentiate between these models based on predictions oil recovery for base and simple low salinity floods. The performance of these models for a wider variety of injectants and more detailed chemical analysis of the effluents would be necessary.

Table 3-4: Minimum threshold values in Eq. (3.18) for chosen the sensitivity analysis purpose

	Base Case	**Case 1**	**Case 2**	**Case 3**
ζ_{min}(moles)	3.8×10^{-4}	4.5×10^{-5}	5.5×10^{-5}	6.5×10^{-5}

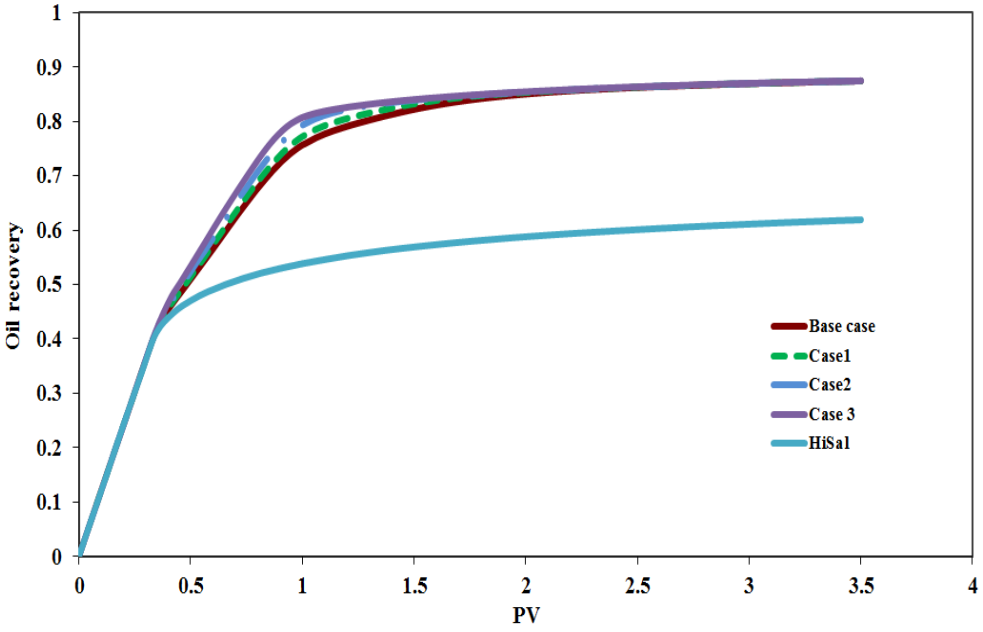

Figure 3-44: Oil recovery at the secondary injection mode (sensitivity analysis on the minimum threshold of the interpolating parameter).

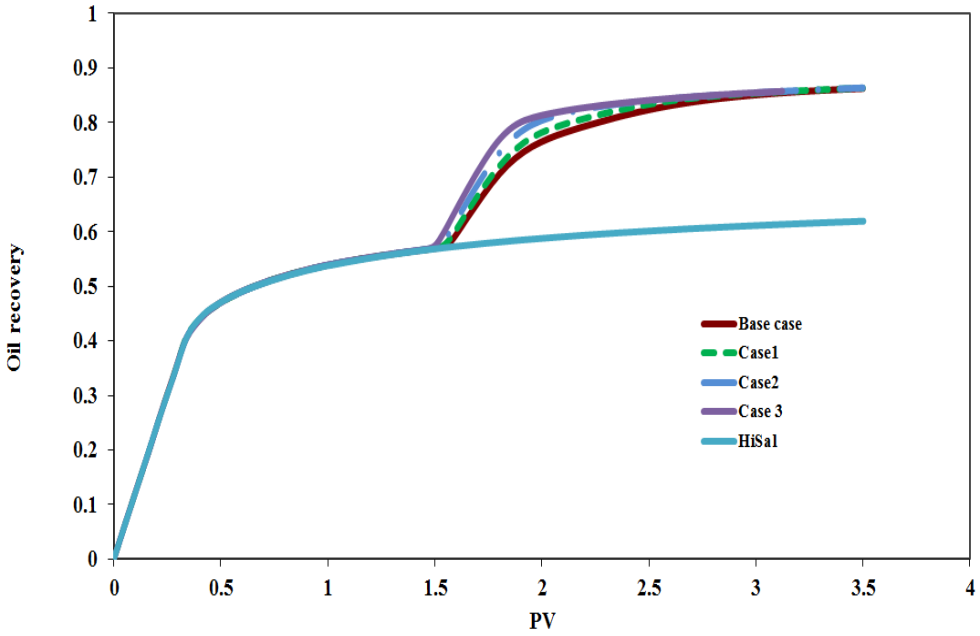

Figure 3-45: Oil recovery at the tertiary injection mode (sensitivity analysis on the minimum threshold of the interpolating parameter).

Chapter 4: Mechanistic Modeling of Modified Salinity Waterflooding in Carbonate Reservoirs

Low primary recovery factor in carbonate reservoirs brings about a tremendous potential for EOR. However, reservoir conditions limit the number of applicable EOR methods in these reservoirs. Recently, several investigations have focused on tuning ion compositions of the injected water to improve oil recovery. While this new process is supported by extensive promising laboratory and single-well chemical tracer tests, the underlying mechanism of this process is still a subject of ardent debate.

In line with Hiorth *et al.* (2010), we believe that during the modified salinity waterflooding in carbonates, calcite is dissolved and it liberates the adsorbed oil from the surface; hence, fresh surface with the wettability towards more water-wet is created. Therefore, we model wettability to be dynamically altered as a function of calcite dissolution in the UTCOMP-IPhreeqc simulator. We then apply our integrated simulator to model and interpret a systematic coreflood published by Chandrasekhar and Mohanty (2013). What follows in this chapter, reviews important findings published in the literature on the modified salinity waterflooding in carbonate reservoirs; describes the model proposed for the modified salinity waterflooding in carbonates; presents the description of experimental and modeling procedures; interprets the coreflood modeled.

4.1 Modified Salinity Waterflooding in Carbonate Reservoirs

Carbonate reservoirs account for more than half of the world's hydrocarbon reserves. However, about 90% of carbonate reservoirs are neutral to oil-wet making the average oil recovery from carbonate reservoir to about 30% which is lower than that of

sandstones (Austad *et al.*, 2008; Chandrasekhar and Mohanty, 2013; Chandrasekhar, 2013). Low primary recovery factor in carbonate reservoirs ushers a tremendous potential for EOR. However, harsh reservoir conditions, such as high temperature and high salinity, high level of heterogeneity, and initial state of the rock wettability (i.e., mostly oil-wet) of carbonate reservoirs, limit the use of recovery processes in the likes of; surfactant-polymer flooding, gas injection, and conventional waterflooding.

Recently, investigations have been directed toward improving the oil recovery from carbonate reservoirs through tuning the injected water salinity (either by modifying the injected water for certain ions or by decreasing a certain lumped geochemical property of the injected water, such as the total salinity or the total ionic strength of injected water). The new proposed process is supported by several laboratory studies (Chandrasekhar and Mohanty, 2013; Chandrasekhar, 2013; Zekri *et al.*, 2011; Yousef *et al.*, 2010; Alotaibi *et al.*, 2010; Al-Attar *et al.*, 2013a; 2013b) and also by a single-well chemical tracer test (Yousef *et al.*, 2012). Some of these reports are discussed:

Al-Attar *et al.* (2013a; 2013b) conducted low salinity water experiment on five carbonate core samples taken from Bu Hasa field in Abu Dhabi. Their results show that reducing the salinity of water from 197,357 to 5,000 ppm enhances the oil recovery from 63 to 84.5%.

Al-Harrasi *et al.* (2012)'s experimental work show that reducing the salinity of the injected or imbibed water improves the oil recovery of a sample taken from a carbonate reservoir (mainly composed calcite with very small amounts of dolomite minerals) in Oman. Incremental oil recoveries for coreflood and imbibition tests are 3 to 5% and 16 to 21% of OOIP, respectively. Measured IFT at room temperature shows

slight decrease (one unit) with the diluted water. The injected water improves the oil recovery where its salinity is at the high level of 97,000 ppm.

Experimental work conducted by Sharifi and Al-Shaikh (2013) shows that oil recovery from calcites is related to the contact angle. However, not necessarily diluted waters lead in lowering the contact angle. Hence, they believe that contact angle is better criteria for the injected water compare with salinity level. Based on the results reported in this work, modified salinity waterflooding improves the oil recovery by 12-18 percentages.

Understanding the mechanisms behind any EOR process is essential for successful oil production modeling. McGuire *et al.* (2005) proposed the interfacial tension (IFT) reduction as the dominant mechanism for modified salinity waterflooding. Based on the observed trend of decreasing IFT with decreasing salinity, Okasha and Al-Shiwaish (2009) also drew the similar conclusion. However, Okasha and Al-Shiwaish (2009) did not notice that oil-water IFT should drop to ultra-low values (e.g., 10^{-3} dyne/cm) to contribute to oil recovery (Lohne *et al.*, 2012; Patacchini *et al.*, 2012; Najafabadi *et al.*, 2008). There are some experimental data in which oil recovery does not show any correlation with the pH increase of the system and the interfacial tension (Al-Attar *et al.*, 2013a; 2013b). This is also consistent with the works of Yousef *et al.* (2010) and Al Harrasi *et al.* (2012) where although the modified salinity waterflooding shows the incremental oil recovery, IFT decreases only for one unit.

Evidence of wettability alteration is more pronounced in recent laboratory observations (Austad *et al.*, 2008; Chandrasekhar and Mohanty, 2013; Chandrasekhar, 2013; Zekri *et al.*, 2011; Yousef *et al.*, 2010; Alotaibi *et al.*, 2010; Al-Attar *et al.*, 2013a; 2013b; Yousef *et al.*, 2012; Al Harrasi *et al.*, 2012; Gupta *et al.*, 2011). However, the

process by which the wettability alteration occurs is still in debate. Researchers have tried to correlate oil recovery to either lumped geochemical properties, such as the total dissolved salts (TDS) and total ionic strength (TIS), or the presence/absence of certain ions, called potential determining ions, in the injected water.

Some researchers have observed the increase in oil recovery when the injected water is simply diluted (Chandrasekhar and Mohanty, 2013; Chandrasekhar, 2013; Al-Attar *et al.*, 2013a; 2013b; Bagci *et al.*, 2001). However, experimental data of Sharifi and Al-Shaikh (2013) show that lowering the salinity of the water has no significant effect on the contact angle; hence, the total salinity might not be the main contributor in improving oil recovery due to modified saline or brackish waterflooding. Furthermore, experimental results of Hognesen *et al.* (2005) also present oil recoveries that are different for waters with identical salinities but different ion compositions. Also, the modified salinity waterflooding shows incremental oil recovery when the salinity of the injected water is at a high value of 97,000 ppm (Al Harrasi *et al.*, 2012). This reveals that under favorable conditions, it is not necessary that the total salinity should be reduced to observe the modified salinity waterflooding effect. Moreover, Gupta *et al.* (2011) observed incremental oil recovery even when water with higher salinity is injected into the core. Experimental results of Fathi *et al.* (2012) also illustrate the detrimental effect of the injected diluted water.

On the other hand, Romanuka *et al.* (2012) believe that the total ionic strength is the controlling factor of the wettability alteration due to modified salinity waterflooding in carbonates. Their belief is contrary to several experimental works in which the incremental oil recovery was observed through tuning ion compositions of the injected

water by keeping the total ionic strength of the solution unchanged (Chandrasekhar and Mohanty, 2013; Chandrasekhar, 2013; Al-Attar *et al.*, 2013a; 2013b).

A large group of researchers pointed out the important role of certain ions during modified salinity waterflooding in carbonates (Austad *et al.*, 2008; Chandrasekhar and Mohanty, 2013; Chandrasekhar, 2013; Alotaibi *et al.*, 2010; Al-Attar *et al.*, 2013a; 2013b; Gupta *et al.*, 2011; Hognesen *et al.*, 2005; Fathi *et al.*, 2012; Romanuka *et al.*, 2012; Zhang *et al.*, 2007; Austad *et al.*, 2005; Austad *et al.*, 2011; Strand *et al.*, 2006; Tweheyo *et al.*, 2006; Shariatpanahi *et al.*, 2011; Fernø *et al.*, 2011; Sultani *et al.*, 2012; Rezaei Gomari and Hamouda, 2006; Hamouda *et al.*, 2008; Gupta and Mohanty; 2011; Chukwudeme and Hamouda, 2009). In their opinion, modified salinity waterflooding is effective if it is just tuned for the potential determining ions. Austad *et al.* (2005) concluded that sulfate (SO_4^{-2}), calcium (Ca^{+2}), and magnesium (Mg^{+2}) are potential determining ions for the modified salinity waterflooding in chalk formations and their effect is more pronounced at elevated temperatures. This hypothesis is further supported by the works of Zhang *et al.* (2007); Austad *et al.* (2008); Austad *et al.* (2011); Fathi *et al.* (2012); Strand *et al.* (2006); Tweheyo *et al.* (2006). In the proposed mechanism by Zhang *et al.* (2007) as the sulphate adsorbs to the positive chalk surface it diminishes the positive charge of the surface and consequently gives the calcium ion the opportunity to get close to the surface and reacts with the carboxylic branches attached to the surface and liberates them from the surface. Through this mechanisms, wettability of rock changes from oil-wet towards the water-wet. This mechanism interprets the temperature dependency of low salinity waterflooding in carbonates in the way that at elevated temperatures Mg^{+2} can directly displace the calcium-carbonate complexes from the rock surface that promotes oil recovery. Strand *et al.* (2006) studied the affinity of the sulfate

ion towards the chalk surface. In this work a non-potential ion, SCN^-, and a potential determining ion, SO_4^{-2}, are simultaneously injected into a chalk core. SCN^- shows earlier breakthrough compare with SO_4^{-2} which clearly shows the affinity of the sulfate ion towards the carbonate surface.

Works of Al-Attar *et al.* (2013a; 2013b), Alotaibi *et al.* (2010), Hognesen *et al.* (2005), and Shariatpanahi *et al.* (2011) also confirm the potential determining effect of sulfate. However, there is an upper limit beyond which sulfate has detrimental effect on oil recovery. On the other hand, experimental results of Fernø *et al.* (2011) show that a not necessarily high sulfate concentration leads to the incremental oil recovery even at high temperature of 130 ^oC. Also, Sultani *et al.* (2012) observed no significant increase in the oil recovery when sulfate concentration is tuned in the seawater; however, the Mg^{+2} ion improves oil recovery significantly. Gupta *et al.* (2011) introduced borate (BO_3^{-3}) and phosphate (PO_4^{-3}) as two new potential determining ions during modified salinity waterflooding in carbonates. Furthermore, they presented a case in which formation water containing no SO_4^{-2}, no Ca^{+2} and Mg^{+2} and even with higher total dissolved salts shows incremental oil recovery over the formation water. Their observation is in line with the work of Alotaibi *et al.* (2010), where Ca^{+2} has the detrimental effect during modified salinity waterflooding. Rezaei Gomary and Hamouda (2006) concluded that potential of Mg^{+2} and SO_4^{-2} ions to alter the wettability of calcite is pH-dependent. Compared with Mg^{+2}, the effect of SO_4^{-2} is more pronounced at low pH values. Mg^{+2} becomes more effective as pH increases while the SO_4^{-2} effect on wettability alteration has an optimum pH value (about 7) beyond which wettability changes towards more oil-wet in the presence of the sulfate ion. Laboratory work of Chandrasekhar and Mohanty (2013) and Chandrasekhar (2013) show that Mg^{+2} and SO_4^{-2} ions alone or combined with other

potential determining ions can change wettability. However, Ca^{+2} ion is effective only if it is used along with both Mg^{+2} and SO_4^{-2}. Also, experiments conducted by Hamouda *et al.* (2008) illustrate that Mg^{+2} and SO_4^{-2} are potential determining ions in chalks and that Mg^{+2} is more effective than SO_4^{-2}. These observations, however, are in contrast with the work of Gupta and Mohanty (2011) where Mg^{+2}, used alone, is not a potential determining ion while Ca^{+2} at high concentration is a wettability modifier for calcite plates. Imbibition experiment of Chukwudeme and Hamouda (2009) presents that Mg^{+2} and SO_4^{-2} have negative and positive effects, respectively, on incremental oil recovery from chalk cores. Based on experimental observations, Hognesen *et al.* (2005) reported the ratio of Ca^{+2} to the SO_4^{-2} concentration as one of the most important parameter in modified salinity waterflooding in carbonates. Fathi *et al.* (2012) pointed out the modified salinity waterflooding is more effective if the injected water is diluted for non-potential determining ions (e.g., Na^{+} and Cl^{-1}). In fact, through this the potential determining ions (i.e., Ca^{+2}, Mg^{+2}, and SO_4^{-2}) have more space on the surface to act efficiently. They believed although Ca^{+2}, Mg^{+2}, and SO_4^{-2} are the potential determining ions in carbonates, non-potential determining ions (i.e., Na^{+} and Cl^{-}) may affect the easy access of these potential determining ions to the rock surface. This hypothesis is in line with their imbibition test where keeping the concentration of Ca^{+2}, Mg^{+2}, and SO_4^{-2} unchanged in the imbibing brine, final oil recovery and the imbibition rate increase by decreasing the Na^{+} and Cl^{-} concentrations. This observation is confirmed at different temperatures of 100, 110, and 120 ^{o}C. However, Romanuka *et al.* (2012) conducted an experiment on a limestone sample showing that injecting seawater without Na^{+} and Cl^{-1} ions has no positive effect on oil recovery over the seawater with Na^{+} and Cl^{-1} ions.

Observations from experiments conducted by Bagci *et al.* (2001) on unconsolidated carbonate sandpack show that addition of KCl makes modified salinity waterflooding more efficient in carbonate reservoirs and $CaCl_2$ has no positive effect.

It is hard to draw a conclusion out of the extensive research performed in this area laden with several contradictions. We believe that the main reason no definitive mechanism has been proposed yet for this process is the fact that most of the researchers have not tried to take into the account the effects of ion compositions of the injected and initial waters, mineralogy of the rock, and type of the oil (composition and dead/live) all together when interpreting their results. In fact, some researchers tried to interpret their results based on just the ion compositions of injected water, the initial water, or the mineralogy of the rock. However, all the factors should be included to better interpret modified salinity waterflooding.

4.2 MECHANISTIC MODELING USING UTCOMP-IPHREEQC

With all these uncertainties, with regards to the underlying mechanism for modified salinity waterflooding, some researchers have still tried to model this process. Aladasani *et al.* (2012) and Gupta *et al.* (2011) applied the model first proposed by Jerauld *et al.* (2008) to model low salinity waterflooding. Jerauld *et al.* (2008)'s model treats the TDS as a lumped inactive tracer in the system. This model introduces the wettability alteration in the system through interpolation between two extreme relative permeability and capillary pressure curves (i.e., water-wet and oil-wet set) using the TDS concentration at each gridblock. However, because of geochemical features present in the system (e.g., dissolution/precipitation of minerals, exchanging of ions with the exchanger and surface complexation), ion compositions of the injected water might be significantly changed when passing through the system. Hence, we believe that even if the lumped

geochemical properties (e.g., TDS or TIS) are assumed to be the controlling parameters for modified salinity waterflooding, these parameters need to be evaluated during simulation by applying the comprehensive geochemical calculation rather than being treated as an inactive tracer. The validity of this assumption is investigated later in the chapter (cf. Section 4.5). Al-Shalabi *et al.* (2014a) applied a different approach to model two sets of corefloods published by Yousef *et al.* (2010). In the Yousef *et al.* (2010)'s experimental work, seawater is first injected into a composite core and then followed by four modified salinity waters with different TDS levels (with the diluting factors of 1/2, 1/10, 1/20, and 1/100 of total seawater salinity). Al-Shalabi *et al.* (2014a) considered different relative permeability exponents and endpoints for each cycle to successfully match the measured oil recoveries.

By injecting water with modified ion compositions, the equilibrated system among crude oil, brine, and rock (COBR) is in fact disturbed. Hence, it appears that the underlying mechanism behind the process should be somehow related to geochemical reactions. Few researchers have tried to model or interpret this process by addressing the geochemistry of the problem (Al-Shalabi *et al.*, 2014b; Andersen *et al.*, 2012a; 2012b; Yu *et al.*, 2009). However, none of these researchers have modeled histories of produced ions, along with the oil recovery, for more robust interpretations.

Hiorth *et al*. (2010) tried to interpret the modified salinity waterflooding effects using surface reactions. However, predictions of their surface model developed were not consistent with several experimental observations documented in the literature. On the other hand, they were able to interpret the observations, assuming calcite dissolution as the dominant controlling parameter in the underlying modified salinity waterflooding. In their opinion, during modified salinity waterflooding in carbonates, calcite is dissolved

and liberates the adsorbed oil from the surface; hence, a fresh surface leaning more towards water-wetting is created. Figure 4-1 compares the rock surface before (top panel) and after (bottom panel) injection of modified saline or brackish water. The proposed model is also supported by Vo *et al.* (2012), Zahid *et al.* (2012), and Gupta *et al.* (2011).

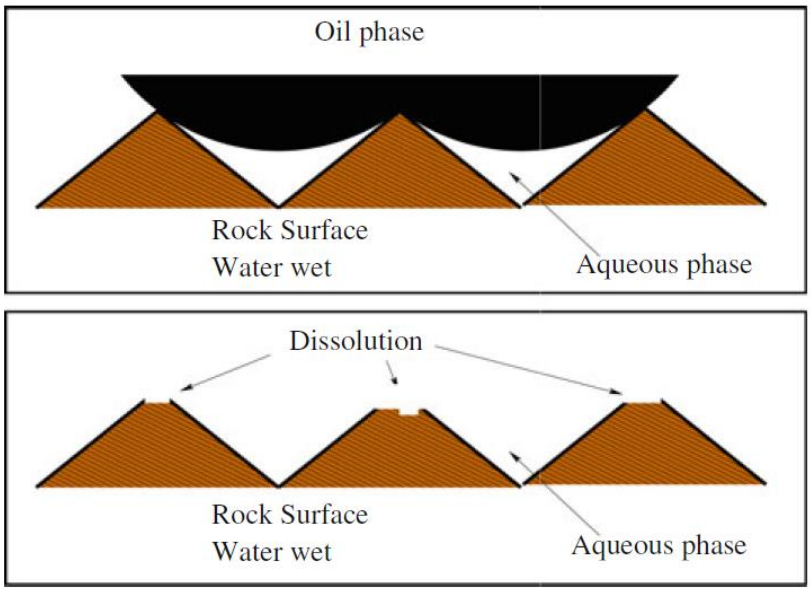

Figure 4-1: Top: Before the modified salinity waterflooding oil is attached to the surface (i.e., oil-wet surface). Bottom: Due to the modified salinity waterflooding, dissolution occurs that takes away the oil attached to the surface (i.e., water-wet surface) (Hiorth *et al.*, 2010).

Based on the model proposed by Hiorth *et al.* (2010), we apply the interpolating technique in UTCOMP-IPhreeqc and dynamically alter the wettability of the rock as a function of calcite dissolution. Hence, in each time step after IPhreeqc provides the equilibrated data of entire gridblocks, UTCOMP evaluates the interpolating parameter for each gridblock using the following equation:

$$\theta = \frac{\xi_{\max} - \xi(x,t)}{\xi_{\max} - \xi_{\min}}, \tag{4.1}$$

where, $\zeta(x,t)$ is the amount of calcite in each gridblock, ζ_{max} is the amount of calcite above which no wettability alteration would occur. In other words, certain amount of calcite should be dissolved for the wettability alteration to occur. ζ_{min} is the value at which enough amount of calcite is dissolved making the rock totally water-wet. Maximum and minimum thresholds in Eq.(4.1) are the matching parameters.

The θ calculated from Eq.(4.1) is then used to interpolate between the two extreme relative permeability and capillary pressure sets (see Eqs. (4.2) and (4.3)) to find the altered relative permeability and capillary pressure at each gridblock.

$$k_{rl}^{altered} = (1-\theta) k_{rl}^{oil-wet} + \theta k_{rl}^{water-wet} \tag{4.2}$$

$$P_c^{altered} = (1-\theta) P_c^{oil-wet} + \theta P_c^{water-wet} \tag{4.3}$$

We need to point out that one feature stands out in this model: calcite dissolution customarily occurs if the injected solution is undersaturated for either the calcium or the carbonate ions; it thus appears that the modified salinity waterflooding effect should be more pronounced should the Ca^{+2} and CO_3^{-2} ions be selectively removed from the injected solution. However, while to the best of author's knowledge, the effect of CO_3^{-2} has not been investigated in any experimental work published anywhere, reports of both detrimental and beneficial effects of Ca^{+2} ions removed from the injected solution can be found (as discussed in Section 4.1).

We assume the dissolution of calcite to be the underlying mechanism for wettability alteration. Furthermore, we hypothesize that this model should perhaps be

generalized to include the dissolution of entire spectrum of existing minerals, not a specific mineral type (e.g., calcite proposed by Hiorth *et al.*, 2010). Dissolution, if occurring on any oil-wet mineral, creates a fresh surface and can alter rock wettability. It should be noted that while in one hand the CO_3^{-2} concentration gives the determining ion controlling calcite dissolution and on the other hand some of CO_3^{-2} are always fed to the aqueous phase, on account of buffering of CO_2 in the hydrocarbon phase, it is crucial to include the effect of hydrocarbon phase on aqueous-rock geochemistry. We quantify this importance later in the chapter (cf. Section 4.5).

UTCOMP-IPhreeqc, with wettability alteration model implemented, applied to model a systematic coreflood published by Chandrasekhar (2013) and Chandrasekhar and Mohanty (2013). Section 4.3 describes the experiment.

4.3 EXPERIMENT DESCRIPTION

Chandrasekhar (2013) documented several modified salinity waterflooding experiments conducted on carbonate cores. One of the corefloods (labeled as "SW/50 in Tertiary Mode" in his thesis) is modeled in this work using UTCOMP-IPhreeqc. Petrophysical properties of the core are shown in Table 4-1. The coreflood was conducted at 120 ^oC. Prior to the waterflooding, core had been aged at 80 ^oC for at least 30 days. The core is first flooded with the formation brine ("FB") for 5 PV followed by "SW/50" (which is 50 times diluted seawater) water for 9 PV. Ion compositions of "SW/50" and "FB" are given in Table 4-2. Oil viscosity and the total acid number are 1cp at 120 ^oC and 2.45 KOH/g oil, respectively. Coreflood configuration is vertical with the injection at the bottom and production at the top. The water viscosity is about 0.9 cp at the experiment temperature[1].

[1] Personal communication with S. Chandrasekhar and K.K. Mohanty. 2014. Austin: The University of

Table 4-1: Core geometry and petrophysical properties (Chandrasekhar and Mohanty, 2013).

Diameter (mm)	37.7
Length (mm)	75.9
Porosity	0.155
S_{oi}	0.76
K_{air}(md)	64.7
K_{brine}(md)	10.3

Table 4-2: Formation brine (FB) and "SW/50" ion concentrations (Chandrasekhar and Mohanty, 2013).

Ion	Formation brine (FB) (ppm)	SW/50 (ppm)
Na^{+}	49933	274
Mg^{+2}	3248	32.4
Ca^{+2}	14501	10.42
Cl^{-}	111810	489.36
SO_4^{-2}	234	66.2
HCO_3^{-}	-	-
Total ionic strength (mol/kgw)	3.658	0.017
TDS (mg/L)	179730	872

4.4 MODEL DESCRIPTION

To mimic heterogeneity inherent in carbonate reservoirs, a 2D (5×1×25) model is designed in UTCOMP-IPhreeqc. Dimension and petrophysical properties considered in UTCOMP-IPhreeqc are all consistent with those reported from the experiment. Injection rate in UTCOMP-IPhreeqc is 3.32×10^{-4} bbl/day (0.0366 cc/min) which produces 1 ft/day (3.53×10^{-6} m/s) for the velocity applied in the experiment. Also, producing pressure is 50 psi (Chandrasekhar, 2013). Similar to the coreflood design, we first flooded the core with 5 PV of the formation water and then followed by 9 PV of "SW/50" (ion compositions

provided in Table 4-2). What follows below presents the assumptions and the matching parameters considered to model the coreflood.

- **Geochemistry**
  - The pitzer.dat database of IPhreeqc is considered for the geochemical calculations. The Pitzer aqueous model is suitable for high-salinity waters where the Debye-Hückel model (the ion-association aqueous model used in the phreeqc.dat database) is not applicable. However, we assume the pitzer.dat database can be used at high temperature of 120 ^{o}C of the experiment.
  - Because the core is carbonate, calcite and dolomite are assumed to be the only minerals present in the core.
  - It is assumed that at lab condition, fluid velocity is high enough that kinetics of the minerals can be introduced into the model through super/undersaturation. Hence, saturation indices of calcite and dolomite are matching parameters.
  - To properly model the effluent pH history, cation exchanger is also included in the model.
  - Ion histories are measured after cooling down the effluent aqueous solution in the presence of atmospheric CO_2 (Chandrasekhar, 2013). Hence, $10^{-2.0}$ atm and 30 ^{o}C are assumed to be the CO_2 partial pressure and the temperature at which ion histories are measured.
  - Inclusion of surface complexation in the model is mandatory to model the effluent ion histories. This confirms the extensive discussion in the literature on the importance of calcium, magnesium, and sulfate surface reactions in carbonates during modified salinity waterflooding (see Section 4.1).

Consistent with observations in the literature, Ca^{+2}, Mg^{+2}, and SO_4^{-2} are the ions assumed on the surface. Stoichiometric coefficients of these ions on the surface are the matching parameters.

- **Core geometry**
  - Although the dimension in the *x*-direction is 0.033 m (the model and the core have the same cross-sectional area). Gridblcok widths in the *x*-direction are adjusted.
- **Transport**
  - A synthetic dead oil composition, which satisfies the oil viscosity of 0.9 cp reported by Chandrasekhar (2013) is used.
  - Absolute permeability in the flow direction (*z*-direction) is constant and equal to the average value reported from the experiment (K_{Brine} = 10.3 md given in Table 4-1). However, the core absolute permeability perpendicular to the flow (*x*-direction) is adjusted to better match the experimental data. Figure 4-2 shows the permeability distribution in *x*-direction of the tuned model. Average permeability in the *x*-direction is 0.1 md with the Dykstra-Parson coefficient of 0.1.
  - As discussed previously, two relative permeability sets (initial state or oil-wet set and final state or water-wet set) are considered to model the wettability alteration. Initial oil saturation (S_{oi}) of the oil-wet set in the model is 0.76 as measured in the experiment. We assume enough pore volumes of oil are injected to saturate the core. Hence, residual water saturation of the oil-wet set is 0.24 in the model. Residual oil saturation (S_{or}) and oil and water endpoints and exponents of the oil-wet set are the matching parameters. Residual oil saturation is the main controlling parameter to match the final oil recovery (S_{or}

= 0.42 in the tuned model). Oil and water residual saturations, exponents, and endpoints of the second (or the water-wet) set are adjusted to better match the coreflood. Figure 4-3 presents the initial and the altered relative permeability curves of the tuned model. We further assume that the pressure gradient in the coreflood is high enough that capillary pressure can be ignored.

- Amounts of calcite dissolution at which wettability alteration is start and completed (ζ_{max} and ζ_{min} in Eq. (3.1)) are the matching parameters.

- **Dispersion**
  - Low order method of discretization is applied in UTCOMP and numerical dispersion (with $\alpha=\Delta x/2$) is assumed to provide the physical dispersion involved in the experiment (Jerauld *et al.* (2008)). In other words, Peclet number is assumed to be 50 at the lab scale.

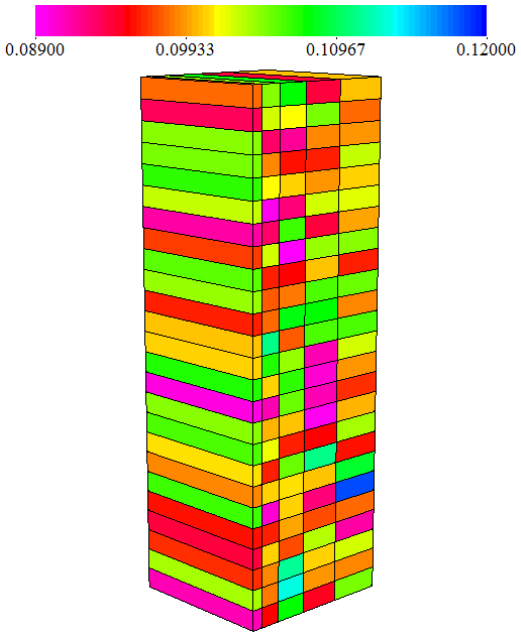

Figure 4-2: Absolute permeability (in md) distribution perpendicular to the flow direction (*x*-direction) in the model.

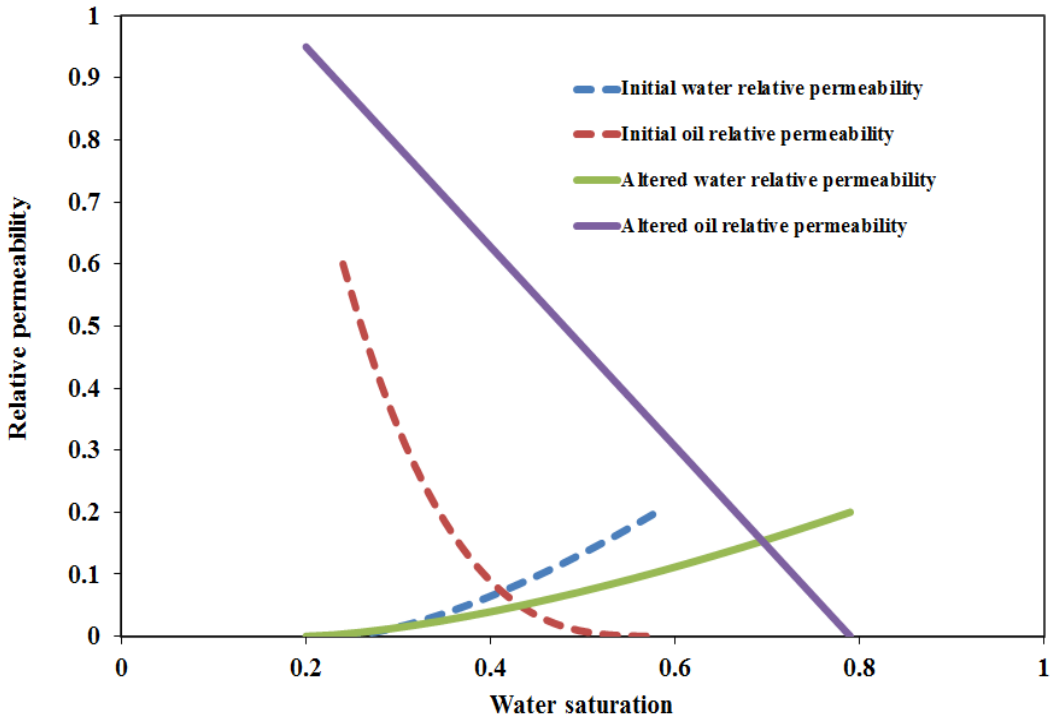

Figure 4-3: Initial (dashed lines) and altered (solid lines) relative permeability curves used in the model.

4.5 RESULTS AND DISCUSSIONS

Figures 4-4 through 4-10 present the UTCOMP-IPhreeqc simulated results for the oil recovery, effluent ion histories, and pH against the experimental data. Initial and injected concentrations are shown with the black dashed lines in the figures. Although we obtain reasonable matches to the oil recovery, ion histories, and pH (to some extent), our match for Ca^{+2} is poor. In fact, if we tried to model the Ca^{+2} ion we would mismatch the Mg^{+2} ion. Our tuned model shows that the wettability alteration starts when 2.5% of the calcite is dissolved and the maximum wettability alteration (extreme water-wet) takes place when 5% of calcite is dissolved. However, we believe that a fraction of these values is actually effective for the modified salinity waterflooding because dissolution continues

at places where they have been already altered to the water-wet condition. It should be also noted that the initial chloride concentration of the formation brine is 111,810 ppm. However, the chloride (Cl^-) concentration initially produced from the core is about 17,143.02 ppm (see Figure 4-9). This is contrary with the fact that Cl^- and Br^- are usually treated as inactive tracer in reactive-transport problems (Cartwright *et al.*, 2006; Alcalá and Custodio, 2008). No solid explanation was presented in the works of Chandrasekhar and Mohanty (2013) and Chandrasekhar (2013) which interpret so much decrease in the chloride concentration. Also, we could not find any physical basis for this phenomenon to occur. Because the solubility product (K_{SP}) of the halite mineral is sufficiently high (about 37.17 at 25 ^oC, the pitzer.dat database of PHREEQC (Parkhurst and Appelo, 2013), halite precipitation cannot also justify this phenomenon. Moreover, the difference is too large to be interpreted as an experimental measurement error. To model the coreflood, rather than the actual value of 111,810 ppm, 17,143.02 ppm is used. We did not consider the actual value because considering high concentration for chloride significantly changes the total ionic strength of the solution which consequently affects the aqueous speciation of the other ions.

To study the importance of the geochemical reaction, particularly the surface reactions during the modified salinity waterflooding, a freshening case (blue dashed line) is also included in Figures 4-4 through 4-10. While calcite and dolomite are still included in the freshening model, the surface complexation and the exchange reactions are excluded from this case. The difference between the freshening case and the full model reveals the significant role of surface reactions in carbonate reservoirs. Interestingly enough, no incremental oil recovery is observed in the freshening case over the formation brine flooding. Based on the results we hypothesize that although calcite dissolution is

the main mechanism controlling the wettability alteration, surface reaction are mandatory for seeing modified salinity effect in carbonate reservoirs. Our hypothesis is in line with the works of Zaretskiy (2012) and Vo *et al.* (2012) where it is concluded that neither rock dissolution nor the ion-exchange (or in general, surface reactions) alone can interpret the incremental oil recovery by conducting modified salinity waterflooding in carbonates.

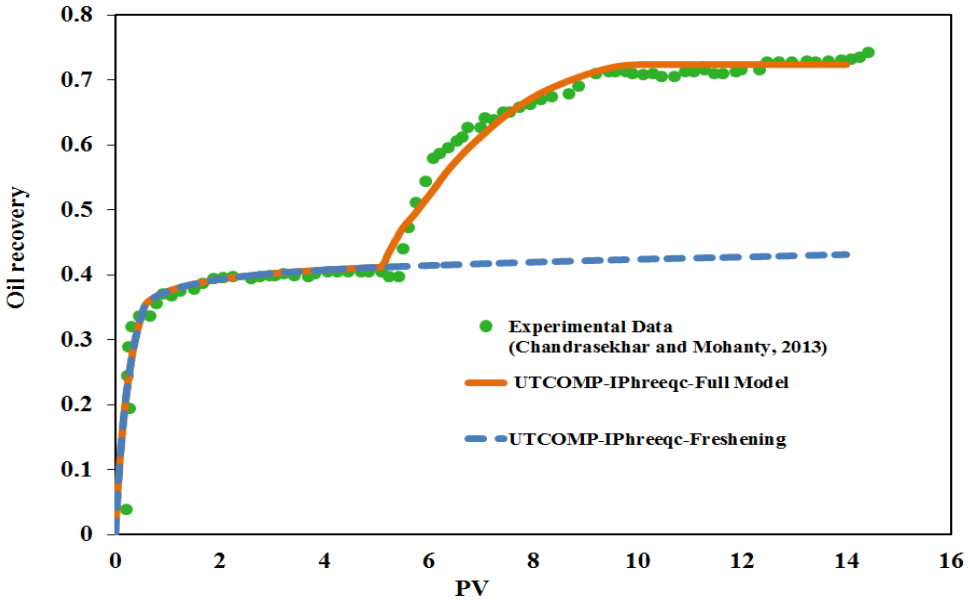

Figure 4-4: UTCOMP-IPhreeqc simulated results against the measured oil recovery data of the coreflood.

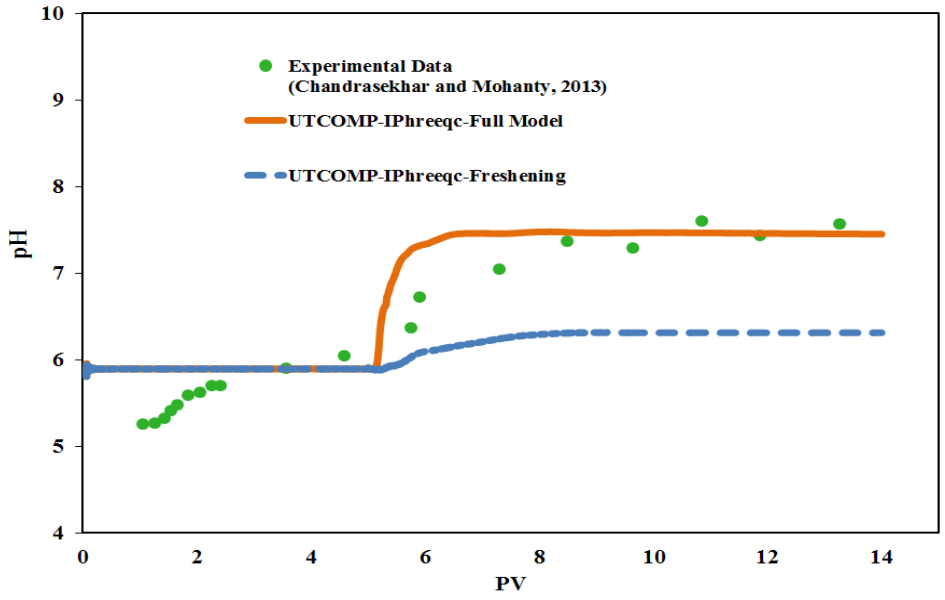

Figure 4-5: UTCOMP-IPhreeqc simulated results against the measured pH of the aqueous solution produced from the core.

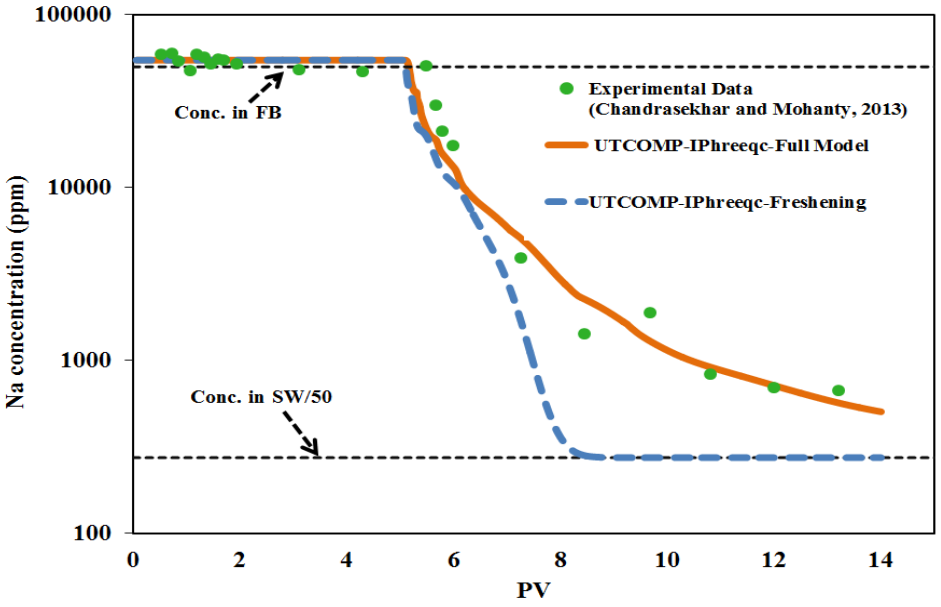

Figure 4-6: UTCOMP-IPhreeqc simulated results against the measured sodium concentration of the aqueous solution produced from the core.

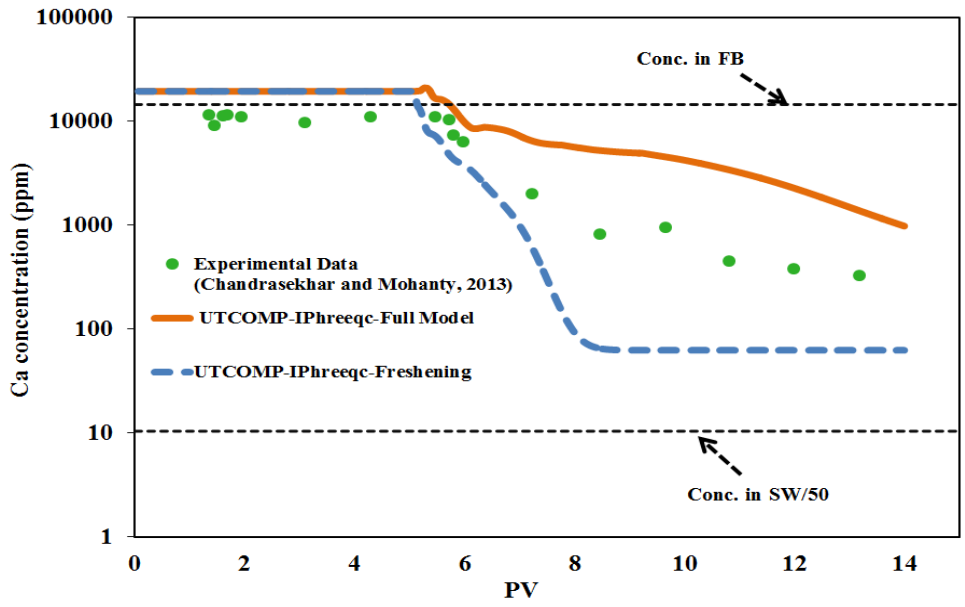

Figure 4-7: UTCOMP-IPhreeqc simulated results against the measured calcium concentration of the aqueous solution produced from the core.

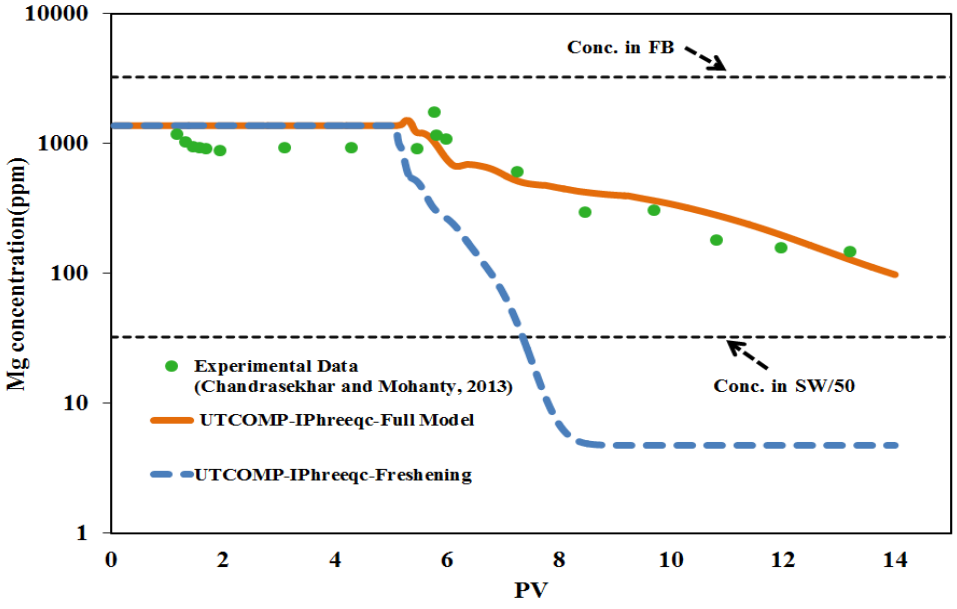

Figure 4-8: UTCOMP-IPhreeqc simulated results against the measured magnesium concentration of the aqueous solution produced from the core.

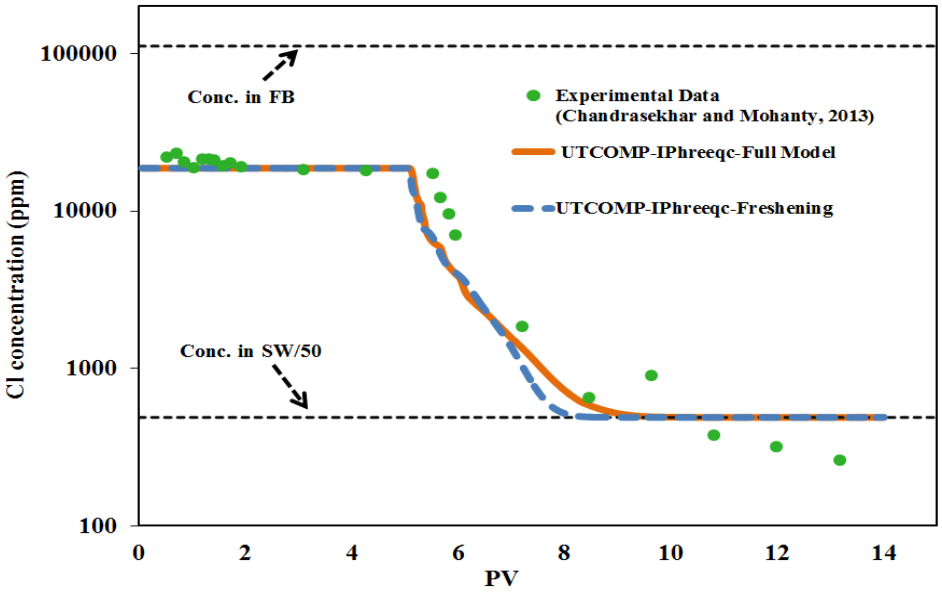

Figure 4-9: UTCOMP-IPhreeqc simulated results against the measured chloride concentration of the aqueous solution produced from the core.

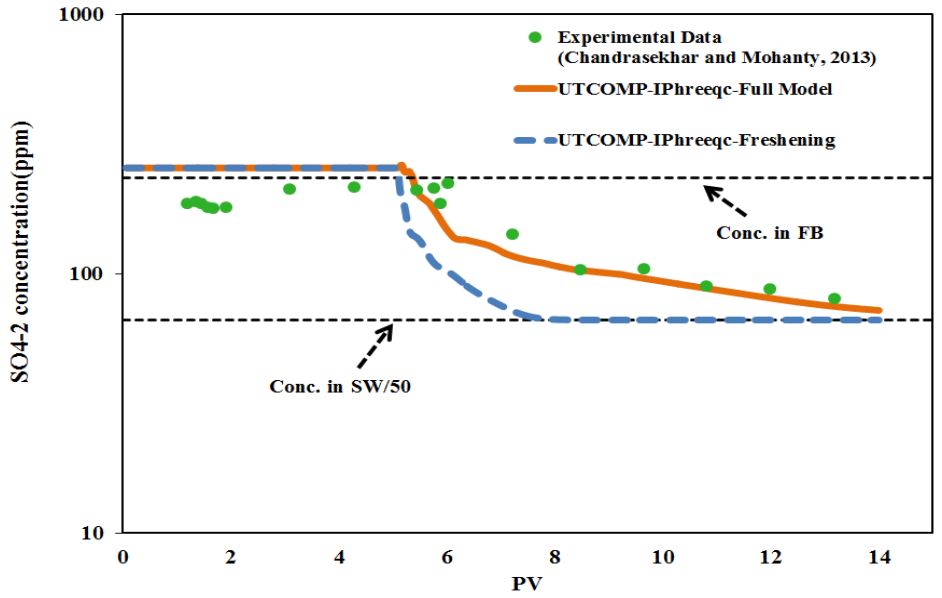

Figure 4-10: UTCOMP-IPhreeqc simulated results against the measured sulfate concentration of the aqueous solution produced from the core.

In contrast to the conclusion drawn by Austad *et al.* (2011), where the anhydrite dissolution is the main controlling parameter for the modified salinity flooding in carbonates, if we include anhydrite in our model, the trend for the sulfate ion is always increasing. Hence, although the modified salinity waterflooding improves the oil recovery in this coreflood, it appears there is no anhydrite present in the core.

Figure 4-11 compares TDS when it is calculated during the simulation with the case in which TDS is treated as an inactive tracer. As the figure shows, because of possible dissolution/precipitation, surface complexation, and exchange reactions occurring in the core, the total dissolved salts might significantly change when passing through the core; hence, treating it as an inactive tracer is not a good assumption. The same conclusion applies to the total ionic strength of the solution (see Figure 4-12).

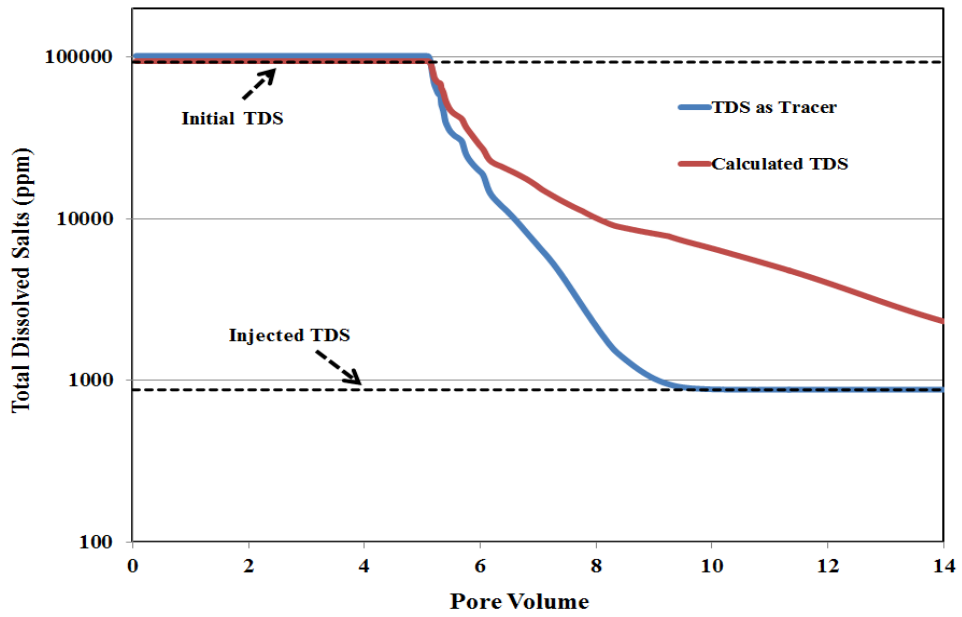

Figure 4-11: Calculated TDS against the case in which TDS is treated as an inactive tracer.

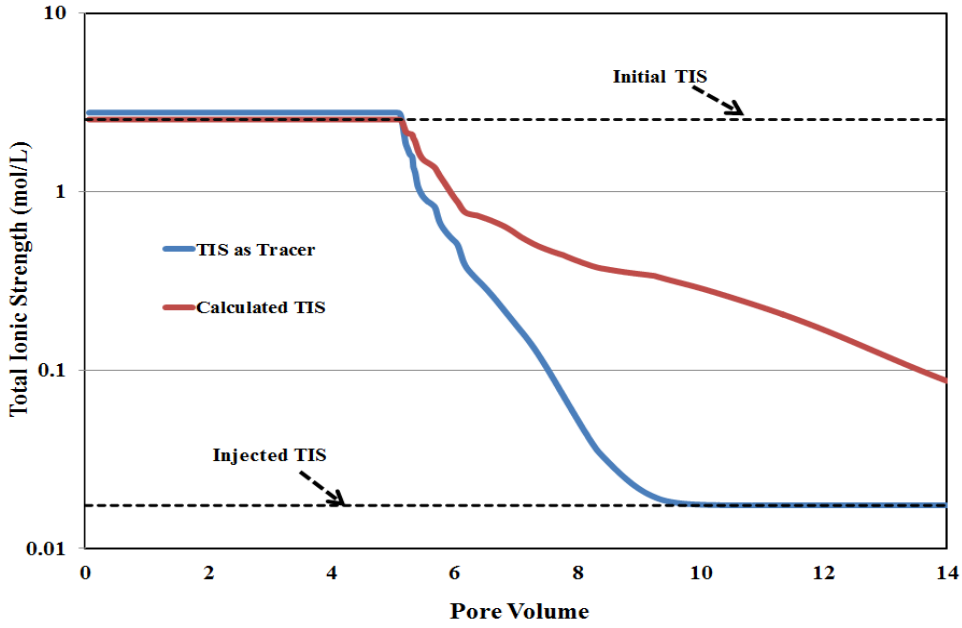

Figure 4-12: Calculated TIS against the case in which TIS is treated as an inactive tracer.

Several laboratory observations clearly illustrate the pronounced effect of elevated temperatures on the modified salinity waterflooding in carbonates (Austad *et al.*, 2008; Hognesen *et al.*, 2005; Fathi *et al.*, 2012; Chukwudeme and Hamouda, 2009; Yi and Sharma, 2012). If the surface complexation included in our model is assumed to be exothermic, our model predicts the right trend of increased oil recovery as temperature increases. Figure 4-13 shows the simulated oil recoveries when 2 PV of "SW/50" with different temperatures is injected into the core in the secondary mode of injection. For each individual case shown in the figure, we assume that the formation brine and the injected water have identical temperatures (i.e., no energy balance equation is solved). With a good approximation, we further assume that the temperature has the similar effect on both water and oil viscosities; so the decrease in the oil viscosity is compensated by the drop in the water viscosity. Hence, the overall effect of temperature in improving oil

recovery through increasing the oil mobility is negligible; particularly for this case in which oil viscosity is fairly small (i.e., 1 cp) and the core configuration is vertical with injection at the bottom and production at the top. Moreover, the measured oil viscosities at different temperatures provided in Chandrasekhar (2013) show that the oil viscosity does not have strong dependency on temperature in the range of 60-120 ^{o}C (i.e., 1.8 cp at 60 ^{o}C compare with 1.0 cp at 120 ^{o}C). Also, we ignore the potential effect of temperature on the wettability of the rock. Hence, all of wettability alteration owe to because of modified salinity waterflooding.

Based on the experimental observation, Austad *et al.* (2008) reported that the temperature effect is more pronounced in the temperature range between 100 and 130 ^{o}C. This is somehow consistent with the work of Hognesen *et al.* (2005), in which modified salinity waterflooding shows more promising results for temperatures of 90 to 120 ^{o}C, compared to the case where temperature increases from 60 to 90 ^{o}C. We have not included any physics into our model to predict this phenomenon; however, our simulation results presented in Figure 4-13 are accidentally consistent with the Hognesen *et al.* (2005) and the Austad *et al.* (2008) experimental observations.

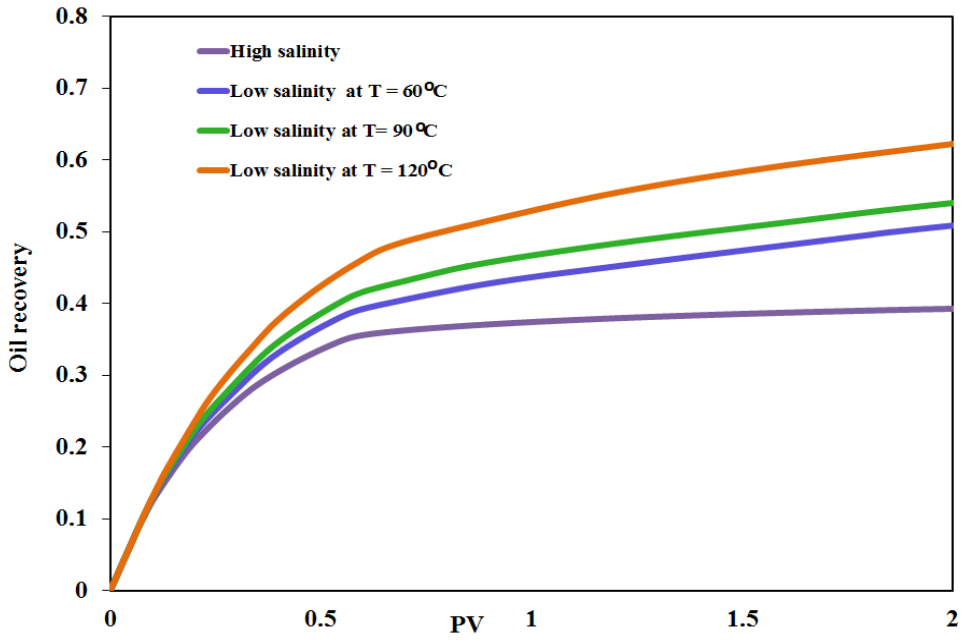

Figure 4-13: UTCOMP-IPhreeqc predictions for the oil recovery due to the modified salinity waterflooding in a carbonate core at different temperatures.

It should also be noted that our model predicts identical oil recoveries when different concentrations (i.e., 4x, 2x, and 0x) of sulfate, calcium, and magnesium are injected into the core. This is in line with several experimental observations, but not entirely consistent with some other laboratory works (see Section 4.1).

Chandrasekhar and Mohanty (2013) and Chandrasekhar (2013) properly hypothesized that if the rock dissolution is the controlling factor in incremental oil recovery due to the modified salinity waterflooding in carbonates, then modified salinity effect should be observed only in lab scales. The reason: the injected water becomes saturated for the ions (i.e., Ca^{+2} and CO_3^{-2}), when it penetrates only small distance into the reservoir; hence, no more dissolution occurs afterwards. Even the single well

chemical tracer test conducted by Yousef *et al.* (2012) cannot decline this hypothesis because the region of study in the single well chemical tracer test is limited to several feet around the well.

To verify this hypothesis, the design of the coreflood is applied to a synthetic quarter five-spot pattern (shown in Figure 4-14). Important reservoir characteristics are presented in Table 4-3. Injection rate is 400 bbl/day and the production well operates with the constant bottomhole pressure of 4925.0 psi. The live oil corresponding to the synthetic dead oil used to model the coreflood is considered in the quarter five-spot pattern. We still assume that kinetics of the mineral can be ignored when scaling up the coreflood to the field case. This might not be a good assumption far from the wells when the fluid velocity is fairly low.

Figure 4-15 compares oil recoveries for cases in which about 1.4 PV of modified salinity (i.e., the blue line) and high salinity (i.e., the orange line) waters are injected into the reservoir in the secondary mode of injection. This figure clearly illustrates that the modified salinity waterflooding shows promising results even in large scales. We believe that although the calcite dissolution is the controlling factor changing the wettability of the rock, however, as discussed in Figure 4-4, the effect does not solely depend on the calcite dissolution. Besides the calcite dissolution, surface reactions play a significant role that makes the process effective. This might be the main reason why the modified salinity waterflooding also shows promising results when applied in large scales.

To show the importance of the CO_2 buffering of the hydrocarbon phase on the aqueous-rock geochemistry and consequently on the performance of the modified salinity waterflooding, the result of the case without the CO_2 effect of the hydrocarbon phase included is also shown in Figure 4-15 (i.e., the green line).

Figure 4-16 presents the same cases as discussed in Figure 4-15, except that the modified saline waters are injected in the tertiary mode of injection (about 0.5 PV of the formation water is injected first and then chased with about 0.8 PV of the modified saline water). The effect of modified salinity waterflooding is also observed during the tertiary mode of injection.

Figures 4-17 and 4-18 illustrate maps of the interpolating parameter (i.e., θ) of the first layer at 0.5 PV (in the secondary mode of injection) for case with the hydrocarbon-CO_2 effect on the aqueous-rock geochemistry included and the case in which the effect is ignored, respectively. The corresponding maps at 1.0 PV are presented in Figure 4-19 and Figure 4-20. The front of the wettability alteration penetrates more into the reservoir for the case in which the CO_2 effect is ignored compared with the case in which the CO_2 effect is included. Hence, more oil recovery is observed when the CO_2 effect is excluded from the simulation.

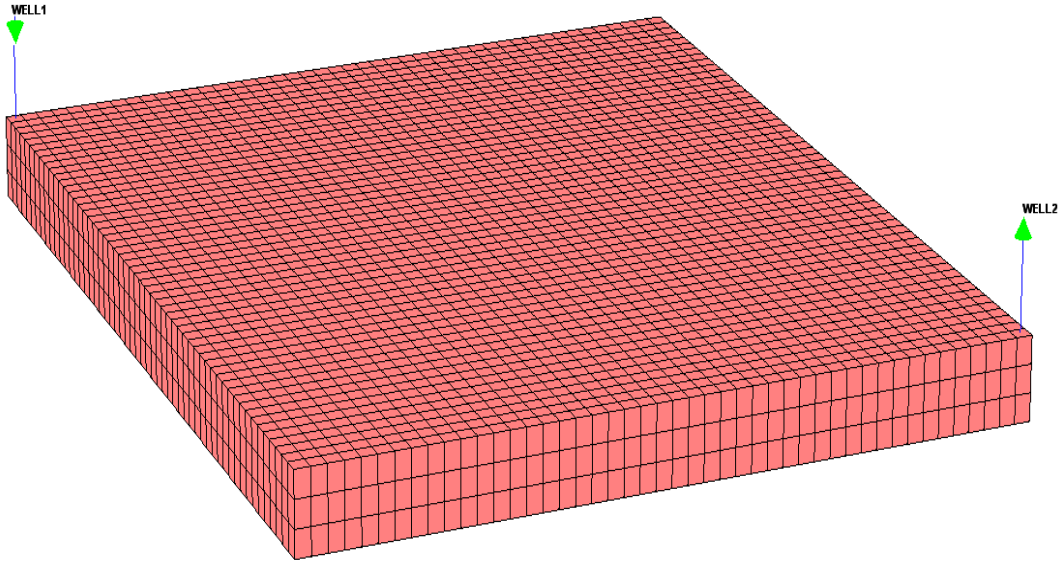

Figure 4-14: A quarter five-spot pattern.

Table 4-3: Geometrical and petrophysical properties of the quarter five-spot.

No. of gridblocks		7452 (46×54×3)
Δx(ft)		25.0
Δy(ft)		25.0
Δz(ft)		4.0
Permeability (md)	*x*-direction	200.0
	y-direction	200.0
	z-direction	30.0
Porosity		0.25
Rock compressibility (psi^{-1})		50.0×10^{-6}
Water compressibility (psi^{-1})		0.
Initial Water saturation		0.3
Irreducible water saturation		0.2
Reservoir temperature (^{o}F)		248.0
Initial pressure (psi)		4925.0
Reservoir depth (ft)		0.
Water viscosity (cp)		0.79
Number of wells	2	1 injector
		1 producer
Simulation time(PV)		1.3

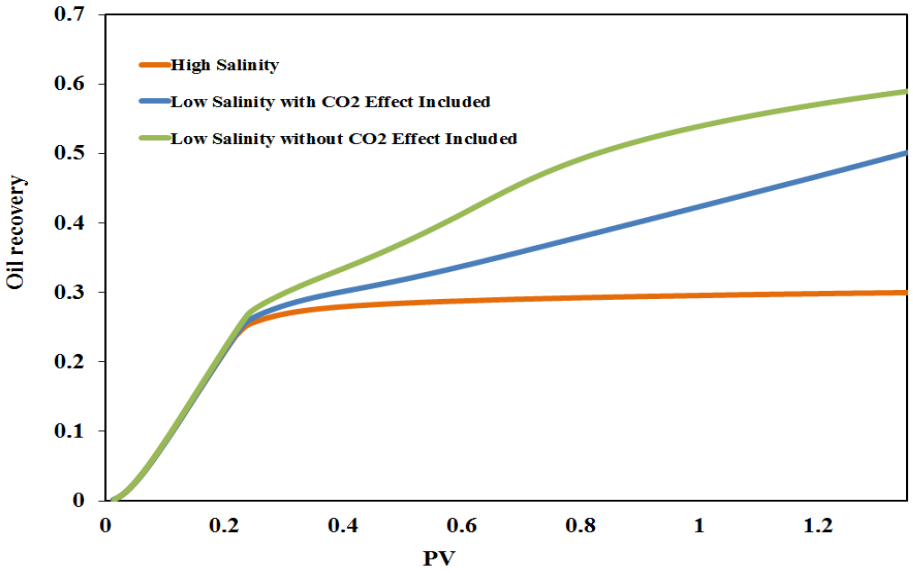

Figure 4-15: Simulated oil recovery of the quarter five-spot pattern when high salinity, low salinity with the CO_2 effect on the aqueous-rock geochemistry included, and low salinity without the CO_2 effect on the aqueous-rock geochemistry included are injected in the secondary mode of injection.

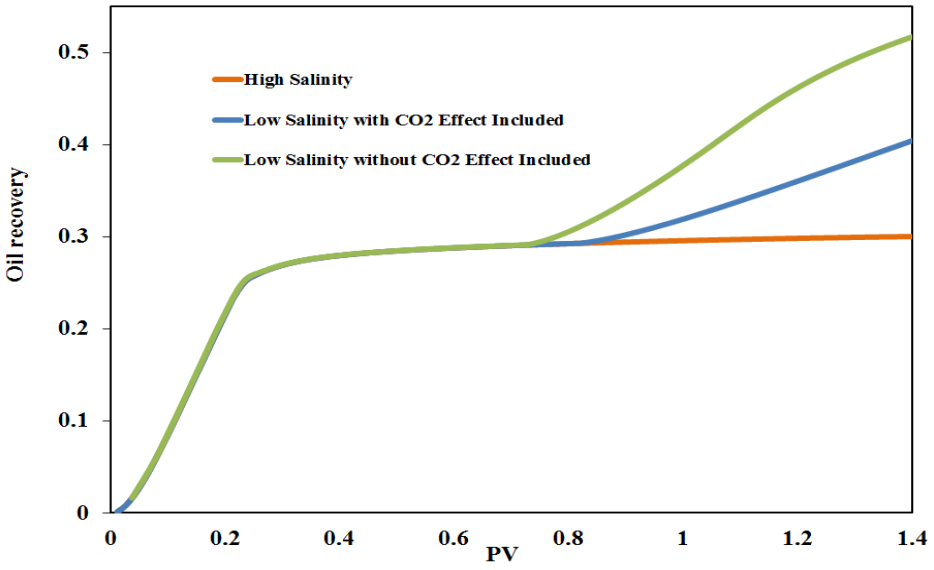

Figure 4-16: Simulated oil recovery of the quarter five-spot pattern when high salinity, low salinity with the CO_2 effect on the aqueous-rock geochemistry included, and low salinity without the CO_2 effect on the aqueous-rock geochemistry included are injected in the tertiary mode of injection.

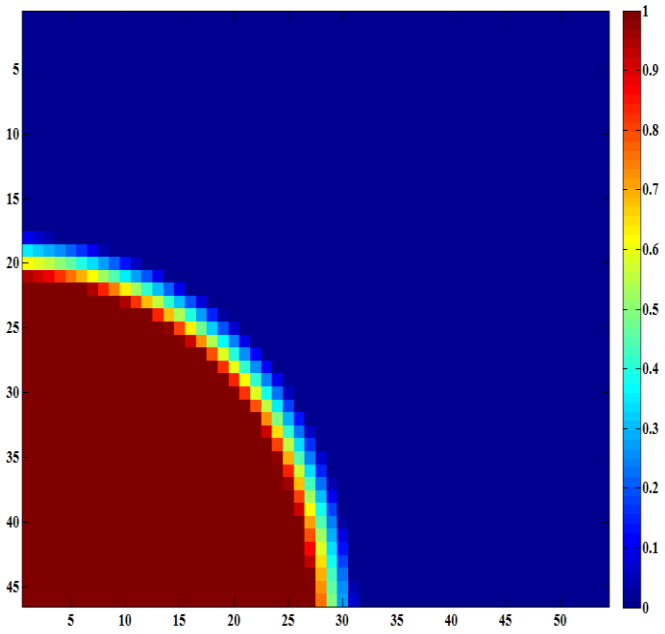

Figure 4-17: Map of the interpolating parameter (1: water-wet, 0: oil-wet) in the first layer at PV = 0.5; with the CO_2 effect on the aqueous-rock geochemistry included.

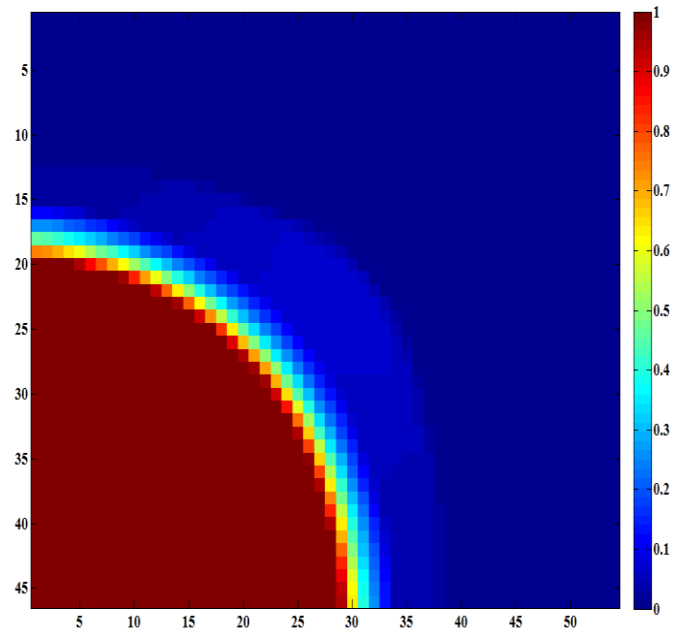

Figure 4-18: Map of the interpolating parameter (1: water-wet, 0: oil-wet) in the first layer at PV = 0.5; without the CO_2 effect on the aqueous-rock geochemistry included.

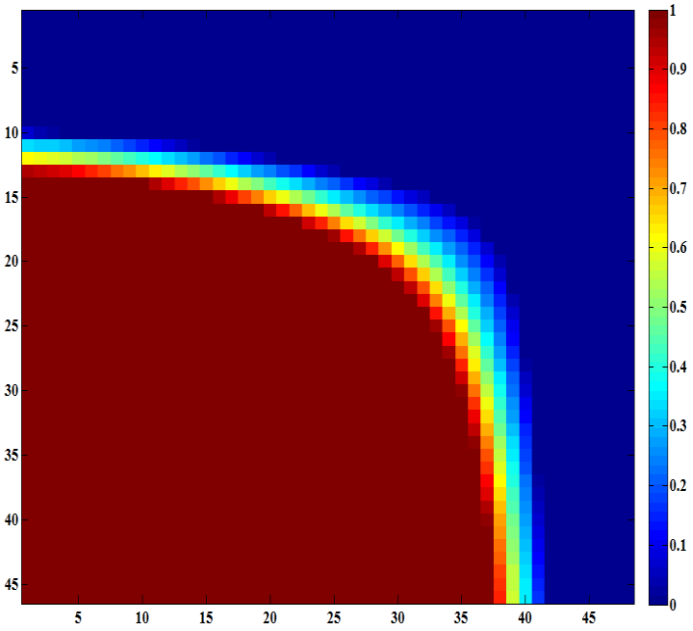

Figure 4-19: Map of the interpolating parameter (1: water-wet, 0: oil-wet) in the first layer at PV = 1.0; with the CO_2 effect on the aqueous-rock geochemistry included

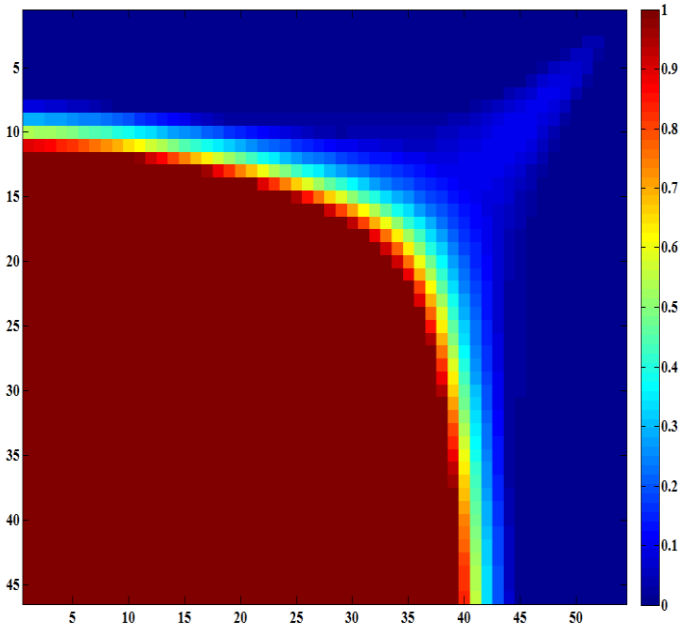

Figure 4-20: Map of the interpolating parameter (1: water-wet, 0: oil-wet) in the first layer at PV = 1.0; without the CO_2 effect on the aqueous-rock geochemistry included.

Figure 4-21 shows oil recovery if the core is saturated with the synthetic live, rather than the dead oil. Obviously green dots are still the experimental data in which the dead oil is used. Results for both cases of with and without the CO_2 effect included are shown in the figure. Results presented in this figure confirm the significant effect of CO_2 on buffering of the aqueous-rock geochemistry. However, if enough pore volumes of the modified saline water are injected, both cases (i.e., with and without the CO_2 effect included) would have the same final oil recovery.

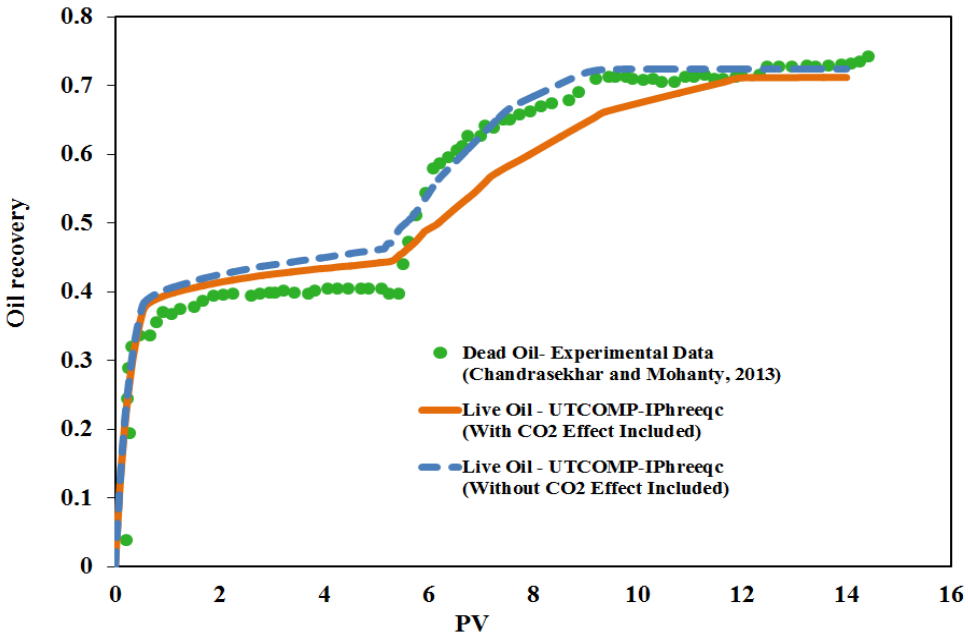

Figure 4-21: Simulated oil recoveries when core is saturated with the synthetic live-oil (with and without the CO_2 effect on the aqueous-rock geochemistry included) against the experimental data with dead oil.

Chapter 5: A Mechanistic Integrated Geochemical and Chemical Flooding Tool for Alkaline/Surfactant/Polymer Floods[1]

Mechanistic simulation of alkaline/surfactant/polymer (ASP) flooding considers chemical reactions between the alkali and the oil to form in-situ soap and reactions between the alkali and the minerals and brine. A comprehensive mechanistic modeling of such process remains a challenge, mainly due to the complicated ASP phase behavior and the complexity of geochemical reactions that occur in the reservoir. Due to the lack of the microemulsion phase and/or lack of reactions that may lead to the consumption of alkali and resulting lag in the pH, a simplified ASP phase behavior is often used.

In this chapter we couple IPhreeqc with UTCHEM for a robust, flexible, and accurate integrated tool to mechanistically model ASP floods. UTCHEM has a comprehensive three phase (water, oil, microemulsion) flash calculation package for the mixture of surfactant and soap as a function of salinity, temperature, and co-solvent concentration. IPhreeqc has rich databases of chemical species and also the flexibility to include the alkaline reactions required for modeling ASP floods. Hence, to the best of our knowledge, for the first time, the important aspects of ASP flooding are truly considered.

[1] Some parts of Chapter 5 are published in the following citation:

Korrani, A. K. N., Sepehrnoori, K., and Delshad, M. 2014b. A Mechanistic Integrated Geochemical and Chemical Flooding Tool for Alkaline/Surfactant/Polymer Floods. Society of Petroleum Engineers. doi:10.2118/169094-MS.

Below briefly describes nature of coathors'contribution.

- Kamy Sepehrnoori: The idea of coupling PHREEQC with UTCHEM for mechanistic modeling of Alkaline/Surfactant/Polymer floods, technical support, and revising the manuscript.

- Mojdeh Delshad: Technical support in applying the UTCHEM simulator for chemical floods and revising the manuscript.

In this chapter we first review the important findings published in the literature on ASP flooding. An algorithm is then presented for modeling the geochemistry in an IMPEC (implicit in pressure and explicit in concentration) solution algorithm. Finally, we show how to apply the integrated tool, UTCHEM-IPhreeqc, to match three different reaction-related chemical flooding processes: ASP flooding in an acidic active crude oil, ASP flooding in a non-acidic crude oil, and alkaline/co-solvent/polymer (ACP) flooding.

5.1 ALKALINE/SURFACTANT/POLYMER FLOODING

Surfactant/polymer (SP) flooding is an EOR process in which surfactant is added to the injected water to lower the interfacial tension (IFT) between the aqueous and oil phases, increase the capillary number and consequently mobilize the residual oil saturation beyond that of waterflood (Tavassoli *et al.*, 2014a; 2014b). Polymer is included in this EOR process for the mobility control purpose. Although the SP process is very well-established and technically successful, because of high chemical costs, it is not considered as one of the cost-efficient EOR processes (Kon *et al.*, 2002). For years, researchers have tried to come up with promising modifications to make the SP process more economical. Alkaline/polymer (AP) flood is an alternative process proposed to the SP flooding because the cost of alkali is considerably lower than that of surfactant. The essence of the AP flooding is to react alkaline agents (e.g., Na_2CO_3, NaOH, $NaBO_2$, K_2CO_3, and KOH) with acidic components in the crude oil and generate the in-situ surfactant (soap). Similar to the SP process, the role of the polymer is to increase the sweep efficiency.

Figure 5-1 presents how acidic component of the crude oil is partitioned between the aqueous and the oleic phases and how soap (A_w^-) is generated in the aqueous phase. The partitioning reaction of the acidic component is given in Eq. (5.1):

$$HA_w \rightleftharpoons HA_o. \tag{5.1}$$

where

A_w = acid component in the aqueous phase

A_o = acid component in the oleic phase

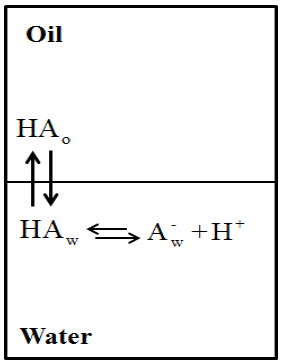

Figure 5-1: Equilibria in water/oil/naphthenic acid systems at low pH (Havre *et al.*, 2003).

This geochemical reaction is known as partitioning reaction with the equilibrium constant given in Eq. (5.2):

$$K_{wo} = \frac{[HA_w]}{[HA_o]}, \tag{5.2}$$

where

$K_{wo} =$ partition coefficient of the acid component between the aqueous and oleic phase

The partitioned acid in the aqueous phase will dissociate in the aqueous phase according to Eq. (5.3):

$$HA_w \rightleftharpoons A_w^- + H^+. \tag{5.3}$$

With the reaction constant following the equilibrium relationship:

$$K_a = \frac{\left[H^+\right]\left[A_w^-\right]}{\left[HA_w\right]}, \tag{5.4}$$

where

$K_a =$ equilibrium constant for the dissociation reaction of the acid component in the aqueous phase.

Alkaline agents are injected into the reservoir to raise the pH and generate soap when crude oil has high acid number and to lower the surfactant adsorption among other benefits. Le Chatelier's principle for geochemical reactions proposes that when a system at equilibrium experiences a change (e.g., in concentration, partial pressure, and temperature), the equilibrium shifts to counteract the imposed change and establish a new equilibrium (Le Chatelier, 1884; Monk, 2008). Hence, based on the Le Chatelier's principle, more soap (A_w^-) is generated if the H^+ concentration of the system is decreased (see Eq. (5.3)).

The H^+ concentration can be diminished through injecting the alkaline agents. For example, injecting Na_2CO_3 increases the CO_3^{-2} concentration of the aqueous phase which

shifts the carbonic acid reaction (Eq. (5.5)) to the left (based on the Le Chatelier's principle); hence, H^+ concentration of the system decreases and consequently, more soap is generated. The same principle is applied for other alkaline agents such as NaOH and $NaBO_2$.

$$H_2CO_3 \rightleftharpoons 2H^+ + CO_3^{-2} \tag{5.5}$$

In the AP process, in one hand, the generated soap (A_w^-) has very low optimum salinity and narrow salinity window (Nelson *et al.*, 1984; Mohammadi, 2008); hence, the brine salinity should be low enough to achieve the ultra-low IFT. On the other hand, sufficiently high amount of alkaline agents should be injected to compensate the alkali consumption by the acidic component; divalent ions in the aqueous; and ion-exchange. Injecting large amount of alkaline agents increases the salinity of the brine (Peru and Lorenz, 1990; Mohammadi, 2008; Fortenberry *et al.*, 2013). The dilemma involved in the AP process makes the process impractical most of the times. It seems that the AP flooding can be applied only in reservoirs with low salinity brine. Nelson *et al.* (1984) solved the AP flooding dilemma by adding small concentration of co-surfactant in the chemical slug. Co-surfactant favorably increases the optimum salinity to alkali concentration high enough for deep propagation into the reservoir (Nelson *et al.*, 1984; Kon *et al.*, 2002; Sheng, 2013). Including the alkaline agents in the SP process makes the process cost-efficient not only through generating the soap but also the injected alkali can significantly decrease the surfactant (Song *et al.*, 1995; Al-Hashim *et al.*, 1996; Wang and Gu, 2003; Hirasaki *et al.*, 2004; Liu *et al.*, 2008; Liu, 2007; Mohan, 2009; Sheng, 2013) and polymer (Song *et al.*, 1995) adsorptions on the rock, alter the wettability of the

rock (Kon *et al.*, 2002; Wang and Gu, 2003; Liu, 2007; Sundstrom, 2011; Sheng, 2013; Fortenberry *et al.*, 2013), and accelerate the equilibrium time, shortening the coalesce time (Jackson, 2006). Several researchers have reported successful laboratory and field pilot studies of the ASP flooding. Some of these reports are discussed:

Gao *et al.* (1995) conducted a coreflood using Daqing reservoir core. They reported incremental oil recovery of 20% and 33% original oil in place (OOIP) after injecting 0.2 and 0.3 PV of ASP into the core, respectively. Mohammadi (2008) documented several ASP corefloods conducted at The University of Texas at Austin. Injecting ASP shows promising results in all the corefloods reported in her dissertation (with more than 90% recovery of the residual oil in most cases). We model and present the simulation results of one of the coreflood reported by Mohammadi (2008). Song *et al.* (1995) applied ASP flooding on a pilot area (containing 4 inverted five-spot patterns) in the waterflooded Gudong oil field with the oil viscosity and the acid number of 41.25 cp and 3.11 mg of KOH/g of oil, respectively. ASP successfully reduced the watercut from 98% to 74.2% with the cumulative oil production of 20,667.7 t (tonnes) from the pilot (Song *et al.*, 1995). The feasibility of implementing ASP on the Saudi Arabian carbonate reservoirs was studied in the work of Al-Hashim *et al.* (1996). Crude oil in this field has the acid number of 0.3 mg of KOH/g of oil and the viscosity of 0.7 at 90 ^{o}C. Na_2CO_3 and $NaHCO_3$, the alkaline agents used in this work, showed very promising results in decreasing the surfactant adsorption. Their results showed that ASP could significantly improve the oil recovery even in carbonate reservoirs with harsh reservoir condition. Results presented for one of their coreflood showed 18.2% of OOIP additional oil recovery after injecting 0.6 PV of ASP chased with 5.66 PV of water in the Arab-D sample core. Demin *et al.* (1997) reported the results of the implementation of two ASP

pilot tests (i.e., PO and XF pilots) in Daqing oil field (with the acid number of 0.1 KOH mg/g of oil). Early response was observed when injecting only 0.07 PV and 0.05 PV of ASP solution in the PO and XF pilots, respectively. Due to the ASP injection, average watercut of the PO pilot reduced from 88.4% to 68.8% with the 20.8% OOIP incremental oil recovery over the waterflood. Their estimation for the XF pilot gave 25% OOIP incremental oil recovery over the waterflood. Due to the promising results observed for the PO and XF pilot tests, the ASP flooding was further expanded to a larger scale in Daqing oil field (Yang *et al.*, 2003). Field results were also in line with the pilot tests where the maximum reduction in the watercut was about 40% (Yang *et al.*, 2003). Demin *et al*. (1998) applied the ASP flooding in four inverted five-spot patterns with 4 injectors and 9 producers. The reduction in watercut started after 0.09 PV ASP injected. By 1998, the additional oil recovery for the pilot was 12.8% OOIP and the ultimate oil recovery was estimated to be about 16 to 17% OOIP. ASP flooding in Cambridge Minnelusa field (located in Wyoming, USA) gave 1.143 MM bbls incremental oil recovery (Vargo *et al.*, 2000). The implemented design on this pilot was 0.307 PV of the ASP solution that was followed by 0.297 PV of the polymer slug. Qi *et al.* (2000) documented the ASP flooding in the Karamay oil field in China. ASP flooding in this pilot started in 1995 and lasted for three years. Prior to the ASP injection, NaCl brine was injected for about a year. Incremental oil recovery due to the ASP injection is 23.15% OOIP with the watercut of 92.5%. The pilot test in Qi *et al.* (2000) contained 9 production and 4 injection wells in an inverted five-spot pattern. Xu (2012) simulated two corefloods performed at The University of Texas at Austin by Pope *et al.* using ACP flooding (Weerasooriya and Pope, 2011; Fortenberry, 2013; Fortenberry *et al.*, 2013; Taghavifar, 2014). As the result of the ACP injection, residual oil saturation reduced from about 45% to 14% in one core

(labeled “PCN-1”) and from about 36% to nearly 0% in the another one (labeled “PCN-4”). PCN-1 is modeled and discussed in this chapter.

Optimization, interpretation, and design of EOR processes require a predictive model. A predictive model is needed to fully understand the underlying mechanisms driving the EOR processes. Mechanistic modeling of the ASP flooding is highly challenging mainly due to the complicated ASP phase behavior and complexity of the geochemical reactions that occur in the reservoir. UTCHEM, an in-house research chemical flooding reservoir simulator has a comprehensive three-phase (water, oil, microemulsion) phase behavior model for the mixture of surfactant and soap as a function of salinity, temperature, and co-solvent concentration (Bhuyan, 1989; Mohammadi, 2008). Geochemical module (hereafter, EQBATCH) of UTCHEM was developed by Bhuyan (1989) and later generalized (UTCHEM Technical Documentation, 2000). EQBATCH takes into account not all but essential geochemical reactions relevant to ASP flooding such as soap generation, alkali precipitation with aqueous divalents, and alkaline consumption in ion exchange reactions. Assumptions and limitations of EQBATCH were previously discussed in Chapter 2. IPhreeqc (Charlton and Parkhurst, 2011) overcomes all the simplifying assumptions and limitations inherent in EQBATCH. Hence, we coupled IPhreeqc with UTCHEM to build a comprehensive simulator for mechanistic modeling of ASP floods. Sections below present the procedure through which we coupled IPhreeqc with UTCHEM.

5.2 COUPLING IPHREEQC WITH UTCHEM FOR MECHANISTIC MODELING OF ASP

Figure 5-2 gives UTCHEM flowchart where we start the simulation at time t after the initialization step is completed. We solve pressure equation implicitly first and then solve component concentrations explicitly. The overall concentrations (defined per unit

gridblock pore volume) for the volume occupying components (oil, water, co-solvent, surfactant, and gas) are then used to find phase saturations at each gridblock using Hand's rule. The phase saturations are used to calculate the relative permeability and capillary pressure. For non-isothermal cases, the energy balance equation is solved to compute the gridblock temperature (see Lashgari *et al.*, 2014a; 2014b for details on thermal flooding using UTCHEM). Finally, reservoir rock and fluid properties are updated for the new component concentrations and temperature. For example, if polymer is considered, water viscosity is calculated as a function of polymer concentration, effective salinity (which is function of total salinity and divalent concentrations), and shear rate (see Li and Delshad (2013) and UTCHEM Technical Documentation (2000) for details on the UTCHEM polymer models). The same algorithm will be followed for the next time-step until the end of the simulation (UTCHEM Technical Documentation, 2000; Korrani *et al.*, 2013).

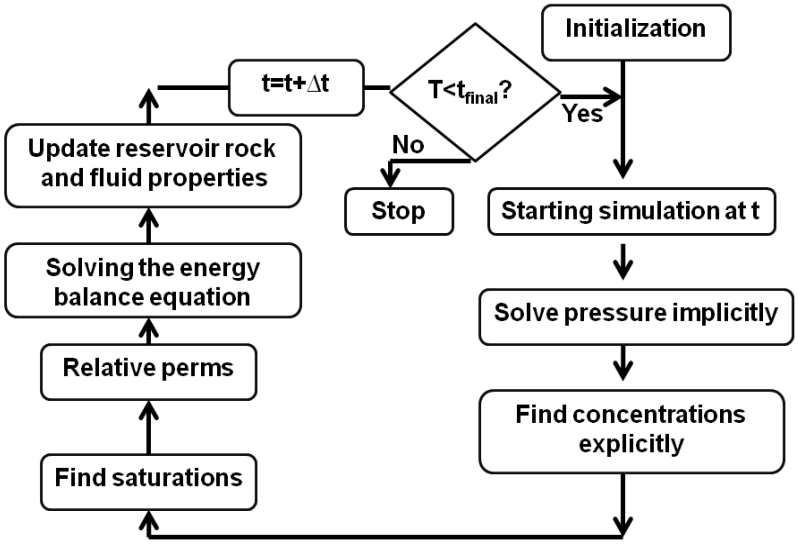

Figure 5-2: Simplified UTCHEM calculation flowchart (Korrani *et al.*, 2013).

To integrate IPhreeqc with UTCHEM, the UTCHEM computing algorithm is modified based on the work of Charlton and Parkhurst (2011) as follows:

- Once the aqueous geochemical species in UTCHEM are calculated (the mass conservation equation was previously implemented and verified for the geochemical elements in UTCHEM by Bhuyan (1989), the IPhreeqc input is accumulated in the computer memory using *AccumulateLine* method available in IPhreeqc;
- IPhreeqc is run using *RunAccumulated* method to calculate the new equilibrium state for all batch cells;
- Use *GetSelectedOutputValue* method to transfer the results from IPhreeqc to UTCHEM. The latter includes concentrations for the ions in the aqueous phase, moles for solid phases, and concentrations of ions on ion-exchangers, if there is any. We discussed the IPhreeqc methods with more details in Chapter 2. Figure 5-3 highlights the modified solution algorithm.

Similar to UTCOMP-IPhreeqc, element concentrations in the aqueous phase, moles for solid phases, and moles for exchangers of each simulation gridblock are defined in the first time-step through using **SOLUTION**, **EQUILIBRIUM_PHASES**, and **EXCHANGE** keywords, respectively. For the next time steps, IPhreeqc uses **SOLUTION_MODIFY**, **EQUILIBRIUM_PHASES_MODIFY** (if it is required), and **EXCHANGE_MODIFY** (if it is required) rather than the corresponding keywords of **SOLUTION**, **EQUILIBRIUM_PHASES**, and **EXCHANGE**, respectively, In addition, we must transport charge balance (**CHARGE_BALANCE** of IPhreeqc returns this for each gridblock), total moles of hydrogen (**TOTMOLE("H")** is used), and oxygen (**TOTMOLE("O")** is used) along with the elements present in the system.

Similar to PHAST (Parkhurst *et al.*, 2010) transport and the chemical-reaction calculation are separate in the UTCOMP-IPhreeqc and UTCHEM-IPhreeqc simulators. There is no iteration between the transport and reaction calculation during a time step. If kinetic reactions are included in the model, IPhreeqc applies the operator splitting and separates the chemical equilibrium reactions from the kinetic reactions. In this case, Newton-Raphson method is first applied to solve the nonlinear chemical equilibrium equations. An Explicit Runge-Kutta method or CVODE algorithm (Cohen and Hindmarsh, 1996), for stiff differential equations, are then followed to solve the ordinary differential equations of the kinetic-reaction equations. Using Runge-Kutta or CVODE algorithms, IPhreeqc evaluates the reaction rates at several intermediate times within the overall time interval equal to the transport time step (i.e., the time step in UTCHEM). To control the errors, IPhreeqc applies an automatic time stepping algorithm when integrating the kinetic reaction rates (Parkhurst *et al*., 2010). It is worth noting that the transport time-step size (i.e., time-step in UTCHEM) is selected based on relative changes for all the components (UTCHEM User's Guide, 2011).

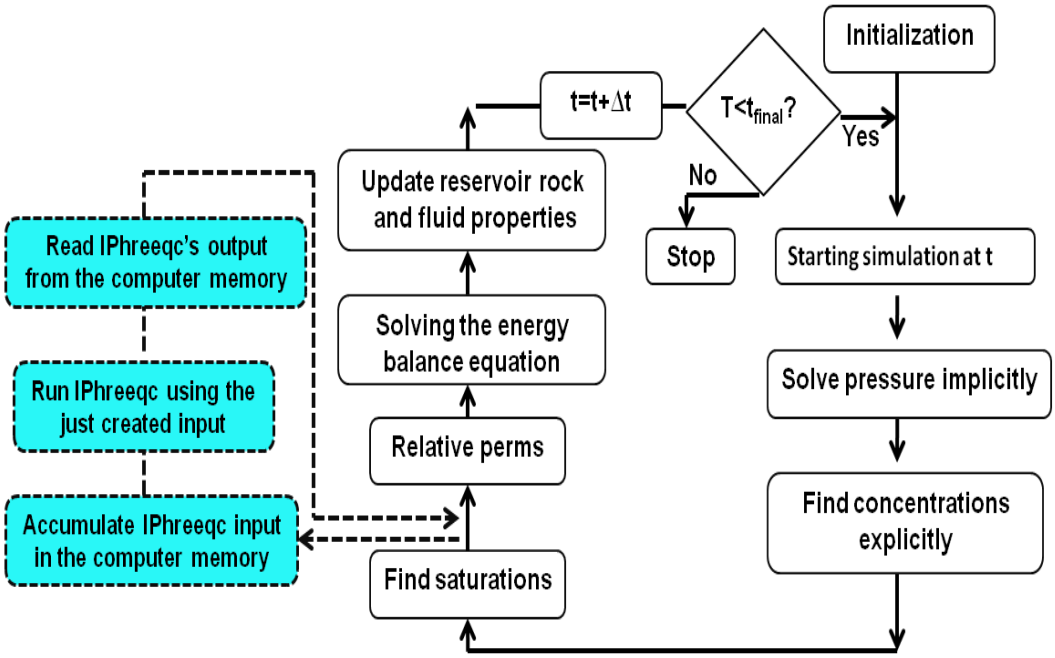

Figure 5-3: Simplified UTCHEM flowchart after coupling with IPhreeqc (Korrani *et al.*, 2013).

Including the exchange of the acidic component among the aqueous, microemulsion, and oil phases is the most important development that needs to be implemented in UTCHEM-IPhreeqc for mechanistic modeling of ASP. At the equilibrium state, the acid element (A) is partitioned into three fluid species as HA_w, HA_o, and A_w^- (soap). These fluid species are respectively carried along with the water, oil, and surfactant components. Concentrations of HA_w, HA_o, and A_w^- are related to each other through the aqueous-oleic partitioning and acid dissociation reactions. Hence, these two reactions (i.e., Eqs. (5.1) and (5.3)) must be properly included in the IPhreeqc database when modeling an ASP process using UTCHEM-IPhreeqc.

SOLUTION_MASTER_SPECIES and **SOLUTION_SPECIES** of IPhreeqc are used to define new components as representative of the acid component in the aqueous

and oleic phases (the total moles of the acid element (A) is the sum of moles in the aqueous (A_w) and oleic phases (A_o)). Because aqueous reactions in the IPhreeqc database are defined in the association rather than dissociation form (Parkhurst and Appelo, 2013), association form of Eq. (5.3) is simply included in the IPhreeqc database.

By default, all reactions defined in IPhreeqc must be balanced in both charge and elemental. However, the identifier "**-NO_CHECK**" can be used to disable checking the elemental balance. The aqueous-oleic partitioning reaction (Eq. (5.1)) is not completely balanced in the elements. While equivalent for the hydrogen element is the same in both sides; this reaction is not balanced in terms of the acid element (A_w in the left side while A_o in the right side). Hence, we must use the "**-NO_CHECK**" identifier to be able to include this reaction in the IPhreeqc thermodynamic database.

The following shows how the acidic/oleic reaction as well as the acid dissociation reactions can be defined in the IPhreeqc database. In this example, the partitioning constant and the equilibrium constant for the acid dissociation reaction are assumed to be $10^{-3.6}$ and 10^{-8}, respectively. The value of 59.05 is the molecular weight of the acid component. IPhreeqc uses molecular weights of the elements only if the concentration units are mass unit (Parkhurst and Appelo, 1999; 2013).

```
SOLUTION_MASTER_SPECIES
    Aw     Aw-      1.0    59.05     59.05
    Ao     Ao-      1.0    59.05     59.05
SOLUTION_SPECIES
    Aw- = Aw-;      log_k 0
    Ao- = Ao-;      log_k 0
Aw- + H+ = HAw;   log_k   +8.0
HAw = HAo;    log_k      +3.6;   -no_check; -mole_balance   Aw
```

These reactions are considered along with other aqueous geochemical reactions in modeling an ASP process in UTCHEM-IPhreeqc. Acid concentration in the oleic phase (HA_o) is defined as an independent aqueous species when Newton-Raphson is applied to find the equilibrium state (Bhuyan, 1989). That is why the equilibrium constant of both the partitioning and the acid dissociation reactions are function of relative volumes of water and oil (Bhuyan, 1989; Mohammadi, 2008). However, in UTCHEM-IPhreeqc only the constant partition coefficient needs to be defined as a function of volumes of water and oil. Hence, at each simulation time-step, the partition coefficient is updated and stored in the computer memory through *AccumulateLine* of IPhreeqc.

In general water saturation might be different in reservoir gridblocks. Hence, the equilibrium constant of the partitioning reaction (which is a function of water saturation of gridblocks) is different for each gridblock. On the other hand, if the same geochemical reaction with different equilibrium constants is stored in the computer memory, IPhreeqc considers the last equilibrium constant for geochemical calculations. To this end, if we accumulate the geochemistry data of the entire gridblocks in the computer memory all at once, the equilibrium constant of the partitioning reaction evaluated based on the water saturation of the last gridblock is applied to find the equilibrium state of all gridblocks. To avoid this inconsistency, we evaluate the new equilibrium state of gridblocks one by one rather than all together. In other words, when using UTCHEM-IPhreeqc for ASP floods, the modified geochemistry data of a single gridblock is accumulated in the computer memory using *AccumulateLine*. The stored data is then run using *RunAccumulated*. Finally, *GetSelectedOutputValue* is used to transfer the new equilibrium state of that gridblock to UTCHEM. The same procedure is followed for

other gridblocks. Finding the equilibrium state of gridblocks individually, rather than all together, slows down the simulation to some extent.

As mentioned above, in using IPhreeqc, charge balance and total moles of hydrogen and oxygen must be transported along with other geochemical elements present in the system (Charlton and Parkhurst, 2011; Korrani *et al.*, 2013; Korrani *et al.*, 2014c). For ASP simulations, care must be taken to partition the charge balance and the total moles of hydrogen and oxygen among different phases. At the equilibrium state, the total acid element (A) is partitioned into three fluid species as HA_w, HA_o, and A_w^-. A_w^- is the generated soap and will be used along with the injected synthetic surfactant for the phase behavior calculations. Phase behavior of the in-situ generated surfactant (soap) can be defined either the same as or different from that of the injected synthetic surfactant. If the phase behavior of the soap is different from the injected surfactant, nonlinear mixing rule is applied to find the combined surfactant and soap phase behavior (Delshad *et al.*, 2013).

Because hydrogen (H) and acid (A) elements are involved in HA_w, HA_o, and A_w^- fluid species, hydrogen (H) and acid (A) elements must be transported differently than other geochemical elements present in the system. Geochemical elements other than "H" and "A" are carried by the water component; depending on how water component is partitioned between aqueous and microemulsion phases corresponding to different Winsor types, these geochemical elements are partitioned correspondingly. However, the hydrogen element is not carried only by the water component but also by the oil component (hydrogen element in the HA_w and HA_o fluid species are carried along with water and oil components, respectively). Hence, some amount of hydrogen is partitioned among the phases corresponding to the water component (i.e., hydrogen element in the HA_w fluid species) and the rest is shared between the phases corresponding to the oil

component (i.e., hydrogen element in the HA_o fluid species). The same concept applies for the acid element (A) and the charge balance. Because the acid component is carried along with water, oil, and surfactant components, HA_w, HA_o, and A_w^- are respectively shared among the phases containing water, oil, and surfactant components. Finally, because A_w^- fluid species carries charge, charge balance is carried along with the water and surfactant components. The amount of charge balance that is transported along with the surfactant component is A_w^- and that for the water component is the total charge balance minus the amount that is transported by the surfactant component (i.e., A_w^-). Table 5-1 summarizes the amount of each geochemical species (i.e., hydrogen, acid component, charge balance, and other geochemical species including oxygen) carried along with the volume-occupying components (i.e., water, oil, and surfactant) in UTCHEM-IPhreeqc.

Table 5-1: How the geochemical species are partitioned among the phases and transported in UTCHEM-IPhreeqc

Geochemical Element	Amount of the geochemical element carried along with the volume-occupying components to be partitioned among the phases		
	Water	Surfactant	Oil
Hydrogen (H)	Total hydrogen of the system minus the amount of hydrogen in HA_o	-	HA_o
Acid component (A)	Total acid component of the system minus the amount of the acid component in A_w^- and HA_o	A_w^-	HA_o
Charge balance	Lumped charge balance of the aqueous solution minus the amount charge in A_w^-	A_w^-	-
Other geochemical species including oxygen (O)	Entirely by the water component	-	-

Similar to UTCOMP-IPhreeqc, we also parallelized the geochemistry module of UTCHEM-IPhreeqc (hereafter, the parallel version of UTCHEM-IPhreeqc). Restart option is also available in both single- and multiple-processor version of UTCHEM-IPhreeqc.

5.3 VERIFYING UTCHEM-IPHREEQC AGAINST PHREEQC

We verified our integrated tool, UTCHEM-IPhreeqc against PHREEQC's single phase and one-dimensional reactive-transport case studies. UTCHEM-IPhreeqc is verified for the example problem 11 from Parkhurst and Appelo (2013). The case description was previously discussed in Section 2.7.2. Figures 5-4 and 5-5 verify the UTCHEM-IPhreeqc results against PHREEQC for two different dimensionless Peclet numbers of infinity (or dispersion-free case) and 40, respectively.

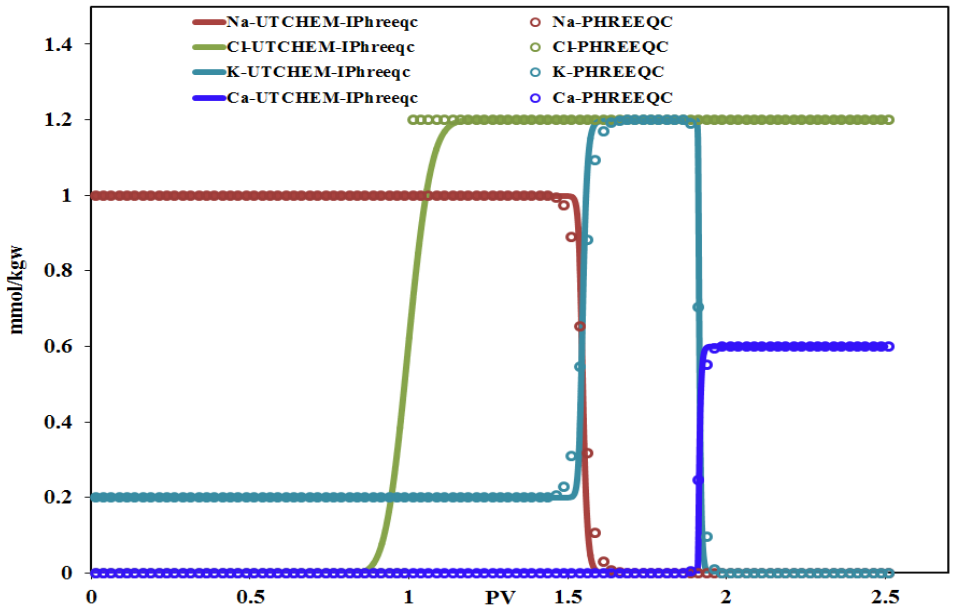

Figure 5-4: UTCHEM-IPhreeqc verification for example problem 11 of PHREEQC (Parkhurst and Appelo, 2013) at $P_e=\infty$.

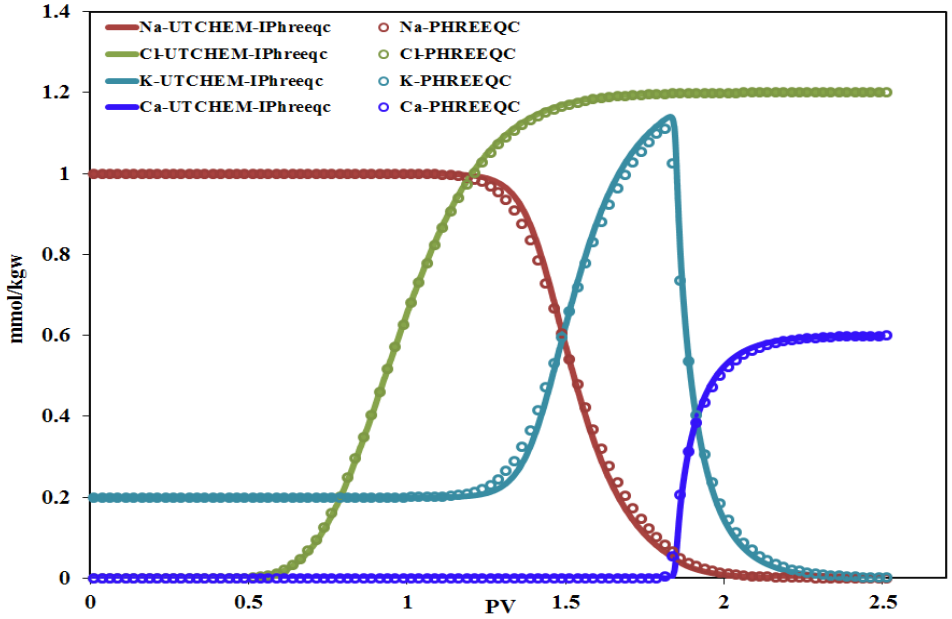

Figure 5-5: UTCHEM-IPhreeqc verification for example problem 11 of PHREEQC (Parkhurst and Appelo, 2013) at P_e=40.

We verify UTCHEM-IPhreeqc against PHREEQC for another realistic case. The characteristics for this case are similar to the case previously used in Section 2.8. A 1D single phase model with 100 gridblocks is used in both UTCHEM-IPhreeqc and PHREEQC. Aragonite, calcite, celestite, dolomite, halite, strontianite, sylvite, and witherite are the minerals that are considered. Except calcite and dolomite with initial concentration of 0.1 moles/kg of water, initial concentrations for other minerals are zero. It is also assumed that a cation-exchanger with cation exchange capacitance (CEC) of 0.01 moles/kg of water is at equilibrium with the initial solution. Injection rate is 0.0023 ft^3/day and the producing well is operating with the constant bottomhole pressure of 4000.0 psi. Produced water from the South American formation water is assumed to be initially present. Waters with different ion compositions are injected into the case: 0.5 pore volume of IW1 (injection water), 0.5 PW1 (produced water), 0.5 SW1 (fresh water),

and finally 1.5 PV of PW1 (produced water). Water compositions for IW1, PW1, and SW1 are shown in Table 2-23. The phreeqc.dat database of IPhreeqc is applied in this simulation and around 150 geochemical reactions are activated during this process. The dimensionless Peclet number is 50.0 in this case. Figures 5-6 through 5-13 present the verification results between the parallel version of UTCHEM-IPhreeqc (using different number processor) and PHREEQC for Na^{+}, Ca^{+2}, Cl^{-}, HCO_3^{-}, Mg^{+2}, and Sr^{+2}, as well as the pH histories of the aqueous solution produced from the 100^{th} gridblock.

Table 5-2 shows the computational time of the total simulation versus different number of processors applied in the simulation (plot is provided in Figure 5-14). Figure 5-15 presents the plot of speedup.

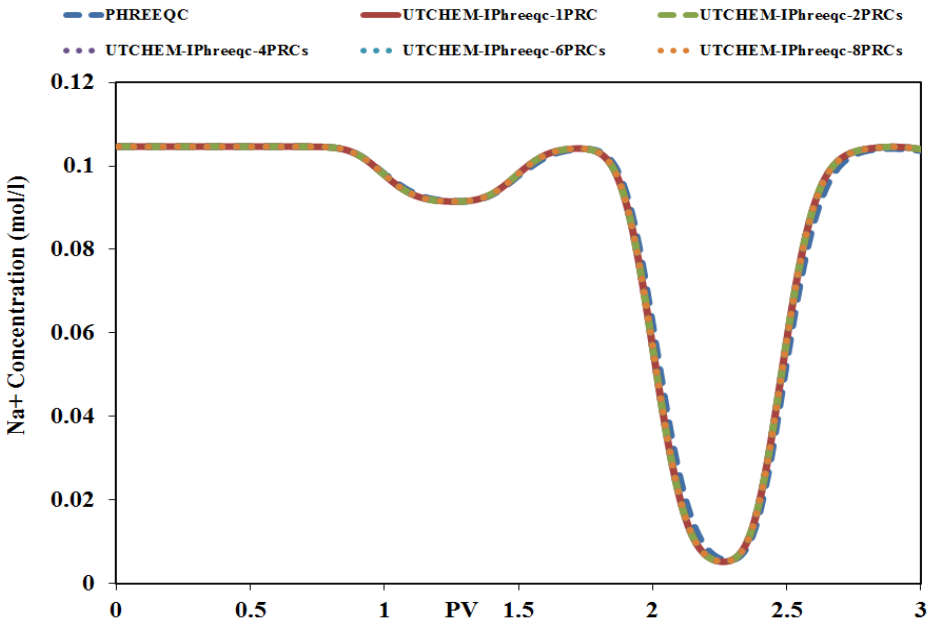

Figure 5-6: History of effluent Na^{+} concentration (the parallel version of UTCHEM-IPhreeqc verification against PHREEQC).

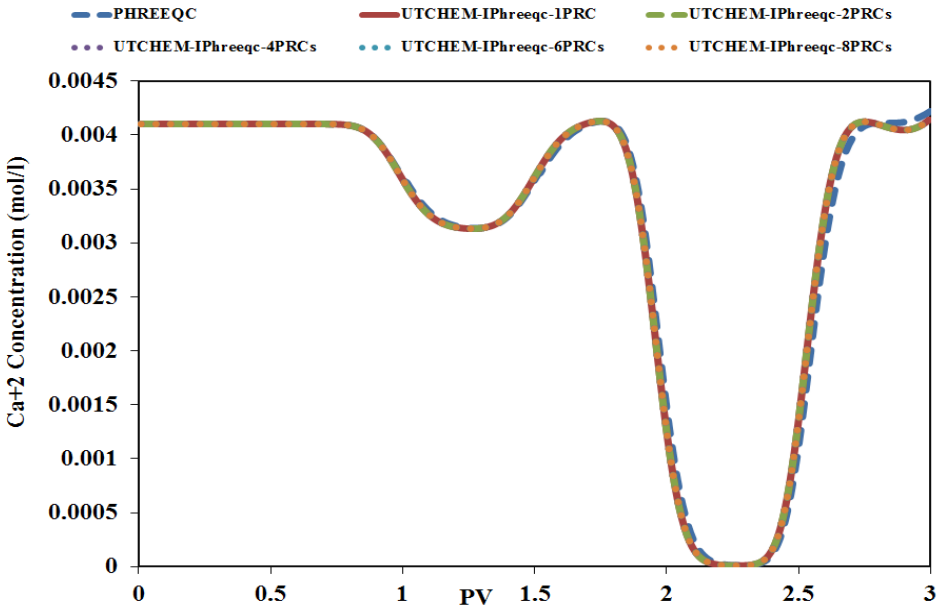

Figure 5-7: History of effluent Ca^{+2} concentration (the parallel version of UTCHEM-IPhreeqc verification against PHREEQC).

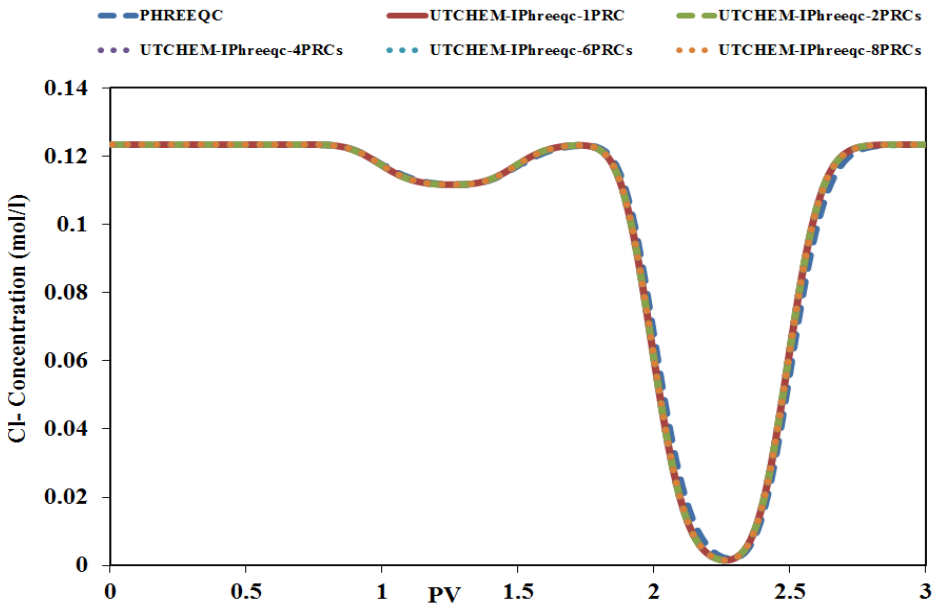

Figure 5-8: History of effluent Cl^{-} concentration (the parallel version of UTCHEM-IPhreeqc verification against PHREEQC).

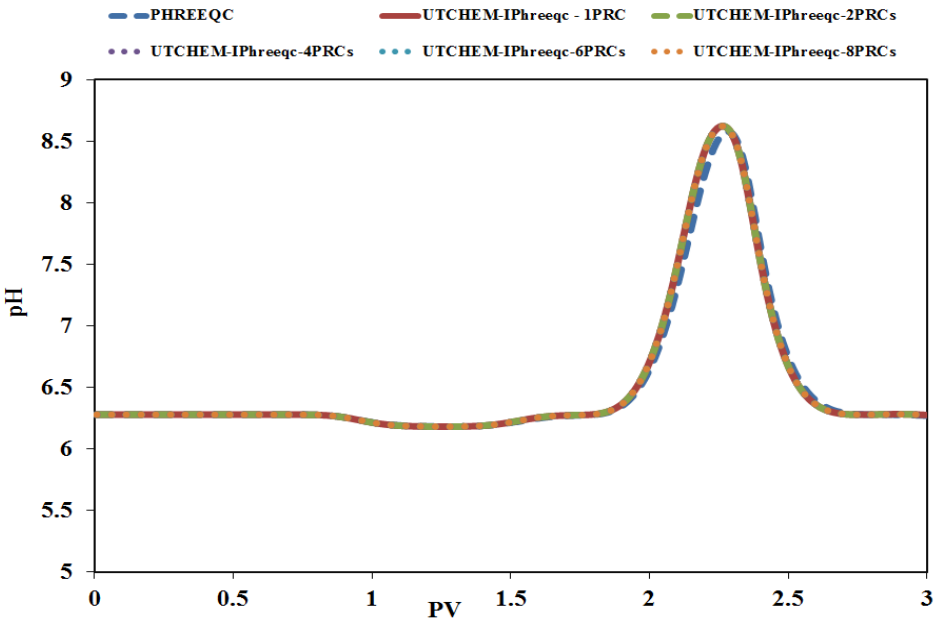

Figure 5-9: History of effluent pH (the parallel version of UTCHEM-IPhreeqc verification against PHREEQC).

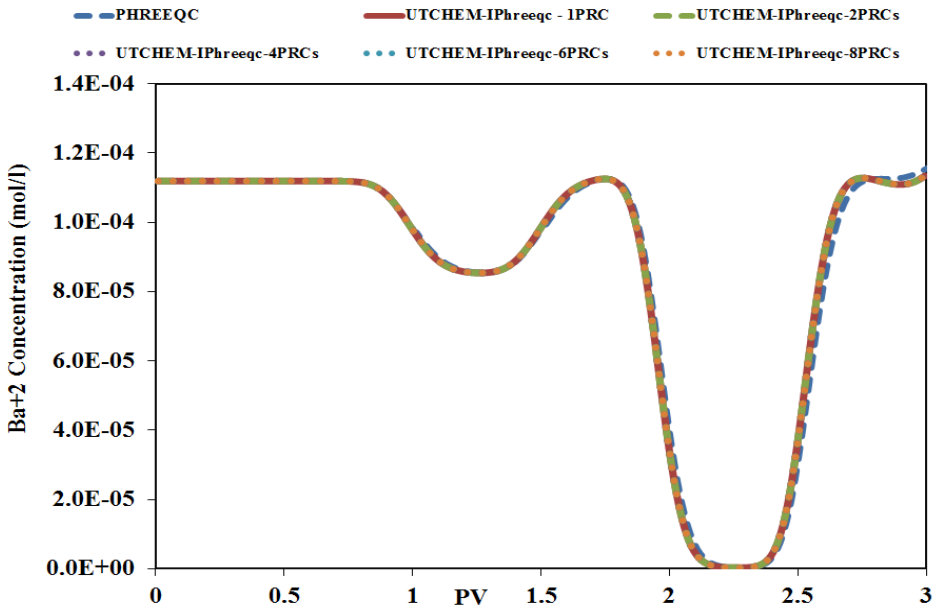

Figure 5-10: History of effluent Ba^{+2} concentration (the parallel version of UTCHEM-IPhreeqc verification against PHREEQC).

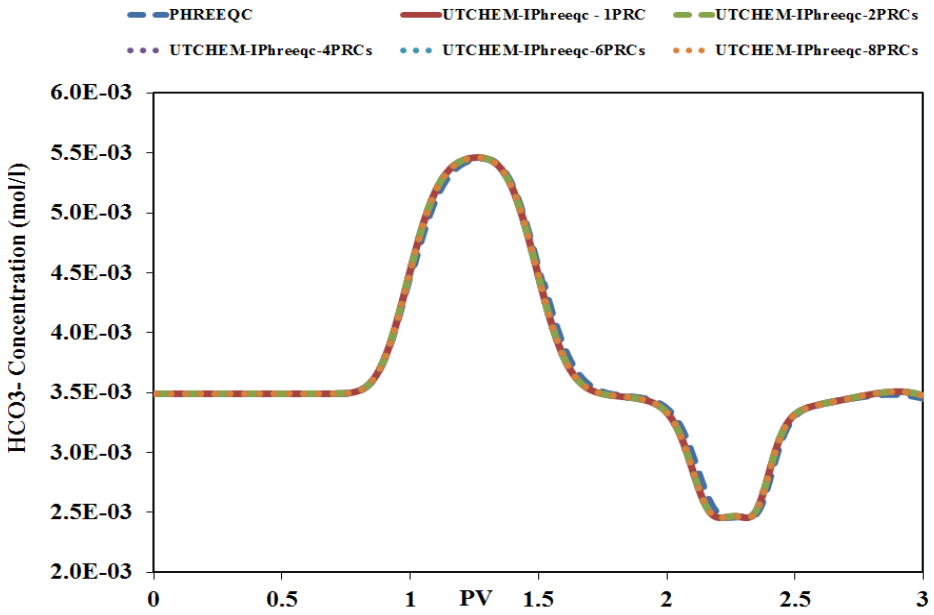

Figure 5-11: History of effluent HCO_3^- concentration (the parallel version of UTCHEM-IPhreeqc verification against PHREEQC).

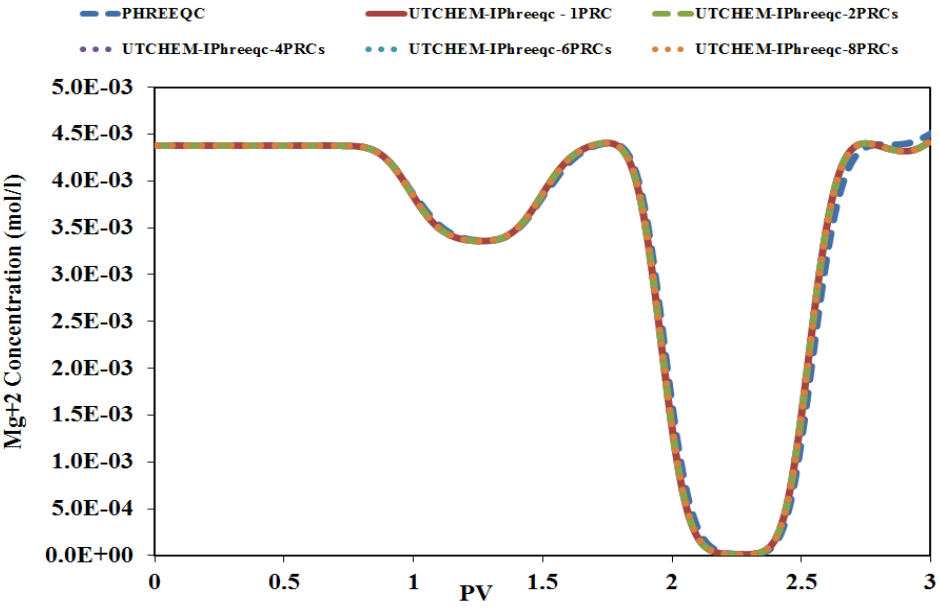

Figure 5-12: History of effluent Mg^{+2} concentration (the parallel version of UTCHEM-IPhreeqc verification against PHREEQC).

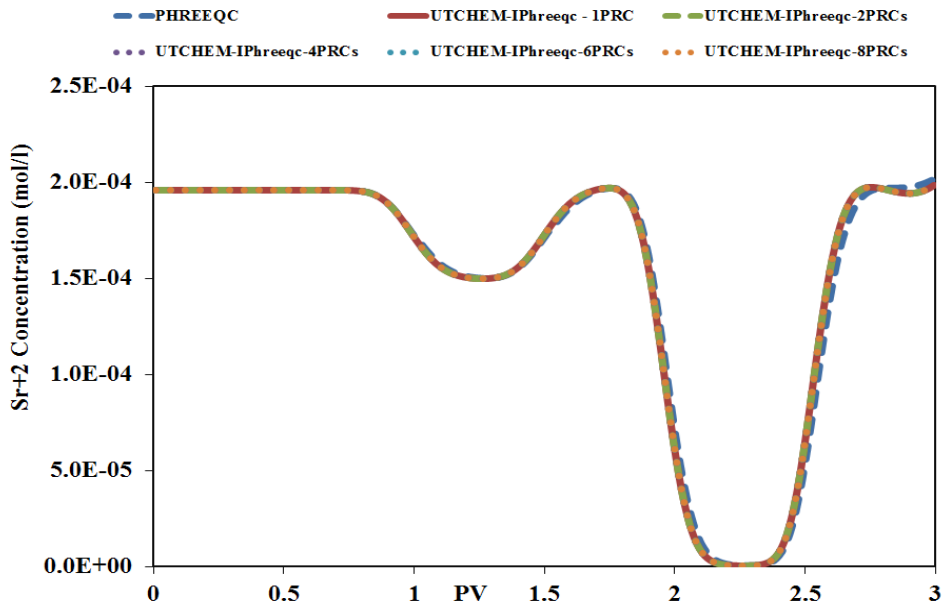

Figure 5-13: History of effluent Sr^{+2} concentration (the parallel version of UTCHEM-IPhreeqc verification against PHREEQC).

Table 5-2: total computational time

No. of processor(s) in UTCHEM-IPhreeqc	Total computational time (seconds)
1PRC	297.9
2PRCs	166.82
4PRCs	81.05
6PRCs	58.57
8PRCs	45.77
10PRCs	36.80
12PRCs	34.82

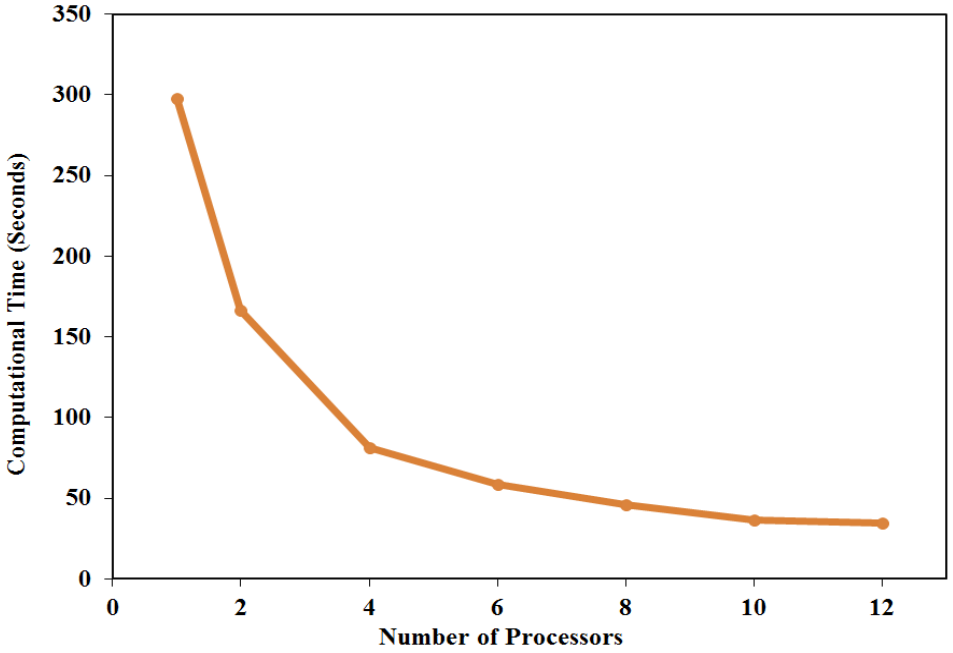

Figure 5-14: Total computational time versus number of processors.

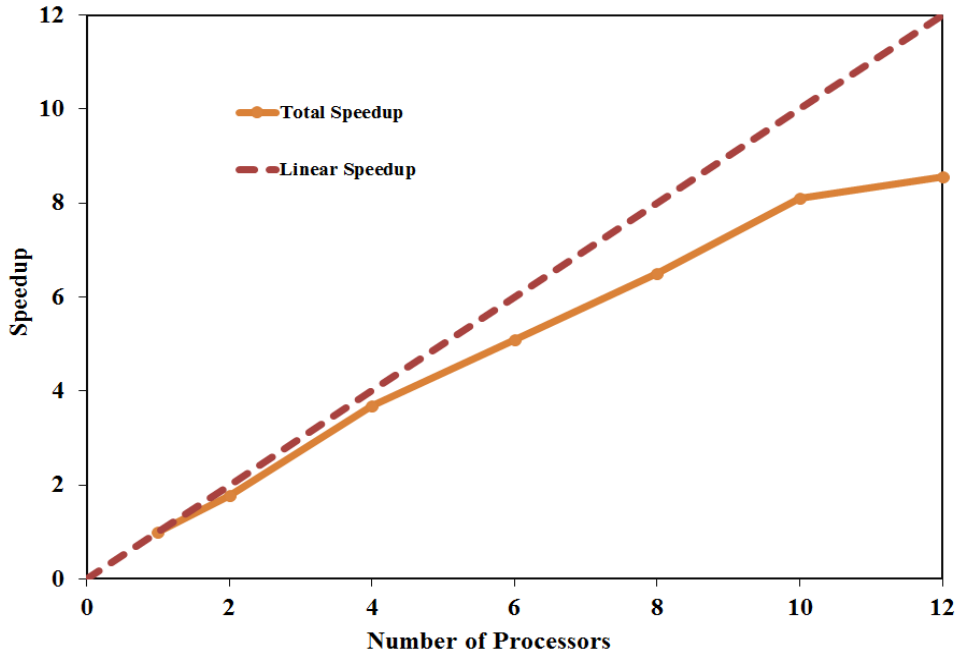

Figure 5-15: Speedup curve for the total simulation versus number of processors.

5.4 UTCHEM-IPHREEQC VERSUS UTCHEM-EQBATCH

EQBATCH lacks several capabilities that are included (e.g., considering super- and under-saturation reactions for the minerals; kinetic; surface complexation; and irreversible reactions). None of these capabilities can be used when verifying UTCHEM-IPhreeqc against UTCHEM-EQBATCH (refers to the original UTCHEM where EQBATCH is used for the geochemical calculations). However, EQBATCH solves aqueous, solid (with zero for the saturation index), and the exchange reactions. Due to specific assumptions in EQBATCH, it is not straightforward to verify UTCHEM-IPhreeqc against UTCHEM-EQBATCH. While IPhreeqc uses activities in finding the equilibrium state, molalities are used for both aqueous and exchange species in EQBATCH. Davies (Davies, 1962; Parkhurst and Appelo, 1999; 2013) and the extended or WATEQ Debye-Huckel (Truesdell and Jones, 1974; Parkhurst and Appelo, 1999; 2013) that is the extended form of Debye-Huckel model (Debye and Huckel, 1954) are the models (see Appendix A) through which IPhreeqc calculates the activity coefficients of the aqueous and exchange species. Pitzer and SIT aqueous-association models can be also used through two separate databases (i.e., pitzer.dat and sit.dat) released with IPhreeqc.

IPhreeqc uses the product of the activity coefficient times the molality to calculate the activity of the aqueous species (Parkhurst and Appelo, 1999; 2013). To verify UTCHEM-IPhreeqc against UTCHEM-EQBATCH, the IPhreeqc database is modified to make ion activity coefficients of the aqueous species close to one. This approach is discussed in the work of Farajzadeh *et al.* (2012) when verifying MPRS-PHREEQC against UTCHEM-EQBATCH. Towards this goal, WATEQ Debye-Huckel activity

coefficient model is applied with a high value (say 1×10^{9}) for a^{o}_{i} and zero for b_i[1]. However, this approach does not make the exchange reaction modeling identical in IPhreeqc and EQBATCH. IPhreeqc calculates the activity of the exchange species by multiplying the activity coefficients times the equivalent fraction (Parkhurst and Appelo, 1999; 2013). Hence, even with the activity coefficients of the exchange species equal to unity, IPhreeqc applies the equivalent fractions while EQBATCH uses molalities for the species on the exchange site. For example, what follows below presents how the Na-Ca exchange reaction (i.e., $2NaX + Ca^{+2} \rightleftharpoons CaX_2 + 2Na^{+}$) is modeled in EQBATCH and IPhreeqc. This exchange reaction is defined through two half-reactions in IPhreeqc (Parkhurst and Appelo, 1999; 2013, Farajzadeh *et al.*, 2012):

EQBATCH	IPhreeqc
$K^{ex} = \frac{\left[Na^{+}\right]^{2}\left[CaX_2\right]}{\left[Ca^{+2}\right]\left[NaX\right]^{2}}$	$K^{ex} = \frac{\left[\gamma_{Na^{+}} Na^{+}\right]^{2}\left[\gamma_{CaX_2}\frac{2\left[CaX_2\right]}{2\left[CaX_2\right]+\left[NaX\right]}\right]}{\left[\gamma_{Ca^{+2}} Ca^{+2}\right]\left[\gamma_{NaX}\frac{\left[NaX\right]}{2\left[CaX_2\right]+\left[NaX\right]}\right]^{2}}$

where

γ_{CaX_2} = activity coefficient of the calcium on the ion exchange X

γ_i = activity coefficient of the aqueous species *i*, dimensionless

γ_{NaX} = activity coefficient of the sodium on the ion exchange X

K^{ex} = equilibrium constant of the exchange reaction

[1] Personal communication with D. L. Parkhurst of the USGS. 2014 (through email).

[ ]= molality of species in the aqueous, mol/kgw (molality is assumed to equal molarity in this work, mol/L)

An identical single-phase and 1D model is simulated in UTCHEM-IPhreeqc, UTCHEM-EQBATCH, and PHREEQC. Tables 5-3 and 5-4 present initial and injected ion concentrations and initial solid concentrations, respectively. Table 5-5 gives the list of geochemical reactions of the aqueous phase. Figures 5-16 through 5-21 illustrate pH and fluid species concentration profiles at 0.5 PV of UTCHEM-IPhreeqc, UTCHEM-EQBATCH, and PHREEQC. In this case, no exchange reaction is included and ion activities are close to unity in UTCHEM-IPhreeqc and PHREEQC. As the figures show, results of the three geochemical tools are in good agreements.

Table 5-3: Initial and injected (i.e., pure water) ion concentrations.

Ion	$C_{Initail}$ (mol/l)	$C_{Injected}$ (mol/l)
pH	12.63	7.0
Ca	0.1092	0.
S	0.0092	0.
Cl	Charge balance element	
Na	0.1	0.
CO_3^{-2}	0.01	0.

Table 5-4: Initial solid concentrations.

Solid Name	Formula	$C_{Initail}$ (mol/l of PV)
Anhydride	$CaSO_4$	0.091
Calcite	$CaCO_3$	0.1

Table 5-5: Aqueous and solid reactions.

Reaction	K_{eq}
$H_2O \rightleftharpoons H^+ + OH^-$	$10^{-14.0}$
$SO_4^{-2} + H^+ \rightleftharpoons HSO_4^-$	$10^{1.988}$
$Ca^{+2} + SO_4^{-2} \rightleftharpoons CaSO_4$	$10^{2.30}$
$Na^+ + SO_4^{-2} \rightleftharpoons NaSO_4^-$	$10^{0.7}$
$Na^+ + CO_3^{-2} \rightleftharpoons NaCO_3^-$	$10^{1.27}$
$Na^+ + H^+ + CO_3^{-2} \rightleftharpoons NaHCO_3$	$10^{10.079}$
$H^+ + CO_3^{-2} \rightleftharpoons HCO_3^-$	$10^{10.329}$
$Ca^{+2} + CO_3^{-2} \rightleftharpoons CaCO_3$	$10^{3.224}$
$Ca^{+2} + H_2O \rightleftharpoons CaOH^+ + H^+$	$10^{-12.78}$
$Ca^{+2} + CO_3^{-2} + H^+ \rightleftharpoons CaHCO_3^+$	$10^{11.435}$
$Ca^{+2} + SO_4^{-2} + H^+ \rightleftharpoons CaHSO_4^+$	$10^{3.068}$
$Na^+ + H_2O \rightleftharpoons NaOH + H^+$	$10^{-24.0}$
$CaSO_4(S) \rightleftharpoons Ca^{+2} + SO_4^{-2}$	$10^{-4.36}$
$CaCO_3(S) \rightleftharpoons Ca^{+2} + CO_3^{-2}$	$10^{-8.48}$

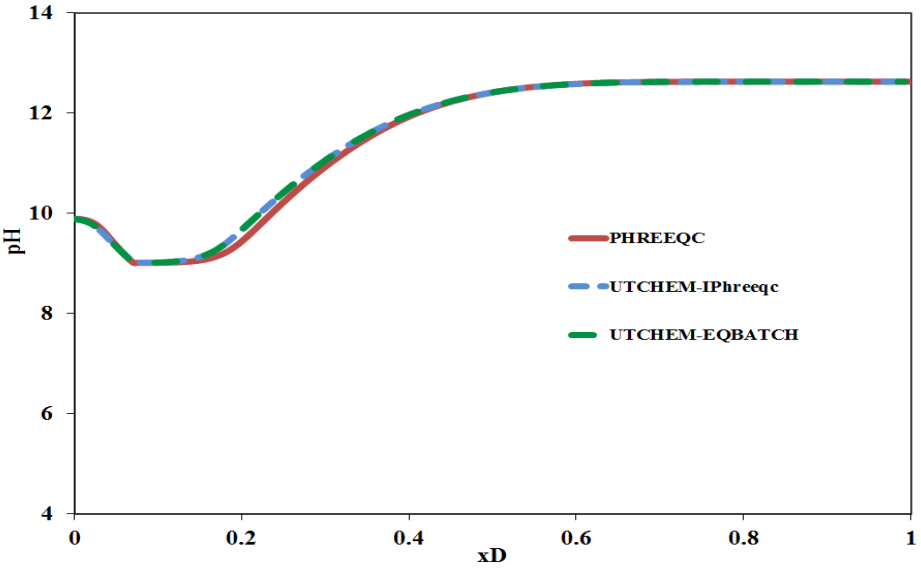

Figure 5-16: pH profile at 0.5 PV of UTCHEM-IPhreeqc, UTCHEM-EQBATCH, and PHREEQC - the same reactions are considered in three tools with no exchange site included in the model. Moreover, activity coefficients of the aqueous species are close to unity in UTCHEM-IPhreeqc and PHREEQC.

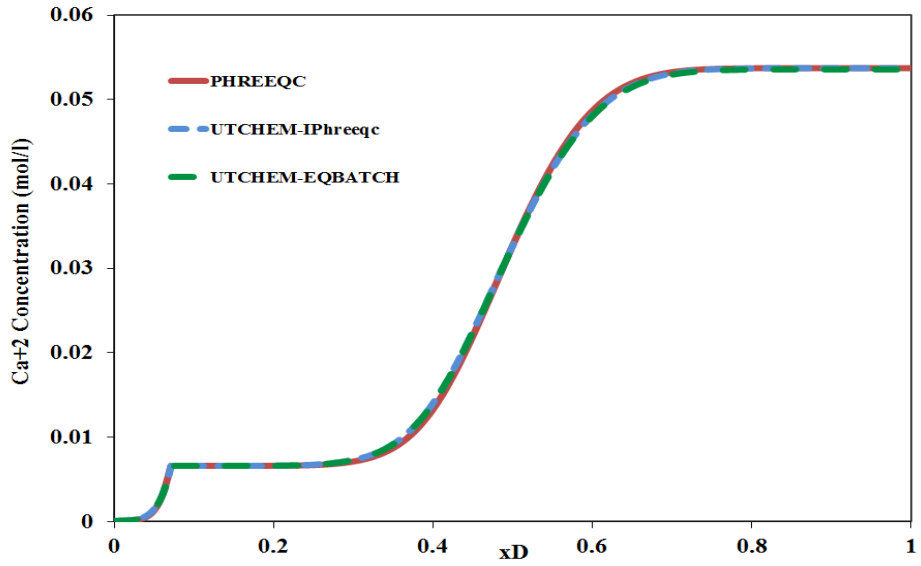

Figure 5-17: Ca^{+2} concentration profile at 0.5 PV of UTCHEM-IPhreeqc, UTCHEM-EQBATCH, and PHREEQC - the same reactions are considered in three tools with no exchange site included in the model. Moreover, activity coefficients of the aqueous species are close to unity in UTCHEM-IPhreeqc and PHREEQC.

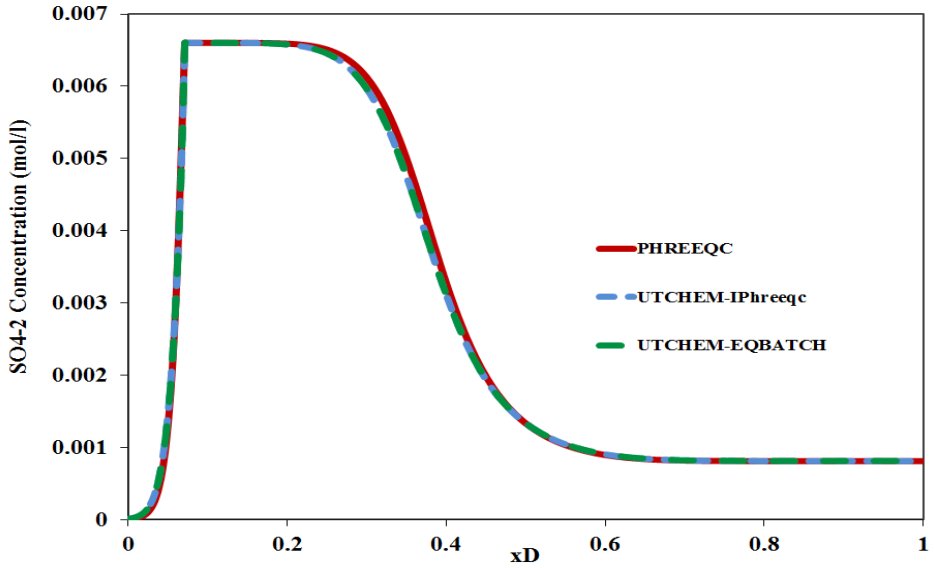

Figure 5-18: SO_4^{-2} concentration profile at 0.5 PV of UTCHEM-IPhreeqc, UTCHEM-EQBATCH, and PHREEQC - the same reactions are considered in three tools with no exchange site included in the model. Moreover, activity coefficients of the aqueous species are close to unity in UTCHEM-IPhreeqc and PHREEQC.

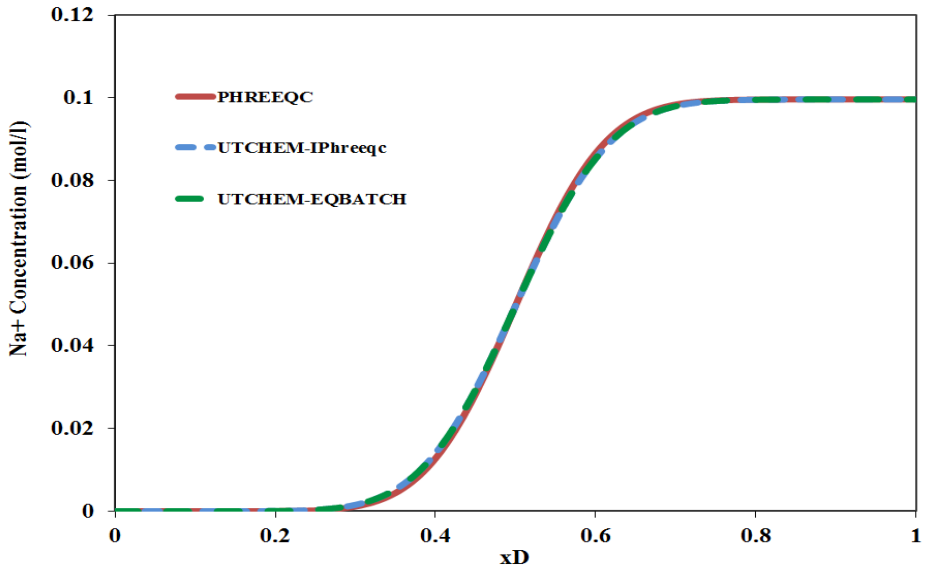

Figure 5-19: Na^+ concentration profile at 0.5 PV of UTCHEM-IPhreeqc, UTCHEM-EQBATCH, and PHREEQC - the same reactions are considered in three tools with no exchange site included in the model. Moreover, activity coefficients of the aqueous species are close to unity in UTCHEM-IPhreeqc and PHREEQC.

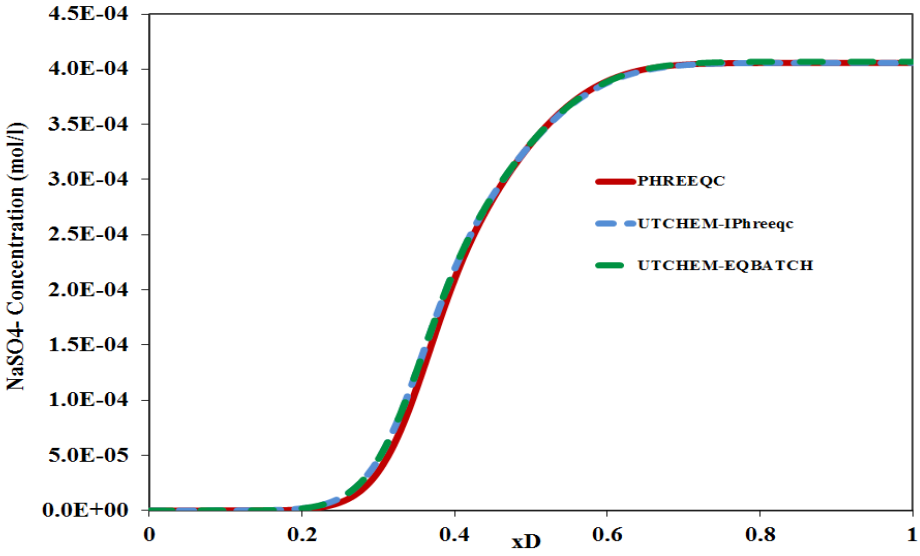

Figure 5-20: $NaSO_4^-$ concentration profile at 0.5 PV of UTCHEM-IPhreeqc, UTCHEM-EQBATCH, and PHREEQC - the same reactions are considered in three tools with no exchange site included in the model. Moreover, activity coefficients of the aqueous species are close to unity in UTCHEM-IPhreeqc and PHREEQC.

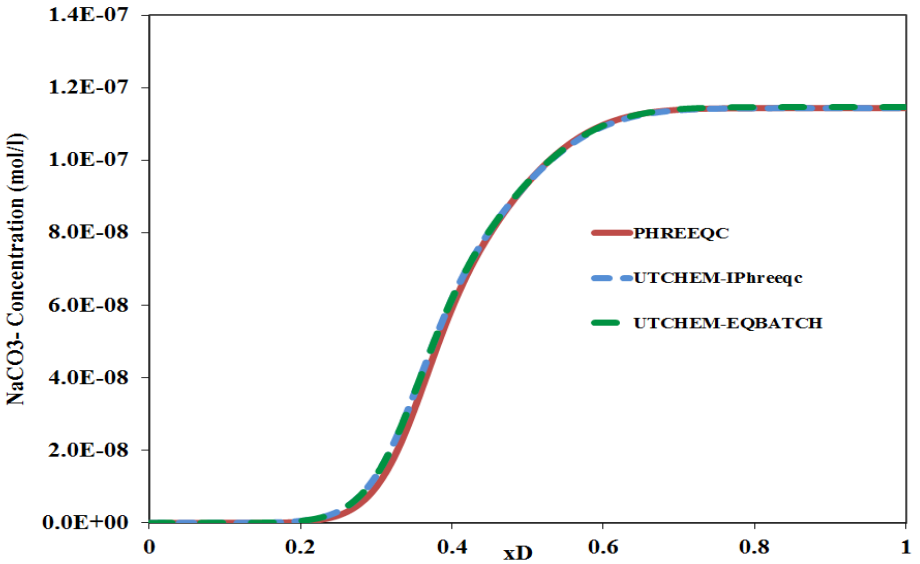

Figure 5-21: $NaCO_3^-$ concentration profile at 0.5 PV of UTCHEM-IPhreeqc, UTCHEM-EQBATCH, and PHREEQC - the same reactions are considered in three tools with no exchange site included in the model. Moreover, activity coefficients of the aqueous species are close to unity in UTCHEM-IPhreeqc and PHREEQC.

Figures 5-22 through 5-27 compare the results when the exchange reactions shown in Table 5-6 are included. In solid blue and red lines activity coefficients are assumed to be one for both aqueous and exchange species in UTCHEM-IPhreeqc and PHREEQC, respectively. However, as discussed above, even in this case molalities are used for the aqueous species and fractions of molalities are applied for the exchange species in UTCHEM-IPhreeqc and PHREEQC. On the other hand, molalities are considered for the aqueous and exchange species in the current version of UTCHEM-EQBATCH. Although this has not been pointed out in the work of Farajzadeh *et al.* (2012), for the case studied, the discrepancies between the solid green line (i.e., UTCHEM-EQBATCH) and solid red (i.e., PHREEQC) and blue (i.e., UTCHEM-IPhreeqc) lines are insignificant (some discrepancies can be seen for Na^+ and Ca^{+2} ions). Included in the Figures 5-22 through 5-27 are also UTCHEM-IPhreeqc and PHREEQC results (i.e., blue and red dashed lines) in which activity coefficients of both aqueous and exchange species are included. Table 5-7 summarizes the WATEQ or extended Debye-Huckel activity coefficient parameters considered for the aqueous and exchange reactions (values are taken from the phreeqc.dat database of PHREEQC (Parkhurst and Appelo, 2013)). pH, $NaSO_4^-$, and $NaCO_3^-$ show some discrepancies when the activity coefficients are included and the difference is more pronounced for Ca^{+2}, and SO_4^{-2} ions. This clearly shows the fundamental role of activities in reactive-transport modeling.

Table 5-6: Exchange reactions

Exchange Reaction	K_{ex}
$Na^+X^- + H^+ \rightleftharpoons H^+X^- + Na^+$	$10^{1.0}$
$2Na^+X^- + Ca^{+2} \rightleftharpoons Ca^+X_2^- + Na^+$	$10^{0.8}$

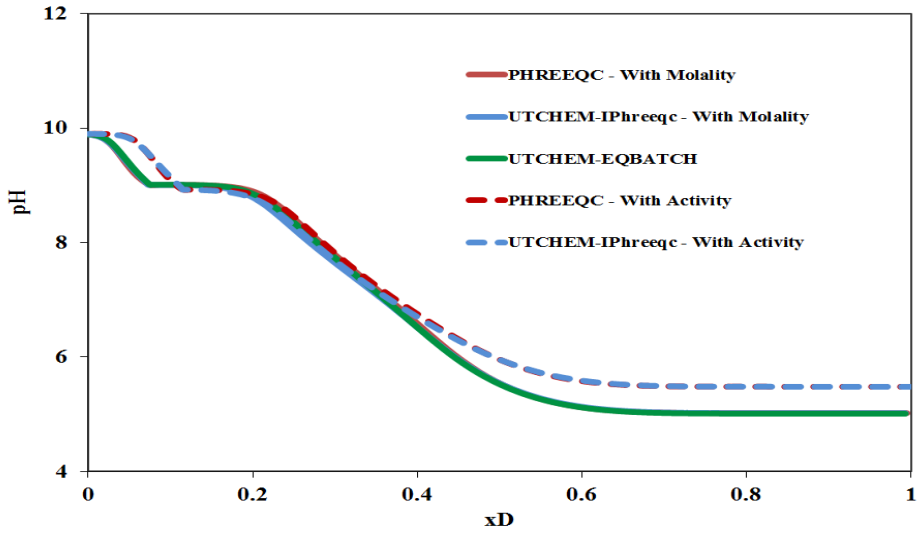

Figure 5-22: pH profile at 0.5 PV of UTCHEM-IPhreeqc, UTCHEM-EQBATCH, and PHREEQC when an exchange site is included in the model– In solid lines molalities are used for both aqueous and exchange species where in the dashed lines activities (for both aqueous and exchange species) are applied (no activities have been implemented in the current version of UTCHEM-EQBATCH).

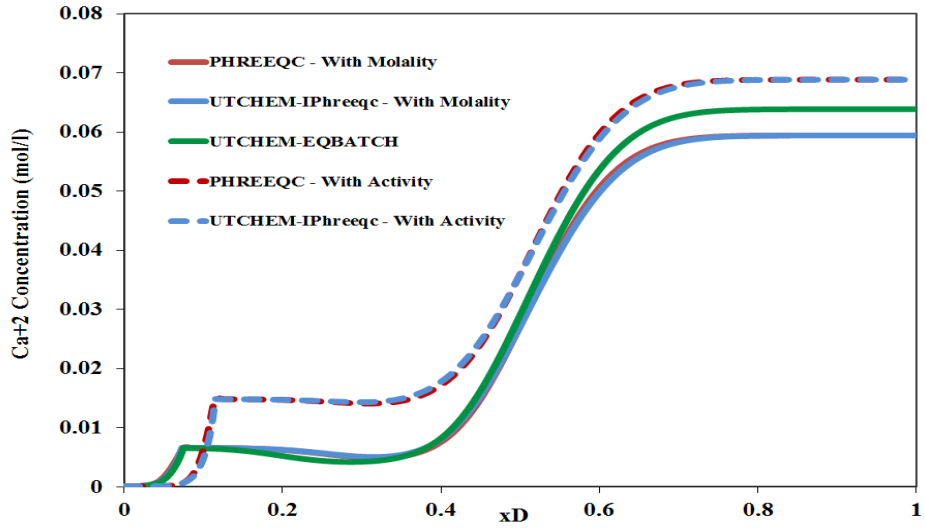

Figure 5-23: Ca^{+2} concentration profile at 0.5 PV of UTCHEM-IPhreeqc, UTCHEM-EQBATCH, and PHREEQC when an exchange site is included in the model– In solid lines molalities are used for both aqueous and exchange species where in the dashed lines activities (for both aqueous and exchange species) are applied (no activities have been implemented in the current version of UTCHEM-EQBATCH).

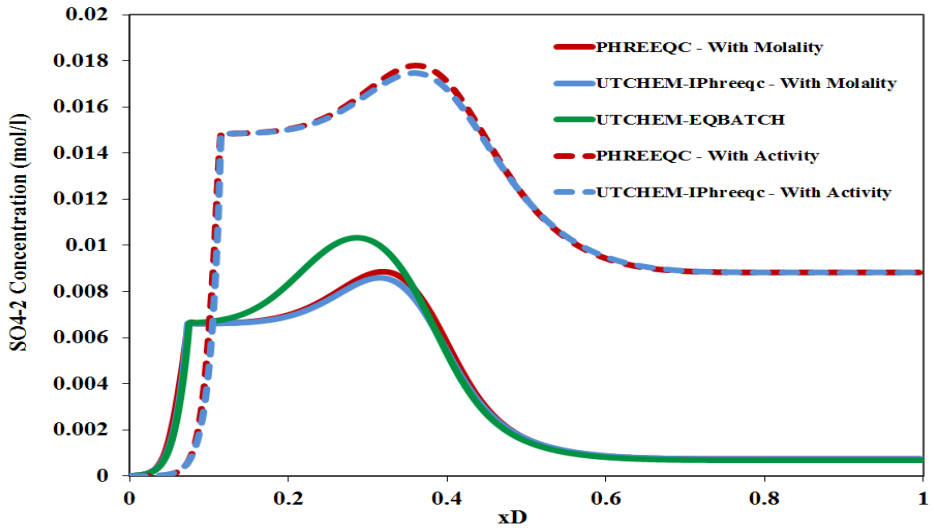

Figure 5-24: SO_4^{-2} concentration profile at 0.5 PV of UTCHEM-IPhreeqc, UTCHEM-EQBATCH, and PHREEQC when an exchange site is included in the model– In solid lines molalities are used for both aqueous and exchange species where in the dashed lines activities (for both aqueous and exchange species) are applied (no activities have been implemented in the current version of UTCHEM-EQBATCH).

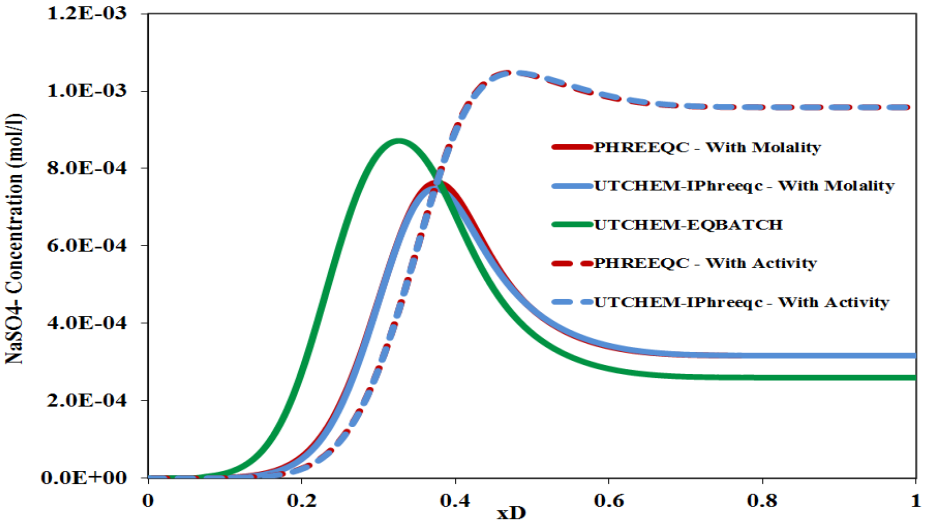

Figure 5-25: $NaSO_4^-$ concentration profile at 0.5 PV of UTCHEM-IPhreeqc, UTCHEM-EQBATCH, and PHREEQC when an exchange site is included in the model– In solid lines molalities are used for both aqueous and exchange species where in the dashed lines activities (for both aqueous and exchange species) are applied (no activities have been implemented in the current version of UTCHEM-EQBATCH).

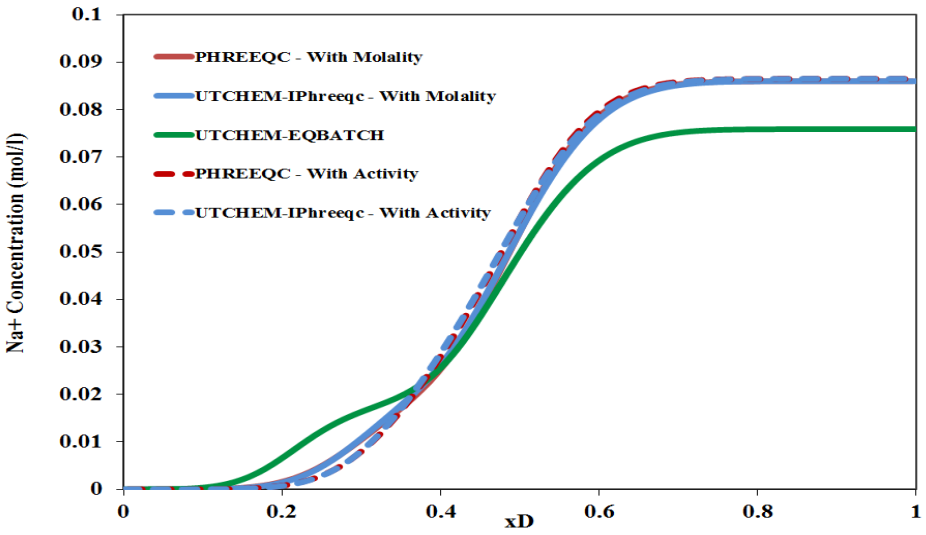

Figure 5-26: Na^+ concentration profile at 0.5 PV of UTCHEM-IPhreeqc, UTCHEM-EQBATCH, and PHREEQC when an exchange site is included in the model– In solid lines molalities are used for both aqueous and exchange species where in the dashed lines activities (for both aqueous and exchange species) are applied (no activities have been implemented in the current version of UTCHEM-EQBATCH).

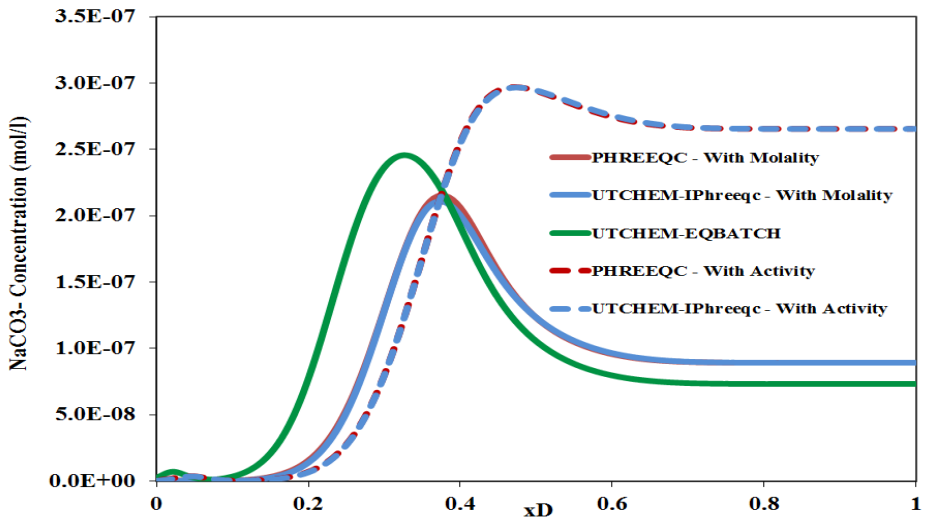

Figure 5-27: $NaCO_3^-$ concentration profile at 0.5 PV of UTCHEM-IPhreeqc, UTCHEM-EQBATCH, and PHREEQC when an exchange site is included in the model– In solid lines molalities are used for both aqueous and exchange species where in the dashed lines activities (for both aqueous and exchange species) are applied (no activities have been implemented in the current version of UTCHEM-EQBATCH).

Table 5-7: WATEQ or Extended activity coefficient parameters used in the model (values are taken from phreeqc.dat (Parkhurst and Appelo, 2013))

Reactions	a_i^0	b	**Reactions**	a_i^0	b
$H_2O \rightleftharpoons H^+ + OH^-$	3.5	0	$H^+ + CO_3^{-2} \rightleftharpoons HCO_3^-$	5.4	0
$H^+ \rightleftharpoons H^+$	9.0	0.	$Ca^{+2} + CO_3^{-2} \rightleftharpoons CaCO_3$	-	-
$Na^+ \rightleftharpoons Na^+$	4.0	0.075	$Ca^{+2} + H_2O \rightleftharpoons CaOH^+ + H^+$	-	-
$Cl^- \rightleftharpoons Cl^-$	3.5	0.015	$Ca^{+2} + CO_3^{-2} + H^+ \rightleftharpoons CaHCO_3^+$	6.0	0.
$SO_4^{-2} \rightleftharpoons SO_4^{-2}$	5.0	-0.04	$Ca^{+2} + SO_4^{-2} + H^+ \rightleftharpoons CaHSO_4^+$	-	-
$CO_3^{-2} \rightleftharpoons CO_3^{-2}$	5.4	0.	$Na^+ + H_2O \rightleftharpoons NaOH + H^+$	-	-
$SO_4^{-2} + H^+ \rightleftharpoons HSO_4^-$	-	-	$CaSO_4(S) \rightleftharpoons Ca^{+2} + SO_4^{-2}$	-	-
$Ca^{+2} + SO_4^{-2} \rightleftharpoons CaSO_4$	-	-	$CaCO_3(S) \rightleftharpoons Ca^{+2} + CO_3^{-2}$	-	-
$Na^+ + SO_4^{-2} \rightleftharpoons NaSO_4^-$	5.4	0	$Na^+ + X^- \rightleftharpoons Na^+X^-$	4.08	0.082
$Na^+ + CO_3^{-2} \rightleftharpoons NaCO_3^-$	-	-	$H^+ + X^- \rightleftharpoons H^+X^-$	9.0	0.
$Na^+ + H^+ + CO_3^{-2} \rightleftharpoons NaHCO_3$	-	-	$Ca^{+2} + X^- \rightleftharpoons Ca^{+2}X_2^-$	5.0	0.165

The difference between UTCHEM-IPhreeqc and UTCHEM-EQBATCH results is more pronounced as more geochemical elements and reactions are included.

Two notes on UTCHEM-IPhreeqc:

- Similar to UTCHEM-EQBATCH, geochemical calculations are skipped for the gridblocks with porosity of less than 0.01 and/or with water saturation of less than 10^{-4}.
- Although UTCHEM-EQBATCH includes the surfactant associated cation reactions in batch reaction calculations (UTCHEM Technical Documentation, 2000), no surfactant associated cations are modeled in the current version of UTCHEM-IPhreeqc. However, we believe these reactions can be included in the UTCHEM-IPhreeqc simulator through

using the **SURFACE** keyword available in IPhreeqc.

We use UTCHEM-IPhreeqc to model three coreflood experiments: 1) ASP flooding of an acidic crude oil (active oil), 2) ASP flooding of a non-reactive crude oil, and 3) ACP flooding of an acidic crude.

5.5 ASP COREFLOOD USING AN ACIDIC CRUDE OIL

Mohammadi (2008) simulated several ASP corefloods with acidic crude oils. We use UTCHEM-IPhreeqc to model the coreflood labeled "Case AII." Crude oil has an acid number of 0.5 mg KOH/g oil. Oil and water viscosities are 19 and 0.5 cp, respectively. The coreflood configuration is vertical with the injection at the bottom and production at the top. ASP slug is injected into the core with the oil is at its residual saturation to water of 0.43. The ASP slug is injected for 0.3 PV and chased with about 1.5 PVs of the polymer slug. C20-24 IOS (0.1 wt%) and C16 bABS (0.1 wt%) are the injected surfactants and 0.1wt% Diethylene Glycol Butyl Ether (DGBE) is injected as co-solvent. 3000 ppm of Flopaam 3630S polymer is included in the ASP slug for the mobility control. Brine salinity of the ASP slug is 27500 ppm Na_2CO_3 in 0.6 wt% NaCl and that of polymer slug is 0.6 wt% NaCl. pH of the ASP slug is about 11.5. Further details about the coreflood are given in Mohammadi (2008).

Using the experimental data, surfactant phase behavior and polymer properties were previously modeled (Mohammadi, 2008) and directly used in our model. Below presents the assumptions and matching parameters applied by Mohammadi (2008) in modeling this coreflood:

- Geochemistry: Only the essential reactions for the ASP flooding are considered, which includes; oil/aqueous partitioning reaction of the acid component,

dissociation reaction of the acid component in the aqueous phase; exchange reaction which exchanges only the hydrogen and sodium ions. Reaction for H_2CO_3 and HCO_3^- were also added to the model. It is assumed that the injection rate is high enough at the lab scale, which makes the effect of kinetics of the mineral negligible on the geochemistry of the problem. Hence, no solid reaction is included when modeling the coreflood (the significance of the kinetic reaction will be discussed later in this chapter). However, this assumption might not be valid at the field scale where the fluid velocity is fairly low far from the wells. Partitioning coefficient, dissociation coefficient of the acid component in the aqueous phase, cation exchange capacitance of the exchanger, and equilibrium constant of the Na-H exchange reaction are the adjusting parameters.

- Surfactant and Soap Phase Behavior: Upper (CSEU) and lower salinities (CSEL); and the equivalent weight of the generated soap are matching parameters (equivalent weight of the surfactant and soap are used when applying the mixing rule to the surfactant and soap phase behaviors).
- Surfactant Adsorption on the Rock: Consistent with the literature, in UTCHEM, between certain pH threshold values, surfactant adsorption decreases linearly with increasing pH. The surfactant adsorption is pH-independent for values less than the lower threshold value and becomes a small constant fraction for the values higher than the upper threshold (see Mohammadi, 2008). Upper and lower thresholds used in this model are matching parameters (7 and 13 are values of the lower and upper thresholds in the tuned model, respectively).
- Relative Permeability Curves: Microemulsion residual saturation and endpoint relative permeability at high IFT (or low capillary number) and water, oil, and

microemulsion phase exponents at high IFT are tuning parameters. At low IFT, relative permeabilities of the oil, water, and microemulsion phases are assumed to be linear with no residual saturation and 1.0 for both endpoint and exponent. Experimental measurements are used for the residual oil (i.e., 0.43) and residual water saturations (i.e., 0.32); and water (i.e., 0.05) and oil (i.e., 0.6) endpoint relative permeabilities.

To verify UTCHEM-IPhreeqc against UTCHEM-EQBATCH, except for the ion-exchange parameters and dispersivity coefficients (explained below), everything is identical to the input file provided by Mohammadi (2008). Hence, similar to Mohammadi (2008)'s model, we consider only essential reactions such as in-situ generation of soap and aqueous reactions involving the alkali. An ion exchanger is also included. Sodium and hydrogen are the only elements involved in the ion exchange reaction. Moreover, ion activity coefficients of the aqueous and exchange species are close to unity in UTCHEM-IPhreeqc. Table 5-8 presents the reactions considered in the UTCHEM-IPhreeqc thermodynamic database to model this coreflood. As discussed earlier in this chapter, because exchange reactions are modeled differently between IPhreeqc and EQBATCH, exchange parameters in UTCHEM-IPhreeqc are adjusted to reproduce the same pH lag as that for UTCHEM-EQBATCH. Physical dispersion (longitudinal dispersivities) was modified to improve the match.

Figures 5-28 and 5-29 present simulated results against the experimental measurements for cumulative oil recovery, oil cut, and pressure drop. Figure 5-30 shows a plot of Winsor's Type III region salinity and the IFT profiles at 0.5 PV. Ultra-low IFT is achieved when the salinity is between the upper and the lower salinity boundaries (i.e., Winsor Type III).

Table 5-8: Reactions considered to model the Case AII coreflood

Reaction	K_{eq}
$HA_o \rightleftharpoons HA_w$	$10^{-3.966}$
$HA_w \rightleftharpoons H^+ + A_w^-$	$10^{-8.0}$
$CO_3^{-2} + H^+ \rightleftharpoons HCO_3^-$	$10^{10.324}$
$CO_3^{-2} + 2H^+ \rightleftharpoons H_2CO_3$	$10^{16.689}$
$Na^+ + HX \rightleftharpoons NaX + H^+$	$10^{-6.731}$

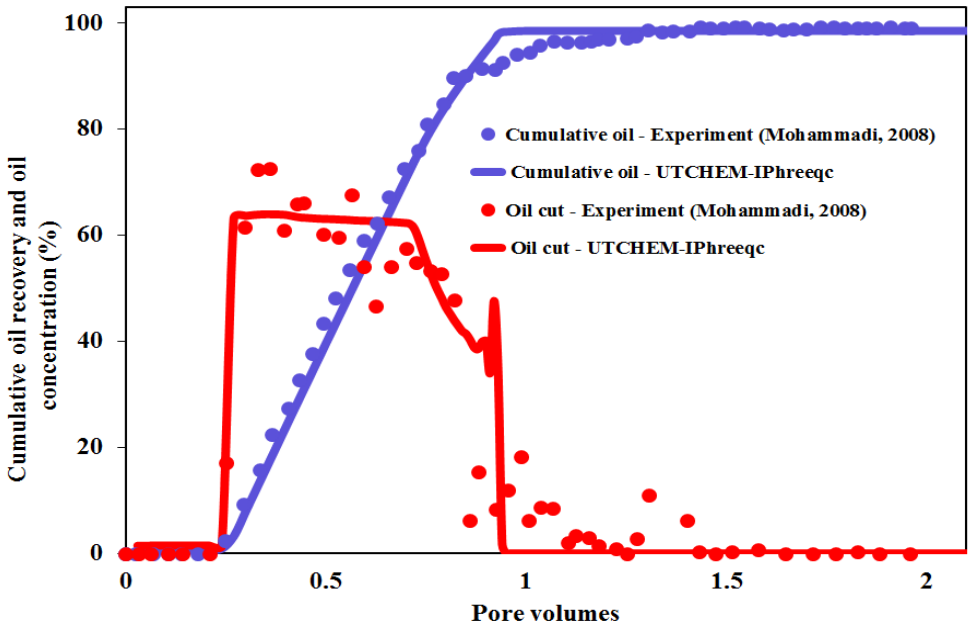

Figure 5-28: UTCHEM-IPhreeqc simulation results versus measured data for cumulative oil recovery and oil cut.

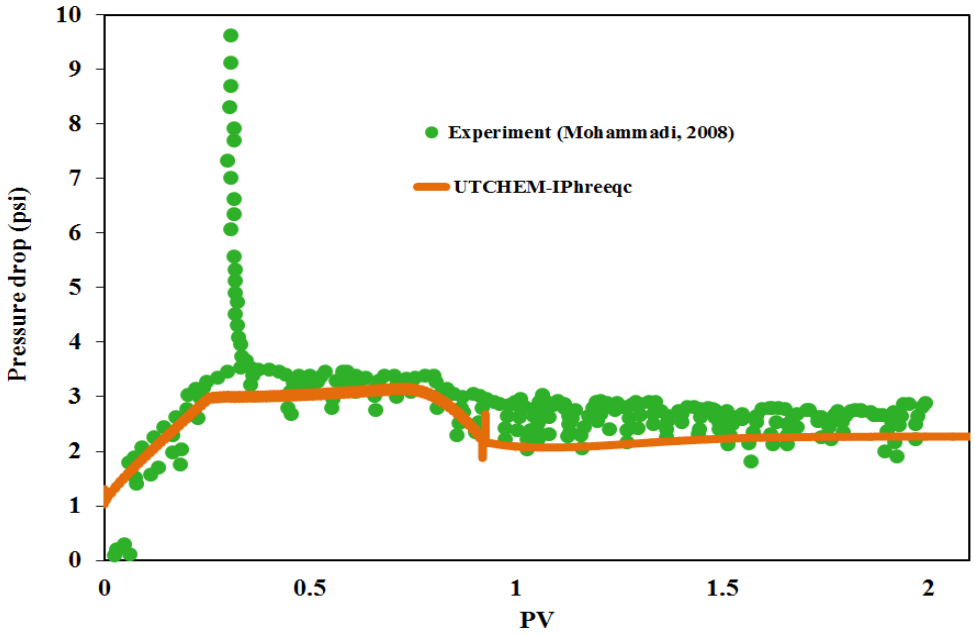

Figure 5-29: UTCHEM-IPhreeqc simulation results versus measured data for pressure drop.

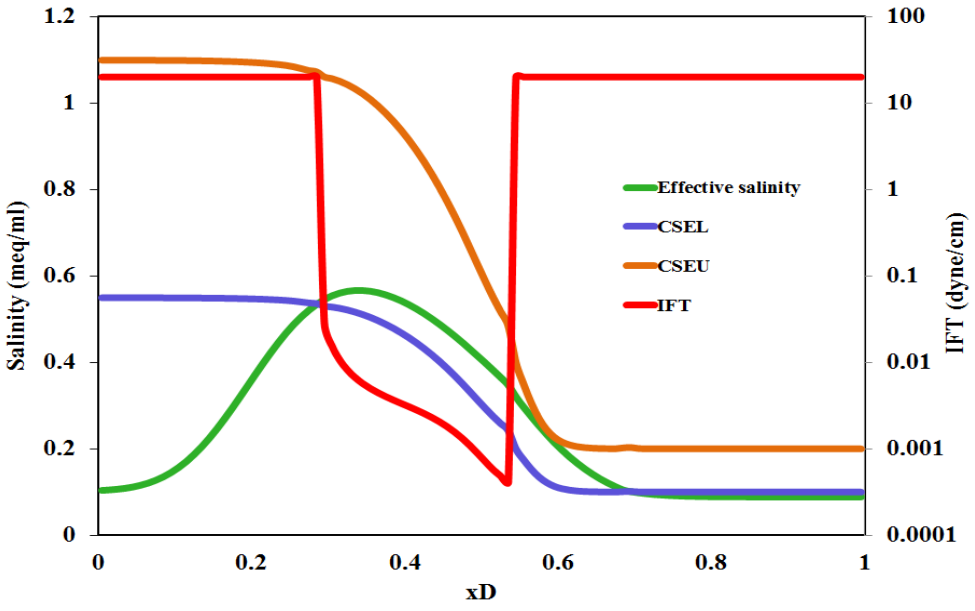

Figure 5-30: UTCHEM-IPhreeqc simulation results for effective salinity, CSEL, CSEU, and IFT at 0.5 PV.

To model this coreflood different mechanisms are considered. Injecting alkaline agents increase pH, which results in generating more soap. The generated soap along with the injected surfactant decreases the IFT between oil and water and consequently mobilizes and produces the residual oil saturation. Also included in the model is the dependency of the surfactant adsorption on pH. Figure 5-31 quantifies the contribution of the different mechanisms in increasing the oil recovery during the ASP flooding in this coreflood.

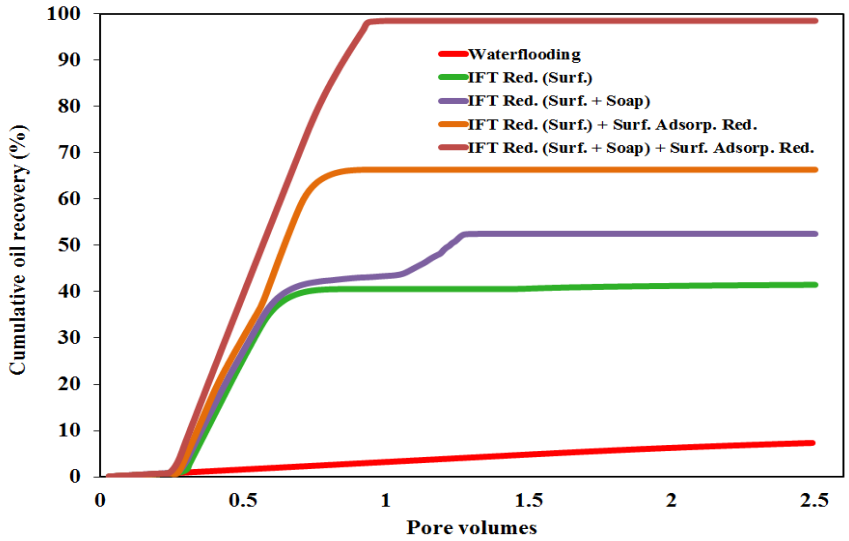

Figure 5-31: Contribution of different mechanisms in increasing the oil recovery.

To emphasize on the importance of the geochemistry during ASP processes, sensitivity studies are performed on the pH of the ASP slug and initial acid concentration of the crude oil (i.e., CAC2I). It is noted that the pH of the ASP slug and the initial acid concentration in the experiment were 11.5 and 0.00729 mol/l of oil, respectively. Figures 5-32 through 5-35 present the effect of pH of the ASP slug on the cumulative oil

recovery, oil cut, the effluent pH history, and the soap total concentration profile at 0.5 PV. As these figures show, the soap total concentration increases by increasing the pH which results in higher oil recovery. Below certain pH value (9.5 in this case) alkaline effect is more pronounced in decreasing the surfactant adsorption on the rock surface than generating soap in-situ. These numerical results and their trend need to be verified against systematic laboratory experiments. Figure 5-36 illustrates how the oil recovery changes as a function of the initial acid concentration of the crude oil. Consistent with the literature, more benefit, can be achieved during injecting ASP in acidic crude oils.

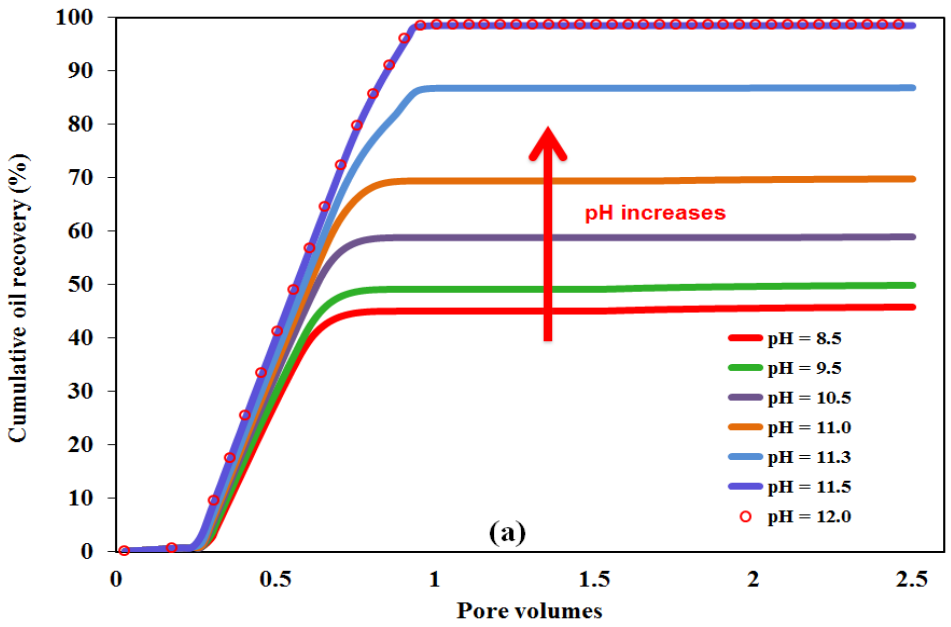

Figure 5-32: The effect of change in the "pH of the injected ASP slug" on Cumulative oil recovery.

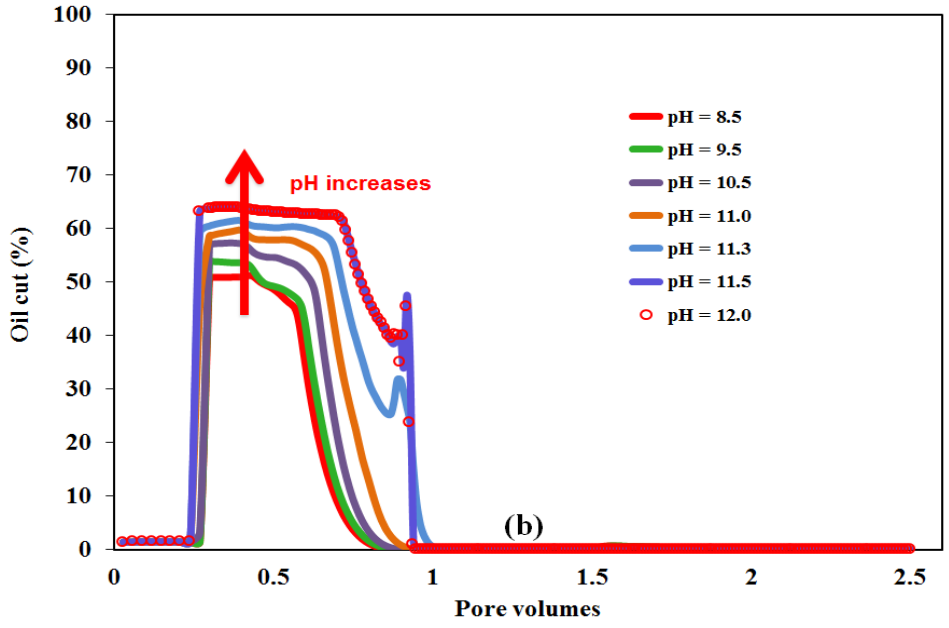

Figure 5-33: The effect of change in the "pH of the injected ASP slug" on Oil cut.

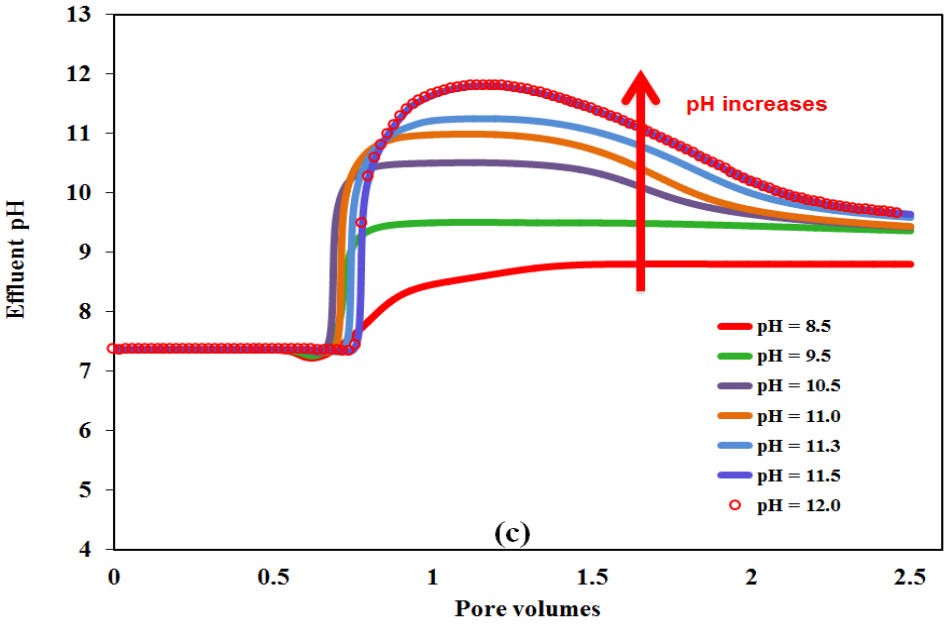

Figure 5-34: The effect of change in the "pH of the injected ASP slug" on Effluent pH history.

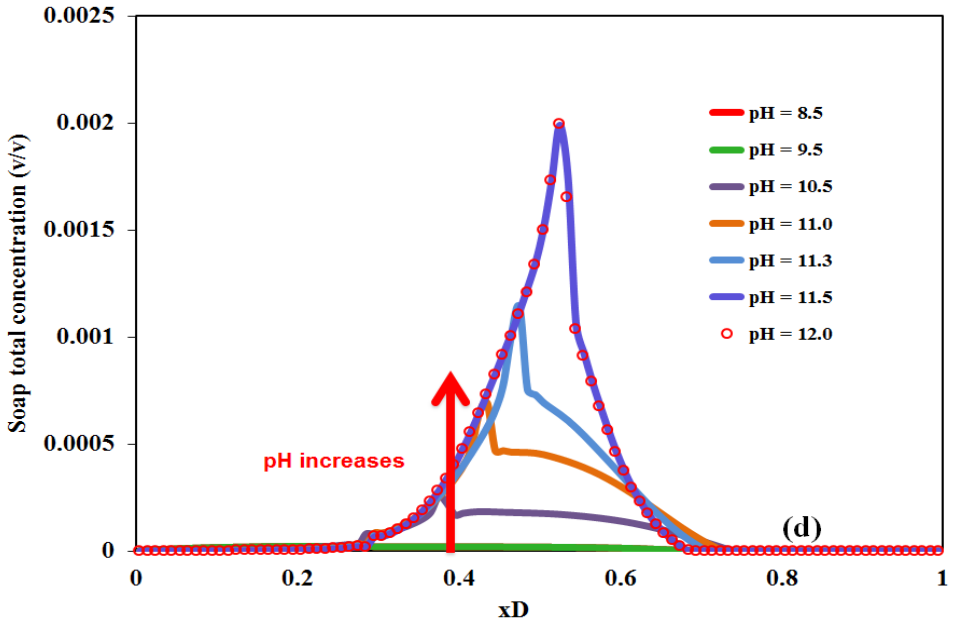

Figure 5-35: The effect of change in the "pH of the injected ASP slug" on Soap total concentration profile at 0.5 PV.

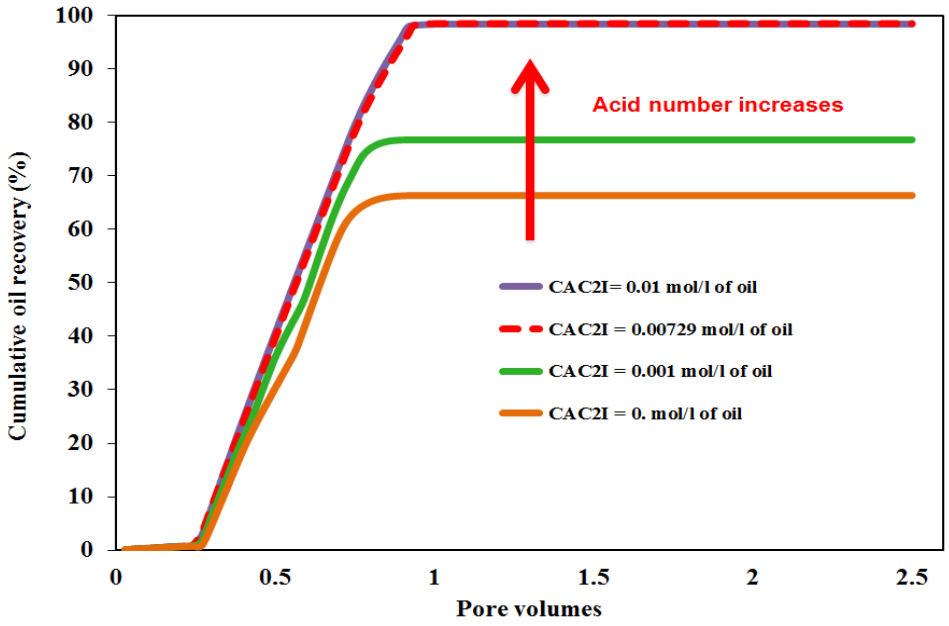

Figure 5-36: The effect of change in "the initial acid concentration in the crude oil (CAC2I)" on cumulative oil recovery.

The tuned model is used to investigate the significance of common assumptions made during modeling an ASP process. To emphasize on the importance of the including Type III during the ASP modeling, we run the tuned model (through which we match the experimental data) by considering equal values for Type III upper (CSEU) and lower (CSEL) effective salinities for both the surfactant and soap. By doing this we ignore the salinity window and subsequently Type III during the simulation. Figures 5-37 and 5-38 present UTCHEM-IPhreeqc simulation results when Type III is excluded from the simulation versus the experimental data. There is a significant mismatch in the oil recovery and pressure drop when Type III is excluded in the simulations. This emphasizes the importance of the Type III during an ASP process. It is worth noting that to the best of the author's knowledge, MPRS-PHREEQC (Wei, 2011; 2012; Farajzadeh *et al.*, 2012) excludes Type III. This may explain MPRS-PHREEQC difficulties in matching the pressure drop (see the work of Farajzadeh *et al.*, 2012). The importance of modeling Type III region was also discussed in the work of Mohammadi (2008).

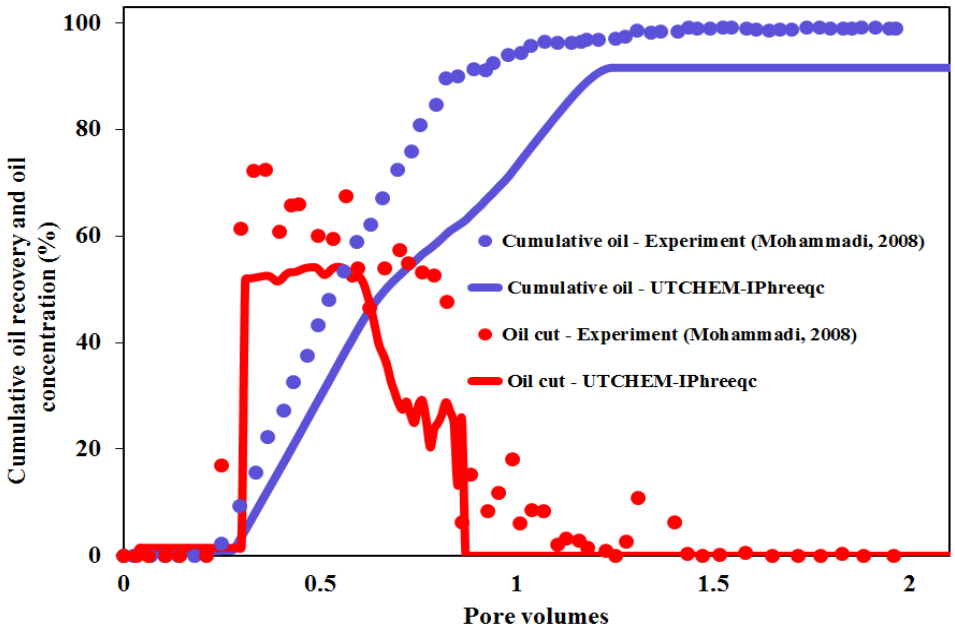

Figure 5-37: UTCHEM-IPhreeqc simulation results when Type III is excluded from the simulation versus measured data for cumulative oil recovery and oil cut.

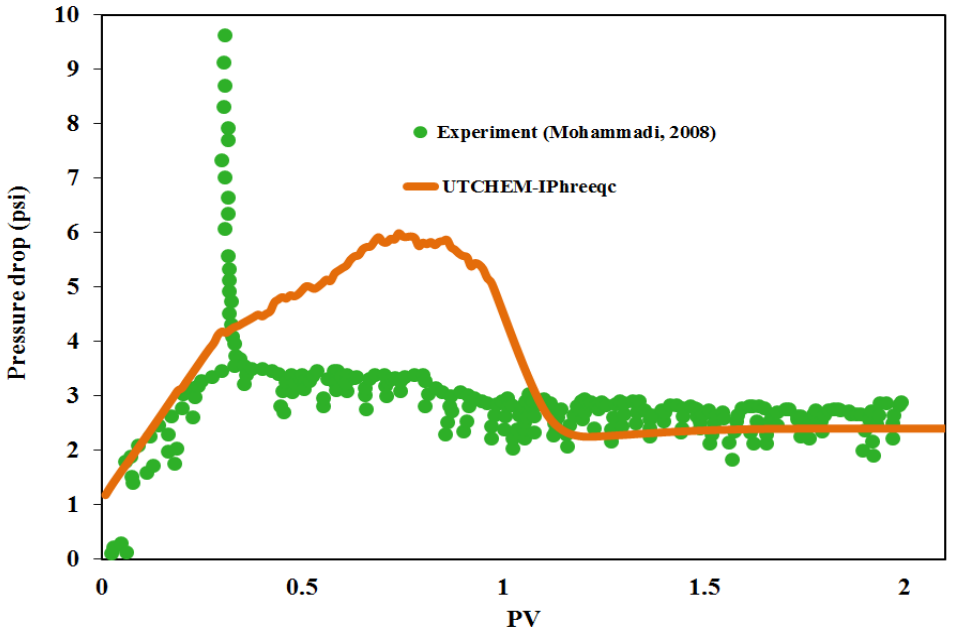

Figure 5-38: UTCHEM-IPhreeqc simulation results when Type III is excluded from the simulation versus measured data for pressure drop.

Ideal solution is another assumption made in ASP modeling (i.e., UTCHEM-EQBATCH). Also, rather than considering the entire thermodynamically equilibrated system, the most important reactions (i.e., acid component/alkali reaction and alkali consumption due to the exchanger or precipitation reactions) are selectively considered. To investigate the important role of geochemical reactions during an ASP flood, rather than the limited number of reactions used to model the coreflood, we use different thermodynamic databases released along with the IPhreeqc geochemical package. Figures 5-39 and 5-40 show the simulated oil recovery and pressure drop, respectively, when phreeqc.dat, pitzer.dat, llnl.dat, sit.dat, and wateq4.dat geochemistry databases are used. These databases are different in number of reactions as well as their approach to evaluate the ion activities. More details on these databases can be found in Parkhurst and Appelo (1999; 2013). Figures 5-39 and 5-40 show the significance of the number of reactions as well as ion-association model considered on the performance of the ASP processes. To make the plots clearer, oil cut plots are excluded from Figure 5-39.

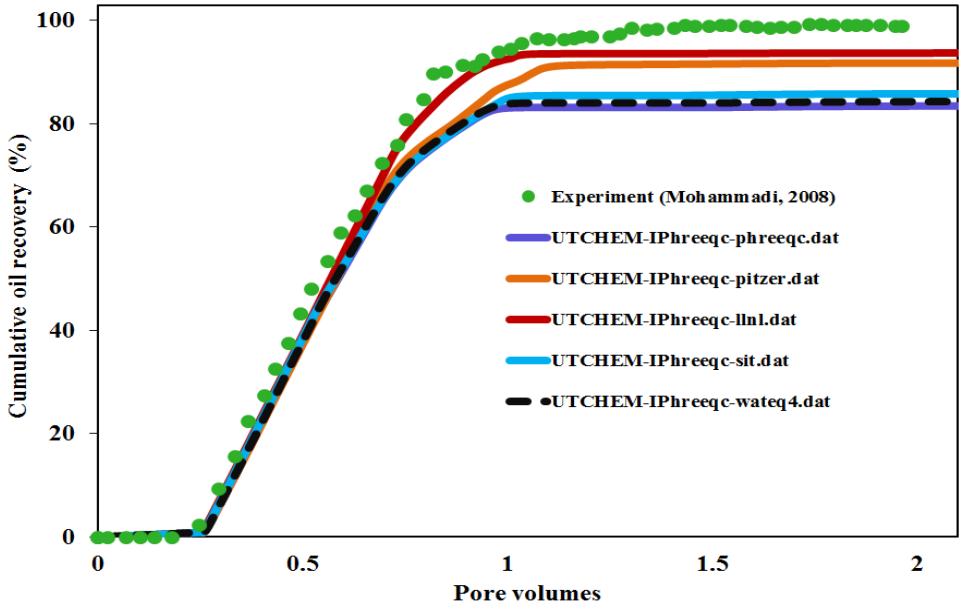

Figure 5-39: UTCHEM-IPhreeqc simulation results using different thermodynamic databases (with different types of ion-association aqueous models and number of reactions) versus measured data for cumulative oil recovery.

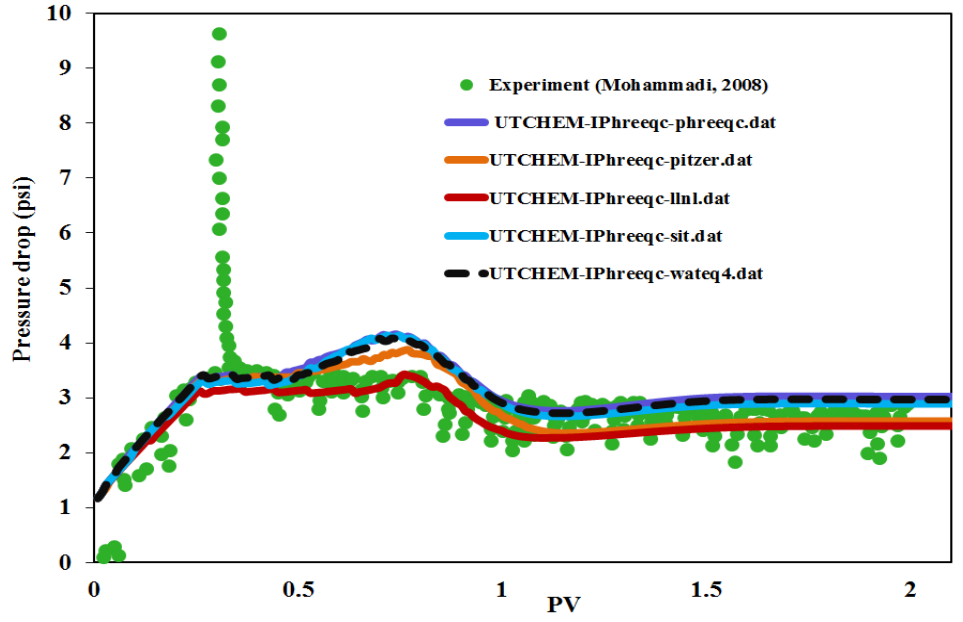

Figure 5-40: UTCHEM-IPhreeqc simulation results using different thermodynamic databases (with different types of ion activities and number of reactions) versus measured data for pressure drop.

The effects of temperature and pressure on geochemical reactions are usually neglected in reactive-transport modeling. In our previous work, we studied the temperature and pressure effects in reactive-transport modeling in general (Korrani *et al.*, 2014c). In this chapter their effects are specifically investigated for ASP processes. Towards this goal, the tuned model of Case AII is run at different temperatures. Initial and injected waters have the same temperature (i.e., no energy equation is solved in UTCHEM-IPhreeqc). Although a non-isothermal case can be modeled using UTCHEM-IPhreeqc, to isolate the effect of the temperature for the geochemistry of the problem, transport-related parameters such as viscosity, surfactant and soap phase behaviors, etc. are assumed to be temperature-independent. Hence, any change in the oil recovery is solely due to the effect of the temperature on the geochemical reactions. Figures 5-41 and 5-42 present UTCHEM-IPhreeqc simulation results at different temperatures versus the measured data for the cumulative oil recovery and pressure drop. It is worth noting that pitzer.dat database is used for all the temperatures. These figures clearly show the significant effect of the temperature on the geochemical reactions and consequently on the oil recovery and the pressure drop (i.e., oil recovery decreases by increasing the temperature). Again, we emphasize on the fact that we assumed the temperature has no effect on the viscosities and surfactant and soap phase behaviors.

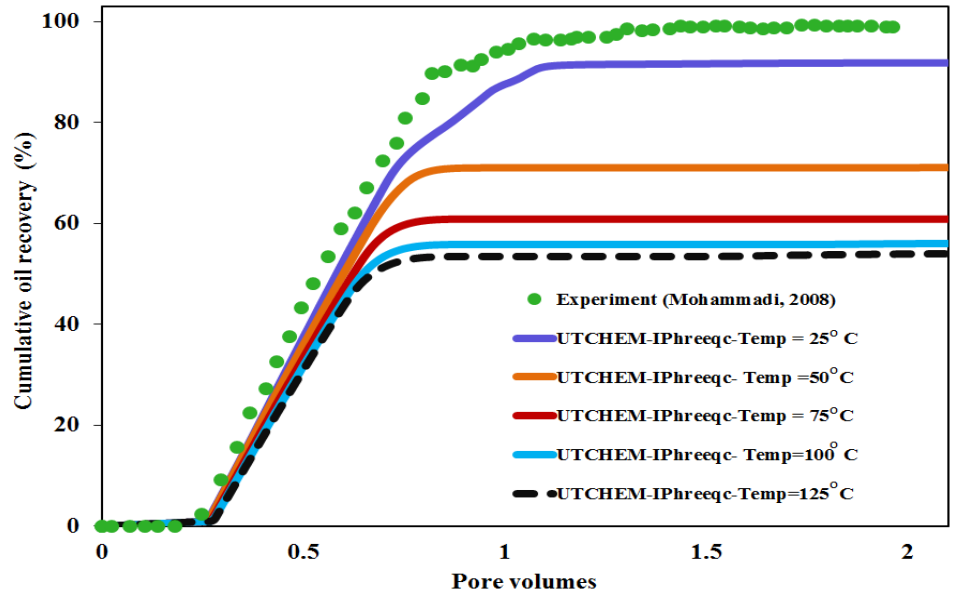

Figure 5-41: UTCHEM-IPhreeqc simulation results at different temperatures using Pitzer thermodynamic database versus measured data for cumulative oil recovery – temperature effect is isolated to the geochemical reactions.

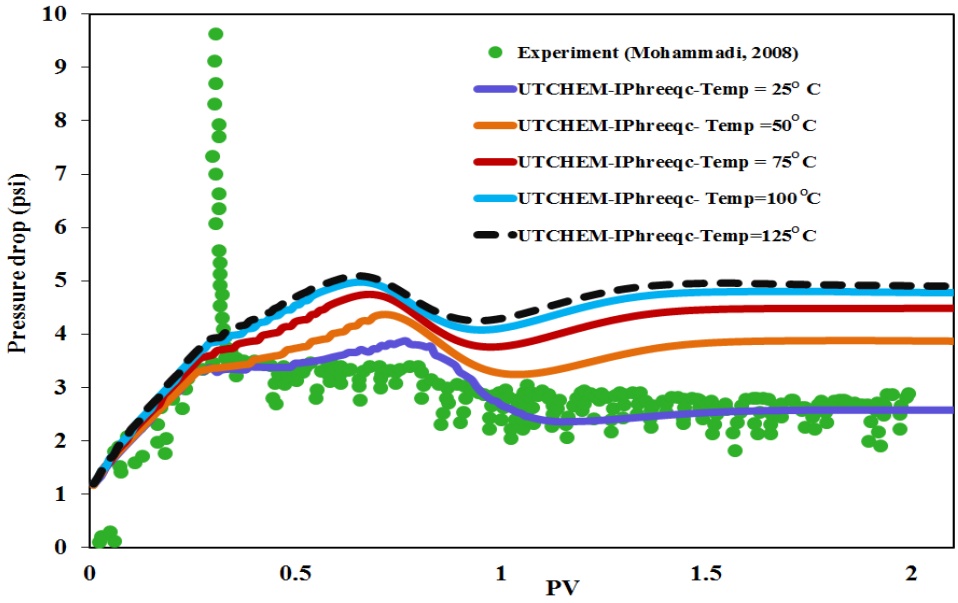

Figure 5-42: UTCHEM-IPhreeqc simulation results at different temperatures using Pitzer thermodynamic database versus measured data for pressure drop - temperature effect is isolated to the geochemical reactions.

Figures 5-43 and 5-44 compare simulated results for the oil recovery and the pressure drop when pressure effect is included in the geochemical calculation. Pressures shown in the figures are approximately the average pressure during the simulation. To change the average pressure in the core, we modify the initial and injecting pressures. Based on the results shown in Figures 5-43 and 5-44 we conclude that the pressure has minor effect on the geochemical reactions and its effect can be neglected in modeling ASP processes.

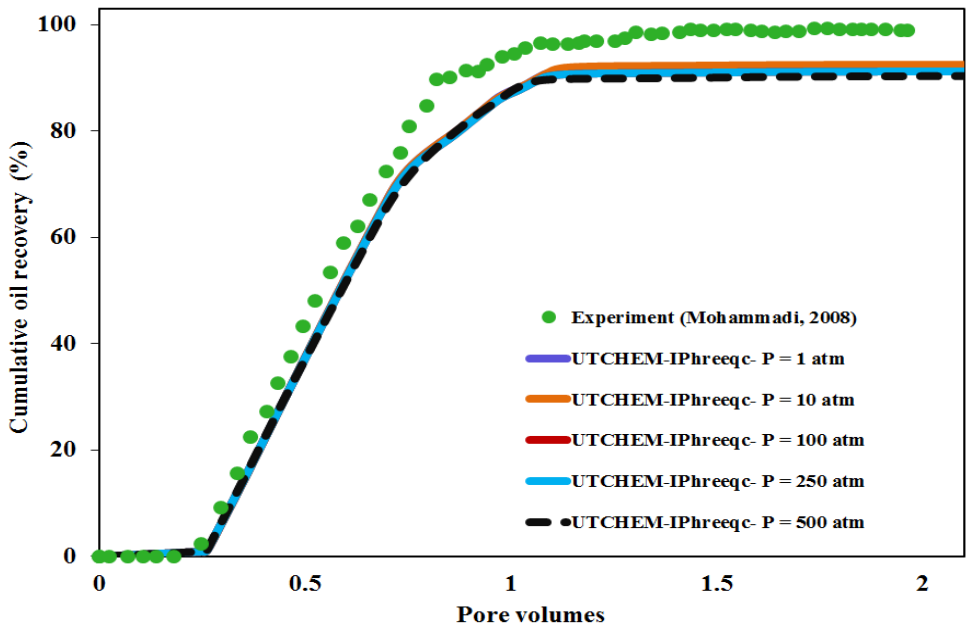

Figure 5-43: UTCHEM-IPhreeqc simulation results at different pressure using Pitzer thermodynamic database versus measured data for cumulative oil recovery.

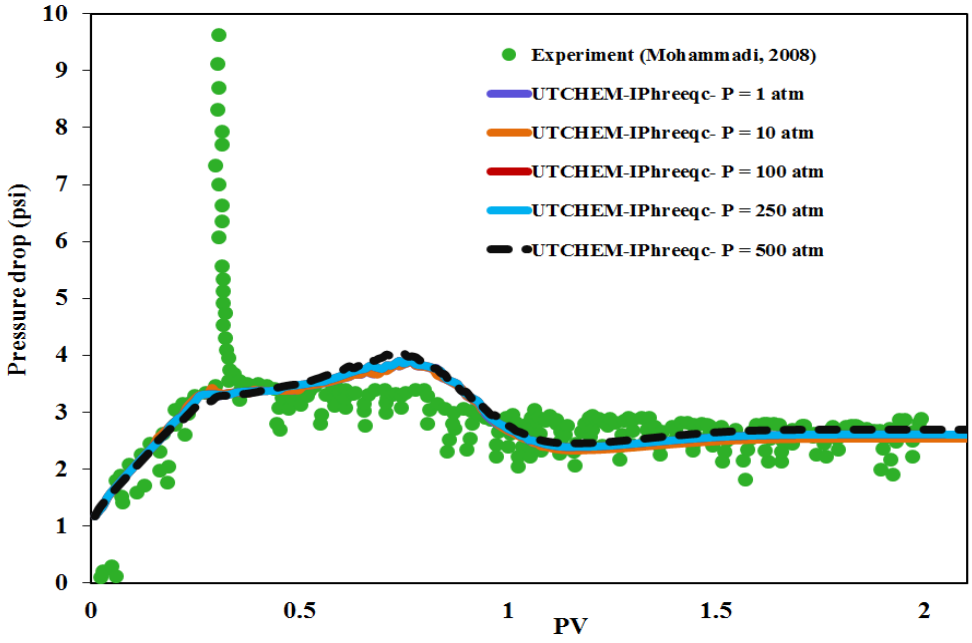

Figure 5-44: UTCHEM-IPhreeqc simulation results at different pressure using Pitzer thermodynamic database versus measured data for pressure drop.

In modeling the coreflood "Case AII" and also the two more corefloods that will be presented later in this chapter we assume the injection flowrate at the lab condition is high enough that with a good approximation we can neglect the kinetics of the minerals from the geochemistry of the problem (the same assumption was also applied in the work of Farajzadeh *et al.* (2012) and Mohammadi *et al.* (2009)). However, this assumption might not be valid at the field scale far from the wellbore where the velocity is very low compared with the velocity at the lab scale. To study the significance of the kinetics in reactive-transport problems (e.g., ASP flooding and AP flooding) the UTCHEM-IPhreeqc case based on the example 11 of PHREEQC is considered (this case was previously used to verify UTCHEM-IPhreeqc against PHREEQC). We include calcite with initial moles of 7×10^{-4} in all the cells through using the **KINETICS** keyword of IPhreeqc. PHREEQC proposed kinetic reaction rate for the calcite

precipitation/dissolution (Parkhurst and Appelo, 1999; 2013) is considered. Figures 5-45 through 5-48 present the produced ion histories at different injection rates. Injection flow rate of the base case (shown as "q" in the figures) is about 2.3×10^{-3} ft^3/day. Also, included in the figures is a case in which no calcite is present in the system (shown with circles). These figures show as the injection rate increases aqueous solution does not have enough time to equilibrate with the calcite, hence produced ion histories are approaching towards the case with no calcite included. These figures clearly show that the local equilibrium assumption holds only at low velocities.

Setting aside the complexity of the modeling of kinetic reactions, including the kinetics drastically increases the simulation time (5 times or even more). This might be the main reason that the local equilibrium assumption is usually preferred in modeling reactive-transport problems. When the local equilibrium is assumed, the kinetic nature of the minerals can be introduced in the problem through the supersaturation (at low velocities) and undersaturation (at high velocities) of the minerals. To show this, the UTCHEM-IPhreeqc case based on example 11 of PHREEQC is again considered but now calcite is included in the model through the **EQUILIBRIUM_PHASES** keyword (rather than **KINETICS**) of IPhreeqc. Figures 5-49 through 5-52 present the produced ion histories when different saturation indices are assumed for calcite of the system. Produced ion histories for the case with the local equilibrium assumption (i.e., zero saturation index) are shown with circles in the figures. As these figures illustrate, when the saturation index is negative (i.e., undersaturation) produced calcium concentration is lower than the case in which the local equilibrium is assumed. On the other hand, more calcium is produced when the calcite saturation index is positive (i.e., supersaturation).

More details on kinetics versus local equilibrium assumption can be found in Zhu and Anderson (2002).

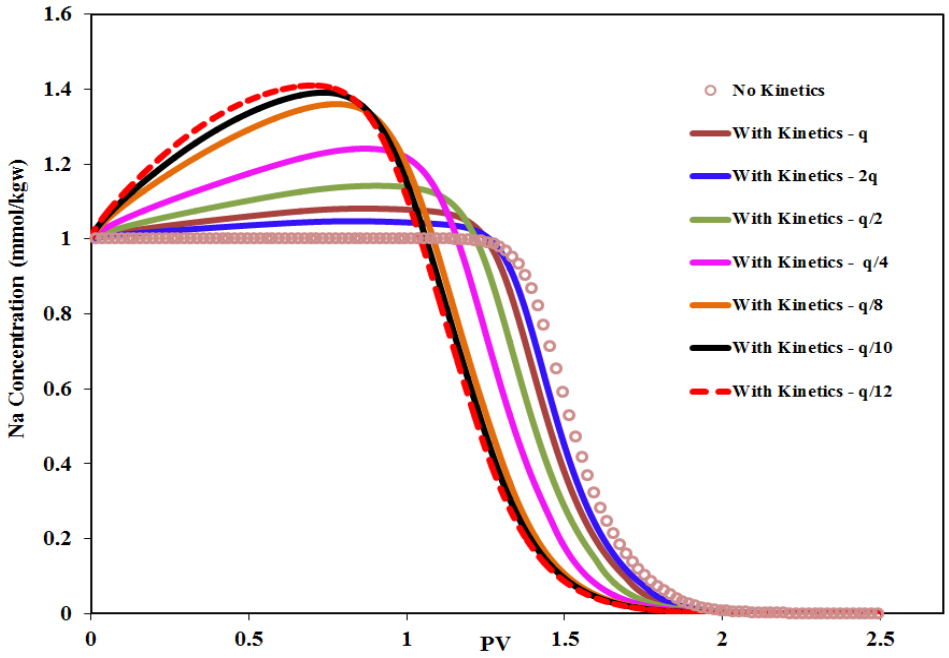

Figure 5-45: Sodium produced ion history for the example 11 of PHREEQC when the calcite kinetic reaction is included at different injection rates.

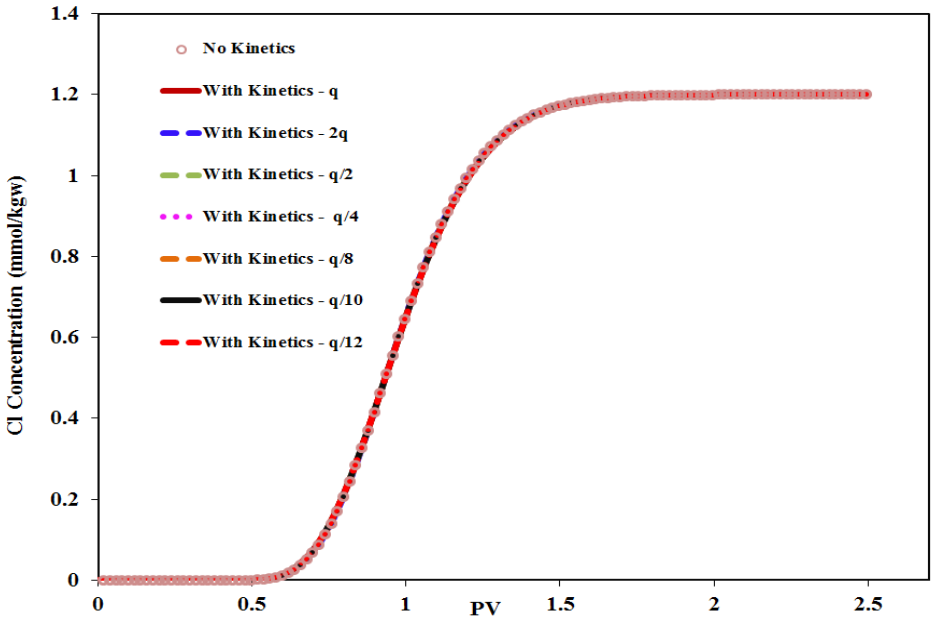

Figure 5-46: Chloride produced ion history for the example 11 of PHREEQC when the calcite kinetic reaction is included at different injection rates.

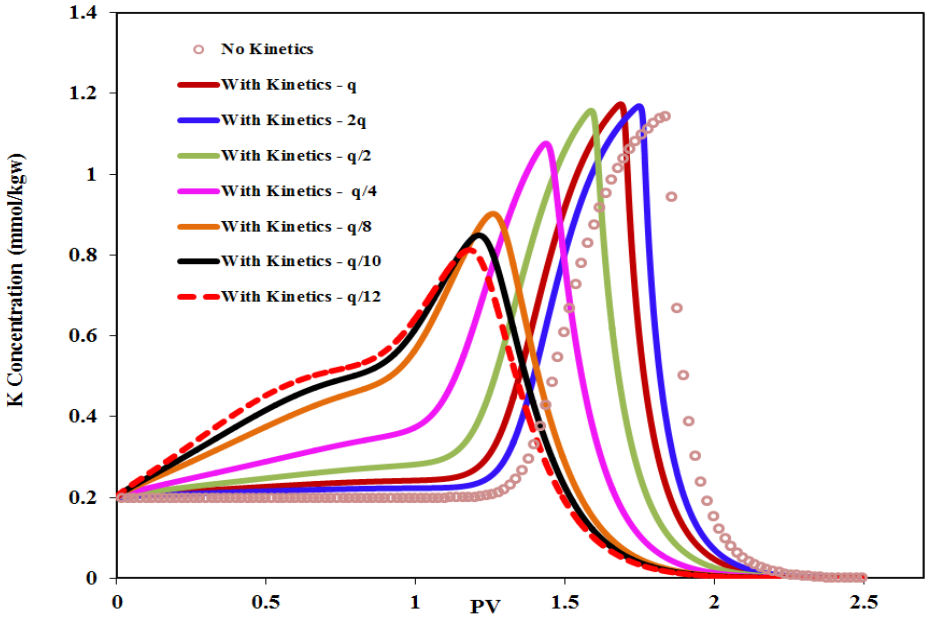

Figure 5-47: Potassium produced ion history for the example 11 of PHREEQC when the calcite kinetic reaction is included at different injection rates.

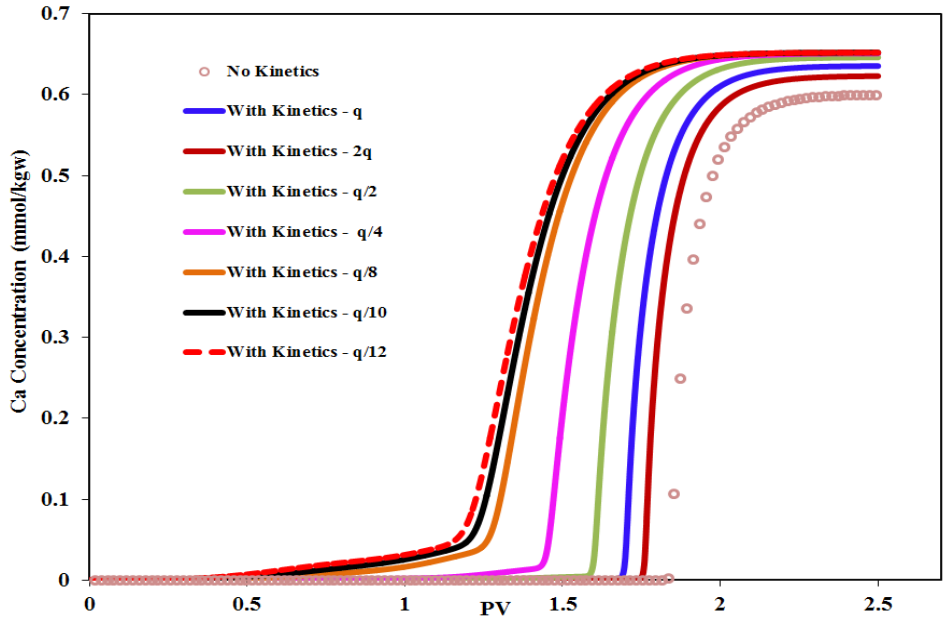

Figure 5-48: Calcium produced ion history for the example 11 of PHREEQC when the calcite kinetic reaction is included at different injection rates.

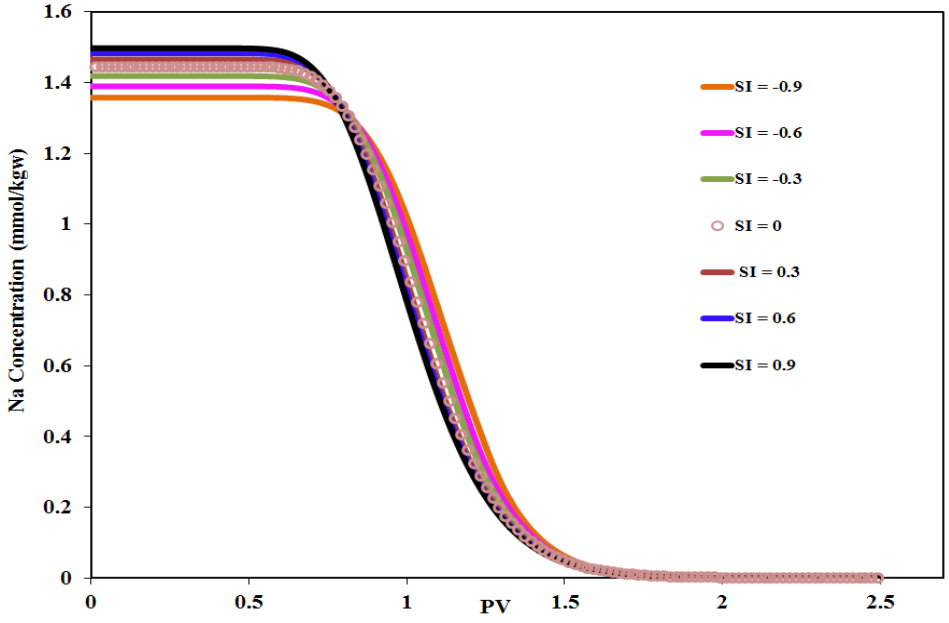

Figure 5-49: Sodium produced ion history for the example 11 of PHREEQC when the calcite mineral is included with different saturation index.

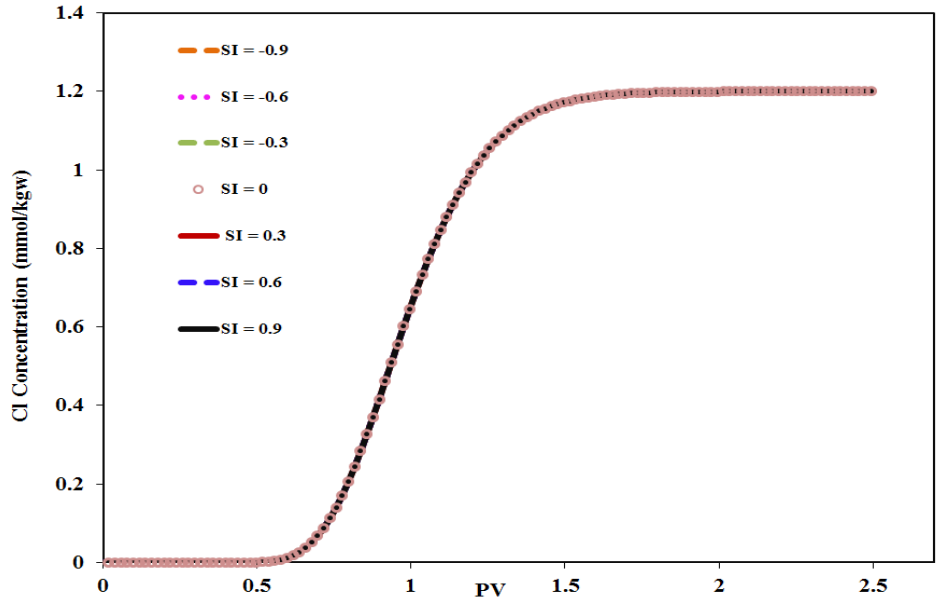

Figure 5-50: Chloride produced ion history for the example 11 of PHREEQC when the calcite mineral is included with different saturation index.

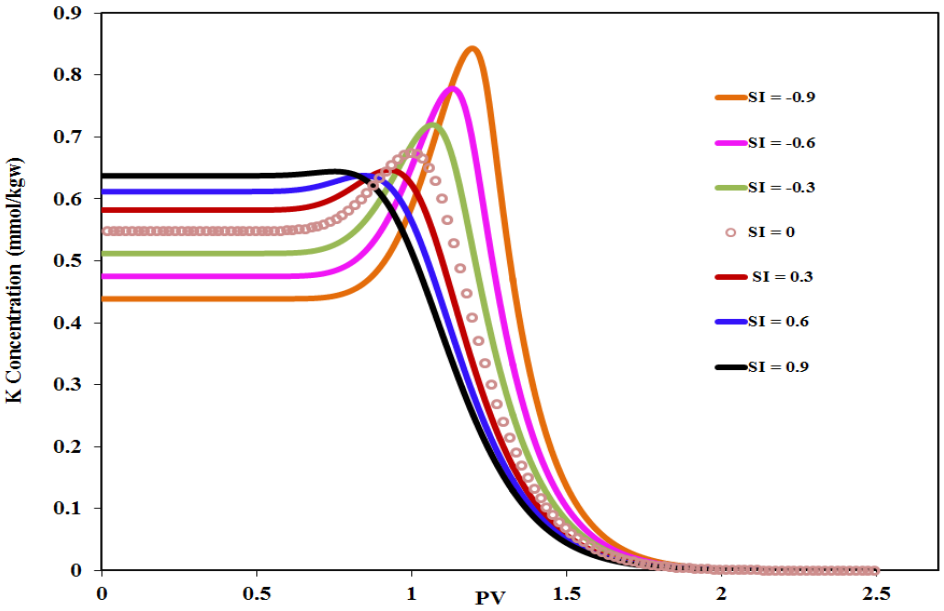

Figure 5-51: Potassium produced ion history for the example 11 of PHREEQC when the calcite mineral is included with different saturation index.

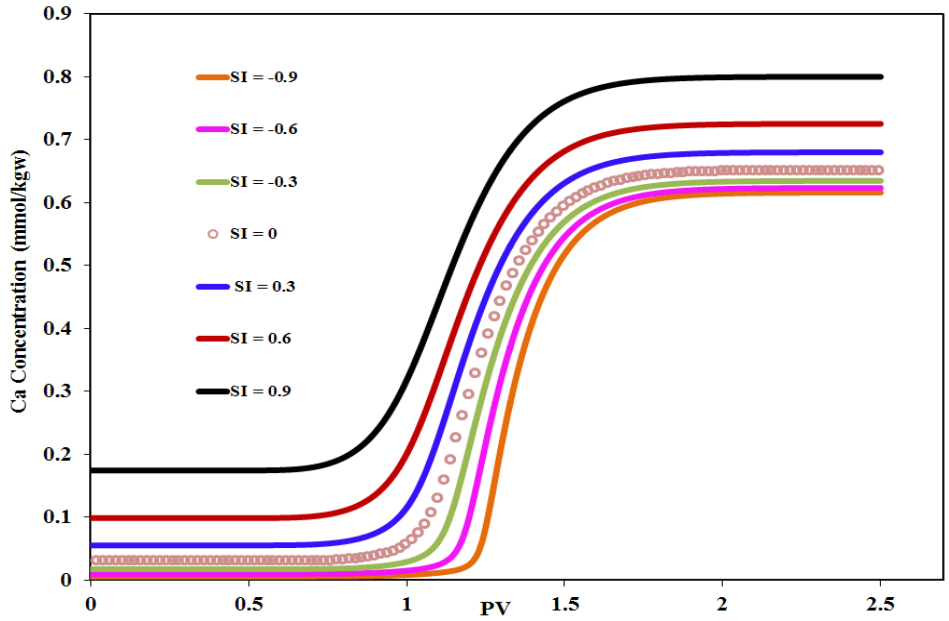

Figure 5-52: Calcium produced ion history for the example 11 of PHREEQC when the calcite mineral is included with different saturation index.

As mentioned earlier in Chapter 2, IPhreeqc provides kinetic, supersaturation and undersaturation capabilities and also geochemical reactions are the temperature- and pressure-dependent. Moreover, there are many discussions in the literature on the importance of surface reactions in carbonate reservoirs (Strand *et al.*, 2006; Austad *et al.*, 2008; Hiorth *et al.*, 2010; Fathi *et al.*, 2012). While EQBATCH lacks the surface complexation modeling, IPhreeqc has the capability to model the surface complexation through different generalized two-layer model (Dzombak and Morel; 1990), a two-layer model that explicitly calculates the diffuse-layer composition (Borkovec and Westall, 1983), and a non-electrostatic surface-complexation model (Davis and Kent, 1990). Details on these surface complexation models are beyond the scope of this work and can be found in Parkhurst and Appelo (1999; 2013).

5.6 ASP COREFLOOD USING NON-ACIDIC CRUDE OIL

ASP flood in non-acidic crude oil reservoirs (crude oils with low acid number) is usually referred to high-pH surfactant/polymer flood. In this process, alkaline agent is injected as sacrificial agent to improve the phase behavior and decrease the surfactant adsorption on the rock.

High-pH surfactant/polymer corefloods were performed at UT chemical flooding laboratory and were simulated by Mohammadi (2008). A coreflood, labeled "BM-07", is modeled in this chapter using UTCHEM-IPhreeqc. Table 5-9 presents detailed ion compositions of the synthetic brine. The ASP slug is injected for 0.15 PV and contains 2 wt% surfactant, 3 wt% ethylene glycol butyl ether (EGBE), 0.85 wt% sodium carbonate, and 2500 ppm AN125 polymer. The ASP slug is then chased with 0.2 PV of polymer drive with polymer concentration of 2200 ppm and 1.5 wt% EGBE and 0.65 wt% sodium carbonate and then followed by 1.5 PV of 1800 ppm polymer. The ASP slug and two polymer slugs are injected along with the synthetic brine into the core. Using the experimental data, Mohammadi (2008) documented surfactant phase behavior, surfactant adsorption, and polymer parameters to model this coreflood using UTCHEM-EQBATCH. The same parameters are considered in our work. Following presents the assumptions and matching parameters used in the model:

- Geochemistry: Contrary to the work of Mohammadi (2008) where only certain ions and reactions are considered, we use "phreeqc.dat" database where about 35 reactions are activated. However, the phreeqc.dat database of PHREEQC is designed for the low-temperature geochemical calculation (Parkhurst and Appelo, 1999). Hence, we assume this database is applicable at 115 ^{o}F at which the coreflood was conducted. Furthermore, we assume the ion-association aqueous

model included in the phreeqc.dat database is sufficient to model the coreflood. A cation exchange site (initially equilibrated with the aqueous solution) is included in the model. The cation exchange capacitance of the exchanger is a tuning parameter. To better match the pH, hydrogen is also assumed to be an existing cation on the exchanger (hydrogen is not an exchanging cation in phreeqc.dat). The equilibrium constant of the hydrogen half-reaction (i.e., $H^+ + X^- \leftrightarrow HX$) is adjusted in our model. Similar to the coreflood AII, no kinetic reaction is included. We also tune the partitioning coefficient of the acid component (K_{wo}) and the equilibrium constant of the acid component in the aqueous phase.

- Relative Permeability Curves: While measured values are applied for the oil and water residual saturations and endpoint relative permeabilities (Mohammadi, 2008); the oil, water, and microemulsion relative permeability exponents and the microemulsion residual saturation and endpoint at low capillary number are the matching parameters. Moreover, linear relative permeabilities are assumed for the three phases at high capillary number (i.e., zero residual saturation and 1.0 for the endpoint and exponent).
- Surfactant and Soap Phase Behavior: Upper (CSEU) and lower effective salinities (CSEL) for Type III; and the equivalent weight of the generated soap are matching parameters.
- Surfactant Adsorption on the Rock Surface: Upper and lower thresholds of the model through which the dependency of surfactant adsorption on the rock surface is defined in UTCHEM are adjusting parameters (6 and 11 are the lower and upper thresholds in the tuned model, respectively).

Table 5-9: Synthetic brine composition (Mohammadi, 2008)

Ion	Concentration (ppm)
Na	900
Ca	20.
Mg	5
K	15
Cl	800
SO_4	18
HCO_3^-	1100
Total dissolved solids	2858

Figures 5-53 through 5-59 present UTCHEM-IPhreeqc (solid lines) and UTCHEM-EQBATCH (dashed lines), modeled by Mohammadi (2008), simulation results against the measured data. Having several capabilities in IPhreeqc, we significantly improve the match for pH, carbonate, and bicarbonate compared with the work of Mohammadi (2008). We believe the main reason for this is introducing more physics to the numerical models by including activities and all possible geochemical reactions.

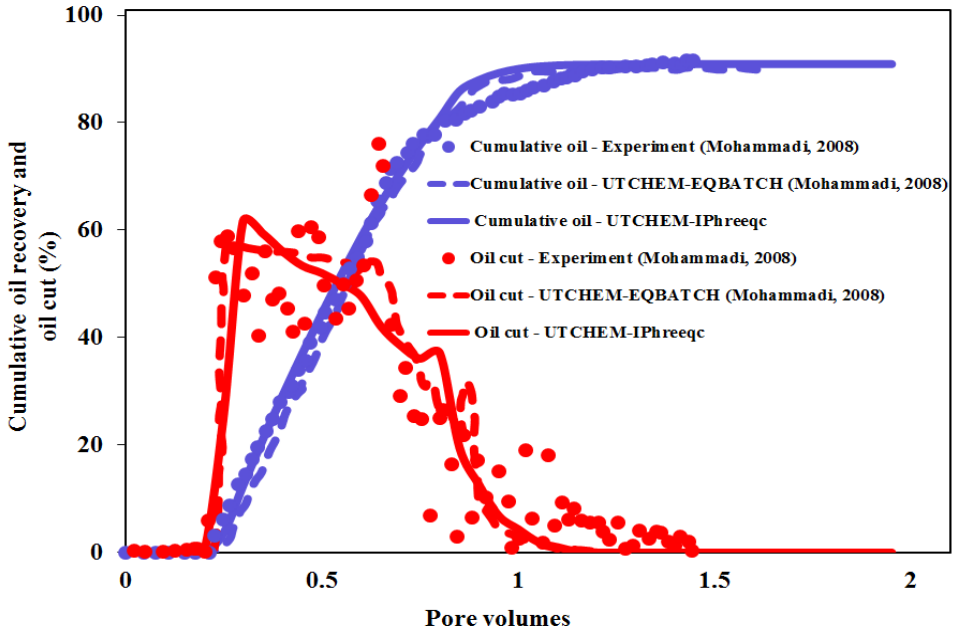

Figure 5-53: Simulation results using UTCHEM-IPhreeqc and UTCHEM-EQBATCH (Mohammadi, 2008) versus measured data for cumulative oil recovery and oil cut.

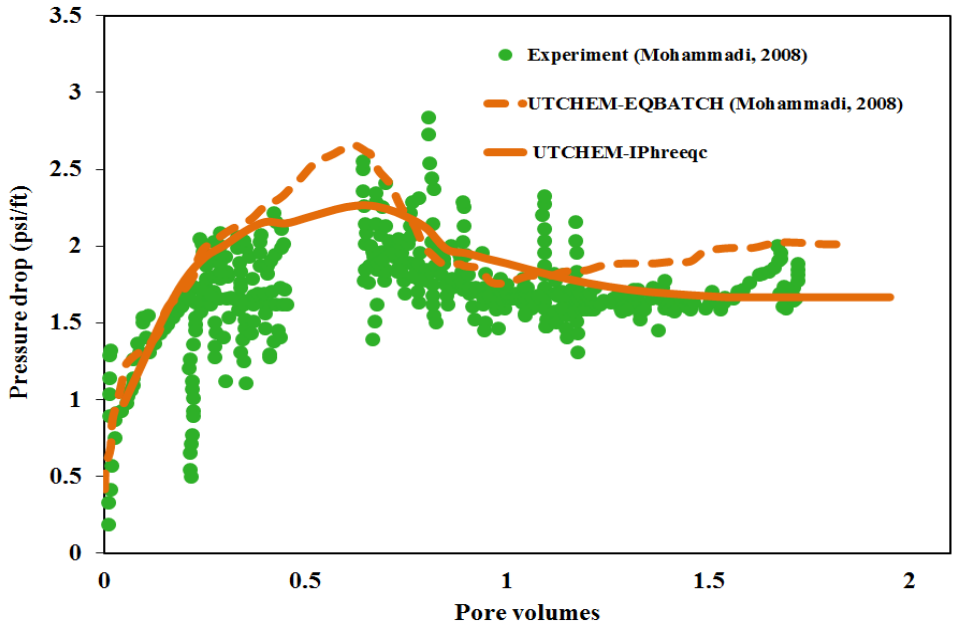

Figure 5-54: Simulation results using UTCHEM-IPhreeqc and UTCHEM-EQBATCH (Mohammadi, 2008) versus measured data for pressure drop.

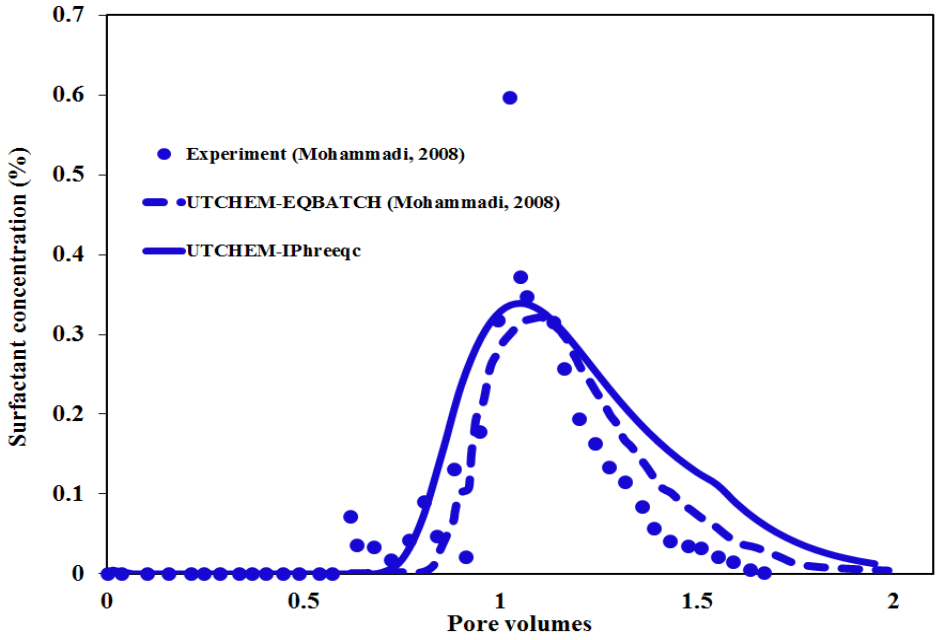

Figure 5-55: Simulation results using UTCHEM-IPhreeqc and UTCHEM-EQBATCH (Mohammadi, 2008) versus measured data for surfactant concentration.

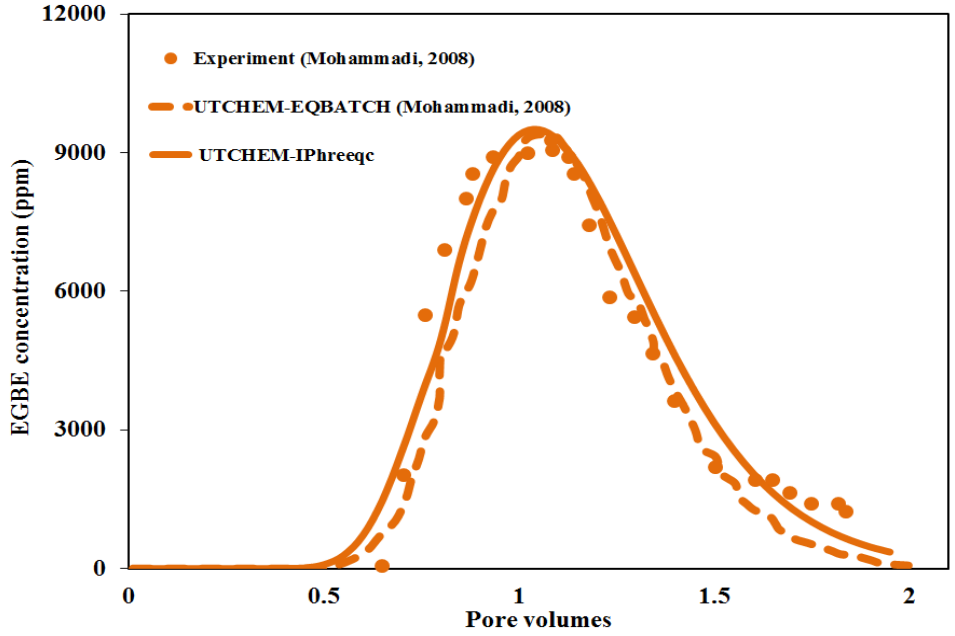

Figure 5-56: Simulation results using UTCHEM-IPhreeqc and UTCHEM-EQBATCH (Mohammadi, 2008) versus measured data for EGBE concentration.

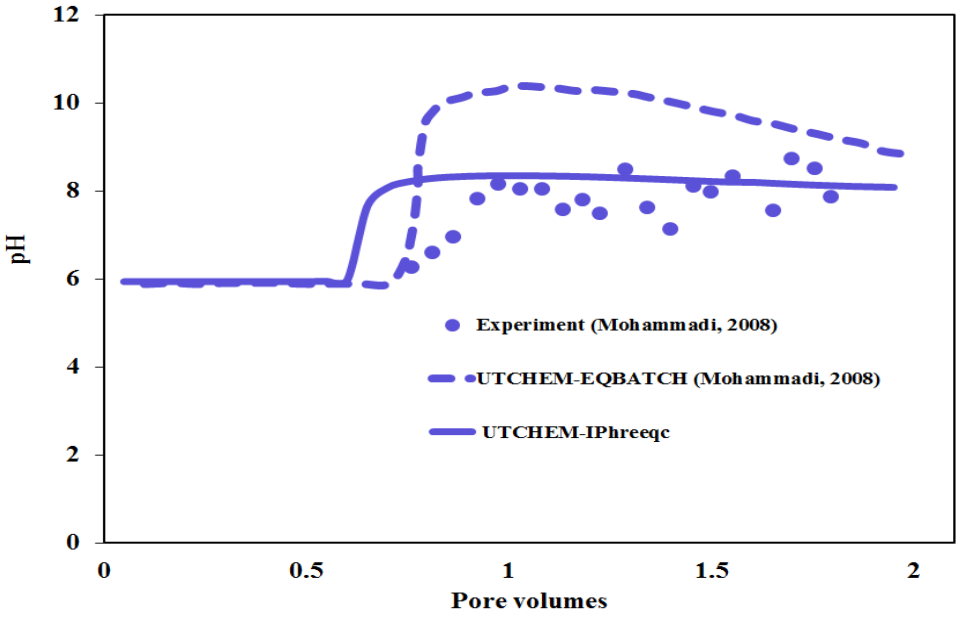

Figure 5-57: Simulation results using UTCHEM-IPhreeqc and UTCHEM-EQBATCH (Mohammadi, 2008) versus measured data for effluent pH.

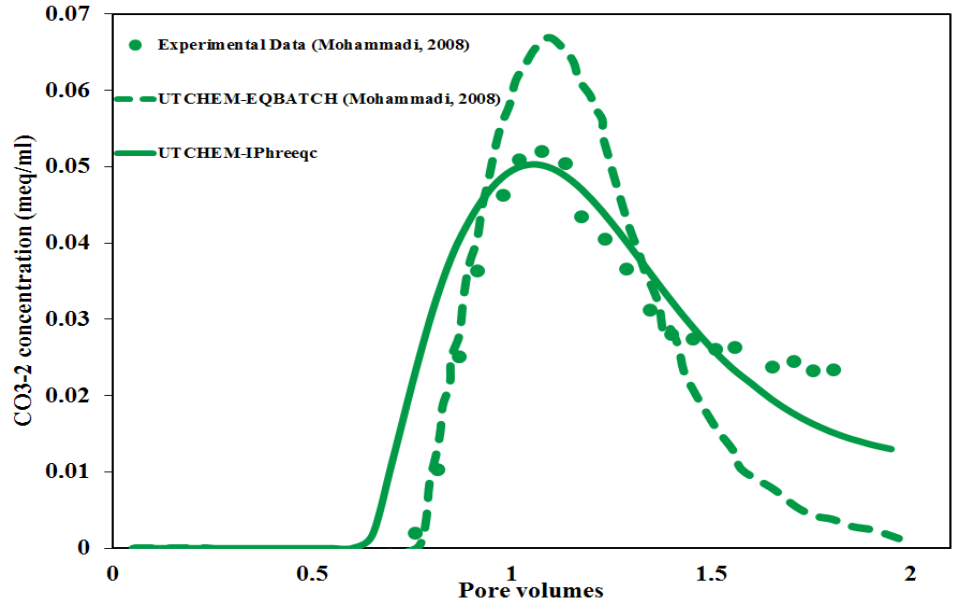

Figure 5-58: Simulation results using UTCHEM-IPhreeqc and UTCHEM-EQBATCH (Mohammadi, 2008) versus measured data for CO_3^{-2}.

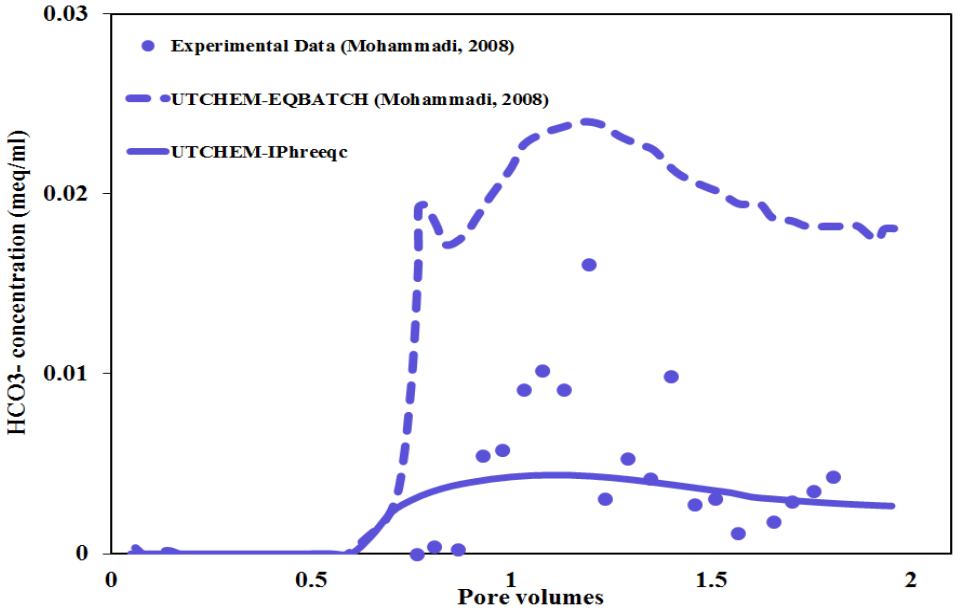

Figure 5-59: Simulation results using UTCHEM-IPhreeqc and UTCHEM-EQBATCH (Mohammadi, 2008) versus measured data for HCO_3^-.

To show how successfully the injected alkaline agent decreased the surfactant adsorption, this case is compared against a case where no alkaline agent is injected. Figures 5-60 and 5-61 present effluent surfactant concentration and the cumulative oil recovery for the cases compared. As we expect, when no alkaline agent is injected, the surfactant adsorption increases and consequently oil recovery decreases.

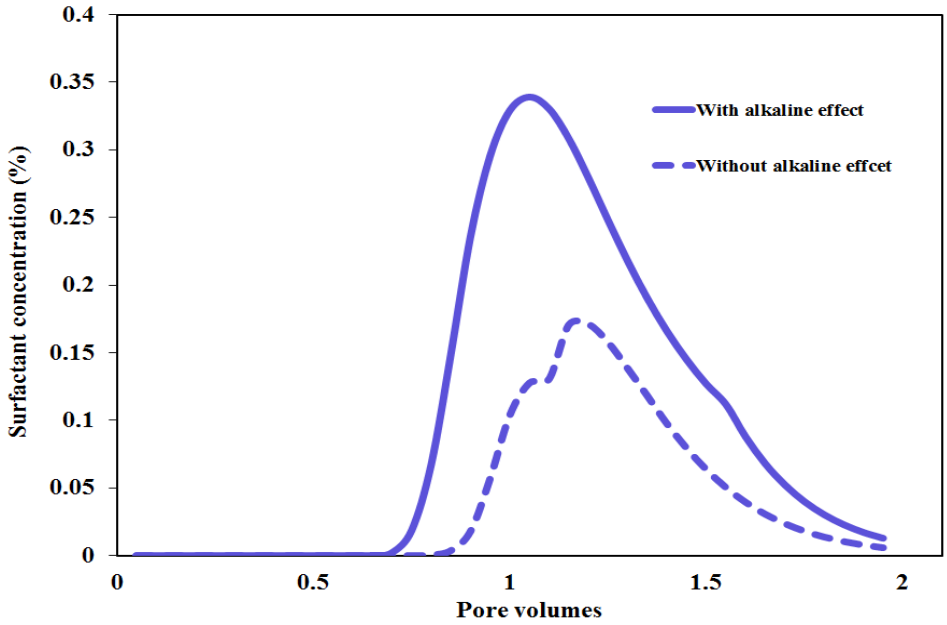

Figure 5-60: The effect of "alkaline agent injection" on surfactant adsorption.

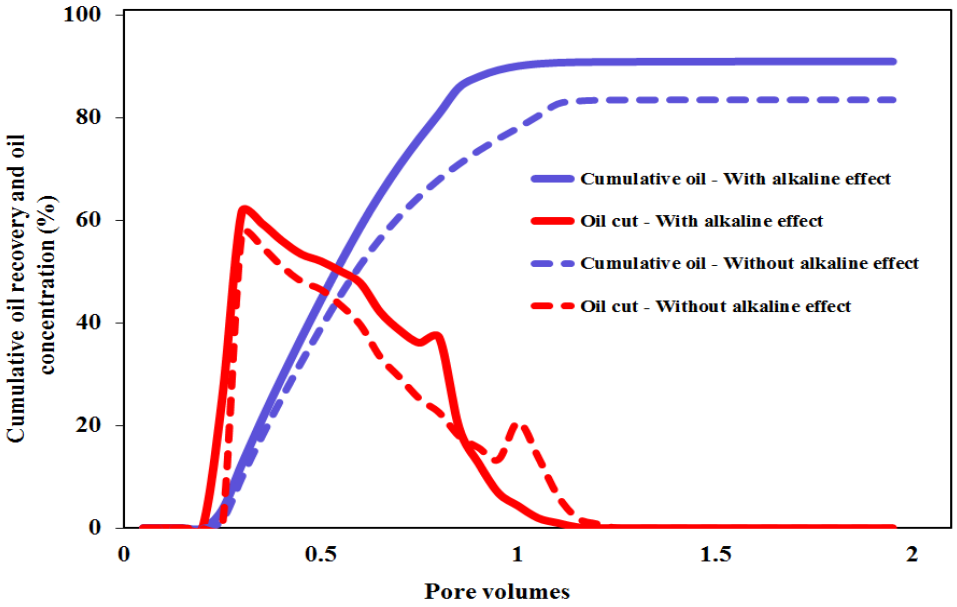

Figure 5-61: The effect of "alkaline agent injection" on cumulative oil recovery and oil cut.

To investigate the performance of this coreflood in a large-scale application, similar design is applied to a real field case with 33×35×16 gridblocks. Out of 18480 gridblocks, 2323 are inactive cells. The permeability/porosity maps are shown in Figures 5-62 through 5-64. This pilot contains 8 production and 3 injection wells. However, 4 injection and 2 production wells are hydraulic wells for conformance. The hydraulic injection wells are injecting water, which is already at equilibrium with the reservoir brine. The pilot of study is a five-spot pattern with 4 injection and 1 production wells (see Figure 5-65). Hydraulic wells are not shown in this figure. Each pilot injection well is injecting at constant flow rate of about 500 bbl/day and the production well is operating with the constant bottomhole pressure of 700 psi. Relative permeabilities and initial oil saturation of the field is used. However, oil; surfactant phase behavior; polymer rheology; initial brine salinity and composition are based on the coreflood results. Prior to the ASP flooding, this field was waterflooded for 13.5 years. 2 wt% surfactant, 3 wt% ethylene glycol butyl ether (EGBE), 0.85 wt% sodium carbonate, and 2500 ppm AN125 polymer is flooded for 125 days. Polymer drive (i.e., 2200 ppm and 1.5 wt% EGBE and 0.65 wt% sodium carbonate) is then injected for 119 days. Rather than injecting the last polymer drive as the design of the coreflood (i.e., 1800 ppm polymer), water is injected for 76 days in the field. The pilot test takes about 320 days.

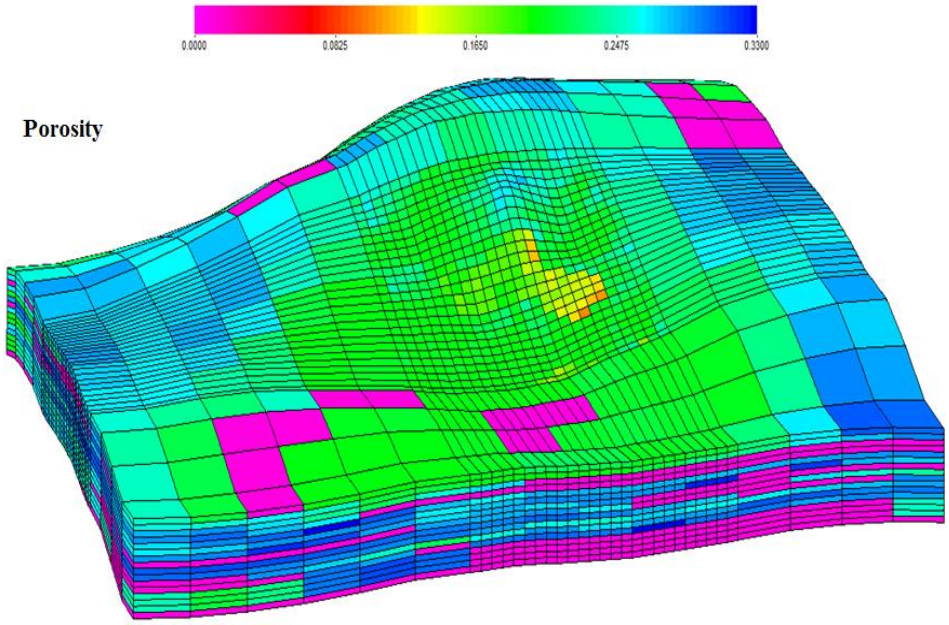

Figure 5-62: Porosity distribution of the field.

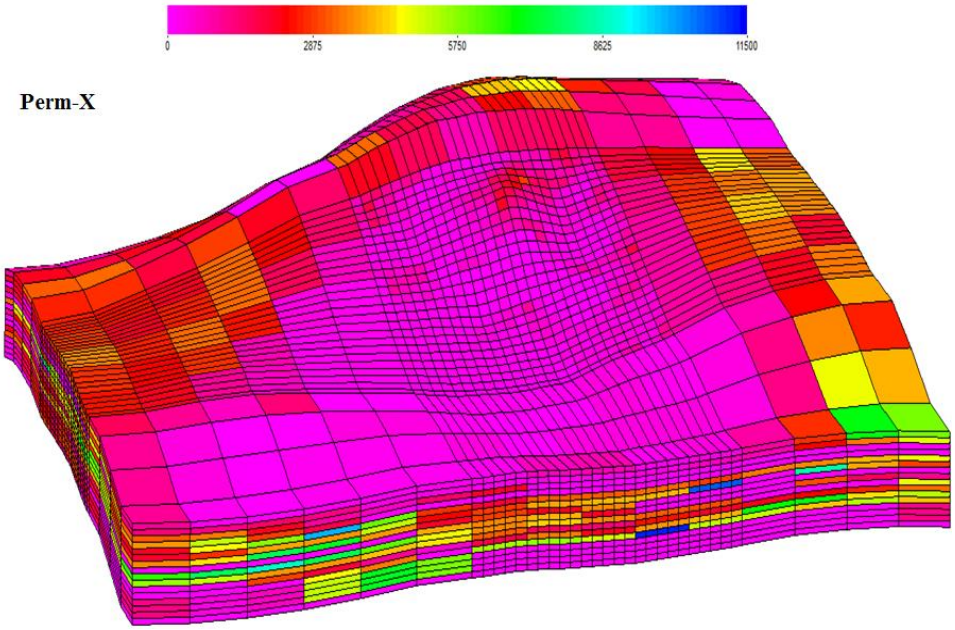

Figure 5-63: Absolute permeability (in md) distribution in *x*- and *y*-direction of the field.

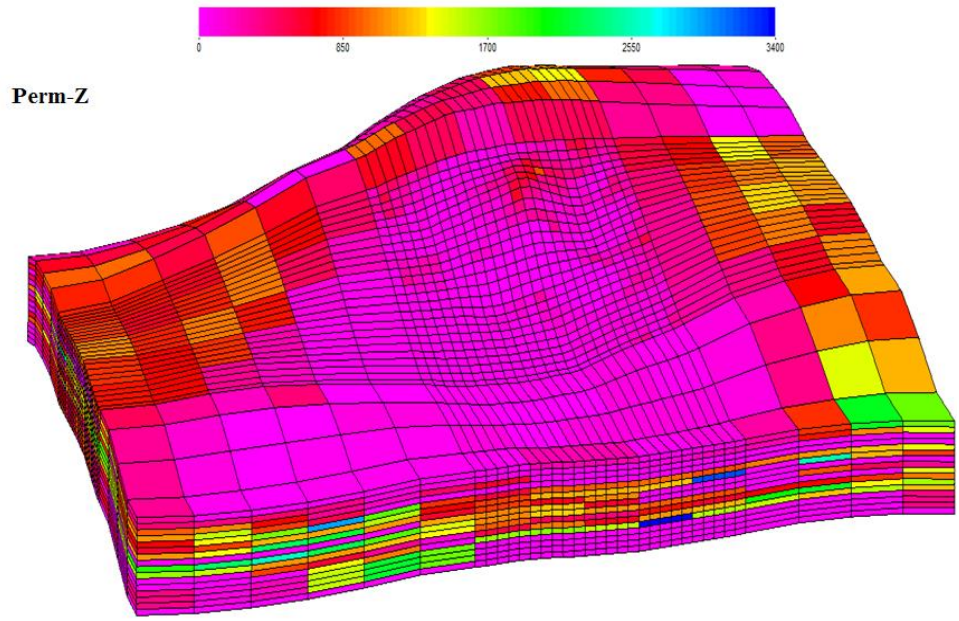

Figure 5-64: Absolute permeability (in md) distribution in *z*-direction of the field.

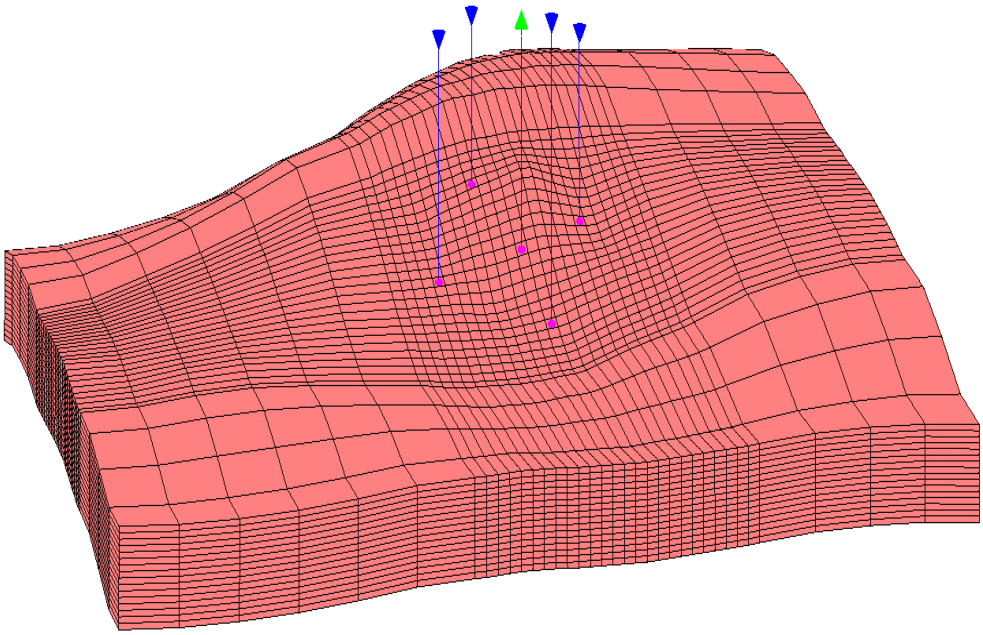

Figure 5-65: A five-spot designed for the ASP flooding in the field (hydraulic wells are not shown).

Figures 5-66 through 5-69 show the simulated oil rate produced from the pilot wells (not the whole field), cumulative oil production produced from the pilot, bottomhole pressure of one of the pilot injection well, and pH of the produced aqueous solution using both UTCHEM-IPhreeqc and UTCHEM-EQBATCH. Simulation results for 320 days waterflooding are also included in these figures for comparison. Although the simulated cumulative oil recoveries are different between UTCHEM-IPhreeqc and UTCHEM-EQBATCH, both tools show significant increase in oil recovery for ASP. UTCHEM-IPhreeqc simulation results appear to be more accurate because more comprehensive geochemistry is applied in this integrated tool compare with the simplified EQBATCH geochemistry module in the original UTCHEM. The simulated produced pH history confirms the difference observed between UTCHEM-IPhreeqc and UTCHEM-EQBATCH in modeling the coreflood. Figures 5-70 through 5-72 show the maps of the initial oil saturation; oil saturation before the ASP flooding (i.e., after 13.5 years of water injection); and oil saturation after ASP flooding for the layer 9. The images indicate a successfully ASP with significant reduction in the residual oil saturation to nearly zero.

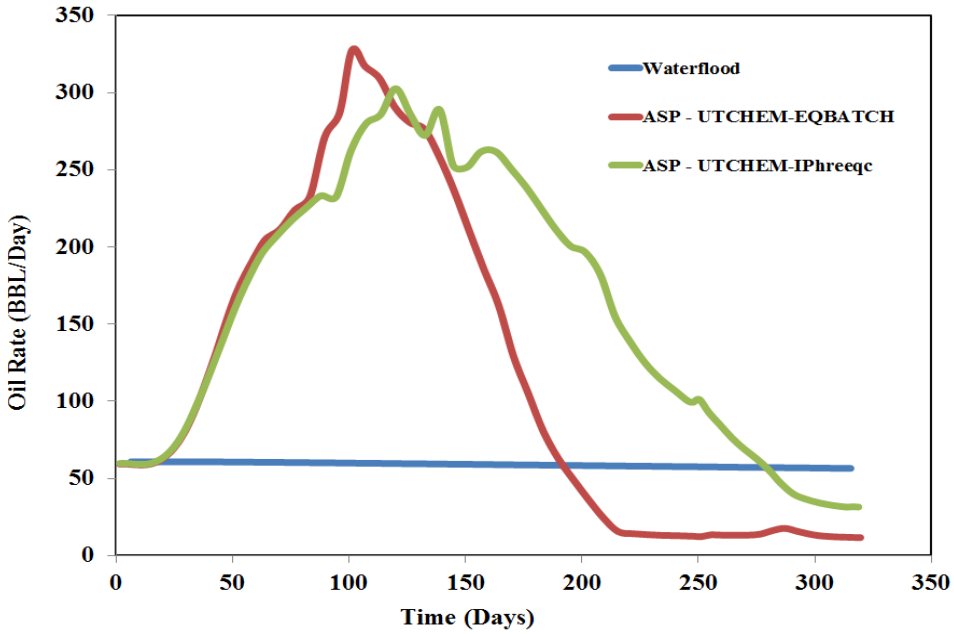

Figure 5-66: UTCHEM-IPhreeqc and UTCHEM-EQBATCH simulation results for the oil rate from the pilot.

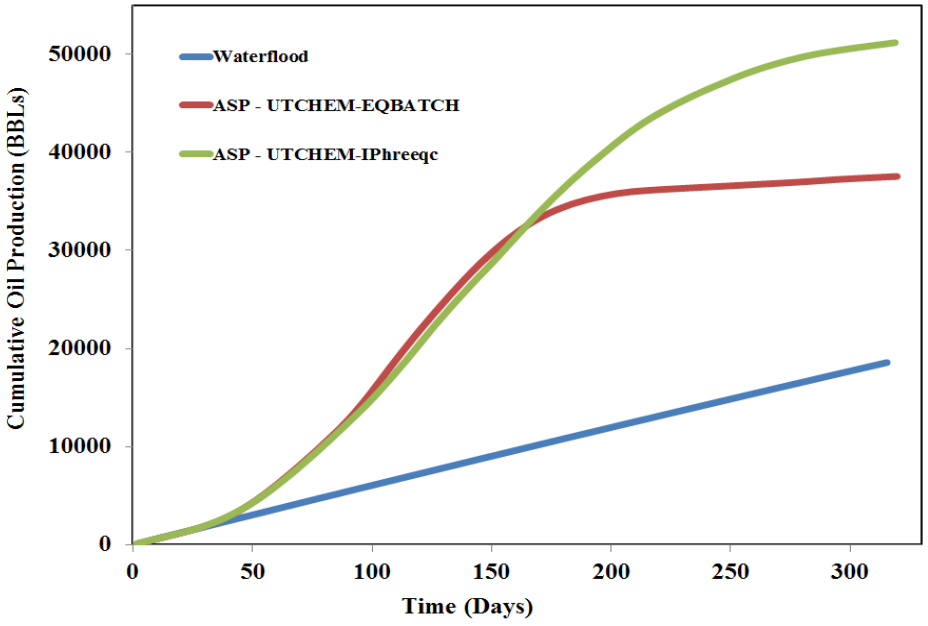

Figure 5-67: UTCHEM-IPhreeqc and UTCHEM-EQBATCH simulation results for the cumulative oil recovery from the pilot.

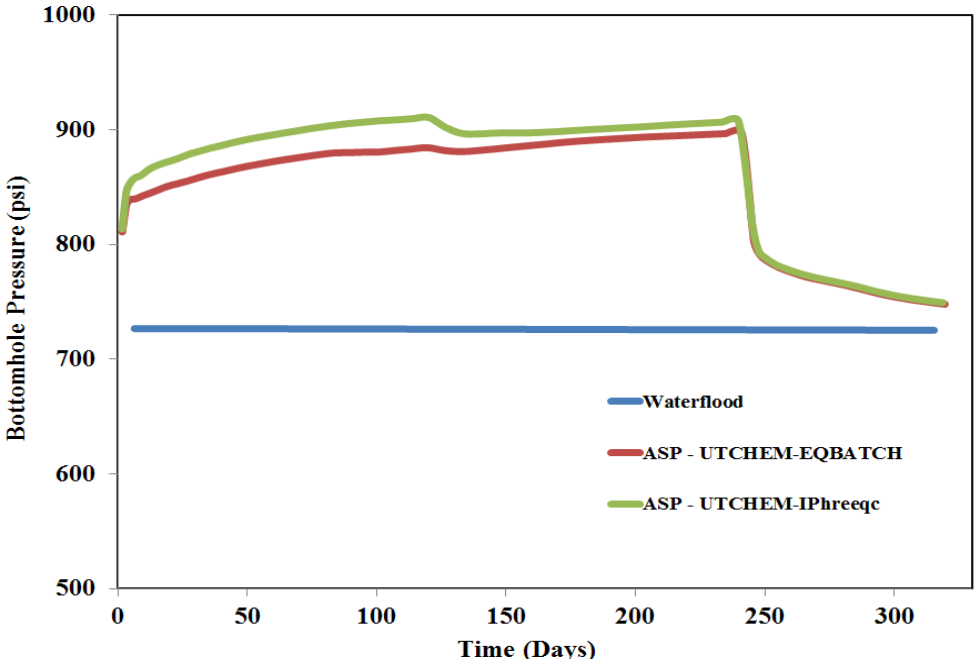

Figure 5-68: UTCHEM-IPhreeqc and UTCHEM-EQBATCH simulation results for bottomhole pressure of one of injection well of the pilot.

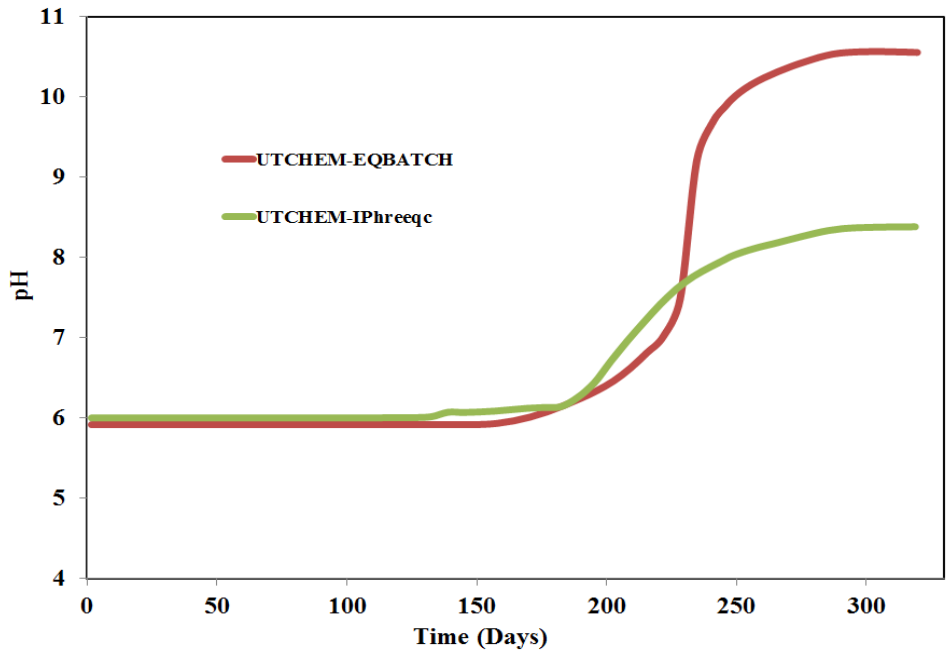

Figure 5-69: pH of the produced water.

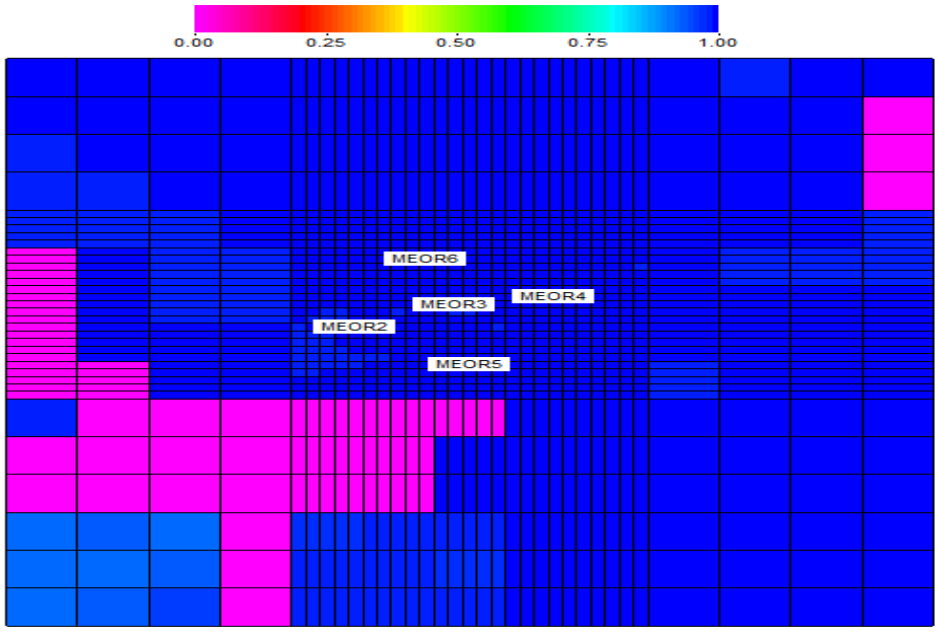

Figure 5-70: Oil saturation map of layer 9th before waterflooding.

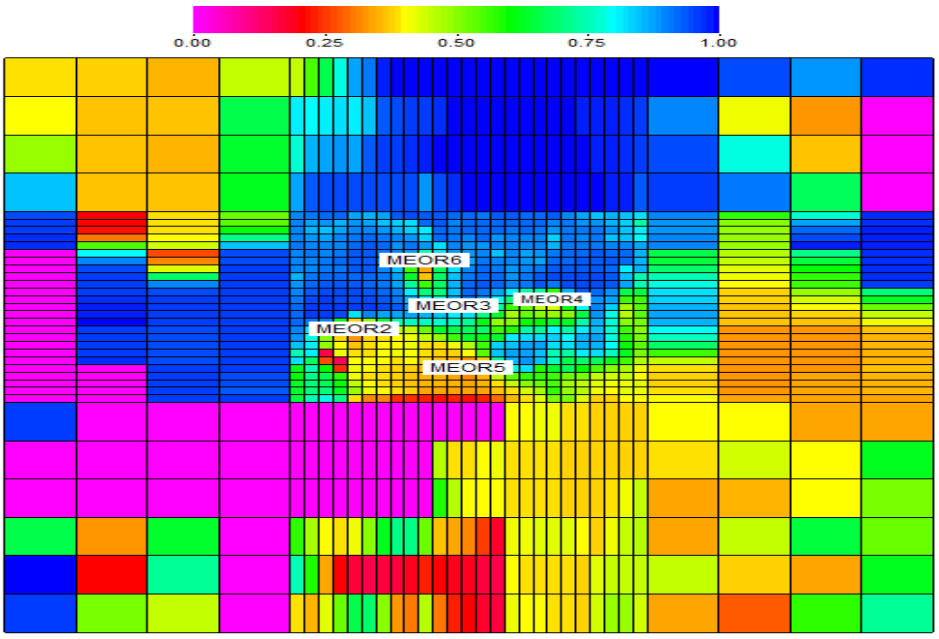

Figure 5-71: Oil saturation map of layer 9th after 13.5 years of waterflooding.

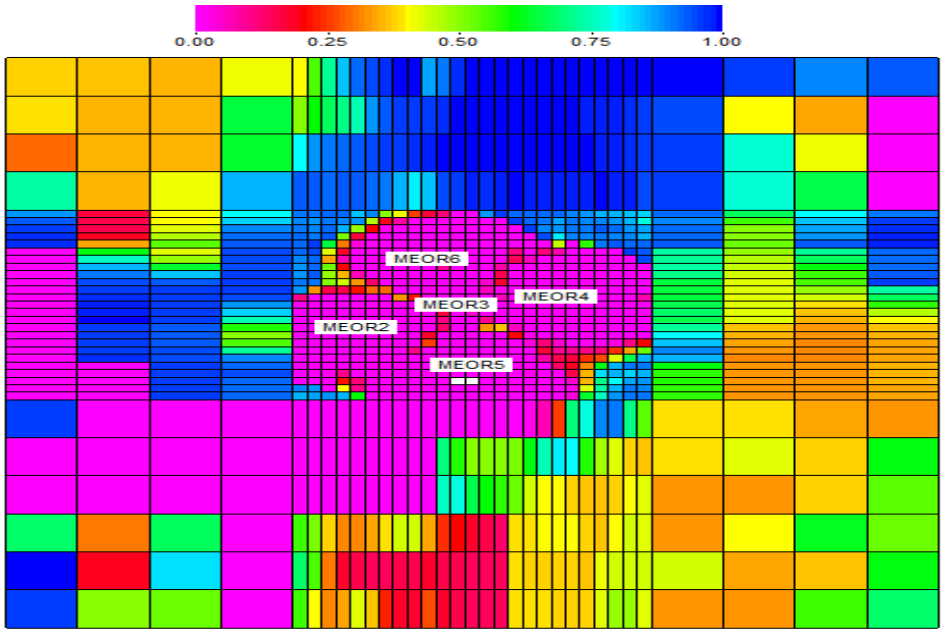

Figure 5-72: Oil saturation map of layer 9th after ASP flooding.

It is worth noting that when scaling up an ASP coreflood to a field application, care must be taken to properly include the effect of the solution and free gas on the surfactant and soap phase behavior as well as on the geochemical reactions. We neglected the effect of gas in the field case studied. The effect of the gas on performance of the ASP flooding has been discussed in the work of Farajzadeh *et al.* (2013) and Jang *et al.* (2014). It should be also noted that no kinetics of the minerals is included in the model when scaling up the coreflood to the field. The significance of kinetics of minerals on the performance of ASP flooding is the scope of our future work.

5.7 ACP COREFLOOD USING ACIDIC CRUDE OIL

ACP flood, if applicable, is a cost efficient alternate process to ASP flooding (Weerasooriya and Pope, 2011; Fortenberry, 2013; Fortenberry *et al.*, 2013; Taghavifar, 2014). In this process no synthetic surfactant is injected and the alkaline agent-oil

reaction is intended to provide adequate amount of surfactant in-situ. Polymer is responsible for the mobility control and co-solvent is added to the slug to make the in-situ soap compatible with the polymer injected and also to reduce the microemulsion viscosity (Xu *et al.,* 2013; Fortenberry *et al.,* 2013). It seems that this process is applicable in high acidic crude oil with relatively fresh water.

Xu (2012) and Xu *et al*. (2013) applied the simplified ASP module of UTCHEM (Delshad *et al.,* 2013) and successfully simulated two ACP corefloods (labeled "PCN-1" and "PCN-4"). We use UTCHEM-IPhreeqc ("phreeqc.dat" database is used) and model the "PCN-1" coreflood reported and simulated by Xu *et al*. (2013). The core is initially at the residual oil saturation of 0.443. Water and oil viscosities at the reservoir conditions are 0.53 and 170 cp, respectively. The ACP slug contains 1.5% Huntsmann n-Butyl-5EO as co-solvent; 6,000 ppm Na_2CO_3; and 2750 ppm Flopaam 3630S polymer. ACP slug is injected for 0.5 PV and then followed by 1.4 PV of polymer drive with the composition of 2250 ppm Flopaam 3630S. Synthetic brine (PCNSSB) with total dissolved solids of 934 ppm is initially in the core (see Table 5-10). More details about this coreflood (e.g., activity map, polymer, and microemulsion properties, etc.) can be found in Xu *et al.* (2013). Assumptions and matching parameters considered to model the coreflood are listed below (UTCHEM-IPhreeqc input files are provided in Appendix H):

- Geochemistry: We use the phreeqc.dat database to model the PCN-1 coreflood and all the assumptions addressed for the coreflood BM-07 are applied here. Also, similar to the BM-07 coreflood, an exchange site is included in the model; and the hydrogen exchange reaction is considered.
- Soap Phase Behavior: The co-solvent and soap phase behavior parameters; and polymer and microemulsion viscosity and adsorption parameters are matching

parameters.

- Relative Permeability Curves: The oil, water, and microemulsion relative permeability exponents and the microemulsion residual saturation and endpoint at low capillary number are matching parameters and linear relative permeabilities are assumed for the three phases at high capillary number.

Table 5-10: Composition of synthetic brine (PCNSSB) (Xu, 2012)

Ion	Concentration (ppm)
Potassium	11.59
Sodium	300.00
Magnesium	0
Calcium	0
Chlorine	140.81
Sulfate	310.41
Bicarbonate	176.95
Total Dissolved Solid	939.77

Figures 5-73 through 5-76 compare UTCHEM-IPhreeqc (solid lines) and UTCHEM-simplified ASP module (dashed lines), modeled by Xu *et al.* (2013), simulation results against measured oil recovery, oil cut, pressure drop, average oil saturation in the core, and the effluent pH history. It is worth noting that the simulated pH for the simplified ASP module has not been reported by Xu *et al.* (2013) and modeled in the current work using the provided input file. Through tuning the microemulsion viscosity parameters in UTCHEM-IPhreeqc, we significantly improved the match for the pressure drop and to some extent the effluent pH compared with the work of Xu (2012) and Xu *et al*. (2013). The profile of total soap concentration (simulated using UTCHEM-IPhreeqc) at 0.5 PV is shown in Figure 5-77.

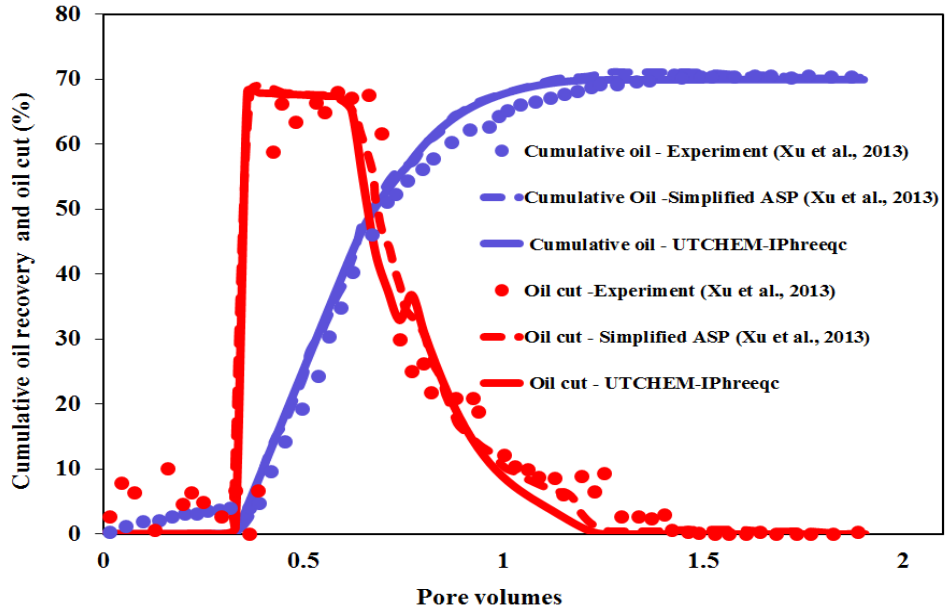

Figure 5-73: Simulation results using UTCHEM-IPhreeqc and UTCHEM-simplified ASP module (Xu *et al.*, 2013) versus measured data for cumulative oil recovery and oil cut of the ACP experiment.

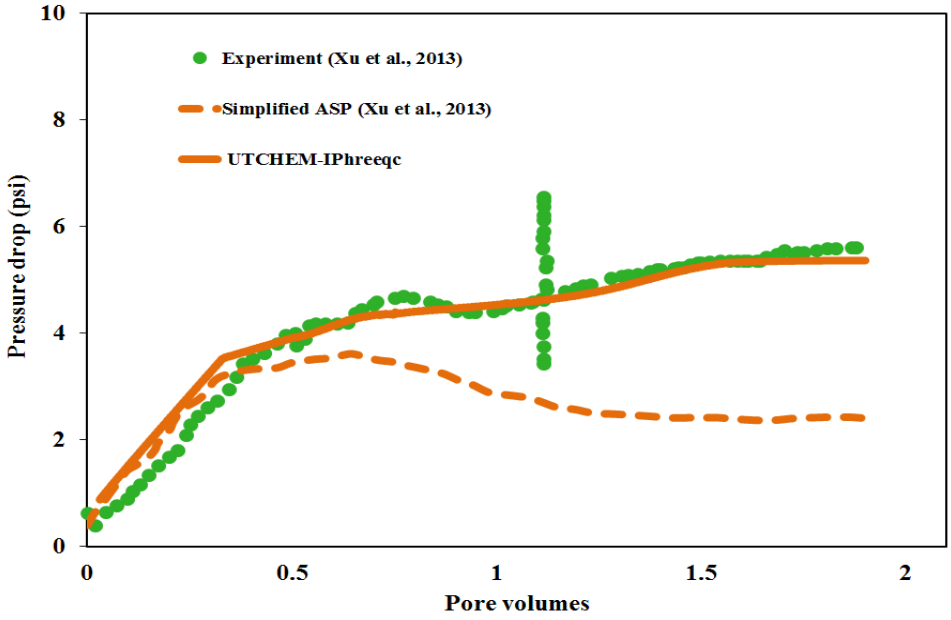

Figure 5-74: Simulation results using UTCHEM-IPhreeqc and UTCHEM simplified ASP module (Xu *et al.*, 2013) versus measured data for pressure drop of the ACP experiment.

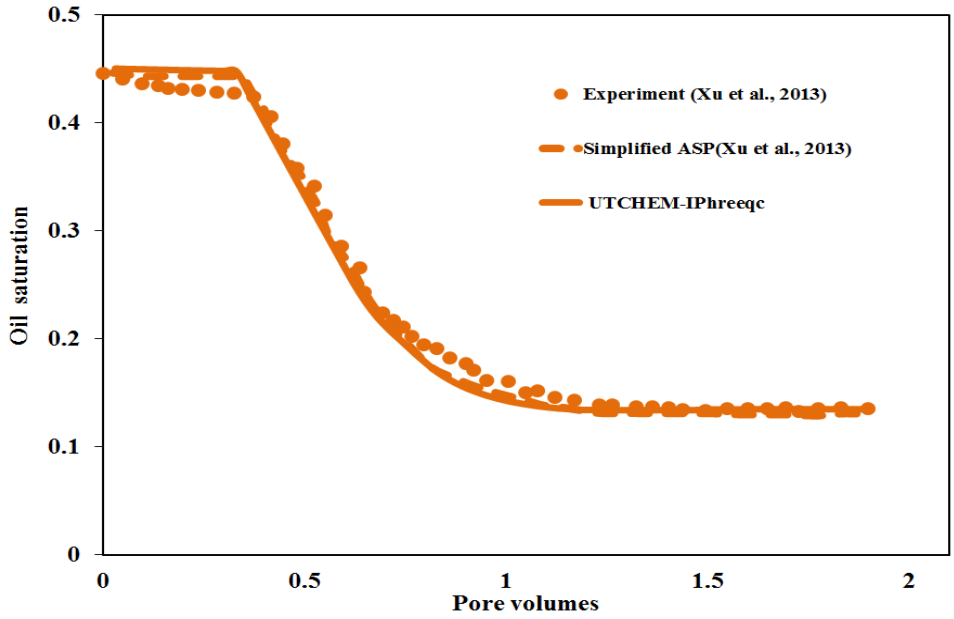

Figure 5-75: Simulation results using UTCHEM-IPhreeqc and UTCHEM simplified ASP module (Xu *et al.*, 2013) versus measured data for oil saturation of the ACP experiment.

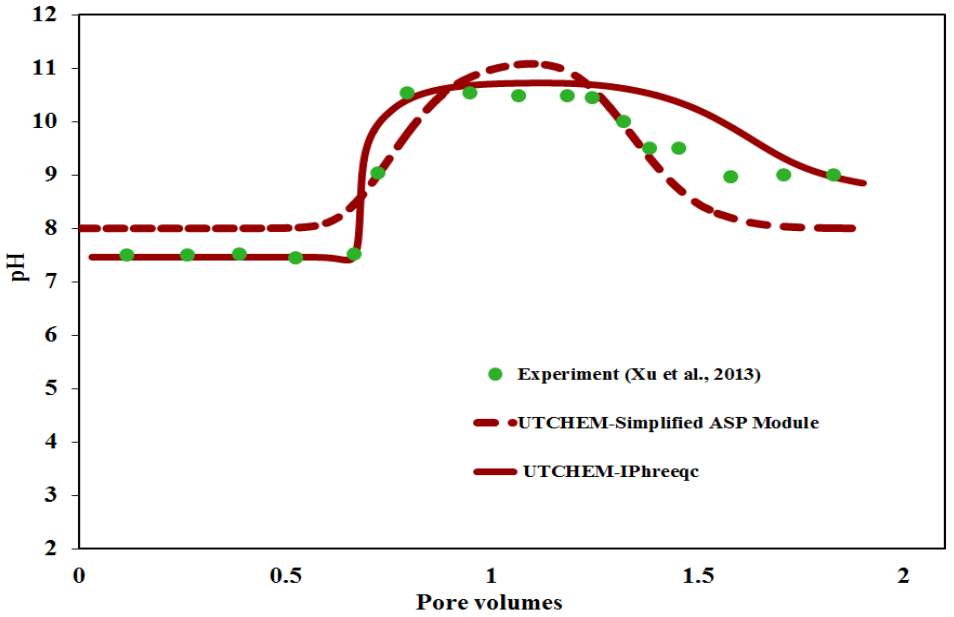

Figure 5-76: Simulation results using UTCHEM-IPhreeqc and UTCHEM simplified ASP module versus measured data for effluent pH for the ACP experiment. (pH for the simplified ASP module was modeled in the current work).

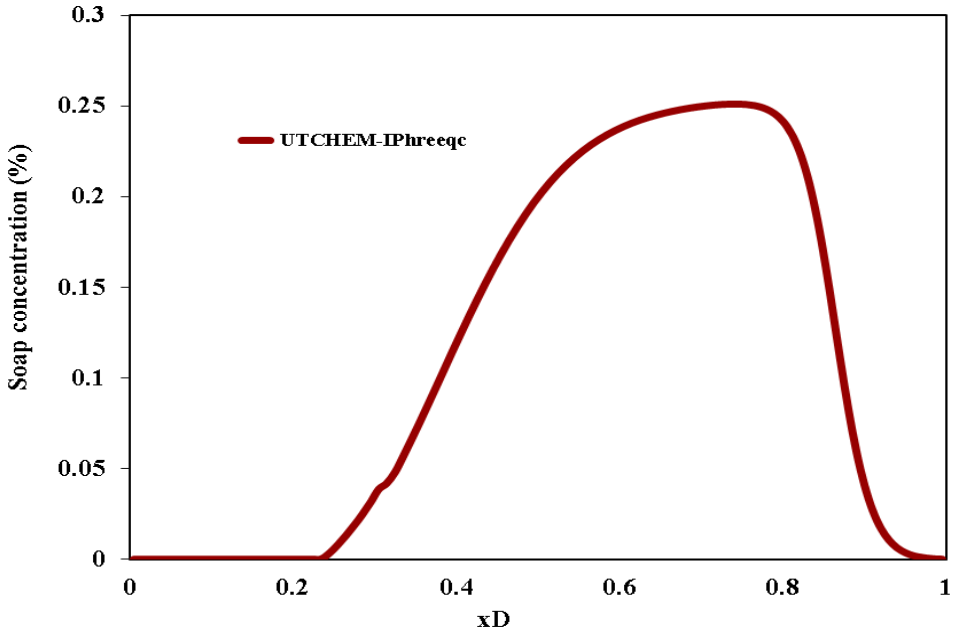

Figure 5-77: Soap total concentration profile at 0.5 PV.

5.8 PROS AND CONS OF UTCHEM-IPHREEQC

Assumptions made in developing EQBATCH are not always valid. For example, the ideal solution assumption is not valid unless the water salinity is low. This makes EQBATCH applicable to limited conditions. EQBATCH is not robust and has numerical convergence problems for some simulation case studies. This geochemical module is limited to modeling aqueous, solid (mineral), and exchange (micelles and rock) reactions. The original intention was for modeling ASP floods with some limited reactions that may have significant impact on the process. The module is not connected to a geochemical database and the users need to set up the input which can be tedious. On the other hand, the full capabilities of IPhreeqc, discussed earlier in this chapter and Chapter 2, (Charlton and Parkhurst, 2011) are functional in UTCHEM-IPhreeqc. Compared to UTCHEM-EQBATCH, UTCHEM-IPhreeqc is robust and user-friendly to setup the initial and injection geochemical states. Geochemical reactions are coupled and highly nonlinear.

Iterative methods like the Newton-Raphson method is used to find the solution to this set of nonlinear equations (i.e., EQBATCH). Two problems should be noted when the Newton-Raphson method is used for chemical equilibria. First, for this method to converge the initial guess values must be sufficiently close to the equilibrium values; second, if the chemical reactions for a set of phases are not linearly independent, this method may encounter with the singularity in the matrix (Parkhurst and Appelo, 1999). Both of these problems are frequently occurring in EQBATCH. To avoid the occurrence of the singular matrix, IPhreeqc/PHREEQC applies an optimization technique proposed by Barrodale and Roberts (1980) based on modification of the simplex linear programming algorithm. This optimization technique also provides the opportunity for IPhreeqc/PHREEQC to add inequality constraints of the solid phases to the problem (Parkhurst and Appelo, 1999). Moreover, while EQBATCH always uses the aqueous concentrations of the previous time-step as the initial guesses, PHREEQC applied rigorous strategies in selecting the initial estimates. More details on how IPhreeqc/PHREEQC handles the numerical convergence are well documented in Parkhurst and Appelo (1999; 2013). Similar to UTCOMP-IPhreeqc (described in Chapter 2), the way by which a reactive-transport problem is designed in UTCHEM-IPhreeqc has been tried to be very close to PHAST, the USGS groundwater simulator (Parkhurst *et al.*, 2010). In UTCHEM-IPhreeqc, transport parameters, thermodynamic database, and the initial geochemical states of gridblocks are defined through individual input files which are respectively equivalent to "*prefix*.trans.dat", "phast.dat", and "*prefix*.chem.dat" files in PHAST.

Although the algorithm applied to couple IPhreeqc with UTCHEM is efficient (see Charlton and Parkhurst, 2011; Muller *et al.*, 2011), UTCHEM-IPhreeqc normally

will require longer CPU times and larger amounts of computer memory than UTCHEM-EQBATCH. For cases studied, the increased computational time using UTCHEM-IPhreeqc compare with UTCHEM-EQBATCH per time step and for the total simulation time ranges from a factor of 1.0 to 2.9 and 1.5 to 8.9, respectively. The CPU time required to model a reactive-transport model using UTCHEM-IPhreeqc depends on the number of gridblocks; number of aqueous species (this was not observed in MPRS-PHREEQC (Wei, 2012)); number of reactions and the ion-association aqueous model applied or in other words the database used for the simulation (e.g., Table 5-11 shows the CPU time when different databases used to produce the results presented in Figures 5-39 and 5-40); the initial gridblock conditions (e.g., kinetics significantly slows down the simulation, as it has been also reported for MPRS-PHREEQC (Wei, 2012)); and the injected fluid composition. It appears that the difference between the total simulation time of UTCHEM-IPhreeqc and UTCHEM-EQBATCH is more pronounced for large cases (the more gridblocks the larger difference). For the field case studied in this work (with 16157 active gridblocks), UTCHEM-EQBATCH is about 36 times faster than UTCHEM-IPhreeqc (3.9 hrs versus 143.2 hrs, see Table 5-12). However, it should be noted that for the field case the number of geochemical reactions (in other words, number of equations in terms of geochemistry that is solved per time-step) in UTCHEM-IPhreeqc (i.e., 35 reactions) and UTCHEM-EQBATCH (i.e., 9 reactions) is different. As shown in Table 5-11, the computational time to model a reactive-transport model highly depends on the number of active reactions and the ion-association aqueous model applied (the phreeqc.dat database of PHREEQC was used for the field case). The observed increased in the CPU time of UTCHEM-IPhreeqc (in which the coupling approach is close to hard coupling) is consistent with that of PHAST of the USGS (Parkhurst *et al.*, 2010) and

PHT3D (Appelo and Rolle, 2010) but not consistent with the claim reported for MPRS-PHREEQC in which geochemical calculation, through calling PHREEQC, slows down the simulation by less than three times in a 3D case with 29934 active gridblocks when a single processor is used (Wei, 2012). In PHAST, PHREEQC has been hard coupled with HST3D (i.e., a transport simulator) (Parkhurst *et al.*, 2010) and in PHT3D, PHREEQC is hard coupled with MODFLOW-2000 and MT3DMS, as the transport simulator, (Appelo and Rolle, 2010). PHAST and PHT3D have been designed for groundwater modeling.

The difference between the increase in CPU time per time step and for the total simulation time in UTCHEM-IPhreeqc reveals the fact that "time-step" does not build up in UTCHEM-IPhreeqc as it increases in UTCHEM-EQBATCH. Our investigations show that frequently, charge balance is the controlling element for the time step size. It is reminded that charge balance and total moles of hydrogen and oxygen must be transported in UTCHEM-IPhreeqc (Charlton and Parkhurst, 2011; Korrani *et al.*, 2013; Korrani *et al.*, 2014c). For the time being, charge balance and total hydrogen and oxygen affect the time-step through the same automatic time-step algorithm used for other geochemical species. Literature shows other strategies that can be applied to diminish the CPU time involved in modeling reactive-transport problems (De Lucia and Kuhn, 2013).

We applied Message Passing Interface (MPI) (Barney, 2009) and parallelized the geochemistry module of UTCHEM-IPhreeqc to compensate for the increase in the CPU time. Figures 5-78 and 5-79 respectively present the total simulation time and speedup using different number of processors to simulate the same field case presented earlier in this chapter (corresponding CPU time values are shown in Table 5-12). Simulations were run on Lonestar-cluster of Texas Advanced Computing Center (TACC) at The University of Texas at Austin. TACC characteristics were previously described in Chapter 2. As

Figure 5-79 shows, the speedup is; super-linear when number of processors is less than 16; is linear when the number of processor is equal to 16; and sub-linear afterwards. The same trend was observed for other large cases studied in Chapter 2 on UTCOMP-IPhreeqc (particularly when the number of gridblocks is above 10,000). The maximum time limit for the jobs submitted to TACC is 24 hours. Hence, for the cases when 1, 2, and 4 processors is used the total simulation time beyond 24 hours is estimated using the remaining number of time steps (which can be found from the cases finished within 24 hours) multiplied by the average time spent per each time step. The average time spent in each time step is 13.6, 5.9, and 3.3 seconds when 1, 2, and 4 processors are used, respectively. Based on the results presented, we conclude that UTCHEM-IPhreeqc with single processor is suitable for lab scales (less than 1000 gridblocks). However, at least 10 processors (the most decrease in the CPU time occurs when 10 processors are considered) are required to use UTCHEM-IPhreeqc integrated tool for large-scale field applications.

Table 5-11: Comparison of the CPU time using UTCHEM-IPhreeqc with different thermodynamic databases released with IPhreeqc (Charlton and Parkhurst, 2011)

Database	Total CPU time (seconds)
sit.dat	6598.4
llnl.dat	4647.2
wateq4f.dat	1165.3
pitzer.dat	805.9
phreeqc.dat	633.3

Table 5-12: Comparison of the CPU time between UTCHEM-IPhreeqc with different number of processors and UTCHEM-EQBATCH

No. of processer(s)	Total computational time (hrs)	Speedup
UTCHEM-EQBATCH-1PRC	3.9	
UTCHEM-IPhreeqc-1PRC	143.2*	1.0
UTCHEM-IPhreeqc-2PRCs	58.6*	2.4
UTCHEM-IPhreeqc-4PRCs	30.1*	4.8
UTCHEM-IPhreeqc-6PRCs	19.6	7.3
UTCHEM-IPhreeqc-8PRCs	14.8	9.7
UTCHEM-IPhreeqc-10PRCs	12.7	11.2
UTCHEM-IPhreeqc-12PRCs	11.2	12.7
UTCHEM-IPhreeqc-16PRCs	9.0	16.0
UTCHEM-IPhreeqc-20PRCs	7.9	18.2
UTCHEM-IPhreeqc-24PRCs	7.2	19.9
UTCHEM-IPhreeqc-30PRCs	6.5	22.1
UTCHEM-IPhreeqc-40PRCs	5.8	24.7
UTCHEM-IPhreeqc-50PRCs	5.3	26.8
UTCHEM-IPhreeqc-60PRCs	5.1	28.1
UTCHEM-IPhreeqc-70PRCs	4.9	29.3
UTCHEM-IPhreeqc-80PRCs	4.8	30.1
UTCHEM-IPhreeqc-100PRCs	4.6	31.4
UTCHEM-IPhreeqc-120PRCs	4.4	32.2

*time beyond 24 hrs is estimated based on the average time spent in each time step.

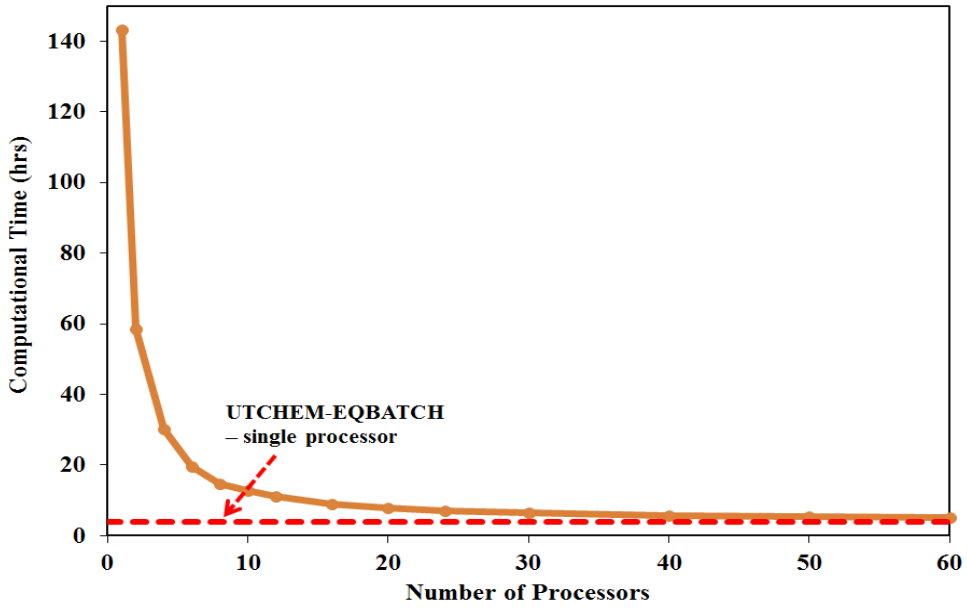

Figure 5-78: Computational time versus number of processors using UTCHEM-IPhreeqc for the field case.

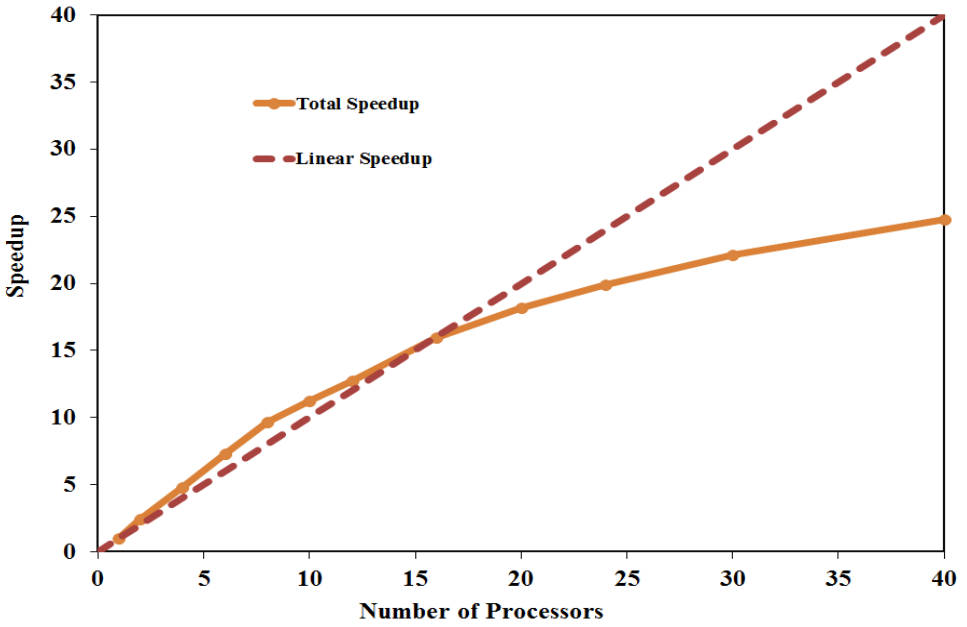

Figure 5-79: Speedup versus number of processors using UTCHEM-IPhreeqc for the field case.

Chapter 6: Scale Deposition and Groundwater Modeling Using UTCOMP-IPhreeqc and UTCHEM-IPhreeqc

Both UTCHEM-IPhreeqc and UTCOMP-IPhreeqc simulators can be applied to comprehensively model variety of reactive-transport problems such as scale deposition, groundwater, matrix acidizing, and CO_2 sequestration modelings. Scale deposition and groundwater modelings are briefly discussed in the chapter.

6.1 SCALE DEPOSITION MODELING

The precipitation of solid minerals from brine is known as scale precipitation in the oil industry. Oilfield scales result from changes in the physicochemical properties (pH, temperature, pressure, etc.) of the produced fluids and/or the major source of scale which is the chemical incompatibility between waters of different compositions (e.g., formation brine and injection brine) (Mitchell *et al.*, 1980; Mackay, 2003; Moghadasi *et al.*, 2003b; Moghadasi *et al.*, 2003a; Merdhah and Yassin, 2008; Merdhah and Yassin, 2009; Elmorsey, 2013). Hence, before injecting water into the reservoir, it must be monitored for chemical compatibility with the reservoir brine particularly nowadays that the new technology of low (or modified) salinity waterflooding has become popular in the oil field industry (as discussed in Chapters 3 and 4).

Scale deposition inflicts the most serious oilfield problems to water injection systems primarily when two incompatible waters are involved. Moreover, the risk posed by deposition of mineral scales to the injection and production wells during such operations has been studied extensively. Precipitation of mineral scales causes many problems in oil and gas production operations, such as formation damage, production

losses, increased workovers in producers and injectors, poor injection water quality, and equipment failures due to deposit due to corrosion.

Common scales include calcium carbonate and barium and strontium sulfates (Wright *et al.*, 1994; Yeboah *et al.*, 1993; Merdhah and Yassin, 2009). The sulfate scales are generally the result of mixing incompatible waters (Merdhah and Yassin, 2009). Sulfate scales can cause severe operational problems when sulfate-rich water, such as seawater, is used to waterflood oil reservoirs with high concentrations of barium and/or strontium in the formation water. Calcium carbonate may be formed in reservoirs containing CO_2 in the associated gas. However, scales are not limited to these minerals and there have recently been reports of unusual scale types, such as zinc and lead sulfides (Collins and Jordan, 2003; Okocha and Sorbie, 2013) or iron oxides, iron sulfides and iron carbonate (Merdhah and Yassin, 2008; Okocha and Sorbie, 2013). The most common oilfield scales are listed in Table 6-1 along with the primary variables that affect their solubility (Moghadasi *et al.*, 2003b).

Table 6-1: Common scales in oilfield damage (Moghadasi *et al.*, 2003b)

Name	Chemical Formula	Primary Variables
Calcium Carbonate	$CaCO_3$	Partial pressure of CO_2, temperature, total dissolved salts, pH
Calcium Sulphate: • Gypsum • Hemi hydrate • Anhydrite	$CaSO_4.2H_2O$ $CaSO_4.1/2H_2O$ $CaSO_4$	Temperature, total dissolved salts
Barium Sulfate	$BaSO_4$	Temperature, pressure, total dissolved salts
Iron Compounds: • Ferrous Carbonate • Ferrous Sulphate • Ferrous Hydroxide • Ferric Hydroxide	$FeCO_3$ FeS $Fe(OH)_2$ $Fe(OH)_3$	Corrosion, dissolved gases, pH

The severity of scales may significantly change from one reservoir to another and even in the same field over time due to variation of temperature and pressure. Many cases of oil well damages due to scales of calcium carbonate, calcium sulfate, strontium sulfate, and barium sulfate have been reported. Some of these reports are discussed next.

Mitchell *et al.* (1980) reported serious plugging of the wells in the Forties field due to scales caused by mixing of Forties formation and injection waters and precipitation of calcium carbonate from due to variations in pressure and temperature in the production system.

Both carbonate and sulfate scales have had a major influence on production from the Glamis field. Carbonate deposited within tubes during water production and sulfate scales appeared at the perforations, following seawater breakthrough. Downhole injection and inhibitor squeezing are tried to inhibit scaling problems (Wright *et al.*, 1994).

Tjomsland *et al.* (2001) reported the scaling problem in the Veslefrikk field of the Norwegian sector of the North Sea. Seawater was injected into this field for the purpose of pressure maintenance. Comparing to other North Sea formation waters, severe scale formation had been identified. This is probably due to high reservoir temperature of 125 ^{o}C and comingled production. $BaSO_4$ is reported to be the most important type of scale in this field. However, carbonate scale may also cause problems as pressure decreases in this field.

Injected seawater mixing with aquifer brines is the main reason behind the scaling in the Alba field in the North Sea (Paulo *et al.*, 2001). Sulfate scale deposition near the injection and production wellbores caused considerable disruption to hydrocarbon production after water breakthrough.

Qing *et al.* (2002) documented the scale precipitation during ASP flooding in the Daqing oil field in China. Silicate deposition caused frequent downhole operation failures in the producer tubings. The alkaline agent (NaOH) reacts and dissolves the reservoir rock, the dissolved materials plug the porous media or will propagate towards the production wells. Wang *et al.* (2004), Kazempour *et al.* (2012; 2013), Alwi *et al.* (2013), and Hunter *et al.* (2013) also investigated the significance of scales and/or the water-rock interaction during the ASP or high-pH enhanced oil recovery floods.

Continuous precipitation of calcium sulfate caused the oil production to decrease to almost one tenth of the typical rate in Gemsa oil field in Egypt. Water incompatibility between the formation water and the injection water was offered as the main reason for the calcium sulfate precipitation. Several screening tests were conducted to find a suitable chemical to remove this scale. Elmorsey proposed a highly efficient new chemical, SAG-01, as a good calcium sulfate remover (Elmorsey, 2013).

Moghadasi *et al.* (2003b) reported severe formation damage occurred in Siri field in Iran. Water injection in Siri commenced in 1984 with 9100 bbl/day for pressure maintenance and increasing oil recovery purposes. However, a rapid decrease was seen in the injectivity of the injection well, where by 1990 they were able to inject only 2200 bbl/day and finally stopped the water injection in this field. Sulfate and carbonate are two main types of scale reported for this field.

Scale removal is not only expensive but sometimes nearly impossible to achieve (particularly for $BaSO_4$), it is therefore scale prevention is preferred compared to its removal using chemical inhibitors or mechanical treatments. Hence, modeling and prediction of scale is needed for field developments. Several researchers have tried to quantify the reservoir permeability impairment due to scale precipitations. For example,

Ohen and Civan (1989) proposed a model for the prediction of petroleum reservoir permeability impairment based on the solid-liquid interactions. They considered combined effects of clay swelling, external particles invasion, fines generation, migration, and retention in their model. Mikhailov and Chirkov (2010) also studied methods to upscale the scaling from the laboratory to the field by taking into account the process of formation damage during reservoir development. Their analysis on the laboratory experiments results shows that permeability has similar kinetics of alteration for different damaging mechanisms. Many other researchers have tried to quantify the scaling problems (Liu and Civan, 1995; Chekani and Mackay, 2006; Civan, 2007; Fadairo *et al*., 2008; Lohne *et al*., 2009; Bedrikovetsky *et al*., 2010).

In general, due to the complexity of the precipitation kinetics and ion exchange/chemical reaction processes, geochemical-based models to quantify amount of scales are fairly simplistic. They have neglected various important aspects, such as ion activity coefficients (by assuming ideal solutions), temperature, and pressure effects on geochemical reactions. As a result, large errors may occur in scale prediction in some cases. In some other models, a specific ion effect is considered where solubility and scale formation is predicted only for one mineral. In these models, the effect of scale formation of other minerals in the same solution is simply ignored. Hence, the need to develop an accurate, reliable, and easy-to-use model for predicting the formation of the common oilfield scales is the aim of this section. IPhreeqc provides factors neglected by the current models. In this work, we develop UTCHEM-IPhreeqc further to consider the comprehensive geochemistry for the scales predictions for field applications. However, similar developments can be implemented in the UTCOMP-IPhreeqc simulator.

6.1.1 Quantifying Scales

Scales are quantified by including the dissolution or the precipitation of all minerals (either initially present or precipitated later due to the injected waters) on the reservoir porosity and consequently on the permeability. Eq. (6.1) updates the porosities in each gridblock and time-step

$$\phi_i^{n+1} = \phi_i^n - \frac{\sum_k \frac{\Delta n_k Mw_k}{\rho_k}}{V_{Bi}}, \tag{6.1}$$

where

ϕ_i^{n+1} = time update of porosity in i^{th} gridblock

ϕ_i^n = current time step porosity of the i^{th} gridblock

Δn_k = change in concentrations (moles) of the κ^{th} solid of the current time-step (**EQUI_DELTA** of IPhreeqc is used to find this value for each solid)

Mw_k = gram formula weight of the solid κ (**GFW** along with **PHASE_FORMULA** of IPhreeqc return this value for each solid phase)

ρ_k = density for the κ^{th} solid

V_{Bi} = the i^{th} gridblock bulk volume

Δn_k in Eq. (6.1) is negative (porosity increases) while Δn_k is positive (porosity decreases) for solids that are precipitating.

Three common permeability-porosity approaches (Modified Fair-Hatch, MFH, (Chadam *et al.*, 1986), Kozeny-Carman, KC, (Kozeny, 1927; Carman, 1956), and Verma-Pruess, VP, (Verma and Pruess, 1988)) are implemented in UTCHEM-IPhreeqc to reflect the change in porosities and the resulting change in permeabilities (the same relationship is used to modify the *x*-, *y*-, and *z*-direction permeabilities). These models are described

as follows (in all of the models, k_i and ϕ_i are absolute permeability and porosity of gridblock *i* and (n+1) and (n) superscripts are time-steps).

The permeability-porosity model was proposed by Kozeny (1927) and later modified by Carman (1956) referred to KC. KC model considered the porous medium as a bundle of cylindrical pores. The KC equation has the form of

$$\frac{k_i^{n+1}(\phi)}{k_i^{n}} = \left(\frac{\phi_i^{n+1}}{\phi_i^{n}}\right)^3 \left(\frac{1-\phi_i^{n}}{1-\phi_i^{n+1}}\right)^2 . \tag{6.2}$$

Fair-Hatch, FH, model was derived from dimensional analysis and validated experimentally (Bear, 2013). Later Chadam *et al.* (1986) modified this model as

$$\frac{k_i^{n+1}(\phi)}{k_i^{n}} = \frac{\phi_i^{n+1}}{\phi_i^{n}} \left[\frac{\left(1-\phi_i^{n}\right)^{2/3} + E_1\left(\phi_f - \phi_i^{n}\right)^{2/3}}{\left(1-\phi_i^{n+1}\right)^{2/3} + E_1\left(\phi_f - \phi_i^{n+1}\right)^{2/3}} \right]^2 , \tag{6.3}$$

where ϕ_f is the final porosity after all the dissolutions (or the precipitations) have occurred and E_1 is an arbitrary constant (matching parameter).

Verma and Pruess (1988) derived a permeability-porosity relationship from a pore-body-and-throat model in which permeability can be reduced to zero with a finite (critical) porosity remaining as follows (see Eq. (6.4)):

$$\frac{k_i^{n+1}(\phi)}{k_i^{n}} = \left(\frac{\phi_i^{n+1} - \phi_c}{\phi_i^{n} - \phi_c}\right)^n , \tag{6.4}$$

where

$\phi_c =$ critical porosity at which permeability reduces to zero (it was proposed to be 0.8 of the initial porosity of gridblock *i*

$n =$ a power law exponent

Parameters ϕ_c and n in Eq. (6.4) are medium-dependent.

6.1.2 Synthetic Case Study

A synthetic five-spot pattern (see Figure 6-1) is modeled using the UTCHEM-IPhreeqc integrated simulator. High resolution grid near the injection well is recommended. Reservoir formation is carbonate (50 vol% dolomite and 50 vol% calcite) with the initial porosity of 0.25. The initial pressure, temperature, and water saturation are 4890 psi, 219 ^{o}F, and 0.3, respectively. The permeability is homogenous and isotropic and equal to 100 md. Four production wells are operating with constant bottomhole pressure, while the injection well is injecting water at the reservoir temperature with constant flowrate of 0.1 PV/year. T-Block formation water with ion compositions presented in Table 6-2 (Mazzolini *et al.*, 1992) is assumed to be the water initially present in this reservoir. Seven different water compositions (see Tables 6-3 and 6-4) are then injected to investigate their impact in generating scales in the reservoir. Verma-Pruess model (Verma and Pruess, 1988) with the power law exponent of 3.0 is used in this simulation study (based on the initial porosity; the critical porosity is 0.2). As pointed out previously, keeping the same initial water, depending on the injection water, the possible solids considered in Eq. (6.1) are different. For example, when the injection water is Solution#1 (see Table 6-3), solids considered are: anhydrite, aragonite, barite, calcite, celestite, dolomite, gypsum, halite, strontianite, sylvite, and witherite, while if the injection water is Solution#5 (see Table 6-4), 10 more solid phases ($Fe(OH)_3$(a), FeS(ppt), goethite, gypsum, hematite, jarosite-K, mackinawite, melanterite, pyrite, and

siderite) should be included in the simulation. PHREEQC (Parkhurst and Appelo, 2013) is run externally using the initial (connate) and the injection solutions to find all the possible solids involved.

Figures 6-2 and 6-3 present porosity and permeability of the injection gridblock during injection of different solutions into the reservoir. As these figures demonstrate, different solutions show significantly different effects on the reservoir properties. The precipitation of different scales, solutions numbers 1, 3, 5, 6, and 7 drastically reduce porosity and permeability of the injection gridblock whereas solutions numbers 2 and 4 seem compatible with the connate water without reducing porosity and permeability. In fact, when solution #4 is injected, solid dissolution, rather than precipitation, occurs which enhances the porosity and permeability of the injection gridblock. However, it should be noted that our model is very simple that does not take into account the damage due to potential clay swelling, if any present in the system. Figures 6-4 and 6-5 demonstrate permeability maps of near the injection well at PV=0.1 for solutions #1 and 7, respectively. As these figures present, the main precipitations (or dissolutions) occur near the injection well and reduces away from the well.

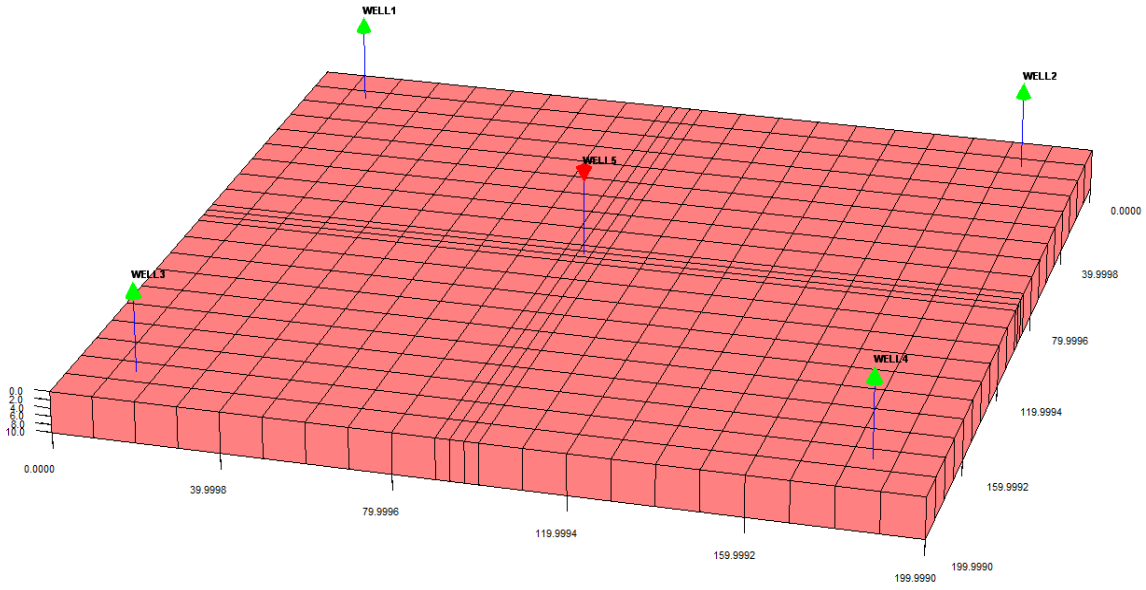

Figure 6-1: The schematic of 2D model and well locations for synthetic case study.

Table 6-2: Initial water composition used in the synthetic case study

Ions	T-Block formation water (Mazzollni *et al.*, 1992) (mg/l)
Na	36360
K	1720
Mg	365
Ca	3790
Sr	355
Ba	930
Cl	65840
S	2
HCO_3^-	--
Alkalinity	560

Table 6-3: Water analysis of the injection waters (Solutions #1 through 4) used in the synthetic case study

Ions	Solution#1 (Al-Harrasi *et al.*, 2012) (kg/m^3)	Solution#2 (Dang *et al.*, 2013) (LoSal®[1]-composition) (mol/l)	Solution#3 (Dang *et al.*, 2013) (Sea water-composition) (mol/l)	Solution#4 (de Bruin, 2012) (LSW composition) (ppm)
Na	59.970	0.01326	0.45011	295
K	--	0.00006	0.01006	--
Mg	2.153	0.00018	0.04451	--
Ca	11.618	0.00148	0.01299	--
Sr	--	--	--	--
Ba	--	--	--	--
Cl	118.791	0.01661	0.52513	455
S	0.689	0.00001	0.02401	--
HCO_3^-	0.009	--	--	--

Table 6-4: Water analysis of the injection waters (Solutions #5 through 7) used in the synthetic case study

Ions	Solution#5 (Elmorsey *et al.*, 2013) (Nukhul Formation) (mg/l)	Solution#6 (Kazempour *et al.*, 2013) (Injection water) (ppm)	Solution#7 (Kazempour *et al.*, 2013) (Produced water) (ppm)
Na	60146	2083	2430
K	12709	75	66
Mg	1145	50	47
Ca	6625	310	300
Fe	4.46	--	--
Sr	393	28	26
Ba	1.296	70	20
Cl	120104.6	3926	4343
F	47.50	--	--
Br	519	--	--
S	685.25	--	--
HCO_3^-	199.8	928	512

[1] LoSal® is the trademark of BP p.l.c

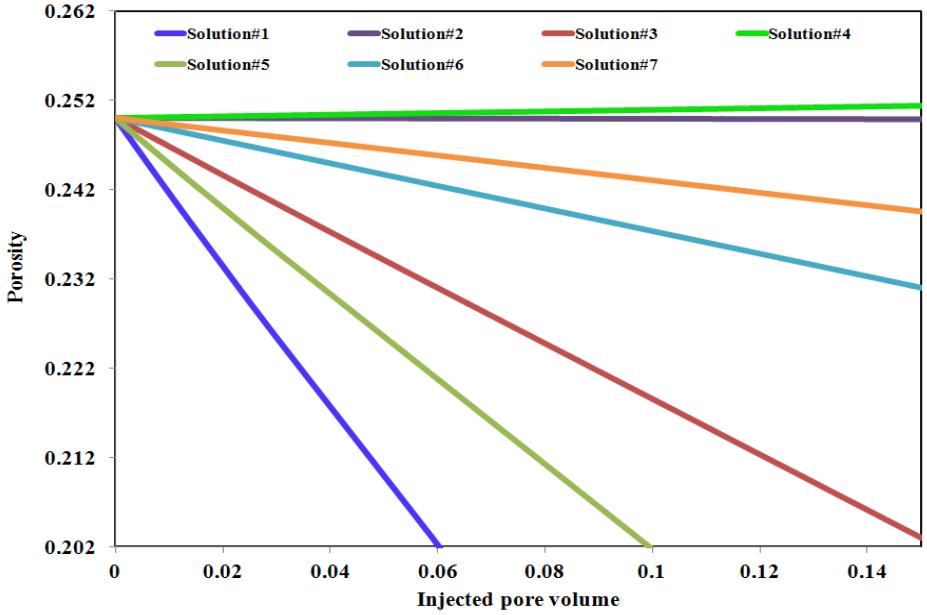

Figure 6-2: Porosity of the injection gridblock versus injected pore volume for different solutions.

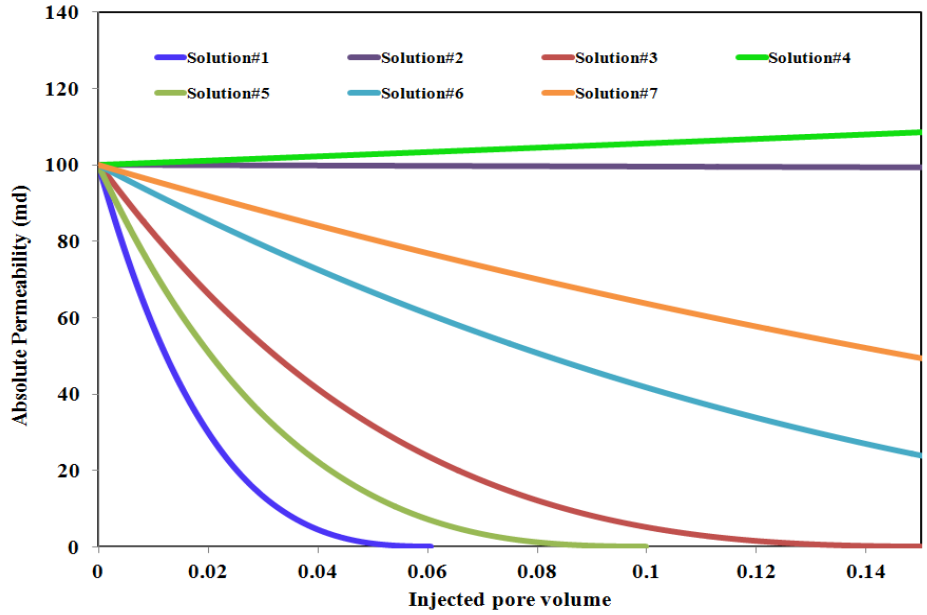

Figure 6-3: Permeability of the injection gridblock versus injected pore volume for different solutions.

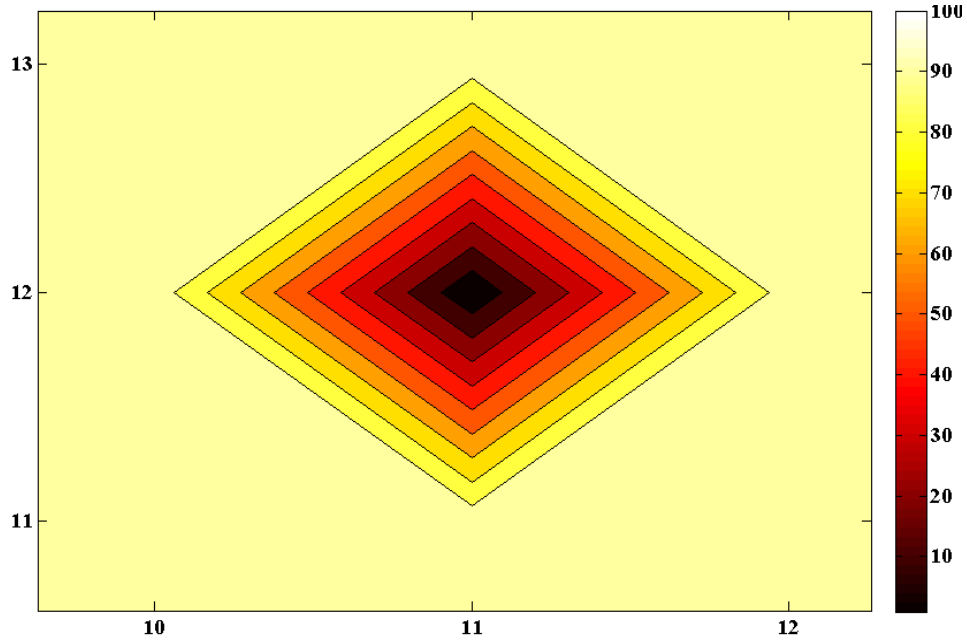

Figure 6-4: Permeability map (in md) of the zoomed area near the injection well (point (11,12) is where the injection well located) for the injection solution#1 at PV=0.1.

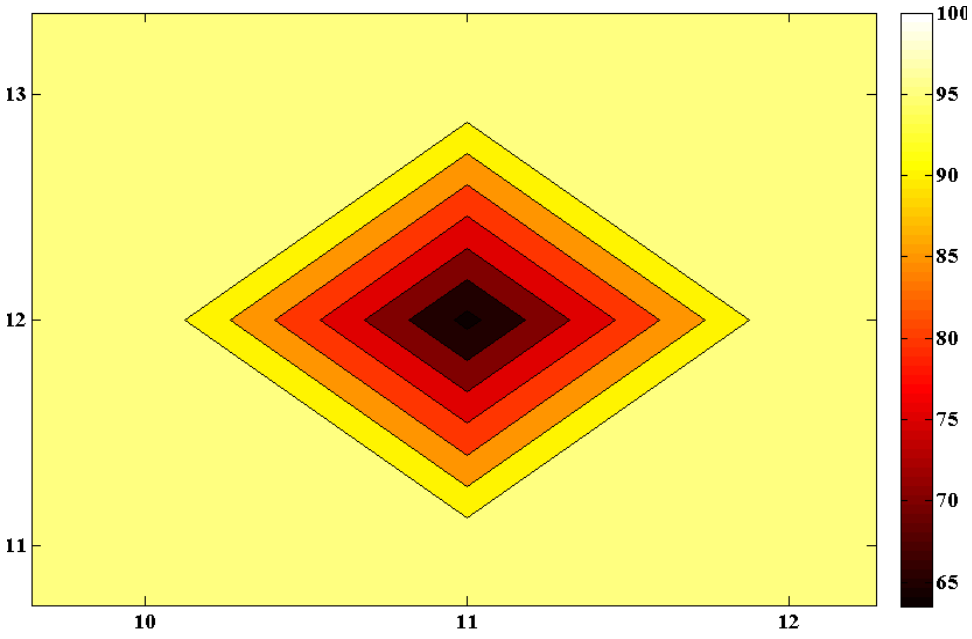

Figure 6-5: Permeability map (in md) of the zoomed area near the injection well (point (11,12) is where the injection well located) for the injection solution#7 at PV=0.1.

6.2 GROUNDWATER MODELING

Considering water saturation equal to one, both the UTCHEM-IPhreeqc and UTCOMP-IPhreeqc (water saturation is 0.999 for water single-phase flow in UTCOMP-IPhreeqc) simulators can be applied for groundwater modeling. As mentioned previously, these simulators have been tried to be very similar to PHAST of the USGS groundwater simulator (Parkhurst *et al.*, 2010), in terms of designing a model and the computational algorithm. However, UTCHEM-IPhreeqc is preferred over UTCOMP-IPhreeqc for groundwater modeling. The reason is, through ICF keyword available in UTCHEM-IPhreeqc, one can skip extra calculations for components excluded from the simulation. For example, oleic, surfactant phase behavior, and polymer calculations can be easily excluded from the simulation using UTCHEM-IPhreeqc. However, UTCOMP-IPhreeqc has been designed based on the assumption that the hydrocarbon phase is always present in the system. Hence, hydrocarbon phase behavior calculations are performed at all times (by using the ISINGL keyword available in UTCOMP we can skip the phase composition calculations for single hydrocarbon phase). That is why water saturation must be 0.999, rather than 1.0, even for single-phase flow of water in UTCOMP-IPhreeqc.

A synthetic case is designed using UTCHEM-IPhreeqc. Figure 6-6 shows reservoir geometry and wells locations and Table 6-5 summarizes case descriptions. Also, Figure 6-7 illustrates *x*- and *y*-direction permeability distributions and Figure 6-8 presents the porosity distribution of the model (porosity and permeability distribution data are taken from Case Study 28 of Li (2012)). The Endicott connate water (see Table 2-20) is initially present in the system. All the solids presented in Table 2-21 are included in the model. Saturation index and initial mole of the entire solids are set to zero. Six injection wells are injecting Endicott seawater (see Table 2-20 for the ion compositions)

at constant flowrate of 1123 ft^3/day into the reservoirs. Production wells are operating at constant bottomhole pressure of 1000.0 psi. The simulation was carried out on TACC facilities (see Chapter 2 for TACC characteristics). Using 120 computing processors, after 24 hours, which is the upper limit to submit a job in TACC, about 0.325 PV of the Endicott seawater is injected into the reservoir.

Figures 6-9 through 6-14 illustrate maps of some fluid species (Ba^{+2}, Ca^{+2}, $CaSO_4$, Cl^{-1}, Mg^{+2}) and pH of the solution for the last layer at about 0.325 PV. Contrary to the fluid species that show either continuous decreasing (e.g., Ba^{+2}) or increasing (e.g., Ca^{+2}) trend from the injection to the production well, solution pH is low at the front and starts increasing near the injection wells.

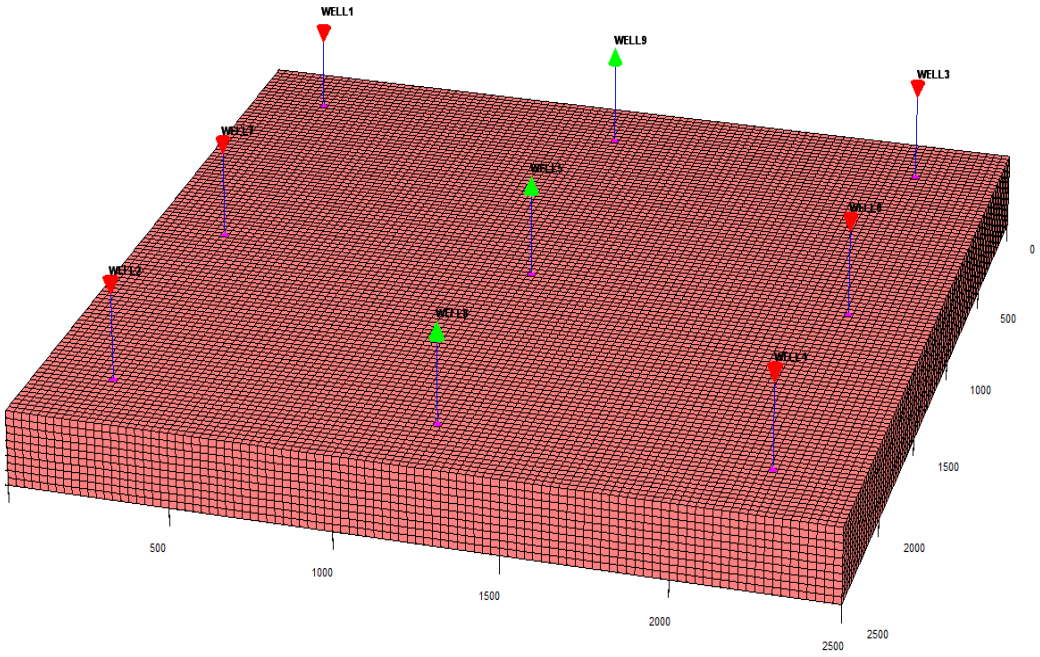

Figure 6-6: Well locations in the 3D case considered for groundwater modeling.

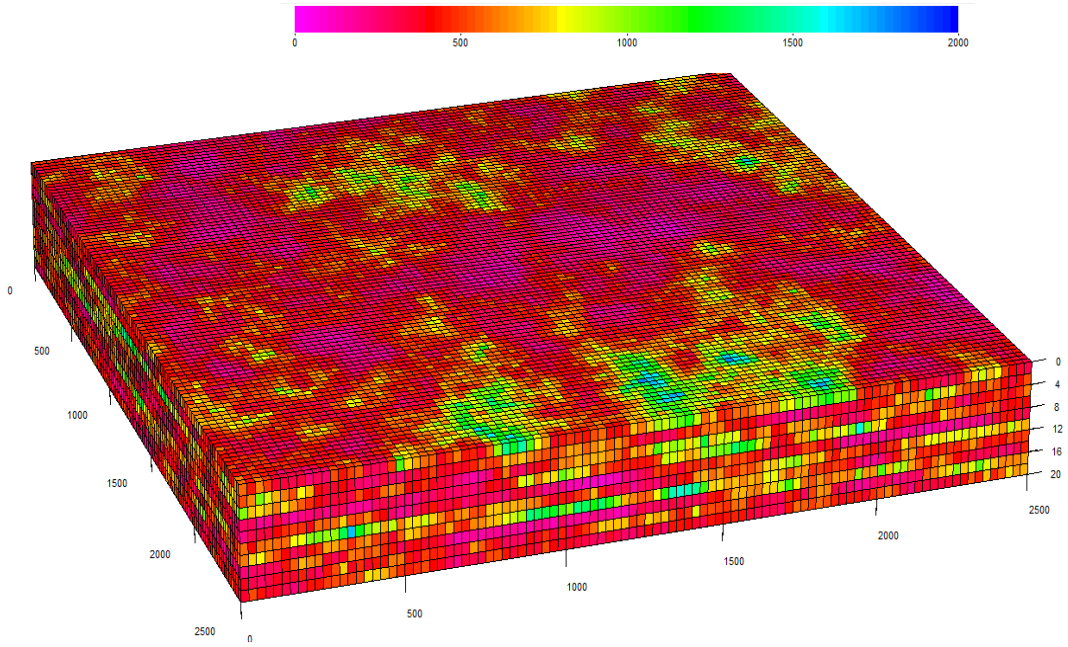

Figure 6-7: Distribution of the absolute permeability (in md) in the *x*- and *y*-direction for the 3D case.

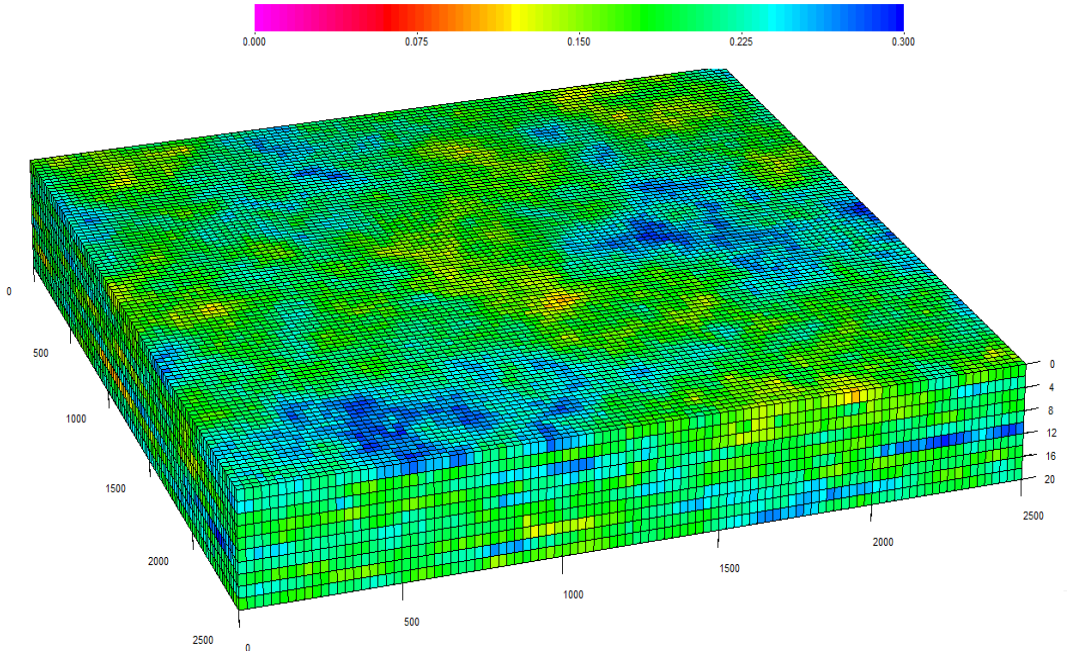

Figure 6-8: Distribution of the porosity in the 3D case.

Table 6-5: Case descriptions for the 3D Case

No. of gridblocks		100,000 (100×100×10)	
Δx(ft)		25.0	
Δy(ft)		25.0	
Δz(ft)		2.0	
Permeability (md)	*x*-direction	Heterogeneous	
	y-direction	Heterogeneous	
	z-direction	10.0	
Porosity		Heterogeneous	
Rock compressibility (psi^{-1})		0.	
Water compressibility (psi^{-1})		0.	
Initial pressure (psi)		1100.0	
Reservoir depth (ft)		0.	
Water viscosity (cp)		0.79	
Number of wells		9	6 injectors
			3 producers
Simulation time(PV)		0.325	

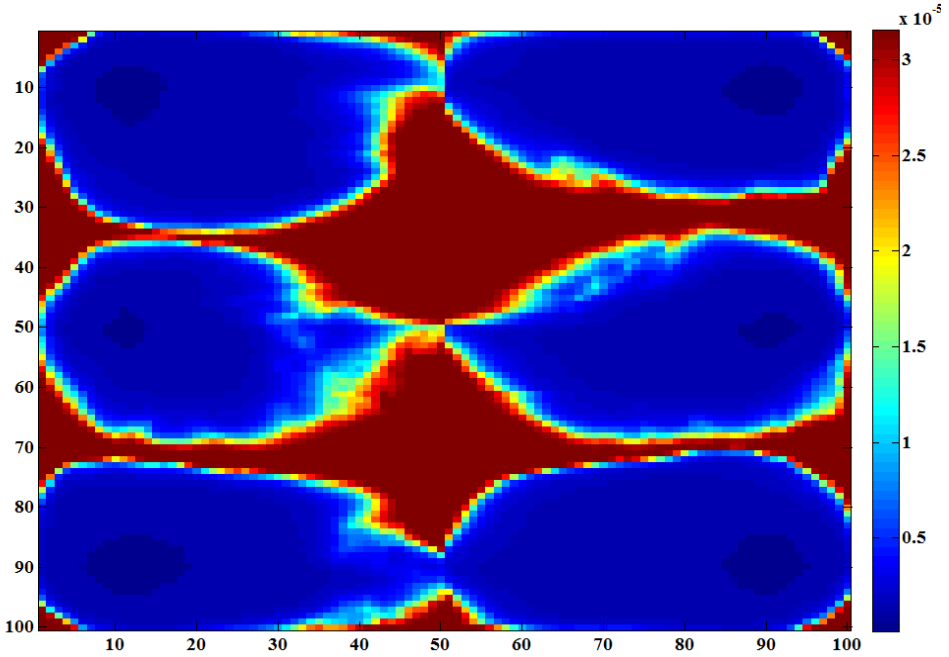

Figure 6-9: Ba^{+2} concentration (in mol/l) map of layer 10^{th} at 0.325 PV.

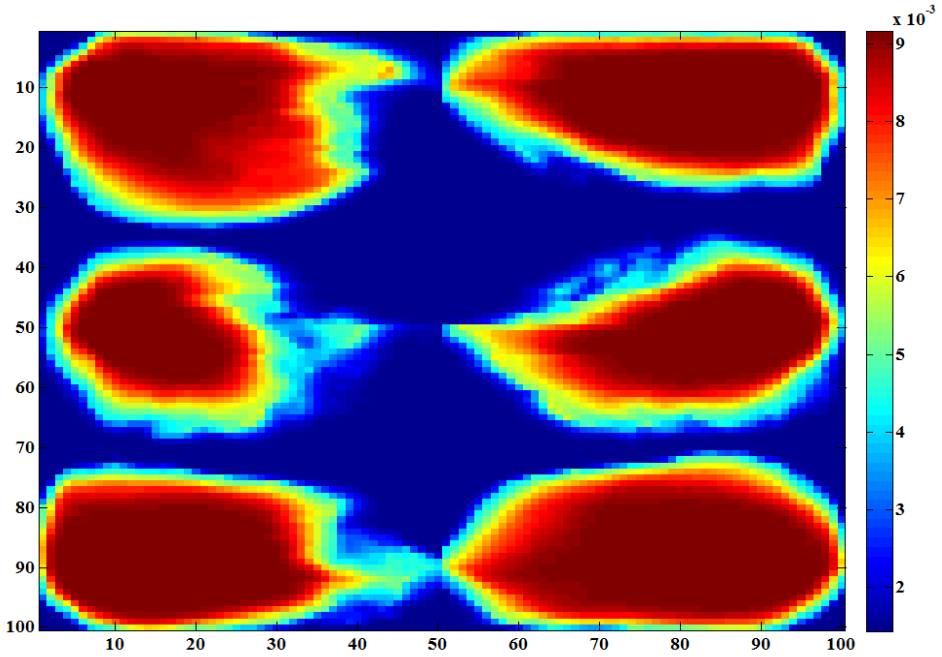

Figure 6-10: Ca^{+2} concentration (in mol/l) map of layer 10^{th} at 0.325 PV.

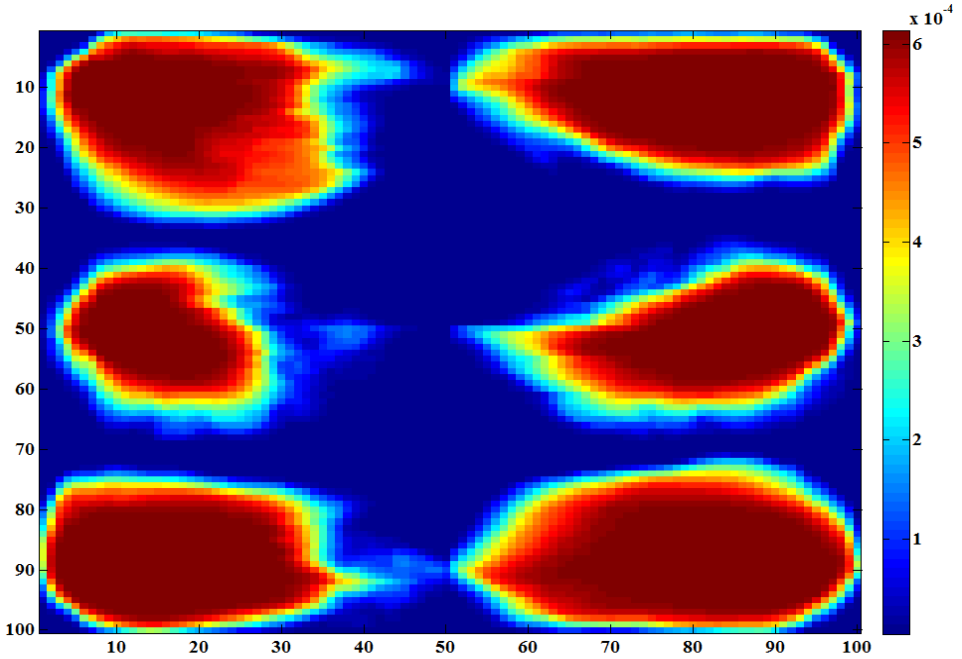

Figure 6-11: $CaSO_4$ concentration (in mol/l) map of layer 10^{th} at 0.325 PV.

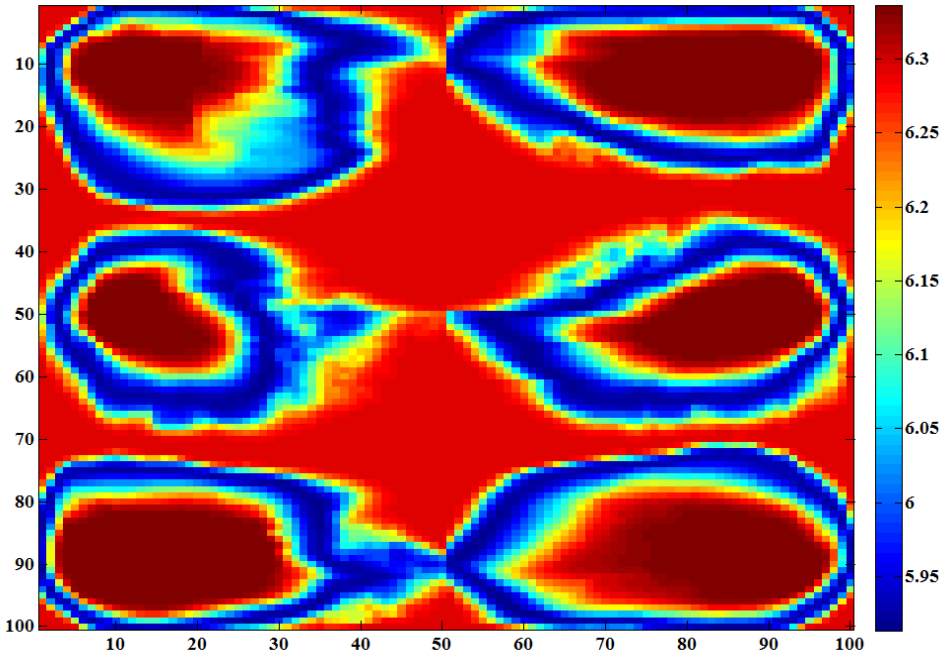

Figure 6-12: pH map of layer 10^{th} at 0.325 PV.

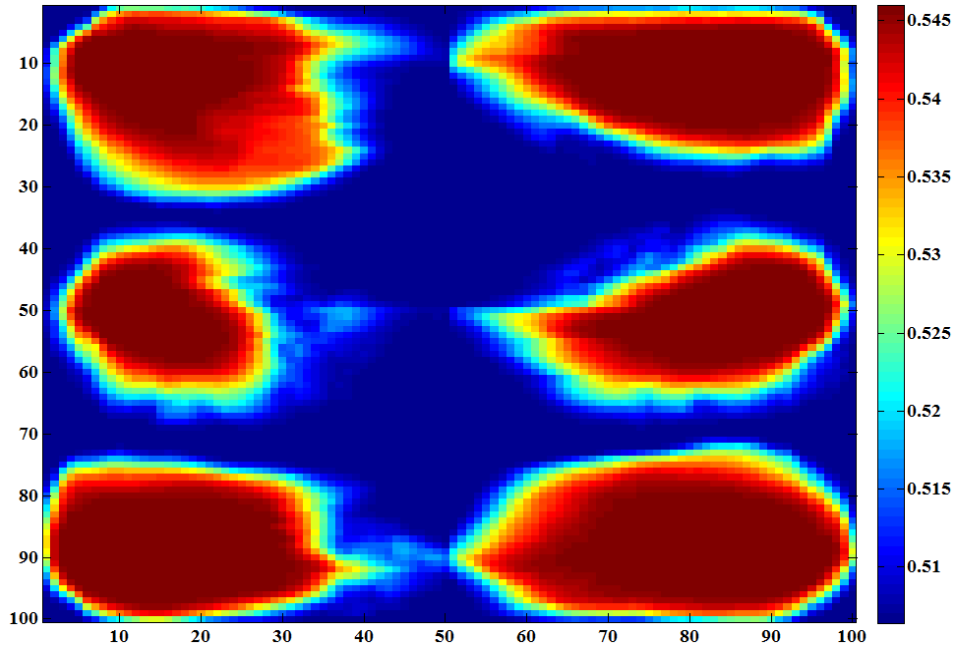

Figure 6-13: Cl^{-1} concentration (in mol/l) map of layer 10^{th} at 0.325 PV.

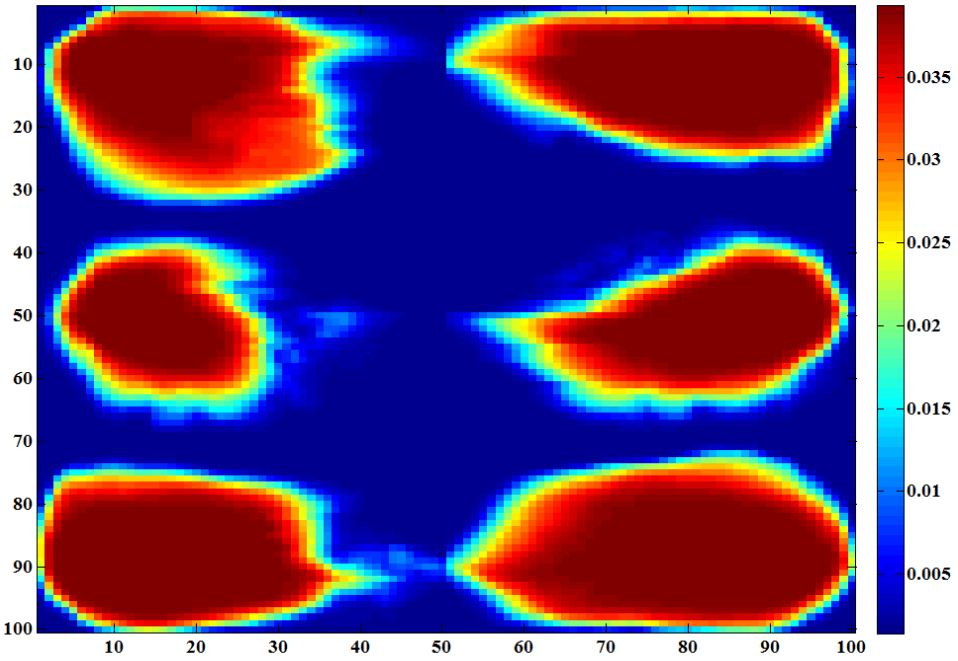

Figure 6-14: Mg^{+2} concentration (in mol/l) map of layer 10^{th} at 0.325 PV.

Chapter 7: Conclusions and Recommendations for Future Research

This chapter presents the summary and the conclusions of this dissertation and provides some recommendations for further extensions of this work.

7.1 SUMMARY AND CONCLUSIONS

In the following, we present the summary and conclusions of this study:

- In this dissertation, we modeled low (or modified) salinity waterflooding mechanistically and comprehensively.
- Because in low salinity water injection, only water with the modified ion concentrations is injected into the reservoir, it appears no matter the manner and details of the mechanism, the improved oil recovery must be due to the ions and geochemical reactions. Hence, we believe mechanistic modeling of this process is possible only by including geochemical reactions.
- In line with several experimental observations published in the literature we hypothesized that wettability alteration is the underlying mechanism in low (or modified) salinity waterflooding in both sandstone and carbonate reservoirs. However, the mechanism through which rock wettability changes is different in sandstone and carbonate reservoirs.
- To handle the complicated geochemical reactions involved in low salinity waterflooding, we first integrated EQBATCH, a geochemical module previously developed by Bhuyan (1989), to UTCOMP, The University of Texas at Austin in-house compositional reservoir simulator. However, the physics in EQBATCH is limited and also EQBATCH is not robust due to numerical convergence problems. To overcome the issues involved in

EQBATCH, we coupled IPhreeqc (Charlton and Parkhurst, 2011), the state-of-the-art geochemical package of the USGS, with UTCOMP, to generate a robust, accurate, and flexible integrated simulator (i.e., UTCOMP-IPhreeqc) to model low salinity waterflooding mechanistically based on geochemical reactions. We parallelized the geochemistry module of UTCOMP-IPhreeqc for large scale reservoir simulation applications.

- Thermodynamic constraints, equality of components fugacities and pseudo-fugacities (defined in this dissertation) in all phases, were used to explicitly include the buffering effect of the hydrocarbon phase on the aqueous-rock geochemistry in UTCOMP-IPhreeqc.
- We presented the importance of ion activities, temperature, and pressure on reactive transport modeling.
- UTCOMP-IPhreeqc is flexible enough to allow implementation of a variety of geochemically based models of low salinity water injection. A model based on the interpolating relative permeability and capillary pressure as a function of total ionic strength was implemented along with two more direct and mechanistic models (based on the fraction of organometallic components on the exchanger; based on change in moles of the organic oil component in the surface complex) in UTCOMP-IPhreeqc to model low salinity waterflooding in sandstone reservoirs.
- UTCOMP-IPhreeqc was used to match both oil recovery and produced ion histories for Kozaki (2012)'s experimental coreflood (Berea sandstone core) as well as the Endicott field trial (sandstone reservoir). Key conclusions from the modeling are

- Buffering of CO_2 from the oil phase accounts for the trend of decreasing pH seen at the Endicott trial
- Quantitative modeling shows that the mechanisms proposed by RezaeiDoust *et al.* (2011) do not account for the observed alkalinity and production of iron during the Endicott trial.

- We implemented the model proposed by Hiorth *et al.* (2010) in UTCOMP-IPhreeqc to take into the account the wettability alteration and mechanistically model the modified salinity waterflooding in carbonate reservoirs. This model assumes during this process, calcite is dissolved and liberates the adsorbed oil from the surface; hence, a fresh surface leaning more towards water-wetting is created.
- We hypothesized that calcite dissolution model should perhaps be generalized to include the dissolution of entire spectrum of existing minerals, not a specific mineral type. Dissolution, if occurring on any oil-wet mineral, creates a fresh surface and can alter rock wettability.
- Fairly reasonable, UTCOMP-IPhreeqc matches the experimental data recently published by Chandrasekhar and Mohanty (2013) conducted on a carbonate core. For the time being, we cannot interpret the significant decrease in the initial chloride concentration produced from the core. Surface reactions play significant role in carbonate reservoirs. Moreover, if we assume surface complex reaction is exothermic, our model predicts the right trend of increased oil recovery with increasing temperature.
- We believe although the calcite dissolution is the controlling factor that changes the rock wettability, the effect does not solely depend on the calcite

dissolution but also the surface reactions. Hence, the modified salinity waterflooding effect is not limited to small scales. The effect of hydrocarbon phase (e.g., CO_2 component) must be included in multi-phase reactive-transport modeling.

- We coupled IPhreeqc with our in-house chemical flooding simulator, UTCHEM, to develop a mechanistic integrated simulator, UTCHEM-IPhreeqc, to model ASP flooding.
- We coupled IPhreeqc to the UTCHEM simulator to be used in conjunction with the comprehensive three phase (water, oil, microemulsion) flash package for the mixture of surfactant and soap option in the UTCHEM simulator. However, the proposed procedure can be implemented in any existing reservoir simulator.
- Coupling of IPhreeqc with a client simulator (i.e., UTCHEM) becomes more difficult if there are partitioning and exchange of certain species between fluid phases (e.g., acidic component in ASP). For these cases, special care must be taken to properly transport geochemical elements (including total H and O) as well as the charge balance in the system.
- UTCHEM-IPhreeqc successfully history matched three laboratory corefloods: ASP for an acidic crude oil, ASP for a non-acidic crude oil, and ACP for an acidic oil.
- We scaled up the ASP coreflood conducted using non-acidic crude oil and applied it with similar chemical injection design to a model based on real field data. Both UTCHEM-IPhreeqc and UTCHEM-EQBATCH (i.e., the original version of UTCHEM where EQBATCH is used for geochemical calculations)

show very promising results when ASP is injected compared with the waterflooding.

- We studied the importance of common assumptions made in modeling ASP floods. Our investigations show that geochemistry plays a very important role in modeling ASP process i.e. different IPhreeqc thermodynamic databases predict different oil recovery. The local equilibrium can be applied only at low fluid velocities in reactive-transport modeling. Modeling Type III microemulsion phase is critical. Moreover, while the pressure effect on the geochemical calculation can be neglected, temperature significantly affects the geochemical calculation and consequently the performance of the ASP flooding.
- The importance of geochemistry during the ASP process was addressed through performing sensitivity studies.
- Although UTCHEM-IPhreeqc is robust, accurate, and flexible in terms of the geochemistry calculations, this integrated tool requires longer CPU times and larger computer memory compared to UTCHEM-EQBATCH. However, through parallelization of the geochemistry module of UTCHEM-IPhreeqc, it can be used for large scale field cases.
- We illustrated that both UTCOMP-IPhreeqc and UTCHEM-IPhreeqc can be applied for groundwater modeling (UTCHEM-IPhreeqc is preferred) and also to comprehensively model oil-field scales. However, these integrated simulators can also be used to model variety of reactive-transport problems, particularly matrix-acidizing and CO_2 sequestration (only UTCOMP-IPhreeqc).

- We quantified the scale through inclusion of dissolution/precipitation of all possible minerals on porosity and permeability.
- We implemented three commonly used permeability-porosity models (Modified Fair-Hatch, Kozeny-Carman, and Verma-Pruess models) to quantify the impact of scales on reservoir permeability.

7.2 RECOMMENDATIONS FOR FUTURE RESEARCH

In the following the recommendations for further study in this area are presented:

- In Chapter 3, we described several direct and mechanistic approaches to model low (or modified) salinity waterflooding (based on detachment of acid components from the rock surface). However, we did not validate our mechanistic and direct approaches against any experimental results. Hence, it would be of more interest if low salinity waterflooding is modeled using direct models.
- Throughout this dissertation, we assumed local-equilibrium between the minerals and the aqueous solution. Nevertheless, the reactions may not be always in equilibrium within the time and space of interest. Hence, we recommend applying the kinetics approach when local equilibrium assumption is violated (e.g., high velocity flow).
- The UTCOMP version used in this dissertation was isothermal. However, several laboratory observations clearly illustrate the pronounced effect of elevated temperatures on the modified salinity waterflooding in carbonates. Hence, it would be more realistic if the energy balance equation is also included in the UTCOMP-IPhreeqc simulator to properly model the modified salinity waterflooding in carbonates.

- Several laboratory and field studies show the significant effect of low salinity waterflooding in improving the oil recovery. However, there is always a salinity threshold below which clay swelling becomes a serious problem in sandstone reservoirs. For the time being, the UTCOMP-IPhreeqc simulator does not model the clay swelling in sandstone reservoirs. Hence, we recommend a clay swelling model to be implemented in UTCOMP-IPhreeqc so with that clay swelling is also taken into account when modeling low salinity waterflooding.
- We neglected the effect of gas on the surfactant and soap phase behavior calculations when modeling ASP floods. We recommend investigating the effect of the gas phase on the surfactant and soap phase behaviors and consequently on SP and ASP processes.
- In reality, cations resided on the surfactant micelles might be exchanged with those in the aqueous phase (similar to the aqueous-rock exchange reactions). The surfactant associated cation reactions have been included in the UTCHEM-EQBATCH simulator by Bhuyan (1989). However, no surfactant associated cations are modeled in the current version of UTCHEM-IPhreeqc.
- For some cases, time-step does not increase in UTCHEM-IPhreeqc as it builds up in UTCHEM-EQBATCH. Our investigations show that frequently, charge balance is the controlling element for the time step size (charge balance must be transported along with geochemical species in UTCHEM-IPhreeqc). Hence, different time-step criteria should be investigated for the charge balance to resolve the time-step issue in the UTCHEM-IPhreeqc simulator.
- Feasibility of using the Gibbs free energy approach (Venkatraman, 2014)

rather than the sequential iterative approach, presented in this research, for multi-phase reactive-transport modeling can be also studied.

Appendix A: Basic Geochemistry Definitions

Unless otherwise cited specifically, all definitions below are taken from Zhu and Anderson (2002):

Activity coefficient: is a dimensionless quantity through which the deviation from the ideal state of an aqueous species is defined. Below presents the Davies (Davies, 1962; Parkhurst and Appelo, 1999; 2013) and the extended or WATEQ Debye-Huckel (extended form of Debye-Huckel model (Debye and Huckel, 1954)) models through which IPhreeqc calculates the activity coefficients of the aqueous and exchange species:

Davies equation (Davies, 1962; Parkhurst and Appelo, 1999; 2013):

$$\log \gamma_i = -Az_i^2 \left(\frac{\sqrt{I}}{1+\sqrt{I}} - 0.3I \right). \tag{A.1}$$

Extended or WATEQ Debye-Huckel equation (Truesdell and Jones, 1974; Parkhurst and Appelo, 1999; 2013):

$$\log \gamma_i = -\frac{Az_i^2 \sqrt{I}}{1+Ba_i^o \sqrt{I}} + b_i I, \tag{A.2}$$

where

γ_i = activity coefficient of the aqueous or exchange species *i*

z_i = ionic charge of aqueous phase species *i*

A, B = constants dependent only on temperature

a_i^o, b_i ion-specific parameters

I = total ionic strength of the solution (mol/kgw)

A and B in the Eqs. (A.1) and (A.2) are constant at a given temperature and are defined as follows: (Parkhurst and Appelo, 1999; 2013).

$$B = \left(\frac{2e^2 N_A}{\varepsilon_0 \varepsilon_r k_B T} \right)^{0.5} \tag{A.3}$$

$$A = \frac{e^2 B}{2.303 \times 8\pi \varepsilon_r \varepsilon_0 k_B T} \tag{A.4}$$

where

$e =$ electrostatic unit of charge, 4.803×10^{-10} esu

$N_A =$ Avogadro's number, 6.022×10^{23} molecules per mole

$\varepsilon_0 =$ the permittivity of the free space (or vacuum), also called the electric constant, 8.85×10^{-12} F/m

$\varepsilon_r =$ the relative permittivity of the material in which the charges are immersed, dimensionless, the relative permittivity of the water is about 80 at 20 ^{o}C

$k_B =$ the Boltzmann constant, 1.38×10^{-16} erg/Kelvin

$T =$ temperature, kelvin

$\pi =$ pi number, a mathematical constant, 3.14159

A and B at 25 ^{o}C are 0.51 $mol^{-1/2}dm^{3/2}$ and 3.29 $nm^{-1}mol^{-1/2}dm^{3/2}$, respectively.

Activity: for an aqueous species is defined as molalities times the activity coefficient of that aqueous species (Parkhurst and Appelo, 1999; 2013).

Equivalent fraction of a species on the ion exchange: is equivalent of a species on the ion exchange divided by the sum equivalents of the entire cations present on the

exchanger (or the cation exchange capacitance (CEC) of an exchanger because at equilibrium the total equivalents of the cations present on the exchanger is equal to CEC).

***Equivalent*:** for a species is the molality of the species multiplied by the ionic charge of that species.

Exchange reaction: is a reaction between a geochemical species in the solution and an electrolyte attached to a solid surface. A general exchange reaction is shown as Eq. (A.5):

$$X^{-}A^{+} + B^{+} \rightleftharpoons X^{-}B^{+} + A^{+} \tag{A.5}$$

Ion exchange reaction is similar to the adsorption phenomenon. Clays are one of the most important exchangers in the petroleum reservoirs (Green and Willhite, 1998).

Ionic strength: for a solution is a function of the entire ions concentration present in the solution and defined as follows:

$$I = \frac{1}{2}\sum_{i} m_i z_i^2 \tag{A.6}$$

where

$m_i =$ molality of aqueous species *i* (mole/kgw)

$z_i =$ ionic charge of aqueous phase species *i*

Irreversible reaction: geochemical reactions in which reactants convert to the products while the products cannot convert back to the reactants.

Kinetic reaction: is defined versus the local equilibrium assumption. While thermodynamic is defined at equilibrium, kinetics explains the rate (or how fast) a reaction takes place.

Local equilibrium: assumes both homogenous (aqueous reactions) and heterogeneous (precipitation/dissolution of the solids) reactions occur at the same reaction rate (Zhu and Anderson, 2002). This assumption is valid at low velocities.

Molality: the amount of substance (in mole) in one kilogram of solvent.

Molarity: the amount of substance (in mole) in one liter of solution. Molarity is usually assumed to be equal to molality.

pH: the decimal logarithm of reciprocal of the hydrogen ion activity. pH is defined as follows:

$$pH = -Log\left[a_{H^+}\right] \tag{A.7}$$

where a_{H+} is the hydrogen ion activity.

Redox reaction: reaction between the same element but different state(s) of oxidation or valance(s) (e.g., Fe^{+2} and Fe^{+3}).

Reversible reaction: geochemical reactions in which reactants and products are never fully consumed. In fact, they are dynamically reacting and being produced.

Saturation index (SI): is the logarithm of ratio of the ion activity product (IAP) of a solid divided by the solubility product (K_{SP}) of that solid. Saturation index is defined as follows (Eq. (A.8)):

$$SI = Log\frac{IAP}{K_{SP}} \tag{A.8}$$

Eq. (A.9) shows definition of the saturation index for calcite,

$$SI_{Calcite} = Log \frac{\left[\gamma_{Ca^{+2}} C_{Ca^{+2}}\right]\left[\gamma_{CO_3^{-2}} C_{CO_3^{-2}}\right]}{K_{SP}} \qquad (A.9)$$

Solubility product reaction: the dissolution/precipitation equilibrium reaction of solids is called solubility product reaction and shown with K_{sp}. At zero saturation index equilibrium, the solubility product (K_{SP}) of a solid is equal to the ion activity product (IAP) of the constituting species of that solid. For example, the solubility product of calcite at zero saturation index is shown in Eq. (A.10):

$$CaCO_3(S) \rightleftharpoons Ca^{+2} + CO_3^{-2} \qquad K_{SP} = \left[\gamma_{Ca^{+2}} C_{Ca^{+2}}\right]\left[\gamma_{CO_3^{-2}} C_{CO_3^{-2}}\right]. \qquad (A.10)$$

Super/under saturation: if the saturation index (SI) of a solid is positive, solution is supersatured with respect to that solid hence, solid is precipitated in the system. On the other hand, if the saturation index (SI) of the solid is negative, solution is undersaturated with respect to that solid hence, solid, if presented in the system, is dissolved to the aqueous phase.

Surface complexation: is a general form of the ion-exchanger except the fact that species are attached to the existing functional group of the solid surface of amorphous aluminosilicates, metal oxides/hydroxides and organic matters (Deutsch, 1997). In reactive-transport modeling, ion-exchange concept is usually applied for the major ions while the surface complexation concepts are used for minor and trace components (Zhu and Anderson, 2002). Moreover, in the surface complexation the electrical potential of the surface is taken into account in the sorption of species on the surface (Appelo and Rolle, 2010).

Appendix B: UTCOMP-EQBATCH and UTCHEM-EQBATCH Sample Input Files

B.1 UTCOMP-EQBATCH INPUT FILES

To run UTCOMP-EQBATCH two input files are required (INPUT.DAT and GCINPUT.DAT). INPUT.DAT is the main UTCOMP input file and the geochemistry data are defined in the GCINPUT.DAT file. Both the INPUT.DAT and GCINPUT.DAT files are provided below. UTCHEM-EQBATCH input file for the same case is also given.

B.1.1 INPUT.DAT

```
CC*************************************************************************
**
CC                                                                       *
CC  BRIEF DESCRIPTION OF DATA SET: UTCOMP ( VERSION 3.8)
*
CC
*
CC*************************************************************************
**
CC
*
CC
*
CC
*
CC LENGTH(FT):                    INJECTION FLUID  : WATERFLOOD
*
CC HEIGHT(FT):                  INJECTION RATE   :                  *
CC WIDTH(FT) :                W/O REL. PERM    : Corey             *
CC POROSITY  :                G/O REL. PERM    : Corey             *
CC ABS. PERM :                 3-PHASE REL. PERM: Corey            *
CC TEMP(F)   :                 WETTIBILITY:       none             *
CC PRE(PSI)  :                                                     *
CC SOR       :                                                     *
CC SWC       :                                                     *
CC AVG. DEPTH(FT) :                                                *
```

```
CC
*
CC      "FFT"                    *
CC                                 *
CC
*
CC
*
CC
*
CC*********************************************************************
**
CC
*
CC         HYDROCARBON DATA AND FLASH CALCULATION OPTIONS
*
CC
*
CC*********************************************************************
**
CC
CC..+....1....+....2....+....3....+....4....+....5....+....6...+...7..
CC***********SOME CONSTANTS AND MAXIMUM VALUES FOR MODELS**************
CC
CC NXM, NYM, NZM, NPM, NCM, NWM POSTPROCESSOR
   100  1   1    3     12    2   2
CC
CC NS1M,NBWM,NPRM,NPFM,NCTM,NHSM
    1    401   50    10   10   10000
CC
CC IC2,NCMT,NREG,NTAB
    2  4    6   25
CC
CC EE, NZPM
   0.5761 3
CC
CC TOLP, TOLVOL, QLIM
   0.5D-1 0.5D-4 1.0D-30
CC
CC NUMAX,INQUA,INCON,INVEL,NOSWTM,NUMPRE,NUMOUT,NUMPVT,NST,IFLIP
    10     3     3     5     10     30     12     30    20   0
CC*********************************************************************
CC CASE NAME WITH FORMAT ( 17A4, A2 ) OF TOTAL 70 COLUMNS.
*----HEADER
1D CO2+NG INJECTION INVOLVING 3 HC PHASES
CC
CC NUMBER OF COMPONENTS.
*--------NC
         12
CC COMPONENT NAMES WITH FORMAT ( 1X, A8 ), NC CARDS.
CC..+..8
```

```
*----NAME
    CO2
    C1N2
    C2
    C3
    C4
    C5
    C6
    C710
    C1113
    C1419
    C2029
    C30P
CC
CC BLACK OIL OPTION; AQUIFER SALINITY (ppm); AQUIFER OPTION
*-----IBOST     SLNTY    IAQUIF
         0        0.         0
CC CRITICAL PRESS. (PSI), TEMP. (R) AND  VOL. (CU FT/LB-MOLE),
CC MOLECULAR WT. (LB/LB-MOLE), ACENTRIC FACTOR, PARACHOR. NC CARDS.
*--------PC         TC          VC        MW         OM      PARACH
VSP
        1070.535624     547.5 2.243201575 44    0.2276      49    0
        666.972984      342.5 1.442237287 16.1  0.0109      71    0
      707.6591358 549.6 2.371294757 30.1  0.099 134.825     0
      616.2902348 665.6 3.252343124 44.1  0.1518      233.048     0
      544.3147329 756.4 4.122115282 58.1  0.1885      394.499     0
      489.3334468 838.4 4.883768876 72.1  0.24  707.76      0
      476.1379381 913.8 5.423128436 84    0.2711      1035.85     0
      412.859476  1048.7      6.959539271 113.3 0.3683      1035.85
      0
      318.1916979 1196.4      10.20105981 161.9 0.5239      1035.85
      0
      249.6150391 1328.9      14.31231704 226   0.6932      1035.85
      0
      192.4345015 1475.9      21.23608053 331.5 0.9   1035.85     0
      133.6545083 1574.9      37.15367911 588   1.2   1035.85     0
CC EOS parameters (Ac and Bc)
CC NC CARDS.
*----    PARAA           PARAB
      0.457236    0.077796
      0.457236    0.077796
      0.457236    0.077796
      0.457236    0.077796
      0.457236    0.077796
      0.457236    0.077796
      0.457236    0.077796
      0.457236    0.077796
      0.457236    0.077796
      0.457236    0.077796
      0.457236    0.077796
      0.457236    0.077796
```

```
CC
CC BINARY INTERACTION COEFFICIENTS, CIJ. NC CARDS.
*-----DELTA
      0
      0.105 0
      0.125 0.0028      0

      0.12  0.0089      0.0017      0

      0.12  0.0156      0.0053      0.001 0

      0.12  0.0216      0.009 0.0029      0.0005      0

      0.12  0.0257      0.0118      0.0045      0.0013      0.0002
      0
      0.12  0.0369      0.0198      0.01  0.0047      0.0022
      0.0011      0
      0.13  0.0575      0.0359      0.0223      0.0141      0.0093
      0.0069      0.0025      0
      0.13  0.0789      0.0538      0.037 0.0263      0.0198
      0.0161      0.009 0.002 0
      0.13  0.1072      0.0784      0.0584      0.045 0.0365
      0.0316      0.0213      0.0093      0.0027      0
      0.13  0.1523      0.1193      0.0954      0.0788      0.0677
      0.0612      0.0469      0.0284      0.0156      0.0054      0
CC
CC BINARY INTERACTION COEFFICIENTS, DIJ. NC CARDS.
*-------DIJ
      0
      0     0
      0     0     0
      0     0     0     0
      0     0     0     0     0
      0     0     0     0     0     0
      0     0     0     0     0     0     0
      0     0     0     0     0     0     0     0
      0     0     0     0     0     0     0     0     0
      0     0     0     0     0     0     0     0     0     0
      0     0     0     0     0     0     0     0     0     0     0
      0     0     0     0     0     0     0     0     0     0     0
      0
CC
CC reduction method: (0: OFF, 1: ON)
*-------IFLASHTYPE  irfla  irsa
          1           0      0
CC
CC MAXIMUM NUMBER OF PHASES ( 3 OR 4 )
*--------NP      IVISC  IVISC_COEF   ISINGL   ISOLU
         3         1      0           0        0
CC IEOS: 1,    IPEM: 0 OR 1
CC ISTAM: -1, 0 OR 1, IEST: 0 OR 1  KI: 0, 1 OR 2
```

```
*---IEOS   IPEM     ISTAM   IEST  IVSP   KI
     1      1        -1      1      0     0
CC
CC ITERATION TOLERANCES FOR PERSCHKE'S FLASH ROUTINES.
*----TOLFLA    TOLFLM     TOLPD    TOLSAM    TOLSAS    TOLSUM
     1.0E-08  1.0E-8    1.0E-10  1.0E-8   1.0E-8   1.0E-08
CC
CC MAXIMUM NUMBER OF ITERATIONS FOR PERSCHKE'S FLASH ROUTINES.
*----MAXFLA    MAXFLM     MAXPD    MAXSAM    MAXSAS
      30000     1000      1000      1000     30000      20
CC
CC VECTOR FLASH OPTION
*--IVCFL   TOLVFL     MAXVFL
     0      1.E-10     30
CC
CC SWITCHING PARAMETERS FOR PERSCHKE'S FLASH ROUTINES.
*----SWIPCC    SWIPSA
     1.e-3     1.e-3
CC
CC PHASE IDENTIFICATION PARAMETERS FOR PERSCHKE'S FLASH ROUTINES.
*------IOIL      ITRK   DMSLIM
         1        2      25.
CC
CC IFLAGT ( 0 : OFF,   1 : ON )
*------IFLAGT  IGEOCHEM IPhreeqc    IASPR
            0     1        0          0
CC
CC*****************************************************************
**
CC                                                              *
CC OUTPUT OPTIONS                                               *
CC                                                              *
CC*****************************************************************
**
CC
CC
CC HISTORY PRINTING PARAMETER FOR <<HISTORY.CPR>>.
*--- NHSSKIP   NSTSKIP     IPV
      20        20          1
CC
CC REFERENCE CONCENTRATION, CONC0, USED FOR EFFLUENT CONCENTRATION.
*-----CONC0
  1.0  1.0  1.0  1.0  1.0  1.0  1.0  1.0   1.0  1.0  1.0  1.0
CC
CC
*------
      0
CC
CC NUMBER OF PRINTS FOR <<PROFILE.CPR>>.
*-------NPF
         0
```

```
CC
CC NUMBER OF PRINTS FOR <<CONTOUR.CPR>>.
*-------NCT
         0
CC
CC**********************************************************************
**
CC                                                                    *
CC RESERVOIR AND WELL DATA                                                *
CC                                                                    *
CC**********************************************************************
**
CC
CC A FLAG FOR RESERVOIR GEOMETRY:
CC 2-D: 11(Y), 12(X), 13(Z), 2-D: 21(XY), 22(YZ), 23(XZ), 3-D: 31
*-----IGEOM       INUG
        12          0
CC
CC NUMBER OF GRID BLOCKS IN X, Y, AND Z.
*--------NX        NY        NZ
         100        1         1
CC
CC NUMBER OF WELLS, AND FLAG FOR WELLBORE MODEL
*--------NW       IWM
         2         1
CC
CC WELLBORE RATIUS (FT). NW NUMBERS.
*--------RW: (NW)
        0.33         0.33
CC
CC WELL LOCATIONS. NW CARDS.
*-------LXW       LYW    IDIR   LZWF      LZWL
          1        1        3      1         1
         100       1        3      1         1
CC
CC A FLAG ( 0 OR 1 ) FOR GRID BLOCK SIZE IN X-DIRECTION.
*-------MDX
         0
CC
CC CONSTANT GRID BLOCK SIZE IN X-DIRECTION (FT).
*--------DX
         0.04
CC
CC A FLAG ( 0 OR 1 ) FOR GRID BLOCK SIZE IN Y-DIRECTION.
*-------MDY
        0
CC
CC CONSTANT GRID BLOCK SIZE IN Y-DIRECTION (FT).
*--------DY
        0.15
CC
```

```
CC A FLAG ( 0 OR 1 ) FOR GRID BLOCK SIZE IN Z-DIRECTION.
*-------MDZ
        0
CC
CC CONSTANT GRID BLOCK SIZE IN Z-DIRECTION (FT).
*--------DZ
        0.15
CC
CC A FLAG ( 0 OR 1 ) FOR FORMATION DEPTH.
*--------MD
         0
CC
CC DEPTH (FT) OF THE MOST UPPER LAYER.
*---------D
       0.
CC
CC A FLAG ( 0 OR 1 ) FOR FORMATION POROSITY.
*------MPOR
       0
CC
CC HOMOGENEOUS POROSITY (FRACTION) AT PF.
*----PORSTD
     0.25
CC
CC A FLAG ( 0 OR 1 ) FOR PERMEABILITY IN X-DIRECTION.
*----MPERMX
       0
CC
CC HOMOGENEOUS PERMEABILITY (MD) IN X-DIRECTION.
*-----PERMX
100
CC
CC A FLAG ( 0 OR 1 ) FOR PERMEABILITY IN Y-DIRECTION.
*----MPERMY
       0
CC
CC HOMOGENEOUS PERMEABILITY (MD) IN Y-DIRECTION.
*-----PERMY
100
CC
CC FLAG ( 0 OR 1 ) FOR PERMEABILITY IN Z-DIRECTION.
*----MPERMZ
       0
CC
CC HOMOGENEOUS PERMEABILITY (MD) IN Z-DIRECTION.
*-----PERMZ
     10.00
CC
CC FORMATION COMPRESSIBILITY (1/PSI) AND REFERENCE PRESSURE (PSI).
*--------CF           PF
       0.          14.67
```

```
CC H2O COMPRESSIBILITY (1/PSI), REFERENCE PRESSURE (PSI) AND
CC MOLAR DENSITY (LB-MOLE/CU FT).
*--------CW       PW     DENMWS
      0.     14.67      3.467
CC
CC WATER MOLECULAR WT. (LBM/LBM-MOLE) AND VISCOSITY (CP).
*-------WTW     VISCW
        18.       0.79
CC
CC FORMATION TEMPERATURE (F).
*-----TEMPF
       212.0
CC
CC STANDARD TEMPERATURE (F) AND STANDARD PRESSURE (PSI).
*-----TFSTD      PSTD
        60.      14.67
CC
CC A FLAG ( 1, 2, 3 OR 4 ) FOR NUMERICAL DISPERSION CONTROL.
*----IUPSTW
        1
CC
CC ITC ( 0 : NO 2ND ORDER TIME,   1 : 2ND ORDER TIME ON )
*----ITC
       0
CC RESTART OPTIONS.
CC ISTART ( 1 OR 2 ), ISTORE ( 0 OR 1 ).
*----ISTART    ISTORE
        1       1
CC
CC A FLAG ( 0 OR 1 ) FOR AUTOMATIC TIME-STEP SELECTION ( = 1 ).
*-------MDT
         1
CC
CC A FLAG ( 0 OR 1 ) FOR PHYSICAL DISPERSION CALCULATION.
*-----MDISP
        1
CC MOLECULAR DIFFUSION COEFFICIENTS ( FT*FT/DAY ).
CC NP CARDS AND EACH CARD HAS NC NUMBERS.
*----DIFFUN
       0. 0. 0. 0.  0. 0. 0. 0.  0. 0. 0. 0.
       0. 0. 0. 0.  0. 0. 0. 0.  0. 0. 0. 0.
       0. 0. 0. 0.  0. 0. 0. 0.  0. 0. 0. 0.
CC
CC TORTUOSITY FACTOR.
*-------TAU
         1.
CC
CC LONGITUDINAL AND TRANSVERSE DISPERSIVITIES (FT). NP CARDS.
*----ALPHAL ALPHAT
      0.08    0.0
      0.    0.0
```

```
      0.    0.0
CC
CC YOUNG'S DISPERSION MODEL
*-----BETAL BETAT ALMAX ATMAX
       0.0   0.0   0.2  0.005
CC FLAGS FOR RELATIVE PERMEABILITY MODEL AND CAPILLARY PRESSURE.
CC IPERM ( 1 OR 2 ), ICPRES ( 0 OR 1 ).
*-----IPERM    ICPRES      ICAP    IRPERM
       4         0          0          0
CC CAPILLARY PRESSURE PARAMETERS AND
CC WATER/OIL INTERFACIAL TENSION (DYNES/CM).
*-------EPC       CPC    RIFTWO    RIFTWG    RIFTWL
         2.        2.0    20.        24.       30.
CC
CC HIGH IFT RESIDUAL SATURATIONS.
*-----S1RW     S2RW1     S2RW2      S3RW     S4RW1     S4RW2
         0.05      0.18       .25       0.05     0.2       0.2
CC
CC LOW IFT RESIDUAL SATURATIONS.
*------S1RC     S2RC1     S2RC2      S3RC     S4RC1     S4RC2
       0    .0       .0         0.        0.        0.
CC
CC HIGH IFT END POINT RELATIVE PERMEABILITY.
*------P1RW      P2RW      P3RW      P4RW
        0.383     1.0       0.35       0.35
CC
CC LOW IFT END POINT RELATIVE PERMEABILITY.
*------P1RC       P2RC         P3RC         P4RC
        1.        1              1           1.
CC
CC HIGH IFT EXPONENT OF RELATIVE PERMEABILITY.
*-------E1W      E2W1      E2W2       E3W      E4W1      E4W2
         1.59       3.22     2.5      2.5       2.5       2.5
CC
CC LOW IFT EXPONENT OF RELATIVE PERMEABILITY.
*-------E1C      E2C1      E2C2       E3C      E4C1      E4C2
         1.        1.        1.        1.        1.        1.
CC
CC WATER AND L1 PHASE CAPILLARY DESATURATION PARAMETERS.
*-------T11       T12      T211      T221      T212      T222
        -.4       1.6      -0.5       2.2      -.04       1.6
CC
CC GAS AND L2 PHASE CAPILLARY DESATURATION PARAMETERS.
*-------T31       T32      T411      T421      T412      T422
        -0.5      2.2      -0.5       2.2       -.4       1.6
CC
CC
*------  IWALT    IWALF
            0       0
CC
CC A FLAG FOR PRESSURE EQUATION SOLVER ( 1, 2, 3, 4 OR 5 ).
```

```
*----IPRESS    IPREC   METHSL   OMEGA    IHYPRE
        4       2       1       1.0      1      0
CC
CC ITERATIVE PRESSURE SOLVER PARAMETERS.
*-----ITMAX  LEVLIT  IDGTS   NS1       NS2      ZETA
      1000      1      1      5      1000000   1.E-07
CC
CC INITIAL TIME (DAYS).
*---------T
          0
CC
CC A FLAG ( 0 OR 1 ) FOR INITIAL PRESSURE.
*--------MP
         0
CC
CC CONSTANT INITIAL PRESSURE (PSIA).
*---------P
        4890
CC
CC A FLAG ( 0 OR 1 ) FOR INITIAL WATER SATURATION.
*------MSAT
        0
CC
CC CONSTANT INITIAL WATER SATURATION (FRACTION).
*-------SAT
      0.999
CC
CC A FLAG ( 0 OR 1 ) FOR INITIAL OVERALL COMPOSITION.
*-----MOMFR
        0
CC
CC CONSTANT INITIAL COMPOSITION (MOLE FRACTION).
*------OMFR
      0.12837     0.42134     0.05557     0.02662     0.01535
      0.00985     0.00835     0.06971     0.03578     0.07131
      0.07629     0.08146
CC
CC*************************************************************************
**
CC                                                                      *
CC RECURRENT DATA
*
CC                                                                      *
CC*************************************************************************
**
CC                  Sea   Water Injection
*
CC*************************************************************************
**
CC MAXIMUM TIME (DAYS), TIME STEP (DAYS) AND WELL DATA.
*--------TM         DT       NWELLS    GORLIM    WORLIM
```

```
        1.5         1E-3     2          -1       -1
CC
CC
*-----DTMAX     DTMIN     DSLIM     DPLIM      DVLIM    DMFACT
DMFACTG
       0.1      0.001     0.05      0.005       0.05      0.03     0.05
CC
CC WELL NO. AND WELL TYPE.
*--------LW    IQTYPE
          1      4
CC
CC   (B/D)  (MSCF/D)
*----QPSVC(1)   QPSVC(3)   NCOMP   ISWITCH   PBHC
      4E-5       0         0        0        6000
CC
CC
*---
0.0003      1.660228      0.00002      0.004    0.048046   0.0013
5.036216E-03      7.799387E-03      0.0013      0.048      9.006128E-03
0.04826
CC
CC WELL NO. AND WELL TYPE.
*--------LW    IQTYPE
         2       -2
CC
CC CONSTANT BHP PRODUCER (PSI)
*--------PBHC
        4890.0
CC
CC END OF INPUT.
*--------TM     DT    NWELLS   GORLIM   WORLIM ----------------
         -1.0   -1.     -1     -1.E10    -1.E10
```

B.1.2 GCINPUT.DAT

```
CC
CC*******************************************************
CC                                                      *
CC             GEOCHEMISTRY SECTION                     *
CC                                                      *
CC*******************************************************
CC
CC
*-----NELET NFLD NSLD NSORB ITCHARGE
        12    51  7      0     0
CC
CC
*----- NIAQ NEX NSLEL NOXY
       12    0    9   12
```

```
CC
CC NAME AND CHARGE FOR THE ELEMENTS
*----
Cr+3                                3
H+1                                 1
Pb+2                                2
MG+2                                2
Ca+2                                2
Na+1                                1
Al+3                                3
Si+4                                4
Cl-1                               -1
CO3-2                              -2
SO4-2                              -2
OXYGEN                             -2
CC
CC
*------ FLDSPS(I)
 Cr(OH)2+
 H+1
 Pb+2
 Mg+2
 Ca+2
 Na+1
 Al+3
 H4SiO4
 Cl-1
 CO3-2
 SO4-2
 WATER
 OH-
 H3SiO4 -
 MgOH +
 MgCO3 AQ
 MgHCO3 +
 MgSO4 AQ
 CaOH +
 CaHCO3 +
 CaCO3 AQ
 CaSO4 AQ
 NaCO3 -
 NaHCO3 AQ
 NaSO4 -
 AlOH +2
 Al(OH)2 +
 AlSO4 +
 Al(SO4)2 -
 PbCl +
 PbCl2 AQ
 PbCl3 -
 PbCl4 -2
```

```
 Pb(CO3)2-2
 PbOH +
 Pb2OH +3
 PbSO4 AQ
 PbCO3 AQ
 Pb(SO4)2-2
 PbHCO3 +
 HCO3 -
 H2CO3 AQ
 HSO4 -
 Cr+3
 Cr(OH)+2
 CrCl+2
 CrCl2 +
 CrSO4 +
 CrOHSO4 AQ
 Cr2OH2SO4+2
 Cr2OH2SO42
CC
CC-
*-------- SLDPS(I)
 CALCITE
 GIBBSITE (C)
 GYPSUM
 SIO2(A,PT)
 CERRUSITE
 ANGLESITE
 CR(OH)3 (A)
CC
CC
*------- SORBSP(I)

CC
CC- (IF NSORB>0)
*-------- NSORBX(I)

CC
CC
*----- AR(I,J)
 1.  0.  0.  0.  0.  0.  0.  0.  0.  0.  0.  0.  0.  0.  0.
 0.  0.  0.  0.  0.  0.  0.  0.  0.  0.  0.  0.  0.  0.  0.
 0.  0.  0.  0.  0.  0.  0.  0.  0.  0.  0.  0.  0.  1.  1.
 1.  1.  1.  1.  2.  2.
 2.  1.  0.  0.  0.  0.  0.  4.  0.  0.  0.  2.  1.  3.  1.
 0.  1.  0.  1.  1.  0.  0.  0.  1.  0.  1.  2.  0.  0.  0.
 0.  0.  0.  0.  1.  1.  0.  0.  0.  1.  1.  2.  1.  0.  1.
 0.  0.  0.  1.  2.  2.
 0.  0.  1.  0.  0.  0.  0.  0.  0.  0.  0.  0.  0.  0.  0.
 0.  0.  0.  0.  0.  0.  0.  0.  0.  0.  0.  0.  0.  0.  1.
 1.  1.  1.  1.  1.  2.  1.  1.  1.  1.  0.  0.  0.  0.  0.
 0.  0.  0.  0.  0.  0.
```

```
 0.  0.  0.  1.  0.  0.  0.  0.  0.  0.  0.  0.  0.  0.  1.
 1.  1.  1.  0.  0.  0.  0.  0.  0.  0.  0.  0.  0.  0.  0.
 0.  0.  0.  0.  0.  0.  0.  0.  0.  0.  0.  0.  0.  0.  0.
 0.  0.  0.  0.  0.  0.
 0.  0.  0.  0.  1.  0.  0.  0.  0.  0.  0.  0.  0.  0.  0.
 0.  0.  0.  1.  1.  1.  1.  0.  0.  0.  0.  0.  0.  0.  0.
 0.  0.  0.  0.  0.  0.  0.  0.  0.  0.  0.  0.  0.  0.  0.
 0.  0.  0.  0.  0.  0.
 0.  0.  0.  0.  0.  1.  0.  0.  0.  0.  0.  0.  0.  0.  0.
 0.  0.  0.  0.  0.  0.  0.  1.  1.  1.  0.  0.  0.  0.  0.
 0.  0.  0.  0.  0.  0.  0.  0.  0.  0.  0.  0.  0.  0.  0.
 0.  0.  0.  0.  0.  0.
 0.  0.  0.  0.  0.  0.  1.  0.  0.  0.  0.  0.  0.  0.  0.
 0.  0.  0.  0.  0.  0.  0.  0.  0.  0.  1.  1.  1.  1.  0.
 0.  0.  0.  0.  0.  0.  0.  0.  0.  0.  0.  0.  0.  0.  0.
 0.  0.  0.  0.  0.  0.
 0.  0.  0.  0.  0.  0.  0.  1.  0.  0.  0.  0.  0.  1.  0.
 0.  0.  0.  0.  0.  0.  0.  0.  0.  0.  0.  0.  0.  0.  0.
 0.  0.  0.  0.  0.  0.  0.  0.  0.  0.  0.  0.  0.  0.  0.
 0.  0.  0.  0.  0.  0.
 0.  0.  0.  0.  0.  0.  0.  0.  1.  0.  0.  0.  0.  0.  0.
 0.  0.  0.  0.  0.  0.  0.  0.  0.  0.  0.  0.  0.  0.  1.
 2.  3.  4.  0.  0.  0.  0.  0.  0.  0.  0.  0.  0.  0.  0.
 1.  2.  0.  0.  0.  0.
 0.  0.  0.  0.  0.  0.  0.  0.  0.  1.  0.  0.  0.  0.  0.
 1.  1.  0.  0.  1.  1.  0.  1.  1.  0.  0.  0.  0.  0.  0.
 0.  0.  0.  2.  0.  0.  0.  1.  0.  1.  1.  1.  0.  0.  0.
 0.  0.  0.  0.  0.  0.
 0.  0.  0.  0.  0.  0.  0.  0.  0.  0.  1.  0.  0.  0.  0.
 0.  0.  1.  0.  0.  0.  1.  0.  0.  1.  0.  0.  1.  2.  0.
 0.  0.  0.  0.  0.  0.  1.  0.  2.  0.  0.  0.  1.  0.  0.
 0.  0.  1.  1.  1.  2.
 2.  0.  0.  0.  0.  0.  0.  4.  0.  0.  0.  1.  1.  4.  1.
 0.  0.  0.  1.  0.  0.  0.  0.  0.  0.  1.  2.  0.  0.  0.
 0.  0.  0.  0.  1.  1.  0.  0.  0.  0.  0.  0.  0.  0.  1.
 0.  0.  0.  1.  2.  2.
CC
CC
*---- BR(I,J)
 0.  0.  0.  0.  0.  0.  1.
 0.  3.  4.  0.  0.  0.  3.
 0.  0.  0.  0.  1.  1.  0.
 0.  0.  0.  0.  0.  0.  0.
 1.  0.  1.  0.  0.  0.  0.
 0.  0.  0.  0.  0.  0.  0.
 0.  1.  0.  0.  0.  0.  0.
 0.  0.  0.  1.  0.  0.  0.
 0.  0.  0.  0.  0.  0.  0.
 1.  0.  0.  0.  1.  0.  0.
 0.  0.  1.  0.  0.  1.  0.
 0.  3.  2.  2.  0.  0.  3.
```

```
CC
CC
*----------- DR(I,J)

CC
CC
*------------ BB(I,J)
 1.0  0.0  0.0  0.0  0.0  0.0  0.0  0.0  0.0  0.0  0.0  0.0
 0.0  1.0  0.0  0.0  0.0  0.0  0.0  0.0  0.0  0.0  0.0  0.0
 0.0  0.0  1.0  0.0  0.0  0.0  0.0  0.0  0.0  0.0  0.0  0.0
 0.0  0.0  0.0  1.0  0.0  0.0  0.0  0.0  0.0  0.0  0.0  0.0
 0.0  0.0  0.0  0.0  1.0  0.0  0.0  0.0  0.0  0.0  0.0  0.0
 0.0  0.0  0.0  0.0  0.0  1.0  0.0  0.0  0.0  0.0  0.0  0.0
 0.0  0.0  0.0  0.0  0.0  0.0  1.0  0.0  0.0  0.0  0.0  0.0
 0.0  0.0  0.0  0.0  0.0  0.0  0.0  1.0  0.0  0.0  0.0  0.0
 0.0  0.0  0.0  0.0  0.0  0.0  0.0  0.0  1.0  0.0  0.0  0.0
 0.0  0.0  0.0  0.0  0.0  0.0  0.0  0.0  0.0  1.0  0.0  0.0
 0.0  0.0  0.0  0.0  0.0  0.0  0.0  0.0  0.0  0.0  1.0  0.0
 0.0  0.0  0.0  0.0  0.0  0.0  0.0  0.0  0.0  0.0  0.0  1.0
 0.0 -1.0  0.0  0.0  0.0  0.0  0.0  0.0  0.0  0.0  0.0  0.0
 0.0 -1.0  0.0  0.0  0.0  0.0  0.0  1.0  0.0  0.0  0.0  0.0
 0.0 -1.0  0.0  1.0  0.0  0.0  0.0  0.0  0.0  0.0  0.0  0.0
 0.0  0.0  0.0  1.0  0.0  0.0  0.0  0.0  0.0  1.0  0.0  0.0
 0.0  1.0  0.0  1.0  0.0  0.0  0.0  0.0  0.0  1.0  0.0  0.0
 0.0  0.0  0.0  1.0  0.0  0.0  0.0  0.0  0.0  0.0  1.0  0.0
 0.0 -1.0  0.0  0.0  1.0  0.0  0.0  0.0  0.0  0.0  0.0  0.0
 0.0  1.0  0.0  0.0  1.0  0.0  0.0  0.0  0.0  1.0  0.0  0.0
 0.0  0.0  0.0  0.0  1.0  0.0  0.0  0.0  0.0  1.0  0.0  0.0
 0.0  0.0  0.0  0.0  1.0  0.0  0.0  0.0  0.0  0.0  1.0  0.0
 0.0  0.0  0.0  0.0  0.0  1.0  0.0  0.0  0.0  1.0  0.0  0.0
 0.0  1.0  0.0  0.0  0.0  1.0  0.0  0.0  0.0  1.0  0.0  0.0
 0.0  0.0  0.0  0.0  0.0  1.0  0.0  0.0  0.0  0.0  1.0  0.0
 0.0 -1.0  0.0  0.0  0.0  0.0  1.0  0.0  0.0  0.0  0.0  0.0
 0.0 -2.0  0.0  0.0  0.0  0.0  1.0  0.0  0.0  0.0  0.0  0.0
 0.0  0.0  0.0  0.0  0.0  0.0  1.0  0.0  0.0  0.0  1.0  0.0
 0.0  0.0  0.0  0.0  0.0  0.0  1.0  0.0  0.0  0.0  2.0  0.0
 0.0  0.0  1.0  0.0  0.0  0.0  0.0  0.0  1.0  0.0  0.0  0.0
 0.0  0.0  1.0  0.0  0.0  0.0  0.0  0.0  2.0  0.0  0.0  0.0
 0.0  0.0  1.0  0.0  0.0  0.0  0.0  0.0  3.0  0.0  0.0  0.0
 0.0  0.0  1.0  0.0  0.0  0.0  0.0  0.0  4.0  0.0  0.0  0.0
 0.0  0.0  1.0  0.0  0.0  0.0  0.0  0.0  0.0  2.0  0.0  0.0
 0.0 -1.0  1.0  0.0  0.0  0.0  0.0  0.0  0.0  0.0  0.0  0.0
 0.0 -1.0  2.0  0.0  0.0  0.0  0.0  0.0  0.0  0.0  0.0  0.0
 0.0  0.0  1.0  0.0  0.0  0.0  0.0  0.0  0.0  0.0  1.0  0.0
 0.0  0.0  1.0  0.0  0.0  0.0  0.0  0.0  0.0  1.0  0.0  0.0
 0.0  0.0  1.0  0.0  0.0  0.0  0.0  0.0  0.0  0.0  2.0  0.0
 0.0  1.0  1.0  0.0  0.0  0.0  0.0  0.0  0.0  1.0  0.0  0.0
 0.0  1.0  0.0  0.0  0.0  0.0  0.0  0.0  0.0  1.0  0.0  0.0
 0.0  2.0  0.0  0.0  0.0  0.0  0.0  0.0  0.0  1.0  0.0  0.0
 0.0  1.0  0.0  0.0  0.0  0.0  0.0  0.0  0.0  0.0  1.0  0.0
 1.0  2.0  0.0  0.0  0.0  0.0  0.0  0.0  0.0  0.0  0.0  0.0
```

```
 1.0  1.0  0.0  0.0  0.0  0.0  0.0  0.0  0.0  0.0  0.0  0.0
 1.0  2.0  0.0  0.0  0.0  0.0  0.0  0.0  1.0  0.0  0.0  0.0
 1.0  2.0  0.0  0.0  0.0  0.0  0.0  0.0  2.0  0.0  0.0  0.0
 1.0  2.0  0.0  0.0  0.0  0.0  0.0  0.0  0.0  0.0  1.0  0.0
 1.0  1.0  0.0  0.0  0.0  0.0  0.0  0.0  0.0  0.0  1.0  0.0
 2.0  2.0  0.0  0.0  0.0  0.0  0.0  0.0  0.0  0.0  1.0  0.0
 2.0  2.0  0.0  0.0  0.0  0.0  0.0  0.0  0.0  0.0  2.0  0.0
CC
CC
*------- EXSLD(I,J)
 0.0  0.0  0.0  0.0  1.0  0.0  0.0  0.0  0.0  1.0  0.0  0.0
 0.0 -3.0  0.0  0.0  0.0  0.0  1.0  0.0  0.0  0.0  0.0  0.0
 0.0  0.0  0.0  0.0  1.0  0.0  0.0  0.0  0.0  0.0  1.0  0.0
 0.0  0.0  0.0  0.0  0.0  0.0  0.0  1.0  0.0  0.0  0.0  0.0
 0.0  0.0  1.0  0.0  0.0  0.0  0.0  0.0  0.0  1.0  0.0  0.0
 0.0  0.0  1.0  0.0  0.0  0.0  0.0  0.0  0.0  0.0  1.0  0.0
 1.0 -1.0  0.0  0.0  0.0  0.0  0.0  0.0  0.0  0.0  0.0  0.0
CC
CC
*-------- CHARGE(I), FOR I=1, NFLD
 1.0  1.0  2.0  2.0  2.0  1.0  3.0  0.0 -1.0 -2.0 -2.0  0.0
-1.0 -1.0  1.0  0.0  1.0  0.0  1.0  1.0  0.0  0.0 -1.0  0.0
-1.0  2.0  1.0  1.0 -1.0  1.0  0.0 -1.0 -2.0 -2.0  1.0  3.0
 0.0  0.0 -2.0  1.0 -1.0  0.0 -1.0  3.0  2.0  2.0  1.0  1.0
 0.0  2.0  0.0
CC
CC (IF NSORB>0)
*------- SCHARGE (I,J)

CC
CC
*------- EQK(I)
0.1000000000000E+01 0.1000000000000E+01 0.1000000000000E+01
0.1000000000000E+01 0.1000000000000E+01 0.1000000000000E+01
0.1000000000000E+01 0.1000000000000E+01 0.1000000000000E+01
0.1000000000000E+01 0.1000000000000E+01 0.1000000000000E+01
0.1000000000000E-13 0.1175000000000E-09 0.1622000000000E-11
0.9550000000000E+03 0.2512000000000E+12 0.1778000000000E+03
0.2512000000000E-12 0.2138000000000E+12 0.1412000000000E+04
0.2042000000000E+03 0.1862000000000E+02 0.1905460000000E+11
0.5011872300000E+01 0.1023293000000E-04 0.7943282000000E-10
0.1047128500000E+04 0.8317637700000E+05 0.3981071700000E+02
0.6309573400000E+02 0.5011872300000E+02 0.2398832900000E+02
0.4365158000000E+11 0.1949844000000E-07 0.4365158000000E-06
0.5623413300000E+03 0.1737800800000E+08 0.2951209200000E+04
0.1584893000000E+14 0.2137962000000E+11 0.4786300000000E+17
0.9772372200000E+02 0.4168693000000E+10 0.4168693800000E+06
0.2344228000000E+10 0.4570881000000E+09 0.9332543000000E+11
0.1905460000000E+09 0.1445439000000E+17 0.8511380000000E+18
CC
CC-
```

```
*----------EXK(I,J)

CC
CC-
*-------- EXEX(I,J,K)

CC
CC- (IF NEX>0)
*------- REDUC(I,J)

CC
CC-
*-------- EXCAI(I)

CC
CC- (IF NSLD>0)
*--------- SPK(I)
0.3388441000000E-08 0.5888438000000E+09 0.1412537000000E-04
0.1949844600000E-02 0.7413107300000E-13 0.1621810000000E-07
0.1778279400000E+00
CC
CC
*-------- CELAQI(J)
0.3000000000000E-07 0.1530386041025E-01 0.2000000000000E-07
0.4000000000000E-02 0.1551935201385E-01 0.1300000000000E-02
0.3360166316048E-07 0.7803332339265E-02 0.1300000000000E-02
0.1130958182209E-01 0.1316977019176E-01  0.2540363606000E-02
CC
CC-
*------- CAQI(J)
0.8133276056620e-08 0.2317756800271E-06 0.5542315747452E-09
0.1268460852414E-02 0.4702576290752E-02 0.1276700137574E-02
0.7331683328725E-11 0.1949844600000E-02 0.1299999971197E-02
0.7205499263593E-06 0.3003751375130E-02 0.2673101911424E-07
CC
CC-
*-------- NSLDI(I)
0.1834950908896E-01 0.2499999991088E-02 0.8994349041223E-03
0.3979999669152E+00 0.0000000000000E+00 0.0000000000000E+00
0.0000000000000E+00
CC
CC-
*------ CSORBI(I)
```

B.2 UTCHEM-EQBATCH INPUT FILE

```
CC*****************************************************************
CC                                                                *
CC    BRIEF DESCRIPTION OF DATA SET : UTCHEM (VERSION 2011)       *
```

```
CC                                                                    *
CC*********************************************************************
CC                                                                    *
CC  GEOCHEMISTRY 1D TEST RUN                                          *
CC                                                                    *
CC  LENGTH (FT) :                    PROCESS :                        *
CC  THICKNESS (FT) :                 INJ. RATE (FT3/DAY) :            *
CC  WIDTH (FT) :                     COORDINATES :                    *
CC  POROSITY :                                                        *
CC  GRID BLOCKS :                                                     *
CC  DATE :                                                            *
CC                                                                    *
CC*********************************************************************
CC
CC*********************************************************************
CC                                                                    *
CC    RESERVOIR DESCRIPTION                                           *
CC                                                                    *
CC*********************************************************************
CC
CC Run number
*---- RUNNO
UTEX45
CC
CC Title and run description
*---- title(i)
run ex45
GEOCHEMISTRY - PB AND CR
SINGLE PHASE FLOW
CC
CC SIMULATION FLAGS
*---- IMODE IMES IDISPC ICWM ICAP IREACT IBIO ICOORD ITREAC ITC  IGAS
IENG   IPhreeqc
        1    1     0     0    0     2     0     1      0     1    0
0         0
CC
CC no. of gridblocks,flag specifies constant or variable grid size,unit
*---- NX    NY    NZ  IDXYZ  IUNIT
      100     1    1     0      0
CC
CC constant grid block size in x,y,and z
*---- dx1           dy1           dz1
       0.04          0.15          0.15
CC
CC total no. of components,no. of tracers,no. of gel components
*----n    no    ntw    nta    ngc    ng    noth
     19    0      0      0      11     0      0
CC
CC Name of the components
*----spname(i) for i=1 to n
Water
```

```
Oil
Surf.
Polymer
Chloride
Calcium
Alcohol 1
Alcohol 2
gc-1
gc-2
gc-3
gc-4
gc-5
gc-6
gc-7
gc-8
gc-9
gc-10
gc-11
CC
CC flag indicating if the component is included in calculations or not
*----icf(kc) for kc=1,n
      1  1  1  1  1  1  0  0  1  1  1  1  1  1  1  1  1  1  1
CC
CC*****************************************************************
CC                                                                 *
CC    OUTPUT OPTIONS                                               *
CC                                                                 *
CC*****************************************************************
CC
CC
CC FLAG TO WRITE TO UNIT 3,FLAG FOR PV OR DAYS TO PRINT OR TO STOP THE
RUN
*---- ICUMTM  ISTOP  IOUTGMS
        0       1       0
CC
CC FLAG INDICATING IF THE PROFILE OF KCTH COMPONENT SHOULD BE WRITTEN
*---- IPRFLG(KC),KC=1,N
        1  1  1  1  1  1  0  0  1  1  1  1  1  1  1  1  1  1  1
CC
CC FLAG FOR PRES.,SAT.,TOTAL CONC.,TRACER CONC.,CAP.,GEL, ALKALINE
PROFILES
*---- IPPRES IPSAT IPCTOT IPBIO IPCAP IPGEL IPALK IPTEMP IPOBS
        0      0      1      0     0     0     1     0      0
CC
CC FLAG FOR WRITING SEVERAL PROPERTIES TO UNIT 4 (Prof)
*---- ICKL IVIS IPER ICNM ICSE IHYSTP IFOAMP INONEQ
       0    0    0    0    0    0    0    0
CC
CC FLAG  for variables to PROF output file
*---- IADS IVEL IRKF IPHSE
       0    0    0    0
```

```
CC
CC*********************************************************************
CC                                                                     *
CC    RESERVOIR PROPERTIES                                             *
CC                                                                     *
CC*********************************************************************
CC
CC
CC MAX. SIMULATION TIME ( DAYS)
*---- TMAX
       1.5
CC
CC ROCK COMPRESSIBILITY (1/PSI), STAND. PRESSURE(PSIA)
*---- COMPR                PSTAND
        0                    0
CC
CC FLAGS INDICATING CONSTANT OR VARIABLE POROSITY, X,Y,AND Z
PERMEABILITY
*---- IPOR1  IPERMX IPERMY IPERMZ IMOD
        0      0      0      0     0    0   0 0
CC
CC CONSTANT POROSITY FOR WHOLE RESERVOIR
*---- PORC1
       0.25
CC
CC CONSTANT X-PERMEABILITY FOR WHOLE RESERVOIR
*---- PERMXC
        100
CC
CC CONSTANT Y-PERMEABILITY FOR WHOLE RESERVOIR
*---- PERMYC
        100
CC
CC CONSTANT Z-PERMEABILITY FOR WHOLE RESERVOIR
*---- PERMZC
        10
CC
CC FLAG FOR CONSTANT OR VARIABLE DEPTH, PRESSURE, WATER
SATURATION,INITIAL AQUEOUS PHASE cOMPOSITIONS
*----IDEPTH  IPRESS  ISWI  ICWI
       0       0      0     -1
CC
CC CONSTANT DEPTH (FT)
*---- D111
       0
CC
CC CONSTANT PRESSURE (PSIA)
*---- PRESS1
       4890
CC
CC CONSTANT INITIAL WATER SATURATION
```

```
*---- SWI
      1
CC
CC BRINE SALINITY AND DIVALENT CATION CONCENTRATION (MEQ/ML)
*---- C50       C60
       0.05892   0.00271
CC
CC*********************************************************************
CC                                                                     *
CC    PHYSICAL PROPERTY DATA                                           *
CC                                                                     *
CC*********************************************************************
CC
CC
CC OIL CONC. AT PLAIT POINT FOR TYPE II(+)AND TYPE II(-), CMC
*---- c2plc  c2prc   epsme   ihand
        0      1     0.0001     0
CC
CC flag indicating type of phase behavior parameters
*---- ifghbn
        0
CC SLOPE AND INTERCEPT OF BINODAL CURVE AT ZERO, OPT., AND 2XOPT
SALINITY
CC FOR ALCOHOL 1
*---- hbns70   hbnc70   hbns71   hbnc71   hbns72   hbnc72
        0    0.016       0     0.016     0     0.016
CC SLOPE AND INTERCEPT OF BINODAL CURVE AT ZERO, OPT., AND 2XOPT
SALINITY
CC FOR ALCOHOL 2
*---- hbns80  hbnc80  hbns81  hbnc81  hbns82  hbnc82
        0       0       0       0       0       0
CC
CC LOWER AND UPPER EFFECTIVE SALINITY FOR ALCOHOL 1 AND ALCOHOL 2
*---- csel7   cseu7   csel8   cseu8
       0.65    0.9     0       0
CC
CC THE CSE SLOPE PARAMETER FOR CALCIUM AND ALCOHOL 1 AND ALCOHOL 2
*---- beta6    beta7    beta8
        0        0       0
CC
CC FLAG FOR ALCOHOL PART. MODEL AND PARTITION COEFFICIENTS
*---- ialc   opsk7o   opsk7s   opsk8o   opsk8s
        0      0        0        0        0
CC
CC NO. OF ITERATIONS, AND TOLERANCE
*---- nalmax     epsalc
        20       0.0001
CC
CC ALCOHOL 1 PARTITIONING PARAMETERS IF IALC=1
*---- akwc7     akws7    akm7     ak7      pt7
       4.671    1.79      48     35.31    0.222
```

```
CC
CC ALCOHOL 2 PARTITIONING PARAMETERS IF IALC=1
*---- akwc8     akws8    akm8    ak8     pt8
        0         0        0      0       0
CC
CC ift model flag
*----  ift
        0
CC
CC INTERFACIAL TENSION PARAMETERS
*----  g11     g12     g13     g21     g22      g23
       13    -14.8    0.007     13     -14.5     0.01
CC
CC LOG10 OF OIL/WATER INTERFACIAL TENSION
*---- xiftw
       1.477
CC
CC ORGANIC MASS TRANSFER FLAG
*---- imass icor
        0       0
CC
CC
*--- IWALT  IWALF
      0      0
CC
CC CAPILLARY DESATURATION PARAMETERS FOR PHASE 1, 2, AND 3
*---- itrap      t11      t22      t33
        0        1865    28665.46    364.2
CC
CC  FLAG FOR RELATIVE PERMEABILITY AND CAPILLARY PRESSURE MODEL
*---- iperm
        0   0
CC
CC FLAG FOR CONSTANT OR VARIABLE REL. PERM. PARAMETERS
*---- isrw    iprw    iew
        0      0       0
CC
CC CONSTANT RES. SATURATION OF PHASES 1,2,AND 3 AT LOW CAPILLARY NO.
*---- s1rwc    s2rwc     s3rwc
       0.147      0.4      0.147
CC
CC CONSTANT ENDPOINT REL. PERM. OF PHASES 1,2,AND 3 AT LOW CAPILLARY
NO.
*---- p1rwc     p2rwc    p3rwc
       0.13771       0.9148      0.13771
CC
CC CONSTANT REL. PERM. EXPONENT OF PHASES 1,2,AND 3 AT LOW CAPILLARY
NO.
*---- e1wc     e2wc     e3wc
       2.1817       1.40475       2.1817
CC
```

```
CC WATER AND OIL VISCOSITY , RESERVOIR TEMPERATURE
*---- VIS1    VIS2   TSTAND
      0.79      2.5      0
CC
CC COMPOSITIONAL PHASE VISCOSITY PARAMETERS
*----   ALPHAV1   ALPHAV2   ALPHAV3   ALPHAV4  ALPHAV5
         2.25812   0.9967113   0         0.9       0.7
CC
CC PARAMETERS TO CALCULATE POLYMER VISCOSITY AT ZERO SHEAR RATE
*---- AP1      AP2      AP3
       74.3      1106     6376
CC
CC PARAMETER TO COMPUTE CSEP,MIN. CSEP, AND SLOPE OF LOG VIS. VS. LOG
CSEP
*---- BETAP    CSE1     SSLOPE
       2      0.01      0
CC
CC PARAMETER FOR SHEAR RATE DEPENDENCE OF POLYMER VISCOSITY
*---- GAMMAC   GAMHF   POWN
       0       10      1.8  0 0 0 0  0
CC
CC CC FLAG FOR POLYMER PARTITIONING, PERM. REDUCTION PARAMETERS
*---- IPOLYM    EPHI3    EPHI4    BRK     CRK
        1         1       0.9      1000    0.0186  0
CC
CC SPECIFIC WEIGHT FOR COMPONENTS 1,2,3,7,8 ,Coeffient of oil and
GRAVITY FLAG
*---- DEN1     DEN2    DEN23     DEN3    DEN7    DEN8    IDEN
      0.4368     0.3462     0.3462     0.4333     0.346    0        1
CC
CC FLAG FOR CHOICE OF UNITS ( 0:BOTTOMHOLE CONDITION , 1: STOCK TANK)
*----- ISTB
        0
CC
CC COMPRESSIBILITY FOR VOL. OCCUPYING COMPONENTS 1,2,3,7,AND 8
*---- COMPC(1)  COMPC(2)  COMPC(3)  COMPC(7)  COMPC(8)
         0        0         0         0         0
CC
CC CONSTANT OR VARIABLE PC PARAM., WATER-WET OR OIL-WET PC CURVE FLAG
*---- ICPC    IEPC   IOW
       0       0      0
CC
CC CAPILLARY PRESSURE PARAMETER, CPC0
*---- CPC0
       0
CC
CC CAPILLARY PRESSURE PARAMETER, EPC0
*---- EPC0
       2
CC
CC MOLECULAR DIFFUSION COEF. KCTH COMPONENT IN PHASE 1
```

```
*---- D(KC,1),KC=1,N
         0        0        0        0        0        0        0
0        0        0        0        0        0
         0        0        0        0        0        0
CC
CC MOLECULAR DIFFUSION COEF. KCTH COMPONENT IN PHASE 2
*---- D(KC,2),KC=1,N
         0        0        0        0        0        0        0
0        0        0        0        0        0
         0        0        0        0        0        0
CC
CC MOLECULAR DIFFUSION COEF. KCTH COMPONENT IN PHASE 3
*---- D(KC,3),KC=1,N
         0        0        0        0        0        0        0
0        0        0        0        0        0
         0        0        0        0        0        0
CC
CC LONGITUDINAL AND TRANSVERSE DISPERSIVITY OF PHASE 1
*---- ALPHAL(1)     ALPHAT(1)
         0.08           0
CC
CC LONGITUDINAL AND TRANSVERSE DISPERSIVITY OF PHASE 2
*---- ALPHAL(2)     ALPHAT(2)
         0.           0
CC
CC LONGITUDINAL AND TRANSVERSE DISPERSIVITY OF PHASE 3
*---- ALPHAL(3)     ALPHAT(3)
         0.           0
CC
CC flag to specify organic adsorption calculation
*---- iadso
        0
CC
CC SURFACTANT AND POLYMER ADSORPTION PARAMETERS
*---- AD31    AD32   B3D    AD41   AD42   B4D   IADK  IADS1   FADS
REFK
      0.17      0    1000    0.17     0     100     0     0      0
0
2  0  804
12    51  7      0     0     0
12  0  9  0
2  6  5  4 10
7  8       12
Cr+3                                3
H+1                                 1
Pb+2                                2
MG+2                                2
Ca+2                                2
Na+1                                1
Al+3                                3
Si+4                                4
```

```
Cl-1                                -1
CO3-2                               -2
SO4-2                               -2
OXYGEN                              -2
 Cr(OH)2+
 H+1
 Pb+2
 Mg+2
 Ca+2
 Na+1
 Al+3
 H4SiO4
 Cl-1
 CO3-2
 SO4-2
 WATER
 OH-
 H3SiO4 -
 MgOH +
 MgCO3 AQ
 MgHCO3 +
 MgSO4 AQ
 CaOH +
 CaHCO3 +
 CaCO3 AQ
 CaSO4 AQ
 NaCO3 -
 NaHCO3 AQ
 NaSO4 -
 AlOH +2
 Al(OH)2 +
 AlSO4 +
 Al(SO4)2 -
 PbCl +
 PbCl2 AQ
 PbCl3 -
 PbCl4 -2
 Pb(CO3)2-2
 PbOH +
 Pb2OH +3
 PbSO4 AQ
 PbCO3 AQ
 Pb(SO4)2-2
 PbHCO3 +
 HCO3 -
 H2CO3 AQ
 HSO4 -
 Cr+3
 Cr(OH)+2
 CrCl+2
 CrCl2 +
```

```
CrSO4 +
CrOHSO4 AQ
Cr2OH2SO4+2
Cr2OH2SO42
CALCITE
GIBBSITE (C)
GYPSUM
SIO2(A,PT)
CERRUSITE
ANGLESITE
CR(OH)3 (A)
1.  0.  0.  0.  0.  0.  0.  0.  0.  0.  0.  0.  0.  0.
0.  0.  0.  0.  0.  0.  0.  0.  0.  0.  0.  0.  0.  0.
0.  0.  0.  0.  0.  0.  0.  0.  0.  0.  0.  0.  1.  1.
1.  1.  1.  1.  2.  2.
2.  1.  0.  0.  0.  0.  0.  4.  0.  0.  0.  2.  1.  3.  1.
0.  1.  0.  1.  1.  0.  0.  0.  1.  0.  1.  2.  0.  0.  0.
0.  0.  0.  0.  1.  1.  0.  0.  0.  1.  1.  2.  1.  0.  1.
0.  0.  0.  1.  2.  2.
0.  0.  1.  0.  0.  0.  0.  0.  0.  0.  0.  0.  0.  0.  0.
0.  0.  0.  0.  0.  0.  0.  0.  0.  0.  0.  0.  0.  0.  1.
1.  1.  1.  1.  1.  2.  1.  1.  1.  1.  0.  0.  0.  0.  0.
0.  0.  0.  0.  0.  0.
0.  0.  0.  1.  0.  0.  0.  0.  0.  0.  0.  0.  0.  0.  1.
1.  1.  1.  0.  0.  0.  0.  0.  0.  0.  0.  0.  0.  0.  0.
0.  0.  0.  0.  0.  0.  0.  0.  0.  0.  0.  0.  0.  0.  0.
0.  0.  0.  0.  0.  0.
0.  0.  0.  0.  1.  0.  0.  0.  0.  0.  0.  0.  0.  0.  0.
0.  0.  0.  1.  1.  1.  1.  0.  0.  0.  0.  0.  0.  0.  0.
0.  0.  0.  0.  0.  0.  0.  0.  0.  0.  0.  0.  0.  0.  0.
0.  0.  0.  0.  0.  0.
0.  0.  0.  0.  0.  1.  0.  0.  0.  0.  0.  0.  0.  0.  0.
0.  0.  0.  0.  0.  0.  0.  1.  1.  1.  0.  0.  0.  0.  0.
0.  0.  0.  0.  0.  0.  0.  0.  0.  0.  0.  0.  0.  0.  0.
0.  0.  0.  0.  0.  0.
0.  0.  0.  0.  0.  0.  1.  0.  0.  0.  0.  0.  0.  0.  0.
0.  0.  0.  0.  0.  0.  0.  0.  0.  0.  1.  1.  1.  1.  0.
0.  0.  0.  0.  0.  0.  0.  0.  0.  0.  0.  0.  0.  0.  0.
0.  0.  0.  0.  0.  0.
0.  0.  0.  0.  0.  0.  0.  1.  0.  0.  0.  0.  0.  1.  0.
0.  0.  0.  0.  0.  0.  0.  0.  0.  0.  0.  0.  0.  0.  0.
0.  0.  0.  0.  0.  0.  0.  0.  0.  0.  0.  0.  0.  0.  0.
0.  0.  0.  0.  0.  0.
0.  0.  0.  0.  0.  0.  0.  0.  1.  0.  0.  0.  0.  0.  0.
0.  0.  0.  0.  0.  0.  0.  0.  0.  0.  0.  0.  0.  0.  1.
2.  3.  4.  0.  0.  0.  0.  0.  0.  0.  0.  0.  0.  0.  0.
1.  2.  0.  0.  0.  0.
0.  0.  0.  0.  0.  0.  0.  0.  0.  1.  0.  0.  0.  0.  0.
1.  1.  0.  0.  1.  1.  0.  1.  1.  0.  0.  0.  0.  0.  0.
0.  0.  0.  2.  0.  0.  0.  1.  0.  1.  1.  1.  0.  0.  0.
0.  0.  0.  0.  0.  0.
```

0. 0. 0. 0. 0. 0. 0. 0. 0. 0. 1. 0. 0. 0. 0.
0. 0. 1. 0. 0. 0. 1. 0. 0. 1. 0. 0. 1. 2. 0.
0. 0. 0. 0. 0. 0. 1. 0. 2. 0. 0. 0. 1. 0. 0.
0. 0. 1. 1. 1. 2.
2. 0. 0. 0. 0. 0. 0. 4. 0. 0. 0. 1. 1. 4. 1.
0. 0. 0. 1. 0. 0. 0. 0. 0. 0. 1. 2. 0. 0. 0.
0. 0. 0. 0. 1. 1. 0. 0. 0. 0. 0. 0. 0. 0. 1.
0. 0. 0. 1. 2. 2.
0. 0. 0. 0. 0. 0. 1.
0. 3. 4. 0. 0. 0. 3.
0. 0. 0. 0. 1. 1. 0.
0. 0. 0. 0. 0. 0. 0.
1. 0. 1. 0. 0. 0. 0.
0. 0. 0. 0. 0. 0. 0.
0. 1. 0. 0. 0. 0. 0.
0. 0. 0. 1. 0. 0. 0.
0. 0. 0. 0. 0. 0. 0.
1. 0. 0. 0. 1. 0. 0.
0. 0. 1. 0. 0. 1. 0.
0. 3. 2. 2. 0. 0. 3.
1.0 0.0 0.0 0.0 0.0 0.0 0.0 0.0 0.0 0.0 0.0 0.0
0.0 1.0 0.0 0.0 0.0 0.0 0.0 0.0 0.0 0.0 0.0 0.0
0.0 0.0 1.0 0.0 0.0 0.0 0.0 0.0 0.0 0.0 0.0 0.0
0.0 0.0 0.0 1.0 0.0 0.0 0.0 0.0 0.0 0.0 0.0 0.0
0.0 0.0 0.0 0.0 1.0 0.0 0.0 0.0 0.0 0.0 0.0 0.0
0.0 0.0 0.0 0.0 0.0 1.0 0.0 0.0 0.0 0.0 0.0 0.0
0.0 0.0 0.0 0.0 0.0 0.0 1.0 0.0 0.0 0.0 0.0 0.0
0.0 0.0 0.0 0.0 0.0 0.0 0.0 1.0 0.0 0.0 0.0 0.0
0.0 0.0 0.0 0.0 0.0 0.0 0.0 0.0 1.0 0.0 0.0 0.0
0.0 0.0 0.0 0.0 0.0 0.0 0.0 0.0 0.0 1.0 0.0 0.0
0.0 0.0 0.0 0.0 0.0 0.0 0.0 0.0 0.0 0.0 1.0 0.0
0.0 0.0 0.0 0.0 0.0 0.0 0.0 0.0 0.0 0.0 0.0 1.0
0.0 -1.0 0.0 0.0 0.0 0.0 0.0 0.0 0.0 0.0 0.0 0.0
0.0 -1.0 0.0 0.0 0.0 0.0 0.0 1.0 0.0 0.0 0.0 0.0
0.0 -1.0 0.0 1.0 0.0 0.0 0.0 0.0 0.0 0.0 0.0 0.0
0.0 0.0 0.0 1.0 0.0 0.0 0.0 0.0 0.0 1.0 0.0 0.0
0.0 1.0 0.0 1.0 0.0 0.0 0.0 0.0 0.0 1.0 0.0 0.0
0.0 0.0 0.0 1.0 0.0 0.0 0.0 0.0 0.0 0.0 1.0 0.0
0.0 -1.0 0.0 0.0 1.0 0.0 0.0 0.0 0.0 0.0 0.0 0.0
0.0 1.0 0.0 0.0 1.0 0.0 0.0 0.0 0.0 1.0 0.0 0.0
0.0 0.0 0.0 0.0 1.0 0.0 0.0 0.0 0.0 1.0 0.0 0.0
0.0 0.0 0.0 0.0 1.0 0.0 0.0 0.0 0.0 0.0 1.0 0.0
0.0 0.0 0.0 0.0 0.0 1.0 0.0 0.0 0.0 1.0 0.0 0.0
0.0 1.0 0.0 0.0 0.0 1.0 0.0 0.0 0.0 1.0 0.0 0.0
0.0 0.0 0.0 0.0 0.0 1.0 0.0 0.0 0.0 0.0 1.0 0.0
0.0 -1.0 0.0 0.0 0.0 0.0 1.0 0.0 0.0 0.0 0.0 0.0
0.0 -2.0 0.0 0.0 0.0 0.0 1.0 0.0 0.0 0.0 0.0 0.0
0.0 0.0 0.0 0.0 0.0 0.0 1.0 0.0 0.0 0.0 1.0 0.0
0.0 0.0 0.0 0.0 0.0 0.0 1.0 0.0 0.0 0.0 2.0 0.0
0.0 0.0 1.0 0.0 0.0 0.0 0.0 0.0 1.0 0.0 0.0 0.0
0.0 0.0 1.0 0.0 0.0 0.0 0.0 0.0 2.0 0.0 0.0 0.0

```
 0.0  0.0  1.0  0.0  0.0  0.0  0.0  0.0  3.0  0.0  0.0  0.0
 0.0  0.0  1.0  0.0  0.0  0.0  0.0  0.0  4.0  0.0  0.0  0.0
 0.0  0.0  1.0  0.0  0.0  0.0  0.0  0.0  0.0  2.0  0.0  0.0
 0.0 -1.0  1.0  0.0  0.0  0.0  0.0  0.0  0.0  0.0  0.0  0.0
 0.0 -1.0  2.0  0.0  0.0  0.0  0.0  0.0  0.0  0.0  0.0  0.0
 0.0  0.0  1.0  0.0  0.0  0.0  0.0  0.0  0.0  0.0  1.0  0.0
 0.0  0.0  1.0  0.0  0.0  0.0  0.0  0.0  0.0  1.0  0.0  0.0
 0.0  0.0  1.0  0.0  0.0  0.0  0.0  0.0  0.0  0.0  2.0  0.0
 0.0  1.0  1.0  0.0  0.0  0.0  0.0  0.0  0.0  1.0  0.0  0.0
 0.0  1.0  0.0  0.0  0.0  0.0  0.0  0.0  0.0  1.0  0.0  0.0
 0.0  2.0  0.0  0.0  0.0  0.0  0.0  0.0  0.0  1.0  0.0  0.0
 0.0  1.0  0.0  0.0  0.0  0.0  0.0  0.0  0.0  0.0  1.0  0.0
 1.0  2.0  0.0  0.0  0.0  0.0  0.0  0.0  0.0  0.0  0.0  0.0
 1.0  1.0  0.0  0.0  0.0  0.0  0.0  0.0  0.0  0.0  0.0  0.0
 1.0  2.0  0.0  0.0  0.0  0.0  0.0  0.0  1.0  0.0  0.0  0.0
 1.0  2.0  0.0  0.0  0.0  0.0  0.0  0.0  2.0  0.0  0.0  0.0
 1.0  2.0  0.0  0.0  0.0  0.0  0.0  0.0  0.0  0.0  1.0  0.0
 1.0  1.0  0.0  0.0  0.0  0.0  0.0  0.0  0.0  0.0  1.0  0.0
 2.0  2.0  0.0  0.0  0.0  0.0  0.0  0.0  0.0  0.0  1.0  0.0
 2.0  2.0  0.0  0.0  0.0  0.0  0.0  0.0  0.0  0.0  2.0  0.0
 0.0  0.0  0.0  0.0  1.0  0.0  0.0  0.0  0.0  1.0  0.0  0.0
 0.0 -3.0  0.0  0.0  0.0  0.0  1.0  0.0  0.0  0.0  0.0  0.0
 0.0  0.0  0.0  0.0  1.0  0.0  0.0  0.0  0.0  0.0  1.0  0.0
 0.0  0.0  0.0  0.0  0.0  0.0  0.0  1.0  0.0  0.0  0.0  0.0
 0.0  0.0  1.0  0.0  0.0  0.0  0.0  0.0  0.0  1.0  0.0  0.0
 0.0  0.0  1.0  0.0  0.0  0.0  0.0  0.0  0.0  0.0  1.0  0.0
 1.0 -1.0  0.0  0.0  0.0  0.0  0.0  0.0  0.0  0.0  0.0  0.0
 1.0  1.0  2.0  2.0  2.0  1.0  3.0  0.0 -1.0 -2.0 -2.0  0.0
-1.0 -1.0  1.0  0.0  1.0  0.0  1.0  1.0  0.0  0.0 -1.0  0.0
-1.0  2.0  1.0  1.0 -1.0  1.0  0.0 -1.0 -2.0 -2.0  1.0  3.0
 0.0  0.0 -2.0  1.0 -1.0  0.0 -1.0  3.0  2.0  2.0  1.0  1.0
 0.0  2.0  0.0
0.1000000000000E+01 0.1000000000000E+01 0.1000000000000E+01
0.1000000000000E+01 0.1000000000000E+01 0.1000000000000E+01
0.1000000000000E+01 0.1000000000000E+01 0.1000000000000E+01
0.1000000000000E+01 0.1000000000000E+01 0.1000000000000E+01
0.1000000000000E-13 0.1175000000000E-09 0.1622000000000E-11
0.9550000000000E+03 0.2512000000000E+12 0.1778000000000E+03
0.2512000000000E-12 0.2138000000000E+12 0.1412000000000E+04
0.2042000000000E+03 0.1862000000000E+02 0.1905460000000E+11
0.5011872300000E+01 0.1023293000000E-04 0.7943282000000E-10
0.1047128500000E+04 0.8317637700000E+05 0.3981071700000E+02
0.6309573400000E+02 0.5011872300000E+02 0.2398832900000E+02
0.4365158000000E+11 0.1949844000000E-07 0.4365158000000E-06
0.5623413300000E+03 0.1737800800000E+08 0.2951209200000E+04
0.1584893000000E+14 0.2137962000000E+11 0.4786300000000E+17
0.9772372200000E+02 0.4168693000000E+10 0.4168693800000E+06
0.2344228000000E+10 0.4570881000000E+09 0.9332543000000E+11
0.1905460000000E+09 0.1445439000000E+17 0.8511380000000E+18
0.3388441000000E-08 0.5888438000000E+09 0.1412537000000E-04
0.1949844600000E-02 0.7413107300000E-13 0.1621810000000E-07
```

```
0.1778279400000E+00
0.2540363606000E-02 0.1551935201385E-01
0.3000000000000E-07 0.1530386041025E-01 0.2000000000000E-07
0.4000000000000E-02 0.1300000000000E-02
0.3360166316048E-07 0.7803332339265E-02 0.1300000000000E-02
0.1130958182209E-01 0.1316977019176E-01 0.1560691274518E-01
0.8133276056620e-08 0.2317756800271E-06 0.5542315747452E-09
0.1268460852414E-02 0.4702576290752E-02 0.1276700137574E-02
0.7331683328725E-11 0.1949844600000E-02 0.1299999971197E-02
0.7205499263593E-06 0.3003751375130E-02 0.2673101911424E-07
0.1834950908896E-01 0.2499999991088E-02 0.8994349041223E-03
0.3979999669152E+00 0.0000000000000E+00 0.0000000000000E+00
0.0000000000000E+00
CC
CC*****************************************************************
CC                                                                 *
CC    WELL DATA                                                    *
CC                                                                 *
CC*****************************************************************
CC
CC
CC FLAG FOR SPECIFIED BOUNDARY AND ZONE IS MODELED
*---- IBOUND     IZONE
        0      0
CC
CC TOTAL NUMBER OF WELLS, WELL RADIUS FLAG, FLAG FOR TIME OR COURANT
NO.
*---- NWELL   IRO    ITIME    NWREL
        2      2       1        2
CC
CC WELL ID,LOCATIONS,AND FLAG FOR SPECIFYING WELL TYPE, WELL RADIUS,
SKIN
*---- IDW    IW    JW    IFLAG    RW     SWELL   IDIR   IFIRST   ILAST
IPRF
       1     1     1       1      0.5       0       3      1      1
0
CC
CC WELL NAME
*----  WELNAM
INJECTOR
CC
CC ICHEK , MAX. AND MIN. ALLOWABLE BOTTOMHOLE PRESSURE AND RATE
*---- ICHEK     PWFMIN     PWFMAX    QTMIN    QTMAX
        0          0         5000      0        1000
CC
CC WELL ID,LOCATIONS,AND FLAG FOR SPECIFYING WELL TYPE, WELL RADIUS,
SKIN
*---- IDW    IW    JW    IFLAG    RW     SWELL   IDIR   IFIRST   ILAST
IPRF
       2     100     1       2      0.5       0       3      1      1
0
```

```
CC
CC WELL NAME
*----  WELNAM
PRODUCER
CC
CC ICHEK , MAX. AND MIN. ALLOWABLE BOTTOMHOLE PRESSURE AND RATE
*---- ICHEK     PWFMIN     PWFMAX    QTMIN    QTMAX
        0          0         5000      0        50000
CC
CC  ID,INJ. RATE AND INJ. COMP. FOR RATE CONS. WELLS FOR EACH PHASE
(L=1,3)
*----  ID     QI(M,L)     C(M,KC,L)
       1        7.12378E-06    1      0      0      0      0.04826
0.048046      0      0      0.0003      1.660228      0.00002
0.004      0.0013      5.036216E-03      7.799387E-03      0.0013
0.048      9.006128E-03      1.620164
       1      0      0      0      0      0    0 0 0 0 0 0 0 0 0 0 0 0
0 0 0
       1      0      0      0      0      0     0 0 0 0 0 0 0 0 0 0 0 0
0 0 0
CC
CC ID, BOTTOM HOLE PRESSURE FOR PRESSURE CONSTRAINT WELL (IFLAG=2 OR 3)
*----  ID    PWF
       2     4890
CC
CC CUM. INJ. TIME , AND INTERVALS (PV OR DAY) FOR WRITING TO OUTPUT
FILES
*---- TINJ     CUMPR1     CUMHI1     WRHPV     WRPRF      RSTC
       1.5      150        150        10      50       400
CC
CC FOR IMES=2 ,THE INI. TIME STEP,CONC. TOLERANCE,MAX.,MIN. courant
numbers
*----  DT      DCLIM     CNMAX      CNMIN
       0.01       0.1      0.5         0.0001
```

Appendix C: Using IPhreeqc Methods in a Simplified Code

A simplified code is provided that shows how IPhreeqc methods are applied to communicate between this geochemical package (i.e., IPhreeqc) and a client simulator (i.e., UTCOMP or UTCHEM) through the computer memory. This code is the expanded version of advect.f90 example file released with IPhreeqc (Charlton and Parkhurst, 2011). The simplified code includes two subroutines: main.f90 and ehandler.f90. Both subroutines are provided below. Basically, the same IPhreeqc methods are applied in the UTCOMP-IPhreeqc and UTCHEM-IPhreeqc simulators. Compare with this simplified code in which simple cell shifting is used for the transport, in the UTCOMP-IPhreeqc and UTCHEM-IPhreeqc simulators, mass conservation equation is solved.

C. 1 SIMPLIFIED CODE

C. 1.1 The main.f90 subroutine:

```
!!  THE UNIVERSITY OF TEXAS AT AUSTIN - 2014
!!  ABOULGHASEM KAZEMI NIA KORRANI, MAY 2014
!!  aboulghasem.kazemi@utexas.edu

PROGRAM MAIN

IMPLICIT NONE

INTEGER, ALLOCATABLE :: VT(:,:)

DOUBLE PRECISION, ALLOCATABLE :: AVAR_LIB(:,:)
CHARACTER, ALLOCATABLE :: SV(:,:)
CHARACTER (LEN=32), ALLOCATABLE :: STR_ELE(:)
CHARACTER (LEN=80), ALLOCATABLE :: STR_PRINT(:)
```

```
CHARACTER (LEN=64) :: DUMMY_STR
INTEGER :: DUMMY_INT, NO_CELLS, NO_SLUGS
INTEGER, ALLOCATABLE :: NO_SHIFTS(:), INJ_SOLUTIONS(:)
INTEGER  :: NELE, I, J, IPHREEQC_ID, N_COLUMN, N_ROW, IERR,
SHIFT, KK, JJ
INTEGER :: TOTAL_SHIFTS
INTEGER :: NO_PRINT
DOUBLE PRECISION, ALLOCATABLE:: CONC(:,:),
OTHER_GEOCHEMISTRY_VALUES(:,:)
CHARACTER (LEN=32), ALLOCATABLE :: INJ_SOLUTIONS_STRING(:)
! STRING
LOGICAL :: FILE_EXISTS
DOUBLE PRECISION, ALLOCATABLE :: INJ_CONCENTRATIONS(:,:)

INCLUDE "IPHREEQC.F90.INC"

!   ******    USER INPUT PARAMETERS  ********************

NO_CELLS = 1000   ! USER INPUT PARAMETER
NO_SLUGS = 3     ! USER INPUT PARAMETER
ALLOCATE(NO_SHIFTS(1:NO_SLUGS))
ALLOCATE(INJ_SOLUTIONS(1:NO_SLUGS))
NO_SHIFTS= (/700, 700, 700/)        ! USER INPUT PARAMETER,
NO OF SHIFTS IN EACH SLUG
INJ_SOLUTIONS= (/1001, 1002, 1003/) ! USER INPUT PARAMETER,
NUMBERS MUST BE DIFFERENT
NO_PRINT=8       ! USER INPUT PARAMETER

ALLOCATE(STR_PRINT(1:NO_PRINT))

STR_PRINT(1) = 'MOL("Na+")'     ! USER INPUT PARAMETER
STR_PRINT(2) = 'MOL("Ca+2")'    ! USER INPUT PARAMETER
STR_PRINT(3) = 'MOL("Cl-")'     ! USER INPUT PARAMETER
STR_PRINT(4) = '-LA("H+")'      ! USER INPUT PARAMETER
STR_PRINT(5) = 'MOL("Ba+2")'    ! USER INPUT PARAMETER
STR_PRINT(6) = 'MOL("HCO3-")'   ! USER INPUT PARAMETER
STR_PRINT(7) = 'MOL("Mg+2")'    ! USER INPUT PARAMETER
STR_PRINT(8) = 'MOL("Sr+2")'    ! USER INPUT PARAMETER

!   ******   END OF  USER INPUT PARAMETERS  ***************
```

```
OPEN(UNIT=121, FILE='CONCENTRATIONS.TXT')
 WRITE(121,2268) 'PV', (TRIM(ADJUSTL(STR_PRINT(I))),
I=1,NO_PRINT)
 2268 FORMAT (8X,100(A10,15X))
ALLOCATE(OTHER_GEOCHEMISTRY_VALUES(1:NO_CELLS,1:NO_PRINT))
OTHER_GEOCHEMISTRY_VALUES(1:NO_CELLS,1:NO_PRINT)=0.D0
  IPHREEQC_ID = CREATEIPHREEQC()
  IF (LOADDATABASE(IPHREEQC_ID, "IPHREEQC_DATABASE.DAT")
.NE. 0) CALL EHANDLER(IPHREEQC_ID)
INQUIRE(FILE="IPHREEQC_DATABASE.INC", EXIST=FILE_EXISTS)
IF (FILE_EXISTS) THEN
  IERR=ACCUMULATELINE(IPHREEQC_ID,'INCLUDE$
IPHREEQC_DATABASE.INC')
END IF
IERR=ACCUMULATELINE(IPHREEQC_ID, 'SOLUTION_SPECIES; H2O +
0.01E- = H2O-0.01; LOG_K -8')
    IERR=ACCUMULATELINE(IPHREEQC_ID,'INCLUDE$ INPUT.DAT')
      IF (RUNACCUMULATED(IPHREEQC_ID) .NE. 0) CALL
EHANDLER(IPHREEQC_ID)
       NELE=GETCOMPONENTCOUNT(IPHREEQC_ID)+3  ! 3 IS FOR
CHARGE BALANCE, TOTAL HYDROGEN, AND TOTAL OXYGEN
       ALLOCATE(STR_ELE(1:NELE))
        DO I=1, NELE-3
         CALL GETCOMPONENT(IPHREEQC_ID,I,STR_ELE(I))
        END DO
        ALLOCATE(CONC(0:NO_CELLS,1:NELE))
        CONC(0:NO_CELLS,1:NELE) =0.D0
        STR_ELE(NELE-2)= 'CB'
        STR_ELE(NELE-1)= 'H'
        STR_ELE(NELE)= 'O'
       IERR=ACCUMULATELINE(IPHREEQC_ID,'SELECTED_OUTPUT
1')
       IERR=ACCUMULATELINE(IPHREEQC_ID,'-RESET FALSE')
       IERR=ACCUMULATELINE(IPHREEQC_ID,'USER_PUNCH  1')
       DO I=1, NELE-3
       IERR=ACCUMULATELINE(IPHREEQC_ID,'-HEADING  '//
TRIM(ADJUSTL(STR_ELE(I))))
       END DO
       IERR=ACCUMULATELINE(IPHREEQC_ID,'-HEADING
CHARGE_BALANCE')
       IERR=ACCUMULATELINE(IPHREEQC_ID,'-HEADING
TOTAL_H')
```

```
       IERR=ACCUMULATELINE(IPHREEQC_ID,'-HEADING
TOTAL_O')
       DO I=1, NO_PRINT
       IERR=ACCUMULATELINE(IPHREEQC_ID,'-HEADING    '//
TRIM(ADJUSTL(STR_PRINT(I))))
       END DO
       DO I=1, NELE-3
        WRITE(DUMMY_STR,*) (I)*10
        IERR=ACCUMULATELINE(IPHREEQC_ID,
TRIM(ADJUSTL(DUMMY_STR))//' PUNCH  TOTMOLE("'//
TRIM(ADJUSTL(STR_ELE(I)))//'")')
       END DO
       WRITE(DUMMY_STR,*) (NELE-2)*10

IERR=ACCUMULATELINE(IPHREEQC_ID,TRIM(ADJUSTL(DUMMY_STR))//
'PUNCH   CHARGE_BALANCE')
       WRITE(DUMMY_STR,*) (NELE-1)*10

IERR=ACCUMULATELINE(IPHREEQC_ID,TRIM(ADJUSTL(DUMMY_STR))//'
PUNCH   TOTMOLE("H")')
       WRITE(DUMMY_STR,*) (NELE)*10

IERR=ACCUMULATELINE(IPHREEQC_ID,TRIM(ADJUSTL(DUMMY_STR))//'
PUNCH   TOTMOLE("O")')
       DO I=1, NO_PRINT
        WRITE(DUMMY_STR,*) (NELE+I)*10
        IERR=ACCUMULATELINE(IPHREEQC_ID,
TRIM(ADJUSTL(DUMMY_STR))//' PUNCH  '//
TRIM(ADJUSTL(STR_PRINT(I))))
       END DO

IERR=SETCURRENTSELECTEDOUTPUTUSERNUMBER(IPHREEQC_ID,1)
!CC       CALL OUTPUTACCUMULATEDLINES(IPHREEQC_ID)
         ALLOCATE(INJ_SOLUTIONS_STRING(1:NO_SLUGS)) !
STRING
         DO KK=1, NO_SLUGS
          WRITE(INJ_SOLUTIONS_STRING(KK), *)
INJ_SOLUTIONS(KK)
         END DO
        WRITE(DUMMY_STR,*) NO_CELLS
        IERR=ACCUMULATELINE(IPHREEQC_ID,'RUN_CELLS; -
CELLS;')
```

```
        IERR=ACCUMULATELINE(IPHREEQC_ID,'1-'//
TRIM(ADJUSTL(DUMMY_STR)))
        DO KK=1, NO_SLUGS
         IERR=ACCUMULATELINE(IPHREEQC_ID,
TRIM(ADJUSTL(INJ_SOLUTIONS_STRING(KK))))
        END DO
        IERR=ACCUMULATELINE(IPHREEQC_ID,'END')
       IF (RUNACCUMULATED(IPHREEQC_ID) .NE. 0) CALL
EHANDLER(IPHREEQC_ID)
         N_ROW=GETSELECTEDOUTPUTROWCOUNT(IPHREEQC_ID)
         N_COLUMN=GETSELECTEDOUTPUTCOLUMNCOUNT(IPHREEQC_ID)
        ALLOCATE(AVAR_LIB(1:N_ROW,1:N_COLUMN))
        ALLOCATE(VT(1:N_ROW,1:N_COLUMN))
        ALLOCATE(SV(1:N_ROW,1:N_COLUMN))
        AVAR_LIB(1:N_ROW,1:N_COLUMN)=0.D0
       DO I=1, N_ROW
          DO J=1, N_COLUMN
          IERR =
GETSELECTEDOUTPUTVALUE(IPHREEQC_ID,I,J,VT(I,J),AVAR_LIB(I,J
),SV(I,J))
       END DO
      END DO
       CONC(1:NO_CELLS,1:NELE)= AVAR_LIB(1:NO_CELLS,1:NELE)
       ALLOCATE(INJ_CONCENTRATIONS(1:NO_SLUGS,1:NELE))
       INJ_CONCENTRATIONS(1:NO_SLUGS,1:NELE) =0.D0
        INJ_CONCENTRATIONS(1:NO_SLUGS,1:NELE)=
AVAR_LIB(NO_CELLS+1:N_ROW,1:NELE)
       DEALLOCATE(AVAR_LIB, VT, SV)
!CC-- END OF INITILIZATION
        ALLOCATE(AVAR_LIB(1:NO_CELLS,1:NELE+NO_PRINT))
        ALLOCATE(VT(1:NO_CELLS,1:NELE+NO_PRINT))
        ALLOCATE(SV(1:NO_CELLS,1:NELE+NO_PRINT))
TOTAL_SHIFTS = 0
DO JJ=1, NO_SLUGS
 WRITE(DUMMY_STR,*) JJ
 WRITE(*,*) '-----------------------------------------
---'
 WRITE(*,*) 'START INJECTING SLUG: '//
TRIM(ADJUSTL(DUMMY_STR))
 WRITE(*,*) '-----------------------------------------
----'
 WRITE(122,*) '-----------------------------------------
-----'
```

```
 WRITE(122,*) 'START INJECTING SLUG: '//
TRIM(ADJUSTL(DUMMY_STR))
 WRITE(122,*) '-----------------------------------------
------'
 CONC(0,1:NELE) = INJ_CONCENTRATIONS(JJ,1:NELE)

 DO SHIFT =1, NO_SHIFTS(JJ)

!CC -- SHIFT THE CELLS (I.E., DO THE TRANSPORT)
!CC -- IN UTCOMP-IPHREEQC MASS BALANCE EQUATION IS SOLVED
INSTEAD
          DO I= NO_CELLS,1, -1
           CONC(I,1:NELE) = CONC(I-1,1:NELE)
          END DO
!CC -- END

       DO I=1, NO_CELLS
         WRITE(DUMMY_STR,*) I
        IERR=ACCUMULATELINE(IPHREEQC_ID,'SOLUTION_MODIFY
'// TRIM(ADJUSTL(DUMMY_STR)))
         WRITE(DUMMY_STR,*) CONC(I,NELE-2)
        IERR=ACCUMULATELINE(IPHREEQC_ID,'-CB
'//TRIM(ADJUSTL(DUMMY_STR)))
         WRITE(DUMMY_STR,*) CONC(I,NELE-1)
        IERR=ACCUMULATELINE(IPHREEQC_ID,'-TOTAL_H
'//TRIM(ADJUSTL(DUMMY_STR)))
         WRITE(DUMMY_STR,*) CONC(I,NELE)
        IERR=ACCUMULATELINE(IPHREEQC_ID,'-TOTAL_O
'//TRIM(ADJUSTL(DUMMY_STR)))
        IERR=ACCUMULATELINE(IPHREEQC_ID,'-TOTALS; ')
         DO J=1,NELE-3
          WRITE(DUMMY_STR,*) CONC(I,J)

IERR=ACCUMULATELINE(IPHREEQC_ID,TRIM(ADJUSTL(STR_ELE(J)))//
'   '//TRIM(ADJUSTL(DUMMY_STR)))
          END DO  !! FOR J
       END DO   !! FOR I
         IERR=ACCUMULATELINE(IPHREEQC_ID,'END')
          WRITE(DUMMY_STR,*) NO_CELLS
        IERR=ACCUMULATELINE(IPHREEQC_ID,'RUN_CELLS; -CELLS
1-'// TRIM(ADJUSTL(DUMMY_STR))//';  END')
        IF (RUNACCUMULATED(IPHREEQC_ID) .NE. 0) CALL
EHANDLER(IPHREEQC_ID)
```

```
          N_ROW=GETSELECTEDOUTPUTROWCOUNT(IPHREEQC_ID)
          N_COLUMN=GETSELECTEDOUTPUTCOLUMNCOUNT(IPHREEQC_ID)
         AVAR_LIB(1:N_ROW,1:N_COLUMN)=0.D0
        DO I=1, N_ROW
           DO J=1, N_COLUMN
           IERR =
GETSELECTEDOUTPUTVALUE(IPHREEQC_ID,I,J,VT(I,J),AVAR_LIB(I,J
),SV(I,J))
        END DO
       END DO
        CONC(1:NO_CELLS,1:NELE)= AVAR_LIB(1:NO_CELLS,1:NELE)
        OTHER_GEOCHEMISTRY_VALUES(1:NO_CELLS,1:NO_PRINT)=
AVAR_LIB(1:NO_CELLS,NELE+1:NELE+NO_PRINT)
TOTAL_SHIFTS = TOTAL_SHIFTS + 1
         WRITE(*,*) 'SHIFT NO. =', SHIFT
         WRITE(121,2267) (TOTAL_SHIFTS+0.5)/NO_CELLS,
OTHER_GEOCHEMISTRY_VALUES(NO_CELLS,:)
 END DO !! SHIFT
END DO !! NO_SLUGS
 2267 FORMAT (2X,1000(F20.10,2X))
END PROGRAM MAIN

! END OF KAZEMI NIA, MAY 2014
```

C.1.2 The ehandler.f90 subroutine:

```
      SUBROUTINE EHANDLER(IPHREEQC_ID)
        IMPLICIT NONE
         INTEGER :: IPHREEQC_ID
         INCLUDE "IPHREEQC.F90.INC"
         CALL OUTPUTERRORSTRING(IPHREEQC_ID)
       STOP
       END SUBROUTINE EHANDLER
```

C.2 COMPILING THE SIMPLIFIED CODE IN A WINDOWS®[1]-BASED MACHINE

Follow the procedure below to add IPhreeqc libraries before compiling the code in Microsoft® Visual Studio®: This procedure is based on Microsoft® Visual Studio® (2008). However, we believe the same procedure should work in other versions.

1) Adding the directory of IPhreeqc libraries (see Figure C-1).

"project> project properties>linker>General>Additional Library Directories"

For example, we add the followings:

"D:\Dropbox\Softwares\IPhreeqc\IPhreeqc-3.1.2-8538-vs2005-win32\lib"

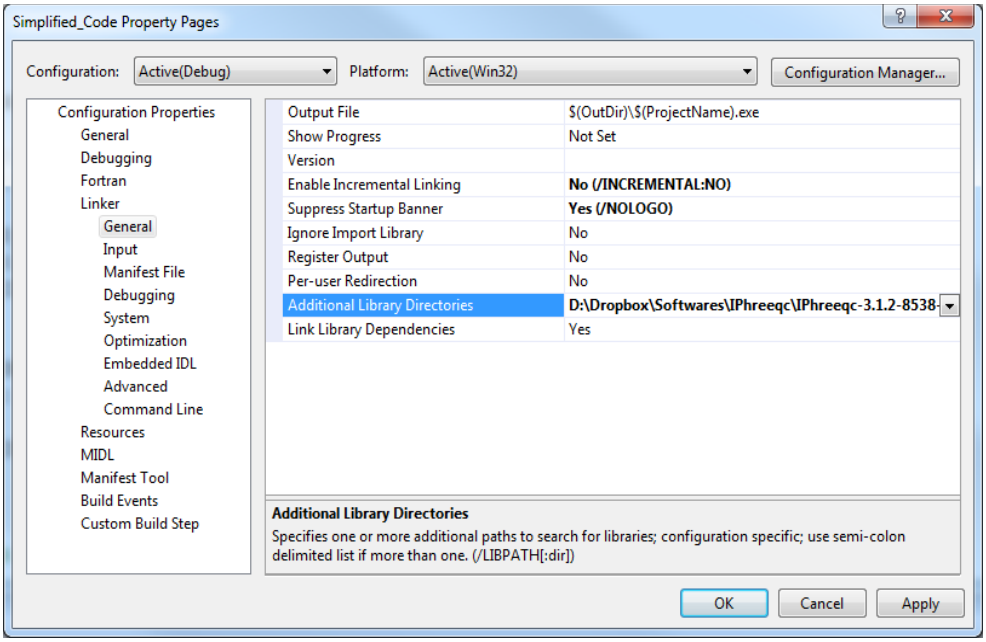

Figure C-1: Adding IPhreeqc library directories in Microsoft® Visual Studio®.

[1] Windows®, Microsoft®, and Visual Studio® are registered trademarks of Microsoft Corporation

2) Adding the IPhreeqc library ("IPhreeqcd.lib" for the Debug mode and "IPhreeqc.lib" for the Release mode) (see Figure C-2).

"project> project properties>linker>General>Input>Additional Dependencies"

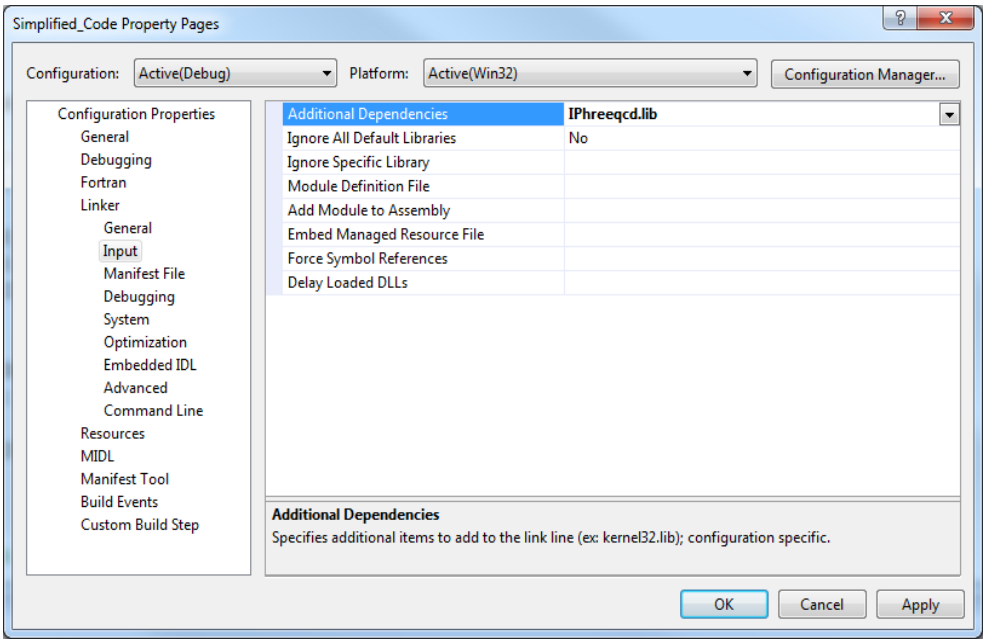

Figure C-2: Adding IPhreeqc library in Microsoft® Visual Studio®.

3) Adding the IPhreeqc include files (i.e., IPhreeqc.f90.inc for Fortran® 90/95) as shown in Figure C-3:

"project> project properties>Fortran>General>Additional Include Directories"

For example, we add the followings:

"D:\Dropbox\Softwares\IPhreeqc\IPhreeqc-3.1.2-8538-vs2005-win32\include"

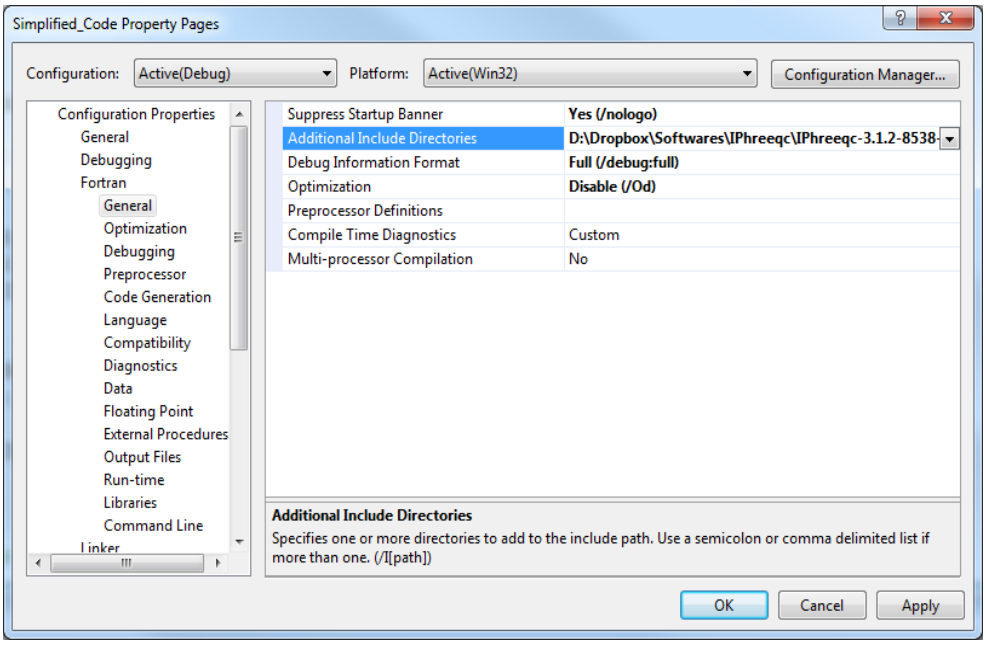

Figure C-3: Adding IPhreeqc include directory in Visual Studio®.

C.3 Compiling the Simplified Code in a Linux®[1]-Based Machine

Use the Makefile provided below.

Important Note: Command lines in Makefile must begin with a tab character (see http://en.wikipedia.org/wiki/Make_%28software%29 for Makefile rules).

```
## THE UNIVERSITY OF TEXAS AT AUSTIN - 2014
## ABOULGHASEM KAZEMI NIA KORRANI, MAY 2014
## aboulghasem.kazemi@utexas.edu
#FFLAGS = -O -pg
#FFLAGS = -O -fast
#FFLAGS = -g
FSRCS = \
main.f90 ehandler.f\
```

[1] Linux® is a registered trademark of Linus Torvalds

```
IPhreeqc_LIB_PATH=/home1/02950/kazemi/lib  ## directory
where IPhreeqc libraries were installed
IPhreeqc_INCLUDE_PATH=/home1/02950/kazemi/include/  ##
directory where IPhreeqc libraries were installed
IPhreeqc_LIBRARIES=-Wl,-rpath $(IPhreeqc_LIB_PATH)  -
L/$(IPhreeqc_LIB_PATH)   $(IPhreeqc_LIB_PATH)/libiphreeqc-
3.1.2.so  $(IPhreeqc_LIB_PATH)/libiphreeqc.a
$(IPhreeqc_LIB_PATH)/libiphreeqc.so
ifdef tight
FFLAGS = -c -CB -r8 -g -traceback -check all -
fltconsistency -align all -debug all   -I
$(IPhreeqc_INCLUDE_PATH)
else
FFLAGS=  -c -g -O3  -I $(IPhreeqc_INCLUDE_PATH)
endif
PROG = exe
FORT =  ifort
FOBJS = $(FSRCS:.f=.o)
PARA_OBJ = $(FSRCS_PARA:.f=.o)
OBJS = $(FOBJS) $(PARA_OBJ)
.f.o:
        $(FORT) $(FFLAGS) $*.f
.F.o:
        $(FORT) $(FFLAGS) $*.F
$(PROG):  $(OBJS)
        $(FORT) -o $(PROG) $(OBJS) $(IPhreeqc_LIBRARIES) -I
$(IPhreeqc_INCLUDE_PATH)
clean:
        rm -f *.o
        rm -f *.mod
        rm -f *.exe
        rm -f $(PROG)
```

C.4 VERIFICATION OF THE SIMPLIFIED CODE

A 1D case with 1000 cells is designed using the simplified code and PHREEQC. This case is initially saturated with the produced water of the South American formation (Kazempour *et al.*, 2013). Aragonite, calcite, celestite, dolomite, halite, strontianite,

sylvite, and witherite are the minerals included in the model. Except calcite and dolomite with initial concentration of 0.1 moles/kg of water, initial concentrations for other minerals are zero. It is also assumed that a cation-exchanger with cation exchange capacitance (CEC) of 0.01 moles/kgw is at equilibrium with the initial solution. The case is then flushed with 0.7 PV IW1 followed by 0.7 PV PW1 and finally 0.7 SW1 (0.7 PV in this case is about 700 shifts). Table C-1 shows ion compositions of the waters. Temperature of the initial and injection solutions is 100 ^{o}C. The phreeqc.dat database is used for the simulation. The PHREEQC input file is also provided. The same input file with no **SELECTED_OUTPUT** and **TRANSPORT** is used in the simplified code. **SELECTED_OUTPUT** is defined in the simplified code (rather than being defined in the input file). Also, because transport is performed by cell shifting in the simplified code, hence, there is no need to use the **TRANSPORT** keyword in the simplified code input file. The input file loaded in the simplified code is also given below. Figures C-4 through C-11 verify the simplified code results (shown as "Advection" in the figures) versus PHREEQC outputs.

Table C-1: Water analysis for South American formation (in ppm) (Kazempour *et al.*, 2013)

Ions	Produced water (PW1)	Injection water (IW1)	Fresh water (SW1)
Na^{+}	2430	2083	40
K^{+}	66	75	< 5
Ca^{+2}	300	310	12
Mg^{+2}	47	50	3
Ba^{+2}	20	70	-
Sr^{+2}	26	28	1
Cl^{-}	4343	3926	18
SO_4^{-2}	-	-	7
HCO_3^{-}	512	928	110
TDS	8410	7680	215

PHREEQC Input File:

```
PRINT
-reset   false
## PRODUCED WATER
SOLUTION 1-1000
-units ppm
-temp     100.0000
-water            1.0   ## kg
Na         2430
K          66
Ca       300
Mg        47
Ba       20
Sr         26
Cl         4343
S(6)           0.
C(4)   512   as HCO3-
END
EQUILIBRIUM_PHASES 1-1000
Aragonite     0.   0.
Calcite       0.    0.1
Celestite      0.   0.
Dolomite      0.    0.1
Halite          0.    0.
Strontianite   0.     0.
Sylvite        0.     0.
Witherite      0.    0.
END
EXCHANGE   1-1000
```

```
X   0.01
-equilibrate  1
END
## INJECTION WATER
SOLUTION 1001
-units ppm
-temp     100.0000   ###        Endicott Reservoir Temperature
-water            1.0
Na         2083
K           75
Ca           310
Mg           50
Ba           70
Sr           28
Cl           3926
S(6)          0.
C(4)  928  as HCO3-
END

##  PRODUCED WATER
SOLUTION  1002
-units ppm
-temp     100.0000
-water            1.0
Na          2430
K           66
Ca        300
Mg         47
Ba        20
Sr          26
Cl          4343
S(6)            0.
C(4) 512  as HCO3-
END
##    FRESH WATER
SOLUTION 1003
-units  ppm
-temp     100.0000
-water            1.0
Na           40
K            5
Ca            12
Mg          3
Ba           0
Sr           1
Cl           18
S(6)            7
C(4) 110  as HCO3-
END
## INJECTION WATER INJECTION
COPY solution 1001 0
```

```
END
SELECTED_OUTPUT
        -file            selected.out
        -reset           false
USER_PUNCH
-Heading     PV
-Heading     Na+
-Heading     Ca+2
-Heading     Cl-
-Heading     pH
-Heading     Ba+2
-Heading     HCO3-
-Heading     Mg+2
-Heading     Sr+2
   1     PUNCH  STEP_NO
   2     PUNCH  MOL("Na+")
   3     PUNCH  MOL("Ca+2")
   4     PUNCH  MOL("Cl-")
   5     PUNCH  -la("H+")
   6     PUNCH  MOL("Ba+2")
   7     PUNCH  MOL("HCO3-")
   8     PUNCH  MOL("Mg+2")
   9     PUNCH  MOL("Sr+2")
END
TRANSPORT
        -cells           1000
        -initial_time      0.
        -length          0.012192      #m
        -shifts          700
        -time_step       1       #s
        -flow_direction  forward
        -boundary_cond   flux    flux
        -diffc           0.0e-9
        -dispersivity    0.    #m
        -punch_cells     1000
        -punch_frequency 1
END
## PRODUCED WATER  INJECTION
COPY solution 1002 0
END
  TRANSPORT;  -shifts          700
END
##   FRESH WATER INJECTION
COPY solution 1003 0
END
TRANSPORT; -shifts          700
END
```

Input File Loaded in the Simplified Code:

```
SOLUTION 1-1000
 -water    1.0   ## water mass in each grid block
```

```
-units  ppm
-temp     100.0000
Na         2430
K           66
Ca        300
Mg         47
Ba        20
Sr          26
Cl          4343
S(6)            0.
C(4)   512   as HCO3-
END
EQUILIBRIUM_PHASES 1-1000
Aragonite      0.   0.
Calcite        0.    10.0
Celestite       0.   0.
Dolomite       0.     10.0
Halite           0.    0.
Strontianite   0.     0.
Sylvite         0.     0.
Witherite       0.    0.
END
EXCHANGE   1-1000
X      0.01
-equilibrate  1
END
SOLUTION 1001
-units   ppm
-temp     100.0000
-water            1.0
Na         2083
K           75
Ca           310
Mg           50
Ba           70
Sr           28
Cl           3926
S(6)          0.
C(4)  928  as HCO3-
END

SOLUTION  1002

-units    ppm
-temp     100.0000
-water            1.0
Na          2430
K           66
Ca        300
Mg         47
Ba        20
```

```
Sr          26
Cl          4343
S(6)            0.
C(4) 512   as HCO3-
END

SOLUTION 1003
-units     ppm
-temp      100.0000
-water              1.0
Na           40
K            5
Ca            12
Mg          3
Ba           0
Sr           1
Cl           18
S(6)            7
C(4) 110   as HCO3-
END
```

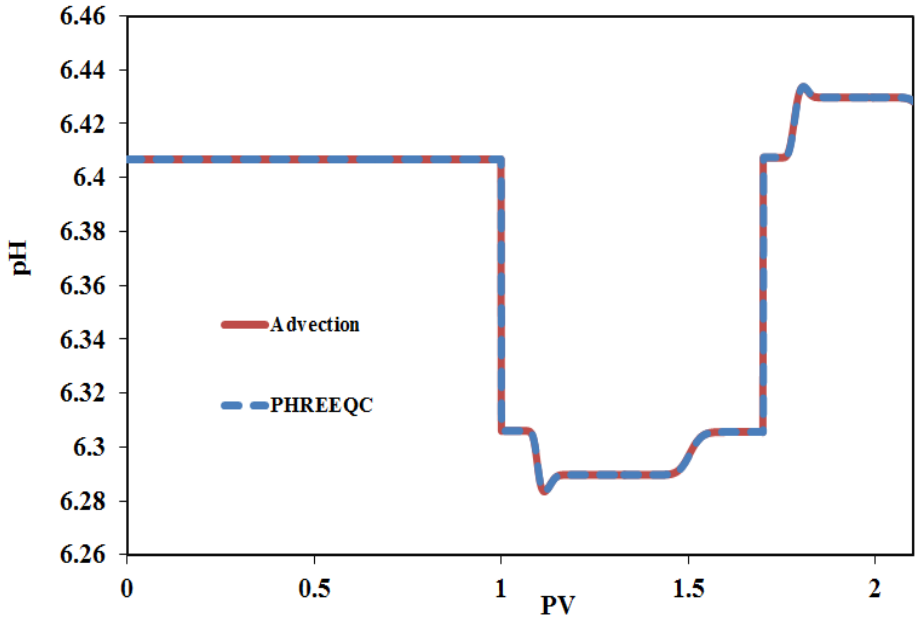

Figure C-4: pH history of the effluent solution (the simplified code verification against PHREEQC).

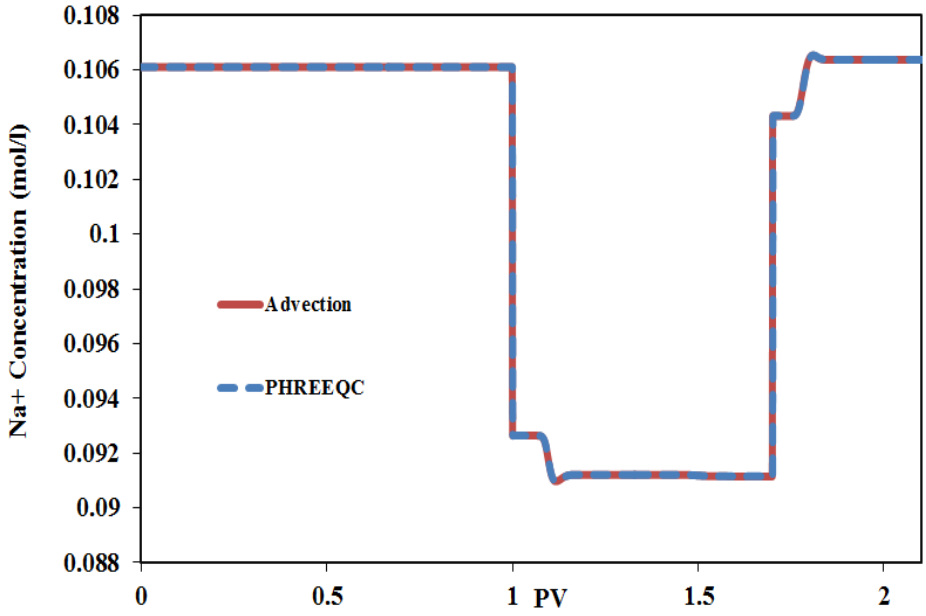

Figure C-5: Na^{+} concentration history of the effluent solution (the simplified code verification against PHREEQC).

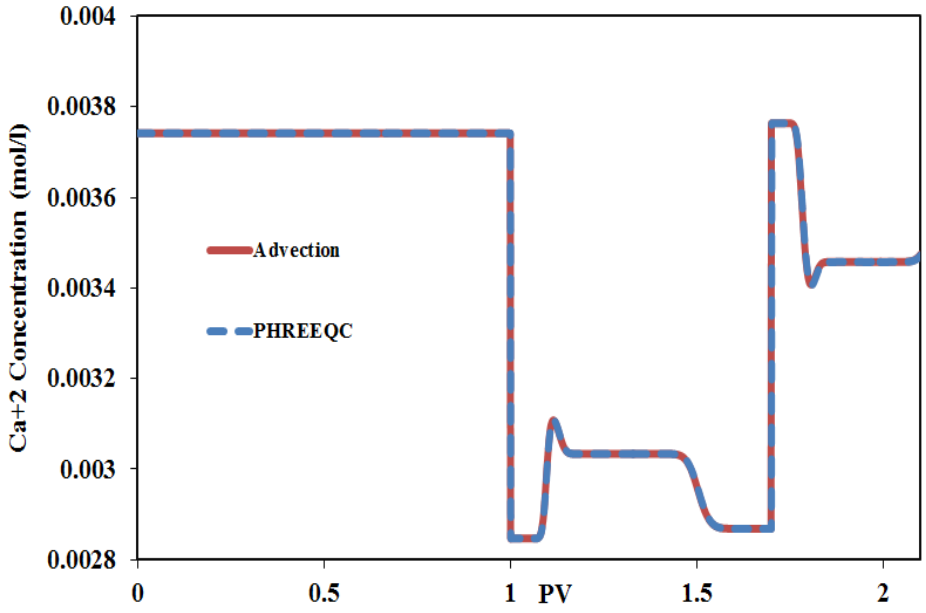

Figure C-6: Ca^{+2} concentration history of the effluent solution (the simplified code verification against PHREEQC).

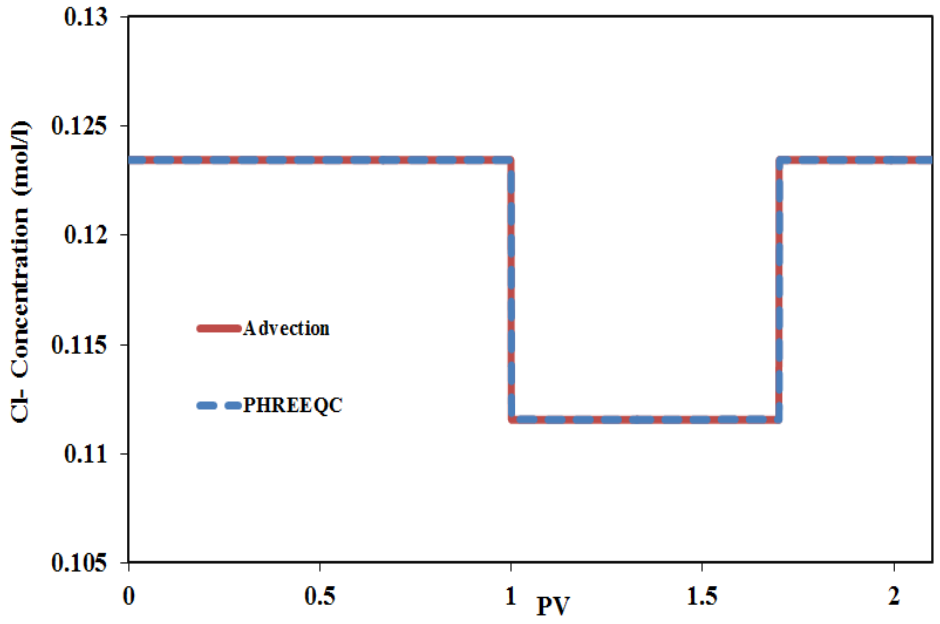

Figure C-7: Cl^- concentration history of the effluent solution (the simplified code verification against PHREEQC).

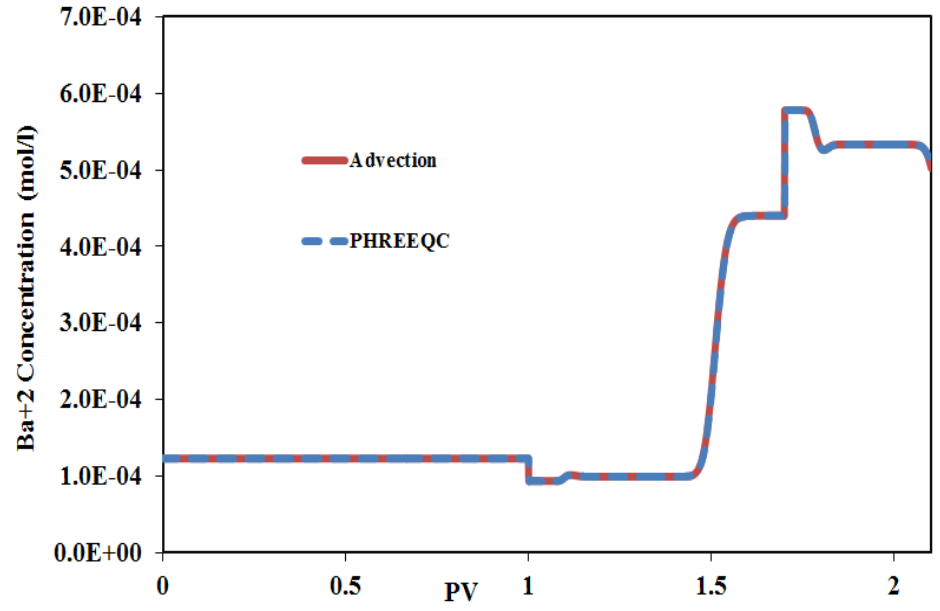

Figure C-8: Ba^{+2} concentration history of the effluent solution (the simplified code verification against PHREEQC).

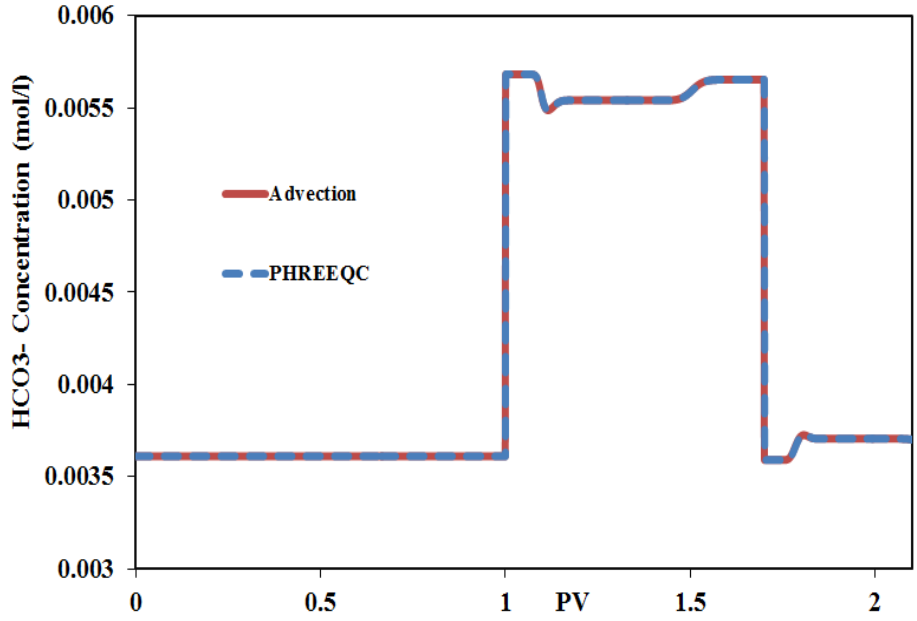

Figure C-9: HCO_3^- concentration history of the effluent solution (the simplified code verification against PHREEQC).

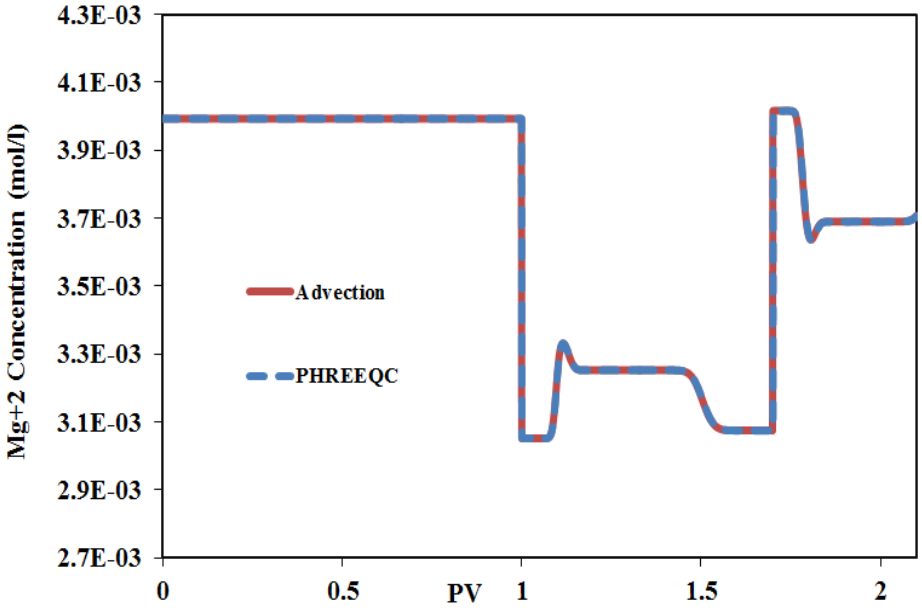

Figure C-10: Mg^{+2} concentration history of the effluent solution (the simplified code verification against PHREEQC).

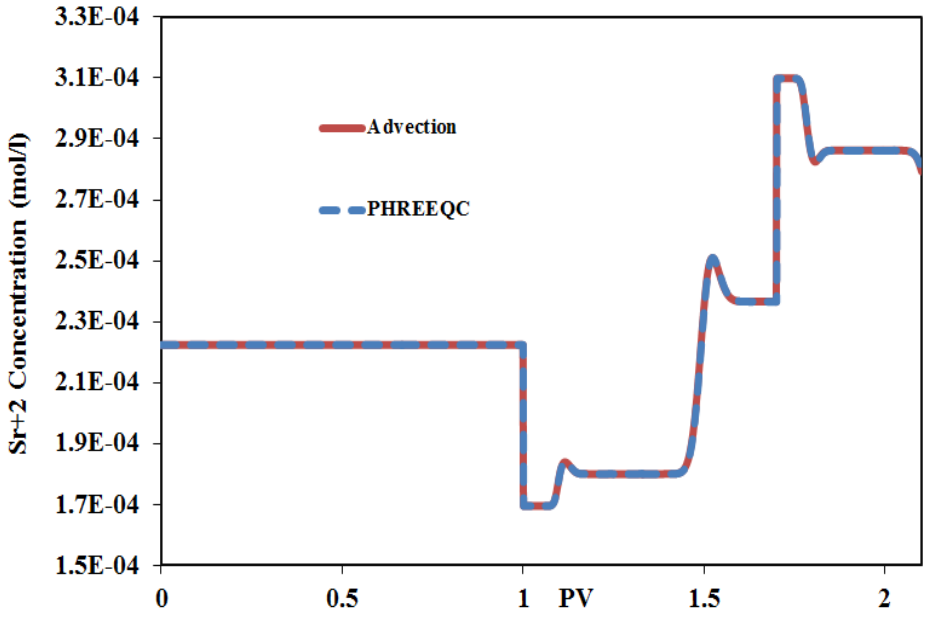

Figure C-11: Sr^{+2} concentration history of the effluent solution (the simplified code verification against PHREEQC).

Appendix D: Detailed UTCOMP-IPhreeqc Computational Flowchart

This appendix presents the UTCOMP-IPhreeqc computational algorithm with more details. In this algorithm only the effect of hydrocarbon-CO_2 on the aqueous-rock geochemistry is considered. However, we apply the same procedure if multiple hydrocarbon components (e.g., CH_4 and H_2S components besides the CO_2 component) are included in calculations. TNK_i, $TNKTG_i$, f_i, and SI_i used in the algorithm are total moles of the hydrocarbon component *i*, total moles of the geochemical element *i*, fugacity of the component *i*, and saturation index of phase *i*, respectively. In IPhreeqc, saturation index for gas is logarithm partial pressure (fugacity in UTCOMP-IPhreeqc).

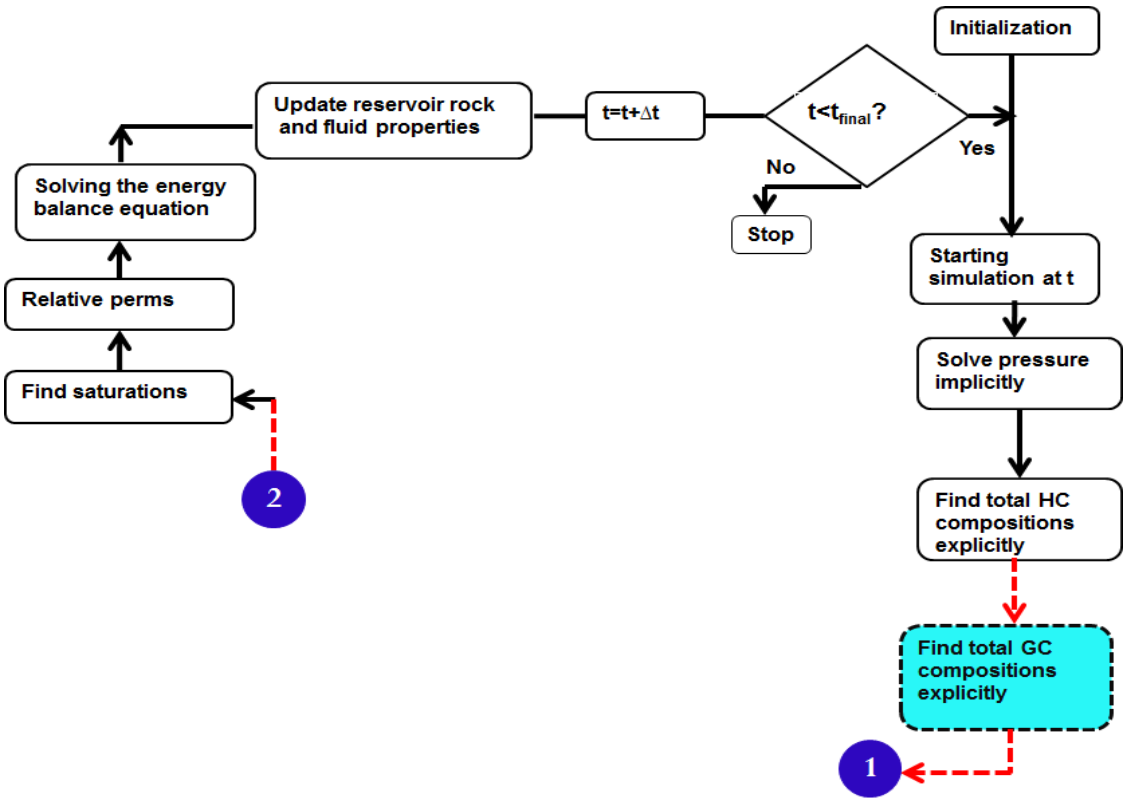

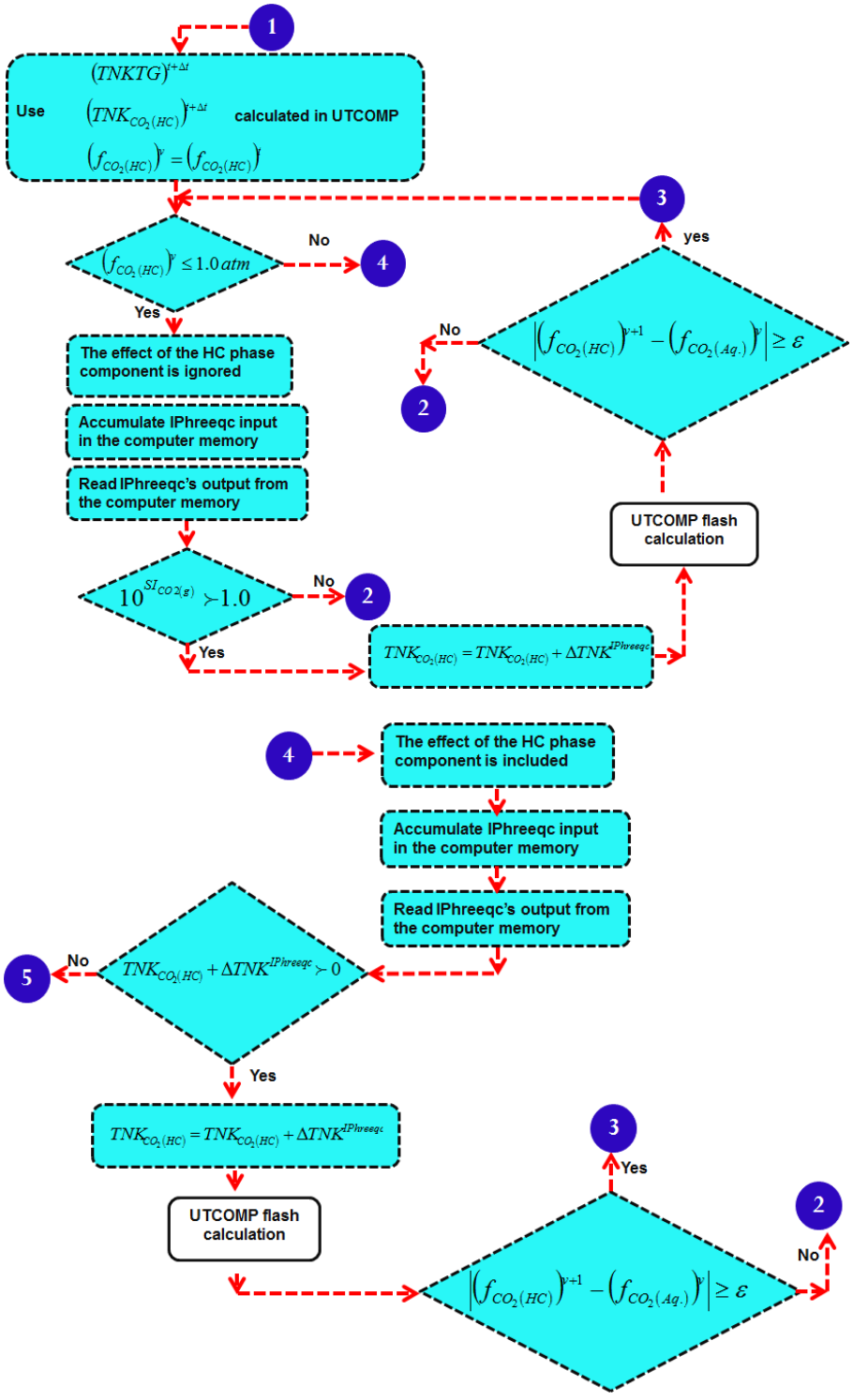
1
Use $(TNKTG)^{t+\Delta t}$ $(TNK_{CO_2(HC)})^{t+\Delta t}$ calculated in UTCOMP $(f_{CO_2(HC)})^{\nu} = (f_{CO_2(HC)})^{t}$
3
$(f_{CO_2(HC)})^{\nu} \le 1.0\,atm$
No
4
Yes
The effect of the HC phase component is ignored
Accumulate IPhreeqc input in the computer memory
Read IPhreeqc's output from the computer memory
$10^{SI_{CO2(g)}} > 1.0$
No
2
Yes
$TNK_{CO_2(HC)} = TNK_{CO_2(HC)} + \Delta TNK^{IPhreeqc}$
UTCOMP flash calculation
yes
$\left|(f_{CO_2(HC)})^{\nu+1} - (f_{CO_2(Aq.)})^{\nu}\right| \ge \varepsilon$
No
2
4
The effect of the HC phase component is included
Accumulate IPhreeqc input in the computer memory
Read IPhreeqc's output from the computer memory
5
No
$TNK_{CO_2(HC)} + \Delta TNK^{IPhreeqc} > 0$
Yes
$TNK_{CO_2(HC)} = TNK_{CO_2(HC)} + \Delta TNK^{IPhreeqc}$
UTCOMP flash calculation
3
Yes
$\left|(f_{CO_2(HC)})^{\nu+1} - (f_{CO_2(Aq.)})^{\nu}\right| \ge \varepsilon$
2
No

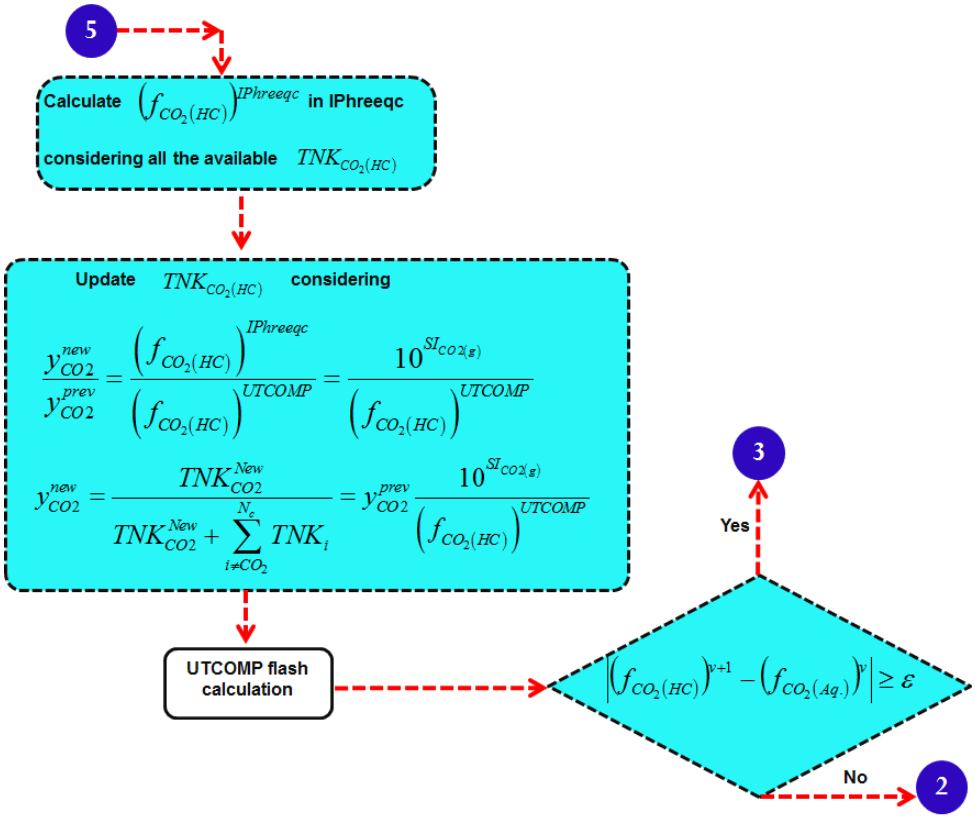
5
Calculate $\left(f_{CO_2(HC)}\right)^{IPhreeqc}$ in IPhreeqc
considering all the available $TNK_{CO_2(HC)}$
Update $TNK_{CO_2(HC)}$ considering
$\frac{y_{CO2}^{new}}{y_{CO2}^{prev}} = \frac{\left(f_{CO_2(HC)}\right)^{IPhreeqc}}{\left(f_{CO_2(HC)}\right)^{UTCOMP}} = \frac{10^{SI_{CO2(g)}}}{\left(f_{CO_2(HC)}\right)^{UTCOMP}}$
$y_{CO2}^{new} = \frac{TNK_{CO2}^{New}}{TNK_{CO2}^{New} + \sum_{i \neq CO_2}^{N_c} TNK_i} = y_{CO2}^{prev} \frac{10^{SI_{CO2(g)}}}{\left(f_{CO_2(HC)}\right)^{UTCOMP}}$
UTCOMP flash calculation
$\left|\left(f_{CO_2(HC)}\right)^{v+1} - \left(f_{CO_2(Aq.)}\right)^{v}\right| \geq \varepsilon$
Yes
3
No
2

Appendix E: UTCOMP-IPhreeqc Input Files

The following presents the description of different sections in Appendix E:

- Appendix E.1 provides UTCOMP-IPhreeqc input files that produce the outputs of PHREEQC example 11. To run UTCOMP-IPhreeqc the following files are required: INPUT.DAT, GCINPUT.DAT, IPhreeqc_Database.DAT, and IPhreeqc_INPUT.DAT. Description of each file is provided in Chapter 2.
- Appendix E.2 shows how gridblocks geochemistry data are stored in the computer memory (for the case presented in Appendix E.1).
- Appendix E.3 presents how we modify the gridblock geochemistry data in the computer memory (for the case presented in Appendix E.1).
- Appendix E.4 illustrates how IPhreeqc outputs are organized in the computer memory to be transferred to UTCOMP (for the case presented in Appendix E.1).

E.1: UTCOMP-IPHREEQC SAMPLE INPUT FILES

E.1.1 INPUT.DAT

```
CC*****************************************************************
**
CC                                                                *
CC  BRIEF DESCRIPTION OF DATA SET: UTCOMP
*
```

```
CC
*
CC*********************************************************************
**
CC
*
CC
*
CC
*
CC LENGTH(FT):                    INJECTION FLUID  :
*
CC HEIGHT(FT):                    INJECTION RATE   :
*
CC WIDTH(FT) :                    W/O REL. PERM    :
*
CC POROSITY  :                    G/O REL. PERM    :
*
CC ABS. PERM :                    3-PHASE REL. PERM:
*
CC TEMP(F)   :                    WETTIBILITY:
*
CC PRE(PSI)  :
*
CC SOR       :
*
CC SWC       :
*
CC AVG. DEPTH(FT) :
*
CC
*
CC
*
CC
*
CC
*
CC
*
CC
*
CC*********************************************************************
**
CC
*
CC        HYDROCARBON DATA AND FLASH CALCULATION OPTIONS
*
CC
*
```

```
CC*********************************************************************
**
CC
CC..+....1....+....2....+....3....+....4....+....5....+....6...+...7..
CC***********SOME CONSTANTS AND MAXIMUM VALUES FOR MODELS**************
CC
CC NXM, NYM, NZM, NPM, NCM, NWM POSTPROCESSOR
   40  1   1    3     12    3   2
CC
CC NS1M,NBWM,NPRM,NPFM,NCTM,NHSM
    1    401   50    10   10   10000
CC
CC IC2,NCMT,NREG,NTAB
    2  4    6   25
CC
CC EE, NZPM
   0.5761 3
CC
CC TOLP, TOLVOL, QLIM
   0.5D-1 0.5D-4 1.0D-30
CC
CC NUMAX,INQUA,INCON,INVEL,NOSWTM,NUMPRE,NUMOUT,NUMPVT,NST,IFLIP
    10     3     3     5     10     30     12     30    20   0
CC*********************************************************************
CC CASE NAME WITH FORMAT ( 17A4, A2 ) OF TOTAL 70 COLUMNS.
*----HEADER
1D CO2+NG INJECTION INVOLVING 3 HC PHASES
CC
CC NUMBER OF COMPONENTS.
*--------NC
         12
CC COMPONENT NAMES WITH FORMAT ( 1X, A8 ), NC CARDS.
CC..+..8
*----NAME
    CO2
    C1N2
    C2
    C3
    C4
    C5
    C6
    C710
    C1113
    C1419
    C2029
    C30P
CC
CC BLACK OIL OPTION; AQUIFER SALINITY (ppm); AQUIFER OPTION
*-----IBOST     SLNTY    IAQUIF
          0        0.         0
CC CRITICAL PRESS. (PSI), TEMP. (R) AND  VOL. (CU FT/LB-MOLE),
```

```
CC MOLECULAR WT. (LB/LB-MOLE), ACENTRIC FACTOR, PARACHOR. NC CARDS.
*--------PC         TC          VC        MW         OM      PARACH
VSP
        1070.535624     547.5 2.243201575 44    0.2276      49    0
        666.972984      342.5 1.442237287 16.1  0.0109      71    0
      707.6591358 549.6 2.371294757 30.1  0.099 134.825     0
      616.2902348 665.6 3.252343124 44.1  0.1518      233.048     0
      544.3147329 756.4 4.122115282 58.1  0.1885      394.499     0
      489.3334468 838.4 4.883768876 72.1  0.24  707.76      0
      476.1379381 913.8 5.423128436 84    0.2711      1035.85     0
      412.859476  1048.7      6.959539271 113.3 0.3683      1035.85
      0
      318.1916979 1196.4      10.20105981 161.9 0.5239      1035.85
      0
      249.6150391 1328.9      14.31231704 226   0.6932      1035.85
      0
      192.4345015 1475.9      21.23608053 331.5 0.9   1035.85     0
      133.6545083 1574.9      37.15367911 588   1.2   1035.85     0
CC EOS parameters (Ac and Bc)
CC NC CARDS.
*----    PARAA           PARAB
      0.457236    0.077796
      0.457236    0.077796
      0.457236    0.077796
      0.457236    0.077796
      0.457236    0.077796
      0.457236    0.077796
      0.457236    0.077796
      0.457236    0.077796
      0.457236    0.077796
      0.457236    0.077796
      0.457236    0.077796
      0.457236    0.077796
CC
CC BINARY INTERACTION COEFFICIENTS, CIJ. NC CARDS.
*-----DELTA
      0
      0.105 0
      0.125 0.0028      0

      0.12  0.0089      0.0017      0

      0.12  0.0156      0.0053      0.001 0

      0.12  0.0216      0.009 0.0029      0.0005      0

      0.12  0.0257      0.0118      0.0045      0.0013      0.0002
      0
      0.12  0.0369      0.0198      0.01  0.0047      0.0022
      0.0011      0
```

```
      0.13  0.0575      0.0359      0.0223      0.0141      0.0093
      0.0069      0.0025      0
      0.13  0.0789      0.0538      0.037 0.0263      0.0198
      0.0161      0.009 0.002 0
      0.13  0.1072      0.0784      0.0584      0.045 0.0365
      0.0316      0.0213      0.0093      0.0027      0
      0.13  0.1523      0.1193      0.0954      0.0788      0.0677
      0.0612      0.0469      0.0284      0.0156      0.0054      0
CC
CC BINARY INTERACTION COEFFICIENTS, DIJ. NC CARDS.
*-------DIJ
      0
      0     0
      0     0     0
      0     0     0     0
      0     0     0     0     0
      0     0     0     0     0     0
      0     0     0     0     0     0     0
      0     0     0     0     0     0     0     0
      0     0     0     0     0     0     0     0     0
      0     0     0     0     0     0     0     0     0     0
      0     0     0     0     0     0     0     0     0     0     0
      0     0     0     0     0     0     0     0     0     0     0
      0
CC
CC reduction method: (0: OFF, 1: ON)
*-------IFLASHTYPE  irfla  irsa
          1           0      0
CC
CC MAXIMUM NUMBER OF PHASES ( 3 OR 4 )
*---------NP     IVISC  IVISC_COEF   ISINGL   ISOLU
         3         1      0            0        0
CC IEOS: 1,    IPEM: 0 OR 1
CC ISTAM: -1, 0 OR 1, IEST: 0 OR 1  KI: 0, 1 OR 2
*---IEOS   IPEM     ISTAM   IEST  IVSP   KI
     1      1        -1      1      0     0
CC
CC ITERATION TOLERANCES FOR PERSCHKE'S FLASH ROUTINES.
*----TOLFLA    TOLFLM     TOLPD    TOLSAM    TOLSAS    TOLSUM
     1.0E-08  1.0E-8    1.0E-10  1.0E-8   1.0E-8   1.0E-08
CC
CC MAXIMUM NUMBER OF ITERATIONS FOR PERSCHKE'S FLASH ROUTINES.
*----MAXFLA    MAXFLM     MAXPD    MAXSAM    MAXSAS
      30000     1000      1000      1000     30000      20
CC
CC VECTOR FLASH OPTION
*--IVCFL   TOLVFL     MAXVFL
     0      1.E-10     30
CC
CC SWITCHING PARAMETERS FOR PERSCHKE'S FLASH ROUTINES.
*----SWIPCC    SWIPSA
```

```
     1.e-3     1.e-3
CC
CC PHASE IDENTIFICATION PARAMETERS FOR PERSCHKE'S FLASH ROUTINES.
*------IOIL      ITRK   DMSLIM
         1        2      25.
CC
CC IFLAGT ( 0 : OFF,   1 : ON )
*------IFLAGT  IGEOCHEM  IPhreeqc  IASPR
            0     1          1       0
CC
CC*********************************************************************
**
CC                                                      *
CC OUTPUT OPTIONS                                       *
CC                                                      *
CC*********************************************************************
**
CC
CC
CC HISTORY PRINTING PARAMETER FOR <<HISTORY.CPR>>.
*--- POSTPROCESSOR  NHSSKIP   NSTSKIP     IPV
                  20        20          1
CC
CC REFERENCE CONCENTRATION, CONC0, USED FOR EFFLUENT CONCENTRATION.
*-----CONC0
  1.0  1.0  1.0  1.0  1.0  1.0  1.0  1.0   1.0  1.0  1.0  1.0
CC
CC
*------
      0
CC
CC NUMBER OF PRINTS FOR <<PROFILE.CPR>>.
*-------NPF
         0
CC
CC NUMBER OF PRINTS FOR <<CONTOUR.CPR>>.
*-------NCT
         0
CC
CC*********************************************************************
**
CC                                                          *
CC RESERVOIR AND WELL DATA                                        *
CC                                                          *
CC*********************************************************************
**
CC
CC A FLAG FOR RESERVOIR GEOMETRY:
CC 2-D: 11(Y), 12(X), 13(Z), 2-D: 21(XY), 22(YZ), 23(XZ), 3-D: 31
*-----IGEOM       INUG
        12          0
```

```
CC
CC NUMBER OF GRID BLOCKS IN X, Y, AND Z.
*--------NX        NY        NZ
         40        1          1
CC
CC NUMBER OF WELLS, AND FLAG FOR WELLBORE MODEL
*--------NW       IWM
         2         1
CC
CC WELLBORE RATIUS (FT). NW NUMBERS.
*--------RW: (NW)
        0.33         0.33
CC
CC WELL LOCATIONS. NW CARDS.
*-------LXW       LYW    IDIR   LZWF      LZWL
          1        1        3      1         1
         40       1        3      1         1
CC
CC A FLAG ( 0 OR 1 ) FOR GRID BLOCK SIZE IN X-DIRECTION.
*-------MDX
         0
CC
CC CONSTANT GRID BLOCK SIZE IN X-DIRECTION (FT).
*--------DX
         0.04
CC
CC A FLAG ( 0 OR 1 ) FOR GRID BLOCK SIZE IN Y-DIRECTION.
*-------MDY
        0
CC
CC CONSTANT GRID BLOCK SIZE IN Y-DIRECTION (FT).
*--------DY
        0.15
CC
CC A FLAG ( 0 OR 1 ) FOR GRID BLOCK SIZE IN Z-DIRECTION.
*-------MDZ
        0
CC
CC CONSTANT GRID BLOCK SIZE IN Z-DIRECTION (FT).
*--------DZ
        0.15
CC
CC A FLAG ( 0 OR 1 ) FOR FORMATION DEPTH.
*--------MD
         0
CC
CC DEPTH (FT) OF THE MOST UPPER LAYER.
*---------D
       0.
CC
CC A FLAG ( 0 OR 1 ) FOR FORMATION POROSITY.
```

```
*------MPOR
       0
CC
CC HOMOGENEOUS POROSITY (FRACTION) AT PF.
*----PORSTD
     0.25
CC
CC A FLAG ( 0 OR 1 ) FOR PERMEABILITY IN X-DIRECTION.
*----MPERMX
       0
CC
CC HOMOGENEOUS PERMEABILITY (MD) IN X-DIRECTION.
*-----PERMX
100
CC
CC A FLAG ( 0 OR 1 ) FOR PERMEABILITY IN Y-DIRECTION.
*----MPERMY
       0
CC
CC HOMOGENEOUS PERMEABILITY (MD) IN Y-DIRECTION.
*-----PERMY
100
CC
CC FLAG ( 0 OR 1 ) FOR PERMEABILITY IN Z-DIRECTION.
*----MPERMZ
       0
CC
CC HOMOGENEOUS PERMEABILITY (MD) IN Z-DIRECTION.
*-----PERMZ
     10.00
CC
CC FORMATION COMPRESSIBILITY (1/PSI) AND REFERENCE PRESSURE (PSI).
*--------CF           PF
       0.          14.67
CC H2O COMPRESSIBILITY (1/PSI), REFERENCE PRESSURE (PSI) AND
CC MOLAR DENSITY (LB-MOLE/CU FT).
*--------CW       PW     DENMWS
      0.     14.67      3.467
CC
CC WATER MOLECULAR WT. (LBM/LBM-MOLE) AND VISCOSITY (CP).
*-------WTW     VISCW
        18.       0.79
CC
CC FORMATION TEMPERATURE (F).
*-----TEMPF
       212.0
CC
CC STANDARD TEMPERATURE (F) AND STANDARD PRESSURE (PSI).
*-----TFSTD      PSTD
        60.      14.67
CC
```

```
CC A FLAG ( 1, 2, 3 OR 4 ) FOR NUMERICAL DISPERSION CONTROL.
*----IUPSTW
       1
CC
CC ITC ( 0 : NO 2ND ORDER TIME,   1 : 2ND ORDER TIME ON )
*----ITC
      0
CC RESTART OPTIONS.
CC ISTART ( 1 OR 2 ), ISTORE ( 0 OR 1 ).
*----ISTART    ISTORE
       1       1
CC
CC A FLAG ( 0 OR 1 ) FOR AUTOMATIC TIME-STEP SELECTION ( = 1 ).
*-------MDT
        1
CC
CC A FLAG ( 0 OR 1 ) FOR PHYSICAL DISPERSION CALCULATION.
*-----MDISP
       1
CC MOLECULAR DIFFUSION COEFFICIENTS ( FT*FT/DAY ).
CC NP CARDS AND EACH CARD HAS NC NUMBERS.
*----DIFFUN
      0. 0. 0. 0.  0. 0. 0. 0.  0.  0. 0. 0.
      0. 0. 0. 0.  0. 0. 0. 0.  0.  0.  0. 0.
      0. 0. 0. 0.  0. 0. 0. 0.  0.  0.  0. 0.
CC
CC TORTUOSITY FACTOR.
*-------TAU
        1.
CC
CC LONGITUDINAL AND TRANSVERSE DISPERSIVITIES (FT). NP CARDS.
*----ALPHAL ALPHAT
     0.02  0.0
     0.    0.0
     0.    0.0
CC
CC YOUNG'S DISPERSION MODEL
*-----BETAL BETAT ALMAX ATMAX
      0.0   0.0   0.2  0.005
CC FLAGS FOR RELATIVE PERMEABILITY MODEL AND CAPILLARY PRESSURE.
CC IPERM ( 1 OR 2 ), ICPRES ( 0 OR 1 ).
*-----IPERM    ICPRES      ICAP    IRPERM
      4         0          0         0
CC CAPILLARY PRESSURE PARAMETERS AND
CC WATER/OIL INTERFACIAL TENSION (DYNES/CM).
*-------EPC       CPC    RIFTWO    RIFTWG    RIFTWL
        2.        2.0    20.        24.       30.
CC
CC HIGH IFT RESIDUAL SATURATIONS.
*-----S1RW     S2RW1     S2RW2      S3RW     S4RW1     S4RW2
        0.05      0.18       .25       0.05     0.2       0.2
```

```
CC
CC LOW IFT RESIDUAL SATURATIONS.
*------S1RC     S2RC1     S2RC2      S3RC     S4RC1     S4RC2
       0    .0       .0         0.        0.        0.
CC
CC HIGH IFT END POINT RELATIVE PERMEABILITY.
*------P1RW      P2RW      P3RW      P4RW
        0.383     1.0       0.35       0.35
C
CC LOW IFT END POINT RELATIVE PERMEABILITY.
*------P1RC       P2RC         P3RC         P4RC
        1.        1              1           1.
CC
CC HIGH IFT EXPONENT OF RELATIVE PERMEABILITY.
*-------E1W      E2W1      E2W2       E3W      E4W1      E4W2
        1.59       3.22       2.5      2.5       2.5       2.5
CC
CC LOW IFT EXPONENT OF RELATIVE PERMEABILITY.
*-------E1C      E2C1      E2C2       E3C      E4C1      E4C2
         1.        1.        1.        1.        1.        1.
CC
CC WATER AND L1 PHASE CAPILLARY DESATURATION PARAMETERS.
*-------T11       T12      T211      T221      T212      T222
        -.4       1.6      -0.5       2.2      -.04       1.6
CC
CC GAS AND L2 PHASE CAPILLARY DESATURATION PARAMETERS.
*-------T31       T32      T411      T421      T412      T422
        -0.5      2.2      -0.5       2.2       -.4       1.6
CC
CC
*------  IWALT    IWALF
            0       0
CC
CC A FLAG FOR PRESSURE EQUATION SOLVER ( 1, 2, 3, 4 OR 5 ).
*----IPRESS    IPREC   METHSL   OMEGA    IHYPRE
        11      2       1       1.0     1     0
CC
CC ITERATIVE PRESSURE SOLVER PARAMETERS.
*-----ITMAX  LEVLIT  IDGTS   NS1       NS2      ZETA
      1000      1      1      5      1000000   1.E-07
CC
CC INITIAL TIME (DAYS).
*---------T
          0
CC
CC A FLAG ( 0 OR 1 ) FOR INITIAL PRESSURE.
*--------MP
         0
CC
CC CONSTANT INITIAL PRESSURE (PSIA).
*---------P
```

```
      4890
CC
CC A FLAG ( 0 OR 1 ) FOR INITIAL WATER SATURATION.
*------MSAT
        0
CC
CC CONSTANT INITIAL WATER SATURATION (FRACTION).
*-------SAT
      0.999
CC
CC A FLAG ( 0 OR 1 ) FOR INITIAL OVERALL COMPOSITION.
*-----MOMFR
        0
CC
CC CONSTANT INITIAL COMPOSITION (MOLE FRACTION).
*------OMFR
      0.12837     0.42134     0.05557     0.02662     0.01535
      0.00985     0.00835     0.06971     0.03578     0.07131
      0.07629     0.08146
CC
CC*************************************************************************
**
CC                                                                       *
CC RECURRENT DATA
*
CC                                                                       *
CC*************************************************************************
**
CC                           LoSal INJECTION
*
CC*************************************************************************
**
CC MAXIMUM TIME (DAYS), TIME STEP (DAYS) AND WELL DATA.
*--------TM         DT       NWELLS    GORLIM    WORLIM
        2.5         0.05      2         -1       -1
CC
CC
*-----DTMAX     DTMIN     DSLIM     DPLIM      DVLIM    DMFACT
DMFACTG
       0.1      0.001     0.05      0.005       0.05      0.03     0.05
CC
CC WELL NO. AND WELL TYPE.
*--------LW    IQTYPE
          1      4
CC
CC   (B/D)  (MSCF/D)
*----QPSVC(1)   QPSVC(3)   NCOMP   ISWITCH   PBHC
      4E-5       0         0        0        6000
CC
CC
*--- INJ_SOLUTION_NO
```

```
          0
CC
CC WELL NO. AND WELL TYPE.
*--------LW    IQTYPE
         2       -2
CC
CC CONSTANT BHP PRODUCER (PSI)
*--------PBHC
        4890.0
CC
CC END OF INPUT.
*--------TM     DT    NWELLS   GORLIM   WORLIM ----------------
         -1.0   -1.     -1     -1.E10    -1.E10
```

E.1.2 GCINPUT.DAT

```
CC
CC*******************************************************
CC                                                      *
CC              GEOCHEMISTRY SECTION                    *
CC                                                      *
CC*******************************************************
CC
CC
*------- RIUNITS   NO_HC_GC   NO_ACID_BASE  IITERATION
            0         0           0            1
CC
CC*******************************************************
CC                                                      *
CC              GEOCHEMISTRY OUTPUT  SECTION            *
CC                                                      *
CC*******************************************************
CC
CC
*--- IPRES   IPWELL  IPTDRM  IPWET
       1        0      0       0
CC****************** RESERVOIR SECTION **********************
CC
*---- PRINT_NUMBER_ELEMENT   ELEMENT_HISTORY   ELEMENT_PROFILE
FREQUENCY_HIS(TIME STEP)  FREQUENCY_PROF(TIME STEP)
             0                  1                 1
1                           1
CC
CC
*---- NSLDP  SOLID_HISTORY   SOLID_PROFILE    FREQUENCY_HIS (TIME STEP)
FREQUENCY_PROF(TIME STEP)
       0      1                 1                   1           1
CC
```

```
CC
*----  NAQSP   AQS_HISTORY   AQS_PROFILE    FREQUENCY_HIS(TIME STEP)
FREQUENCY_PROF(TIME STEP)
        0         1             1                   10
1000
CC
CC
*---- NSORBP  SORBED_HISTORY   ELEMENT_PROFILE    FREQUENCY_HIS (TIME
STEP)   FREQUENCY_PROF (TIME STEP)
        0           1                   1                  1
1
CC
CC
*---- NPRINTG    PRINTG_HISTORY   PRINTG_PROFILE    FREQUENCY_HIS (TIME
STEP)  FREQUENCY_PROF(TIME STEP)
        4              1              0                    1
1
CC
CC
*-------- NO OF GRIDBLOCKS
         1
CC
CC
*----- (I,J,K)
      40
       1
       1
CC
CC
*------ OTHER GEOCHEMICAL PROPERTIES NAMES
TOT("Na")*1E3
TOT("Cl")*1E3
TOT("K")*1E3
TOT("Ca")*1E3
```

E.1.3 IPhreeqc_INPUT.DAT

```
##  GRIDBLOCK INITIALIZATION

SOLUTION 1-40
 -water     1.0   ## water mass in each grid block
        units           mmol/kgw
        temp            25.0
        pH              7.0     charge
        pe              12.5    O2(g)   -0.68
        Na              1.0
        K               0.2
        N(5)            1.2
END
```

```
EXCHANGE 1-40
        -equilibrate 1
        X               0.0011
END

#   INJECTION SOLUTIONS

SOLUTION 0
   -water 1  ## kg
        units           mmol/kgw
        temp            25.0
        pH              7.0     charge
        pe              12.5    O2(g)   -0.68
        Ca              0.6
        Cl              1.2
END
```

E.1.4 IPhreeqc_Database.DAT

```
# PHREEQC.DAT for calculating pressure dependence of reactions, with
#   molal volumina of aqueous species and of minerals, and
#   critical temperatures and pressures of gases used in Peng-
Robinson's EOS.
# Details are given at the end of this file.

SOLUTION_MASTER_SPECIES
#
#element    species     alk   gfw_formula element_gfw
#
H           H+    -1.0  H           1.008
H(0)        H2    0.0   H
H(1)        H+    -1.0  0.0
E           e-    0.0   0.0         0.0
O           H2O   0.0   O           16.0
O(0)        O2    0.0   O
O(-2)       H2O   0.0   0.0
Ca          Ca+2  0.0   Ca          40.08
Mg          Mg+2  0.0   Mg          24.312
Na          Na+   0.0   Na          22.9898
K           K+    0.0   K           39.102
Fe          Fe+2  0.0   Fe          55.847
Fe(+2)            Fe+2  0.0   Fe
Fe(+3)            Fe+3  -2.0  Fe
Mn          Mn+2  0.0   Mn          54.938
Mn(+2)            Mn+2  0.0   Mn
Mn(+3)            Mn+3  0.0   Mn
Al          Al+3  0.0   Al          26.9815
Ba          Ba+2  0.0   Ba          137.34
```

```
Sr          Sr+2  0.0   Sr          87.62
Si          H4SiO4      0.0   SiO2        28.0843
Cl          Cl-   0.0   Cl          35.453
C           CO3-2 2.0   HCO3        12.0111
C(+4)       CO3-2 2.0   HCO3
C(-4)       CH4   0.0   CH4
Alkalinity  CO3-2 1.0   Ca0.5(CO3)0.5     50.05
S           SO4-2 0.0   SO4         32.064
S(6)        SO4-2 0.0   SO4
S(-2)       HS-   1.0   S
N           NO3-  0.0   N           14.0067
N(+5)       NO3-  0.0   N
N(+3)       NO2-  0.0   N
N(0)        N2    0.0   N
N(-3)       NH4+  0.0     N
#Amm        AmmH+ 0.0   AmmH        17.0
B           H3BO3 0.0   B           10.81
P           PO4-3 2.0   P           30.9738
F           F-    0.0   F           18.9984
Li          Li+   0.0   Li          6.939
Br          Br-   0.0   Br          79.904
Zn          Zn+2  0.0   Zn          65.37
Cd          Cd+2  0.0   Cd          112.4
Pb          Pb+2  0.0   Pb          207.19
Cu          Cu+2  0.0   Cu          63.546
Cu(+2)            Cu+2  0.0   Cu
Cu(+1)            Cu+1  0.0   Cu
# redox-uncoupled gases
Hdg         Hdg   0     Hdg   2.016 # H2 gas
Oxg         Oxg   0     Oxg   32 # Oxygen gas
Mtg         Mtg   0.0   Mtg   16.032 # CH4 gas
Sg          H2Sg  1.0   H2Sg  34.08
Ntg         Ntg   0     Ntg   28.0134 # N2 gas

SOLUTION_SPECIES
H+ = H+
      -gamma      9.0   0.0
      -dw    9.31e-9
e- = e-
H2O = H2O
Ca+2 = Ca+2
      -gamma      5.0   0.1650
#     -gamma      4.5   0.23 # anhydrite in NaCl solutions, Freyer and
Voigt, 2004, GCA 68, 307
      -dw    0.793e-9
      -Vm  -0.3456  -7.252  6.149  -2.479  1.239  5  1.60  -57.1  -
6.12e-3  1 # supcrt modified
Mg+2 = Mg+2
      -gamma      5.5   0.20
      -dw    0.705e-9
```

```
      -Vm  -1.410  -8.6  11.13  -2.39  1.332  5.5  1.29  -32.9  -5.86e-
3  1 # supcrt modified
Na+ = Na+
      -gamma      4.0    0.075
      -gamma      4.08 0.082 # halite solubility
      -dw    1.33e-9
      -Vm  1.403  -2.285  4.419  -2.726  -5.125e-5  4.0  0.162  47.67
-3.09e-3  0.725 # supcrt modified
# for calculating densities (rho) when I > 3...
#     -Vm  1.403  -2.285  4.419  -2.726  -5.125e-5  2.0  0.162  47.67
-3.09e-3  0.4
K+ = K+
      -gamma      3.5   0.015
      -dw    1.96e-9
      -Vm  3.322  -1.473  6.534  -2.712  9.06e-2  3.5  0  29.7  0  1 #
supcrt modified
Fe+2 = Fe+2
      -gamma      6.0   0.0
      -dw    0.719e-9
      -Vm  -0.3255  -9.687  1.536  -2.379  0.3033  5.5  -4.21e-2  37.96
0  1 # supcrt modified
Mn+2 = Mn+2
      -gamma      6.0   0.0
      -dw    0.688e-9
      -Vm  -.1016  -8.0295  8.9060  -2.4471  1.4006 6 # supcrt
Al+3 = Al+3
      -gamma      9.0   0.0
      -dw    0.559e-9
      -Vm  -3.3404  -17.1108  14.9917  -2.0716  2.8711 9 # supcrt
Ba+2 = Ba+2
      -gamma  5.0  0
      -gamma      4.0  0.153 # Barite solubility
      -dw 0.848e-9
      -Vm  2.063  -10.06  1.9534  -2.36  0.4218  5  1.58  -12.03  -
8.35e-3  1 # supcrt modified
Sr+2 = Sr+2
      -dw    0.794e-9
      -gamma      5.260 0.121
      -Vm  -1.57e-2  -10.15  10.18  -2.36  0.860  5.26  0.859  -27.0  -
4.1e-3  1.97 # supcrt modified
H4SiO4 = H4SiO4
      -dw    1.10e-9
      -Vm  10.5  1.7  20  -2.7  0.1291 # supcrt + 2*H2O in a1
Cl- = Cl-
      -gamma      3.5     0.015
      -gamma      3.63  0.017 # cf. pitzer.dat
      -dw    2.03e-9
      -Vm  4.465  4.801  4.325  -2.847  1.748  0  -0.331  20.16  0  1 #
supcrt modified
CO3-2 = CO3-2
      -gamma      5.4   0.0
```

```
      -dw    0.955e-9
      -Vm  6.95  0  0  -5.98  8.32  0  -0.115  167  -0.026  1 # supcrt
modified
SO4-2 = SO4-2
      -gamma      5.0   -0.04
      -dw    1.07e-9
      -Vm  8.0  2.51  -42.5 5.41  4.23 0 0 0 0 1 # supcrt modified
NO3- = NO3-
      -gamma      3.0   0.0
      -dw    1.9e-9
      -Vm  6.392  6.78  0  -3.06  0.449  0  0.80  0  -1.05e-2  1 #
supcrt modified
#AmmH+ = AmmH+
#     -gamma      2.5   0.0
#     -dw    1.98e-9
#     -Vm  4.837  2.345  5.522  -2.88 1.096  3  -1.456  75.0  7.17e-3
1 # supcrt modified
H3BO3 = H3BO3
      -dw   1.1e-9
      -Vm 7.0643  8.8547  3.5844  -3.1451 -.2000  # supcrt
PO4-3 = PO4-3
      -gamma      4.0   0.0
      -dw    0.612e-9
      -Vm  -.5259  -9.0654  9.3131  -2.4042  5.6114 # supcrt
F- = F-
      -gamma      3.5   0.0
      -dw    1.46e-9
      -Vm  .6870  1.3588  7.6033  -2.8352  1.787 # supcrt
Li+ = Li+
      -gamma      6.0   0.0
      -dw    1.03e-9
      -Vm  -.0237  -.0690  11.5800  -2.7761 .4862 6 # supcrt
Br- = Br-
      -gamma      3.0   0.0
      -dw    2.01e-9
      -Vm  5.2690  6.5940  4.7450  -3.1430  1.3858 # supcrt
Zn+2 = Zn+2
      -gamma      5.0   0.0
      -dw    0.715e-9
      -Vm  -1.0677  -10.3884  9.8331  -2.3495  1.4574 5 # supcrt
Cd+2 = Cd+2
      -dw    0.717e-9
      -Vm  .0537  -10.7080  16.5176  -2.3363  1.2528 5 # supcrt
Pb+2 = Pb+2
      -dw    0.945e-9
      -Vm  -.0051  -7.7939  8.8134  -2.4568  1.0788 4.5 # supcrt
Cu+2 = Cu+2
      -gamma      6.0   0.0
      -dw    0.733e-9
      -Vm  -1.1021  -10.4726  9.8662  -2.3461  1.4769 6 # supcrt
# redox-uncoupled gases
```

```
Hdg = Hdg # H2
      -dw    5.13e-9
      -Vm 6.52  0.78  0.12 # supcrt
Oxg = Oxg # O2
      -dw    2.35e-9
      -Vm  5.7889  6.3536  3.2528  -3.0417  -0.3943 # supcrt
Mtg = Mtg # CH4
      -dw    1.85e-9
      -Vm 7.7 # CH4 solubility, 25-100C, 1-700atm
Ntg = Ntg # N2
      -dw    1.96e-9
      -Vm 7 # Pray et al., 1952, IEC 44. 1146
H2Sg = H2Sg # H2S
      -dw    2.1e-9
      -Vm  7.81  2.96  -0.46 # supcrt
# aqueous species
H2O = OH- + H+
      -analytic  293.29227  0.1360833  -10576.913  -123.73158  0  -
6.996455e-5
      -gamma      3.5   0.0
      -dw    5.27e-9
      -Vm  -9.66  28.5  80.0 -22.9 1.89 0 1.09 0 0 1 # supcrt modified
2 H2O = O2 + 4 H+ + 4 e-
      -log_k      -86.08
      -delta_h 134.79 kcal
      -dw    2.35e-9
      -Vm  5.7889  6.3536  3.2528  -3.0417  -0.3943 # supcrt
2 H+ + 2 e- = H2
      -log_k      -3.15
      -delta_h -1.759 kcal
      -dw    5.13e-9
      -Vm 6.52  0.78  0.12 # supcrt
CO3-2 + H+ = HCO3-
      -log_k      10.329
      -delta_h -3.561   kcal
      -analytic   107.8871    0.03252849  -5151.79    -38.92561
      563713.9
      -gamma      5.4   0.0
      -dw    1.18e-9
      -Vm  8.60  0  -12.0  0  1.643  0  0  167  0  1 # supcrt modified
CO3-2 + 2 H+ = CO2 + H2O
      -log_k      16.681
      -delta_h -5.738   kcal
      -analytic   464.1965    0.09344813  -26986.16   -165.75951
      2248628.9
      -dw    1.92e-9
      -Vm  20.85  -46.93  -79.0  27.9  -0.193 # supcrt modified
CO3-2 + 10 H+ + 8 e- = CH4 + 3 H2O
      -log_k      41.071
      -delta_h -61.039 kcal
      -dw    1.85e-9
```

```
      -Vm 7.7
SO4-2 + H+ = HSO4-
      -log_k      1.988
      -delta_h 3.85     kcal
      -analytic   -56.889     0.006473    2307.9      19.8858     0.0
      -dw    1.33e-9
      -Vm 8.2 9.2590  2.1108  -3.1618 1.1748  0 -0.3 15 0 1 # supcrt
modified
HS- = S-2 + H+
      -log_k      -12.918
      -delta_h 12.1     kcal
      -gamma      5.0   0.0
      -dw    0.731e-9
SO4-2 + 9 H+ + 8 e- = HS- + 4 H2O
      -log_k      33.65
      -delta_h -60.140 kcal
      -gamma      3.5   0.0
      -dw    1.73e-9
      -Vm  5.0119  4.9799  3.4765  -2.9849  1.4410 # supcrt
HS- + H+ = H2S
      -log_k      6.994
      -delta_h -5.30    kcal
      -analytical  -11.17  0.02386  3279.0
      -dw    2.1e-9
      -Vm  7.81  2.96  -0.46 # supcrt
H2Sg = HSg- + H+
      -log_k      -6.994
      -delta_h 5.30     kcal
      -analytical  11.17  -0.02386  -3279.0
      -dw    2.1e-9
      -Vm  5.0119  4.9799  3.4765  -2.9849  1.4410 # supcrt
NO3- + 2 H+ + 2 e- = NO2- + H2O
      -log_k      28.570
      -delta_h -43.760 kcal
      -gamma      3.0   0.0
      -dw    1.91e-9
      -Vm  5.5864  5.8590  3.4472  -3.0212  1.1847 # supcrt
2 NO3- + 12 H+ + 10 e- = N2 + 6 H2O
      -log_k      207.08
      -delta_h -312.130 kcal
      -dw    1.96e-9
      -Vm 7 # Pray et al., 1952, IEC 44. 1146

NO3- + 10 H+ + 8 e- = NH4+ + 3 H2O
      log_k 119.077
      delta_h -187.055  kcal
      -gamma      2.5   0.0
      -dw    1.98e-9
      -Vm  4.837  2.345  5.522  -2.88 1.096  3  -1.456  75.0  7.17e-3
1 # supcrt modified
#AmmH+ = AmmH+
```

```
#     -gamma      2.5   0.0
#     -dw    1.98e-9
#     -Vm  4.837  2.345  5.522  -2.88 1.096  3  -1.456  75.0  7.17e-3
1 # supcrt modified
NH4+ = NH3 + H+
      -log_k      -9.252
      -delta_h 12.48    kcal
      -analytic  0.6322  -0.001225  -2835.76
      -dw    2.28e-9
      -Vm  5.09  2.8  8.62  -2.88  -0.05 # supcrt
#AmmH+ = Amm + H+
#     -log_k      -9.252
#     -delta_h 12.48    kcal
#     -analytic  0.6322  -0.001225  -2835.76
#     -dw    2.28e-9
#     -Vm  5.09  2.8  8.62  -2.88  -0.05 # supcrt
NH4+ + SO4-2 = NH4SO4-
      log_k 1.11
#        -gamma  5.0     0.0
#AmmH+ + SO4-2 = AmmHSO4-
#     -log_k      1.11
H3BO3 = H2BO3- + H+
      -log_k      -9.24
      -delta_h 3.224    kcal
H3BO3 + F- = BF(OH)3-
      -log_k      -0.4
      -delta_h 1.850    kcal
H3BO3 + 2 F- + H+ = BF2(OH)2- + H2O
      -log_k      7.63
      -delta_h 1.618    kcal
H3BO3 + 2 H+ + 3 F- = BF3OH- + 2 H2O
      -log_k      13.67
      -delta_h -1.614   kcal
H3BO3 + 3 H+ + 4 F- = BF4- + 3 H2O
      -log_k      20.28
      -delta_h -1.846   kcal
PO4-3 + H+ = HPO4-2
      -log_k      12.346
      -delta_h -3.530   kcal
      -gamma      5.0   0.0
      -dw   0.69e-9
      -Vm  3.6315  1.0857  5.3233  -2.8239  3.3363 # supcrt
PO4-3 + 2 H+ = H2PO4-
      -log_k      19.553
      -delta_h -4.520   kcal
      -gamma      5.4   0.0
      -dw    0.846e-9
      -Vm  6.4875  8.0594  2.5823  -3.1122  1.3003 # supcrt
H+ + F- = HF
      -log_k      3.18
      -delta_h 3.18     kcal
```

```
      -analytic   -2.033      0.012645    429.01
      -Vm  3.4753  .7042  5.4732  -2.8081  -.0007 # supcrt
H+ + 2 F- = HF2-
      -log_k      3.76
      -delta_h 4.550    kcal
      -Vm  5.2263  4.9797  3.7928  -2.9849  1.2934 # supcrt
Ca+2 + H2O = CaOH+ + H+
      -log_k      -12.78
Ca+2 + CO3-2 = CaCO3
      -log_k      3.224
      -delta_h 3.545    kcal
      -analytic   -1228.732   -0.299440   35512.75    485.818
      -dw 4.46e-10      # complexes: calc'd with the Pikal formula
      -Vm  -.2430  -8.3748  9.0417  -2.4328  -.0300 # supcrt
Ca+2 + CO3-2 + H+ = CaHCO3+
      -log_k      11.435
      -delta_h -0.871   kcal
      -analytic   1317.0071   0.34546894  -39916.84   -517.70761
      563713.9
      -gamma      6.0   0.0
      -dw 5.06e-10
      -Vm  3.1911  .0104  5.7459  -2.7794  .3084 5.4 # supcrt
Ca+2 + SO4-2 = CaSO4
      -log_k      2.25
      -delta_h 1.325    kcal
      -dw 4.71e-10
      -Vm  2.7910  -.9666  6.1300  -2.7390  -.0010 # supcrt
Ca+2 + HSO4- = CaHSO4+
      -log_k        1.08
Ca+2 + PO4-3 = CaPO4-
      -log_k      6.459
      -delta_h 3.10     kcal
      -gamma  5.4  0.0
Ca+2 + HPO4-2 = CaHPO4
      -log_k      2.739
      -delta_h 3.3 kcal
Ca+2 + H2PO4- = CaH2PO4+
      -log_k      1.408
      -delta_h 3.4 kcal
      -gamma  5.4  0.0
#Ca+2 + F- = CaF+
#     -log_k      0.94
#     -delta_h 4.120    kcal
#     -Vm  .9846  -5.3773  7.8635  -2.5567  .6911 5.5 # supcrt
#     -gamma  5.5  0.0
Mg+2 + H2O = MgOH+ + H+
      -log_k      -11.44
      -delta_h 15.952 kcal
      -gamma      6.5   0.0
Mg+2 + CO3-2 = MgCO3
      -log_k      2.98
```

```
      -delta_h 2.713    kcal
      -analytic   0.9910      0.00667
      -dw 4.21e-10
      -Vm  -.5837  -9.2067  9.3687  -2.3984  -.0300 # supcrt
Mg+2 + H+ + CO3-2 = MgHCO3+
      -log_k      11.399
      -delta_h -2.771   kcal
      -analytic   48.6721     0.03252849  -2614.335   -18.00263
      563713.9
      -dw 4.78e-10
      -Vm  2.7171  -1.1469  6.2008  -2.7316  .5985 4 # supcrt
      -gamma      4.0   0.0
Mg+2 + SO4-2 = MgSO4
      -log_k      2.37
      -delta_h 4.550    kcal
      -dw 4.45e-10
      -Vm  2.4  -0.97  6.1  -2.74  # est'd
Mg+2 + PO4-3 = MgPO4-
      -log_k      6.589
      -delta_h 3.10     kcal
      -gamma      5.4   0.0
Mg+2 + HPO4-2 = MgHPO4
      -log_k      2.87
      -delta_h 3.3 kcal
Mg+2 + H2PO4- = MgH2PO4+
      -log_k      1.513
      -delta_h 3.4 kcal
      -gamma      5.4   0.0
Mg+2 + F- = MgF+
      -log_k      1.82
      -delta_h 3.20     kcal
      -Vm  .6494  -6.1958  8.1852  -2.5229  .9706 4.5 # supcrt
      -gamma      4.5   0.0
      Na+ + OH- = NaOH
      -log_k      -10 # remove this complex
Na+ + CO3-2 = NaCO3-
      -log_k      1.27
      -delta_h 8.91 kcal
      -dw 5.85e-10
      -Vm  3.99  0  15.3  -8.12  3.11  0  2.7  0  0.026  1
      #-gamma     5.4   0.0
Na+ + HCO3- = NaHCO3
      -log_k  -0.25
      -delta_h  -1 kcal
      -dw 6.73e-10
      -Vm  0.51
Na+ + SO4-2 = NaSO4-
      -log_k      0.7
      -delta_h 1.120    kcal
      -dw 6.18e-10
```

```
      -Vm  1e-5  19.3  1.07  -2.05  3.41  0  4.7  0  0  0.77 # not in
supcrt
      -gamma      5.4   0.0
Na+ + HPO4-2 = NaHPO4-
      -log_k      0.29
      -gamma      5.4   0.0
Na+ + F- = NaF
      -log_k      -0.24
      -Vm  2.7483  -1.0708  6.1709  -2.7347  -.030 # supcrt
K+ + SO4-2 = KSO4-
      -log_k      0.85
      -delta_h 2.250    kcal
      -analytical  3.106  0.0  -673.6
      -dw 7.46e-10
      -gamma      5.4   0.0
K+ + HPO4-2 = KHPO4-
      -log_k      0.29
      -gamma      5.4   0.0
Fe+2 + H2O = FeOH+ + H+
      -log_k      -9.5
      -delta_h 13.20    kcal
      -gamma      5.0   0.0
Fe+2 + 3H2O = Fe(OH)3- + 3H+
      -log_k -31.0
      -delta_h 30.3 kcal
      -gamma  5.0 0.0
Fe+2 + Cl- = FeCl+
      -log_k      0.14
Fe+2 + CO3-2 = FeCO3
      -log_k      4.38
Fe+2 + HCO3- = FeHCO3+
      -log_k      2.0
Fe+2 + SO4-2 = FeSO4
      -log_k      2.25
      -delta_h 3.230    kcal
Fe+2 + HSO4- = FeHSO4+
      -log_k      1.08
Fe+2 + 2HS- = Fe(HS)2
      -log_k      8.95
Fe+2 + 3HS- = Fe(HS)3-
      -log_k      10.987
Fe+2 + HPO4-2 = FeHPO4
      -log_k      3.6
Fe+2 + H2PO4- = FeH2PO4+
      -log_k      2.7
      -gamma      5.4   0.0
Fe+2 + F- = FeF+
      -log_k      1.0
Fe+2 = Fe+3 + e-
      -log_k      -13.02
      -delta_h 9.680    kcal
```

```
      -gamma      9.0   0.0
Fe+3 + H2O = FeOH+2 + H+
      -log_k      -2.19
      -delta_h 10.4     kcal
      -gamma      5.0   0.0
Fe+3 + 2 H2O = Fe(OH)2+ + 2 H+
      -log_k      -5.67
      -delta_h 17.1     kcal
      -gamma      5.4   0.0
Fe+3 + 3 H2O = Fe(OH)3 + 3 H+
      -log_k      -12.56
      -delta_h 24.8     kcal
Fe+3 + 4 H2O = Fe(OH)4- + 4 H+
      -log_k      -21.6
      -delta_h 31.9     kcal
      -gamma      5.4   0.0
Fe+2 + 2H2O = Fe(OH)2 + 2H+
      -log_k  -20.57
      -delta_h 28.565 kcal
2 Fe+3 + 2 H2O = Fe2(OH)2+4 + 2 H+
      -log_k      -2.95
      -delta_h 13.5     kcal
3 Fe+3 + 4 H2O = Fe3(OH)4+5 + 4 H+
      -log_k      -6.3
      -delta_h 14.3     kcal
Fe+3 + Cl- = FeCl+2
      -log_k      1.48
      -delta_h 5.6      kcal
      -gamma      5.0   0.0
Fe+3 + 2 Cl- = FeCl2+
      -log_k      2.13
      -gamma      5.0   0.0
Fe+3 + 3 Cl- = FeCl3
      -log_k      1.13
Fe+3 + SO4-2 = FeSO4+
      -log_k      4.04
      -delta_h 3.91     kcal
      -gamma      5.0   0.0
Fe+3 + HSO4- = FeHSO4+2
      -log_k      2.48
Fe+3 + 2 SO4-2 = Fe(SO4)2-
      -log_k      5.38
      -delta_h 4.60     kcal
Fe+3 + HPO4-2 = FeHPO4+
      -log_k      5.43
      -delta_h 5.76     kcal
      -gamma      5.0   0.0
Fe+3 + H2PO4- = FeH2PO4+2
      -log_k      5.43
      -gamma      5.4   0.0
Fe+3 + F- = FeF+2
```

```
      -log_k      6.2
      -delta_h 2.7      kcal
      -gamma      5.0   0.0
Fe+3 + 2 F- = FeF2+
      -log_k      10.8
      -delta_h 4.8      kcal
      -gamma      5.0   0.0
Fe+3 + 3 F- = FeF3
      -log_k      14.0
      -delta_h 5.4      kcal
Mn+2 + H2O = MnOH+ + H+
      -log_k      -10.59
      -delta_h 14.40    kcal
      -gamma      5.0   0.0
Mn+2 + 3H2O = Mn(OH)3- + 3H+
      -log_k  -34.8
      -gamma      5.0   0.0
Mn+2 + Cl- = MnCl+
      -log_k      0.61
      -Vm  2.7448  -1.0793  6.1743  -2.7344  .3686 # supcrt
      -gamma      5.0   0.0
Mn+2 + 2 Cl- = MnCl2
      -log_k      0.25
Mn+2 + 3 Cl- = MnCl3-
      -log_k      -0.31
      -gamma      5.0   0.0
Mn+2 + CO3-2 = MnCO3
      -log_k      4.9
Mn+2 + HCO3- = MnHCO3+
      -log_k      1.95
      -gamma      5.0   0.0
Mn+2 + SO4-2 = MnSO4
      -log_k      2.25
      -delta_h 3.370    kcal
      -Vm  2.4377  -1.8292  6.4690  -2.7034  -.0300 # supcrt
Mn+2 + 2 NO3- = Mn(NO3)2
      -log_k      0.6
      -delta_h -0.396   kcal
Mn+2 + F- = MnF+
      -log_k      0.84
      -gamma      5.0   0.0
Mn+2 = Mn+3 + e-
      -log_k      -25.51
      -delta_h 25.80    kcal
      -gamma      9.0   0.0
Al+3 + H2O = AlOH+2 + H+
      -log_k      -5.0
      -delta_h 11.49    kcal
      -analytic   -38.253     0.0   -656.27     14.327
      -Vm  -1.4649  -11.3582  10.2143  -2.3095  1.6668 5.4 # supcrt
      -gamma      5.4   0.0
```

```
Al+3 + 2 H2O = Al(OH)2+ + 2 H+
      -log_k      -10.1
      -delta_h 26.90    kcal
      -analytic   88.50 0.0   -9391.6     -27.121
      -gamma      5.4   0.0
Al+3 + 3 H2O = Al(OH)3 + 3 H+
      -log_k      -16.9
      -delta_h 39.89    kcal
      -analytic   226.374     0.0   -18247.8    -73.597
Al+3 + 4 H2O = Al(OH)4- + 4 H+
      -log_k      -22.7
      -delta_h 42.30    kcal
      -analytic   51.578      0.0   -11168.9    -14.865
      -gamma      4.5   0.0
Al+3 + SO4-2 = AlSO4+
      -log_k      3.5
      -delta_h 2.29 kcal
      -gamma      4.5   0.0
Al+3 + 2SO4-2 = Al(SO4)2-
      -log_k      5.0
      -delta_h 3.11 kcal
      -gamma      4.5   0.0
Al+3 + HSO4- = AlHSO4+2
      -log_k      0.46
Al+3 + F- = AlF+2
      -log_k      7.0
      -delta_h 1.060    kcal
      -gamma      5.4   0.0
Al+3 + 2 F- = AlF2+
      -log_k      12.7
      -delta_h 1.980    kcal
      -gamma      5.4   0.0
Al+3 + 3 F- = AlF3
      -log_k      16.8
      -delta_h 2.160    kcal
Al+3 + 4 F- = AlF4-
      -log_k      19.4
      -delta_h 2.20     kcal
      -gamma      4.5   0.0
# Al+3 + 5 F- = AlF5-2
      # log_k     20.6
      # delta_h 1.840   kcal
# Al+3 + 6 F- = AlF6-3
      # log_k     20.6
      # delta_h -1.670  kcal
H4SiO4 = H3SiO4- + H+
      -log_k      -9.83
      -delta_h 6.12     kcal
      -analytic   -302.3724   -0.050698   15669.69    108.18466   -
1119669.0
      -Vm  7.94  1.0881  5.3224  -2.8240  1.4767 # supcrt + H2O in a1
```

```
      -gamma      4     0.0
H4SiO4 = H2SiO4-2 + 2 H+
      -log_k      -23.0
      -delta_h 17.6     kcal
      -analytic   -294.0184   -0.072650   11204.49    108.18466   -
1119669.0
      -gamma      5.4   0.0
H4SiO4 + 4 H+ + 6 F- = SiF6-2 + 4 H2O
      -log_k      30.18
      -delta_h -16.260  kcal
      -Vm  8.5311  13.0492  .6211  -3.3185  2.7716 # supcrt
      -gamma      5.0   0.0
Ba+2 + H2O = BaOH+ + H+
      -log_k      -13.47
      -gamma      5.0   0.0
Ba+2 + CO3-2 = BaCO3
      -log_k      2.71
      -delta_h 3.55     kcal
      -analytic   0.113 0.008721
      -Vm  .2907  -7.0717  8.5295  -2.4867  -.0300 # supcrt
Ba+2 + HCO3- = BaHCO3+
      -log_k      0.982
      -delta_h 5.56 kcal
      -analytical -3.0938     0.013669    0.0   0.0   0.0
Ba+2 + SO4-2 = BaSO4
      -log_k      2.7
Sr+2 + H2O = SrOH+ + H+
      -log_k      -13.29
      -gamma      5.0   0.0
Sr+2 + CO3-2 + H+ = SrHCO3+
      -log_k      11.509
      -delta_h 2.489    kcal
      -analytic   104.6391    0.04739549  -5151.79    -38.92561
      563713.9
      -gamma      5.4   0.0
Sr+2 + CO3-2 = SrCO3
      -log_k      2.81
      -delta_h 5.22     kcal
      -analytic   -1.019      0.012826
      -Vm  -.1787  -8.2177  8.9799  -2.4393  -.0300 # supcrt
Sr+2 + SO4-2 = SrSO4
      -log_k      2.29
      -delta_h 2.08     kcal
      -Vm  6.7910  -.9666  6.1300  -2.7390  -.0010 # celestite
solubility
Li+ + SO4-2 = LiSO4-
      -log_k      0.64
      -gamma      5.0   0.0
Cu+2 + e- = Cu+
      -log_k      2.72
      -delta_h 1.65     kcal
```

```
      -gamma      2.5   0.0
Cu+ + 2Cl- = CuCl2-
      -log_k        5.50
      -delta_h -0.42 kcal
      -gamma  4.0  0.0
Cu+ + 3Cl- = CuCl3-2
      -log_k        5.70
      -delta_h 0.26 kcal
      -gamma  5.0  0.0
Cu+2 + CO3-2 = CuCO3
      -log_k        6.73
Cu+2 + 2CO3-2 = Cu(CO3)2-2
      -log_k        9.83
      Cu+2 + HCO3- = CuHCO3+
      -log_k        2.7
Cu+2 + Cl- = CuCl+
      -log_k        0.43
      -delta_h 8.65 kcal
      -gamma  4.0  0.0
Cu+2 + 2Cl- = CuCl2
      -log_k        0.16
      -delta_h 10.56 kcal
Cu+2 + 3Cl- = CuCl3-
      -log_k        -2.29
      -delta_h 13.69 kcal
      -gamma  4.0  0.0
Cu+2 + 4Cl- = CuCl4-2
      -log_k        -4.59
      -delta_h 17.78 kcal
      -gamma  5.0  0.0
Cu+2 + F- = CuF+
      -log_k        1.26
      -delta_h 1.62 kcal
Cu+2 + H2O = CuOH+ + H+
      -log_k      -8.0
      -gamma      4.0   0.0
Cu+2 + 2 H2O = Cu(OH)2 + 2 H+
      -log_k      -13.68
Cu+2 + 3 H2O = Cu(OH)3- + 3 H+
      -log_k      -26.9
Cu+2 + 4 H2O = Cu(OH)4-2 + 4 H+
      -log_k      -39.6
2Cu+2 + 2H2O = Cu2(OH)2+2 + 2H+
      -log_k  -10.359
      -delta_h 17.539 kcal
      -analytical  2.497  0.0  -3833.0  0.0  0.0
Cu+2 + SO4-2 = CuSO4
      -log_k      2.31
      -delta_h 1.220    kcal
Cu+2 + 3HS- = Cu(HS)3-
      -log_k  25.9
```

```
Zn+2 + H2O = ZnOH+ + H+
      -log_k      -8.96
      -delta_h 13.4 kcal
Zn+2 + 2 H2O = Zn(OH)2 + 2 H+
      -log_k      -16.9
Zn+2 + 3 H2O = Zn(OH)3- + 3 H+
      -log_k      -28.4
Zn+2 + 4 H2O = Zn(OH)4-2 + 4 H+
      -log_k      -41.2
Zn+2 + Cl- = ZnCl+
      -log_k      0.43
      -delta_h 7.79 kcal
      -Vm  1.5844  -3.9128  7.2879  -2.6172  .2025 4
      -gamma  4.0  0.0
Zn+2 + 2 Cl- = ZnCl2
      -log_k      0.45
      -delta_h 8.5 kcal
      -Vm  5.0570  4.5665  3.9552  -2.9678  -.0010
Zn+2 + 3Cl- = ZnCl3-
      -log_k      0.5
      -delta_h 9.56 kcal
      -Vm  9.5417  15.5168  -.3487  -3.4205  1.2513
      -gamma  4.0  0.0
Zn+2 + 4Cl- = ZnCl4-2
      -log_k      0.2
      -delta_h 10.96 kcal
      -Vm  14.6628  28.0213  -5.2636  -3.9374  2.6662
      -gamma  5.0  0.0
Zn+2 + H2O + Cl- = ZnOHCl + H+
      -log_k  -7.48
Zn+2 + 2HS- = Zn(HS)2
      -log_k  14.94
Zn+2 + 3HS- = Zn(HS)3-
      -log_k  16.1
Zn+2 + CO3-2 = ZnCO3
      -log_k      5.3
Zn+2 + 2CO3-2 = Zn(CO3)2-2
      -log_k      9.63
Zn+2 + HCO3- = ZnHCO3+
      -log_k      2.1
Zn+2 + SO4-2 = ZnSO4
      -log_k      2.37
      -delta_h 1.36 kcal
Zn+2 + 2SO4-2 = Zn(SO4)2-2
      -log_k      3.28
Zn+2 + Br- = ZnBr+
      -log_k  -0.58
Zn+2 + 2Br- = ZnBr2
      -log_k  -0.98
Zn+2 + F- = ZnF+
      -log_k  1.15
```

```
      -delta_h 2.22 kcal
Cd+2 + H2O = CdOH+ + H+
      -log_k      -10.08
      -delta_h 13.1 kcal
Cd+2 + 2 H2O = Cd(OH)2 + 2 H+
      -log_k      -20.35
Cd+2 + 3 H2O = Cd(OH)3- + 3 H+
      -log_k      -33.3
Cd+2 + 4 H2O = Cd(OH)4-2 + 4 H+
      -log_k      -47.35
2Cd+2 + H2O = Cd2OH+3 + H+
      -log_k  -9.39
      -delta_h 10.9 kcal
Cd+2 + H2O + Cl- = CdOHCl + H+
      -log_k  -7.404
      -delta_h 4.355 kcal
Cd+2 + NO3- = CdNO3+
      -log_k  0.4
      -delta_h -5.2 kcal
Cd+2 + Cl- = CdCl+
      -log_k      1.98
      -delta_h 0.59 kcal
Cd+2 + 2 Cl- = CdCl2
      -log_k      2.6
      -delta_h 1.24 kcal
Cd+2 + 3 Cl- = CdCl3-
      -log_k      2.4
      -delta_h 3.9 kcal
Cd+2 + CO3-2 = CdCO3
      -log_k      2.9
Cd+2 + 2CO3-2 = Cd(CO3)2-2
      -log_k      6.4
Cd+2 + HCO3- = CdHCO3+
      -log_k      1.5
Cd+2 + SO4-2 = CdSO4
      -log_k      2.46
      -delta_h 1.08 kcal
Cd+2 + 2SO4-2 = Cd(SO4)2-2
      -log_k      3.5
Cd+2 + Br- = CdBr+
      -log_k  2.17
      -delta_h -0.81 kcal
Cd+2 + 2Br- = CdBr2
      -log_k  2.9
Cd+2 + F- = CdF+
      -log_k  1.1
Cd+2 + 2F- = CdF2
      -log_k  1.5
Cd+2 + HS- = CdHS+
      -log_k  10.17
Cd+2 + 2HS- = Cd(HS)2
```

```
      -log_k  16.53
Cd+2 + 3HS- = Cd(HS)3-
      -log_k  18.71
Cd+2 + 4HS- = Cd(HS)4-2
      -log_k  20.9
Pb+2 + H2O = PbOH+ + H+
      -log_k      -7.71
Pb+2 + 2 H2O = Pb(OH)2 + 2 H+
      -log_k      -17.12
Pb+2 + 3 H2O = Pb(OH)3- + 3 H+
      -log_k      -28.06
Pb+2 + 4 H2O = Pb(OH)4-2 + 4 H+
      -log_k      -39.7
2 Pb+2 + H2O = Pb2OH+3 + H+
      -log_k      -6.36
Pb+2 + Cl- = PbCl+
      -log_k      1.6
      -delta_h 4.38 kcal
      -Vm  2.8934  -.7165  6.0316  -2.7494  .1281 6
Pb+2 + 2 Cl- = PbCl2
      -log_k      1.8
      -delta_h 1.08 kcal
      -Vm  6.5402  8.1879  2.5318  -3.1175  -.0300
Pb+2 + 3 Cl- = PbCl3-
      -log_k      1.7
      -delta_h 2.17 kcal
      -Vm  11.0396  19.1743  -1.7863  -3.5717  .7356
Pb+2 + 4 Cl- = PbCl4-2
      -log_k      1.38
      -delta_h 3.53 kcal
      -Vm  16.4150  32.2997  -6.9452  -4.1143  2.3118
Pb+2 + CO3-2 = PbCO3
      -log_k      7.24
Pb+2 + 2 CO3-2 = Pb(CO3)2-2
      -log_k      10.64
Pb+2 + HCO3- = PbHCO3+
      -log_k      2.9
Pb+2 + SO4-2 = PbSO4
      -log_k      2.75
Pb+2 + 2 SO4-2 = Pb(SO4)2-2
      -log_k      3.47
Pb+2 + 2HS- = Pb(HS)2
      -log_k  15.27
Pb+2 + 3HS- = Pb(HS)3-
      -log_k  16.57
3Pb+2 + 4H2O = Pb3(OH)4+2 + 4H+
      -log_k  -23.88
      -delta_h 26.5 kcal
Pb+2 + NO3- = PbNO3+
      -log_k      1.17
Pb+2 + Br- = PbBr+
```

```
      -log_k  1.77
      -delta_h 2.88 kcal
Pb+2 + 2Br- = PbBr2
      -log_k  1.44
Pb+2 + F- = PbF+
      -log_k  1.25
Pb+2 + 2F- = PbF2
      -log_k  2.56
Pb+2 + 3F- = PbF3-
      -log_k  3.42
Pb+2 + 4F- = PbF4-2
      -log_k  3.1

PHASES
Calcite
      CaCO3 = CO3-2 + Ca+2
      -log_k      -8.48
      -delta_h -2.297 kcal
      -analytic   -171.9065   -0.077993   2839.319    71.595
      -Vm 36.9 cm3/mol # MW (100.09 g/mol) / rho (2.71 g/cm3)
Aragonite
      CaCO3 = CO3-2 + Ca+2
      -log_k      -8.336
      -delta_h -2.589 kcal
      -analytic   -171.9773   -0.077993   2903.293    71.595
      -Vm 34.04
Dolomite
      CaMg(CO3)2 = Ca+2 + Mg+2 + 2 CO3-2
      -log_k      -17.09
      -delta_h  -9.436 kcal
      -Vm 64.5
Siderite
      FeCO3 = Fe+2 + CO3-2
      -log_k      -10.89
      -delta_h  -2.480 kcal
      -Vm 29.2
Rhodochrosite
      MnCO3 = Mn+2 + CO3-2
      -log_k      -11.13
      -delta_h  -1.430 kcal
      -Vm 31.1
Strontianite
      SrCO3 = Sr+2 + CO3-2
      -log_k      -9.271
      -delta_h -0.400 kcal
      -analytic   155.0305    0.0   -7239.594   -56.58638
      -Vm 39.69
Witherite
      BaCO3 = Ba+2 + CO3-2
      -log_k      -8.562
      -delta_h  0.703 kcal
```

```
      -analytic   607.642     0.121098    -20011.25   -236.4948
      -Vm 46
Gypsum
      CaSO4:2H2O = Ca+2 + SO4-2 + 2 H2O
      -log_k      -4.58
      -delta_h -0.109 kcal
      -analytic   68.2401     0.0   -3221.51    -25.0627
      -Vm 73.9 # 172.18 / 2.33  (Vm H2O = 13.9 cm3/mol)
Anhydrite
      CaSO4 = Ca+2 + SO4-2
      -log_k      -4.36
      -delta_h -1.710 kcal
      -analytic  84.90  0  -3135.12  -31.79 # 50 - 160oC, 1 - 1e3 atm,
anhydrite dissolution, Blount and Dickson, 1973, Am. Mineral. 58, 323.
      -Vm 46.1 # 136.14 / 2.95
Celestite
      SrSO4 = Sr+2 + SO4-2
      -log_k      -6.63
      -delta_h -4.037 kcal
#     -analytic   -14805.9622 -2.4660924  756968.533  5436.3588   -
40553604.0
      -analytic  -7.14 6.11e-3  75 0 0 -1.79e-5  # Howell et al., 1992,
JCED 37, 464.
      -Vm 46.4
Barite
      BaSO4 = Ba+2 + SO4-2
      -log_k      -9.97
      -delta_h  6.35 kcal
      -analytic   136.035     0.0   -7680.41    -48.595
      -Vm 51.9
Hydroxyapatite
      Ca5(PO4)3OH + 4 H+ = H2O + 3 HPO4-2 + 5 Ca+2
      -log_k       -3.421
      -delta_h -36.155 kcal
      -Vm 128.9
Fluorite
      CaF2 = Ca+2 + 2 F-
      -log_k      -10.6
      -delta_h   4.69 kcal
      -analytic   66.348      0.0   -4298.2     -25.271
      -Vm 15.7
SiO2(a)
      SiO2 + 2 H2O = H4SiO4
      -log_k      -2.71
      -delta_h  3.340 kcal
      -analytic   -0.26 0.0   -731.0
Chalcedony
      SiO2 + 2 H2O = H4SiO4
      -log_k      -3.55
      -delta_h  4.720 kcal
      -analytic   -0.09 0.0   -1032.0
```

```
      -Vm 23.1
Quartz
      SiO2 + 2 H2O = H4SiO4
      -log_k      -3.98
      -delta_h  5.990 kcal
      -analytic   0.41  0.0   -1309.0
      -Vm 22.67
Gibbsite
      Al(OH)3 + 3 H+ = Al+3 + 3 H2O
      -log_k        8.11
      -delta_h -22.800 kcal
Al(OH)3(a)
      Al(OH)3 + 3 H+ = Al+3 + 3 H2O
      -log_k       10.8
      -delta_h -26.500 kcal
Kaolinite
      Al2Si2O5(OH)4 + 6 H+ = H2O + 2 H4SiO4 + 2 Al+3
      -log_k        7.435
      -delta_h -35.300 kcal
Albite
      NaAlSi3O8 + 8 H2O = Na+ + Al(OH)4- + 3 H4SiO4
      -log_k      -18.002
      -delta_h 25.896 kcal
Anorthite
      CaAl2Si2O8 + 8 H2O = Ca+2 + 2 Al(OH)4- + 2 H4SiO4
      -log_k      -19.714
      -delta_h 11.580 kcal
K-feldspar
      KAlSi3O8 + 8 H2O = K+ + Al(OH)4- + 3 H4SiO4
      -log_k      -20.573
      -delta_h 30.820   kcal
K-mica
      KAl3Si3O10(OH)2 + 10 H+ = K+ + 3 Al+3 + 3 H4SiO4
      -log_k      12.703
      -delta_h -59.376 kcal
Chlorite(14A)
      Mg5Al2Si3O10(OH)8 + 16H+ = 5Mg+2 + 2Al+3 + 3H4SiO4 + 6H2O
      -log_k      68.38
      -delta_h -151.494 kcal
Ca-Montmorillonite
      Ca0.165Al2.33Si3.67O10(OH)2 + 12 H2O = 0.165Ca+2 + 2.33 Al(OH)4-
+ 3.67 H4SiO4 + 2 H+
      -log_k      -45.027
      -delta_h 58.373   kcal
Talc
      Mg3Si4O10(OH)2 + 4 H2O + 6 H+ = 3 Mg+2 + 4 H4SiO4
      -log_k      21.399
      -delta_h -46.352 kcal
Illite
      K0.6Mg0.25Al2.3Si3.5O10(OH)2 + 11.2H2O = 0.6K+ + 0.25Mg+2 +
2.3Al(OH)4- + 3.5H4SiO4 + 1.2H+
```

```
      -log_k      -40.267
      -delta_h 54.684 kcal
Chrysotile
      Mg3Si2O5(OH)4 + 6 H+ = H2O + 2 H4SiO4 + 3 Mg+2
      -log_k      32.2
      -delta_h -46.800 kcal
      -analytic   13.248      0.0   10217.1     -6.1894
Sepiolite
      Mg2Si3O7.5OH:3H2O + 4 H+ + 0.5H2O = 2 Mg+2 + 3 H4SiO4
      -log_k      15.760
      -delta_h -10.700 kcal
Sepiolite(d)
      Mg2Si3O7.5OH:3H2O + 4 H+ + 0.5H2O = 2 Mg+2 + 3 H4SiO4
      -log_k      18.66
Hematite
      Fe2O3 + 6 H+ = 2 Fe+3 + 3 H2O
      -log_k      -4.008
      -delta_h -30.845 kcal
Goethite
      FeOOH + 3 H+ = Fe+3 + 2 H2O
      -log_k      -1.0
      -delta_h     -14.48 kcal
Fe(OH)3(a)
      Fe(OH)3 + 3 H+ = Fe+3 + 3 H2O
      -log_k      4.891
Pyrite
      FeS2 + 2 H+ + 2 e- = Fe+2 + 2 HS-
      -log_k      -18.479
      -delta_h 11.300 kcal
FeS(ppt)
      FeS + H+ = Fe+2 + HS-
      -log_k      -3.915
Mackinawite
      FeS + H+ = Fe+2 + HS-
      -log_k      -4.648
Sulfur
      S + 2H+ + 2e- = H2S
      -log_k      4.882
      -delta_h -9.5 kcal
Vivianite
      Fe3(PO4)2:8H2O = 3 Fe+2 + 2 PO4-3 + 8 H2O
      -log_k      -36.0
Pyrolusite  # H2O added for surface calc's
      MnO2:H2O + 4 H+ + 2 e- = Mn+2 + 3 H2O
      -log_k      41.38
      -delta_h -65.110 kcal
Hausmannite
      Mn3O4 + 8 H+ + 2 e- = 3 Mn+2 + 4 H2O
      -log_k      61.03
      -delta_h -100.640 kcal
Manganite
```

```
      MnOOH + 3 H+ + e- = Mn+2 + 2 H2O
      -log_k      25.34
Pyrochroite
      Mn(OH)2 + 2 H+ = Mn+2 + 2 H2O
      -log_k      15.2
Halite
      NaCl  =  Cl- + Na+
      log_k   1.570
      -delta_h  1.37
      #-analytic -713.4616   -.1201241   37302.21    262.4583    -
2106915.
      -Vm 27.1
Sylvite
      KCl  = K+ + Cl-
      log_k    0.900
      -analytic     3.984     0.0    -919.55
      Vm 37.5
CO2(g)
      CO2 = CO2
      -log_k      -1.468
      -delta_h -4.776 kcal
      -analytic  109.534  1.9913e-2  -6986.04  -40.83  669370
      -T_c  304.2 # critical T, K
      -P_c   72.86 # critical P, atm
      -Omega 0.225 # acentric factor
H2O(g)
      H2O = H2O
      -log_k  1.506; delta_h -44.03 kJ
      -T_c  647.3
      -P_c  217.60
      -Omega 0.344
      -analytic   -16.5066 -2.0013E-3  2710.7  3.7646  0 2.24E-6

# Gases from LLNL...
O2(g)
      O2 = O2
      -log_k   -2.8983
      -analytic -7.5001 7.8981e-3 0.0 0.0 2.0027e5
      -T_c  154.6
      -P_c   49.80
      -Omega 0.021
H2(g)
      H2 = H2
      -log_k         -3.1050
      -delta_h -4.184  kJ
      -analytic   -9.3114    4.6473e-3   -49.335    1.4341    1.2815e5
      -T_c  33.2
      -P_c   12.80
      -Omega 0.225
N2(g)
      N2 = N2
```

```
      -log_k             -3.1864
      -analytic -58.453 1.818e-3  3199  17.909 -27460
      -T_c  126.2
      -P_c   33.50
      -Omega 0.039
H2S(g)
      H2S  =  H+ + HS-
      -log_k         -7.9759
      -analytic -97.354 -3.1576e-2 1.8285e3 37.44 28.56
      -T_c  373.2
      -P_c  88.20
      -Omega 0.1
CH4(g)
      CH4 = CH4
      -log_k         -2.8502
      -analytic -24.027 4.7146e-3 372.27 6.4264 2.3362e5
      -T_c  190.6
      -P_c   45.40
      -Omega 0.008
NH3(g)
      NH3 = NH3
      -log_k         1.7966
      -analytic -18.758 3.3670e-4 2.5113e3 4.8619 39.192
      -T_c  405.6
      -P_c   111.3
      -Omega 0.25
#Amm(g)
#     Amm = Amm
#     -log_k         1.7966
#     -analytic -18.758 3.3670e-4 2.5113e3 4.8619 39.192
#     -T_c  405.6
#     -P_c   111.3
#     -Omega 0.25

# redox-uncoupled gases
Oxg(g)
      Oxg = Oxg
      -analytic -7.5001 7.8981e-3 0.0 0.0 2.0027e5
      -T_c  154.6 ; -P_c   49.80 ; -Omega 0.021
Hdg(g)
      Hdg = Hdg
      -analytic   -9.3114    4.6473e-3   -49.335    1.4341    1.2815e5
      -T_c  33.2 ; -P_c   12.80 ; -Omega 0.225
Ntg(g)
      Ntg = Ntg
      -analytic -58.453 1.81800e-3  3199  17.909 -27460
      T_c  126.2 ; -P_c   33.50 ; -Omega 0.039
Mtg(g)
      Mtg = Mtg
      -analytic -24.027 4.7146e-3 3.7227e2 6.4264 2.3362e5
      -T_c  190.6 ; -P_c   45.40 ; -Omega 0.008
```

```
H2Sg(g)
      H2Sg  =  H+ + HSg-
      -analytic -97.354 -3.1576e-2 1.8285e3 37.44 28.56
      -T_c  373.2 ; -P_c  88.20 ; -Omega 0.1
Melanterite
      FeSO4:7H2O = 7 H2O + Fe+2 + SO4-2
      -log_k      -2.209
      -delta_h 4.910    kcal
      -analytic   1.447 -0.004153   0.0   0.0   -214949.0
Alunite
      KAl3(SO4)2(OH)6 + 6 H+ = K+ + 3 Al+3 + 2 SO4-2 + 6H2O
      -log_k      -1.4
      -delta_h -50.250 kcal
Jarosite-K
      KFe3(SO4)2(OH)6 + 6 H+ = 3 Fe+3 + 6 H2O + K+ + 2 SO4-2
      -log_k      -9.21
      -delta_h -31.280 kcal
Zn(OH)2(e)
      Zn(OH)2 + 2 H+ = Zn+2 + 2 H2O
      -log_k      11.5
Smithsonite
      ZnCO3 = Zn+2 + CO3-2
      -log_k      -10.0
      -delta_h -4.36    kcal
Sphalerite
      ZnS + H+ = Zn+2 + HS-
      -log_k      -11.618
      -delta_h 8.250    kcal
Willemite   289
      Zn2SiO4 + 4H+ = 2Zn+2 + H4SiO4
      -log_k      15.33
      -delta_h -33.37   kcal
Cd(OH)2
      Cd(OH)2 + 2 H+ = Cd+2 + 2 H2O
      -log_k      13.65
Otavite     315
      CdCO3 = Cd+2 + CO3-2
      -log_k      -12.1
      -delta_h -0.019   kcal
CdSiO3      328
      CdSiO3 + H2O + 2H+ = Cd+2 + H4SiO4
      -log_k      9.06
      -delta_h -16.63   kcal
CdSO4 329
      CdSO4 = Cd+2 + SO4-2
      -log_k      -0.1
      -delta_h -14.74   kcal
Cerrusite   365
      PbCO3 = Pb+2 + CO3-2
      -log_k      -13.13
      -delta_h 4.86     kcal
```

```
Anglesite   384
      PbSO4 = Pb+2 + SO4-2
      -log_k      -7.79
      -delta_h 2.15     kcal
Pb(OH)2     389
      Pb(OH)2 + 2H+ = Pb+2 + 2H2O
      -log_k      8.15
      -delta_h -13.99   kcal

EXCHANGE_MASTER_SPECIES
      X     X-
EXCHANGE_SPECIES
      X- = X-
      -log_k      0.0

      Na+ + X- = NaX
      -log_k      0.0
      -gamma      4.08 0.082

      K+ + X- = KX
      -log_k      0.7
      -gamma      3.5   0.015
      -delta_h  -4.3    # Jardine & Sparks, 1984

      Li+ + X- = LiX
      -log_k      -0.08
      -gamma      6.0   0.0
      -delta_h  1.4     # Merriam & Thomas, 1956

# !!!!!
#     H+ + X- = HX
#     -log_k      1.0
#     -gamma      9.0   0.0


      NH4+ + X- = NH4X
      log_k   0.6
      -gamma  2.5     0.0
      delta_h  -2.4   # Laudelout et al., 1968

#     AmmH+ + X- = AmmHX
#     -log_k      0.6
#     -gamma      2.5   0.0
#     -delta_h  -2.4    # Laudelout et al., 1968

      Ca+2 + 2X- = CaX2
      -log_k      0.8
      -gamma      5.0   0.165
      -delta_h  7.2    # Van Bladel & Gheyl, 1980

      Mg+2 + 2X- = MgX2
```

```
      -log_k      0.6
      -gamma      5.5   0.2
      -delta_h  7.4     # Laudelout et al., 1968

      Sr+2 + 2X- = SrX2
      -log_k      0.91
      -gamma      5.26  0.121
      -delta_h  5.5     # Laudelout et al., 1968

      Ba+2 + 2X- = BaX2
      -log_k      0.91
      -gamma      5.0   0.0
      -delta_h  4.5     # Laudelout et al., 1968

      Mn+2 + 2X- = MnX2
      -log_k      0.52
      -gamma      6.0   0.0

      Fe+2 + 2X- = FeX2
      -log_k      0.44
      -gamma      6.0   0.0

      Cu+2 + 2X- = CuX2
      -log_k      0.6
      -gamma      6.0   0.0

      Zn+2 + 2X- = ZnX2
      -log_k      0.8
      -gamma      5.0   0.0

      Cd+2 + 2X- = CdX2
      -log_k      0.8
      -gamma 0.0  0.0

      Pb+2 + 2X- = PbX2
      -log_k      1.05
      -gamma 0.0  0.0

      Al+3 + 3X- = AlX3
      -log_k      0.41
      -gamma      9.0   0.0

      AlOH+2 + 2X- = AlOHX2
      -log_k      0.89
      -gamma      0.0   0.0

SURFACE_MASTER_SPECIES
      Hfo_s Hfo_sOH
      Hfo_w Hfo_wOH
SURFACE_SPECIES
# All surface data from
```

```
# Dzombak and Morel, 1990
#
#
# Acid-base data from table 5.7
#
# strong binding site--Hfo_s,

      Hfo_sOH = Hfo_sOH
      -log_k      0.0

      Hfo_sOH     + H+ = Hfo_sOH2+
      -log_k      7.29  # = pKa1,int

      Hfo_sOH = Hfo_sO- + H+
      -log_k      -8.93 # = -pKa2,int

# weak binding site--Hfo_w

      Hfo_wOH = Hfo_wOH
      -log_k      0.0

      Hfo_wOH     + H+ = Hfo_wOH2+
      -log_k      7.29  # = pKa1,int

      Hfo_wOH = Hfo_wO- + H+
      -log_k      -8.93 # = -pKa2,int
###############################################
# CATIONS #
###############################################
#
# Cations from table 10.1 or 10.5
#
# Calcium
      Hfo_sOH + Ca+2 = Hfo_sOHCa+2
      -log_k      4.97

      Hfo_wOH + Ca+2 = Hfo_wOCa+ + H+
      -log_k -5.85
# Strontium
      Hfo_sOH + Sr+2 = Hfo_sOHSr+2
      -log_k      5.01

      Hfo_wOH + Sr+2 = Hfo_wOSr+ + H+
      -log_k -6.58

      Hfo_wOH + Sr+2 + H2O = Hfo_wOSrOH + 2H+
      -log_k -17.6
# Barium
      Hfo_sOH + Ba+2 = Hfo_sOHBa+2
      -log_k      5.46
```

```
      Hfo_wOH + Ba+2 = Hfo_wOBa+ + H+
      -log_k      -7.2  # table 10.5
#
# Cations from table 10.2
#
# Cadmium
      Hfo_sOH + Cd+2 = Hfo_sOCd+ + H+
      -log_k      0.47

      Hfo_wOH + Cd+2 = Hfo_wOCd+ + H+
      -log_k      -2.91
# Zinc
      Hfo_sOH + Zn+2 = Hfo_sOZn+ + H+
      -log_k      0.99

      Hfo_wOH + Zn+2 = Hfo_wOZn+ + H+
      -log_k      -1.99
# Copper
      Hfo_sOH + Cu+2 = Hfo_sOCu+ + H+
      -log_k      2.89

      Hfo_wOH + Cu+2 = Hfo_wOCu+ + H+
      -log_k      0.6   # table 10.5
# Lead
      Hfo_sOH + Pb+2 = Hfo_sOPb+ + H+
      -log_k      4.65

      Hfo_wOH + Pb+2 = Hfo_wOPb+ + H+
      -log_k      0.3   # table 10.5
#
# Derived constants table 10.5
#
# Magnesium
      Hfo_wOH + Mg+2 = Hfo_wOMg+ + H+
      -log_k -4.6
# Manganese
      Hfo_sOH + Mn+2 = Hfo_sOMn+ + H+
      -log_k      -0.4  # table 10.5

      Hfo_wOH + Mn+2 = Hfo_wOMn+ + H+
      -log_k -3.5 # table 10.5
# Iron, strong site: Appelo, Van der Weiden, Tournassat & Charlet, EST
36, 3096
      Hfo_sOH + Fe+2 = Hfo_sOFe+ + H+
      -log_k      -0.95
# Iron, weak site: Liger et al., GCA 63, 2939, re-optimized for D&M
      Hfo_wOH + Fe+2 = Hfo_wOFe+ + H+
      -log_k -2.98

      Hfo_wOH + Fe+2 + H2O = Hfo_wOFeOH + 2H+
      -log_k -11.55
```

```
###############################################
# ANIONS #
###############################################
#
# Anions from table 10.6
#
# Phosphate
      Hfo_wOH + PO4-3 + 3H+ = Hfo_wH2PO4 + H2O
      -log_k      31.29

      Hfo_wOH + PO4-3 + 2H+ = Hfo_wHPO4- + H2O
      -log_k      25.39

      Hfo_wOH + PO4-3 + H+ = Hfo_wPO4-2 + H2O
      -log_k      17.72
#
# Anions from table 10.7
#
# Borate
      Hfo_wOH + H3BO3 = Hfo_wH2BO3 + H2O
      -log_k      0.62
#
# Anions from table 10.8
#
# Sulfate
      Hfo_wOH + SO4-2 + H+ = Hfo_wSO4- + H2O
      -log_k      7.78

      Hfo_wOH + SO4-2 = Hfo_wOHSO4-2
      -log_k      0.79
#
# Derived constants table 10.10
#
      Hfo_wOH + F- + H+ = Hfo_wF + H2O
      -log_k      8.7

      Hfo_wOH + F- = Hfo_wOHF-
      -log_k      1.6
#
# Carbonate: Van Geen et al., 1994 reoptimized for D&M model
#
      Hfo_wOH + CO3-2 + H+ = Hfo_wCO3- + H2O
      -log_k      12.56

      Hfo_wOH + CO3-2 + 2H+= Hfo_wHCO3 + H2O
      -log_k      20.62

RATES
#######
# Example of quartz kinetic rates block:
#KINETICS
```

```
#Quartz
#-m0  158.8     # 90 % Qu
#-parms 23.13  1.5
#-step 3.1536e8 in 10
#-tol 1e-12

# Rate definition:
 Quartz
  -start
 #1 rem Specific rate k from Rimstidt and Barnes, 1980, GCA 44,1683
 #2 rem  k = 10^-13.7 mol/m2/s (25 C), Ea = 90 kJ/mol
 #2 rem  sp. rate * parm(2) due to salts (Dove and Rimstidt, MSA Rev.
29, 259)
 #4 rem  parm(1) = A (m2) recalc's to mol/s
 #5 rem  parm(2) salt correction: (1 + 1.5 * c_Na (mM)), < 35

 10 dif_temp = 1/TK - 1/298
  20 pk_w = 13.7 + 4700.4 * dif_temp
  40 moles = parm(1) * parm(2) * (m/m0)^0.67 * 10^-pk_w * (1 -
SR("Quartz"))
#                  Integrate...
  50 save moles * time
  -end

############
#K-feldspar
############
# Example of KINETICS data block for K-feldspar rate:
#     KINETICS 1
#     K-feldspar
#           -m0 2.16  # 10% K-fsp, 0.1 mm cubes
#           -m  1.94
#           -parms 1.36e4  0.1

K-feldspar
      -start
#1 rem specific rate from Sverdrup, 1990, in kmol/m2/s
#2 rem parm(1) = 10 * (A/V, 1/dm) (recalc's sp. rate to mol/kgw)
#3 rem parm(2) = corrects for field rate relative to lab rate
#4 rem temp corr: from p. 162. E (kJ/mol) / R / 2.303 = H in H*(1/T-
1/298)

10    dif_temp = 1/TK - 1/298
20    pk_H = 12.5 + 3134 * dif_temp
30    pk_w = 15.3 + 1838 * dif_temp
40    pk_OH = 14.2 + 3134 * dif_temp
50    pk_CO2 = 14.6 + 1677 * dif_temp
#60   pk_org = 13.9 + 1254 * dif_temp  # rate increase with DOC
70    rate = 10^-pk_H * ACT("H+")^0.5 + 10^-pk_w + 10^-pk_OH * ACT("OH-
")^0.3
71    rate = rate + 10^-pk_CO2 * (10^SI("CO2(g)"))^0.6
```

```
#72   rate = rate + 10^-pk_org * TOT("DOC")^0.4
80    moles = parm(1) * parm(2) * rate * (1 - SR("K-feldspar")) * time
81 rem decrease rate on precipitation
90    if SR("K-feldspar") > 1 then moles = moles * 0.1
100   save moles
      -end

###########
#Albite
###########
# Example of KINETICS data block for Albite rate:
#     KINETICS 1
#     Albite
#           -m0 0.43  # 2% Albite, 0.1 mm cubes
#           -parms 2.72e3  0.1

Albite
      -start
#1 rem specific rate from Sverdrup, 1990, in kmol/m2/s
#2 rem parm(1) = 10 * (A/V, 1/dm) (recalc's sp. rate to mol/kgw)
#3 rem parm(2) = corrects for field rate relative to lab rate
#4 rem temp corr: from p. 162. E (kJ/mol) / R / 2.303 = H in H*(1/T-
1/298)

10    dif_temp = 1/TK - 1/298
20    pk_H = 12.5 + 3359 * dif_temp
30    pk_w = 14.8 + 2648 * dif_temp
40    pk_OH = 13.7 + 3359 * dif_temp
#41 rem      ^12.9 in Sverdrup, but larger than for oligoclase...
50    pk_CO2 = 14.0 + 1677 * dif_temp
#60   pk_org = 12.5 + 1254 * dif_temp # ...rate increase for DOC
70    rate = 10^-pk_H * ACT("H+")^0.5 + 10^-pk_w + 10^-pk_OH * ACT("OH-
")^0.3
71    rate = rate + 10^-pk_CO2 * (10^SI("CO2(g)"))^0.6
#72   rate = rate + 10^-pk_org * TOT("DOC")^0.4
80    moles = parm(1) * parm(2) * rate * (1 - SR("Albite")) * time
81 rem decrease rate on precipitation
90    if SR("Albite") > 1 then moles = moles * 0.1
100   save moles
      -end

########
#Calcite
########
# Example of KINETICS data block for calcite rate:
#     KINETICS 1
#     Calcite
#           -tol    1e-8
#           -m0    3.e-3
#           -m    3.e-3
#           -parms      50      0.6
```

```
Calcite
  -start
   1 rem    parm(1) = A/V, 1/dm     parm(2) = exponent for m/m0

   10 si_cc = si("Calcite")
   20 if (m <= 0  and si_cc < 0) then goto 200
   30  k1 = 10^(0.198 - 444.0 / (273.16 + tc) )
   40  k2 = 10^(2.84 - 2177.0 / (273.16 + tc) )
   50  if tc <= 25 then k3 = 10^(-5.86 - 317.0 / (273.16 + tc) )
   60  if tc > 25 then k3 = 10^(-1.1 - 1737.0 / (273.16 + tc) )
   70   t = 1
   80   if m0 > 0 then t = m/m0
   90   if t = 0 then t = 1
   100   moles = parm(1) * 0.1 * (t)^parm(2)
   110   moles = moles * (k1 * act("H+") + k2 * act("CO2") + k3 *
act("H2O"))
   120   moles = moles * (1 - 10^(2/3*si_cc))
   130   moles = moles * time
   140  if (moles > m) then moles = m
   150 if (moles >= 0) then goto 200
   160  temp = tot("Ca")
   170  mc  = tot("C(4)")
   180  if mc < temp then temp = mc
   190  if -moles > temp then moles = -temp
   200 save moles
  -end

#######
#Pyrite
#######
# Example of KINETICS data block for pyrite rate:
#     KINETICS 1
#     Pyrite
#           -tol    1e-8
#           -m0    5.e-4
#           -m    5.e-4
#           -parms -5.0  0.1   .5    -0.11
Pyrite
  -start
   1 rem    parm(1) = log10(A/V, 1/dm)    parm(2) = exp for (m/m0)
   2 rem    parm(3) = exp for O2          parm(4) = exp for H+

   10 if (m <= 0) then goto 200
   20 if (si("Pyrite") >= 0) then goto 200
   30  rate = -10.19 + parm(1) + parm(3)*lm("O2") + parm(4)*lm("H+") +
parm(2)*log10(m/m0)
   40  moles = 10^rate * time
   50 if (moles > m) then moles = m
   60 if (moles >= (mol("O2")/3.5)) then moles = mol("O2")/3.5
   200 save moles
  -end
```

```
##########
#Organic_C
##########
# Example of KINETICS data block for Organic_C rate:
#     KINETICS 1
#     Organic_C
#           -tol  1e-8
#           # m in mol/kgw
#           -m0   5e-3
#           -m    5e-3
Organic_C
  -start
   10 if (m <= 0) then goto 200
   20  mO2 = mol("O2")
   30  mNO3 = tot("N(5)")
   40  mSO4 = tot("S(6)")
   50   rate = 1.57e-9*mO2/(2.94e-4 + mO2) + 1.67e-11*mNO3/(1.55e-4 +
mNO3)
   60   rate = rate + 1.e-13*mSO4/(1.e-4 + mSO4)
   70  moles = rate * m * (m/m0) * time
   80 if (moles > m) then moles = m
   200 save moles
  -end

###########
#Pyrolusite
###########
#
# Postma, and Appelo., GCA 64, 1237

#
# Example of KINETICS data block for Pyrolusite
#       KINETICS 1-12
#       Pyrolusite
#            -tol    1.e-7
#            -m0     0.1
#            -m      0.1
Pyrolusite
  -start
   5  if (m <= 0.0) then goto 200
   7  sr_pl = sr("Pyrolusite")
   9  if abs(1 - sr_pl) < 0.1 then goto 200
   10 if (sr_pl > 1.0) then goto 100
   #20 rem  initially 1 mol Fe+2 = 0.5 mol pyrolusite. k*A/V = 1/time
(3 cells)
   #22 rem       time (3 cells) = 1.432e4.  1/time = 6.98e-5
   30 Fe_t = tot("Fe(2)")
   32 if Fe_t < 1.e-8 then goto 200
   40 moles =  6.98e-5 * Fe_t  * (m/m0)^0.67 * time * (1 - sr_pl)
   50 if moles > Fe_t / 2 then moles = Fe_t / 2
```

```
   70 if moles > m then moles = m
   90 goto 200
   100      Mn_t = tot("Mn")
   110      moles = 2e-3 * 6.98e-5 * (1-sr_pl) * time
   120      if moles <= -Mn_t then moles = -Mn_t
   200      save moles
  -end
END

# For the reaction aA + bB = cC + dD,
#   with delta_v = c*Vm(C) + d*Vm(D) - a*Vm(A) - b*Vm(B),
# PHREEQC adds the pressure term to log_k: -= delta_v * (P - 1) /
(2.3RT).
#   Vm(A) is volume of A, cm3/mol, P is pressure, atm, R is the gas
constant, T is Kelvin.
# Gas-pressures and fugacity coefficients are calculated with Peng-
Robinson's EOS.
#   Binary interaction coefficients from Soreide and Whitson, 1992, FPE
77, 217 are
#    hard-coded in calc_PR():
#    kij    CH4    CO2    H2S    N2
#    H2O    0.49   0.19   0.19   0.49
#
================================================================================
======================
# The molar volumes of solids are entered with
#                          -Vm vm cm3/mol
#    vm is the molar volume, cm3/mol (default), but dm3/mol and m3/mol
are permitted.
# Data for minerals' vm (= MW (g/mol) / rho (g/cm3)) are defined using
rho from
#   Deer, Howie and Zussman, The rock-forming minerals, Longman.
#                             --------------------
# Temperature- and pressure-dependent volumina of aqueous species are
calculated with a Redlich-
#   type equation (cf. Redlich and Meyer, Chem. Rev. 64, 221), from
parameters entered with
#                         -Vm a1 a2 a3 a4 W a0 i1 i2 i3 i4
# The volume (cm3/mol) is
#    Vm(T, pb, I) = 41.84 * (a1 * 0.1 + a2 * 100 / (2600 + pb)  + a3 /
(T - 228) +
#                            a4 * 1e4 / (2600 + pb) / (T - 228) - W *
QBrn)
#                  + z^2 / 2 * Av * f(I^0.5)
#                  + (i1 + i2 / (T - 228) + i3 * (T - 228)) * I^i4
#   Volumina at I = 0 are obtained using supcrt92 formulas (Johnson et
al., 1992, CG 18, 899).
#   41.84 transforms cal/bar/mol into cm3/mol.
#   pb is pressure in bar.
#   W * QBrn is the energy of solvation, calculated from W and the
pressure dependence of the
```

```
#     Born equation (i.e. of the dielectric constant of water (f(P, T),
see below).
#   z is charge of the solute species.
#   Av is the Debye-Hueckel limiting slope.
#   a0 is the ion-size parameter in the extended Debye-Hueckel
equation:
#     f(I^0.5) = I^0.5) / (1 + a0 * DH_B * I^0.5),
#     a0 = -gamma x for cations, = 0 for anions.
# Av (P, T) is calculated using the dielectric constant of water from
Bradley and Pitzer, 1979, JPC 83, 1599,
#   and the compressibility of pure water.
# The density of pure water at water saturation pressure is calculated
with eqn 2.6 from
#   Wagner and Pruss, 2002, J. Phys. Chem. Ref. Data 31, 387. At higher
P,T with polynomials
#   interpolated from IAPWS table 3 (2007).
#
# Data for species' parameters, commented with '# supcrt modified',
were fitted from data
#   compiled by Laliberte, 2009, J. Chem. Eng. Data 54, 1725, +
additions, see Appelo, Parkhurst and Post (in prep.)
# H+ has the reference volume of 0 at all P, T and I.
# For Cl-, parameters were obtained from densities of HCl solutions up
to 176 oC, 1 - 280 atm.
# The numbers for cations were extracted from the densities of cation-
Cl-solutions.
# Other anions and OH- then follow from the measured densities of
cation-anion solutions.
# Water dissociation was fitted from Bandura and Lvov, 2006, J. Phys.
Chem. Ref. Data, 35, 15, 0-200 oC, 1-2000 atm.
#                              --------------------
# If -Vm is not defined, the a-f values from -Millero a b c d e f (if
available) will be used for calculating
#   Vm(t, I) = a + b * t + c * t^2 + z^2 / 2 * Av * I^0.5 + (d + e * t
+ f * t^2) * I
#   t is temperature in oC.
#
# redox-uncoupled gases have been added for H2 (Hdg), O2 (Oxg), CH4
(Mtg), N2 (Ntg),
#   H2S (H2Sg, species HSg-, etc.).
#
#
================================================================================
=====================
# It remains the responsibility of the user to check the calculated
results, for example with
#   measured solubilities as a function of (P, T).
```

E.2 ACCUMULATED GRIDBLOCKS DATA IN THE COMPUTER MEMORY

Below presents the geochemistry data stored in the computer memory of only the first gridblock.

```
SOLUTION_RAW                1 Solution after simulation 7.
  -temp                     25
  -pressure                 1
  -total_h                  111.012433603
  -total_o                  55.510351939604
  -cb                       -3.417099389371e-16
  -density                  0.9971127227024
  -totals
    K                       0.00020000000000015
    N(0)                    1.7476550759565e-19
    N(3)                    2.4854400960601e-16
    N(5)                    0.0012000000000009
    Na                      0.0010000000000007
    O(0)                    0.00053513810546585
  -pH                       6.9968880929022
  -pe                       13.630010728329
  -mu                       0.001200104501848
  -ah2o                     0.99995464776062
  -mass_water               1
  -soln_vol                 1.0030097496249
  -total_alkalinity         -7.3060382879865e-12
  -activities
    E                       -13.630010728329
    H(0)                    -29.99987998955
    K                       -3.7159437816406
    N(-3)                   -30.017179792123
    N(0)                    -29.99987998955
    N(3)                    -30.01708526827
    N(5)                    -2.9379040222219
    Na                      -3.0167861963007
    O(0)                    -29.99987998955
  -gammas
EXCHANGE_RAW                1 Exchange assemblage after simulation 7.
  # EXCHANGE_MODIFY candidate identifiers #
  -exchange_gammas          1
  -component                X
    # EXCHANGE_MODIFY candidate identifiers #
    -totals
      H                     1.228218068467e-62
      K                     0.00055065220435679
```

```
      N                      3.0705451711675e-63
      Na                     0.00054934779600379
      X                      0.0011000000003606
    -charge_balance          0
    -la                      2.698454701226
    -phase_proportion        0
    -formula_z               0
  # EXCHANGE_MODIFY candidates with new_def=true #
  -new_def                   0
  -solution_equilibria       0
  -n_solution                -999
  # Exchange workspace variables #
  -totals
```

E.3 HOW UTCOMP MODIFIES GRIDBLOCKS GEOCHEMISTRY DATA

OutputAccumulatedLines (see Table A.1 provided in Charlton and Parkhurst, 2011) of IPhreeqc is used to show the data stored in the memory.

```
SOLUTION_MODIFY  1
-total_h  111.0143854887
-total_o  55.5111480283
-cb  0.0000000000
-totals;
Ca    2.998719125473029E-005
Cl    5.997438250943572E-005
K    1.900077860989028E-004
N    1.140046716593692E-003
Na    9.500389304944622E-004
END
SOLUTION_MODIFY  2
-total_h  111.0124336766
-total_o  55.5103519764
-cb  0.0000000000
-totals;
Ca    0.000000000000000E+000
Cl    0.000000000000000E+000
K    2.000000001328174E-004
N    1.200000000797194E-003
Na    1.000000000664033E-003
END
SOLUTION_MODIFY  3
-total_h  111.0124336728
-total_o  55.5103519745
-cb  0.0000000000
-totals;
```

```
Ca    0.000000000000000E+000
Cl    0.000000000000000E+000
K    2.000000001258349E-004
N    1.200000000755299E-003
Na    1.000000000629120E-003
END
SOLUTION_MODIFY  4
-total_h  111.0124336728
-total_o  55.5103519745
-cb  0.0000000000
-totals;
Ca    0.000000000000000E+000
Cl    0.000000000000000E+000
K    2.000000001258349E-004
N    1.200000000755299E-003
Na    1.000000000629120E-003
END
SOLUTION_MODIFY  5
-total_h  111.0124336689
-total_o  55.5103519726
-cb  0.0000000000
-totals;
Ca    0.000000000000000E+000
Cl    0.000000000000000E+000
K    2.000000001188524E-004
N    1.200000000713404E-003
Na    1.000000000594207E-003
END
SOLUTION_MODIFY  6
-total_h  111.0124336728
-total_o  55.5103519745
-cb  0.0000000000
-totals;
Ca    0.000000000000000E+000
Cl    0.000000000000000E+000
K    2.000000001258349E-004
N    1.200000000755299E-003
Na    1.000000000629120E-003
END
SOLUTION_MODIFY  7
-total_h  111.0124336611
-total_o  55.5103519687
-cb  0.0000000000
-totals;
Ca    0.000000000000000E+000
Cl    0.000000000000000E+000
K    2.000000001048873E-004
N    1.200000000629614E-003
Na    1.000000000524382E-003
END
SOLUTION_MODIFY  8
```

```
-total_h  111.0124336689
-total_o  55.5103519726
-cb  0.0000000000
-totals;
Ca    0.000000000000000E+000
Cl    0.000000000000000E+000
K    2.000000001188524E-004
N    1.200000000713404E-003
Na    1.000000000594207E-003
END
SOLUTION_MODIFY  9
-total_h  111.0124336611
-total_o  55.5103519687
-cb  0.0000000000
-totals;
Ca    0.000000000000000E+000
Cl    0.000000000000000E+000
K    2.000000001048873E-004
N    1.200000000629614E-003
Na    1.000000000524382E-003
END
SOLUTION_MODIFY  10
-total_h  111.0124336611
-total_o  55.5103519687
-cb  0.0000000000
-totals;
Ca    0.000000000000000E+000
Cl    0.000000000000000E+000
K    2.000000001048873E-004
N    1.200000000629614E-003
Na    1.000000000524382E-003
END
SOLUTION_MODIFY  11
-total_h  111.0124336611
-total_o  55.5103519687
-cb  0.0000000000
-totals;
Ca    0.000000000000000E+000
Cl    0.000000000000000E+000
K    2.000000001048873E-004
N    1.200000000629614E-003
Na    1.000000000524382E-003
END
SOLUTION_MODIFY  12
-total_h  111.0124336573
-total_o  55.5103519667
-cb  0.0000000000
-totals;
Ca    0.000000000000000E+000
Cl    0.000000000000000E+000
K    2.000000000979048E-004
```

```
N    1.200000000587719E-003
Na    1.000000000489469E-003
END
SOLUTION_MODIFY  13
-total_h  111.0124336573
-total_o  55.5103519667
-cb  0.0000000000
-totals;
Ca    0.000000000000000E+000
Cl    0.000000000000000E+000
K    2.000000000979048E-004
N    1.200000000587719E-003
Na    1.000000000489469E-003
END
SOLUTION_MODIFY  14
-total_h  111.0124336495
-total_o  55.5103519629
-cb  0.0000000000
-totals;
Ca    0.000000000000000E+000
Cl    0.000000000000000E+000
K    2.000000000839397E-004
N    1.200000000503928E-003
Na    1.000000000419644E-003
END
SOLUTION_MODIFY  15
-total_h  111.0124336534
-total_o  55.5103519648
-cb  0.0000000000
-totals;
Ca    0.000000000000000E+000
Cl    0.000000000000000E+000
K    2.000000000909222E-004
N    1.200000000545823E-003
Na    1.000000000454557E-003
END
SOLUTION_MODIFY  16
-total_h  111.0124336534
-total_o  55.5103519648
-cb  0.0000000000
-totals;
Ca    0.000000000000000E+000
Cl    0.000000000000000E+000
K    2.000000000909222E-004
N    1.200000000545823E-003
Na    1.000000000454557E-003
END
SOLUTION_MODIFY  17
-total_h  111.0124336456
-total_o  55.5103519609
-cb  0.0000000000
```

```
-totals;
Ca    0.000000000000000E+000
Cl    0.000000000000000E+000
K    2.000000000769572E-004
N    1.200000000462033E-003
Na    1.000000000384731E-003
END
SOLUTION_MODIFY  18
-total_h  111.0124336456
-total_o  55.5103519609
-cb  0.0000000000
-totals;
Ca    0.000000000000000E+000
Cl    0.000000000000000E+000
K    2.000000000769572E-004
N    1.200000000462033E-003
Na    1.000000000384731E-003
END
SOLUTION_MODIFY  19
-total_h  111.0124336495
-total_o  55.5103519629
-cb  0.0000000000
-totals;
Ca    0.000000000000000E+000
Cl    0.000000000000000E+000
K    2.000000000839397E-004
N    1.200000000503928E-003
Na    1.000000000419644E-003
END
SOLUTION_MODIFY  20
-total_h  111.0124336379
-total_o  55.5103519570
-cb  0.0000000000
-totals;
Ca    0.000000000000000E+000
Cl    0.000000000000000E+000
K    2.000000000629921E-004
N    1.200000000378242E-003
Na    1.000000000314906E-003
END
SOLUTION_MODIFY  21
-total_h  111.0124336418
-total_o  55.5103519590
-cb  0.0000000000
-totals;
Ca    0.000000000000000E+000
Cl    0.000000000000000E+000
K    2.000000000699747E-004
N    1.200000000420138E-003
Na    1.000000000349819E-003
END
```

```
SOLUTION_MODIFY  22
-total_h  111.0124336418
-total_o  55.5103519590
-cb  0.0000000000
-totals;
Ca    0.000000000000000E+000
Cl    0.000000000000000E+000
K    2.000000000699747E-004
N    1.200000000420138E-003
Na    1.000000000349819E-003
END
SOLUTION_MODIFY  23
-total_h  111.0124336379
-total_o  55.5103519570
-cb  0.0000000000
-totals;
Ca    0.000000000000000E+000
Cl    0.000000000000000E+000
K    2.000000000629921E-004
N    1.200000000378242E-003
Na    1.000000000314906E-003
END
SOLUTION_MODIFY  24
-total_h  111.0124336340
-total_o  55.5103519551
-cb  0.0000000000
-totals;
Ca    0.000000000000000E+000
Cl    0.000000000000000E+000
K    2.000000000560096E-004
N    1.200000000336347E-003
Na    1.000000000279993E-003
END
SOLUTION_MODIFY  25
-total_h  111.0124336340
-total_o  55.5103519551
-cb  0.0000000000
-totals;
Ca    0.000000000000000E+000
Cl    0.000000000000000E+000
K    2.000000000560096E-004
N    1.200000000336347E-003
Na    1.000000000279993E-003
END
SOLUTION_MODIFY  26
-total_h  111.0124336301
-total_o  55.5103519532
-cb  0.0000000000
-totals;
Ca    0.000000000000000E+000
Cl    0.000000000000000E+000
```

```
K    2.000000000490270E-004
N    1.200000000294452E-003
Na    1.000000000245081E-003
END
SOLUTION_MODIFY  27
-total_h  111.0124336340
-total_o  55.5103519551
-cb  0.0000000000
-totals;
Ca    0.000000000000000E+000
Cl    0.000000000000000E+000
K    2.000000000560096E-004
N    1.200000000336347E-003
Na    1.000000000279993E-003
END
SOLUTION_MODIFY  28
-total_h  111.0124336263
-total_o  55.5103519512
-cb  0.0000000000
-totals;
Ca    0.000000000000000E+000
Cl    0.000000000000000E+000
K    2.000000000420445E-004
N    1.200000000252557E-003
Na    1.000000000210168E-003
END
SOLUTION_MODIFY  29
-total_h  111.0124336263
-total_o  55.5103519512
-cb  0.0000000000
-totals;
Ca    0.000000000000000E+000
Cl    0.000000000000000E+000
K    2.000000000420445E-004
N    1.200000000252557E-003
Na    1.000000000210168E-003
END
SOLUTION_MODIFY  30
-total_h  111.0124336224
-total_o  55.5103519493
-cb  0.0000000000
-totals;
Ca    0.000000000000000E+000
Cl    0.000000000000000E+000
K    2.000000000350620E-004
N    1.200000000210662E-003
Na    1.000000000175255E-003
END
SOLUTION_MODIFY  31
-total_h  111.0124336263
-total_o  55.5103519512
```

```
-cb  0.0000000000
-totals;
Ca    0.000000000000000E+000
Cl    0.000000000000000E+000
K    2.000000000420445E-004
N    1.200000000252557E-003
Na    1.000000000210168E-003
END
SOLUTION_MODIFY  32
-total_h  111.0124336185
-total_o  55.5103519474
-cb  0.0000000000
-totals;
Ca    0.000000000000000E+000
Cl    0.000000000000000E+000
K    2.000000000280795E-004
N    1.200000000168767E-003
Na    1.000000000140343E-003
END
SOLUTION_MODIFY  33
-total_h  111.0124336224
-total_o  55.5103519493
-cb  0.0000000000
-totals;
Ca    0.000000000000000E+000
Cl    0.000000000000000E+000
K    2.000000000350620E-004
N    1.200000000210662E-003
Na    1.000000000175255E-003
END
SOLUTION_MODIFY  34
-total_h  111.0124336146
-total_o  55.5103519454
-cb  0.0000000000
-totals;
Ca    0.000000000000000E+000
Cl    0.000000000000000E+000
K    2.000000000210969E-004
N    1.200000000126871E-003
Na    1.000000000105430E-003
END
SOLUTION_MODIFY  35
-total_h  111.0124336185
-total_o  55.5103519474
-cb  0.0000000000
-totals;
Ca    0.000000000000000E+000
Cl    0.000000000000000E+000
K    2.000000000280795E-004
N    1.200000000168767E-003
Na    1.000000000140343E-003
```

```
END
SOLUTION_MODIFY  36
-total_h  111.0124336108
-total_o  55.5103519435
-cb  0.0000000000
-totals;
Ca    0.000000000000000E+000
Cl    0.000000000000000E+000
K    2.000000000141144E-004
N    1.200000000084976E-003
Na    1.000000000070517E-003
END
SOLUTION_MODIFY  37
-total_h  111.0124336146
-total_o  55.5103519454
-cb  0.0000000000
-totals;
Ca    0.000000000000000E+000
Cl    0.000000000000000E+000
K    2.000000000210969E-004
N    1.200000000126871E-003
Na    1.000000000105430E-003
END
SOLUTION_MODIFY  38
-total_h  111.0124336069
-total_o  55.5103519415
-cb  0.0000000000
-totals;
Ca    0.000000000000000E+000
Cl    0.000000000000000E+000
K    2.000000000071319E-004
N    1.200000000043081E-003
Na    1.000000000035605E-003
END
SOLUTION_MODIFY  39
-total_h  111.0124336108
-total_o  55.5103519435
-cb  0.0000000000
-totals;
Ca    0.000000000000000E+000
Cl    0.000000000000000E+000
K    2.000000000141144E-004
N    1.200000000084976E-003
Na    1.000000000070517E-003
END
SOLUTION_MODIFY  40
-total_h  111.0124336073
-total_o  55.5103519417
-cb  0.0000000000
-totals;
Ca    0.000000000000000E+000
```

```
Cl    0.000000000000000E+000
K    2.000000000078469E-004
N    1.200000000047371E-003
Na    1.000000000039180E-003
END
RUN_CELLS;-CELLS;1-40;END
```

E.4 How IPhreeqc Outputs Are Organized in the Memory to Be Transferred to UTCOMP

Table E-1 presents how IPhreeqc outputs are arranged in the computer memory (using **SELECTED_OUTPUT**) to be transferred to UTCOMP. *SetSelectedOutputFileOn* method of IPhreeqc was used to print the outputs from the computer memory to Table E-1 (see Table A.1 provided in Charlton and Parkhurst, 2011). Each row in Table E-1 contains the output data of a certain gridblock (i.e., number of rows is equal to the number of gridblocks). Element concentrations (i.e., columns 1 through 5 for this case), charge balance (i.e., column 10), total hydrogen (i.e., column 11), and total oxygen (i.e., column 12) are mandatory outputs that must be obtained from IPhreeqc at each time step. The reason is that element concentrations, charge balance, total hydrogen, and total oxygen must be transported (either by simple cell-shifting or solving the mass conservation equation) at each time step. Columns 6 through 9 are user-defined and obtained from IPhreeqc only to be printed for certain gridblocks. In other words, sodium, chloride, potassium, and calcium concentrations (in mmol/kgw) are transferred from IPhreeqc to UTCOMP to be printed for gridblocks defined by the user.

Table E-1: IPhreeqc output file printed from the computer memory using *SetSelectedOutputFileOn*

Ca	Cl	K	N	Na	TOT("Na")*1E3	TOT("Cl")*1E3	TOT("K")*1E3	TOT("Ca")*1E3	Charge	Total_H	Total_O
3.99E-08	6.00E-05	2.08E-04	1.14E-03	9.92E-04	9.92E-01	6.00E-02	2.08E-01	3.99E-05	2.68E-16	1.11E+02	5.55E+01
0.00E+00	0.00E+00	2.00E-04	1.20E-03	1.00E-03	1.00E+00	0.00E+00	2.00E-01	0.00E+00	-4.78E-16	1.11E+02	5.55E+01

0.00E+00	0.00E+00	2.00E-04	1.20E-03	1.00E-03	1.00E+00	0.00E+00	2.00E-01	0.00E+00	-4.54E-16	1.11E+02	5.55E+01
0.00E+00	0.00E+00	2.00E-04	1.20E-03	1.00E-03	1.00E+00	0.00E+00	2.00E-01	0.00E+00	-4.54E-16	1.11E+02	5.55E+01
0.00E+00	0.00E+00	2.00E-04	1.20E-03	1.00E-03	1.00E+00	0.00E+00	2.00E-01	0.00E+00	-4.28E-16	1.11E+02	5.55E+01
0.00E+00	0.00E+00	2.00E-04	1.20E-03	1.00E-03	1.00E+00	0.00E+00	2.00E-01	0.00E+00	-4.54E-16	1.11E+02	5.55E+01
0.00E+00	0.00E+00	2.00E-04	1.20E-03	1.00E-03	1.00E+00	0.00E+00	2.00E-01	0.00E+00	-3.77E-16	1.11E+02	5.55E+01
0.00E+00	0.00E+00	2.00E-04	1.20E-03	1.00E-03	1.00E+00	0.00E+00	2.00E-01	0.00E+00	-4.28E-16	1.11E+02	5.55E+01
0.00E+00	0.00E+00	2.00E-04	1.20E-03	1.00E-03	1.00E+00	0.00E+00	2.00E-01	0.00E+00	-3.77E-16	1.11E+02	5.55E+01
0.00E+00	0.00E+00	2.00E-04	1.20E-03	1.00E-03	1.00E+00	0.00E+00	2.00E-01	0.00E+00	-3.77E-16	1.11E+02	5.55E+01
0.00E+00	0.00E+00	2.00E-04	1.20E-03	1.00E-03	1.00E+00	0.00E+00	2.00E-01	0.00E+00	-3.77E-16	1.11E+02	5.55E+01
0.00E+00	0.00E+00	2.00E-04	1.20E-03	1.00E-03	1.00E+00	0.00E+00	2.00E-01	0.00E+00	-3.52E-16	1.11E+02	5.55E+01
0.00E+00	0.00E+00	2.00E-04	1.20E-03	1.00E-03	1.00E+00	0.00E+00	2.00E-01	0.00E+00	-3.52E-16	1.11E+02	5.55E+01
0.00E+00	0.00E+00	2.00E-04	1.20E-03	1.00E-03	1.00E+00	0.00E+00	2.00E-01	0.00E+00	-3.01E-16	1.11E+02	5.55E+01
0.00E+00	0.00E+00	2.00E-04	1.20E-03	1.00E-03	1.00E+00	0.00E+00	2.00E-01	0.00E+00	-3.27E-16	1.11E+02	5.55E+01
0.00E+00	0.00E+00	2.00E-04	1.20E-03	1.00E-03	1.00E+00	0.00E+00	2.00E-01	0.00E+00	-3.27E-16	1.11E+02	5.55E+01
0.00E+00	0.00E+00	2.00E-04	1.20E-03	1.00E-03	1.00E+00	0.00E+00	2.00E-01	0.00E+00	-2.77E-16	1.11E+02	5.55E+01
0.00E+00	0.00E+00	2.00E-04	1.20E-03	1.00E-03	1.00E+00	0.00E+00	2.00E-01	0.00E+00	-2.77E-16	1.11E+02	5.55E+01
0.00E+00	0.00E+00	2.00E-04	1.20E-03	1.00E-03	1.00E+00	0.00E+00	2.00E-01	0.00E+00	-3.01E-16	1.11E+02	5.55E+01
0.00E+00	0.00E+00	2.00E-04	1.20E-03	1.00E-03	1.00E+00	0.00E+00	2.00E-01	0.00E+00	-2.27E-16	1.11E+02	5.55E+01
0.00E+00	0.00E+00	2.00E-04	1.20E-03	1.00E-03	1.00E+00	0.00E+00	2.00E-01	0.00E+00	-2.51E-16	1.11E+02	5.55E+01
0.00E+00	0.00E+00	2.00E-04	1.20E-03	1.00E-03	1.00E+00	0.00E+00	2.00E-01	0.00E+00	-2.51E-16	1.11E+02	5.55E+01
0.00E+00	0.00E+00	2.00E-04	1.20E-03	1.00E-03	1.00E+00	0.00E+00	2.00E-01	0.00E+00	-2.27E-16	1.11E+02	5.55E+01
0.00E+00	0.00E+00	2.00E-04	1.20E-03	1.00E-03	1.00E+00	0.00E+00	2.00E-01	0.00E+00	-2.01E-16	1.11E+02	5.55E+01
0.00E+00	0.00E+00	2.00E-04	1.20E-03	1.00E-03	1.00E+00	0.00E+00	2.00E-01	0.00E+00	-2.01E-16	1.11E+02	5.55E+01
0.00E+00	0.00E+00	2.00E-04	1.20E-03	1.00E-03	1.00E+00	0.00E+00	2.00E-01	0.00E+00	-1.77E-16	1.11E+02	5.55E+01
0.00E+00	0.00E+00	2.00E-04	1.20E-03	1.00E-03	1.00E+00	0.00E+00	2.00E-01	0.00E+00	-2.01E-16	1.11E+02	5.55E+01
0.00E+00	0.00E+00	2.00E-04	1.20E-03	1.00E-03	1.00E+00	0.00E+00	2.00E-01	0.00E+00	-1.52E-16	1.11E+02	5.55E+01
0.00E+00	0.00E+00	2.00E-04	1.20E-03	1.00E-03	1.00E+00	0.00E+00	2.00E-01	0.00E+00	-1.52E-16	1.11E+02	5.55E+01

0.00E+00	0.00E+00	2.00E-04	1.20E-03	1.00E-03	1.00E+00	0.00E+00	2.00E-01	0.00E+00	-1.26E-16	1.11E+02	5.55E+01
0.00E+00	0.00E+00	2.00E-04	1.20E-03	1.00E-03	1.00E+00	0.00E+00	2.00E-01	0.00E+00	-1.52E-16	1.11E+02	5.55E+01
0.00E+00	0.00E+00	2.00E-04	1.20E-03	1.00E-03	1.00E+00	0.00E+00	2.00E-01	0.00E+00	-1.01E-16	1.11E+02	5.55E+01
0.00E+00	0.00E+00	2.00E-04	1.20E-03	1.00E-03	1.00E+00	0.00E+00	2.00E-01	0.00E+00	-1.26E-16	1.11E+02	5.55E+01
0.00E+00	0.00E+00	2.00E-04	1.20E-03	1.00E-03	1.00E+00	0.00E+00	2.00E-01	0.00E+00	-7.47E-17	1.11E+02	5.55E+01
0.00E+00	0.00E+00	2.00E-04	1.20E-03	1.00E-03	1.00E+00	0.00E+00	2.00E-01	0.00E+00	-1.01E-16	1.11E+02	5.55E+01
0.00E+00	0.00E+00	2.00E-04	1.20E-03	1.00E-03	1.00E+00	0.00E+00	2.00E-01	0.00E+00	-3.43E-16	1.11E+02	5.55E+01
0.00E+00	0.00E+00	2.00E-04	1.20E-03	1.00E-03	1.00E+00	0.00E+00	2.00E-01	0.00E+00	-7.47E-17	1.11E+02	5.55E+01
0.00E+00	0.00E+00	2.00E-04	1.20E-03	1.00E-03	1.00E+00	0.00E+00	2.00E-01	0.00E+00	-3.43E-16	1.11E+02	5.55E+01
0.00E+00	0.00E+00	2.00E-04	1.20E-03	1.00E-03	1.00E+00	0.00E+00	2.00E-01	0.00E+00	-3.43E-16	1.11E+02	5.55E+01
0.00E+00	0.00E+00	2.00E-04	1.20E-03	1.00E-03	1.00E+00	0.00E+00	2.00E-01	0.00E+00	-3.43E-16	1.11E+02	5.55E+01

Appendix F: Parallel Version of the Simplified Code

The followings are subroutines for the parallel version of the simplified code provided in Appendix C. This code includes one module and three subroutine files. All the files are provided below. Similar to UTCOMP-IPhreeqc and UTCHEM-IPhreeqc, Massage Passing Interface (MPI) (Barney, 2009) is applied for parallelization of the code.

F.1 Routines for the Parallel Version of the Simplified Code

F.1.1 The main.f90 subroutine

```
!!  THE UNIVERSITY OF TEXAS AT AUSTIN - 2014
!!  ABOULGHASEM KAZEMI NIA KORRANI, MAY 2014
!!  aboulghasem.kazemi@utexas.edu

PROGRAM MAIN

USE MODULEPARA

IMPLICIT NONE

INTEGER, ALLOCATABLE :: VT(:,:), VT_NODAL(:,:)
DOUBLE PRECISION, ALLOCATABLE :: AVAR_LIB(:,:),
AVAR_LIB_NODAL(:,:)
CHARACTER, ALLOCATABLE :: SV(:,:), SV_NODAL(:,:)
CHARACTER (LEN=32), ALLOCATABLE :: STR_ELE(:)
CHARACTER (LEN=32), ALLOCATABLE :: INJ_SOLUTIONS_STRING(:)
! STRING
CHARACTER (LEN=80), ALLOCATABLE :: STR_PRINT(:)
CHARACTER (LEN=64) :: DUMMY_STR, DUMMY_STR2, DUMMY_STR3
INTEGER :: DUMMY_INT, NO_CELLS, NO_SLUGS
INTEGER, ALLOCATABLE :: NO_SHIFTS(:), INJ_SOLUTIONS(:)
DOUBLE PRECISION, ALLOCATABLE :: INJ_CONCENTRATIONS(:,:)
```

```
INTEGER  :: NELE, I, J, JJ,KK, IPHREEQC_ID, N_COLUMN,
N_ROW, IERR, SHIFT
INTEGER :: NO_PRINT
DOUBLE PRECISION, ALLOCATABLE:: CONC(:,:),
OTHER_GEOCHEMISTRY_VALUES(:,:)
DOUBLE PRECISION, ALLOCATABLE:: CONC_NODAL(:,:)
INTEGER :: DEST, SRC, TAG
INTEGER,  ALLOCATABLE :: ISTAT(:)
DOUBLE PRECISION :: TIME_END,TIME_START

LOGICAL :: FILE_EXISTS
INTEGER :: NO_CELLS_NODAL, NERR
INTEGER, ALLOCATABLE :: NO_CELLS_NODAL_EXTRA(:),
SUM_CELL_EXTRA(:)
DOUBLE PRECISION :: TEMP_DBL
INTEGER :: TEMP_INT, TOTAL_SHIFTS
DOUBLE PRECISION :: TIME_START_TRANSPORT,
TIME_END_TRANSPORT,&
TIME_TOTAL_TRANSPORT, TIME_START_GEOCHEMISTRY,
TIME_END_GEOCHEMISTRY,&
TIME_TOTAL_GEOCHEMISTRY, TIME_START_TOTAL, TIME_END_TOTAL


INCLUDE "IPHREEQC.F90.INC"
INCLUDE 'MPIF.H'

CALL CPU_TIME(TIME_START_TOTAL)
NERR=0
NUMPRC=1
MYPRC=0

CALL SETPRCS(NERR)
PRINT *, 'PROCESSER ', MYPRC, ' OF ', NUMPRC, ' IS ALIVE'



!   ******    USER INPUT PARAMETERS  ********************
NO_CELLS = 1000    ! USER INPUT PARAMETER
NO_SLUGS = 3       ! USER INPUT PARAMETER
ALLOCATE(NO_SHIFTS(1:NO_SLUGS))
ALLOCATE(INJ_SOLUTIONS(1:NO_SLUGS))
NO_SHIFTS= (/700, 700, 700/)         ! USER INPUT PARAMETER,
NO OF SHIFTS IN EACH SLUG
```

```
INJ_SOLUTIONS= (/1001, 1002, 1003/) ! USER INPUT PARAMETER,
NUMBERS MUST BE DIFFERENT
NO_PRINT=8    ! USER INPUT PARAMETER
ALLOCATE(STR_PRINT(1:NO_PRINT))
STR_PRINT(1) = 'MOL("Na+")'     ! USER INPUT PARAMETER
STR_PRINT(2) = 'MOL("Ca+2")'    ! USER INPUT PARAMETER
STR_PRINT(3) = 'MOL("Cl-")'     ! USER INPUT PARAMETER
STR_PRINT(4) = '-LA("H+")'      ! USER INPUT PARAMETER
STR_PRINT(5) = 'MOL("Ba+2")'    ! USER INPUT PARAMETER
STR_PRINT(6) = 'MOL("HCO3-")'   ! USER INPUT PARAMETER
STR_PRINT(7) = 'MOL("Mg+2")'    ! USER INPUT PARAMETER
STR_PRINT(8) = 'MOL("Sr+2")'    ! USER INPUT PARAMETER
!   ******   END OF  USER INPUT PARAMETERS  ***************


IF (MYPRC .EQ. 0) THEN
 OPEN(UNIT=121, FILE='CONCENTRATIONS.TXT')
 OPEN(UNIT=122, FILE='CPU_TIME.TXT')
END IF  ! MYPRC
IF (MYPRC .EQ. 0) THEN
 WRITE(121,2268) 'PV', (TRIM(ADJUSTL(STR_PRINT(I))),
I=1,NO_PRINT)
 2268 FORMAT (8X,100(A10,15X))
END IF
TEMP_DBL = NO_CELLS/NUMPRC
NO_CELLS_NODAL = FLOOR(TEMP_DBL)
 ALLOCATE(NO_CELLS_NODAL_EXTRA(0:NUMPRC-1))
 NO_CELLS_NODAL_EXTRA(0:NUMPRC-1) = 0
 ALLOCATE(SUM_CELL_EXTRA(0:NUMPRC-1))
 SUM_CELL_EXTRA(0:NUMPRC-1) = 0
IF (MOD(NO_CELLS, NUMPRC) .NE. 0) THEN
 DO I= 0, MOD(NO_CELLS, NUMPRC)-1
  NO_CELLS_NODAL_EXTRA(I) =  1
 END DO
END IF !
DO I=1, NUMPRC-1
  DO J=0, I-1
   SUM_CELL_EXTRA(I) =  SUM_CELL_EXTRA(I) +
NO_CELLS_NODAL_EXTRA(J)
  END DO
END DO
ALLOCATE(ISTAT(MPI_STATUS_SIZE))
  IPHREEQC_ID = CREATEIPHREEQC()
```

```
  IF (LOADDATABASE(IPHREEQC_ID, "IPHREEQC_DATABASE.DAT")
.NE. 0) CALL EHANDLER(IPHREEQC_ID)
INQUIRE(FILE="IPHREEQC_DATABASE.INC", EXIST=FILE_EXISTS)
IF (FILE_EXISTS) THEN
  IERR=ACCUMULATELINE(IPHREEQC_ID,'INCLUDE$
IPHREEQC_DATABASE.INC')
END IF
IERR=ACCUMULATELINE(IPHREEQC_ID, 'SOLUTION_SPECIES; H2O +
0.01E- = H2O-0.01; LOG_K -8')
!CC -- NO OF COMPONENTS
     IERR=ACCUMULATELINE(IPHREEQC_ID,'INCLUDE$ INPUT.DAT')
      IF (RUNACCUMULATED(IPHREEQC_ID) .NE. 0) CALL
EHANDLER(IPHREEQC_ID)
       NELE=GETCOMPONENTCOUNT(IPHREEQC_ID)+3
       ALLOCATE(STR_ELE(1:NELE))
        DO I=1, NELE-3
         CALL GETCOMPONENT(IPHREEQC_ID,I,STR_ELE(I))
        END DO
        STR_ELE(NELE-2)= 'CB'
        STR_ELE(NELE-1)= 'H'
        STR_ELE(NELE)= 'O'
       ALLOCATE(INJ_CONCENTRATIONS(1:NO_SLUGS,1:NELE))
       INJ_CONCENTRATIONS(1:NO_SLUGS,1:NELE) =0.D0
     IF (MYPRC .EQ. 0) THEN
        ALLOCATE(CONC(0:NO_CELLS,1:NELE))
        CONC(0:NO_CELLS,1:NELE) =0.D0

ALLOCATE(OTHER_GEOCHEMISTRY_VALUES(1:NO_CELLS,1:NO_PRINT))

OTHER_GEOCHEMISTRY_VALUES(1:NO_CELLS,1:NO_PRINT)=0.D0
     END IF  !! MYPRC

ALLOCATE(CONC_NODAL(1:NO_CELLS_NODAL+NO_CELLS_NODAL_EXTRA(M
YPRC),1:NELE))

CONC_NODAL(1:NO_CELLS_NODAL+NO_CELLS_NODAL_EXTRA(MYPRC),1:N
ELE) =0.D0
       IERR=ACCUMULATELINE(IPHREEQC_ID,'SELECTED_OUTPUT
1')
       IERR=ACCUMULATELINE(IPHREEQC_ID,'-RESET FALSE')
       IERR=ACCUMULATELINE(IPHREEQC_ID,'USER_PUNCH  1')
       DO I=1, NELE-3
```

```
       IERR=ACCUMULATELINE(IPHREEQC_ID,'-HEADING  '//
TRIM(ADJUSTL(STR_ELE(I))))
       END DO
       IERR=ACCUMULATELINE(IPHREEQC_ID,'-HEADING
CHARGE_BALANCE')
       IERR=ACCUMULATELINE(IPHREEQC_ID,'-HEADING
TOTAL_H')
       IERR=ACCUMULATELINE(IPHREEQC_ID,'-HEADING
TOTAL_O')
       DO I=1, NO_PRINT
       IERR=ACCUMULATELINE(IPHREEQC_ID,'-HEADING   '//
TRIM(ADJUSTL(STR_PRINT(I))))
       END DO
       DO I=1, NELE-3
        WRITE(DUMMY_STR,*) (I)*10
        IERR=ACCUMULATELINE(IPHREEQC_ID,
TRIM(ADJUSTL(DUMMY_STR))//' PUNCH  TOTMOLE("'//
TRIM(ADJUSTL(STR_ELE(I)))//'")')
       END DO
       WRITE(DUMMY_STR,*) (NELE-2)*10

IERR=ACCUMULATELINE(IPHREEQC_ID,TRIM(ADJUSTL(DUMMY_STR))//
'  PUNCH   CHARGE_BALANCE')
       WRITE(DUMMY_STR,*) (NELE-1)*10

IERR=ACCUMULATELINE(IPHREEQC_ID,TRIM(ADJUSTL(DUMMY_STR))//'
PUNCH   TOTMOLE("H")')
       WRITE(DUMMY_STR,*) (NELE)*10

IERR=ACCUMULATELINE(IPHREEQC_ID,TRIM(ADJUSTL(DUMMY_STR))//'
PUNCH   TOTMOLE("O")')
       DO I=1, NO_PRINT
        WRITE(DUMMY_STR,*) (NELE+I)*10
        IERR=ACCUMULATELINE(IPHREEQC_ID,
TRIM(ADJUSTL(DUMMY_STR))//' PUNCH  '//
TRIM(ADJUSTL(STR_PRINT(I))))
       END DO

IERR=SETCURRENTSELECTEDOUTPUTUSERNUMBER(IPHREEQC_ID,1)
!CC       CALL OUTPUTACCUMULATEDLINES(IPHREEQC_ID)
         WRITE(DUMMY_STR,*) NO_CELLS
         IERR=ACCUMULATELINE(IPHREEQC_ID,'RUN_CELLS; -
CELLS   1-'// TRIM(ADJUSTL(DUMMY_STR))//';  END')
```

```
          IF (RUNACCUMULATED(IPHREEQC_ID) .NE. 0) CALL
EHANDLER(IPHREEQC_ID)
        IF (MYPRC .EQ. 0) THEN
           N_ROW=GETSELECTEDOUTPUTROWCOUNT(IPHREEQC_ID)

N_COLUMN=GETSELECTEDOUTPUTCOLUMNCOUNT(IPHREEQC_ID)
          ALLOCATE(AVAR_LIB(1:N_ROW,1:N_COLUMN))
          ALLOCATE(VT(1:N_ROW,1:N_COLUMN))
          ALLOCATE(SV(1:N_ROW,1:N_COLUMN))
          AVAR_LIB(1:N_ROW,1:N_COLUMN)=0.D0
          DO I=1, N_ROW
           DO J=1, N_COLUMN
           IERR =
GETSELECTEDOUTPUTVALUE(IPHREEQC_ID,I,J,VT(I,J),AVAR_LIB(I,J
),SV(I,J))
           END DO
          END DO
         CONC(1:NO_CELLS,1:NELE)=
AVAR_LIB(1:NO_CELLS,1:NELE)
       DEALLOCATE(AVAR_LIB, VT, SV)
! FIND ELEMENT CONCENTRATIONS FOR THE INJECTING SOLUTIONS
         ALLOCATE(INJ_SOLUTIONS_STRING(1:NO_SLUGS)) !
STRING
         DO KK=1, NO_SLUGS
          WRITE(INJ_SOLUTIONS_STRING(KK), *)
INJ_SOLUTIONS(KK)
         END DO
          IERR=ACCUMULATELINE(IPHREEQC_ID,'RUN_CELLS; -
CELLS;')
            DO KK=1, NO_SLUGS
             IERR=ACCUMULATELINE(IPHREEQC_ID,
TRIM(ADJUSTL(INJ_SOLUTIONS_STRING(KK))))
            END DO
          IERR=ACCUMULATELINE(IPHREEQC_ID,'END')
          IF (RUNACCUMULATED(IPHREEQC_ID) .NE. 0) CALL
EHANDLER(IPHREEQC_ID)
          N_ROW=GETSELECTEDOUTPUTROWCOUNT(IPHREEQC_ID)

N_COLUMN=GETSELECTEDOUTPUTCOLUMNCOUNT(IPHREEQC_ID)
          ALLOCATE(AVAR_LIB(1:N_ROW,1:N_COLUMN))
          ALLOCATE(VT(1:N_ROW,1:N_COLUMN))
          ALLOCATE(SV(1:N_ROW,1:N_COLUMN))
          AVAR_LIB(1:N_ROW,1:N_COLUMN)=0.D0
```

```
          DO I=1, N_ROW
           DO J=1, N_COLUMN
           IERR =
GETSELECTEDOUTPUTVALUE(IPHREEQC_ID,I,J,VT(I,J),AVAR_LIB(I,J
),SV(I,J))
           END DO
          END DO
         INJ_CONCENTRATIONS(1:NO_SLUGS,1:NELE)=
AVAR_LIB(1:NO_SLUGS,1:NELE)
       DEALLOCATE(AVAR_LIB, VT, SV)
!! -- END FOR "FIND ELEMENT CONCENTRATIONS FOR THE
INJECTING SOLUTIONS"
       END IF !! MYPRC
!CC-- END OF INITILIZATION

!! DELETE EXTRA CELLS FROM EACH PROCESSOR
  IF (NUMPRC .GT. 1) THEN
    IF (MYPRC .EQ. 0) THEN
     WRITE(DUMMY_STR,*)
NO_CELLS_NODAL+NO_CELLS_NODAL_EXTRA(MYPRC)+1
     WRITE(DUMMY_STR2,*) NO_CELLS
     IERR=ACCUMULATELINE(IPHREEQC_ID,'DELETE;  -CELLS
'//TRIM(ADJUSTL(DUMMY_STR))//'-
'//TRIM(ADJUSTL(DUMMY_STR2)))
    ELSEIF (MYPRC .EQ. NUMPRC-1) THEN
     WRITE(DUMMY_STR,*)
MYPRC*NO_CELLS_NODAL+SUM_CELL_EXTRA(MYPRC)
     IERR=ACCUMULATELINE(IPHREEQC_ID,'DELETE;  -CELLS 1-
'//TRIM(ADJUSTL(DUMMY_STR)))
    ELSE
     WRITE(DUMMY_STR,*)
MYPRC*NO_CELLS_NODAL+SUM_CELL_EXTRA(MYPRC)
     WRITE(DUMMY_STR2,*)
(MYPRC+1)*NO_CELLS_NODAL+SUM_CELL_EXTRA(MYPRC)+NO_CELLS_NOD
AL_EXTRA(MYPRC)+1
     WRITE(DUMMY_STR3,*) NO_CELLS
     IERR=ACCUMULATELINE(IPHREEQC_ID,'DELETE;  -CELLS 1-
'//TRIM(ADJUSTL(DUMMY_STR)))
     IERR=ACCUMULATELINE(IPHREEQC_ID,'DELETE;  -CELLS
'//TRIM(ADJUSTL(DUMMY_STR2))//'-
'//TRIM(ADJUSTL(DUMMY_STR3)))
    END IF
     IERR=ACCUMULATELINE(IPHREEQC_ID,'END')
```

```
     IF (RUNACCUMULATED(IPHREEQC_ID) .NE. 0) CALL
EHANDLER(IPHREEQC_ID)
   END IF ! FOR "IF (NUMPRC .GT. 1) THEN"
!! END FOR "DELETE EXTRA CELLS FROM EACH PROCESSOR"

ALLOCATE(AVAR_LIB_NODAL(1:NO_CELLS_NODAL+NO_CELLS_NODAL_EXT
RA(MYPRC),1:NELE+NO_PRINT))

ALLOCATE(VT_NODAL(1:NO_CELLS_NODAL+NO_CELLS_NODAL_EXTRA(MYP
RC),1:NELE+NO_PRINT))

ALLOCATE(SV_NODAL(1:NO_CELLS_NODAL+NO_CELLS_NODAL_EXTRA(MYP
RC),1:NELE+NO_PRINT))
 CALL WAITALL()
TOTAL_SHIFTS = 0
DO JJ=1, NO_SLUGS
IF (MYPRC .EQ. 0)  THEN
 WRITE(DUMMY_STR,*) JJ
 WRITE(*,*) '-----------------------------------------
---'
 WRITE(*,*) 'START INJECTING SLUG: '//
TRIM(ADJUSTL(DUMMY_STR))
 WRITE(*,*) '-----------------------------------------
----'
 WRITE(122,*) '-----------------------------------------
-----'
 WRITE(122,*) 'START INJECTING SLUG: '//
TRIM(ADJUSTL(DUMMY_STR))
 WRITE(122,*) '-----------------------------------------
------'
CONC(0,1:NELE) = INJ_CONCENTRATIONS(JJ,1:NELE)
END IF
 CALL WAITALL()
DO SHIFT =1, NO_SHIFTS(JJ)
IF (MYPRC .EQ. 0) THEN
CALL CPU_TIME(TIME_START_TRANSPORT)
!CC -- SHIFT THE CELLS (I.E., DO THE TRANSPORT)
!CC -- IN UTCOMP-IPHREEQC MASS BALANCE EQUATION IS SOLVED
INSTEAD
         DO I= NO_CELLS,1, -1
          CONC(I,1:NELE) = CONC(I-1,1:NELE)
         END DO
!CC -- END
```

```
CALL CPU_TIME(TIME_END_TRANSPORT)
TIME_TOTAL_TRANSPORT = TIME_TOTAL_TRANSPORT +
(TIME_END_TRANSPORT-TIME_START_TRANSPORT)

CONC_NODAL(1:NO_CELLS_NODAL+NO_CELLS_NODAL_EXTRA(MYPRC),1:N
ELE)=CONC(1:NO_CELLS_NODAL+NO_CELLS_NODAL_EXTRA(MYPRC),1:NE
LE)
TAG=100
DO J=1, NUMPRC-1
 DEST=J
 CALL
MPI_SEND(CONC(J*NO_CELLS_NODAL+SUM_CELL_EXTRA(J)+1:(J+1)*NO
_CELLS_NODAL+SUM_CELL_EXTRA(J)+NO_CELLS_NODAL_EXTRA(J),1:NE
LE),(NO_CELLS_NODAL+NO_CELLS_NODAL_EXTRA(J))*NELE,MPI_DOUBL
E_PRECISION,DEST,TAG,MPI_COMM_WORLD,IERR)
END DO
ELSEIF (MYPRC .NE. 0) THEN
 TAG=100
 SRC=0
 CALL
MPI_RECV(CONC_NODAL(1:NO_CELLS_NODAL+NO_CELLS_NODAL_EXTRA(M
YPRC),1:NELE),(NO_CELLS_NODAL+NO_CELLS_NODAL_EXTRA(MYPRC))*
NELE,MPI_DOUBLE_PRECISION,SRC,TAG,MPI_COMM_WORLD,ISTAT,IERR
)
END IF  !! MYPRC
CALL WAITALL()
IF (MYPRC .EQ. 0) CALL CPU_TIME(TIME_START_GEOCHEMISTRY)
      DO I=1, NO_CELLS_NODAL + NO_CELLS_NODAL_EXTRA(MYPRC)
        WRITE(DUMMY_STR,*)
I+MYPRC*NO_CELLS_NODAL+SUM_CELL_EXTRA(MYPRC)
       IERR=ACCUMULATELINE(IPHREEQC_ID,'SOLUTION_MODIFY
'// TRIM(ADJUSTL(DUMMY_STR)))
        WRITE(DUMMY_STR,*) CONC_NODAL(I,NELE-2)
       IERR=ACCUMULATELINE(IPHREEQC_ID,'-CB
'//TRIM(ADJUSTL(DUMMY_STR)))
        WRITE(DUMMY_STR,*) CONC_NODAL(I,NELE-1)
       IERR=ACCUMULATELINE(IPHREEQC_ID,'-TOTAL_H
'//TRIM(ADJUSTL(DUMMY_STR)))
        WRITE(DUMMY_STR,*) CONC_NODAL(I,NELE)
       IERR=ACCUMULATELINE(IPHREEQC_ID,'-TOTAL_O
'//TRIM(ADJUSTL(DUMMY_STR)))
       IERR=ACCUMULATELINE(IPHREEQC_ID,'-TOTALS; ')
        DO J=1,NELE-3
```

```
          WRITE(DUMMY_STR,*) CONC_NODAL(I,J)

IERR=ACCUMULATELINE(IPHREEQC_ID,TRIM(ADJUSTL(STR_ELE(J)))//
'  '//TRIM(ADJUSTL(DUMMY_STR)))
          END DO  !! FOR J
        IERR=ACCUMULATELINE(IPHREEQC_ID,'END')
       END DO   !! FOR I
         WRITE(DUMMY_STR,*)
MYPRC*NO_CELLS_NODAL+SUM_CELL_EXTRA(MYPRC)+1
        WRITE(DUMMY_STR2,*)
(MYPRC+1)*NO_CELLS_NODAL+SUM_CELL_EXTRA(MYPRC)+NO_CELLS_NOD
AL_EXTRA(MYPRC)
       IERR=ACCUMULATELINE(IPHREEQC_ID,'RUN_CELLS; -CELLS
'// TRIM(ADJUSTL(DUMMY_STR))//'-
'//TRIM(ADJUSTL(DUMMY_STR2))//';  END')
       IF (RUNACCUMULATED(IPHREEQC_ID) .NE. 0) CALL
EHANDLER(IPHREEQC_ID)
         N_ROW=GETSELECTEDOUTPUTROWCOUNT(IPHREEQC_ID)
         N_COLUMN=GETSELECTEDOUTPUTCOLUMNCOUNT(IPHREEQC_ID)
        AVAR_LIB_NODAL(1:N_ROW,1:N_COLUMN)=0.D0
       DO I=1, N_ROW
          DO J=1, N_COLUMN
          IERR =
GETSELECTEDOUTPUTVALUE(IPHREEQC_ID,I,J,VT_NODAL(I,J),AVAR_L
IB_NODAL(I,J),SV_NODAL(I,J))
       END DO
      END DO
CALL WAITALL()
IF (MYPRC .EQ. 0) THEN
CALL CPU_TIME(TIME_END_GEOCHEMISTRY)
TIME_TOTAL_GEOCHEMISTRY = TIME_TOTAL_GEOCHEMISTRY +
(TIME_END_GEOCHEMISTRY-TIME_START_GEOCHEMISTRY)
END IF
IF (MYPRC .NE. 0)  THEN
TAG=200
DEST=0
 CALL
MPI_SEND(AVAR_LIB_NODAL(1:NO_CELLS_NODAL+NO_CELLS_NODAL_EXT
RA(MYPRC),1:NELE+NO_PRINT),(NO_CELLS_NODAL+NO_CELLS_NODAL_E
XTRA(MYPRC))*(NELE+NO_PRINT),MPI_DOUBLE_PRECISION,DEST,TAG,
MPI_COMM_WORLD,IERR)
ELSEIF (MYPRC .EQ. 0)  THEN
```

```
CONC(1:NO_CELLS_NODAL+NO_CELLS_NODAL_EXTRA(MYPRC),1:NELE)=A
VAR_LIB_NODAL(1:NO_CELLS_NODAL+NO_CELLS_NODAL_EXTRA(MYPRC),
1:NELE)

OTHER_GEOCHEMISTRY_VALUES(1:NO_CELLS_NODAL+NO_CELLS_NODAL_E
XTRA(MYPRC),1:NO_PRINT)=AVAR_LIB_NODAL(1:NO_CELLS_NODAL+NO_
CELLS_NODAL_EXTRA(MYPRC),NELE+1:NELE+NO_PRINT)
TAG=200
DO J=1, NUMPRC-1
SRC =J
 CALL
MPI_RECV(AVAR_LIB_NODAL(1:NO_CELLS_NODAL+NO_CELLS_NODAL_EXT
RA(J),1:NELE+NO_PRINT),(NO_CELLS_NODAL+NO_CELLS_NODAL_EXTRA
(J))*(NELE+NO_PRINT),MPI_DOUBLE_PRECISION,SRC,TAG,MPI_COMM_
WORLD,ISTAT,IERR)

CONC(J*NO_CELLS_NODAL+SUM_CELL_EXTRA(J)+1:(J+1)*NO_CELLS_NO
DAL+SUM_CELL_EXTRA(J)+NO_CELLS_NODAL_EXTRA(J),1:NELE)=AVAR_
LIB_NODAL(1:NO_CELLS_NODAL+NO_CELLS_NODAL_EXTRA(J),1:NELE)

OTHER_GEOCHEMISTRY_VALUES(J*NO_CELLS_NODAL+SUM_CELL_EXTRA(J
)+1:(J+1)*NO_CELLS_NODAL+SUM_CELL_EXTRA(J)+NO_CELLS_NODAL_E
XTRA(J),1:NO_PRINT)=AVAR_LIB_NODAL(1:NO_CELLS_NODAL+NO_CELL
S_NODAL_EXTRA(J),NELE+1:NELE+NO_PRINT)
END DO
END IF  !! MYPRC
TOTAL_SHIFTS = TOTAL_SHIFTS + 1
 CALL WAITALL()
        IF (MYPRC .EQ. 0) THEN
         WRITE(DUMMY_STR,*) SHIFT
         WRITE(*,*) 'SHIFT NO. =  '//
TRIM(ADJUSTL(DUMMY_STR))
         WRITE(122,*) 'SHIFT NO. =  '//
TRIM(ADJUSTL(DUMMY_STR))
         WRITE(121,2267) (TOTAL_SHIFTS+0.5)/NO_CELLS,
OTHER_GEOCHEMISTRY_VALUES(NO_CELLS,:)
        END IF
 CALL WAITALL()
 END DO !! SHIFT
CALL WAITALL()
END DO !! NO_SLUGS
CALL CPU_TIME(TIME_END_TOTAL)
```

```
      IF (MYPRC .EQ. 0) WRITE(*,*) 'TOTAL TIME ELAPSED(S)
=', TIME_END_TOTAL - TIME_START_TOTAL
      IF (MYPRC .EQ. 0) WRITE(*,*) 'TOTAL CPU TIME SPENT
FOR TRANSPPORT CALCULATION(S) =', TIME_TOTAL_TRANSPORT
      IF (MYPRC .EQ. 0) WRITE(*,*) 'TOTAL CPU TIME SPENT
FOR GEOCHEMISTRY CALCULATION(S) =', TIME_TOTAL_GEOCHEMISTRY

      IF (MYPRC .EQ. 0) WRITE(122,*) 'TOTAL TIME ELAPSED(S)
=', TIME_END_TOTAL - TIME_START_TOTAL
      IF (MYPRC .EQ. 0) WRITE(122,*) 'TOTAL CPU TIME SPENT
FOR TRANSPPORT CALCULATION(S) =', TIME_TOTAL_TRANSPORT
      IF (MYPRC .EQ. 0) WRITE(122,*) 'TOTAL CPU TIME SPENT
FOR GEOCHEMISTRY CALCULATION(S) =', TIME_TOTAL_GEOCHEMISTRY
 2267 FORMAT (2X,1000(F20.10,2X))
       CALL KILLPRC()
END PROGRAM MAIN
! END OF KAZEMI NIA, MAY 2014
```

F.1.2 The ehandler.f90 subroutine

```
      SUBROUTINE EHANDLER(IPHREEQC_ID)
        IMPLICIT NONE
         INTEGER :: IPHREEQC_ID
         INCLUDE "IPHREEQC.F90.INC"
         CALL OUTPUTERRORSTRING(IPHREEQC_ID)
       STOP
       END SUBROUTINE EHANDLER
```

F.1.3 The modulepara.f90 module file

```
      MODULE MODULEPARA
      INTEGER :: NUMPRC,MYPRC
      END MODULE MODULEPARA
```

F.1.4 Subroutine Containing the MPI Functions

All the following subroutines are defined in a file labeled “para.f”.

```
     SUBROUTINE SETPRCS (NERR)
C  ROUTINE SETS MULTIPROCESSOR PARAMETERS INCLUDING NUMBER
OF PROCESSORS,
C  PROCESSOR NUMBER, AND PROCESS ID (IF APPROPRIATE).
C  NERR = ERROR NUMBER STEPED BY 1 ON ERROR (INPUT &
OUTPUT, INTEGER)
      USE MODULEPARA
      INCLUDE 'MPIF.H'
      CHARACTER*14 PARROU
      IERR=0
      PARROU='MPI_INIT'
      CALL MPI_INIT (IERR)
      IF (IERR.GT.0) GO TO 13
      PARROU='MPI_COMM_RANK'
      CALL MPI_COMM_RANK (MPI_COMM_WORLD,MYPRC,IERR)
      IF (IERR.GT.0) GO TO 13
      PARROU='MPI_COMM_SIZE'
      CALL MPI_COMM_SIZE (MPI_COMM_WORLD,NUMPRC,IERR)
      IF (IERR.GT.0) GO TO 13
      RETURN
   13 NERR=NERR+1
      WRITE (*,14) PARROU
   14 FORMAT (/' ERROR # 202; PARALLEL ROUTINE ',A14,'
FAILED')

      END
      SUBROUTINE KILLPRC ()
C  ROUTINE TERMINATES A MULTIPROCESSOR SIMULATION.
      LOGICAL FLAG
      INTEGER IERR
      FLAG = .FALSE.
      CALL MPI_INITIALIZED(FLAG,IERR)
      IF (FLAG) THEN
         CALL MPI_FINALIZE(IERR)
      ENDIF
      END
```

```
      SUBROUTINE WAITALL ()
      INCLUDE 'MPIF.H'
      CALL MPI_BARRIER(MPI_COMM_WORLD,IERR)
      END
      SUBROUTINE SPREADI (NUMVAL, IVEC)
C  SENDS ONE OR MORE INTEGER VALUES FROM PROCESSOR ZERO TO
ALL OTHER
C  PROCESSORS.  THIS ROUTINE MUST BE CALLED BY ALL
PROCESSORS IF IT IS
C  CALLED BY ANY PROCESSOR.
C  NUMVAL = NUMBER OF VALUES IN IVEC (INPUT, INTEGER)
C           (MUST BE THE SAME ON ALL PROCESSORS)
C  IVEC() = DATA TO BE TRANSMITTED (INPUT AND OUTPUT,
INTEGER)
C*************************************************************
***********
      INCLUDE 'MPIF.H'
      INTEGER IVEC(*)
      CALL
MPI_BCAST(IVEC,NUMVAL,MPI_INTEGER,0,MPI_COMM_WORLD,IERR)
      END
      SUBROUTINE SPREADD (NUMVAL, RVEC)
C  SENDS ONE OR MORE REAL*8 VALUES FROM PROCESSOR ZERO TO
ALL OTHER
C  PROCESSORS.  THIS ROUTINE MUST BE CALLED BY ALL
PROCESSORS IF IT IS
C  CALLED BY ANY PROCESSOR.
C  NUMVAL = NUMBER OF VALUES IN RVEC (INPUT, INTEGER)
C           (MUST BE THE SAME ON ALL PROCESSORS)
C  RVEC() = DATA TO BE TRANSMITTED (INPUT AND OUTPUT,
REAL*8)
      INCLUDE 'MPIF.H'
      REAL*8 RVEC(*)
      CALL MPI_BCAST(RVEC,NUMVAL,MPI_DOUBLE_PRECISION,0,
     & MPI_COMM_WORLD,IERR)
      END
      SUBROUTINE SPREADS (NUMVAL, RVEC)
C  SENDS ONE OR MORE REAL*8 VALUES FROM PROCESSOR ZERO TO
ALL OTHER
C  PROCESSORS.  THIS ROUTINE MUST BE CALLED BY ALL
PROCESSORS IF IT IS
C  CALLED BY ANY PROCESSOR.
C  NUMVAL = NUMBER OF VALUES IN RVEC (INPUT, INTEGER)
```

```
C            (MUST BE THE SAME ON ALL PROCESSORS)
C  RVEC() = DATA TO BE TRANSMITTED (INPUT AND OUTPUT,
REAL*8)
      INCLUDE 'MPIF.H'
      CHARACTER*32 RVEC(*)
      CALL MPI_BCAST(RVEC,NUMVAL,MPI_CHARACTER,0,
     & MPI_COMM_WORLD,IERR)
      END
```

F.2 Compiling the Simplified Code in a Windows®-Based Machine

We are able to compile and run the parallel version of the simplified code (as well as the UTCOMP-IPhreeqc and UTCHEM-IPhreeqc simulators) in Microsoft® Visual Studio®. The procedure will be reported later by Wensi Fu, MS student, at The University of Texas at Austin.

F.3 Compiling the Simplified Code in a Linux®-Based Machine

Use the Makefile provided below.

Important Note: Command lines in Makefile must begin with a tab character (see http://en.wikipedia.org/wiki/Make_%28software%29 for Makefile rules).

```
## THE UNIVERSITY OF TEXAS AT AUSTIN
## ABOULGHASEM KAZEMI NIA KORRANI, MAY 2014
## aboulghasem.kazemi@utexas.edu
#FFLAGS = -O -pg
#FFLAGS = -O -fast
#FFLAGS = -g
FSRCS = \
modulepara.f main.f90 ehandler.f\
FSRCS_PARA = para.f\

IPhreeqc_LIB_PATH=/home1/02950/kazemi/lib  ## directory
where IPhreeqc libraries were installed
IPhreeqc_INCLUDE_PATH=/home1/02950/kazemi/include/  ##
directory where IPhreeqc libraries were installed
```

```
IPhreeqc_LIBRARIES=-Wl,-rpath $(IPhreeqc_LIB_PATH)  -
L/$(IPhreeqc_LIB_PATH)   $(IPhreeqc_LIB_PATH)/libiphreeqc-
3.1.2.so  $(IPhreeqc_LIB_PATH)/libiphreeqc.a
$(IPhreeqc_LIB_PATH)/libiphreeqc.so
ifdef tight
FFLAGS = -c -CB -r8 -g -traceback -check all -
fltconsistency -align all -debug all   -I
$(IPhreeqc_INCLUDE_PATH)
else
FFLAGS=  -c -g -O3  -I $(IPhreeqc_INCLUDE_PATH)
endif
PROG = exe
FORT =  mpif90  ## IN CASE THIS COMPILER DOES NOT WORK, YOU
MIGHT ALSO TRY mpif77
FOBJS = $(FSRCS:.f=.o)
PARA_OBJ = $(FSRCS_PARA:.f=.o)
OBJS = $(FOBJS) $(PARA_OBJ)
.f.o:
        $(FORT) $(FFLAGS) $*.f
.F.o:
        $(FORT) $(FFLAGS) $*.F
$(PROG):  $(OBJS)
        $(FORT) -o $(PROG) $(OBJS) $(IPhreeqc_LIBRARIES) -I
$(IPhreeqc_INCLUDE_PATH)
clean:
        rm -f *.o
        rm -f *.mod
        rm -f *.exe
        rm -f $(PROG)
```

F.4 VERIFICATION OF THE PARALLEL VERSION OF THE SIMPLIFIED CODE

The same case applied to verify the simplified code in Appendix C is used to verify the parallel version (see Appendix C for the case descriptions). Figures F-1 through F-8 verify results for the parallel version of the simplified code (with different number of processors) against PHREEQC outputs. Table F-1 presents the computational time versus number of processors applied for the simulation (plot is provided in Figure F-

9) and Figure F-10 shows the speedup plot. Simulations were run on TACC computational facilities at The University of Texas at Austin (see Chapter 2 for the TACC characteristics).

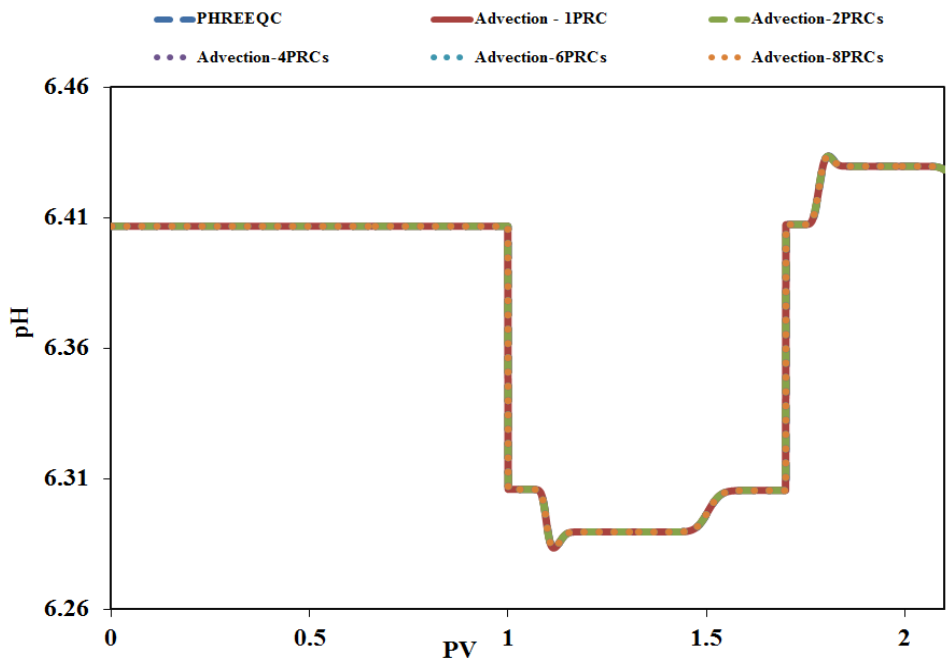

Figure F-1: pH history of the effluent solution (the parallel version of the simplified code verification against PHREEQC).

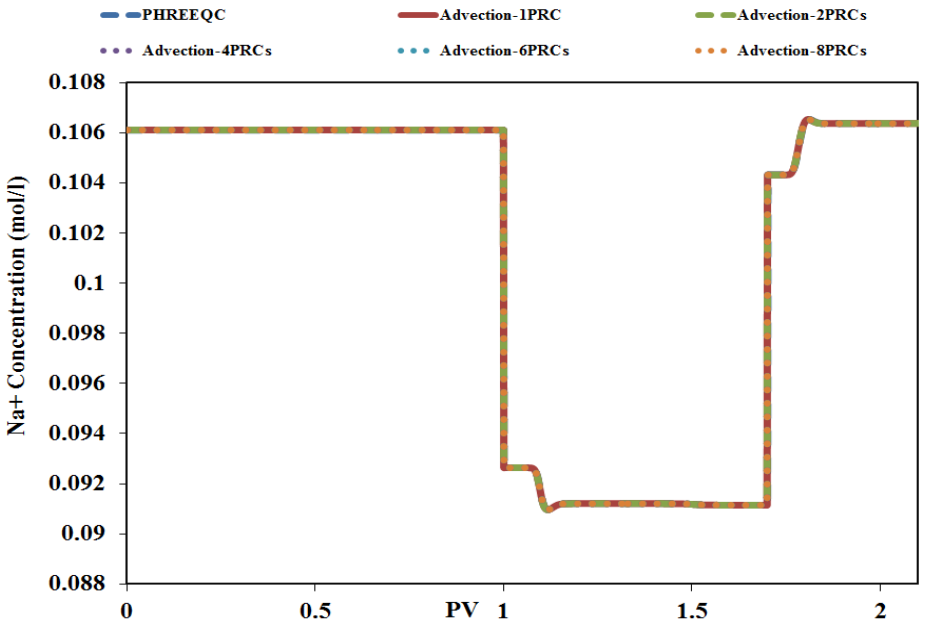

Figure F-2: Na^{+} concentration history of the effluent solution (the parallel version of the simplified code verification against PHREEQC).

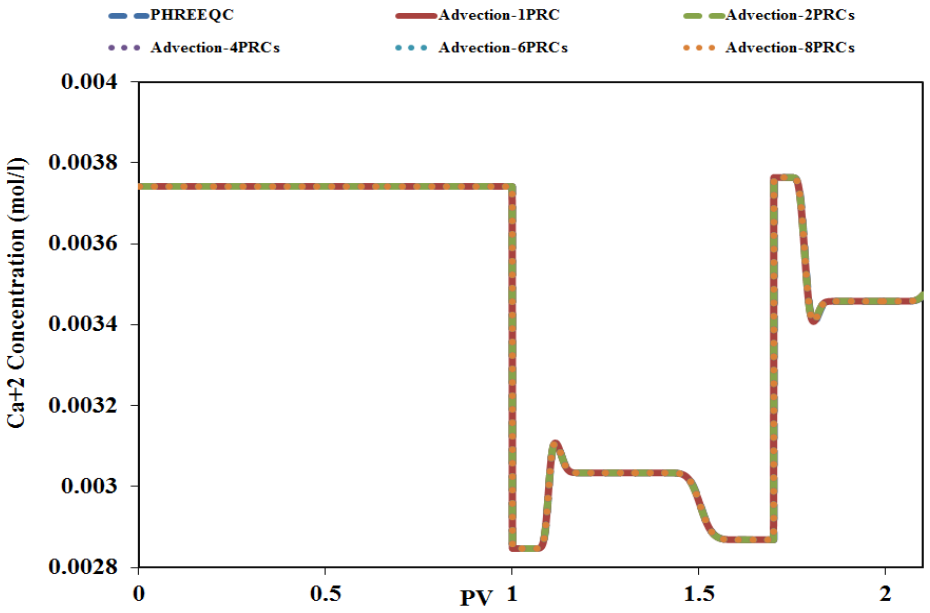

Figure F-3: Ca^{+2} concentration history of the effluent solution (the parallel version of the simplified code verification against PHREEQC).

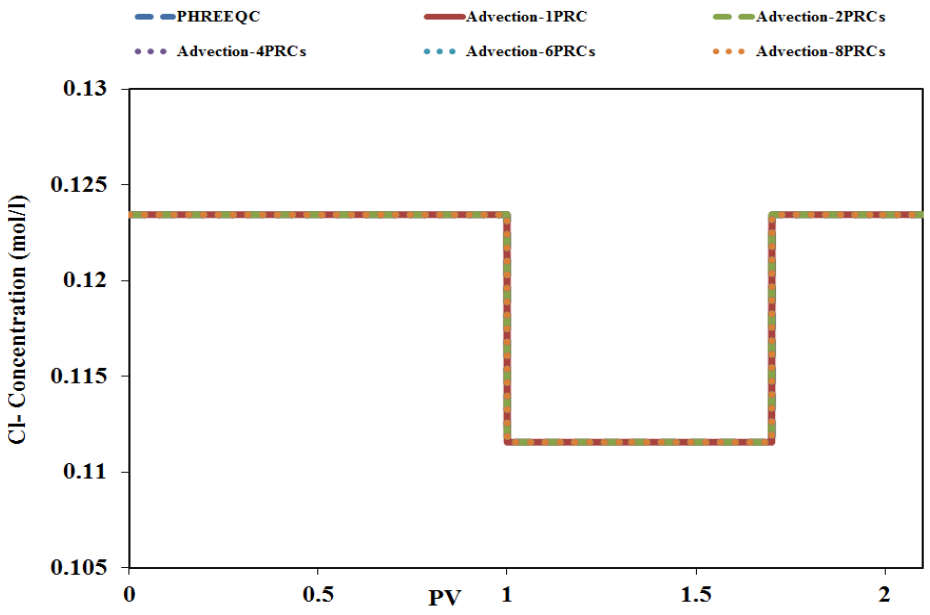

Figure F-4: Cl^- concentration history of the effluent solution (the parallel version of the simplified code verification against PHREEQC).

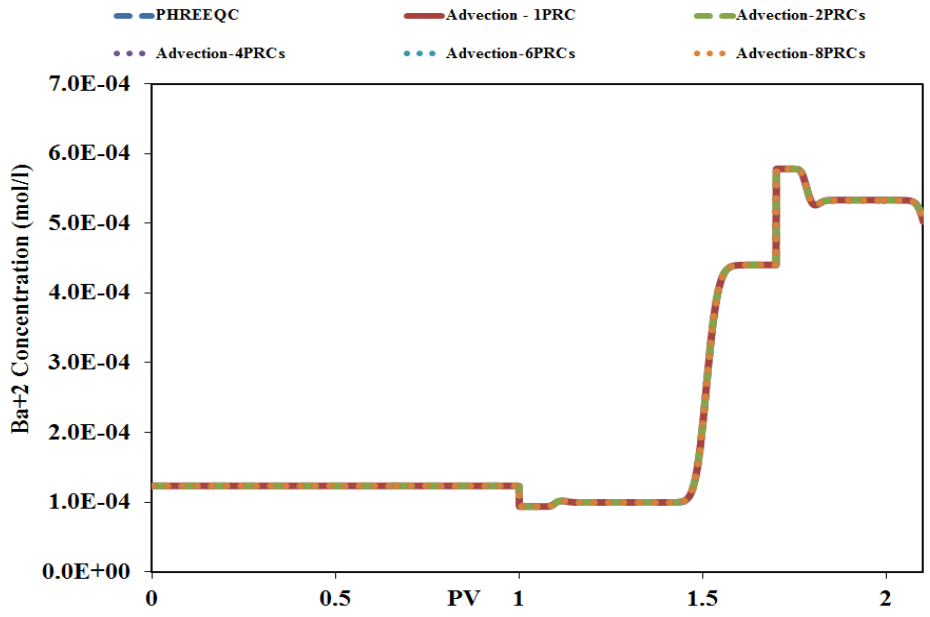

Figure F-5: Ba^{+2} concentration history of the effluent solution (the parallel version of the simplified code verification against PHREEQC).

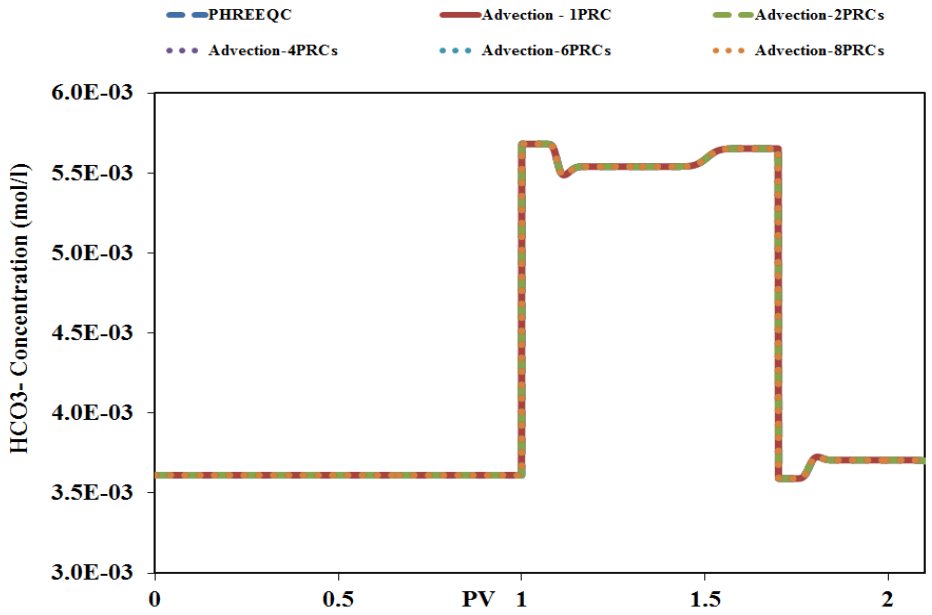

Figure F-6: HCO_3^- concentration history of the effluent solution (the parallel version of the simplified code verification against PHREEQC).

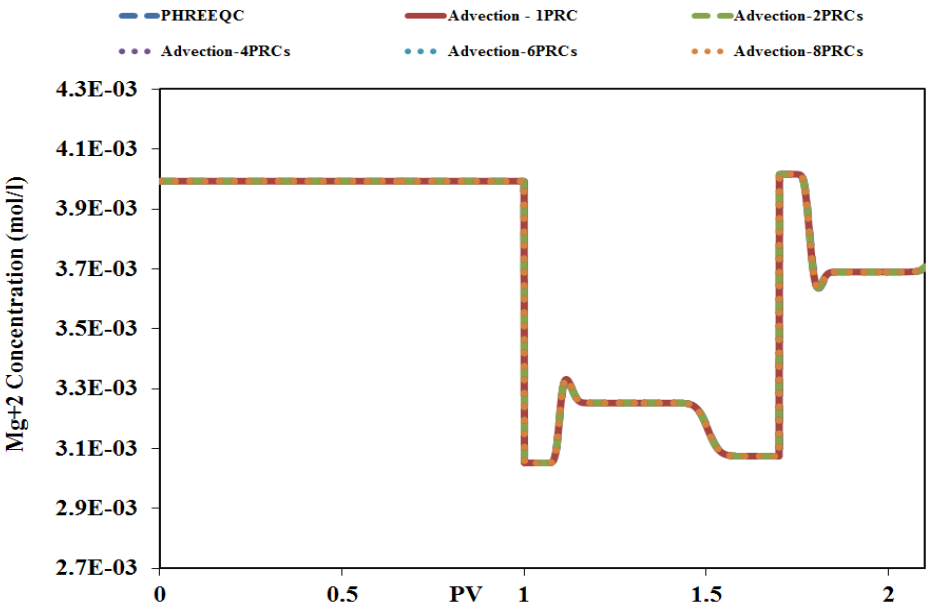

Figure F-7: Mg^{+2} concentration history of the effluent solution (the parallel version of the simplified code verification against PHREEQC).

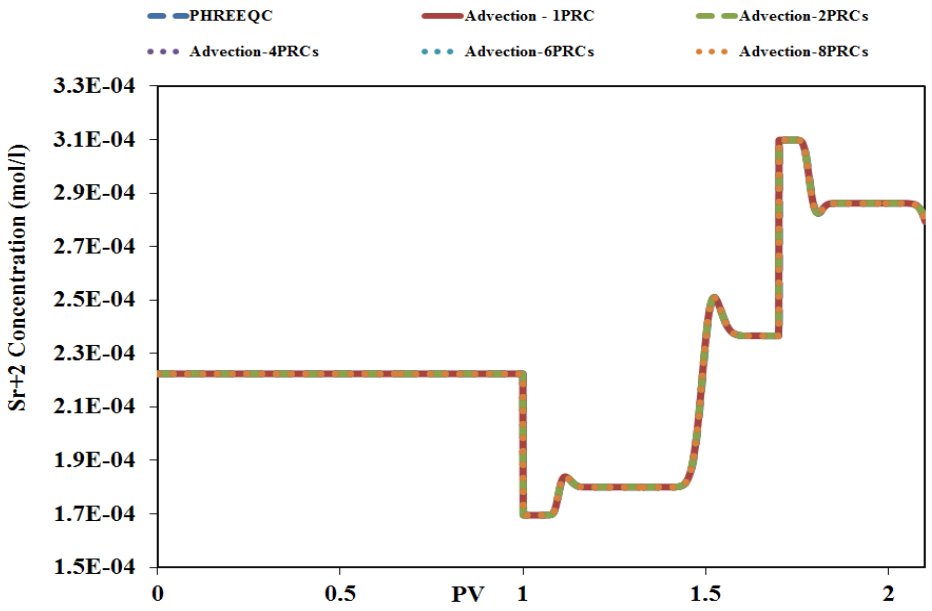

Figure F-8: Sr^{+2} concentration history of the effluent solution (the parallel version of the simplified code verification against PHREEQC).

Table F-1: Total computational time versus number of processors

No. of Processor Simplified Code	Total computational time (seconds)
1PRC	1034.91
2PRCs	537.84
4PRCs	313.69
6PRCs	243.34
8PRCs	203.38
10PRCs	180.47
12PRCs	168.07

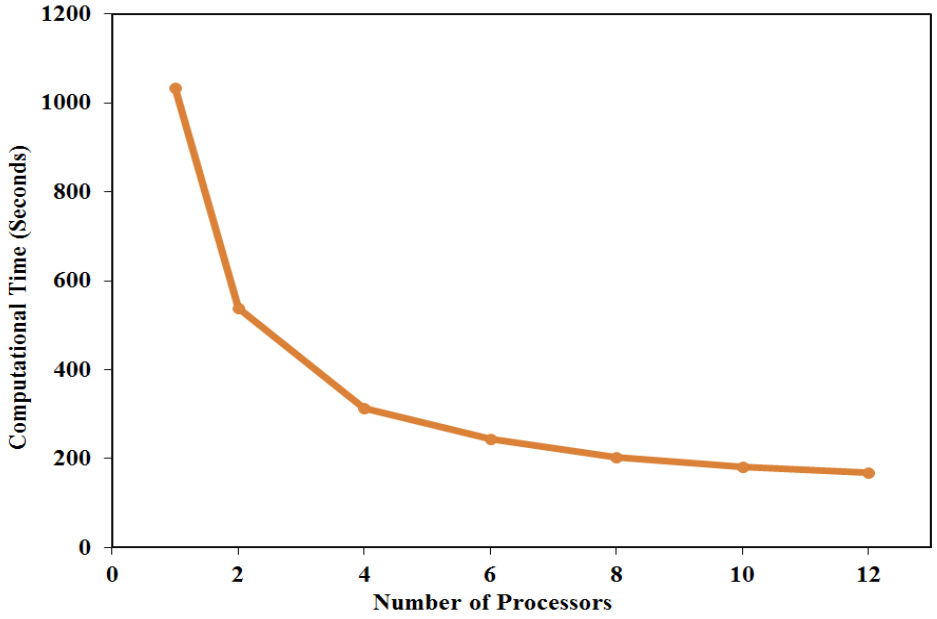

Figure F-9: Total computational time versus number of processors.

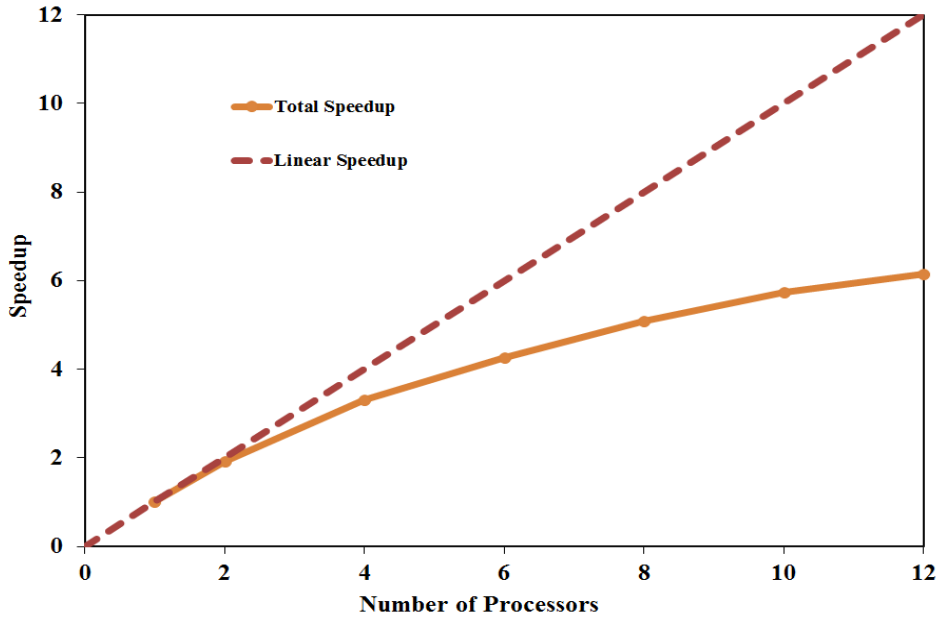

Figure F-10: Speedup curve for the total simulation versus number of processors.

Appendix G: Store Gridblocks Geochemistry Data from Computer Memory into a File in UTCOMP-IPhreeqc

This appendix provides command lines implemented in UTCOMP-IPhreeqc that store gridblocks geochemistry data from the computer memory into the file. Geochemistry data stored in the file can be used along with the UTCOMP restart file to resume the simulation. Appendices G.1 and G.2 present command lines implemented in the single- and multiple-processor versions of UTCOMP-IPhreeqc, respectively.

G.1 Single-Processor Version of UTCOMP-IPhreeqc

```
CC RESTART FILE SECTION IN UTCOMP-IPhreeqc
CC THE UNIVERSITY OF TEXAS AT AUSTIN
CC ABOULGHASEM KAZEMI NIA KORRANI, APRIL 2014
CC aboulghasem.kazemi@utexas.edu

      IF ((MOD(ICNT,NSTSKIP) .EQ. 0).AND. ISTORE.EQ.1 )
THEN
         IERR=ACCUMULATELINE(ID_PHREEQC, 'DUMP;-FILE
     +     TESTGC.STO ; -ALL;  END ')
        IERR = SETDUMPFILEON(ID_PHREEQC,.TRUE.)
        IF (RUNACCUMULATED(ID_PHREEQC) .NE. 0) CALL
     +    EHANDLER(ID_PHREEQC)
        IERR= SETDUMPFILEON(ID_PHREEQC,.FALSE.)
        IF (RUNACCUMULATED(ID_PHREEQC) .NE. 0) CALL
     +    EHANDLER(ID_PHREEQC)
          IGCSTORE = .TRUE.
CC          STOP
      END IF
CC -- END OF KAZEMI NIA KORRANI, APRIL 2014
```

G.2 Multiple-Processor Version of UTCOMP-IPhreeqc

```
CC RESTART FILE SECTION IN UTCOMP-IPhreeqc (PARALLEL
VERSION)
CC THE UNIVERSITY OF TEXAS AT AUSTIN
```

```
CC ABOULGHASEM KAZEMI NIA KORRANI, MAY 2014
CC aboulghasem.kazemi@utexas.edu


      IF (IGEOCHEM .EQ. 1 .AND.
     +    (MOD(ICNT,NSTSKIP) .EQ. 0) .AND. ISTORE .EQ. 1)
THEN
         IERR = SETDUMPSTRINGON(ID_PHREEQC,.TRUE.)
         IERR = ACCUMULATELINE(ID_PHREEQC, 'DUMP; -ALL;
END ')
        IF (RUNACCUMULATED(ID_PHREEQC) .NE. 0) CALL
     +    EHANDLER(ID_PHREEQC)
          DUMP_COUNT_LOCAL =
GETDUMPSTRINGLINECOUNT(ID_PHREEQC)
          ALLOCATE(DUMP_LINE(1:DUMP_COUNT_LOCAL))
         DO J=1, DUMP_COUNT_LOCAL
          CALL GETDUMPSTRINGLINE(ID_PHREEQC,J,DUMP_LINE(J))
         END DO
         IF (MYPRC .EQ. 0) THEN
           ALLOCATE(DUMP_COUNT(0:NUMPRC-1))
           DUMP_COUNT(0:NUMPRC-1) = 0
         END IF
         IF (MYPRC .NE. 0)  THEN
          TAG=100
          DEST=0
          CALL MPI_SEND(DUMP_COUNT_LOCAL
     +   , 1
     +   , MPI_INTEGER,DEST,TAG,MPI_COMM_WORLD,IERR)
        ELSEIF (MYPRC .EQ. 0)  THEN
              WRITE(DUMMY_STR,*) 1
              WRITE(DUMMY_STR2,*) NB_MAIN
              IERR=ACCUMULATELINE(ID_PHREEQC_STORE,
'DELETE; -CELLS '//
     +        TRIM(ADJUSTL(DUMMY_STR))//'-'//
TRIM(ADJUSTL(DUMMY_STR2)))
             IERR=ACCUMULATELINE(ID_PHREEQC_STORE,
'END')
              IF (RUNACCUMULATED(ID_PHREEQC_STORE) .NE.
0)
     +       CALL  EHANDLER(ID_PHREEQC_STORE)
          DUMP_COUNT(MYPRC) = DUMP_COUNT_LOCAL
          TAG=100
```

```
            DO I=1, NUMPRC-1
            SRC = I
            ALLOCATE(ITEMP1(1))
            ITEMP1(1) = 0
            CALL MPI_RECV(ITEMP1(1)
     +     , 1
     +     , MPI_INTEGER, SRC, TAG,
MPI_COMM_WORLD,ISTAT,IERR)
            DUMP_COUNT(I) = ITEMP1(1)
            DEALLOCATE(ITEMP1)
           END DO
          END IF
           CALL WAITALL()
            IF (MYPRC .NE. 0) THEN
             TAG =100
             DEST =0
             CALL MPI_SEND(
     +       DUMP_LINE(1:DUMP_COUNT_LOCAL)
     +     , DUMP_COUNT_LOCAL*80
     +       , MPI_CHARACTER,DEST,TAG,MPI_COMM_WORLD,IERR)
            ELSEIF (MYPRC .EQ. 0) THEN
            TAG =100
            DO J= NUMPRC-1, 1, -1
             SRC = J
             ALLOCATE(DUMP_LINE_TEMP(1:DUMP_COUNT(J)))
             CALL MPI_RECV(
     +      DUMP_LINE_TEMP(1:DUMP_COUNT(J))
     +     , DUMP_COUNT(J)*80
     +     , MPI_CHARACTER, SRC, TAG,
MPI_COMM_WORLD,ISTAT,IERR)
            DO I=1, DUMP_COUNT(J)

IERR=ACCUMULATELINE(ID_PHREEQC_STORE,TRIM(DUMP_LINE_TEMP(I)
))
            END DO
            DEALLOCATE(DUMP_LINE_TEMP)
              DO I=1, NUMBER_GRIDS(J)
               WRITE(DUMMY_STR,*) I
               WRITE(DUMMY_STR2,*) START_GRID(J) + I - 1
               IERR=ACCUMULATELINE(ID_PHREEQC_STORE, 'COPY
CELL '//
     +         TRIM(ADJUSTL(DUMMY_STR)) // '
'//TRIM(ADJUSTL(DUMMY_STR2)))
```

```
            END DO
           IERR=ACCUMULATELINE(ID_PHREEQC_STORE, 'END')
            DO I=1, NUMBER_GRIDS(J)
             WRITE(DUMMY_STR,*) I
             IERR=ACCUMULATELINE(ID_PHREEQC_STORE, 'DELETE;
-CELLS '//
     +       TRIM(ADJUSTL(DUMMY_STR)))
            END DO
            IERR=ACCUMULATELINE(ID_PHREEQC_STORE, 'END')
             IF (RUNACCUMULATED(ID_PHREEQC_STORE) .NE. 0)
     +      CALL  EHANDLER(ID_PHREEQC_STORE)
          END DO ! FOR J
CC ACCUMULATE CELLS OF THE MASTER PROCESSOR
          DO I=1, DUMP_COUNT(0)

IERR=ACCUMULATELINE(ID_PHREEQC_STORE,TRIM(DUMP_LINE(I)))
          END DO
C--

CC ACCUMULATE THE INJECTION SOLUTIONS

        IERR = SETDUMPSTRINGON(ID_PHREEQC_INJECTION,.TRUE.)
        IERR = ACCUMULATELINE(ID_PHREEQC_INJECTION, 'DUMP;
-ALL;  END ')
        IF (RUNACCUMULATED(ID_PHREEQC_INJECTION) .NE. 0)
CALL
     +    EHANDLER(ID_PHREEQC_INJECTION)
        DUMP_COUNT_LOCAL =
GETDUMPSTRINGLINECOUNT(ID_PHREEQC_INJECTION)
         ALLOCATE(DUMP_LINE_INJ(1:DUMP_COUNT_LOCAL))

       DO J=1, DUMP_COUNT_LOCAL
       CALL
GETDUMPSTRINGLINE(ID_PHREEQC_INJECTION,J,DUMP_LINE_INJ(J))
       END DO

          DO I=1, DUMP_COUNT_LOCAL

IERR=ACCUMULATELINE(ID_PHREEQC_STORE,TRIM(DUMP_LINE_INJ(I))
)
          END DO
         IERR =
SETDUMPSTRINGON(ID_PHREEQC_INJECTION,.FALSE.)
```

```
         IF (RUNACCUMULATED(ID_PHREEQC_INJECTION) .NE. 0)
CALL
     +     EHANDLER(ID_PHREEQC_INJECTION)
          DEALLOCATE(DUMP_LINE_INJ)
CC --

          IERR=ACCUMULATELINE(ID_PHREEQC_STORE, 'DUMP;-FILE
     +      TESTGC.STO ; -ALL;  END ')
         IERR = SETDUMPFILEON(ID_PHREEQC_STORE,.TRUE.)
         IF (RUNACCUMULATED(ID_PHREEQC_STORE) .NE. 0) CALL
     +     EHANDLER(ID_PHREEQC_STORE)
         IERR= SETDUMPFILEON(ID_PHREEQC_STORE,.FALSE.)
         IF (RUNACCUMULATED(ID_PHREEQC_STORE) .NE. 0) CALL
     +     EHANDLER(ID_PHREEQC_STORE)
          END IF !  FOR "IF (MYPRC .EQ. 0) THEN"
         CALL WAITALL()
          IERR = SETDUMPSTRINGON(ID_PHREEQC,.FALSE.)
         IF (RUNACCUMULATED(ID_PHREEQC) .NE. 0) CALL
     +     EHANDLER(ID_PHREEQC)
          IF (MYPRC .EQ. 0) IGCSTORE = .TRUE.
          IF (ALLOCATED(DUMP_COUNT)) DEALLOCATE(DUMP_COUNT)
          IF (ALLOCATED(DUMP_LINE)) DEALLOCATE(DUMP_LINE)
       END IF  ! FOR "IF ((MOD(ICNT,NSTSKIP) .EQ. 0) .AND.
ISTORE .EQ. 1) THEN"

       CALL WAITALL()
CC -- END FOR WRITING TESTCG.STO FILE
CC -- END OF KAZEMI NIA KORRANI, MAY 2014
```

Appendix H: UTCHEM-IPhreeqc Input Files for the ACP Coreflood Presented in Chapter 5

To run UTCHEM-IPhreeqc five input files are required (INPUT, HEAD, GCINPUT.DAT, IPhreeqc_Database.DAT, and IPhreeqc_INPUT.DAT). These files are presented below.

H.1 HEAD

```
UTEXAS
NX      NY     NZ     N      NWELL
1       1      100     20     2
NTW        NTA
0          0
NO         NPHAS
0          3
NSUB       MSUB
0          0
```

H.2 INPUT

```
CC*********************************************************************
CC                                                                     *
CC BRIEF DESCRIPTION OF DATA SET : UTCHEM-IPhreeqc (VERSION 2014)      *
CC                                                                     *
CC*********************************************************************
CC                                                                     *
CC  ACP FLOODING                                                     *
CC                                                                     *
CC  LENGTH (FT) :                        PROCESS : A/C/P FLOODING     *
CC  THICKNESS (FT) :                      INJ. PRESSURE (PSI) :       *
CC  WIDTH (FT) :                     COORDINATES : CARTESIAN    *
CC  POROSITY :                                                         *
CC  GRID BLOCKS :                                                      *
CC  DATE :                                                             *
CC                                                                     *
CC*********************************************************************
CC
CC*********************************************************************
CC                                                                     *
CC    RESERVOIR DESCRIPTION                                            *
CC                                                                     *
CC*********************************************************************
CC
CC
*----RUNNO

CC
```

```
CC
*----HEADER
PCN
EXPERIMENT
************************************************************
CC
CC SIMULATION FLAGS
*---- IMODE IMES IDISPC ICWM ICAP IREACT IBIO ICOORD ITREAC ITC IGAS
IENG  IPHREEQC
        1   4    0      0    0     3      0    1     0      0    0   0
1
CC
CC NUMBER OF GRID BLOCKS AND FLAG SPECIFIES CONSTANT OR VARIABLE GRID
SIZE
*----NX   NY  NZ  IDXYZ  IUNIT
     1    1   100   0       0
CC
CC  CONSTANT GRID BLOCK SIZE IN X, Y, AND Z
*----DX        DY         DZ
     0.145489216    0.145489216      0.00971129
CC
CC TOTAL NO. OF COMPONENTS, NO. OF TRACERS, NO. OF GEL COMPONENTS
*----N   NO NTW NTA  NG  NOTH
     8    0  0   0    0    0
CC
CC
*---- SPNAME(I),I=1,N
WATER
OIL
SURFACTANT
POLYMER
ANION
CALCIUM
ALC1
ALC2
CC
CC FLAG INDICATING IF THE COMPONENT IS INCLUDED IN CALCULATIONS OR NOT
*----ICF(KC) FOR KC=1,N
     1  1  1  1  1  1   0  0
CC
CC*****************************************************************
CC                                                                 *
CC    OUTPUT OPTIONS                                               *
CC                                                                 *
CC*****************************************************************
CC
CC
CC  FLAG FOR PV OR DAYS FOR OUTPUT AND STOP THE RUN
*----ICUMTM  ISTOP   IOUTGMS  IS3G
        1         1    0       0
CC
```

```
CC FLAG INDICATING IF THE PROFILE OF KCTH COMPONENT SHOULD BE WRITTEN
*----IPRFLG(KC),KC=1,N
     1  1  1  1  1  1  0  0
CC
CC FLAG FOR PRES,SAT.,TOTAL CONC.,TRACER CONC.,CAP.,GEL, ALKALINE
PROFILES
*----IPPRES IPSAT IPCTOT IPBIO IPCAP IPGEL IPALK ITEMP    IPOBS
      1      1      1      0      0     0    1      0        0
CC
CC FLAG FOR WRITING SEVERAL PROPERTIES
*----ICKL IVIS IPER ICNM  ICSE IFOAM IHYST  INONEQ
      1     1    1    1    1    0     0       0
CC
CC FLAG FOR WRITING SEVERAL PROPERTIES TO PROF
*----IADS  IVEL IRKF IPHSE
      1     0    1    1
CC
CC*********************************************************************
CC                                                                     *
CC    RESERVOIR PROPERTIES                                             *
CC                                                                     *
CC*********************************************************************
CC
CC
CC MAX. SIMULATION TIME ( PV)
*---- TMAX
      1.9
CC
CC ROCK COMPRESSIBILITY (1/PSI), STAND. PRESSURE(PSIA)
*----COMPR   PSTAND
      0.      0.
CC
CC FLAGS INDICATING CONSTANT OR VARIABLE POROSITY, X,Y,AND Z
PERMEABILITY
*----IPOR1 IPERMX IPERMY IPERMZ  IMOD   ITRANZ  INTG
       0      0     3      3      0       0      0
CC
CC CONSTANT POROSITY
*----PORC1
     .21
CC
CC CONSTANT X-PERMEABILITY (MILIDARCY) FOR LAYER K = 1,NZ
*----PERMX
      2507
CC
CC Y DIRECTION PERMEABILITY IS DEPENDENT ON X DIRECTION PERMEABILITY
*---- CONSTANT PERMEABILITY MULTIPLIER FOR Y DIRECTION PERMEABILITY
        1
CC
CC Z DIRECTION PERMEABILITY IS DEPENDENT ON X DIRECTION PERMEABILITY
*---- CONSTANT PERMEABILITY MULTIPLIER FOR Z DIRECTION PERMEABILITY
```

```
        1
CC
CC FLAG FOR CONSTANT OR VARIABLE DEPTH, PRESSURE, WATER SATURATION
*----IDEPTH  IPRESS  ISWI  ICWI
      0        0       0    -1
CC
CC CONSTANT DEPTH (FT)
*----D111
     0.
CC
CC INITIAL PRESSURE (PSIA)
*----PINIT   DEPTH
      14.7    0.0
CC
CC CONSTANT INITIAL WATER SATURATION (RESIDUAL OIL)
*----SWI
     0.565
CC
CC CONSTANT CHLORIDE AND CALCIUM CONCENTRATIONS (MEQ/ML)
*----C50       C60
    0.66296     0.0921
CC
CC*********************************************************************
CC                                                                     *
CC    PHYSICAL PROPERTY DATA                                           *
CC                                                                     *
CC*********************************************************************
CC
CC 3.4.1 OIL CONC. AT PLAIT POINT FOR TYPE II(+)AND TYPE II(-), CMC
CC                     CMC
*---- C2PLC  C2PRC   EPSME   IHAND
        0      1     0.001     0
CC
CC 3.4.2 FLAG INDICATING TYPE OF PHASE BEHAVIOR PARAMETERS
*---- IFGHBN=0 FOR INPUT HEIGHT OF BINODAL CURVE; =1 FOR INPUT SOL.
RATIO
        0
CC 3.4.3 SLOPE AND INTERCEPT OF BINODAL CURVE AT ZERO, OPT., AND 2XOPT
SALINITY
CC FOR ALCOHOL 1
*---- HBNS70   HBNC70   HBNS71   HBNC71   HBNS72   HBNC72
        0      0.15       0       0.13     0        0.15
CC 3.4.5 SLOPE AND INTERCEPT OF BINODAL CURVE AT ZERO, OPT., AND 2XOPT
SALINITY
CC FOR ALCOHOL 2
*---- HBNS80  HBNC80  HBNS81  HBNC81  HBNS82  HBNC82
        0       0       0       0       0       0
CC
CC 3.4.6 LOWER AND UPPER EFFECTIVE SALINITY FOR ALCOHOL 1 AND ALCOHOL 2
*---- CSEL7   CSEU7   CSEL8   CSEU8
      0.1415    0.2264     0       0
```

```
CC 3.4.7 THE CSE SLOPE PARAMETER FOR CALCIUM AND ALCOHOL 1 AND ALCOHOL
2
CC    CA     ALCOHOL#1  ALCOHOL#2
*---- BETA6    BETA7    BETA8
        0        0       0
CC
CC 3.4.8 FLAG FOR ALCOHOL PART. MODEL AND PARTITION COEFFICIENTS
*---- IALC   OPSK7O   OPSK7S   OPSK8O   OPSK8S
        0      0        0        0        0
CC  THESE ARE USED ONLY FOR ALCOHOL PARTITIONING IN A TWO ALCOHOL
SYSTEM:
CC 3.4.9 NO. OF ITERATIONS, AND TOLERANCE
*---- NALMAX     EPSALC
        20       0.0001
CC 3.4.10 ALCOHOL 1 PARTITIONING PARAMETERS IF IALC=1
CC   AQ-OLEIC   AQ-OLEIC  SURF-OLEIC
*---- AKWC7     AKWS7     AKM7       AK7      PT7
       4.671    1.79       48       35.31    0.222
CC
CC 3.4.11 ALCOHOL 2 PARTITIONING PARAMETERS IF IALC=1
*---- AKWC8     AKWS8    AKM8    AK8     PT8
        0         0        0      0       0
CC
CC 3.4.22 IFT MODEL FLAG
*----  IFT=0 FOR HEALY&REED; =1 FOR CHUN HUH CORREL.
        1
CC 3.4.24 INTERFACIAL TENSION PARAMETERS
CC    TYP=.1-.35   TYP=5-20
*---- CHUH         AHUH
      0.3           10
CC 3.4.25 LOG10 OF OIL/WATER INTERFACIAL TENSION
CC     UNITS OF LOG 10 DYNES/CM = MN/M
*---- XIFTW
       1.3
CC 3.4.26 ORGANIC MASS TRANSFER FLAG
CC    IMASS=0 FOR NO OIL SOL. IN WATER.  ICORR=0 FOR CONSTANT MTC
*---- IMASS   ICOR
        0       0
CC
CC
*---  IWALT   IWALF
       0       0
CC 3.4.31 CAPILLARY DESATURATION PARAMETERS FOR PHASE 1, 2, AND 3
CC                AQ     OLEIC     ME
*---- ITRAP      T11      T22      T33
        2        1865    59074    364.2
CC
CC  3.4.32 FLAG FOR RELATIVE PERMEABILITY AND CAPILLARY PRESSURE MODEL
*---- IPERM=0 FOR CONSTANT; =1 VARIES BY LAYER; =2 VARIES BY GRIDBLOCK
        0      0
CC
```

```
CC 3.4.35 FLAG FOR CONSTANT OR VARIABLE REL. PERM. PARAMETERS
*---- ISRW    IPRW    IEW
        0       0       0
CC
CC CONSTANT RES. SATURATION OF PHASES 1,2,AND 3 AT LOW CAPILLARY NO.
*----S1RWC  S2RWC  S3RWC
      .19     .443    .17
CC
CC CONSTANT ENDPOINT REL. PERM. OF PHASES 1,2,AND 3 AT LOW CAPILLARY
NO.
*----P1RW  P2RW  P3RW
      .07   0.95     .07
CC
CC CONSTANT REL. PERM. EXPONENT OF PHASES 1,2,AND 3 AT LOW CAPILLARY
NO.
*----E1W   E2W   E3W
     5.6     1.55   3.0
CC
CC  RES. SATURATION OF PHASES 1,2,AND 3 AT HIGH CAPILLARY NO.
*----S1RC  S2RC  S3RC
     .0    .0    .0
CC
CC ENDPOINT REL. PERM. OF PHASES 1,2,AND 3 AT HIGH CAPILLARY NO.
*----P1RC    P2RC  P3RC
     1.0     1.0   1.0
CC
CC REL. PERM. EXPONENT OF PHASES 1,2,AND 3 AT HIGH CAPILLARY NO.
*----E13CW  E23C  E31C
     1.0     1.0   1.0
CC 3.4.61 WATER AND OIL VISCOSITY , RESERVOIR TEMPERATURE
CC   WATER     OIL       =0 FOR ISOTHERMAL MODELING
*---- VIS1     VIS2   TSTAND
       0.534     170    100.4
CC
CC 3.4.80 COMPOSITIONAL PHASE VISCOSITY PARAMETERS FOR MICROEMULSION
*----   ALPHAV1   ALPHAV2   ALPHAV3   ALPHAV4  ALPHAV5
         0.1       5.0       0.1        0.0      0.0
CC
CC 3.4.81 PARAMETERS TO CALCULATE POLYMER VISCOSITY AT ZERO SHEAR RATE
*---- AP1      AP2      AP3 47.9     346      638
      230      280       1500
CC
CC 3.4.82 PARAMETER TO COMPUTE CSEP,MIN. CSEP, AND SLOPE OF LOG VIS.
VS. LOG CSEP
*---- BETAP    CSE1     SSLOPE
       1      0.01      -0.4435
CC
CC 3.4.83 PARAMETER FOR SHEAR RATE DEPENDENCE OF POLYMER VISCOSITY
*---- GAMMAC   GAMHF  POWN   IPMOD  ISHEAR  RWEFF  GAMHF2
       4        10.0    2.3    0      0       0.25    0.0
CC
```

```
CC 3.4.84  FLAG FOR POLYMER PARTITIONING, PERM. REDUCTION PARAMETERS
*---- IPOLYM    EPHI3    EPHI4    BRK     CRK     RKCUT
        1       1.0      0.93     100      0      10
CC 3.4.85 SPECIFIC WEIGHT FOR COMPONENTS 1,2,3,7,8 ,COEFFIENT OF OIL
AND GRAVITY FLAG
CC   IF IDEN=1 IGNORE GRAVITY EFFECT; =2 THEN INCLUDE GRAVITY EFFECT
*---- DEN1     DEN2      DEN23     DEN3      DEN7    DEN8    IDEN
      0.44     0.40689   0.40689     0.42     0.346    0        2
CC   ISTB=0:BOTTOMHOLE CONDITION , 1: STOCK TANK
CC 3.4.93 FLAG FOR CHOICE OF UNITS WHEN PRINTING
*----- ISTB
        0
CC
CC 3.4.95 COMPRESSIBILITY FOR VOL. OCCUPYING COMPONENTS 1,2,3,7,AND 8
*----   COMPC(1)          COMPC(2)     COMPC(3)  COMPC(7)  COMPC(8)
         0.0000033 0.0000234 0 0 0
CC  IOW=0 WATER WET, =1 OIL WET, =2 MIXED WET
CC 3.4.99 CONSTANT OR VARIABLE PC PARAM., WATER-WET OR OIL-WET PC CURVE
FLAG
*---- ICPC    IEPC   IOW
       0       0      0
CC
CC 3.4.100 CAPILLARY PRESSURE PARAMETER, CPC0
*---- CPC0
       0
CC
CC 3.4.103 CAPILLARY PRESSURE PARAMETER, EPC0
*---- EPC0
       0
CC
CC 3.4.117 MOLECULAR DIFFUSION COEF. KCTH COMPONENT IN PHASE 1
*---- D(KC,1),KC=1,N
         0        0        0        0        0        0         0
0        0        0        0        0
CC
CC 3.4.118 MOLECULAR DIFFUSION COEF. KCTH COMPONENT IN PHASE 2
*---- D(KC,2),KC=1,N
         0        0        0        0        0        0         0
0        0        0        0        0
CC
CC 3.4.119 MOLECULAR DIFFUSION COEF. KCTH COMPONENT IN PHASE 3
*---- D(KC,3),KC=1,N
         0        0        0        0        0        0         0
0        0        0        0        0
CC
CC 3.4.121 LONGITUDINAL AND TRANSVERSE DISPERSIVITY OF PHASE 1
*---- ALPHAL(1)     ALPHAT(1)
         0.005           0.001
CC
CC 3.4.122 LONGITUDINAL AND TRANSVERSE DISPERSIVITY OF PHASE 2
*---- ALPHAL(2)     ALPHAT(2)
```

```
         0.005           0.001
CC
CC 3.4.124 LONGITUDINAL AND TRANSVERSE DISPERSIVITY OF PHASE 3
*---- ALPHAL(3)     ALPHAT(3)
         0.005          0.001
CC
CC 3.4.125 FLAG TO SPECIFY ORGANIC ADSORPTION CALCULATION
*---- IADSO=0 IF ORGANIC ADSORPTION IS NOT CONSIDERED
        0
CC
CC 3.4.130 SURFACTANT AND POLYMER ADSORPTION PARAMETERS
*---- AD31    AD32   B3D      AD41    AD42   B4D   IADK  IADS1   FADS
REFK
      1.6     0.1    1000      0.48    0.      100     0     0      0
50
CC
CC*********************************************************************
CC                                                                     *
CC    WELL DATA                                                        *
CC                                                                     *
CC*********************************************************************
CC
CC
CC FLAG FOR PRESSURE CONST. BOUNDARIES
*---- IBOUND  IZONE
       0     0
CC
CC TOTAL NUMBER OF WELLS, WELL RADIUS FLAG, FLAG FOR TIME OR COURANT
NO.
*----NWELL   IRO   ITIME  NWREL
      2      2      0      2
CC
CC WELL ID,LOCATIONS,AND FLAG FOR SPECIFYING WELL TYPE, WELL RADIUS,
SKIN
*----IDW   IW    JW    IFLAG    RW     SWELL  IDIR   IFIRST  ILAST
IPRF
      1    1      1      1    .003       0.     3     100     100    0
CC
CC WELL NAME
*---- WELNAM
INJECTOR
CC
CC ICHEK MAX. AND MIN. ALLOWABLE BOTTOMHOLE PRESSURE AND RATE
*----ICHEK   PWFMIN   PWFMAX  QTMIN   QTMAX
      0     0.0     5000.   0.0     50000.
CC
CC WELL ID, LOCATION, AND FLAG FOR SPECIFYING WELL TYPE, WELL RADIUS,
SKIN
*----IDW  IW   JW   IFLAG    RW     SWELL  IDIR  IFIRST   ILAST    IPRF
     2    1     1     2       .003     0.      3     1       1       0
CC
```

```
CC WELL NAME
*---- WELNAM
PRODUCER
CC
CC MAX. AND MIN. ALLOWABLE BOTTOMHOLE PRESSURE AND RATE
*----ICHEK  PWFMIN   PWFMAX  QTMIN   QTMAX
      0     0.0     5000.   0.0     50000.
CC
CC ID,INJ. RATE AND INJ. COMP. FOR RATE CONS. WELLS FOR EACH PHASE
(L=1,3)
*----ID  QI(M,L)  C(M,KC,L)  2.75 WT% SODIUM CARBONATE, 1.3 FT/D  CL
CA
       1     0.004445094  0.985  0.   0.015   0.275     0.0132   0.
0.    0.
       1       0.    0.    0.   0.     0.      0.      0.    0.    0.
       1       0.    0.    0.   0.     0.      0.      0.    0.    0.
CC
CC
*---- INJ_SOLUTION
          101
CC
CC ID,
*----ID   PWF
     2    14.7
CC
CC CUM. INJ. TIME , AND INTERVALS (PV OR DAY) FOR WRITING TO OUTPUT
FILES
*----TINJ    CUMPR1   CUMHI1     WRHPV   WRPRF      RSTC
     0.5       0.03      0.03       0.03    0.03      0.3
CC
CC FOR IMES=2 ,THE INI. TIME STEP,CONC. TOLERANCE,MAX.,MIN. COURANT NO.
*----DT      DCLIM     CNMAX   CNMIN
     0.0001   17*0.01     0.01     0.001
CC******     INJECT NO SURFACTANT ********************
CC FLAG FOR INDICATING BOUNDARY CHANGE
*---- IBMOD
        0
CC
CC  IRO, ITIME, NEW FLAGS FOR ALL THE WELLS
*----  IRO    ITIME     IFLAG
        2       0        1  2
CC
CC  NUMBER OF WELLS CHANGES IN LOCATION OR SKIN OR PWF
*----  NWEL1
         0
CC
CC  NUMBER OF WELLS WITH RATE CHANGES, ID
*---- NWEL2     ID
        1        1
CC
```

```
CC  ID,INJ. RATE AND INJ. COMP. FOR RATE CONS. WELLS FOR EACH PHASE
(L=1,3)
*----  ID     QI(M,L) WATER OIL  SURF POLYMER CHLOR DIVALENT  CL
CA
       1    0.004445094  1.0   0.   0.0    0.225      0.0132     0.
0.    0.
       1       0.    0.    0.   0.     0.       0.      0.     0.    0.
       1       0.    0.    0.   0.     0.       0.      0.     0.    0.
CC
CC
*--- INJ_SOLUTION
        102
CC
CC  CUM. INJ. TIME , AND INTERVALS (PV) FOR WRITING TO OUTPUT FILES
*---- TINJ      CUMPR1    CUMHI1     WRHPV   WRPRF       RSTC
      1.9       0.01      0.03       0.03    0.03        2.0
CC
CC  FOR IMES=4 ,THE INI. TIME STEP,CONC. TOLERANCE,MAX.,MIN. TIME STEPS
*----  DT            DCLIM       CNMAX      CNMIN
        0.0001       17*0.01      0.01         0.001
```

H.3 GCINPUT.DAT

```
CC
CC*******************************************************
CC                                                      *
CC             GEOCHEMISTRY SECTION                     *
CC                                                      *
CC*******************************************************
CC
CC
*---- IRSPS   IPHAD  EQW(Equivalent weight of surfactant)
        2      1     804
CC
CC
*--- PHC PHT PHT1 HPHAD(The constant by which the surfactant adsorption
is reduced)
      7   13  13   0.1
CC
CC
*---- CSELP(meq/ml) CSEUP(meq/ml)
         0.2          0.33
CC
CC
*-----IMIX
        0
CC
CC
*------HBN0 HBN1 HBN2
    0.3    0.2  0.3
CC
CC
```

```
*----    AW_MW        EQWPS      Log(Kp) (HAo=HAw)      Log(Kd) (HAw= H+ +
Aw-)
        59.05        600.0         -4.142173494                -8.0
CC
CC*******************************************************
CC                                                       *
CC              GEOCHEMISTRY OUTPUT  SECTION             *
CC                                                       *
CC*******************************************************
CC
CC
*---- PRINT_NUMBER_ELEMENT   ELEMENT_HISTORY   ELEMENT_MAP
FREQUENCY_HIS(TIME STEP)  FREQUENCY_MAP(TIME STEP)
             0                    0                 1
100                       100
CC
CC
*---- NSLDP  SOLID_HISTORY   SOLID_MAP    FREQUENCY_HIS (TIME STEP)
FREQUENCY_MAP(TIME STEP)
       0      1                 1                   1           1
CC
CC
*----  NAQSP   AQS_HISTORY   AQS_MAP    FREQUENCY_HIS(TIME STEP)
FREQUENCY_MAP(TIME STEP)
        0         0             1                   1
1
CC
CC
*---- NSORBP  SORBED_HISTORY   ELEMENT_MAP    FREQUENCY_HIS (TIME STEP)
FREQUENCY_MAP (TIME STEP)
        0          1                 1                  1
1
CC
CC
*---- NPRINTG    PRINTG_HISTORY   PRINTG_MAP    FREQUENCY_HIS (TIME
STEP)  FREQUENCY_MAP(TIME STEP)
        0              0              1                     100000
1
```

H.4 IPHREEQC_DATABASE.DAT

The thermodynamic database used in this case is phreeqc.dat. This database is presented in Appendix E (i.e., Section E.1.4).

H.5 IPHREEQC_INPUT.DAT

```
## GRIDBLOCK INITIALIZATION
SOLUTION 1-100
 -water       1.0
 -units   ppm
```

```
-pH      7.51

K        11.59
Na       300.00
Mg       0.0
Ca       0.0
Cl       140.81
S(6)     310.41
C(4)     176.95
Aw       2879.886276  ## ACID COMPONENT CONCENTRATION

END

EXCHANGE 1-100
        X    0.001302982
        -equilibrate 1
END

##  INJECTION SOLUTIONS

SOLUTION 101   ##   ACP FLOOD
   -water  1.0  ## kg
   -units   ppm
    -pH   7 charge
K        11.59
Na       2903.773585
Mg       0.0
Ca       0.0
Cl       140.81
S(6)     310.41
C(4)    3573.176415

END

SOLUTION 102   ##   POLYMER FLOOD
-water  1.0  ## kg
-units   ppm
-pH       7.51
K        11.59
Na       300.00
Mg       0.0
Ca       0.0
Cl       140.81
S(6)     310.41
C(4)     176.95
END
```

References

Abate, J., Wang, P., and Sepehrnoori, K. 2001. Parallel compositional reservoir simulation on clusters of PCs. International Journal of High Performance Computing Applications, 15(1), 13-21. doi: 10.1177/109434200101500102.

Aksulu, H., Håmsø, D., Strand, S., Puntervold, T., and Austad, T. 2012. Evaluation of low-salinity enhanced oil recovery effects in sandstone: effects of the temperature and pH gradient. Energy & Fuels, 26(6), 3497-3503.

Al Harrasi, A., Al-maamari Rashid Salim, and Masalmeh, S. K. 2012. Laboratory Investigation of Low Salinity Waterflooding for Carbonate Reservoirs. Abu Dhabi International Petroleum Conference and Exhibition. Abu Dhabi, UAE. 11-14 November. doi:10.2118/161468-MS.

Aladasani Ahmad, Bai, B., and Wu, Y.-S. 2012. Investigating Low Salinity Waterflooding Recovery Mechanisms in Carbonate Reservoirs. SPE EOR Conference at Oil and Gas West Asia. Muscat, Oman. 16-18 April. doi:10.2118/155560-MS.

Al-Attar, H. H., Mahmoud, M. Y., Zekri, A. Y., Almehaideb, R. A. and Ghannam, M. T. 2013a. The Impact of LoSal on Oil Recovery from a Selected Carbonate Reservoir in Abu Dhabi-An Experimental Approach. SPE Middle East Oil and Gas Show and Conference, Manama, Bahrain. 10-13 March. http://dx.doi.org/10.2118/164331-MS.

Al-Attar, H. H., Mahmoud, M. Y., Zekri, A. Y., Almehaideb, R., and Ghannam, M. 2013b. Low-salinity flooding in a selected carbonate reservoir: experimental approach. Journal of Petroleum Exploration and Production Technology, 3(2), 139-149. doi: 0.1007/s13202-013-0052-3.

Alcalá, F. J., and Custodio, E. 2008. Using the Cl/Br ratio as a tracer to identify the origin of salinity in aquifers in Spain and Portugal. Journal of Hydrology, 359(1), 189-207. doi: 10.1016/j.jhydrol.2008.06.028.

Al-Hashim, H. S., Obiora, V., Al-Yousef, H. Y., Fernandez, F., and Nofal, W. 1996. Alkaline Surfactant Polymer Formulation for Saudi Arabian Carbonate Reservoirs. SPE/DOE Improved Oil Recovery Symposium, Tulsa, Oklahoma, 21-24 April. http://dx.doi.org/10.2118/35353-MS.

Alotaibi, M. B., Azmy, R., and Nasr-El-Din, H. A. 2010. Wettability Challenges in Carbonate Reservoirs. SPE Improved Oil Recovery Symposium. Tulsa, Oklahoma, USA. 24-28 April. doi:10.2118/129972-MS.

Al-Shalabi, E. W., Sepehrnoori, K., and Delshad, M. 2014a. Mechanisms behind low salinity water injection in carbonate reservoirs. Fuel, 121, 11-19.

Al-Shalabi, E. W., Sepehrnoori, K., and Pope, G. 2014b. Geochemical Interpretation of Low Salinity Water Injection in Carbonate Oil Reservoirs. SPE Improved Oil Recovery Symposium. Tulsa, Oklahoma, USA. 12-16 April. doi:10.2118/169101-MS.

Alwi, N., Salleh, I.K., Irevine-Fortescue, J., Graham, G., Dyer, S., Wright, R., Simpson, C., Kidd, S., and Stalker, R. 2013. Scale and Scale Inhibition Challenges for an Alkaline Surfactant Polymer Flood in a Seawater Flooded Reservoir. SPE: Society of Petroleum Engineers. doi:10.2118/164058-MS.

Andersen, P. Ø., Evje, S., Madland, M. V., and Hiorth, A. 2012a. A geochemical model for interpretation of chalk core flooding experiments. Chemical engineering science, 84, 218-241. doi: 10.1016/j.ces.2012.08.038.

Andersen, P. Ř., and Evje, S. 2012b. A Mathematical Model for Interpretation of Brine-Dependent Spontaneous Imbibition Experiments. In ECMOR XIII-13th European Conference on the Mathematics of Oil Recovery.

Anderson, A. G. 2006. Simulation of Chemical Flood Enhanced Oil Recovery Processes Including the Effects of Reservoir Wettability. MS Thesis, The University of Texas at Austin, Austin, Texas (May 2006).

Appelo, C. A. J., and Rolle, M. 2010. PHT3D: A reactive multicomponent transport model for saturated porous media. Groundwater, 48(5), 627-632. doi: 10.1111/j.1745-6584.2010.00732.x.

Austad, T., RezaeiDoust, A., and Puntervold, T. 2010. Chemical Mechanism of Low Salinity Water Flooding in Sandstone Reservoirs. SPE: Society of Petroleum Engineers. doi:10.2118/129767-MS.

Austad, T., Shariatpanahi, S. F., Strand, S., Black, C. J. J., and Webb, K. J. 2011. Conditions for a low-salinity enhanced oil recovery (EOR) effect in carbonate oil reservoirs. Energy & fuels, 26(1), 569-575. doi: 10.1021/ef201435g.

Austad, T., Strand, S., Høgnesen, E. J., and Zhang, P. 2005. Seawater as IOR fluid in fractured chalk. SPE International Symposium on Oilfield Chemistry. The Woodlands, Texas. 2-4 February. http://dx.doi.org/10.2118/93000-MS.

Austad, T., Strand, S., Madland, M. V., Puntervold, T., and Korsnes, R. I. 2008. Seawater in chalk: An EOR and compaction fluid. SPE Reservoir Evaluation & Engineering, 11(04), 648-654. doi: http://dx.doi.org/10.2118/118431-PA.

Bagci, S., Kok, M. V., and Turksoy, U. 2001. Effect of brine composition on oil recovery by waterflooding. Petroleum science and technology, 19(3-4), 359-372. doi: 10.1081/LFT-100000769.

Barney, B. 2009. Message passing interface (mpi). Lawrence Livermore National Laboratory, https://computing. llnl. gov/tutorials/mpi/, available online, 2010.

Barrodale, I., and Roberts, F. D. K. 1980. Algorithm 552: Solution of the Constrained I 1 Linear Approximation Problem [F4]. ACM Transactions on Mathematical Software (TOMS), 6(2), 231-235. doi:10.1145/355887.355896.

Bear, J. 2013. *Dynamics of fluids in porous media*. Courier Dover Publications.

Bedrikovetsky, P. G., Siqueira, F. D., Furtado, C. J. A., and Serra de Souza, A. L. 2010. Quantitative Theory for Fines Migration and Formation Damage. SPE: Society of Petroleum Engineers. doi:10.2118/128384-MS.

Bhuyan, D. 1989. Development of an Alkaline/Surfactant/Polymer Compositional Reservoir Simulator. PhD dissertation, The University of Texas at Austin, Austin, Texas (December 1989).

Borkovec, M., and Westall, J. 1983. Solution of the Poisson-Boltzmann equation for surface excesses of ions in the diffuse layer at the oxide-electrolyte interface. Journal of Electroanalytical Chemistry and Interfacial Electrochemistry, 150(1), 325-337. DOI: 10.1016/S0022-0728(83)80214-9.

Brady, P. V., and Krumhansl, J. L. 2012. A surface complexation model of oil–brine–sandstone interfaces at 100° C: Low salinity waterflooding. *Journal of Petroleum Science and Engineering*, *81*, 171–176.

Brown, J. 2010. The Portable Extensible Toolkit for Scientific computing.

Buckley, S. E., and Leverett, M. C. 1941. Mechanism of fluid displacement in sands. Trans. Aime, 146.

Callegaro, C., Bartosek, M., Masserano, F., Nobili, M., Parasiliti Parracello, V. P., Pizzinelli, C. S., and Caschili, A. 2013. Opportunity of Enhanced Oil Recovery Low Salinity Water Injection: From Experimental Work to Simulation Study up to Field Proposal. SPE: Society of Petroleum Engineers. doi:10.2118/164827-MS.

Cantucci, B., Montegrossi, G., Vaselli, O., Tassi, F., Quattrocchi, F., and Perkins, E. H. 2009. Geochemical modeling of CO2 storage in deep reservoirs: The Weyburn Project (Canada) case study. *Chemical Geology*, *265*(1), 181–197.

Carman, P. C. 1956. Flow of gases through porous media. Butterworths Scientific Publications London.

Cartwright, I., Weaver, T. R., and Fifield, L. K. 2006. Cl/Br ratios and environmental isotopes as indicators of recharge variability and groundwater flow: an example from the southeast Murray Basin, Australia. Chemical Geology, 231(1), 38-56. doi: 10.1016/j.chemgeo.2005.12.009.

Chadam, J., Hoff, D., Merino, E., Ortoleva, P., and Sen, A. 1986. Reactive infiltration instabilities. *IMA Journal of Applied Mathematics*, *36*(3), 207–221.

Chandrasekhar, S. 2013. Wettability alteration with brine composition in high temperature carbonate reservoirs. MS Thesis. The University of Texas at Austin, Austin, Texas (August 2013).

Chandrasekhar, S., and Mohanty, K. K. 2013. Wettability Alteration with Brine Composition in High Temperature Carbonate Reservoirs. SPE Annual Technical Conference and Exhibition. New Orleans, Louisiana, USA. 30 September-2 October. doi:10.2118/166280-MS.

Chang, Y. B. 1990. Development and application of an equation of state compositional simulator. PhD dissertation. Austin, Texas, University of Texas at Austin (August 1990).

Charlton, S. R., and Parkhurst, D. L. 2011. Modules based on the geochemical model PHREEQC for use in scripting and programming languages. Computers & Geosciences, 37(10), 1653–1663. doi:10.1016/j.cageo.2011.02.005.

Chekani, M., and Mackay, E. J. 2006. Impact on Scale Management of the Engineered Depressurization of Waterflooded Reservoirs: Risk Assessment Principles and Case Study. *SPE-86472-PA*. doi:10.2118/86472-PA.

Cheng, L., Reme, A. B., Shan, D., Coombe, D. A., and Rossen, W. R. 2000. Simulating Foam Processes at High and Low Foam Qualities. SPE/DOE Improved Oil Recovery Symposium. Tulsa, Oklahoma. 3-5 April. doi:10.2118/59287-MS.

Chukwudeme, E. A., and Hamouda, A. A. 2009. Oil recovery from polar components (asphaltene and SA) treated chalk rocks by low salinity water and water containing SO_4^{-2} and Mg^{2+}at different temperatures. Colloids and Surfaces A: Physicochemical and Engineering Aspects, 336(1), 174-182. doi: 10.1016/j.colsurfa.2008.11.051.

Cissokho, M., Boussour, S., Cordier, P., Bertin, H., and Hamon, G. 2010. Low salinity oil recovery on clayey sandstone: Experimental study. *Petrophysics*, *51*(5), 305.

Civan, F. 2007. Formation Damage Mechanisms and Their Phenomenological Modeling-An Overview. SPE: Society of Petroleum Engineers. doi:10.2118/107857-MS.

Cohen, S.D., and Hindmarsh, A.C. 1996, CVODE, A stiff/nonstiff ODE solver in C. Computers in Physics.10(2). 138.

Collins, I. R., and Jordan, M. M. 2003. Occurrence, Prediction, and Prevention of Zinc Sulfide Scale Within Gulf Coast and North Sea High-Temperature and High-Salinity Fields. *SPE-84963-PA*. doi:10.2118/84963-PA.

Dang, C. T. Q., Nghiem, L. X., Chen, Z. J., and Nguyen, Q. P. 2013. Modeling Low Salinity Waterflooding: Ion Exchange, Geochemistry and Wettability Alteration. SPE: Society of Petroleum Engineers. doi:10.2118/166447-MS.

Darabi, H. 2014. Development of a Non-Isothermal Compositional Reservoir Simulator to Model Asphaltene Precipitation, Flocculation, and Deposition and Remediation. PhD dissertation. Austin, Texas, University of Texas at Austin. (May 2014).

Darabi, H., Sepehrnoori, K., and Kalaei, M. H. 2012. Modeling of Wettability Alteration Due to Asphaltene Deposition in Oil Reservoirs. SPE: Society of Petroleum Engineers. doi:10.2118/159554-MS.

Davies, C. W. 1962. Ion association (p. 190). London: Butterworths.

Davis, J. A., and Kent, D. B. 1990. Surface complexation modeling in aqueous geochemistry. Reviews in Mineralogy and Geochemistry, 23(1), 177-260.

De Bruin BSc, W. J. 2012. Simulation of Geochemical Processes during Low Salinity Water Flooding by Coupling Multiphase Buckley-Leverett Flow to the

Geochemical Package PHREEQC. MS Thesis. Delft University of Technology. Delft, The Netherland (August 2012).

De Lucia, M., and Kühn, M. 2013. Coupling R and PHREEQC: an interactive and extensible environment for efficient programming of geochemical models. In *EGU General Assembly Conference Abstracts* Vol. 15, p. 9719.

Debye, P., and Huckel, E. 1954. Translated from Physikalische Zeitschrift, 24(q), 1923, pages 185-206. The Collected Papers of Peter JW Debye, 217.

Delshad, M., Han, C., Veedu, F., et al. 2013. A simplified model for simulations of alkaline–surfactant–polymer floods. Journal of Petroleum Science and Engineering, 108(0), 1–9. doi:10.1016/j.petrol.2013.04.006.

Delshad, M., Pope, G. A., and Sepehrnoori, K. 1996. A compositional simulator for modeling surfactant enhanced aquifer remediation, 1 formulation. Journal of Contaminant Hydrology, 23(4), 303–327. doi:10.1016/0169-7722(95)00106-9.

Demin, W., Zhenhua, Z., Jiecheng, C., Jingchun, Y., Shutang, G., and Li, L. 1997. Pilot Test of Alkaline Surfactant Polymer Flooding in Daqing Oil Field. SPE Reservoir Engineering 12(4): 229-233. SPE-36748-PA. http://dx.doi.org/10.2118/36748-PA.

Deutsch, W. J. 1997. Groundwater geochemistry: fundamentals and applications to contamination. CRC press.

deZabala, E. F., Vislocky, J. M., Rubin, E., and Radke, C. J. 1982. A Chemical Theory for Linear Alkaline Flooding. *SPE-8997-PA*. doi:10.2118/8997-PA.

Duan, Z., and Sun, R. 2003. An improved model calculating CO2 solubility in pure water and aqueous NaCl solutions from 273 to 533 K and from 0 to 2000 bar. *Chemical Geology*, *193*(3), 257–271.

Dzombak, D.A., and Morel, F.M.M.. 1990. Surface complexation modeling-Hydrous ferric oxide: New York, John Wiley.

Elakneswaran, Y., and Ishida, T. 2014. Development and Verification of an Integrated Physicochemical and Geochemical Modelling Framework for Performance Assessment of Cement-Based Materials. Journal of Advanced Concrete Technology, 12(4): 111-126. http://dx.doi.org/10.3151/jact.12.9.

Elmorsey, S. A. 2013. Challenge and Successful Application for Scale Removal Gemsa Oil Field, Egypt: Field Study. SPE: Society of Petroleum Engineers. doi:10.2118/164274-MS.

Emadi, A., and Sohrabi, M. 2013. Visual Investigation of Oil Recovery by Low Salinity Water Injection: Formation of Water Micro-Dispersions and Wettability Alteration. SPE: Society of Petroleum Engineers. doi:10.2118/166435-MS.

Fadairo, A. S., Omole, O., and Falode, O. 2008. Effect of Oilfield Scale Deposition on Mobility Ratio. SPE: Society of Petroleum Engineers. doi:10.2118/114488-MS.

Farajzadeh, R., Ameri, A., Faber, M. J., Van Batenburg, D. W., Boersma, D. M., and Bruining, J. 2013. Effect of Continuous, Trapped, and Flowing Gas on Performance of Alkaline Surfactant Polymer (ASP) Flooding. SPE Enhanced Oil Recovery Conference. Kuala Lumpur, Malaysia, 2-4 July. doi:10.2118/165238-MS.

Farajzadeh, R., Matsuura, T., van Batenburg, D., and Dijk, H. 2012. Detailed Modeling of the Alkali/Surfactant/Polymer (ASP) Process by Coupling a Multipurpose Reservoir Simulator to the Chemistry Package PHREEQC. SPE Reservoir Evaluation & Engineering. 15(4): 423-435. SPE-143671. http://dx.doi.org/10.2118/143671-PA.

Farooq, U., Asif, N., Tweheyo, M. T., Sjöblom, J., and Øye, G. 2011. Effect of low-saline aqueous solutions and pH on the desorption of crude oil fractions from silica surfaces. *Energy & Fuels*, *25*(5), 2058–2064.

Fathi, S. J., Austad, T., and Strand, S. 2012. Water-Based Enhanced Oil recovery (EOR) by "Smart Water" in Carbonate Reservoirs. SPE EOR Conference at Oil and Gas West Asia. Muscat, Oman. 16-18 April. doi:10.2118/154570-MS.

Fernø, M. A., Grønsdal, R., Åsheim, J., Nyheim, A., Berge, M., and Graue, A. 2011. Use of Sulfate for Water Based Enhanced Oil Recovery during Spontaneous Imbibition in Chalk. Energy & fuels, 25(4), 1697-1706. doi: 10.1021/ef200136w.

Fjelde, I., Asen, S. M., and Omekeh, A. V. 2012. Low Salinity Water Flooding Experiments and Interpretation by Simulations. SPE: Society of Petroleum Engineers. doi:10.2118/154142-MS.

Fortenberry, R. P. 2013. Experimental Demonstration and Improvement of Chemical EOR Techniques in Heavy Oils. MS Thesis, The University of Texas at Austin, Austin, Texas (May 2013).

Fortenberry, R. P., Kim, D. H., Nizamidin, N., Adkins, S., Pinnawala Arachchilage, G. W. P., Koh, H. S., Weerasooria, U., and Pope, G. A. 2013. Use of Co-Solvents to Improve Alkaline-Polymer Flooding. SPE Annual Technical Conference and

Exhibition, New Orleans, Louisiana, 30 September-2 October. http://dx.doi.org/10.2118/166478-MS.

Gamage, S., Hasanka, P., and Thyne, G. D. 2011. Comparison of oil recovery by low salinity waterflooding in secondary and tertiary recovery modes. In SPE Annual Technical Conference and Exhibition. Society of Petroleum Engineers.

Gao, S., Li, H., and Li, H. 1995. Laboratory Investigation of Combination of Alkaline-Surfactant-Polymer for Daqing EOR. SPE Reservoir Engineering. 10(3): 194-197. SPE-27631-PA. http://dx.doi.org/10.2118/27631-PA.

Ghasemi Doroh, M. 2012. Development and application of a parallel compositional reservoir simulator. MS Thesis, The University of Texas at Austin, Austin, Texas (August 2012).

Goudarzi, A., Delshad, M., and Sepehrnoori, K. 2013. A Critical Assessment of Several Reservoir Simulators for Modeling Chemical Enhanced Oil Recovery Processes. Society of Petroleum Engineers. doi:10.2118/163578-MS.

Goudarzi, A., Delshad, M., Mohanty, K. K., and Sepehrnoori, K. 2012. Impact of Matrix Block Size on Oil Recovery Response Using Surfactants in Fractured Carbonates. Society of Petroleum Engineers. doi:10.2118/160219-MS.

Green, D. W., and Willhite, G. P. 1998. Enhanced oil recovery. Richardson, Tex.: Henry L. Doherty Memorial Fund of AIME, Society of Petroleum Engineers.

Gupta, R., and Mohanty, K. K. 2011. Wettability alteration mechanism for oil recovery from fractured carbonate rocks. Transport in porous media, 87(2), 635-652. doi: 10.1007/s11242-010-9706-5.

Gupta, R., Smith, G. G., Hu, L., Willingham, T., Lo Cascio, M., Shyeh, J. J., and Harris, C. R. 2011. Enhanced Waterflood for Carbonate Reservoirs - Impact of Injection Water Composition. SPE Middle East Oil and Gas Show and Conference. Manama, Bahrain. 25-28 September. doi:10.2118/142668-MS.

Hadia, N., Lehne, H. H., Kumar, K. G., Selboe, K. A., Stensen, F. Å., and Torsater, O. 2011. Laboratory Investigation of Low Salinity Waterflooding on Reservoir Rock Samples from the Frøy Field. SPE: Society of Petroleum Engineers. doi:10.2118/141114-MS.

Hamouda, A. A., and Valderhaug, O. M. 2014. Investigating Enhanced Oil Recovery from Sandstone by Low-Salinity Water and Fluid/Rock Interaction. Energy & Fuels, 28(2), 898-908.

Hamouda, A. A., Karoussi, O., and Chukwudeme, E. A. 2008. Relative permeability as a function of temperature, initial water saturation and flooding fluid compositions for modified oil-wet chalk. Journal of Petroleum Science and Engineering, 63(1), 61-72. doi: 10.1016/j.petrol.2008.10.002.

Havre, T. E., Sjöblom, J., and Vindstad, J. E. 2003. Oil/water-partitioning and interfacial behavior of naphthenic acids. *Journal of dispersion science and technology*, *24*(6), 789-801. doi:10.1081/DIS-120025547.

Hiorth, A., Cathles, L. M., and Madland, M. V. 2010. The impact of pore water chemistry on carbonate surface charge and oil wettability. Transport in porous media. 85(1), 1-21. doi: 10.1007/s11242-010-9543-6.

Hirasaki, G., and Zhang, D. L. 2004. Surface Chemistry of Oil Recovery From Fractured, Oil-Wet, Carbonate Formations. SPE Journal 9(2): 151-162. SPE-88365-PA. http://dx.doi.org/10.2118/88365-PA.

Hognesen, E. J., Strand, S., and Austad, T. 2005. Waterflooding of preferential oil-wet carbonates: Oil recovery related to reservoir temperature and brine composition. SPE Europec/EAGE Annual Conference. Madrid, Spain. 13-16 June. doi:10.2118/94166-MS.

Huber, P., Nivelon, S., Ottenio, P., and Nortier, P. 2012. Coupling a chemical reaction engine with a mass flow balance process simulation for scaling management in papermaking process waters. *Industrial & Engineering Chemistry Research*, *52*(1), 421-429. DOI: 10.1021/ie300984y.

Hunter, K. D., Kerr, S. H., Ellis-Toddington, T. T., and McInnis, L. E. 2013. The Use of Modeling and Monitoring to Control Scale in Alberta ASP Floods. SPE: Society of Petroleum Engineers. doi:10.2118/165285-MS.

Jackson, A.C. 2006. Experimental Study of the Benefits of Sodium Carbonate on Surfactants for Enhanced Oil Recovery. MS Thesis, The University of Texas at Austin, Austin, Texas (December 2006).

Jang, S. H., Liyanage, P. J., Lu, J., Kim, D. H., Arachchilage, G. W. P. P., Britton, C., … Pope, G. A. 2014. Microemulsion Phase Behavior Measurements Using Live Oils at High Temperature and Pressure. SPE Improved Oil Recovery Symposium, Tulsa, Oklahoma, USA. 12-16 April. doi:10.2118/169169-MS.

Jerauld, G. R., Webb, K. J., Lin, C.Y., and Seccombe, J. C. 2008. Modeling Low-Salinity Waterflooding. SPE Reservoir Evaluation & Engineering. 11(06): 1000-1012. SPE-102239-PA. doi:10.2118/102239-PA.

Jerauld, G., Mohammadi, H., and Webb, K. J. 2010. Interpreting Single Well Chemical Tracer Tests. SPE: Society of Petroleum Engineers. doi:10.2118/129724-MS.

Kazempour, M., Manrique, E. J., Alvarado, V., Zhang, J., and Lantz, M. 2013. Role of active clays on alkaline–surfactant–polymer formulation performance in sandstone formations. *Fuel*, *104*, 593–606.

Kazempour, M., Sundstrom, E., and Alvarado, V. 2012. Geochemical modeling and experimental evaluation of high-pH floods: Impact of Water–Rock interactions in sandstone. *Fuel*, *92*(1), 216–230.

Khan, S. A. 1992. An expert system to aid in compositional simulation of miscible gas flooding. PhD dissertation. Austin, Texas, University of Texas at Austin.

Kon, W., Pitts, M. J., and Surkalo, H. 2002. Mature Waterfloods Renew Oil Production by Alkaline-Surfactant-Polymer Flooding. SPE Eastern Regional Meeting, Lexington, Kentucky, 23-26 October. http://dx.doi.org/10.2118/78711-MS.

Korrani, A. K. N., Jerauld, G. R., and Sepehrnoori, K. 2014a. Coupled Geochemical-Based Modeling of Low Salinity Waterflooding. SPE Improved Oil Recovery Symposium, Tulsa, Oklahoma, USA, 12-16 April. http://dx.doi.org/10.2118/169115-MS.

Korrani, A. K. N., Sepehrnoori, K., and Delshad, M. 2013. A Novel Mechanistic Approach for Modeling Low Salinity Water Injection. SPE: Society of Petroleum Engineers. doi:10.2118/166523-MS.

Korrani, A. K. N., Sepehrnoori, K., and Delshad, M. 2014b. A Mechanistic Integrated Geochemical and Chemical Flooding Tool for Alkaline/Surfactant/Polymer Floods. Society of Petroleum Engineers. doi:10.2118/169094-MS.

Korrani, A. K. N., Sepehrnoori, K., and Delshad, M. 2014c. A Comprehensive Geochemical-Based Approach to Quantify the Scale Problems. SPE: Society of Petroleum Engineers. doi:10.2118/168196-MS.

Kozaki, C. 2012. Efficiency of low salinity polymer flooding in sandstone cores. MS Thesis, Austin, Texas, The University of Texas at Austin. (May 2012).

Kozeny, J. 1927. Uber kapillare Leitung der Wasser in Boden, Sitzungsber. Sitzungsberichte der Akademie der Wissenschaften in Wien 136: 271–306.

Lager, A., Webb, K. J., Black, C. J. J., Singleton, M., and Sorbie, K. S. 2008a. Low salinity oil recovery--An experimental investigation. *Petrophysics*, *49*(1), 28.

Lager, A., Webb, K. J., Collins, I. R., and Richmond, D. M. 2008b. LoSal Enhanced Oil Recovery: Evidence of Enhanced Oil Recovery at the Reservoir Scale. SPE: Society of Petroleum Engineers. doi:10.2118/113976-MS.

Lager, A., Webb, K., and Seccombe, J. 2011. Low Salinity Waterflood, Endicott, Alaska: Geochemical Study & Field Evidence of Multicomponent Ion Exchange. In *IOR 2011*.

Lake, L.W., *Enhanced Oil Recovery*, Prentice-Hall, Inc, Englewood Cliffs, NJ, 1989, 142-148.

Lashgari, H. 2014. Development of a Four-Phase Thermal-Chemical Reservoir Simulator for Heavy Oil. PhD dissertation. Austin, Texas, University of Texas at Austin. (December 2014).

Lashgari, H., Delshad, M., Sepehrnoori, K., and De Rouffignac, E. P. 2014a. Development of Electrical Joule''s Heating Simulation for Heavy Oil Reservoirs. Society of Petroleum Engineers. doi:10.2118/170173-MS.

Lashgari, H., Lotfollahi, M., Delshad, M., Sepehrnoori, K., and De Rouffignac, E. P. 2014b. Steam-Surfactant-Foam Modeling in Heavy Oil Reservoirs. Society of Petroleum Engineers. doi:10.2118/170178-MS.

Le Chatelier, H. L. 1884. Comptes rendus. 99, 786-789.

Lee, S. Y., Webb, K. J., Collins, I., Lager, A., Clarke, S., O'Sullivan, M., Routh, A. F., Wang, X. 2010. Low Salinity Oil Recovery: Increasing Understanding of the Underlying Mechanisms. Society of Petroleum Engineers. doi:10.2118/129722-MS.

Li, X. 2012. A collection of case studies for verification of reservoir simulators. MS Thesis, Austin, Texas, The University of Texas at Austin. (August 2012).

Li, Z., and Delshad, M. 2013. Development of an Analytical Injectivity Model for Non-Newtonian Polymer Solutions. Society of Petroleum Engineers. doi:10.2118/163672-MS.

Ligthelm, D. J., Gronsveld, J., Hofman, J., Brussee, N., Marcelis, F., and van der Linde, H. 2009. Novel Waterflooding Strategy By Manipulation Of Injection Brine Composition. SPE: Society of Petroleum Engineers. doi:10.2118/119835-MS.

Liu, J., Delshad, M., Pope, G. A., and Sepehrnoori, K. 1994. Application of higher-order flux-limited methods in compositional simulation. Transport in Porous media, 16(1), 1-29.

Liu, Q., and Maroto-Valer, M. M. 2010. Investigation of the pH effect of a typical host rock and buffer solution on CO2 sequestration in synthetic brines. *Fuel Processing Technology*, *91*(10), 1321–1329.

Liu, S. 2007. Alkaline Surfactant Polymer Enhanced Oil recovery Process. PhD dissertation. Rice University, Houston, Texas (December 2007).

Liu, S., Zhang, D., Yan, W., Puerto, M., Hirasaki, G. J., and Miller, C. A. 2008. Favorable Attributes of Alkaline-Surfactant-Polymer Flooding. SPE Journal. 13(1): 5-16. SPE-99744-PA. http://dx.doi.org/10.2118/99744-PA.

Liu, X., and Civan, F. 1995. Formation Damage by Fines Migration Including Effects of Filter Cake, Pore Compressibility, and Non-Darcy Flow - A Modeling Approach to Scaling From Core to Field. SPE: Society of Petroleum Engineers. doi:10.2118/28980-MS.

Lohne, A., Han, L., van der Zwaag, C., van Velzen, H., Mathisen, A.-M., Twyman, A., … Hatzignatiou, D. G. 2009. Formation-Damage and Well-Productivity Simulation. *SPE-122241-PA*. doi:10.2118/122241-PA.

Lohne, A., Purwanto, E., and Fjelde, I. 2012. Gravity Segregated Flow in Surfactant Flooding. SPE Europec/EAGE Annual Conference. Copenhagen, Denmark. 4-7 June. doi:10.2118/154495-MS.

Lohrenz, J., Bray, B. G., and Clark, C. R. 1964. Calculating viscosities of reservoir fluids from their compositions. Journal of Petroleum Technology, 16(10), 1-171.

Luo, H., Al-Shalabi, E. W., Delshad, M., Panthi, K., Sepehrnoori, K. 2015. A Robust Geochemical Simulator to Model Improved Oil Recovery Methods. To be presented in SPE Reservoir Simulation Symposium, 23-25 February 2015, Houston, Texas.

Mackay, E. J. 2003. Modeling In-Situ Scale Deposition: The Impact of Reservoir and Well Geometries and Kinetic Reaction Rates. *SPE-81830-PA*. doi:10.2118/81830-PA.

Mahani, H., Sorop, T., Ligthelm, D. J., Brooks, D., Vledder, P., Mozahem, F., and Ali, Y. 2011. Analysis of field responses to low-salinity waterflooding in secondary and tertiary mode in Syria. SPE: Society of Petroleum Engineers. doi:10.2118/142960-MS.

Mangold, D.C., and Tsang, C.F. 1991. A Summary of Subsurface Hydrological and Hydrochemical Models. Review of Geophysics.

Maroongroge, V. 1994. Modeling and application of tracers for reservoir characterization. PhD dissertation. Austin, Texas, The University of Texas at Austin (December 1994).

Mazzolini, E. I., Bertero, L., and Truefitt, C. S. 1992. Scale prediction and laboratory evaluation of BaSO4 scale inhibitors for seawater flood in a high-barium environment. SPE production engineering, 7(02), 186-192.

McGuire, P. L., Chatham, J. R., Paskvan, F. K., Sommer, D. M., and Carini, F. H. 2005. Low Salinity Oil Recovery: An Exciting New EOR Opportunity for Alaska's North Slope. SPE Western Regional Meeting. Irvine, California. 30 March-1 April. doi:10.2118/93903-MS.

Merdhah, A. B. B., and Yassin, A. A. M. 2009. Scale Formation Due to Water Injection in Malaysian Sandstone Cores. *American Journal of Applied Sciences*, *6*(8).

Merdhah, A. B., and Yassin, A. M. 2008. Formation damage due to scale formation in porous media resulting water injection. *System*, *14*, 15.

Mikhailov, N., and Chirkov, M. 2010. Formation Damage Kinetics and its Effect on Oil Reservoir Productivity. SPE: Society of Petroleum Engineers. doi:10.2118/128403-MS.

Mitchell, R. W., Grist, D. M., and Boyle, M. J. 1980. Chemical Treatments Associated With North Sea Projects. *SPE-7880-PA*. doi:10.2118/7880-PA.

Moghadasi, J., Jamialahmadi, M., Müller-Steinhagen, H., and Sharif, A. 2003a. Scale Formation in Oil Reservoir and Production Equipment during Water Injection (Kinetics of CaSO4 and CaCO3 Crystal Growth and Effect on Formation Damage). SPE: Society of Petroleum Engineers. doi:10.2118/82233-MS.

Moghadasi, J., Jamialahmadi, M., Müller-Steinhagen, H., Sharif, A., Ghalambor, A., Izadpanah, M. R., and Motaie, E. 2003b. Scale Formation in Iranian Oil Reservoir and Production Equipment During Water Injection. SPE: Society of Petroleum Engineers. doi:10.2118/80406-MS.

Mohammadi, H. 2008. Mechanistic Modeling, Design, and Optimization of Alkaline/Surfactant/Polymer Flooding. PhD dissertation. The University of Texas at Austin, Austin, Texas (December 2008).

Mohammadi, H., Delshad, M., and Pope, G. A. 2009. Mechanistic Modeling of Alkaline/Surfactant/Polymer Floods. SPE Reservoir Evaluation & Engineering 12(4): 518-527. SPE-110212-PA. http://dx.doi.org/10.2118/110212-PA.

Mohan, K. 2009. Alkaline Surfactant Flooding for Tight Carbonate Reservoirs. SPE Annual Technical Conference and Exhibition, New Orleans, Louisiana, 4-7 October. http://dx.doi.org/10.2118/129516-STU.

Mohebbinia, S. 2013. Advanced Equation of State Modeling for Compositional Simulation of Gas Floods. PhD dissertation. Austin, Texas, University of Texas at Austin (December 2013).

Mohebbinia, S., Sepehrnoori, K., and Johns, R. T. 2013. Four-Phase Equilibrium Calculations of Carbon Dioxide/Hydrocarbon/Water Systems With a Reduced Method. *SPE-154218-PA*. doi:10.2118/154218-PA.

Mohebbinia, S., Sepehrnoori, K., and Johns, R. T., and Korrani, A. K. N. 2014. Simulation of Asphaltene Precipitation during Gas Injection Using PC-SAFT EOS. SPE: Society of Petroleum Engineers.

Monk, P. M. 2008. Physical chemistry: understanding our chemical world. John Wiley and Sons.

Muller, M., Parkhurst, D., L., and Charlton, S., R. 2011. Programming PHREEQC Calculations with C++ and Python a Comparative Study.

Najafabadi, F. N. 2009. Modeling Chemical EOR Processes Using IMPEC and Fully Implicit Reservoir Simulators. PhD dissertation. Austin, Texas, University of Texas at Austin (August 2009).

Najafabadi, N. F., Delshad, M., Sepehrnoori, K., Nguyen, Q. P., and Zhang, J. 2008. Chemical Flooding of Fractured Carbonates Using Wettability Modifiers. Society of Petroleum Engineers. SPE Symposium on Improved Oil Recovery. Tulsa, Oklahoma, USA. 20-23 April. doi:10.2118/113369-MS.

Nardi, A., Idiart, A., Trinchero, P., de Vries, L. M., and Molinero, J. 2014. Interface COMSOL-PHREEQC (iCP), an efficient numerical framework for the solution of coupled multiphysics and geochemistry. Computers & Geosciences, 69(0), 10–21. doi:10.1016/j.cageo.2014.04.011.

Nardi, A., Trinchero, P., de Vries, L., Idiart, A., and Molinero, J. 2012. Coupling multiphysics with geochemistry: The COMSOL-PHREEQC interface. In *COMSOL Conference*.

Nasralla, R. A., Alotaibi, M. B., and Nasr-El-Din, H. A. 2011a. Efficiency of Oil Recovery by Low Salinity Water Flooding in Sandstone Reservoirs. SPE: Society of Petroleum Engineers. doi:10.2118/144602-MS.

Nasralla, R. A., and Nasr-El-Din, H. A. 2011b. Impact of Electrical Surface Charges and Cation Exchange on Oil Recovery by Low Salinity Water. SPE: Society of Petroleum Engineers. doi:10.2118/147937-MS.

Nasralla, R. A., Bataweel, M. A., and Nasr-El-Din, H. A. 2011c. Investigation of Wettability Alteration by Low Salinity Water. Offshore Europe.

Nelson, R. C., Lawson, J. B., Thigpen, D. R., and Stegemeier, G. L. 1984. Cosurfactant-Enhanced Alkaline Flooding. SPE Enhanced Oil Recovery Symposium, Tulsa, Oklahoma, 15-18 April. http://dx.doi.org/10.2118/12672-MS.

Nghiem, L., Sammon, P., Grabenstetter, J., and Ohkuma, H. 2004. Modeling CO2 Storage in Aquifers with a Fully-Coupled Geochemical EOS Compositional Simulator. SPE: Society of Petroleum Engineers. doi:10.2118/89474-MS.

Ohen, H. A., and Civan, F. 1989. Formation Damage In Petroleum Reservoirs I: Modeling. *SPE-19380-MS*.

Okasha, T. M., and Al-Shiwaish, A. A. 2009. Effect of Brine Salinity on Interfacial Tension in SPE Middle East Oil and Gas Show and Conference Society of Petroleum Engineers. Bahrain, Bahrain. 15-18 March. doi:10.2118/119600-MS.

Okocha, C. and Sorbie, K. 2013. Scale Prediction for Iron, Zinc, and Lead Sulfides and Its Relation to Scale Test Design. SPE: Society of Petroleum Engineers. doi:10.2118/164111-MS.

Okuno, R., Johns, R.T., and Sepehrnoori, K. 2010. Three-Phase Flash in Compositional Simulation Using a Reduced Method. SPE Journal, 15(3), 689-703. doi: http://dx.doi.org/10.2118/125226-PA.

Omekeh, A. V., Evje, S., Fjelde, I., and Friis, H. A. 2011. Experimental and modeling investigation of ion exchange during low salinity waterflooding. In *SCA 2011-038 presented at the International Symposium of the Society of Core Analysts, Austin, Texas, USA* (pp. 18–21).

Parkhurst, D. L., and Appelo, C. A. J. 1999. User's guide to PHREEQC (Version 2): A computer program for speciation, batch-reaction, one-dimensional transport, and inverse geochemical calculations.

Parkhurst, D. L., and Appelo, C. A. J. 2013. Description of Input and Examples for PHREEQC Version 3--a Computer Program for Speciation, Batch-reaction, One-dimensional Transport, and Inverse Geochemical Calculations.

Parkhurst, D. L., Kipp, K. L., and Charlton, S. R. 2010. PHAST Version 2-A program for simulating groundwater flow, solute transport, and multicomponent geochemical reactions. US Geological Survey Techniques and Methods, 6, A35.

Parkhurst, D.L., Thorstenson, D.C., and Plummer, L.N. 1980. PHREEQE--A computer program for geochemical calculations.

Patacchini, L., De Loubens, R., and Moncorge, A. 2012. Four-fluid-phase, fully implicit simulation of surfactant flooding. Society of Petroleum Engineers. Abu Dhabi International Petroleum Conference and Exhibition. Abu Dhabi, UAE. 11-14 November. doi:10.2118/161630-MS.

Patil, S. B., Dandekar, A. Y., Patil, S., and Khataniar, S. 2008. Low Salinity Brine Injection for EOR on Alaska North Slope (ANS). IPTC: International Petroleum Technology Conference. doi:10.2523/12004-MS.

Paulo, J., Mackay, E. J., Menzies, N., and Poynton, N. 2001. Implications of Brine Mixing in the Reservoir for Scale Management in the Alba Field. SPE: Society of Petroleum Engineers. doi:10.2118/68310-MS.

Peaceman, D. W. 1978. Interpretation of well-block pressures in numerical reservoir simulation (includes associated paper 6988). Society of Petroleum Engineers Journal, 18(03), 183-194.

Peng, D. Y., and D. B. Robinson. 1976. A New Two-Constant Equation of State. Industrial & Engineering Chemistry Fundamentals 15(1): 59-64.

Peru, D. A., and Lorenz, P. B. 1990. Surfactant-Enhanced Low-pH Alkaline Flooding. SPE Reservoir Engineering. 5(3): 327 - 332. SPE-17117-PA. http://dx.doi.org/10.2118/17117-PA.

Pu, H., Xie, X., Yin, P., and Morrow, N. R. 2010. Low-Salinity Waterflooding and Mineral Dissolution. SPE: Society of Petroleum Engineers. doi:10.2118/134042-MS.

Qi, Q., Gu, H., Li, D., and Dong, L. 2000. The Pilot Test of ASP Combination Flooding in Karamay Oil Field. International Oil and Gas Conference and Exhibition in China, Beijing, China, 7-10 November. doi:10.2118/64726-MS.

Qing, J., Zhou, B., Zhang, R., Chen, Z., and Zhou, Y. 2002. Development and Application of a Silicate Scale Inhibitor for ASP Flooding Production Scale. SPE: Society of Petroleum Engineers. doi:10.2118/74675-MS.

Rezaei Gomari, K. A., and Hamouda, A. A. 2006. Effect of fatty acids, water composition and pH on the wettability alteration of calcite surface. Journal of petroleum science and engineering, 50(2), 140-150. doi: 10.1016/j.petrol.2005.10.007.

RezaeiDoust, A., Puntervold, T., and Austad, T. 2011. Chemical verification of the EOR mechanism by using low saline/smart water in sandstone. *Energy & Fuels*, *25*(5), 2151–2162.

Rezaveisi, M., Johns, R. T., and Sepehrnoori, K. 2014a. Application of Multiple Mixing-Cell Method to Improve Speed and Robustness of Compositional Simulation. SPE Improved Oil Recovery Symposium. Tulsa, Oklahoma, USA. 12-16 April. doi:10.2118/169063-MS.

Rezaveisi, M., Sepehrnoori, K., and Johns, R. T. 2014b. Tie-Simplex-Based Phase-Behavior Modeling in an IMPEC Reservoir Simulator. SPE Journal. 19(02): 327-339. SPE-163676-PA. doi:10.2118/163676-PA.

Rivet, S., Lake, L. W., and Pope, G. A. 2010. A Coreflood Investigation of Low-Salinity Enhanced Oil Recovery. SPE: Society of Petroleum Engineers. doi:10.2118/134297-MS.

Robertson, E. P. 2007. Low-Salinity Waterflooding to Improve Oil Recovery-Historical Field Evidence. SPE: Society of Petroleum Engineers. doi:10.2118/109965-MS.

Romanuka, J., Hofman, J., Ligthelm, D. J., Suijkerbuijk, B., Marcelis, F., Oedai, S., … Austad, T. 2012. Low Salinity EOR in Carbonates. SPE Improved Oil Recovery Symposium. Tulsa, Oklahoma, USA. 14-18 April. doi:10.2118/153869-MS.

Saad, N. 1989. Field Scale Simulation of Chemical Flooding. PhD dissertation, The University of Texas at Austin, Austin, Texas (August 1989).

Seccombe, J. C., Lager, A., Webb, K. J., Jerauld, G., and Fueg, E. 2008. Improving Wateflood Recovery: LoSalTM EOR Field Evaluation. SPE: Society of Petroleum Engineers. doi:10.2118/113480-MS.

Seccombe, J., Lager, A., Jerauld, G., Jhaveri, B., Buikema, T., Bassler, S., … Fueg, E. 2010. Demonstration of Low-Salinity EOR at Interwell Scale, Endicott Field, Alaska. SPE: Society of Petroleum Engineers. doi:10.2118/129692-MS.

Shakiba, M. 2014. Modeling and Simulation of Fluid Flow in Naturally and Hydraulically Fractured Reservoirs Using Embedded Discrete Fracture Model

(EDFM). MS Thesis, Austin, Texas, The University of Texas at Austin. (December 2014).

Shariatpanahi, S. F., Strand, S., and Austad, T. 2011. Initial wetting properties of carbonate oil reservoirs: effect of the temperature and presence of sulfate in formation water. Energy & Fuels, 25(7), 3021-3028. doi: 10.1021/ef200033h.

Sharifi, M., and Shaikh, M. 2013. Investigation of Optimum Salinity of Injected Water in Carbonate Reservoirs using Wettability Measurement and Core Flooding. SPE Reservoir Characterization and Simulation Conference and Exhibition. Abu Dhabi, UAE. 16-18 September. doi:10.2118/165992-MS.

Sheng, J. J. 2013. A Comprehensive Review of Alkaline-Surfactant-Polymer (ASP) Flooding. SPE Western Regional & AAPG Pacific Section Meeting 2013 Joint Technical Conference, Monterey, California, USA, 19-25 April. http://dx.doi.org/10.2118/165358-MS.

Shirdel, M. 2013. Development of a Coupled Wellbore-Reservoir Compositional Simulator for Damage Prediction and Remidiation. PhD dissertation. Austin, Texas, University of Texas at Austin. (August 2013).

Song, W., Yang, C., Han, D., Qu, Z., Wang, B., and Jia, W. 1995. Alkaline-Surfactant-Polymer Combination Flooding For Improving Recovery of the Oil with High Acid Value. International Meeting on Petroleum Engineering, Beijing, China, 14-17 November. http://dx.doi.org/10.2118/29905-MS.

Steefel, C.I., and Lasaga, A.C. 1992. Putting Transport into Water-Rock Interaction Models. Journal of Geology.

Strand, S., Standnes, D. C., and Austad, T. 2006. New wettability test for chalk based on chromatographic separation of SCN^- and SO_4^{2-}. 2006. Journal of Petroleum Science and Engineering, 52(1), 187-197. doi: 10.1016/j.petrol.2006.03.021.

Sultani, B., Szabo, G., Zeng, H., and Abdallah, W. 2012. Novelty in Smart Water Screening and Designing. SPE EOR Conference at Oil and Gas West Asia. Muscat, Oman. 16-18 April. doi:10.2118/155643-MS.

Sundstrom, E. A. 2011. Impact of Rock-Fluid and Fluid-Fluid Interaction in Chemical Flooding. MS Thesis. University of Wyoming, Laramie, Wyoming (August 2011).

TACC (Texas Advanced Computing Center). 2014. https://www.tacc.utexas.edu/user-services/user-guides/lonestar-user-guide.

Taghavifar, M. 2014. Enhanced Heavy Oil Recovery by Hybrid Thermal-Chemical Processes. PhD dissertation. Austin, Texas, University of Texas at Austin. (May 2014).

Tang, G. Q., and Morrow, N. R. 1996. Effect of temperature, salinity and oil composition on wetting behavior and oil recovery by waterflooding. In *SPE annual technical conference* (pp. 45–60).

Tavassoli, S., Lu, J., Pope, G. A., and Sepehrnoori, K. 2014a. Investigation of the Critical Velocity Required for a Gravity-Stable Surfactant Flood. SPE Journal. 19(5): 931-942. http://dx.doi.org/10.2118/163624-PA.

Tavassoli, S., Pope, G. A., and Sepehrnoori, K. 2014b. Frontal Stability Analysis of Surfactant Floods. Paper SPE 169118 presented at the SPE Improved Oil Recovery Symposium, Tulsa, OK, USA.

Tjomsland, T., Grotle, M. N., and Vikane, O. 2001. Scale Control Strategy and Economical Consequences of Scale at Veslefrikk. SPE: Society of Petroleum Engineers. doi:10.2118/68308-MS.

Truesdell, A. H., and Jones, B. F. 1974. WATEQ, a computer program for calculating chemical equilibria of natural waters (p. 73). US Department of the Interior, Geological Survey.

Turek, E. A., R. S. Metcalfs, L. Yarborough, and R. L. Robinson Jr. 1984. Phase Equilibria in CO_2 - Multicomponent Hydrocarbon Systems: Experimental Data and an Improved Prediction Technique. SPE Journal 24(3): 308-324.

Tweheyo, M. T., Zhang, P., and Austad, T. 2006. The Effects of Temperature and Potential Determining Ions Present in Seawater on Oil Recovery From Fractured Carbonates. SPE/DOE Symposium on Improved Oil Recovery. Tulsa, Oklahoma, USA. 22-26 April. doi:10.2118/99438-MS.

UTCHEM Technical Documentation 9. 2000. The University of Texas at Austin.

UTCHEM User's Guide 7. 2011. The University of Texas at Austin.

UTCOMP Technical Documentation 3.8. 2011. The University of Texas at Austin.

UTCOMP User's Guide. 2012. The University of Texas at Austin.

Vargo, J., Turner, J., Bob, V., Pitts, M. J., Wyatt, K., Surkalo, H., and Patterson, D. 2000. Alkaline-Surfactant-Polymer Flooding of the Cambridge Minnelusa Field. SPE

Reservoir Evaluation & Engineering. 3(6): 552-558. SPE-68285-PA. http://dx.doi.org/10.2118/68285-PA.

Venkatraman, A. 2014. Gibbs free energy minimization for flow in porous media. PhD dissertation, The University of Texas at Austin, Austin, Texas (May 2014).

Verma, A., and Pruess, K. 1988. Thermohydrological conditions and silica redistribution near high-level nuclear wastes emplaced in saturated geological formations. *Journal of Geophysical Research: Solid Earth (1978–2012), 93*(B2), 1159–1173.

Vikas. 2002. Simulation of CO2 Sequestration. PhD dissertation. Austin, Texas. University of Texas at Austin (2002).

Vledder, P., Gonzalez, I. E., Carrera Fonseca, J. C., Wells, T., and Ligthelm, D. J. 2010. Low Salinity Water Flooding: Proof of Wettability Alteration On A Field Wide Scale. SPE: Society of Petroleum Engineers. doi:10.2118/129564-MS.

Vo, L. T., Gupta, R., and Hehmeyer, O. J. 2012. Ion Chromatography Analysis of Advanced Ion Management Carbonate Coreflood Experiments. Abu Dhabi International Petroleum Conference and Exhibition. Abu Dhabi, UAE. 11-14 November. doi:10.2118/161821-MS.

Wang, W., and Gu, Y. 2003. Detection and Reuse of the Produced Chemicals in Alkaline-Surfactant-Polymer Floods. SPE Annual Technical Conference and Exhibition, Denver, Colorado, 5-8 October. http://dx.doi.org/10.2118/84075-MS.

Wang, Y., Liu, J., Liu, B., Liu, Y., Wang, H., and Chen, G. 2004. Why Does Scale Form in ASP Flood? How to Prevent from It?--A Case Study of the Technology and Application of Scaling Mechanism and Inhibition in ASP Flood Pilot Area of N-1DX Block in Daqing. SPE: Society of Petroleum Engineers. doi:10.2118/87469-MS.

Webb, K. J., Black, C. J. J., and Al-Ajeel, H. 2004. Low Salinity Oil Recovery - Log-Inject-Log. SPE: Society of Petroleum Engineers. doi:10.2118/89379-MS.

Webb, K. J., Black, C. J. J., and Edmonds, I. J. 2005. Low salinity oil recovery–The role of reservoir condition corefloods. In *13th European Symposium on Improved Oil Recovery*.

Weerasooriya, U. P., and Pope, G. A. 2011. Surfactant-Less Alkaline-Polymer Formulations for Recovering Reactive Crude Oil. U.S. Patent Application 13/115,433.

Wei, L. 2011. Interplay of capillary, convective mixing and geochemical reactions for long-term CO_2 storage in carbonate aquifers. First Break, 29(1).

Wei, L. 2012. Sequential Coupling of Geochemical Reactions with Reservoir Simulations for Waterflood and EOR Studies. SPE Journal. 17(2): 469-484. SPE-138037-PA. http://dx.doi.org/10.2118/138037-PA.

Williams, G. J. J., Mansfield, M., MacDonald, D. G., and Bush, M. D. 2004. Top-Down Reservoir Modelling. SPE: Society of Petroleum Engineers. doi:10.2118/89974-MS.

Wissmeier, L., and Barry, D. A. 2011. Simulation tool for variably saturated flow with comprehensive geochemical reactions in two-and three-dimensional domains. Environmental Modelling & Software, 26(2), 210-218. doi: 10.1016/j.envsoft.2010.07.005.

Wright, R. J., and Hall, J. R. F. 1994. Scale Prediction, Measurement, and Control in a Subsea Satellite Field. SPE: Society of Petroleum Engineers. doi:10.2118/27606-MS.

Wu, Y.S., and Bai, B. 2009. Efficient Simulation for Low Salinity Waterflooding in Porous and Fractured Reservoirs. SPE: Society of Petroleum Engineers. doi:10.2118/118830-MS.

Xiao, S. 1994. Multigrid methods with application to reservoir simulation. PhD dissertation. Austin, Texas. University of Texas at Austin (May 1994).

Xiao, Y., Xu, T., and Pruess, K. 2009. The effects of gas-fluid-rock interactions on CO_2 injection and storage: Insights from reactive transport modeling. *Energy Procedia, 1*(1), 1783–1790.

Xie, Q., Liu, Y., Wu, J., and Liu, Q. 2014. Ions tuning water flooding Experiments and interpretation by thermodynamics of wettability. Journal of Petroleum Science and Engineering. DOI: 10.1016/j.petrol.2014.07.015.

Xu, H. 2012. Potential for Non-Thermal Cost-Effective Chemical Augmented Waterflood for Producing Viscous oils. MS thesis. The University of Texas at Austin, Austin, Texas, (December 2012).

Xu, H., Kim, D. H., and Delshad, M. 2013. Potential for Non-thermal Cost-effective Chemical Augmented Waterflood for Producing Viscous Oils. SPE Western Regional & AAPG Pacific Section Meeting 2013 Joint Technical Conference, Monterey, California, USA, 19-25 April, http://dx.doi.org/10.2118/165350-MS.

Xu, T., Kharaka, Y. K., Doughty, C., Freifeld, B. M., and Daley, T. M. 2010. Reactive transport modeling to study changes in water chemistry induced by CO2 injection at the Frio-I Brine Pilot. *Chemical Geology*, *271*(3), 153–164.

Xu, T., Zheng, L., and Tian, H. 2011. Reactive transport modeling for CO2 geological sequestration. *Journal of Petroleum Science and Engineering*, *78*(3), 765–777.

Yang, X., Liao, G., Han, P., Yang, Z., and Yao, Y. 2003. An Extended field Test Study on Alkaline-surfactant-polymer flooding in Beiyiduanxi of Daqing Oilfield. SPE Asia Pacific Oil and Gas Conference and Exhibition, Jakarta, Indonesia. 9-11 September. http://dx.doi.org/10.2118/80532-MS.

Yeboah, Y. D., Somuah, S. K., and Saeed, M. R. 1993. A New and Reliable Model for Predicting Oilfield Scale Formation. SPE: Society of Petroleum Engineers. doi:10.2118/25166-MS.

Yeh, G.T., and Tripathi, V.S. 1989, A critical evaluation of recent developments in hydrogeochemical transport models of reactive multichemical components. Water Resources Research, 25(1), 93–108.

Yi, Z., and Sarma, H. K. 2012. Improving Waterflood Recovery Efficiency in Carbonate Reservoirs through Salinity Variations and Ionic Exchanges: A Promising Low-Cost "Smart-Waterflood" Approach. Abu Dhabi International Petroleum Conference and Exhibition. Abu Dhabi, UAE. 11-14 November. doi:10.2118/161631-MS.

Yildiz, H. O., and Morrow, N. R. 1996. Effect of brine composition on recovery of Moutray crude oil by waterflooding. *Journal of Petroleum Science and Engineering*, *14*(3), 159–168.

Yousef, A. A., Al-Saleh, S., Al-Kaabi, A. U., and Al-Jawfi, M. S. 2010. Laboratory Investigation of Novel Oil Recovery Method for Carbonate Reservoirs. Canadian Unconventional Resources and International Petroleum Conference. Calgary, Alberta, Canada. 19-21 October. doi:10.2118/137634-MS.

Yousef, A. A., Liu, J. S., Blanchard, G. W., Al-Saleh, S., Al-Zahrani, T., Al-Tammar, H., Al-Mulhim, N. 2012. Smart Waterflooding: Industry's First Field Test in Carbonate Reservoirs. SPE Annual Technical Conference and Exhibition. San Antonio, Texas, USA. 8-10 October. doi:10.2118/159526-MS.

Yu, L., Evje, S., Kleppe, H., Kårstad, T., Fjelde, I., and Skjaeveland, S. M. 2009. Spontaneous imbibition of seawater into preferentially oil-wet chalk cores-

Experiments and simulations. Journal of petroleum science and engineering, 66(3), 171-179. doi: 10.1016/j.petrol.2009.02.008.

Zahid, A., Stenby, E. H., and Shapiro, A. A. 2012. Smart Waterflooding (High Sal/Low Sal) in Carbonate Reservoirs. SPE Europec/EAGE Annual Conference. Copenhagen, Denmark. 4-7 June. doi:10.2118/154508-MS.

Zaretskiy, Y. 2012. Towards Modeling Physical and Chemical Effects during Wettability Alteration in Carbonates at pore and Continuum Scales. PhD Dissertation, Heriot-Watt University, (May 2012).

Zekri, A. Y., Nasr, M. S., and Al-Arabai, Z. I. 2011. Effect of LoSal on Wettability and Oil Recovery of Carbonate and Sandstone Formation. International Petroleum Technology Conference. Bangkok, Thailand. 15-17 November. doi:10.2523/14131-MS.

Zhang, G., and Villegas, E. I. 2012. Geochemical Reactive Transport Modeling in Oil & Gas Industry-Business Drivers, Challenges and Solutions. Proceedings, tough Symposium.

Zhang, P., Tweheyo, M. T., and Austad, T. 2007. Wettability alteration and improved oil recovery by spontaneous imbibition of seawater into chalk: Impact of the potential determining ions Ca^{2+}, Mg^{2+}, and SO_4^{2-}. Colloids and Surfaces A: Physicochemical and Engineering Aspects, 301(1), 199-208. doi: 10.1016/j.colsurfa.2006.12.058.

Zhang, W., Li, Y., and Omambia, A. N. 2011. Reactive transport modeling of effects of convective mixing on long-term CO2 geological storage in deep saline formations. *International Journal of Greenhouse Gas Control*, *5*(2), 241–256.

Zhu, C., and Anderson, G. 2002. Environmental applications of geochemical modeling. Cambridge University Press. 393 p.